Rock Magnetic and Palaeomagnetic Investigations of the Gardar Lava Succession, South Greenland

Thesis submitted in accordance with the requirements of the University of Liverpool for the degree of Doctor in Philosophy

by

Neil Thomas

February 1992

ABSTRACT

This thesis describes the results, and geomagnetic significance, of detailed rock magnetic and palaeomagnetic investigations of the Eriksfjord Group lavas within the Mid-Proterozoic Gardar Igneous Province of South Greenland.

Stepwise thermal demagnetisation and Principal Component Analysis of magnetic remanence has identified mean directions and pole positions for all three lava formations from the Group. The Lower Lava Formation has a mean direction of D/I = 293.4/25.4, (α_{95} = 6.3, k = 52.9) and a corresponding palaeomagnetic pole position of 28.1° N, 194.7°E, (dp = 3.8, dm = 6.7). Two polarity reversals are present in the Lower Formation - one at the base (R→N) and one at the top (N→R), with only a single flow recording the reversed polarity in each case. Two mean directions of magnetisation were isolated for the stratigraphically-thin Middle Lava Formation - the 'A' direction of D/I = 161.8/42.0, (α_{95} = 5.1, k = 141.1) with a corresponding Virtual Geomagnetic Pole (VGP) at 8.6°N, 313.5° E, (dp = 3.1, dm = 6.6) and the 'B' direction of D/I = 139.7/-16.0, (α_{95} = 7.2, k = 87.9) and a VGP at 35.4°N, 344.3° E, (dp = 4.3, dm = 7.2). Two successive complete reversals (N →R→N) are present in the Upper Lava Formation, with evidence for two more, which appear to correlate with reversals identified in a previous study. The mean directions for the normal and reversed flows are D/I = 284.6/36.9 (α_{95} = 9.9, k = 14.1) and D/I = 97.3/-17.4 (α_{95} = 7.1, k = 90.1) with corresponding pole positions at 29.7°N, 207.0°E. and 16.0° N, 206.1°E respectively. The normal and reversed fields show an average inclination asymmetry of 20° .

Palaeomagnetic contact tests were performed on Late Gardar dykes and an alkaline intrusive complex emplaced into the Lower and Upper Lava Formations respectively. Results of these tests confirm that the remanence held by the lava flows of these Formations predates these Late Gardar intrusions.

Extensive rock magnetic investigations show that the majority of flows in all three Lava Formations contain a single magnetic mineral, which is magnetite for some flows and haematite for others. The flows of the Lower Lava Formation are characterised by magnetite with mixed grain sizes dominated by multi-domain (MD) but including varying amounts of single-domain (SD) and cation- deficient (CD) material. Ten flows from the Middle Lavas contain haematite and eight contain magnetite. In the Upper Lava Formation, fourteen flows contain haematite and fifteen contain magnetite, the latter being dominated by MD grains. There is a tendency for normally magnetised flows to contain magnetite and reversely magnetised flows to contain haematite, which provides further support for the oxidation- polarity correlation. The magnetic mineralogy of all three Lava Formations can be explained in terms of high temperature (deuteric) oxidation, which has resulted in the acquisition and retention of a primary thermo- chemical remanence (TCRM). However, low temperature oxidation is also witnessed but is unique to the flows of the Lower Lava Formation. This is characterised by the development of maghaemite.

Flows from the Lower Lava Formation provide the most reliable field intensity estimates, since they possess a magnetic mineralogy which is most

suited to successful palaeointensity work. Consequently, intensity estimates were made using the modified versions of both the Thellier and Shaw techniques. Good agreement was observed between the mean Thellier and Shaw results ($34.3 \pm 1.6\mu T$ and $33.8 \pm 1.8\mu T$ respectively) corresponding to mean Virtual Dipole Moments (VDMs) of $(8.2 \pm 0.5) \times 10^{22} Am^2$ and $(8.0 \pm 0.7) \times 10^{22} Am^2$. These are similar to VDM estimates from other Precambrian rocks. No reliable field intensity estimates were obtained from the Upper Lava Formation using the Shaw technique. The mean Thellier palaeointensities for the normal and reversed flows from this formation are $31.4 \pm 1.7\mu T$ and $10.8 \pm 0.9\mu T$ (mean VDMs of $(6.9 \pm 0.3) \times 10^{22} Am^2$ and $(2.7 \pm 0.2) \times 10^{22} Am^2$). This large difference in N and R intensities, coupled with the inclination asymmetry, suggests that the field may not have been a simple geocentric axial dipole at the time of emplacement of these lavas. Spherical Harmonic Analysis of the field reveals that these anomalies are consistent with a geomagnetic model comprising a reversing geocentric dipole, a partly-reversing quadrupole and a partly- reversing octupole, with the octupole being stronger than the quadrupole in the reversed field.

The Middle Lava Formation shows the lowest mean palaeointensity values of $8.1 \pm 0.6\mu T$ and $9.0 \pm 1.0\mu T$ (VDMs $= (1.7 \pm 0.1) \times 10^{22} Am^2$ and $(2.3 \pm 0.2) \times 10^{22} Am^2$ respectively). This observation, allied with the palaeodirectional, rock magnetic and supporting geological evidence implies that the basal seven flows of this Formation were erupted during a polarity inversion.

A new method for assessing the suitability of magnetite-bearing basalts, with mixed magnetic grain sizes, is described.. This method, more thorough in its approach than previous methods, correlates the behaviour of samples during palaeointensity analysis with their rock magnetic properties and defines selection/rejection criteria based on these correlations. This new method may have general applicability for assessing the suitability of ancient basalts for palaeointensity investigations.

Declaration

I declare that the work submitted is entirely the results of my own investigations and that the work has not already been accepted in substance for any degree, and is not concurrently submitted in candidature for any degree.

Dennis Neil Thomas ..... (candidate)

This thesis is dedicated to the memory of my beloved father.

"Stay close to us until we meet again....."

ACKNOWLEDGEMENTS

"I never cared for the sound of being alone"

(Neil Diamond, 1971)

This project was completed during the tenure of a N.E.R.C research studentship and I am grateful to the council for its financial assistance by way of both my grant and the expenses which allowed me to visit Copenhagen and Vienna for two International Conferences.

I am deeply indebted to my supervisors Dr. John Piper and Dr. John Shaw, who have guided me through a very enjoyable project. Thanks also to Dr. Peter Dagley for helping to keep the "Geomagnetism ship" sailing and for his valuable discussions. Special mention should be given to John Piper for his expertise in the field but particularly for putting up with my occasional homesickness and moods in Greenland. His patience and understanding made for two very productive field seasons and his love for South Greenland infected even me. I am grateful to Prof. Brian Upton and Dr. Sue Mingard of the Grant Institute at Edinburgh for their initial help with the logistics of the first Greenland visit. I am also grateful to Dr. John Share for supplying me with Danish currency and travellers cheques at very short notice! John Piper and I are both indebted to our good friend Ole Plesner for his logistical expertise in Greenland and most of all for his incomparable humour - a truly great man! Thanks also to his wife Marie for feeding us so well after fieldwork.

I would like to thank the staff and students of the Southampton University Geophysical Sciences and Geology departments for providing me with a love of the subject and a desire to pursue postgraduate studies. Special thanks to Andy Langridge, Andy Clitheroe, Greg Jones, Gruff Dodd, Dave Proudlove, Andy Barker, Bob Foster, Derek Moore, John Marshall, and most of all, to Prof. Norman Hamilton and Dr. Ernie Hailwood. I am also grateful to Murty for his valuable discussions which stimulated my interest in rock magnetism.

There are many people, too numerous to mention, whose presence in my life during last few years have kept me sane and have made the transition from "life down south" to "life up north" an experience and a pleasure. My thanks especially go to Rich, Graham, Dave, and Suzanne for their friendship and particularly to Rich for René's late night café! Thanks to Mary for keeping my flat in shape during my bouts of number-crunching and thanks to the porters and security staff for helping to make a tutor's job a little easier.

Special words of thanks go to my friends and team-mates in the Birkenhead Park F.C. Oxton XV. Cheers lads for re-incarnating my rugby career and for keeping Saturday afternoons sacred.

I am deeply indebted to all my friends and colleagues at the Geomagnetism Laboratory who have helped in many ways during the past 3 years, particularly to Tim Rolph, Graham Sherwood, Del Atkinson, Jenny Tait, Jenny King, Derek France, Candy Bevan-Lean, Dot Rolland, Marj Brash and Joan Dean. Special thanks are due to Tim Rolph who has suffered greatly whilst proof reading this thesis! His help and intelligent discussions have been invaluable. I am also grateful to Drs. A.E. Mussett and R.D.J. Oglethorpe for their help with the radiometric dating performed as part of this project.

I have had the pleasure of being a Hall Tutor at Roscoe and Gladstone for three years and during this time, I have been lucky to have the friendship of some wonderful people. Thanks to Dominic, Ashley, Pete, Yvonne, Joanne, Mark A, Mark B, John, Sue, Marianne and everyone else for being good pals and, of course, to Gordon for keeping us all in line!

On a personal note, during the past three years, my family have been extremely supportive to me, and particularly to my mother, in what has been the most trying period of our lives. I will never be able to thank David, Janice, Stan, Carole, Margaret, Mark, Alison, Raymond and Angela enough for all they have done.

Finally, some people who deserve a special mention. Dominic Hames has shown admirable patience and forbearance for many hours during the writing up stage and I thank him deeply for all the work he has put in. To all my friends in Llanelli and Wick Ferry, particularly to Leysh, Rich Chin and Martin for being excellent drinking partners and to Maria, Carol and Andy for being wonderful house mates in Southampton and for putting up with my singing!

My heartfelt thanks and love go to Paula-Lee, who has nursed me through the bad times, both academically and personally and has enjoyed the good times with me. The love she has given me will never be forgotten.

Lastly, and most importantly, to the two people who this is all for - Mam and Dad, who have supported me financially and emotionally throughout my education. Mam, you have suffered the greatest loss of all but, no one could have done more than you. Dad, I only wish you could have seen it through to the end but I know you'll always be with me. To you both, my love always.

LIST OF ABBREVIATIONS

EG = Eriksfjord Group
NRM = Natural Remanent Magnetisation
TRM = Thermoremanent Magnetisation
PTRM = Partial Thermoremanent Magnetisation
CRM = Chemical Remanent Magnetisation
TCRM = Thermochemical Remanent Magnetisation
VRM = Viscous Remanent Magnetisation
IRM = Isothermal Remanent Magnetisation
SIRM = Saturation Isothermal Remanent Magnetisation
ARM = Anhysteretic Remanent Magnetisation
DRM = Detrital (Depositional) Remanent Magnetisation
PDRM = Post-depositional Remanent Magnetisation
GRM = Gyroremanent Magnetisation
T_c = Curie temperature
T_b = Blocking temperature
T_R = Room temperature (30°C)
K_{RT} = Room temperature susceptibility
AMS = Anisotropy of susceptibility
TIFR = Tata Institute of Fundamental Research
RM = Rock Magnetic
SP = Superparamagnetic
SD = Single domain
MD = Multi-domain
PM = Paramagnetic
M_{rs} = Saturation remanence
M_s = Saturation magnetisation
H_c = Coercivity (Coercive force)
KLT = Low temperature susceptibility
KHT = High temperature susceptibility
VSM = Vibrating Sample Magnetometer
AFD = Alternating Field Demagnetisation
MDF = Median Destructive Field
D = Declination

I = Inclination

Lat = Latitude

Long = Longitude

APWP = Apparent Polar Wander Path

B_a = Palaeointensity

SQUID = Superconducting Quantum Interference Detector

VDM = Virtual Dipole Moment

VGP = Virtual Geomagnetic Pole

GAD = Geocentric Axial Dipole

OAD = Offset Axial Dipole

CMB = Core-mantle boundary

Table of Contents

"There is a principle which is a barr against all information, which is a proof against all argument and which cannot fail to keep a man in everlasting influence. That is - contempt prior to investigation."

Herbert Spencer

INTRODUCTION

Since the development of magnetometers as an outcome of research motivated by the Second World War, a large volume of investigations have been made into the Earth's magnetic field over the past forty years or so. The outcome of this research has elevated the study of the Earth's magnetism to one of the most interesting and important of the geophysical sciences.

Three main research areas can be defined in this field: rock and mineral magnetism, Palaeomagnetism and Archaeomagnetism, and Geomagnetism. Rock and mineral magnetism is the branch of the subject which studies the various magnetic minerals which preserve a record of the characteristics of the Earth's magnetic field. Palaeomagnetism is the study of the strength and direction of the Earth's magnetic field, as recorded by rocks, during geological times. Archaeomagnetism is the study of the Earth's magnetic field, recorded by archaeological artefacts, during archaeological times. The third area, Geomagnetism, is the branch of the subject which combines palaeomagnetic and archaeomagnetic observations with the contemporary record of the magnetic field at magnetic observatories around the world to investigate the geometry and source of the magnetic field during recent, historical and geological time.

In order to determine whether the geometry and source of the Earth's magnetic field during the most recent and best-understood part of Earth history are comparable to the field during its remote history, it is important to undertake studies of ancient rocks. In practise, this is made difficult because the rock record becomes generally more scanty and sparsely-preserved with increasing age. This thesis attempts to perform such a study for a small interval of the longest, and oldest, era of geological time - the Precambrian - for which a suitable range of rocks is well preserved.

If an analogy is made, whereby the whole of geological time is represented by one calendar year and one day is equivalent to about 13 Ma of time, the Precambrian era would extend from January 1st. to approximately November 15th. and our own lives would cover a mere fraction of the last second of the year. This simple analogy illustrates that approximately 87% of geological time is represented by the Precambrian era. In contrast, only a very small percentage of the total research into the Earth's magnetic field has originated from studies of Precambrian rocks. This project has aimed to go some way towards redressing the balance by performing a rock magnetic, and palaeomagnetic study of basaltic lavas from the Eriksfjord Group within the Gardar Igneous Province of South Greenland. In our calendar analogy, these rocks formed in just under two hours sometime around September 22nd.

The aims of the project

The initial aims of the project were as follows:

1. To palaeomagnetically sample the entire lava succession exposed within the Eriksfjord Group and perform a detailed study of the variation of the direction of the geomagnetic field during the time of formation of these rocks. A detailed magnetostratigraphy for the Gardar lava succession could thus be defined. Particular emphasis was placed upon the middle of the three Lava Formations comprising the succession, where a previous study (Piper, 1977) identified anomalous results.

2. To examine the reality and significance of the reversal asymmetry witnessed in the previous study.

3. To perform a detailed study of the magnetic mineralogy of the flows comprising the Gardar lavas so that the magnetic characteristics of the remanence carriers could be identified. This information is essential to the understanding of the palaeomagnetic results obtained in the remainder of the project.

4. To investigate the variation in the strength (intensity) of the geomagnetic field during the time of formation of the Gardar lavas. Two standard techniques were used for this palaeointensity analysis.

5. To collate all palaeomagnetic results in order to examine the nature of the geomagnetic field source which prevailed during the formation of the Gardar lavas.

6. To make recommendations, based on the experiences of the present study, to aid future palaeomagnetic work using rocks of comparable age and magnetic mineralogy.

As with all research ventures, new objectives were identified as the project developed. The major new objective was to perform a detailed study of the suitability of basalt samples, with mixed grain sizes of magnetite, for use in palaeointensity experiments. This study provides a rapid but thorough approach to the popular palaeomagnetic problem of selecting samples which are most suitable for palaeointensity work, thus decreasing the time wasted on measuring unsuitable samples during palaeointensity experiments, which are very time-consuming.

The scope of the thesis

This thesis has been written in a format which attempts to describe the results and implications of each separate section of the project. It also emphasises that the separate sections follow in a logical order and combine to describe a picture of the geomagnetic field during the Gardar period. The techniques and theory relevant to each chapter are described within that chapter and not in a general chapter at the beginning of the thesis. This allows the reader to focus on a particular chapter without needing to refer to a general chapter to understand the theory involved.

All the separate chapters of this thesis are inter-related. In Chapter 1, the fundamental general theory of the Earth's magnetic field, rock magnetism and palaeomagnetism are described. This general theory is applied to the Gardar lavas in Chapters 3-8, which describe the results of the present study.

Chapter 2 introduces the reader to the geology of the Gardar Province, in general, and specifically to the geology of Eriksfjord Group which was identified for the present study. Geological features described in this chapter are constantly referenced throughout the project and have an important bearing on the results of the palaeomagnetic study.

Chapters 3-6 describe the results of rock magnetic and palaeomagnetic investigations on the Gardar lavas. These chapters should be treated as a large inter-related section. Chapter 3 describes the theory and experimental results from rock magnetic investigations on the Gardar lavas. These results give information on the composition and sizes of the magnetic remanence carriers in the lavas and their oxidation states. This information is crucial to understanding the nature and origin of the magnetic remanence held by the

lavas. Chapter 4 describes the sampling of, and palaeodirectional results from, the Gardar lavas. A detailed magnetostratigraphy for the succession is defined and pole positions for the three lava groups calculated and compared with previous data. Chapter 5 describes results from palaeomagnetic field tests on the Upper and Lower Lava formations, including baked contact tests, an agglomerate test and results from an unsuccessful attempt to date the lavas using the $^{39}Ar - ^{40}Ar$ stepwise degassing method. The results from the field tests are crucial to establishing the age of the remanence held by the lavas and, consequently, dictate whether or not the palaeomagnetic results can be be interpreted in the context of the geomagnetic field during Early Gardar times. In Chapter 6, the palaeointensity of the Early Gardar geomagnetic field, as recorded by the lavas, is investigated. Two palaeointensity methods are used - the modified versions of the Thellier and Shaw techniques. These results describe the variation in field strength and Virtual Dipole Moment during the time covered by the formation of the Gardar lavas.

In Chapters 7 and 8 results of the preceeding chapters are brought together and analysed in the wider context of the project as a whole. Chapter 7 combines the results from Chapters 3 and 6 to propose a new method for determining the suitability of samples for use in palaeointensity work based on their behaviour during rock magnetic and palaeointensity experiments. This method does not involve any new experimental techniques but examines a new way of analysing rock magnetic and palaeointensity data. In Chapter 8, the geomagnetic significance of all palaeomagnetic results (direction and intensity) is examined. Possible explanations for the differences observed in the palaeomagnetic results for normally and reversely magnetised lavas are discussed and a model is proposed which best represents the observed data.

This project therefore brings together the three disciplines involved in the analysis of the Earth's magnetic field - rock and mineral magnetism, palaeomagnetism (palaeodirections and palaeointensities) and geomagnetism - and applies them to a geological situation from part of the oldest era of geological time in order to evaluate the nature of the Earth's magnetic field, some 1300 Ma ago.

CHAPTER 1 : GENERAL THEORY

1.1 THE EARTH'S MAGNETIC FIELD

1.1.1 Main features of the field

If the Earth's magnetic field (the geomagnetic field) is measured at the surface of the planet, it is found to be a very weak feature. Even near the poles, where it is at its strongest, it is several hundred times weaker than the field between the poles of a toy horseshoe magnet. The elements of the geomagnetic field are illustrated and defined in Figure 1.1 (a). The total intensity F, the declination D and the inclination I completely describe the field at any point on the Earth's surface. The line along which the inclination is zero is called the magnetic equator and the points at which the inclination is $\pm 90°$, i.e. where the field is vertical, are the magnetic poles. At the north magnetic pole, $I = +90°$ and at the south magnetic pole, $I = -90°$.

The present geomagnetic field approximates to that of a bar magnet at the centre of the Earth, tilted at an angle of 11.5° to the axis of rotation. A line passing through the axis of this magnet intersects the surface of the Earth at two points known as the geomagnetic poles (Figure 1.1 (b)). The magnetic and geomagnetic poles would coincide if the Earth's field was perfectly described by a geocentric dipole. However, this is not the case since approximately 10% of the field remains when the effect of this dipole is removed. The remaining field is called the non-dipole field which, along with the dipole field, changes with time. This change is known as the secular variation of the geomagnetic field and is nowadays an important research topic in itself.

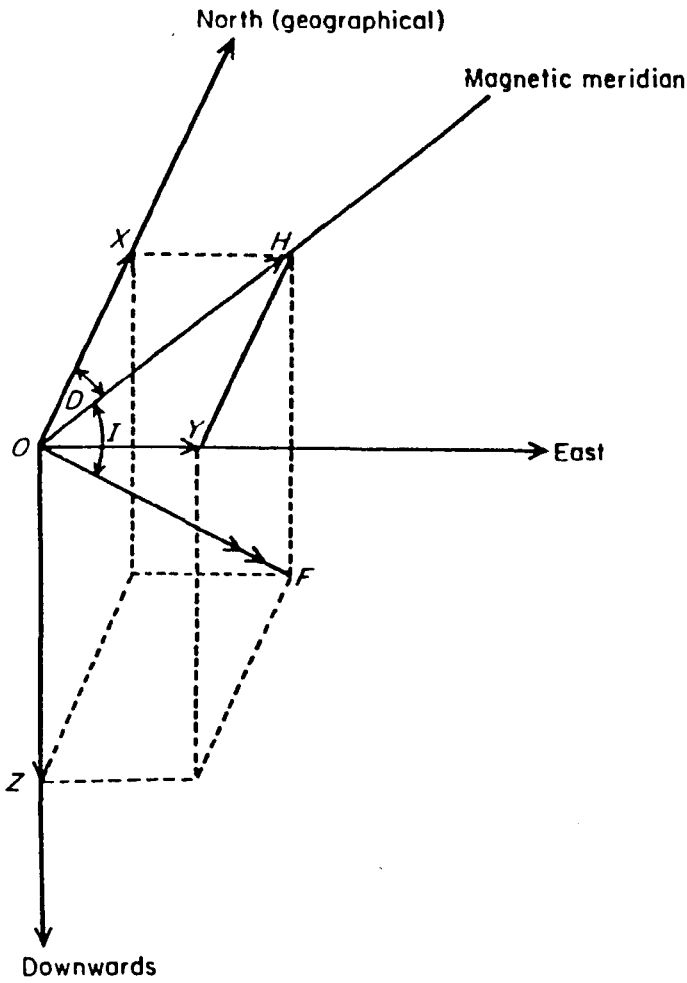

Figure 1.1a : The main elements of the geomagnetic field. The deviation, D, of a compass needle from true north is the declination (reckoned positive east of true north). The compass lies in the magnetic meridian containing the total field F which makes an angle I with the horizontal, termed the inclination (or dip). The inclination is reckoned positive downwards (as in the northern hemisphere) and negative upwards (as in the southern hemisphere). The horizontal and vertical components of F are denoted by $H = F\cos I$ and $Z = F\sin I$ respectively. Z is reckoned positive downwards as for I. The horizontal component can be resolved into two components $X = H\cos D$ (northwards) and $Y = H\sin D$ (eastwards), $F^2 = H^2 + Z^2$. Then $\tan D = Y/X$ and $\tan I = Z/H$ (from Merrill and McElhinny, 1983).

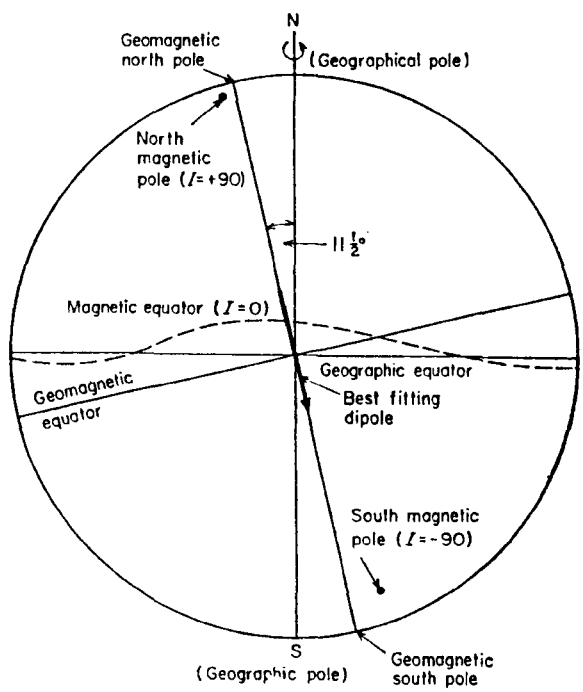

Figure 1.1b : An illustration of the distinction between the magnetic geomagnetic and geographic poles and equators (from McElhinny 1973)

1.1.2 Description of the present field by Spherical Harmonic Analysis (SHA)

A common method of describing the total magnetic field at the Earth's surface is by Spherical Harmonic Analysis (SHA) which was first used by Gauss in 1839. Assuming the Earth to be a sphere of radius **a** (**a** = 6371 km), the magnetic field at the surface can be expressed as the magnetic scalar potential V, where:

$$V = \frac{a}{\mu_0} \sum_{n=0}^{\infty} \sum_{m=0}^{n} P_n^m(\cos\theta) \left\{ \left[C_n^m \left(\frac{r}{a}\right)^n + (1 - C_n^m)\left(\frac{a}{r}\right)^{n+1} \right] g_n^m \cos(m\phi) + \left[S_n^m \left(\frac{r}{a}\right)^n + \left(1 - S_n^m \left(\frac{a}{r}\right)^{n+1}\right) \right] h_n^m \sin(m\phi) \right\} \quad [1.1]$$

C_n^m and S_n^m are positive numbers between 0 and 1 representing the contribution to the potential from external sources, $(1-C_n^m)$ and $(1-S_n^m)$ refer to sources of internal origin, P_n^m are Schmidt functions and θ and ϕ are the colatitude and longitude respectively.

If the field measurements are averaged over a few years, the external effect is negligible and equation 1.1 reduces to:

$$V = \frac{a}{\mu_0} \sum_{n=0}^{\infty} \sum_{m=0}^{n} \left(\frac{a}{r}\right)^{n+1} P_n^m(\cos\theta)(g_n^m \cos(m\phi) + h_n^m \sin(m\phi)) \quad [1.2]$$

The coefficients g_n^m and h_n^m are known as the Gauss coefficients, where n is the harmonic degree and m is the harmonic order. Harmonics are often calculated to degree 6 in models of the present field.

Physically, the g_1^0 term refers to a dipole of strength $\{(4\pi a^3/\mu_0)g_1^0\}$ directed along the rotation axis (z axis) in the positive direction. Similarly, the g_1^1 and

h_1^1 terms refer to dipoles along the +x and +y axes respectively in the equatorial plane of the sphere, orthogonal to the Greenwich Meridian. The present geocentric non-axial dipole can thus be described as a combination of g_1^1, g_1^1 and h_1^1 terms. The terms with n = 2 and n = 3 refer to the geocentric quadrupole and octupole respectively, and so on. Terms which have n = 0 and no longitudinal dependence are known as zonal harmonics. Bullard et al (1950) established that the non-dipole field was drifting westwards at a rate of 0.18° per year during the first half of this century. Alternative calculations, summarised by Yukutake (1962) and Rikitake (1966) confirm that this westward drift of the non-dipole field is close to 0.2° per year. There is no evidence to suggest that any non-dipole feature has lasted long enough to complete a full circuit of the Earth, which would take about 2000 years. (Merrill and McElhinny, 1983).

The dipole has also drifted westwards over the past 180 years at a rate of 0.01° per year (Barraclough, 1974) and its intensity has decreased by ≃8% over this period.

1.1.3 The ancient geomagnetic field

One of the most interesting outcomes of palaeomagnetic research is to show that many rocks record a permanent magnetisation in a direction opposite to that of the present field. Brunhes (1906) first discovered this "reversed" magnetisation in a lava flow from France. Subsequently, as the volume of palaeomagnetic results increased, more reversely magnetised rocks were discovered but it was not until the early 1960s that this phenomenon was proved to be an expression of the field rather than a property of the magnetic minerals in the rocks. Wilson (1962a) confirmed this when he discovered that a baked laterite intruded and reheated by a dyke recorded a reversed

direction similar to that of the dyke, whereas the unbaked part of the laterite recorded a different direction. Dagley et al (1967) recorded at least 60 polarity reversals in some 900 Icelandic lava flows, covering a period of about 20 m.y. This represents an average reversal rate of 3 m.y.$^{-1}$.

Usually, the directions of opposite polarity are anti-parallel (i.e. declination flips 180° and inclination changes sign) which suggests that the ancient field was essentially dipolar on average. This is compatible with the geocentric axial dipole (GAD) hypothesis which predicts that the Earth's magnetic field, when averaged over a period of time sufficiently long to cancel out secular variation ($\simeq 10^4$ years), will approximate to a geocentric dipole orientated along the Earth's rotational axis (Figure 1.2). Thus, at any given palaeolatitude, λ the inclination, I, is given by:

$$\tan I = 2 \tan \lambda \qquad (1.3)$$

In order to compare palaeomagnetic results for the ancient field from different localities, a palaeomagnetic pole is calculated, which represents the point where the dipole axis, defined from the locality, cuts the Earth's surface. Such poles, on the basis of the GAD hypothesis, should occupy the same position for each observing locality.

For any time-averaged field direction (D,I) at a site (λ, ϕ) the co-ordinates (λ', ϕ') of the palaeomagnetic pole are given by:

$$\sin \lambda' = \sin \lambda \cos \theta + \cos \lambda \sin \theta \cos D \qquad (1.4)$$

$$\text{where} \qquad -90 \leq \lambda' \leq +90 \quad \text{and} \quad 2 \cot \theta = \tan I$$

and,

$$\begin{aligned} \phi' &= \phi + \beta \quad \text{when} \quad \cos\theta \geq \sin\lambda \sin\lambda' \\ \text{or} \quad \phi' &= \phi + 180 - \beta \quad \text{when} \quad \cos\theta < \sin\lambda \sin\lambda' \end{aligned} \tag{1.5}$$

$$\text{where} \quad \sin\beta = \frac{\sin\theta \sin D}{\cos\lambda'} \quad (-90 \leq \beta \leq +90)$$

The pole described by these parameters is only a true palaeomagnetic pole if the data cover a time interval sufficient to average out the secular variation of the field ($> 10^4$ years). Spot measurements of the field, for example from a single lava flow, represent only an instantaneous record of the field at the time when the lava cooled. The 'pole' calculated from such a flow, using equations 1.4 and 1.5, is termed a Virtual Geomagnetic Pole (VGP). A number of VGPs, for lava flows recording a suitable time period, must be determined and averaged for a palaeomagnetic pole to be calculated.

The strength, B, of the GAD field at a colatitude θ is given by:

$$B = \frac{\mu_0 P}{4\pi a^3}\left(1 + 3\cos^2\theta\right)^{1/2} \tag{1.6}$$

where P = the magnetic dipole moment
a = radius of the earth
μ_0 = permeability of free space.

It is useful to express the field intensity in terms of its dipole moment, which is independent of latitude and thus allows direct comparison of intensity data, from any locality, to be made. This dipole moment is known as the Virtual Dipole Moment (VDM) (Smith, 1967a) and is given by:

$$\text{VDM} = \frac{Ba^3 4\pi}{\mu_0}\left(1 + 3\cos^2\theta\right)^{-1/2} \tag{1.7}$$

The variation of the VDM throughout geological time, and specifically for the Precambrian, will be discussed in Chapter 8.

1.1.4 Reversals of the geomagnetic field

The reversals of polarity experienced by the Earth's field are a separate subject in their own right and texts such as Jacobs (1984) address this topic in detail. The following section is merely designed to illustrate the basic features of field reversals.

There are certain instances where the declination and/or the inclination of the field have shown deviations in excess of that expected during normal secular variation. Such deviations are known as geomagnetic excursions. Among the best documented excursions are the Laschamp (Bonhommet and Babkine, 1967), the Lake Mungo (Barbetti and McElhinny, 1972,1976) and the Mono Lake excursions (Liddicoat and Coe, 1979). There has been extensive debate about the authenticity and cause of these excursions, and it remains possible that they are either global or localised events caused by fluctuations in the dipole or non-dipole field respectively. It is also possible that excursions are failed reversals (Hoffman, 1986).

Complete reversals of the field are unquestionably global events. The recognition of this fact made it possible to establish polarity time scales by correlating reversals in well-dated rocks from different geographical localities. Reversals are also able to account for the existence of "magnetic stripes", or marine magnetic anomalies, observed over the ocean basins. Detailed mapping of these anomalies has permitted definition of a Geomagnetic Polarity Time Scale (GPTS) which documens the magnetostratigraphy for approximately the last 180 Ma (e.g. Hailwood, 1989).

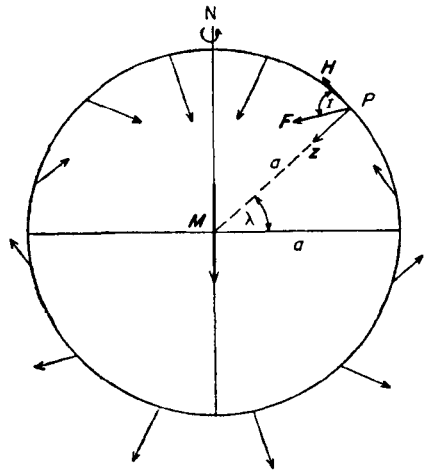

Figure 1.2 : The field due to an axial geocentric dipole (from McElhinny, 1973). M = Magnetic moment of the dipole, a = Radius of the Earth, λ = palaeolatitude at point P. All others symbols as for Figure 1.1(a).

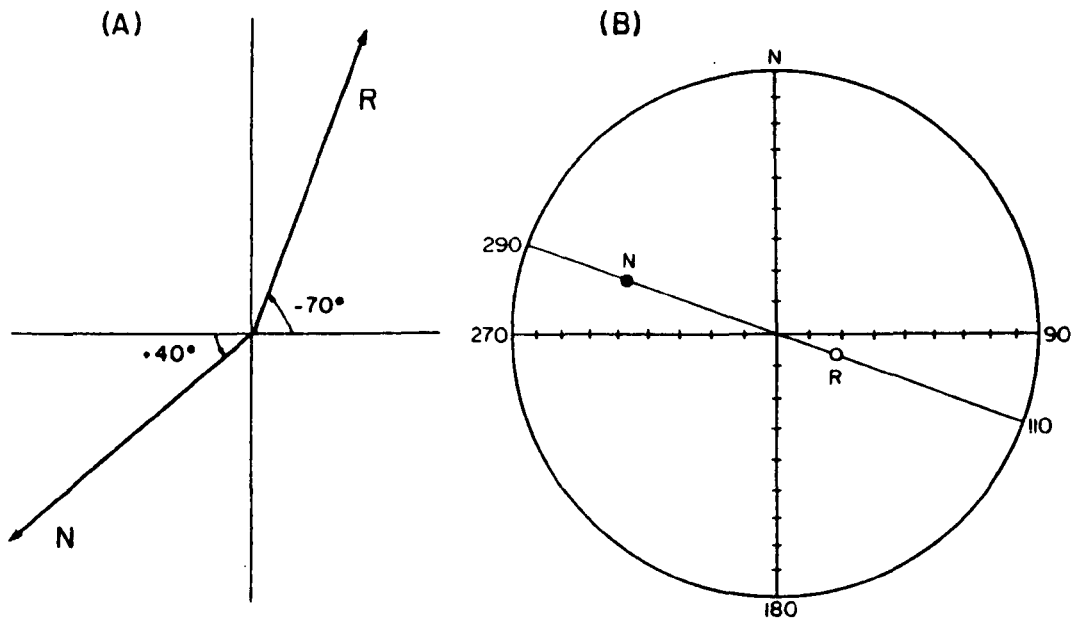

Figure 1.3 : Keweenawan asymmetric reversal. (A) Vector diagram (B) directions on a Lambert equal area projection. Open (closed) symbols indicate reversed (normal) polarity (from Pesonen, 1978).

It has been observed by several workers (e.g. Pesonen and Nevanlinna, 1981; Roy and Robertson, 1978; Vlasov and Popova, 1968; Piper, 1975) that reversals of the geomagnetic field are not always symmetrical. In other words, the two polarity states do not produce exactly anti-parallel magnetic field directions at a given site. For example, reversals in the Keweenawan Province of Canada have normal and reversed directions which differ by 180° in declination, but the reversed inclination is always steeper than the normal inclination. This field asymmetry is illustrated in Figure 1.3. The occurrence of asymmetric fields may be accounted for in terms of the departure of the Earth's field from its time-averaged simple GAD configuration, with the non-dipole field contributing to the permanent aspect of the geomagnetic field. The implications of asymmetry to geomagnetic field models in the context of the present study are discussed fully in Chapter 8.

1.1.5 Polarity Transitions

The period during which the geomagnetic field is in the process of changing from one polarity state to another is called a polarity transition, and the corresponding field behaviour is referred to as "transitional" or "intermediate". Polarity reversals are known to take $10^3 - 10^4$ years, a small time in geological terms. Since polarity transitions occupy only a small fraction of the time spent in normal and reversed states, finding formations which fully record polarity transitions is difficult. Generally, a quasi-regular extrusion of lava flows is required to accurately map the change in direction and intensity of the field. Sediments, whilst often continuously-deposited, generally have rates of sedimentation which were too slow to resolve the changes in detail. Complexities in the sedimentary record include those associated with post-depositional remanent magnetisation (Section 1.2.3), the

'inclination error' resulting from compaction effects, possible 'bedding-errors' resulting from the deposition of sediment on irregular and sloping surfaces, as well as diagenetic effects. Despite these difficulties, a number of polarity transitions have been documented, many of which are described in Jacobs (1984). Probably the most detailed study of both directional and intensity changes during a transition is that of Prévot et al (1985) for the Steens Mountain R-N polarity transition of Miocene age.

The definition of what constitutes a transitional field direction varies between authors. Hoffman (1984) defined a transitional direction as one which deviates by $> 30°$ from the expected GAD direction. McFadden and McElhinny (1982) regard it as a direction which deviates by $> 45°$ from the GAD direction and Wilson et al (1972), and later Roberts and Shaw (1984), define it as being one where the VGP colatitude lies between 40° and 140°.

The non-dipole field appears to dominate during a reversal, with the dipole field apparently decaying towards zero and then growing again in the opposite direction. Thus, the strength of the field would be expected to decrease during a reversal, and this is supported by a vast amount of palaeointensity data. Studies on Icelandic lavas (Dagley and Wilson, 1971; Wilson et al, 1972; Shaw et al, 1982; Roberts and Shaw, 1984) found that the intensity decreased to about 25% during a reversal. Prévot et al (1985) also recognised a decrease in intensity during the Steens mountain transition. They, and Hoffman (1986), suggested that the reversal process consists of a small number of geomagnetic impulses, with large changes in field direction interspersed with periods of relative stability, as opposed to a process occuring at a constant rate. Shaw (1975, 1977), however, found high intensities during field reversals recorded in lavas from Iceland and Nevada.

Clearly then, a great deal still needs to be determined about the behaviour of the field during polarity transitions.

The geomagnetic field is thought to originate within the core of the earth by means of a self-exciting dynamo. Gubbins (1984) concluded that no simple model for the field can explain all the features which are believed to be caused by motions within the liquid outer core. However, secular variation, reversals and field intensity changes are consistent with the dynamo theory.

For a more detailed account of aspects concerning the Earth's magnetic field, the reader is referred to Merrill and McElhinny (1983) and Jacobs (1984).

1.2 BASIC ROCK MAGNETIC THEORY

1.2.1 Types of magnetism in rocks

When a rock forms, it acquires a magnetisation in a direction parallel to the Earth's magnetic field provided that it has isotropic magnetic properties. Such a magnetisation, known as a primary magnetisation, gives information on the strength and direction of the magnetic field in which the rock formed. However, subsequent to its formation, the rock may be subjected to physical and/or chemical processes which result in the acquisition of a secondary magnetisation adding to, or replacing, the primary magnetisation. The total magnetisation initially measured in a laboratory is called the natural remanent magnetisation (NRM). A major problem in palaeomagnetic studies is the isolation of the primary and secondary components which make up the NRM.

An electron, in its path around an atomic nucleus creates a dipole field referred to as the orbital magnetic moment. In addition to this, the electron spins about its own axis, creating an additional magnetic moment called the spin moment. The resultant of the orbital and spin moments defines the magnetic dipole moment of the atom.

The magnetic behaviour of materials can be grouped into five types. When an atom is subjected to a magnetic field, the electrons precess about the applied field. These precessions cause a magnetic moment to be induced in the atom in a direction opposite to that of the applied field. This type of magnetism, exhibited by all substances, is called diamagnetism and is independent of temperature. Some substances have magnetic dipoles arising from unpaired electron spins. This magnetism is known as paramagnetism. The spin dipoles align with the applied field and the intensity of the resulting magnetisation is proportional to the strength of the applied field. The constant of proportionality is termed the magnetic susceptibility and is a measure of the ease with which a substance is magnetised. When the applied field is removed, the thermal energy of the paramagnetic material is sufficient to randomise the spin dipoles, resulting in a zero net magnetisation (O'Reilly, 1984).

Some substances exhibit a permanent (spontaneous) magnetisation even in the absence of an external magnetic field. Such substances exhibit ferromagnetism, ferrimagnetism or anti-ferromagnetism. In ferromagnetic materials, the spontaneous magnetisation is destroyed when the energy of interaction between atoms is smaller than the thermal energy of the system. This occurs at a critical temperature known as the Curie temperature (T_c), after which the ferromagnetic material behaves as a paramagnet.

In substances which are characterised by subdivision into two lattices referred to as A and B, the atomic moments of each lattice are aligned but are anti-parallel to one another. When the moments of A and B are equal, they cancel each other out and the net magnetism is zero (Figure 1.4). This is known as anti-ferromagnetism. Such substances do not have Curie temperatures because there is no net ferromagnetism. The critical temperature above which they become paramagnetic is called the Néel temperature. If, however, the atomic moments of the sub-lattices A and B are unequal then a net spontaneous magnetisation exists and a weak ferromagnetism results. This magnetism is called ferrimagnetism. Alternatively, the equal moments of A and B may not be exactly anti-parallel and a small spontaneous magnetisation results (Figure 1.4) due to this slight 'canting' in alignment. This type of magnetism is known as imperfect, or canted, anti-ferromagnetism. Both ferrimagnetic and canted anti-ferromagnetic substances behave as ferromagnets and have Curie temperatures. The important magnetic minerals are of these two types to which theories of ferromagnetism can be applied.

1.2.2 Magnetic grains and their energy

A number of factors affect the energy of a magnetic grain, they are:

1. Magnetostatic energy

This is the energy resulting from the magnetic poles which form on the surface of a grain. The larger the grain, the larger the magnetostatic energy.

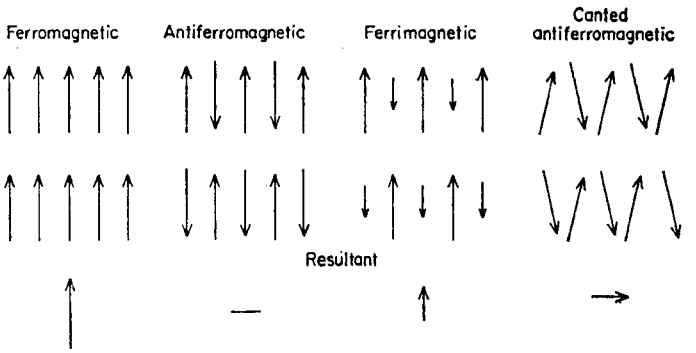

Figure 1.4 : An illustration of the spontaneous magnetisation vectors in crystals. The resultant spontaneous magnetisation is given at the bottom of the diagram (from McElhinny, 1973).

2. Magnetoelastic energy (Magnetostriction)

This is the strain which develops in a grain as a result of magnetic interaction between atoms when placed in an applied field. O'Reilly (1984) notes that the crystal lattice may deform by extending in the direction of the magnetisation of the grain or by contracting. Magnetoelastic strain energy is acquired if the deformation is impeded by the structure or magnetisation of the grain.

3. Magnetocrystalline anisotropy

In a magnetic grain, there are usually magnetic 'easy axes' and 'hard axes'. The easy axes are directions of minimum energy along which magnetic dipoles preferentially align. Thus, the magnetic properties of a material may vary with direction, resulting in a magnetocrystalline anisotropy, which is measured as the difference between the magnetisation in the easiest and hardest axes and is dependent only on crystal structure and composition.

Which of the above forces dominates will vary according to the size and shape of the grains. Once a critical grain size is exceeded, the magnetostatic energy is so great that it is energetically preferable for the grain to sub-divide into a number of regions of ordered magnetic spins known as domains. These domains will order themselves so that the magnetostatic energy is reduced to a minimum. Separating the domains, in which the spontaneous magnetisation is in different directions, are domain walls which possess a wall energy. Walls will continue to form until the energy required to form the wall exceeds the associated reduction in magnetostatic energy.

Domain walls are small (0.01-0.1 μm) compared with the size of the domains. If a magnetic grain has dimensions smaller than the domain wall, then it will comprise only one domain and is thus a single-domain (SD) or monodomain grain. Single domain grains can be divided into stable single domain (SSD) and superparamagnetic (SP) grains. The latter are so small that the thermal energy of the system is enough to prevent their magnetic moment from retaining a permanent alignment. The critical grain sizes of these transitions depend on temperature, the type and intensity of the magnetisation and the size, shape and magnetic mineralogy of the grain itself (Levi and Merrill, 1978). Dunlop (1973) showed experimentally that the upper limit for the SP-SSD transition is 0.035-0.05 μm for spherical grains at room temperature. At some critical size, the grain will be large enough to divide into two or more domains thus becoming a multi-domain (MD) grain. There is a region, just above the SD limit where grains are strictly speaking MD grains but exhibit SD behaviour. These are termed pseudo-single domain (PSD) grains (Dunlop, 1981). It is the magnetically hard PSD and SD grains which are able to preserve magnetic remanence for long periods of time and are therefore of primary importance in palaeomagnetism (Evans and McElhinny, 1969; Dunlop and West, 1969).

Butler and Banerjee (1975) and subsequently Soffel and Appel (1982) calculated that the one to two domain transition occurred in cubes exceeding 0.08 μm in dimension and in elongate grains of 2.5 : 1 length to width ratio which exceed 0.4 μm in length. Scherbakov and Lamash (1988) proposed that the metastable SD to MD transition is at 0.14 μm for cubes of magnetite. They note that all elongate magnetite grains with a length to width ratio of greater than 2.6 : 1 may support a metastable SD state.

1.2.3 Types of remanence in rocks

(1) Thermoremanent magnetisation (TRM)

On cooling from temperatures above their Curie temperatures in the presence of a magnetic field, igneous rocks typically acquire a remanent magnetisation parallel to the applied field; the magnitude of this remanence is also proportional to it provided that the field magnitude is less than about 100 μT (Nagata, 1943). This remanence is known as a thermoremanent magnetisation (TRM). For a certain grain volume, there is a temperature at which the magnetic grain becomes superparamagnetic and has a relaxation time (equation 1.8) of less than 1000s. This is known as the critical blocking temperature, T_b. The magnetic grains in a rock will cover a range of volumes which will have an associated range of blocking temperatures known as the blocking temperature spectrum. As a rock cools from its Curie temperature to the ambient temperature, the relaxation times of the associated grains will increase rapidly and their magnetic moments become effectively blocked. (equation 1.8). At the ambient temperature, the relaxation time of the grain will have increased greatly. The total TRM of a rock is the sum of the individual TRMs of the constituent magnetic grains of the rock. Thus as a rock cools and passes through the blocking temperature spectrum, its remanence will gradually increase, the rate of increase depending on the distribution of the blocking temperatures and hence the grain size distribution. The TRM is acquired over a range of blocking temperatures from the Curie temperature to room temperature as a series of partial thermoremanences (PTRMs) (Figure 1.5). The PTRM acquired in each interval is independent of that acquired over any other blocking temperature interval. The sum of the PTRMs is equal to the total TRM acquired from

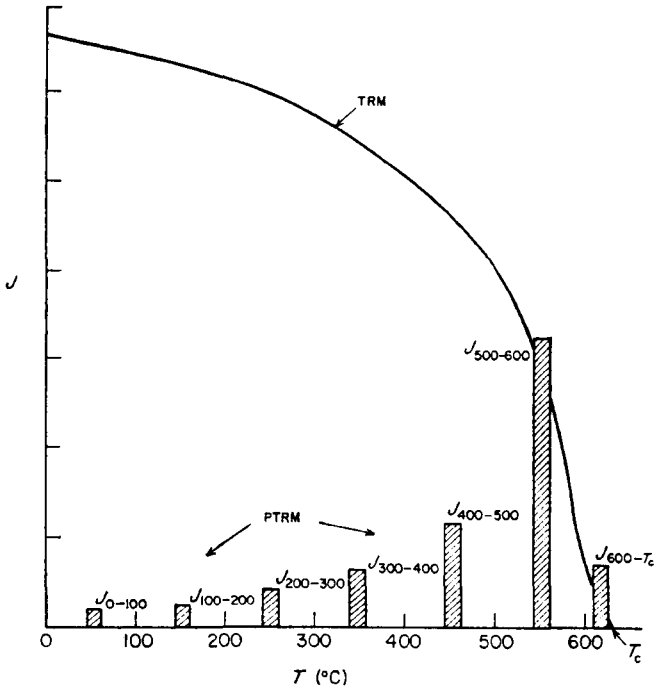

Figure 1.5 : The acquisition of a thermoremanent magnetisation (TRM). The partial TRMs acquired over successive temperature intervals add (JT1-T2) up to give the total TRM curve.

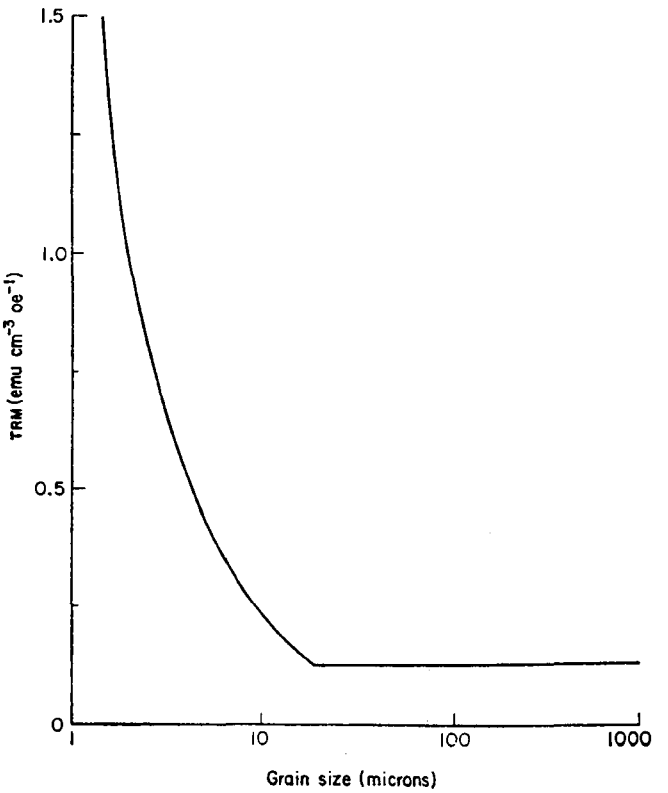

Figure 1.6 : Theoretical variation of TRM with grain size induced by low fields in approximately equidimensional magnetite grains from the multi-domain and pseudo-single domain theories of Stacey (1963) (from McElhinny (1973)).

the Curie point down to room temperature. This is expressed as the law of additivity of TRM (Thellier, 1951).

A rock can acquire a natural TRM in two different ways. The first is a TRM acquired by an extrusive or an intrusive igneous rock when it cools from its molten state ($T > T_c$) to the ambient temperature in the presence of the Earth's field. The second is when a rock is heated by a later event. If the temperature attained is greater than the Curie temperature of the rock then it may become totally remagnetised and acquire a new TRM in the prevailing field. If temperatures are not high enough to reach the blocking temperatures of some of the magnetic grains in the rock, it will acquire a partial TRM which is held by the grains with blocking temperatures below the temperature reached. Old rocks may well have been subjected to more than one heating event and may therefore possess several PTRMs, each originating in different orientations of the Earth's field. The presence of these later PTRMs makes it difficult or impossible to isolate the strength and direction of the field in which the original (primary) TRM was acquired.

For an igneous rock cooling from above its Curie temperature, the thermal energy becomes less than the anisotropy energy terms of the constituent magnetic grains, with the result that the magnetic moments of the grains become 'locked' in the direction of the Earth's field. The stronger the Earth's field, the greater the degree of alignment of magnetic moments and hence the stronger the TRM. For PTRMs acquired during metamorphism, an increase in thermal energy allows increasing numbers of magnetic grains to obtain sufficient thermal energy to move out of their original orientations and towards the new orientation of the Earth's field. These new orientations become 'locked' in when the rock cools down after the heating event. Grains

which are raised above their blocking temperatures by the metamorphism will not obtain this orientation until they fall below the metamorphic temperature.

For non-interacting SD grains of haematite and magnetite up to a few microns in size, the TRM is proportional to the applied field (Stacey, 1963). For grains in the PSD region ($\simeq 20\mu m$), Stacey (1963) recognised that the TRM is proportional to 1/d, where d is the diameter of the grain. For true MD grains, Dickson et al (1966) calculated that the TRM is roughly independent of grain size and is given by $J_{TRM} = F/8$, where F is the field strength. Figure 1.6 shows the variation of TRM with grain size based on theory and supported by experiments such as those of Parry (1965).

(2) Chemical remanent magnetisation (CRM)

A CRM is acquired by a rock when new magnetic minerals are formed, or old magnetic minerals altered, as a result of chemical changes occurring in the presence of a magnetic field at temperatures below the Curie temperature. In newly formed minerals, the CRM is acquired not as a result of passing through the blocking temperature but because the newly forming mineral increases beyond a critical volume, known as the blocking volume, V_b, below which it behaves superparamagnetically at the ambient temperature.

In lava flows, a chemical remanence is often acquired as a consequence of low temperature oxidation (Section 1.3.3) below the Curie point. Thus, the CRM is a secondary magnetisation which contaminates the primary TRM acquired during cooling and may record a different field direction to that of the TRM.

(3) Viscous remanent magnetisation (VRM)

A viscous remanence is acquired by magnetic grains which are able, at ambient temperatures, to change their magnetisation with time. Subsequent to the acquisition of a primary magnetisation, some magnetic grains are able to move from the primary remanence direction and reach equilibrium with the ambient geomagnetic field, resulting in the acquisition of a secondary viscous magnetisation. VRM is normally considered to be the remanence acquired viscously since the last polarity inversion, i.e. during the last 0.73 Ma. It is normally a soft remanence affecting grains of low coercivity or blocking temperature and is acquired as a result of the thermal activation of the grains (Néel, 1955). The time taken by a grain to equilibrate with a new magnetic field is described by its relaxation time, τ, where:

$$\frac{1}{\tau} = C \exp \frac{(-vH_cM_s)}{(2kT)} \qquad (1.8)$$

where
v = volume of grain
H_c = coercivity
M_s = saturation magnetisation
kT = Boltzmann factor
C = frequency factor $(\simeq 10^{10} s^{-1})$

VRM is dependent on grain size (Walton, 1980) and ambient temperature. Superparamagnetic grains have shorter relaxation times than stable SD grains and are thus more likely to contribute to VRM. The acquisition of a VRM follows the expression:

$$VRM = S_a \log_e t \qquad (1.9)$$

Where S_a is a temperature dependent acquisition coefficient and t is time.

This theoretical relationship is supported by experimental observation (Stacey and Banerjee, 1974).

(4) Isothermal remanent magnetisation (IRM)

Magnetic substances may also acquire a remanence without heating if subjected to a strong magnetic field. The effect of the field on the magnetic grains is to reduce the height of the anisotropy energy barriers parallel to the field and to increase the height of the barriers anti-parallel to the field. For a sufficiently strong field, the energy minima anti-parallel to the field will become maxima and those parallel to it will become minima. In this state, for SD grains, small thermal fluctuations are sufficient to displace the magnetisation vectors from their original positions to the direction of the new minima. For MD grains, domains having a magnetisation opposite to the field will be increased in energy and those parallel will be decreased. Domain walls will move in such a way that the volume of domains with parallel components is increased and that for domains with anti-parallel components is decreased. For sufficiently strong fields, the domain walls are pushed out of the grain which effectively behaves as a SD grain aligned parallel to the applied field. In both cases, removal of the strong field allows some magnetisation vectors to return to their original orientations but many remain in their new orientations giving rise to an IRM.

Magnetic grains with low coercivities are more susceptible to acquiring IRMs, thus an IRM can easily be removed by a.f. demagnetisation to low peak alternating fields. In nature, rocks may locally acquire an IRM by lightning strikes.

(5) Detrital (Depositional) remanent magnetisation (DRM)

A DRM occurs in sediments as a result of gravitational settling of previously magnetised grains in aqueous or aeolian media in the presence of the Earth's field. The grains experience a torque, due to the Earth's field, which tends to rotate and align them parallel to the field as they settle. The degree of alignment depends on a number of physical factors, discussed by McElhinny (1973). Grains further rotate under the influence of the Earth's magnetic field, during compaction and dewatering of the sediment, which modifies the DRM or is responsible for a new post-depositional remanence (PDRM). DRM and PDRM are not relevant to the magnetisation processes witnessed in igneous rocks and need not be considered further here.

(6) Anhysteretic remanent magnetisation (ARM)

ARM is an artificial remanence induced in a rock by applying an alternating field in the presence of a constant field. All magnetic grains with coercivities less than the peak alternating field, H_p, will follow the field direction as it alternates, passing around hysteresis loops. On each half cycle, the alternating field reduces anisotropy energy barriers in the direction of the field so that the net magnetic moments of grains with sufficiently low coercivities will flip into line with the applied field. On the second half cycle, the magnetic moments flip back into the opposite direction, in line with the field on this half of the cycle. When a constant field is superimposed on top of the a.f. it increases the field value in one half cycle and decreases it in the other resulting in an increase in the number of net magnetic moments that flip into the one direction relative to the other. The effect of the constant field is to further decrease the anisotropy energy barriers in the direction parallel to the constant field and to counteract the decrease in the opposite

direction. Thus, a sample that is subjected to combined alternating and constant fields has more magnetic moments flipping in the direction in which these two fields are parallel and less in the directions which they are anti-parallel.

When the a.f. is gradually reduced to zero, the field strength falls below the coercivity of a grain and it will cease to flip in response to the field and remain fixed in one of the mutually anti-parallel directions of the a.f. Eventually, all grains will cease to flip and there will be a greater number of magnetic moments parallel to the constant field than anti-parallel to it. The sample will then exhibit a magnetisation in the direction of the applied field. This is an anhysteretic remanence, or ARM. A total ARM is induced when the alternating field strength exceeds the coercivities of all grains in the sample, whereas a partial ARM results when the coercivities of only a fraction of the grains are exceeded.

1.3 THE MAGNETIC MINERALS

The magnetic minerals which are largely responsible for carrying the NRM in rocks are the iron-titanium oxides within the $FeO - TiO_2 - Fe_2O_3$ ternary system (Figure 1.7)

There are three single phases within this system - wustite (FeO), rutile (TiO_2) and haematite (Fe_2O_3). The three solid solution series within the system are:

1. The titanomagnetites (magnetite-ulvospinel)

2. The titanohaematites (haematite-ilmenite)

3. Pseudobrookite

Members of the pseudobrookite series are paramagnetic above liquid oxygen temperature (-210°C) and are not important to palaeomagnetism.

1.3.1 The Titanomagnetite Series

The end members of this series, magnetite (Fe_3O_4) and ulvospinel (Fe_2TiO_4) are cubic minerals and both possess an inverse spinel structure with the cations located in two sub-lattices A and B (Figure 1.8). The magnetite end member has the cation distribution $Fe^{3+}[Fe^{2+}Fe^{3+}]O_4$ where the cation outside the brackets is in the tetrahedral sites of the spinel structure and the cations inside the brackets are in the octahedral sites. The former are in four-fold co-ordination with the oxygen ions and the latter are in six-fold co-ordination. There are two B cations for every A cation, so that the interacting sub-lattices are unequal, resulting in the observed ferromagnetic behaviour for magnetite. Magnetite has a Curie temperature of 575°C.

Titanomagnetites have a composition $Fe_{3-x}Ti_xO_4$ where $0 < x < 1$, with the magnetic and physical properties changing with composition. The Curie temperature varies almost linearly with composition. In the titanomagnetite series, complete solid solution occurs in excess of 600°C, with more restricted solid solution at lower temperatures.

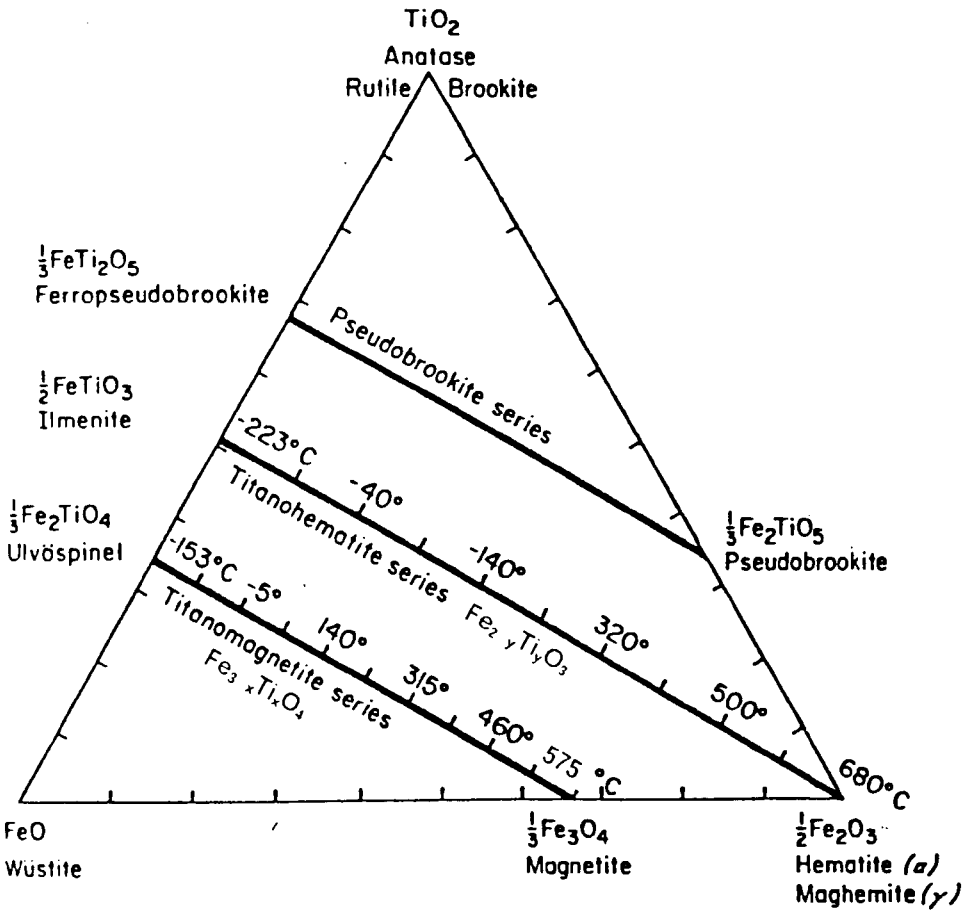

Figure 1.7 : The ternary diagram for the Fe-Ti oxide minerals: showing the two major solid solution series of magnetic oxides, the titanomagnetites and the titanohaematites. The Curie (Néel) temperatures of the various compositions are indicated. Maghaemite is chemically equivalent to haematite but is the metastable product of low temperature oxidation (from Merrill and McElhinny, 1983).

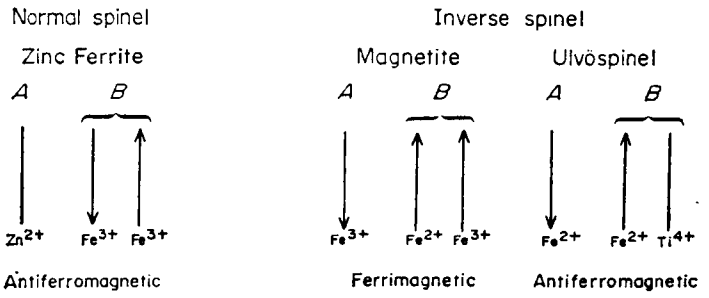

Figure 1.8 : Magnetisation vectors in the two sub-lattices A and B in the inverse spinel structure

The ionic replacement in the series takes the form of:

$$2Fe^{3+} = Fe^{2+} + Ti^{4+} \qquad (1.10)$$

Consequently, the ulvospinel end member is anti-ferromagnetic at low temperatures but paramagnetic at room temperature, having a Néel temperature of − 153°C. The cation distribution is $Fe^{2+}[Ti^{4+}Fe^{2+}]O_4$.

1.3.2 The Titanohaematite Series

Haematite (Fe_2O_3) and ilmenite ($FeTiO_3$) form a solid solution series which is complete at high temperatures (> 960°C) but restricted at lower temperatures when intermediate compositions are represented by intergrowths of the end members. Ionic replacement is the same as for the titanomagnetite series (equation 1.10). The series is characterised by rhombohedral symmetry, and the composition has the form $Fe_{2-y}Ti_yO_3$ where $0 < y < 1$. The properties vary with composition and the Curie temperature varies linearly in a similar manner to the titanomagnetites.

Haematite is composed of hexagonally close-packed layers of oxygen ions and layers of cations. It is anti-ferromagnetic because alternate planes of Fe^{3+} ions are magnetised in opposite directions (Néel, 1949). Haematite also possesses a weak ferromagnetism caused by spin moments of oppositely magnetised Fe^{3+} ions being slightly canted, so as to produce a net magnetisation directed perpendicular to the basal plane of the lattice. This canted ferromagnetic contribution is weak and variable, and the variations are thought to be due to structural defects. The Curie temperature and Néel temperatures of haematite are 680°C and 725°C respectively. A further transition, the Morin transition, occurs in haematite at −20°C at which

temperature, the spin vectors flip from being in the basal plane of the haematite structure and become aligned antiferromagnetically parallel to the trigonal axis perpendicular to the basal plane. The Morin transition is often absent in fine particles of haematite.

Ilmenite ($FeTiO_3$), the other end member of the series, is anti-ferromagnetic at very low temperatures but paramagnetic above liquid nitrogen temperatures. Ilmenite has a Néel temperature of −233°C (O'Reilly, 1984). Members of the series, with compositions of Ti = 0.5-0.7, show self-reversing TRMs (Lawson et al, 1981).

The magnetic structure of ilmentite itself is of little importance to palaeomagnetism although the mineral is of intrinsic importance to this subject because it often occurs as intergrowths with other magnetic minerals.

1.3.3 The oxidation of magnetic minerals

The dominant primary magnetic minerals in basaltic rocks belong to the titanomagnetite solid solution series but the effects of oxidation will generally shift the composition closer to the haematite sector of Figure 1.7. Two types of oxidation are witnessed in igneous rocks:

1. High temperature (deuteric) oxidation, which occurs at temperatures above 600°C and is a sub-solidus exsolution which forms intergrowths incorporating more ferric-rich members.

2. Low temperature oxidation (maghaemitization), which forms cation-deficient spinels of the metastable titanomaghaemite series.

High temperature oxidation.

Buddington and Lindsley (1974) proposed a model to account for the occurrence of ilmenite-magnetite intergrowths in lavas. They demonstrated that titanomagnetites and titanohaematites can co-exist under certain conditions of temperature and oxygen fugacity (fO_2). The intersection of titanomagnetite and titanohaematite curves on Figure 1.9 gives the unique fO_2 and temperature conditions for the co-existence of the two components.

Six classes of high temperature oxidation for titanomagnetites have been recognised by reflected light microscopy (Wilson and Watkins, 1967; Watkins and Haggerty, 1968). The magnetic mineralogy for each class is as follows:

Class I : Homogeneous titanomagnetite grains which are brown or pinky in colour. No intergrowths are visible at x1200 magnification.

Class II : Titanomagnetite containing a small number of exsolved ilmenite lamellae (< 50% of the grain)

Class III : The process started in Class II is complete. The titanomagnetite grain is filled with many ilmenite lamellae (> 50% of the grain).

Class IV : The sharp, well defined ilmenite lamellae of Class III now become mottled and distinctly lighter in colour. Much silicate reddening is present especially in and near olivines.

Class V : Ilmenite lamellae going to pseudobrookite (grey) and enveloping the titanomagnetite grains.

Class VI : This class represents the maximum degree of oxidation. The original titanomagnetite-ilmenite intergrowth at this stage is completely pseudomorphed by an assemblage of pseudobrookite in a host of titanohaematite.

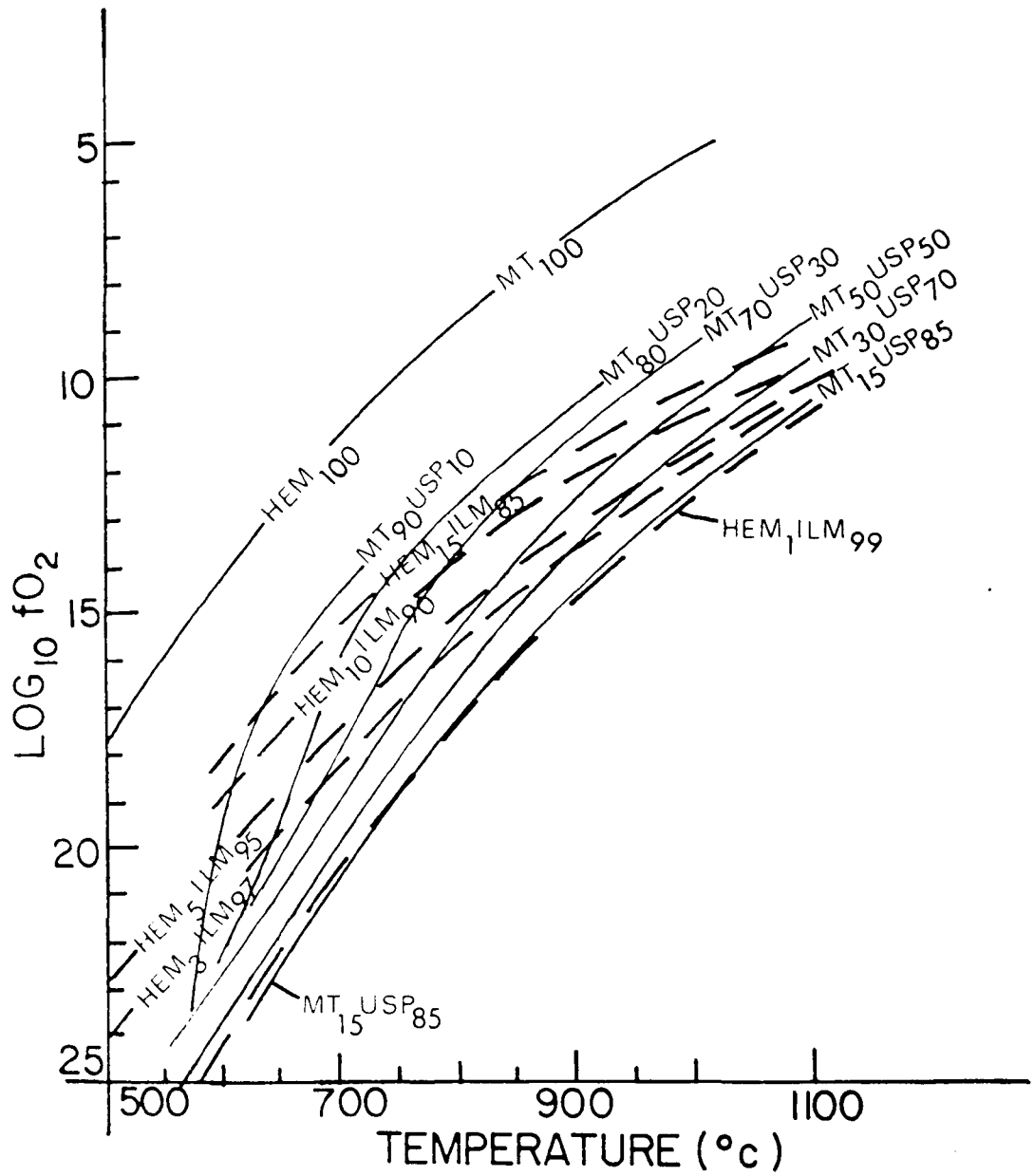

Figure 1.9 : Diagram of oxygen fugacity vs. temperature for titanomagnetites and ilmenite-haematite series (from Buddington and Lindsley, 1964).

Changes in temperature and oxygen fugacity subsequent to crystallisation of the titanomagnetite grain is accompanied by change of the Ti/Fe ratio. Above 600°C, as the temperature decreases, ilmenite is formed which is structurally incompatible with the titanomagnetite host and diffuses into the (111) planes of the host where it forms lamellae. As the temperature continues to fall and oxidising conditions prevail, most of the ulvospinel component will have been altered to ilmenite and most of the original titanomagnetite will have been converted to pure magnetite. Further oxidation causes the alteration of ilmenite and magnetite to haematite, pseudobrookite and possibly rutile. If the oxygen fugacity increases sufficiently, it may be possible for original titanomagnetite to oxidise directly to titanohaematite (Larson et al, 1969).

The end result of deuteric oxidation is the development of essentially non-magnetic ilmenite lamellae within titanomagnetite grains. Since magnetostatic and exchange interactions are probably minimal across the lamellae, they effectively sub-divide larger grains into a number of smaller, magnetically-independent regions which are usually elongate in shape.

It seems probable that deuteric oxidation occurs mostly or entirely above the Curie temperature of magnetite; the resulting remanence in deuterically-oxidised samples is therefore a highly stable thermochemical remanent magnetisation (TCRM) acquired during, or shortly after, initial cooling.

Low temperature oxidation.

Oxidation may also occur a long time after a rock has formed. This may be during the low temperature portion of the cooling process ($\simeq$400°C) or later

during circulation by ground water or hydrothermal fluids, or during subsequent weathering when the unoxidised Fe/Ti grains are still vulnerable to oxidation. The product of such an oxidation process for titanomagnetites is often a cation-deficient titanomagnetite phase belonging to the titanomaghaemite series which is also known as non-stoichiometric titanomagnetite. The low temperature oxidation process is thus referred to as maghaemitization.

The general composition of a titanomaghaemite is $Fe_aTi_b\blacksquare_cO_4$, where $a+b+c=3$ and $\blacksquare$ is the cation vacancy created in order to retain the cubic structure during oxidation. These vacancies are thought to be at the octahedral cation sites but it appears that there is little vacancy ordering in many cases.

Pure maghaemite (γFe_2O_3) is metastable and possesses a haematite composition but has an inverse spinel structure, similar to that of magnetite (Section 1.3.2). As oxidation occurs, the bulk composition of a titanomagnetite phase moves off the ulvospinel-magnetite join towards the ilmenite-haematite join along an oxidation line (Figure 1.10). High grade titanomaghaemite would be found near and beyond the ilmenite-haematite join.

Readman and O'Reilly (1970) note that saturation magnetisation decreases with increasing oxidation and the Curie temperature of the titanomaghaemite phase increases with increasing oxidation (Nishitani and Kono, 1983). Between 350 and 450°C, titanomaghaemites invert irreversibly to a stable phase; for example pure maghaemite inverts to haematite. For most titanomaghaemites, inversion will result in the formation of magnetite or a titanomagnetite as the main magnetic phase, along with some non-magnetic

phases (O'Reilly, 1983). The existence of titanomaghaemites is diagnosed by their characteristic thermomagnetic curves, examples of which can be found in Section 3.2. This is a good rock magnetic test for the occurrence of low temperature oxidation in lavas.

In the remainder of this thesis, the basic theory described in this chapter will be used to examine and interpret the geomagnetic field behaviour recorded by lavas from the Eriksfjord Group within the Gardar Igneous Province of South Greenland, during a short interval of Mid-Proterozoic times.

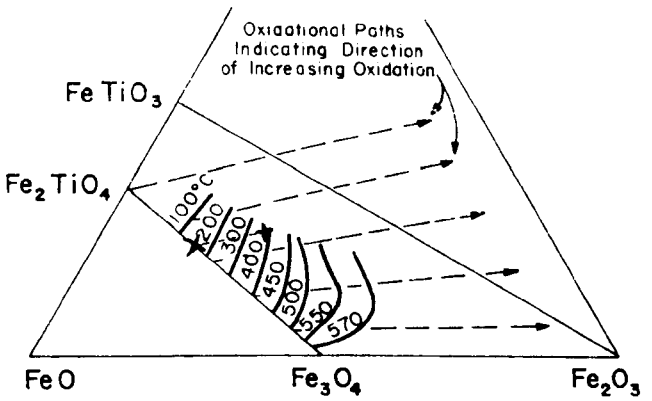

Figure 1.10 : The variation of Curie Temperature with Ti-content and low temperature oxidation; progressive oxidation path of a sample from position x to position + (from Larson et al, 1969).

CHAPTER 2 : THE GEOLOGICAL FRAMEWORK OF THE ERIKSFJORD GROUP

2.1 INTRODUCTION

The majority of the rock magnetic, palaeomagnetic and palaeointensity studies of this project were performed on samples from lava flows of the Eriksfjord Group. This is an important component of the Mid-Proterozoic Gardar Igneous Province in South Greenland. This Province was first investigated in detail by Wegmann (1938), who established a chronology which is still essentially accepted today. He assigned all the sediments, volcanics and intrusives in this region to a single igneous province and called it the "Gardar Province" after the ancient Norse Bishopric of Gardur - the present day village of Igaliko (Figure 2.1).

This chapter will describe the geological setting of the Eriksfjord Group within the Gardar Province and the petrological characteristics of the Gardar lavas. It will also discuss, to a lesser extent, the sandstone members of the Group and the dykes which intrude it. The detailed mineralogy and geochemistry of the many Gardar intrusive igneous complexes will not be described here as they are not relevant to this work; however, detailed descriptions of these rocks can be found in articles by Emeleus and Upton (1976) and Upton and Emeleus (1987).

2.2 GEOLOGICAL SETTING AND TECTONO-MAGMATIC EVOLUTION OF THE GARDAR IGNEOUS PROVINCE

The Gardar igneous province of South Greenland (Figure 2.1) is of Middle Proterozoic age and has an east-west extent of approximately 200 km. It covers a distance of about 80 km. from the southern coastline to the extremities of the inland ice and probably continues further to the northeast beneath the ice cover (Upton and Emeleus, 1987).

The province is emplaced into a basement complex largely assigned to the Julianehåb Granite which was generated during the latter part of the Middle Proterozoic Ketilidian orogeny between 1800 and 1600 Ma (van Breeman et al, 1974). The northwestern part of the province intrudes much older Archaean gneisses.

Extensive Rb-Sr isochron dating of the Gardar intrusive rocks (Blaxland et al, 1978) has identified three tectono-magmatic episodes (Figure 2.2) in the evolution of the province, separated by quiescent intervals, and spanning a period of more than 150 Ma between 1320 Ma and 1140 Ma. During each of these episodes, repeated crustal movements and alkaline magmatism resulted in a wide diversity of both intrusive and extrusive igneous rocks, with the latter confined to the earliest phase. The tectonism and alkaline magmatism, together with the thick sediment-lava piles and axial dyke swarms observed, are analogous to those seen in Phanerozoic continental rift environments, such as the East African rift and the Oslo graben (Sorensen, 1970; Upton and Blundell, 1978).

The three stages in the evolution of the Gardar province are described, in sequence, below.

2.2.1 The Early Gardar (1300 Ma) Episode

This episode is the most significant in the context of this study because it was during the opening part of this earliest phase of Gardar activity that the sequence of continental sandstones, subaerial lavas and subordinate pyroclastics comprising the Eriksfjord Group (EG) were formed. Although much of the original supracrustal sequence is now eroded, a 3 km

Figure 2.1 : Generalised geological map of the Gardar Province, South Greenland, indicating the major intrusive complexes, dyke swarms and the supracrustal rocks of the Eriksfjord Group.

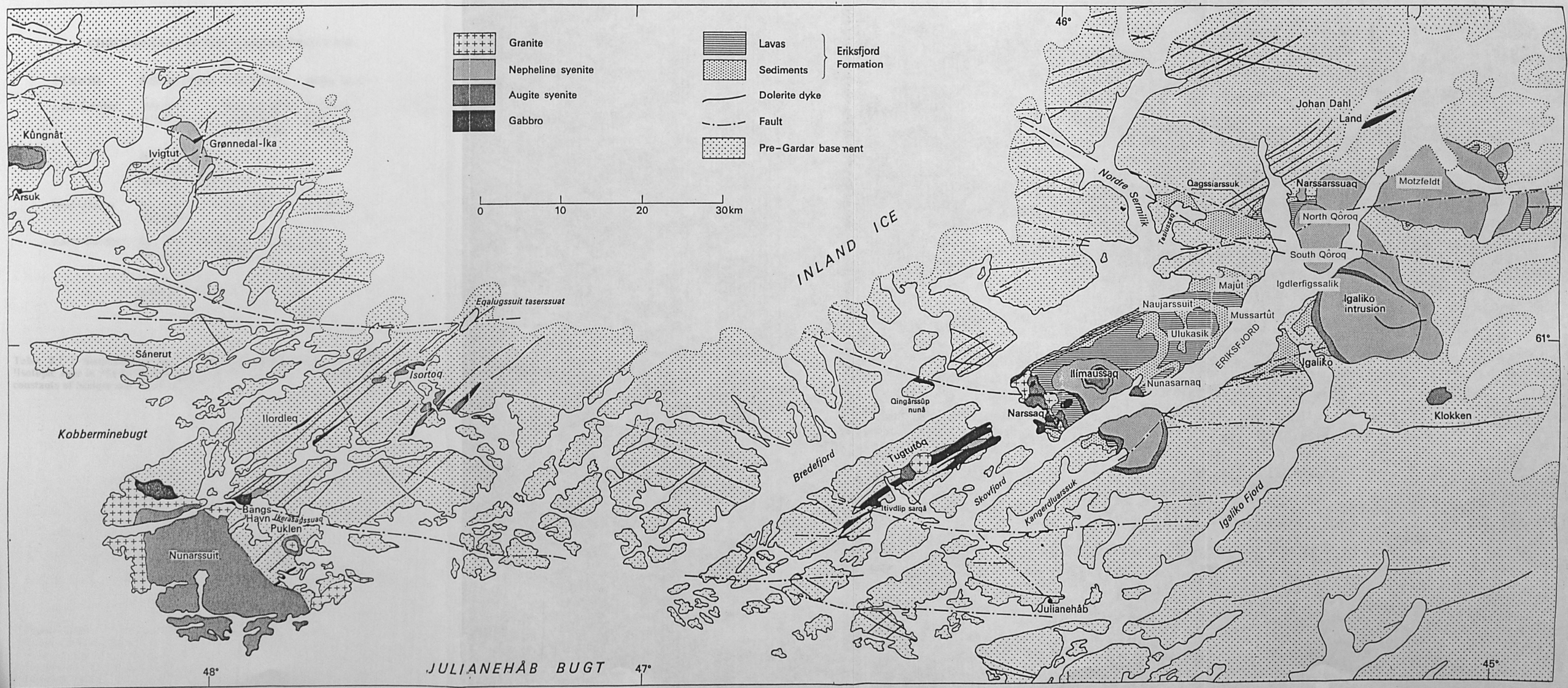
Granite
Nepheline syenite
Augite syenite
Gabbro
Lavas
Sediments
Eriksfjord Formation
Dolerite dyke
Fault
Pre-Gardar basement
0
10
20
30km
Kûngnât
Ivigtut
Grønnedal-Ika
Arsuk
Eqalugssuit taserssuat
Sânerut
Isortoq
Ilordleq
Kobberminebugt
Bangs Havn
Puklen
Nunarssuit
JULIANEHÅB BUGT
48°
47°
46°
45°
61°
INLAND ICE
Nordre Sermilik
Tasiusaq
Qagssiarssuk
Johan Dahl Land
Narssarssuaq
Motzfeldt
North Qôroq
South Qôroq
Igdlerfigssalik
Igaliko intrusion
Majût
Naujarssuit
Mussartût
Ulukasik
ERIKSFJORD
Igaliko
Ilimaussaq
Nunasarnaq
Narssaq
Qingârssûp nunâ
Klokken
Bredefjord
Tugtutôq
Itivdlip sarqâ
Skovfjord
Kangerdluarssuk
Igaliko Fjord
Julianehåb

CHRONOLOGY OF THE GARDAR PROVINCE

PERIOD	ROCK TYPE	LOCALITY	Rb-Sr AGE[1]
Late Gardar	Intrusive complexes	Igdlerfigssalik	1154±15
		Ilímuassaq	1143±21
		South Qôroq	1160±8
	ENE dykes (Dolerite,trachyte, lamprophyre,phonolite)		
Mid Gardar	Intrusive complexes	Kûngnât	1219±17
		Ivigtut	1222±25
Early Gardar	Intrusive complexes	North Qôroq	1291±61
		Motzfeldt	1291±31
		Gronnedal-Ika	1299±17
	ERIKSFJORD GROUP	Ilímaussaq peninsula	

Table 2.1 : Simplified geological succession within the Gardar province. [1]Isotopic ages in Ma from Blaxland et al (1978) recalculated using the decay constants of Steiger and Jager (1977).

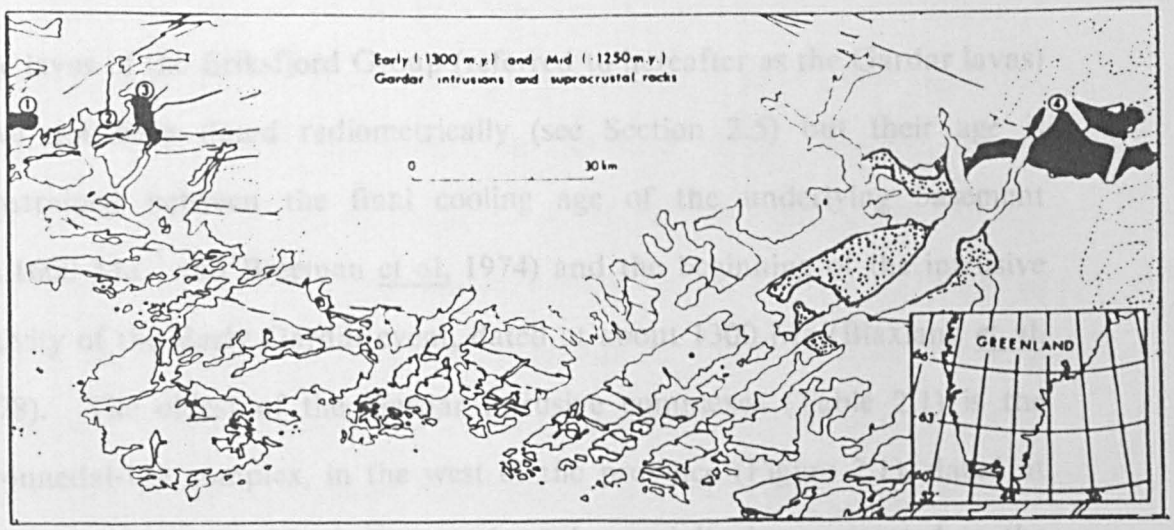

Figure 2.2a : Distribution of early and Mid-Gardar igneous rocks: dotted areas-Eriksfjord lavas; black areas- (1) Kûngât (2) Ivigtut (3) Grønnedal-Ika N.Q ôroq and Motzfeldt (Early Igaliko) nepheline syenite complexes. WNW-ESE-trending mid-Gardar BD0 dykes traverse the region. Younger mid-Gardar dykes are mainly concentrated in the Ivigtut region (from Upton and Blundell, 1978).

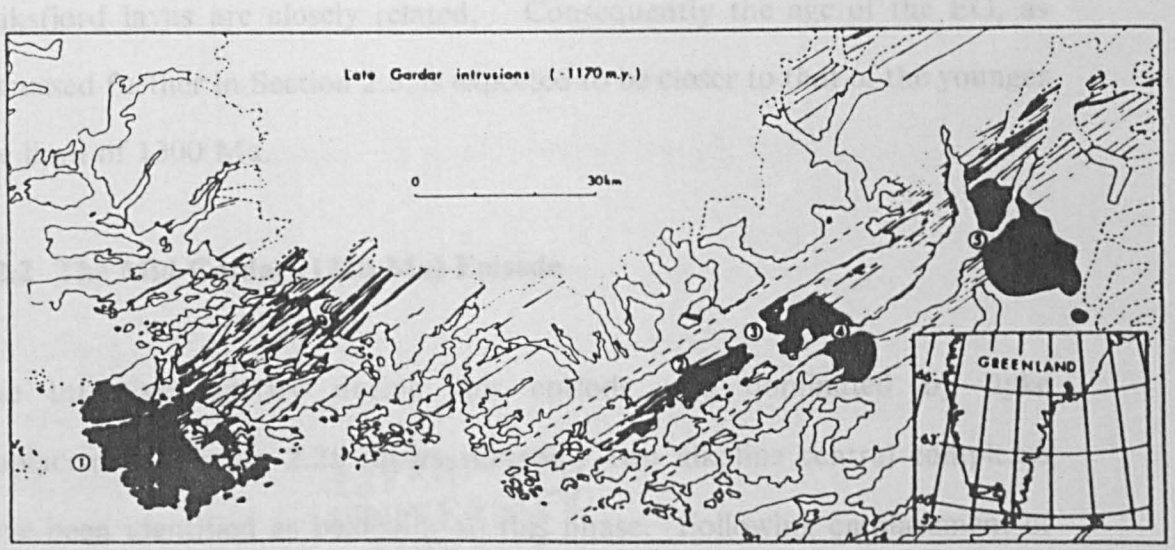

Figure 2.2b : Distribution of late-Gardar igneous intrusions. The principal WSW-ENE swarms are indicated : the Nunarssuit-Isortôq (NI) swarm lies to the west of the Tugtutôq-Ilímaussaq (TI) swarm. Intrusive complexes are (1) Nunarssuit (2) Central Tugtutôq (3) Narssaq (4) Ilímaussaq (from Upton and Blundell, 1978).

thick sequence of intercalated sediments and volcanics is preserved in a downfaulted block comprising the Ilimaussaq Peninsula (Figure 2.1).

The lavas of the Eriksfjord Group (referred to hereafter as the Gardar lavas) have not been dated radiometrically (see Section 2.5) but their age is constrained between the final cooling age of the underlying basement (ca.1600 Ma, van Breeman et al, 1974) and the beginning of the intrusive activity of the Early Gardar event, dated at about 1300 Ma (Blaxland et al, 1978). The oldest of the Gardar intrusive complexes (Table 2.1) is the Grønnedal-Ika complex, in the west of the province (Figure 2.1), dated at 1299 ± 17 Ma. The Early Gardar intrusive activity is represented in the eastern part of the province by the Motzfeldt and North Qôroq complexes (commonly referred to as the Early Igaliko intrusions), dated at 1291 ± 31 Ma and 1291 ± 61 Ma by Blaxland et al (1978). These two complexes cut outliers of the Eriksfjord Group. Furthermore, it has been recognised (Upton and Blundell, 1978) that the petrogenesis of these intrusions and the Eriksfjord lavas are closely related. Consequently the age of the EG, as discussed further in Section 2.5, is expected to be closer to that of the younger age limit of 1300 Ma.

2.2.2 The Mid Gardar (1220 Ma) Episode

The intrusive activity during this episode was dominated by dyke emplacement. Figure 2.2a shows that only two alkaline central complexes have been identified as belonging to this phase. Following emplacement of the Early Gardar complexes and a quiescent interval which may have lasted up to 70 Ma, a period of dyke intrusion ensued in response to crustal extension. Initially, lamprophyric and subsequently olivine doleritic swarms were intruded. The latter, known as the "brown dykes", or "BD" swarm, due

to the colour of their weathering products, are subdivided into four generations - BD_0, BD_1, BD_2, and BD_3. Isolated E-W dykes assigned to the BD_0 swarm in the east of the Province are cut by the Early intrusions of Motzfeldt and North Qôroq and appear to be one of the earliest signatures of activity. The BD_0 generation, in the west of the province, trends WNW-ESE (Fig. 2.2a), while the trend of the younger generations are rotated towards a SW-NE orientation (Berthelsen and Henriksen, 1975) and tend to cut the BD_0 dykes. The main concentration of these dyke swarms is in the vicinity of the boundary between the Archaean basement in the north and the Proterozoic Ketilidian basement in the south comprising the major Early Precambrian crustal boundary in South Greenland.

Some of the dykes intrude the Early Gardar Grønnedal-Ika complex and others are cut by the Mid Gardar Kûngnât intrusion, dated at 1299 ± 17 Ma and 1219 ± 17 Ma respectively. Thus, the age of the dyke emplacement is bracketed between 1299 and 1219 Ma. Both the Kûngnât and the smaller Ivigtut complex (1222 ± 25 Ma) mark the termination, in the Gardar Province, of an extensive magmatic event which spanned much of the Laurentian and Fennoscandian shields (Patchett et al, 1978).

The intrusive complexes of the Mid Gardar period are petrologically-distinct from those of the Early Gardar phase. The former are silica-oversaturated, whereas the latter are larger bodies and are silica-undersaturated (Emeleus and Upton, 1976).

2.2.3 The Late Gardar (1150Ma) Episode

The commencement of the final, and by far the most productive, period of the igneous cycle was marked by the intrusion of a major dyke swarm,

developed along WSW-ENE and SW-NE trends, sub-parallel to the margins of the inferred graben boundaries. These dykes are concentrated along two main zones - the Nunarssuit-Isortoq (NI) zone in the south and the Tugtutôq-Ilímaussaq (TI) zone in the north. The dykes of the NI zone are younger than the Mid Gardar BD swarms but no date for their intrusion is available. The TI dyke episode, however, is dated at 1154 ± 16 Ma (Upton et al, 1985) and began with the intrusion of the Hviddal (or Tugtutôq) giant dyke. Both the NI and TI dyke swarms are believed to reflect crustal extension in ENE trending fault blocks, which are geographically defined by the fjords (Fig. 2.2b). The NI block is approximately twice the width of the TI block (Fig. 2.2b); both blocks exhibit "giant dykes", greater than 0.5 km in width, generally composed of alkali gabbros and syenites. There are petrological differences between the dykes from the two zones; dykes in the TI zone are more evolved than those of the NI zone, where hawaiites predominate (Upton and Emeleus, 1987). The petrologically-varied ENE trending swarm on the Ilímaussaq peninsula is important in the context of this study because it cuts, and consequently has a thermal influence on, the Eriksfjord Group (see Chapter 5).

The intrusion of several alkaline central complexes also occurred during this Late Gardar period. The oldest, the South Qôroq, is dated at 1160 ± 8 Ma (Blaxland et al, 1978). Hence, there is a time gap of approximately 100 Ma between the ages of the Early Gardar North Qôroq and the Late Gardar South Qôroq intrusions. However, the time interval between the emplacement of South Qôroq and the late units of the Igdlerfigssalik complex (1154 ± 15 Ma) evident from field relationships is unresolvable even with high precision isochron dating techniques. Most of the NE trending dykes were intruded just before the emplacement of the Igdlerfigssalik complex, but

some members of this swarm are found within the South Qôroq complex where they have sinuous outcrops and were probably emplaced into a still semi-ductile pluton.

The multi-phase Nunarssuit complex, sited at the south-west of this axial zone (Fig. 2.2c) along with the Tugtutôq central complex and the Ilímaussaq intrusion in the east are regarded as essentially contemporaneous (Blaxland et al, 1978). The older complexes of the Late Gardar event, such as the Narssaq and the South Qôroq intrusions are dislocated by the effect of vigorous E-W, left lateral faulting. Termination of this faulting, however, was complete before the emplacement of the youngest intrusions (the Igdlerfigssalik, Central Tugtutôq, Ilímaussaq and Klokken complexes) which show no signs of dislocation.

Figure 2.3 shows a schematic representation of the chronological relationships between the Gardar intrusive rocks with the division into early, middle and late phases based on the geochronological evidence outlined above.

2.2.4 Summary

The major conclusions to be drawn from geological and geophysical studies of the tectono-magmatic evolution of the province are:

1. Three separate episodes of igneous activity are recognised, dated ca 1300 Ma, 1250 Ma and 1150 Ma. These appear to be brief episodes of intense magmatism separated by long intervals characterised by little activity. The late episode accounts for the majority of the igneous rocks produced during Gardar times.

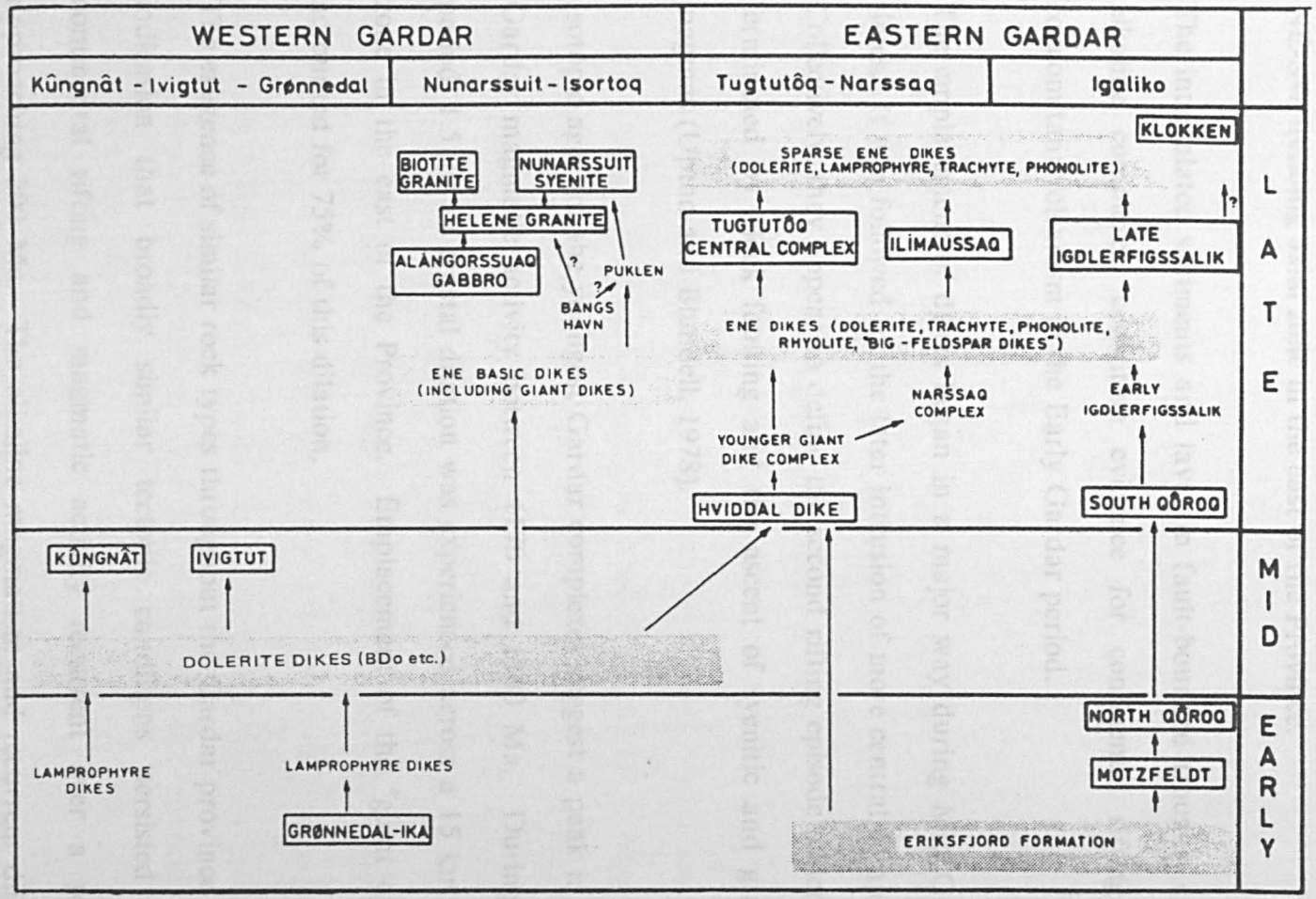

Figure 2.3 : Chronologic scheme for the Gardar region. Only relative chronology is shown (for absolute age values, see Table 2.1). An arrow indicates that the top event is known to be younger than the bottom event on field or isotopic evidence. Rocks within boxes have a Rb-Sr isochron age (from Blaxland et al, 1978).

2. There appears to be no obvious relationship between age, geographical location or emplacement mechanisms of the Gardar intrusives (Blaxland et al, 1978), although all the late activity is concentrated along the NE-SW trending axial zone in the east of the Province.

3. The intercalated sediments and lavas in fault-bounded troughs, cut by alkaline complexes, constitute evidence for continental rifting and concomitant volcanism in the Early Gardar period.

4. The emplacement of dykes began in a major way during Mid Gardar times. It was followed by the later intrusion of more central complexes. Collectively, they appear to define the second rifting episode which was terminated by block faulting and the ascent of syenitic and granitic magmas (Upton and Blundell, 1978).

5. Isotopic ages for the youngest Gardar complexes suggest a peak in Late Gardar magmatic activity between 1170 and 1140 Ma. During this period, 1.5 km of crustal dilation was experienced across a 15 km wide zone in the east of the Province. Emplacement of the "giant dykes" accounted for 75% of this dilation.

6. The existence of similar rock types throughout the Gardar province is an indication that broadly similar tectonic conditions persisted with continental rifting and magmatic activity recurrent over a period approaching 200 Ma. The alkaline magmatism and recurrent dilation implies that the history of the Province was controlled by fluctuations in a prevailing regional tension within the underlying lithosphere, with the orientation of this stress system rotating through approximately 90° during the cycle.

2.3 THE ERIKSFJORD GROUP

The Eriksfjord Group (EG) comprises a thick sequence of supracrustal rocks, with continental red beds and subordinate rudites intercalated with volcanic units. The formation lies unconformably on a basement of Julianehåb Granite and is believed to have accumulated rapidly in a steadily-subsiding graben during the opening stage of the Early Gardar (ca.1300 Ma) episode (Section 2.2.1).

Accounts of the geology of the EG are given by Ussing (1912), Wegmann (1938), Poulsen (1964) and Stewart (1964, 1970). These studies are summarised and reviewed by Emeleus and Upton (1976).

The original thickness of the group was probably greater and it covered a much larger geographical area, possibly in excess of 2500 km^2 (Upton et al, 1974). At the present time, however, outcrop is confined to a number of localities within the eastern sector of the Gardar Province (Figure 2.1). Only the deepest parts of the former basin are now preserved, with the best exposure being on the fault-bounded Ilímaussaq peninsula. Here, the sequence covers an outcrop area of about 150 km^2 and comprises an approximately 3 km thickness of lavas, sediments and pyroclastic rocks. It was in this area that all the sampling for palaeomagnetic purposes was undertaken (Section 3.3).

Three thick sub-aerial volcanic units occur: from oldest to youngest, they are the Mussartût, Ulukasik and Ilímaussaq Formations. These formations are well separated by thick sequences of continental sandstones (Poulsen, 1964). The three Lava Formations have a combined thickness of approximately 1500 m, accounting for half the total exposed EG sequence on the Ilímaussaq

peninsula. The majority (70%) of the lava flows comprise basalts and hawaiites; more differentiated basic lavas account for 7% of the flows and 23% are of trachytic composition (Larsen, 1977). The composition of the lava flows becomes more evolved upwards; the Mussartût and Ulukasik lavas consist entirely of basalts and hawaiites, whereas the Ilímaussaq Formation also contains trachybasalts, trachyandesites, trachytes and phonolites. This evidence suggests that eruptions throughout the EG generally became more evolved with time. All of the lava flows have suffered low grade metamorphism, with epidote extensively developed as a secondary mineral. The assemblages of the metamorphic minerals and their distribution indicate that contact metamorphism (with the Ilímaussaq intrusion) combined with regional hydrothermal activity, motivated by burial, dominated in the alteration of the lavas (see Section 2.4).

The environment which prevailed during the eruption of each volcanic formation is described in detail within the relevant section, but the general absence of palaeosols and the presence of undisturbed, uneroded pahoehoe lava surfaces in each group suggest a volcanic source of high productivity with rapid extrusion of successive flows and minimum intervening time intervals. Each of the three formations may have erupted within 1/4 Ma and each flow, even the thickest, was probably wholly crystallised and cooled within a few tens of years (B.G.J. Upton, pers. comm.).

The sediments of the EG were derived from erosion of the surrounding granitic highlands, during periods of volcanic quiescence after lavas had spilled from vents within the subsiding blocks of the graben. Upton (pers. comm.) suggests that the palaeoenvironment for the early sandstone deposition was a slowly subsiding basin (or basins) with braided river

systems, sand dunes and occasional lakes originating from damming by lavas, dunes or tectonic scarps. Most of the visible sequence is fine-medium grained and conglomerates are rarely seen.

There is uncertainty about the time interval taken for the EG to form. The three lava formations show a generalised increase in differentiation from oldest to youngest, suggesting derivation from a single magma chamber, or a closely related nest of chambers, that was cooling and evolving compostionally. Such volcanic systems rarely have lifespans in excess of 5 Ma (Upton, pers. comm.). The three formations are geochemically similar and could have been related to a single conduit or conduits in the North Qôroq or Motzfeldt centres. Consequently, it is inferred that the entire Eriksfjord Group probably formed in less than 10 Ma, and conceivably in less than 5 Ma.

Figure 2.4 and Table 2.2 summarise the outcrop and stratigraphic sequence of the EG on the Ilímaussaq peninsula, from which all the samples for use in this study were taken. Of the other outcrops of the formation seen in Fig. 2.1, those at Qagssiarssuk and Narssarssuaq are tentatively correlated with the Mâjût and Mussartût formations of the main outcrop. The bulk of the lavas on the northern shores of Eriksfjord, between the Narssaq and Ilímaussaq intrusions correlate with the Ulukasik and Ilímaussaq formations of the EG (Upton et al, 1974).

The lithological characteristics of each of the six formations of the Eriksfjord Group are quite distinctive and in all instances, they reflect changes in tectonic activity. These characteristics are sufficiently important in the context of this study to warrant further discussion, in chronostratigraphical order from oldest to youngest.

2.3.1 The Mâjût Sandstone Formation (Thickness 390m)

This formation overlies a basal conglomerate, which rests unconformably on a basement of Julianehåb Granite, and consists entirely of feldspathic and quartz arenites (arkoses and quartzites) deposited in intra-montaine basins. The granitic material in the arkoses represents weathered products derived from the Julianehåb Granite. During graben formation, the weathering products were washed into the basin from surrounding uplands. The arenites filled hollows in the uneven surface and sedimentation continued with deposition of conglomerates and fine-medium grained quartz arenites. Towards the end of Mâjût sedimentation, a sequence of "mottled" or "white spotted" red sandstones was deposited. This sequence contains primary sedimentary structures such as ripple marks, herring bone cross-lamination and trough cross-bedding, indicating an environment dominated by wave and current action. The red colouration of these sandstones is due to haematite pigmentation. The white spots and general decolouring which produce the characteristic mottled appearance of this rock, occur preferentially along joints, fissures and bedding planes in the vicinity of NE trending Late Gardar dykes. The decolouration is evidently due to leaching of the haematite and probably resulted from the mobilisation of fluids by dyke emplacement.

2.3.2 The Mussartût Formation (745 m)

This formation comprises a series of alternating volcanic rocks and sediments. The first appearance of volcanics defines the base of the sequence. The mottled red beds of the Mâjût Sandstone pass up into a coarse sandstone breccia overlain by two agglomerate bands, separated by a thin siltstone. The agglomerate bands contain quartzite fragments, scoriaceous clasts of glassy basic volcanic material and crudely rounded clasts of crystalline basic igneous

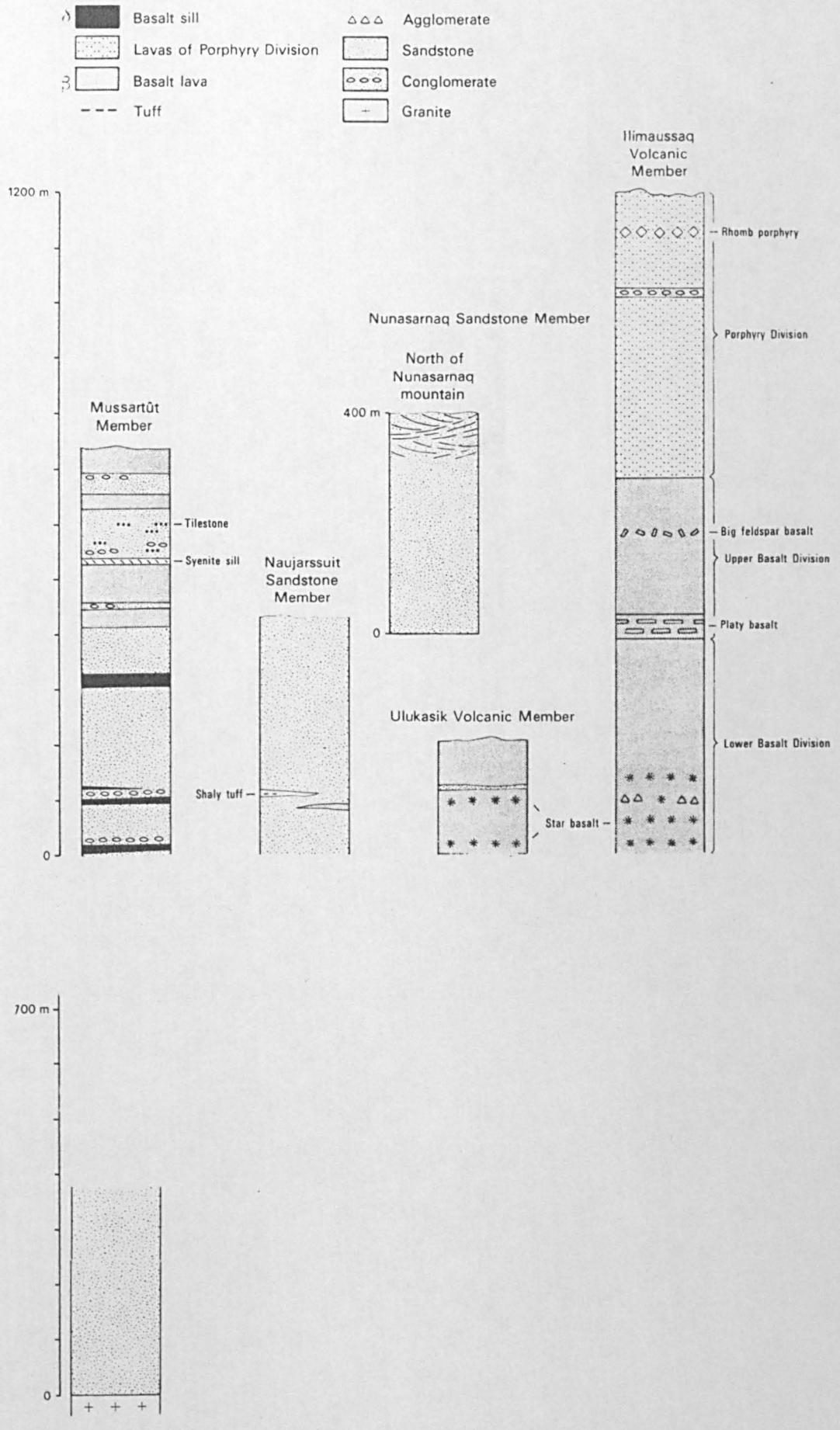

Figure 2.4 : Geological sections through the Eriksfjord Group, cropping out on the Ilimaussaq peninsula (redrawn from Poulsen (1964) .

THE ERIKSFJORD GROUP

GROUP NAME	PETROLOGICAL DESCRIPTION	ENVIRONMENT
Ilímaussaq Formation (Upper lavas)	Aphyric and feldspar-phyric basalts and trachytes (ca. 1030m thick)	Tectonically quiescent Quasi-horizontal plains
Nunasarnaq Formation (Upper sandstones)	Massive quartzitic aeolian sandstone (ca. 350m thick)	Desert
Ulukasik Formation (Middle lavas)	Aphyric and feldspar-phyric basalts. Cavities filled with wind blown sand. (ca. 250m thick)	Tectonically quiescent. Quasi-horizontal arid plains.
Naujarssuit Formation (Middle sandsones)	Medium-fine grained grey quartzitic sandstones (ca.420m thick)	Fluviatile
Mussartût Formation (Lower lavas)	alkaline ultramafics initially but glassy basalts later. Interleaved thin fluviatile and lacustrine sediments occur. (ca. 745m thick).	Rapidly subsiding basin supporting standing bodies of water
Majût Formation (Lower sandstones)	arkoses, quartzites Mottled red sandstones (ca. 390m thick)	Wave and current action predominent

**********Unconformity**********

Ketilidian Basement - including the Julianehåb granite

****

Table 2.2 : Stratigraphical detail of the Eriksfjord Group

rocks, up to 10 cm in diameter. The basic clasts were used in this study to test the origin of the magnetic remanence of the Gardar lavas (see Chapter 5). This layer lacks bedding and is believed to reflect the explosive opening phase of Mussartût volcanism. The agglomerate is overlain by massive columnar jointed basalt units which, in turn, pass up into an alternating sequence of lava flows and conglomerates indicating that the tectonic disturbances which characterised Mussartût times, resulted from the initial opening of magmatic conduits and the periodic rejuvenation of fault scarps (Upton et al, 1974).

The lowermost (columnar jointed) units are very thick (>30m) and were originally believed to be sills (Stewart, 1964). However, Upton et al (1974) found no evidence to corroborate this and prefer to regard these units as lavas. Only a single sill could be identified in this lower formation and the remainder of these units show the characteristics of lava flows. Above these flows, the lava units become thinner (≃10m), with preserved ropy pahoehoe surfaces indicating minimal time periods before subsequent lava outpourings or sediment deposition. The occurrence of crude pillow structures at the base of the lava pile are the only evidence for sub-aqueous eruption in the entire Eriksfjord Group. Thus, substantial bodies of water were present in the depositional basin **only during Mussartût times**. Flow direction measurements indicate that the source for the Mussartût lavas lay to the west, in the region of Bredefjord (Upton et al, 1974). Conglomerate bands are found towards the top of the formation and the thickness of these bands varies from a few centimetres to as much as 20m. The matrix consists of sandstone and the well rounded pebbles, which are normally coated with haematite, comprise pure quartz, quartzites and sandstones. Pebbles of volcanic material are absent, thus precluding the possibility of using the standard palaeomagnetic

conglomerate test (Graham, 1949) to resolve the origin of the lava remanence. Conglomerate pebbles sometimes reach 50 cm in diameter and large transport velocities are inferred: in some places 1m blocks of the underlying sandstone are torn up and incorporated as part of the conglomerate.

The character of the sandstone units of the Mussartût Formation varies throughout the formation. Generally, though, red-grey arenites and grey fissile shaley sandstones predominate; the latter are impossible to sample for palaeomagnetic purposes due to their fissility. The lavas and sediments of the unit are cut by large trachytic and doleritic dykes, up to 10m wide, belonging to the Late Gardar NE-SW trending swarm. The contacts of these dykes with the sediments are relatively well exposed but those with the lavas are badly weathered.

2.3.3 The Naujarssuit Formation (420 m)

The lower 100 m of this formation consist of relatively soft red beds and the remainder is made up of very hard, quartzitic sandstone. Tectonic movements were slow during the deposition of this formation and occasional ripple marks show that shallowing continued and, at certain stages, total emergence may have occurred (Poulsen, 1964). A limited number of palaeomagnetic samples were taken from the lower, softer, horizons but the whiter, more quartzitic sediments were undrillable.

2.3.4 The Ulukasik Formation (250 m)

After the tectonically-quiescent period of Naujarssuit sedimentation, volcanism recommenced with the rapid extrusion of basic lavas which constitute the major part of the Ulukasik Formation. These lavas are

predominantly uniform, coarser grained grey-purple olivine basalts, with the olivine weathered to iddingsite. Sandstones are absent save for a series of thin (≃5-8m) horizons towards the top of the formation. Columnar jointing is poorly developed in the flows. Pillow lavas, pyroclastics and intervening sediments are absent, and pahoehoe surfaces are well preserved. Thus, the Ulukasik flows appear to have erupted across a quasi-horizontal arid plain, with minimal weathering before the succeeding unit was erupted or deposited (Upton et al, 1974). Flow directions are variable and it is likely that the Ulukasik lavas were erupted from low angle fissures and/or shield volcanoes. The lavas are believed to be associated with aeolian sandstones seen as sandstone "dykes" within the lavas. Allart (1970) discovered wind-blown sand filling cavities in the vesicular flow tops, suggesting that change from an aqueous to an aeolian palaeoenvironment occurred during these times.

2.3.5 The Nunasarnaq Formation (350 m)

Continued subsidence resulted in the deposition of this formation during a period of volcanic quiescence. The Nunasarnaq Formation sandstones are white dune relics and open cross-bedding present in the upper part of the sequence (Allart, 1970). They are now thoroughly cemented to quartzite. The sedimentary structures are characteristic of an aeolian environment. Thus, the transition from aqueous to aeolian conditions, probably initiated during the eruption of the Ulukasik lavas, was complete by the time the Nunasarnaq sandstones were deposited.

2.3.6 The Ilímaussaq Formation (1030 m)

This unit is the most petrographically-varied in the EG and comprises a thick sequence of lava flows, of varying composition, uninterrupted by sediment deposition. A major magmatic phase, post-dating the Nunasarnaq event, resulted in the extrusion of a thickness of over 1 km of lava. Individual flows rarely exceed 8 m in thickness and are thinner than those from either of the other two lava groups, but have a broad lateral extent. The superb preservation of ropy pahoehoe surfaces and the absence of clearly developed palaeosols and intervening clastics again suggests rapid extrusion of successive flows across areas of low relief.

The Ilímaussaq Formation can be crudely divided into three sections - lower, middle and upper. The lower section comprises flows of predominantly basaltic and, to a lesser extent, hawaiitic composition. The similarities in petrography and general appearance between these flows and those of the Ulukasik formation suggest that the same mildly alkaline olivine basalt magma was the source of eruption for these flows in the sinking desert basin (Upton et al, 1974). The flows of the lower section of the Ilímaussaq formation are characterised by radiating aggregates of plagioclase phenocrysts, giving them the name - "star basalts". A small number of flows in this section are characterised by large epidote-filled amygdales. The groundmass is dominated by plagioclase, altered olivine, clinopyroxene, apatite and chlorite. Importantly, in the context of this study, the groundmass also contains magnetite and in some flows haematite and partially altered titanomagnetites (Larsen, 1977).

The middle section of the Ilímaussaq formation contains some aphyric flows but is characterised by the occurrence of strikingly porphyritic flows. These

have flow-aligned tabular plagioclase phenocrysts, normally between 1 and 5 cm long but very occasionally megacrysts up to tens of centimetres long are seen. These flows are termed "platy basalts" (Stewart, 1964). The highest flows of the formation, constituting the upper section, were described by Stewart (1964) and Larsen (1977) and shown to comprise trachybasalts, trachyandesites, trachytes and phonolites. The petrologic differences between these rock types are not important to this study; what is important, however, is that the groundmass of each type contains varying amounts of feldspars, altered olivine and opaque minerals, including magnetite and haematite.

2.4 METAMORPHIC STATE OF THE GARDAR LAVAS

Ade-Hall et al (1971) have shown that Proterozoic lavas often have characteristic suites of secondary hydrothermal minerals, where temperature effects rather than those of pressure seem to be the controlling factor. The lavas of the Eriksfjord Group are no exception to this. All have experienced low grade metamorphism, to varying degrees, with epidote extensively developed throughout the succession and implying a minimum hydrothermal temperature of 300° C. The secondary mineral assemblages resulting from contact metamorphism and regional hydrothermal activity have been described for the Mussartût and Ulukasik lavas by Upton et al (1974) and for the Ilímaussaq lavas by Larsen (1977). The effect of alteration on the magnetic minerals of the lavas is discussed in Chapters 3-5.

2.4.1 Mussartût and Ulukasik lavas

The Mussartût lavas contain up to 50% chlorite matrix which has apparently replaced primary glass. Olivine phenocrysts are scarce or completely absent; any prorphyritic lavas exhibit sparse, large plagioclase phenocrysts. The

Ulukasik flows, however, are holocrystalline and contain pseudomorphed olivine phenocrysts and distinctive star aggregates of plagioclase phenocrysts.

The plagioclase in flows from both formations is extensively sericitised. Olivine is pseudomorphed by chlorite and carbonates and most former pyroxene is replaced by chlorite. Amygdales are composed principally of epidote but chlorite, calcite and chalcedony also occur.

2.4.2 Ilímaussaq lavas

The close proximity of the flows from the upper lavas to the younger Ilímaussaq intrusion has resulted in a complex thermal history. Larsen (1977) identified three metamorphic zones, with increasing distance to the east of the intrusion:

1. An andesine-actinolite-biotite zone, 0.2-0.5 km from the intrusion,

2. An albite-oligoclase-epidote-chlorite zone, 1-2 km from the intrusion,

3. A sericite-chlorite zone, more than 2 km away.

These zones correspond to low-grade hornblende-hornfels facies, albite-epidote-hornfels facies and low grade albite-epidote-hornfels facies respectively. Recrystallisation is incomplete in all of these zones, thus labradorite relics may occur in zone (1) and both the original plagioclase and pyroxene may have survived in zones (2) and (3). More than 2 km away from the intrusion, massive parts of the flows are fresh, save for the altered olivine. Porous lava tops, however, contain completely sericitised plagioclase due to the effects of hydrothermal activity. This factor constrains the collection of suitable palaeomagnetic samples from the bulk of the flows. A

single occurrence of prehnite-pumpellyite facies on Ilímaussaq clearly indicates low pressure metamorphism, thus supporting the observation of Ade-Hall et al. (1971) that temperature is the important factor. The mineral assemblages and their distribution indicate that contact metamorphism, combined with hydrothermal activity, dominated the alteration of the Ilímaussaq lavas. Burial metamorphism is not a factor, in contrast to the Mussartût and Ulukasik flows, where its effect is important due to their burial beneath several kilometres of younger sediments and volcanics. The majority of palaeomagnetic samples collected from the Ilímaussaq formation were located in zones (2) and (3). Only flows from the very top of the sequence originate from zone (1).

2.5 THE AGE OF THE ERIKSFJORD GROUP

At present, no radiometric ages are available for the lavas of the Eriksfjord Group. Due to their complex thermal history, an attempt, in this study, to date them using the $^{39}Ar - {}^{40}Ar$ stepwise degassing method (Section 5.5) was unsuccessful. Nd/Sm dating of pyroxenes from the lavas is currently underway (B.G.J. Upton, pers. comm.) in addition to dating of zircons and baddeleyites, by U-Pb techniques (B. Paterson, pers. comm.). No data are yet available from these studies.

The only indication of the age for the Eriksfjord Group we have at present, therefore, is from field relationships with Rb-Sr dated intrusive complexes. As previously mentioned, the EG lies unconformably on the 1600 Ma basement and is cut by the 1299 ± 31 Ma Motzfeldt complex. No unconformities are known within the Group and Upton and Emeleus (1987) believe that the youngest lavas of the Ilímaussaq formation may have been erupted from a conduit or conduits in the North Qôroq or Motzfeldt centres.

Consequently, the entire EG may be no older than 1320 Ma. Despite this uncertainty, it would seem that the Gardar lavas are probably slightly older than comparable Middle-Upper Proterozoic magmatism in the Laurentian shield, including the Seal Lake lavas of Labrador (1280 Ma), the Zig-Zag Dal lavas of North Greenland (1230 Ma), the Coppermine Bay (1215 Ma) lavas and the Keweenawan basalts (1150-1000 Ma). The Eriksfjord Group lavas of the Gardar Province probably rank among the earliest known continental flood basalts.

CHAPTER 3 : ROCK MAGNETIC INVESTIGATIONS OF THE GARDAR LAVAS

3.1 INTRODUCTION

Radhakrishnamurty and Likhite (1987) demonstrated that the magnetic mineralogy of most basalts comprises a mixture of minerals and domain states. Consequently, they often exhibit complex magnetic behaviour. Radhakrishnamurty et al. (1991) believe that to obtain a more complete idea of the magnetic mineralogy, several rock magnetic (RM) techniques should be employed.

This chapter describes the results from five rock magnetic techniques which, for convenience, are divided into thermal RM techniques (thermomagnetic and high temperature susceptibility) and non-thermal RM techniques (low temperature susceptibility, hysteresis and alternating field demagnetisation). The aim of this chapter is to identify the magnetic composition and domain states of the remanence carriers in the flows of the Gardar lavas and to identify whether they carry a primary thermoremanent magnetisation (TRM), a primary thermochemical remanence (TCRM), or a chemical remanent magnetisation (CRM). Also, this chapter demonstrates that results from RM techniques are of maximum use when considered collectively, as opposed to separately.

3.2 THERMOMAGNETIC MEASUREMENTS

3.2.1 Theory

The temperature above which a ferri- or ferromagnetic material becomes paramagnetic is known as the Curie temperature, T_c. In some magnetic minerals, such as magnetite and haematite, this temperature is distinctive and can be a diagnostic rock magnetic property. The Curie temperatures of the

magnetic minerals important in the context of the present study are listed in Table 3.1.

MINERAL	T_c (°C)	SOURCE	ALTERATION PRODUCTS	ALTERATION TEMPERATURE
Magnetite	575	1	Haematite	> 500°C
Titano-haematites	-218 to 675	1	Magnetite	> 300°C
Maghaemite	≃645	2	Haematite	350 – 450°C
Titano-magnetites	-153 to 575	1	Magnetite	> 300°C

Table 3.1 : Curie temperatures and alteration products of some magnetic minerals important in the context of the present study. 1 = O'Reilly (1984); 2 = Ozdemir & Banerjee (1981).

Rock samples which contain a single magnetic mineral phase such as magnetite or haematite will have well defined thermomagnetic curves; typically they show a small loss of magnetisation at low temperatures which increases as the Curie temperature is approached and the magnetisation is destroyed. More complicated thermomagnetic curves arise when more than one mineral is present, with the shape of the resultant curve reflecting the relative contributions and Curie temperatures of the different minerals. The presence of paramagnetic minerals also complicates the issue. The temperature-dependent magnetisation of paramagnetic minerals is governed by the Curie law (equation 3.4) which results in concave thermomagnetic curves.

Table 3.1 also indicates the alteration products of the various magnetic minerals which result from heating to, or above, the temperatures indicated. The oxidation of magnetite (Fe_3O_4) to haematite (Fe_2O_3) for older basalts and

titanomagnetite to magnetite for younger basalts are common features of thermal treatment during palaeomagnetic studies.

3.2.2 Uses of thermomagnetic measurements

Thermomagnetic analysis of a rock sample can provide valuable information about its magnetic mineralogy and resistance to thermal alteration. As previously mentioned, the Curie temperatures of certain minerals are diagnostic and can thus be used to distinguish between, for example, a magnetite-bearing and a haematite-bearing rock. In the present study, all Curie temperatures have been estimated using the intersecting tangents method of Grommé et al (1969). This involves drawing tangents to the maximum gradient of the heating curve and to the part of the curve resulting from the remaining paramagnetic signal (Figure 3.1) and noting the temperature at which they intersect. This method is considered to be more accurate than simply dropping a perpendicular from the point of inflection on the heating curve because it takes into account the effect of the paramagnetic component.

Because these experiments involve heating small samples in air, alteration is a common feature of thermomagnetic analysis. When present it will cause the cooling curve to deviate from the heating curve and the magnitude of the deviation reflects the degree of alteration. Samples may be heated in a vacuum or in a nitrogen atmosphere to reduce the alteration, which is normally caused by oxidation. However, several workers have shown that doing this has little effect on the shape of the thermomagnetic curves (e.g. Pesonen, 1978; Prévot et al, 1985).

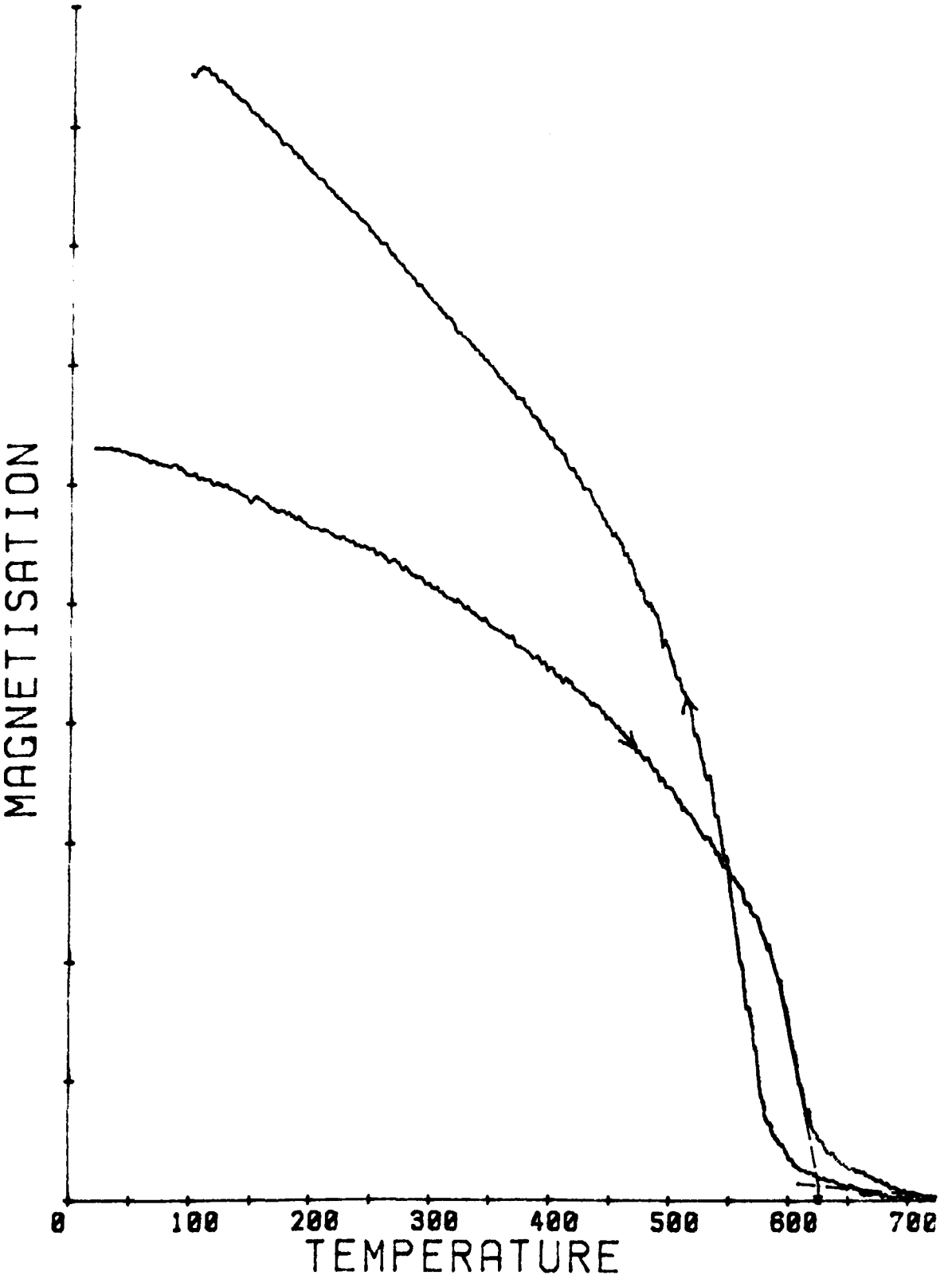

Figure 3.1 : Illustration of the method used for determining Curie temperatures from thermomagnetic curves in the present study.

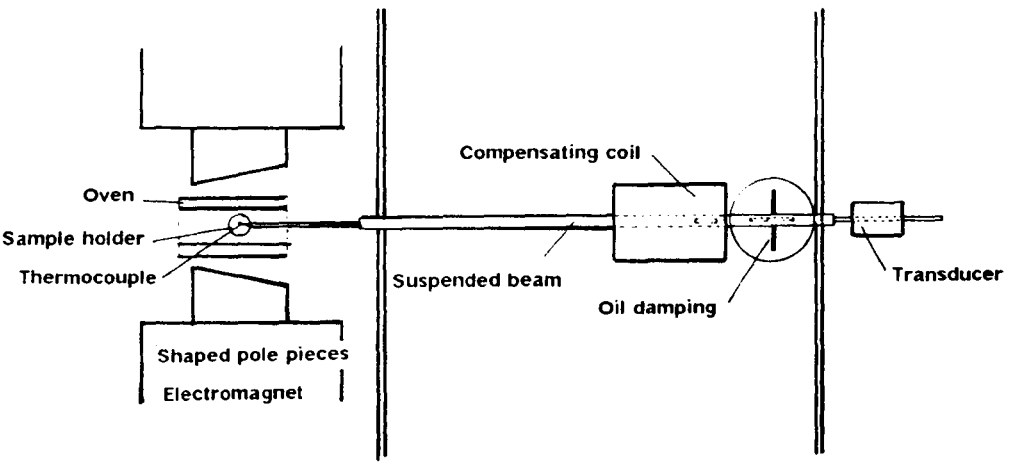

Figure 3.2 : Schematic diagram of the Curie balance used in the present study.

3.2.3 The Liverpool Curie balance

The variation of strong field induced magnetisation with temperature (heating and cooling) was measured using a horizontal translation force Curie balance. This balance, built in Leeds and adapted at Liverpool by Dr. J. A. Share, uses a small amount of material in a non-magnetic holder situated in a non-uniform magnetic field. The balance measures the feedback current caused by the movement of the sample and holder. The saturation magnetisation of the sample changes with temperature and the sample and the holder move to regain equilibrium with the applied field. The sample holder is suspended on fine threads so that it can move freely in order to accurately measure this movement. A schematic diagram of the balance is shown in Figure 3.2.

Samples are placed in a non-magnetic quartz cup mounted on the end of a horizontally suspended rod, and the cup is placed in an oven which is positioned between the pole pieces of an electromagnet. The pole pieces are shaped to produce a strong field gradient, and this causes the sample to move between the pole pieces. The movement is detected by a feedback circuit. As the sample is heated and the magnetisation destroyed the amount of movement, and hence feedback current, will change.

The samples used for thermomagnetic analysis comprised small chips of basalt, ranging from 0.1 to 0.5g depending on the magnetic strength of the sample. Samples were usually measured in fields of 0.68 T (calibrated using a Hall probe - see section 3.2.5.6).

3.2.4 Interpretation of thermomagnetic behaviour

Mankinen et al (1985) described the thermomagnetic behaviour of basalts from the Miocene Steens mountain, Oregon and subsequently classified this behaviour on the basis of the shape thermomagnetic curves. In the present study, the Mankinen et al. classification is used when appropriate, but an alternative classification is used when behaviour not witnessed in the Steens mountain study occurs. Of the six curve types described by Mankinen et al, only two are witnessed in the thermomagnetic study of the Gardar lavas - namely types 2 and 3. Type 1 curves, corresponding to Ti-rich titanomagnetites, are absent. This is not surprising, since it has been widely reported that ancient basalts do not give rock magnetic results characteristic of Ti-rich titanomagnetites (Radhakrishnamurty et al, 1978); it is believed that deuteric ($T > T_c$) oxidation during cooling has converted the primary titanomagnetites to Ti-poor titanomagnetites. Type 4 curves, corresponding to two ferrimagnetic phases - one Ti rich and one Ti-poor titanomagnetite - are also absent from the Gardar lavas. Type 2 curves (Fig. 3.3a,b) are characterised by single high Curie temperatures, invariably greater than 550° C, and a decrease in magnetisation after heating ($J_{sf} < J_{si}$), so that the cooling curve returns below the heating curve. This behaviour is indicative of a single Ti-poor titanomagnetite (i.e. magnetite) phase. Samples with type 2 curves are subdivided, according to the degree of reversibility of the curve:

Type 2a (Fig.3.3a) :
- Little or no change in the shape of the curve is observed after heating.
- Final magnetisation, J_{sf}, is $< 10\%$ lower than the initial magnetisation J_{si}.

Type 2b (not witnessed) :
- Marked change of shape on the cooling curve.
- $J_{sf} < 10\%$ lower than J_{si}.

Type 2c (Fig.3.3b) :
- Marked change of shape on the cooling curve.

- J_{sf} > 10% lower than J_{si}.

The origin of the single magnetic phase which characterises the type 2 curves is either primary or (more likely) a result of the deuteric oxidation of primary Ti-rich titanomagnetites (with Ti≃0.5) to Ti-poor titanomagnetites (with $x < 0.15$) with exsolved ilmenite lamellae (Haggerty, 1976). This oxidation occurs either during or immediately after initial cooling, at temperatures above 700°C. The different shapes of type 2 cooling curves reflect varying degrees of alteration of the magnetic phase on heating in the Curie balance. Type 2a curves represent an essentially unaltered magnetic phase, types 2b and 2c are indicative of magnetic phases which alter significantly after heating.

Type 3 thermomagnetic curves (Fig. 3.3c) are also characterised by a single high Curie temperature, invariably greater than 550°C. This again reflects a single ferrimagnetic phase, with the magnetic mineral similar to that responsible for type 2 behaviour. The type 3 curve only differs from the type 2 curve in that the cooling curve crosses the heating curve, usually in the temperature interval of 400 – 450°C, with the result that J_{sf} is not more than 10-20% higher than J_{si}. The reason for this cross-over is unclear. Perhaps, type 3 curves reflect the conversion of a slightly Ti-enriched titanomagnetite phase to magnetite, which has a greater J_s, causing the cooling curve to return above the heating curve. For type 2 curves, the oxidation of some magnetite to haematite may be the cause of the cooling curve returning below the heating curve.

Type 6 curves (Fig. 3.3d), not witnessed by Mankinen et al (1985), show some interesting features. An inflection is clearly visible on the heating curve but always absent on the cooling cycle. This feature occurs in the region of

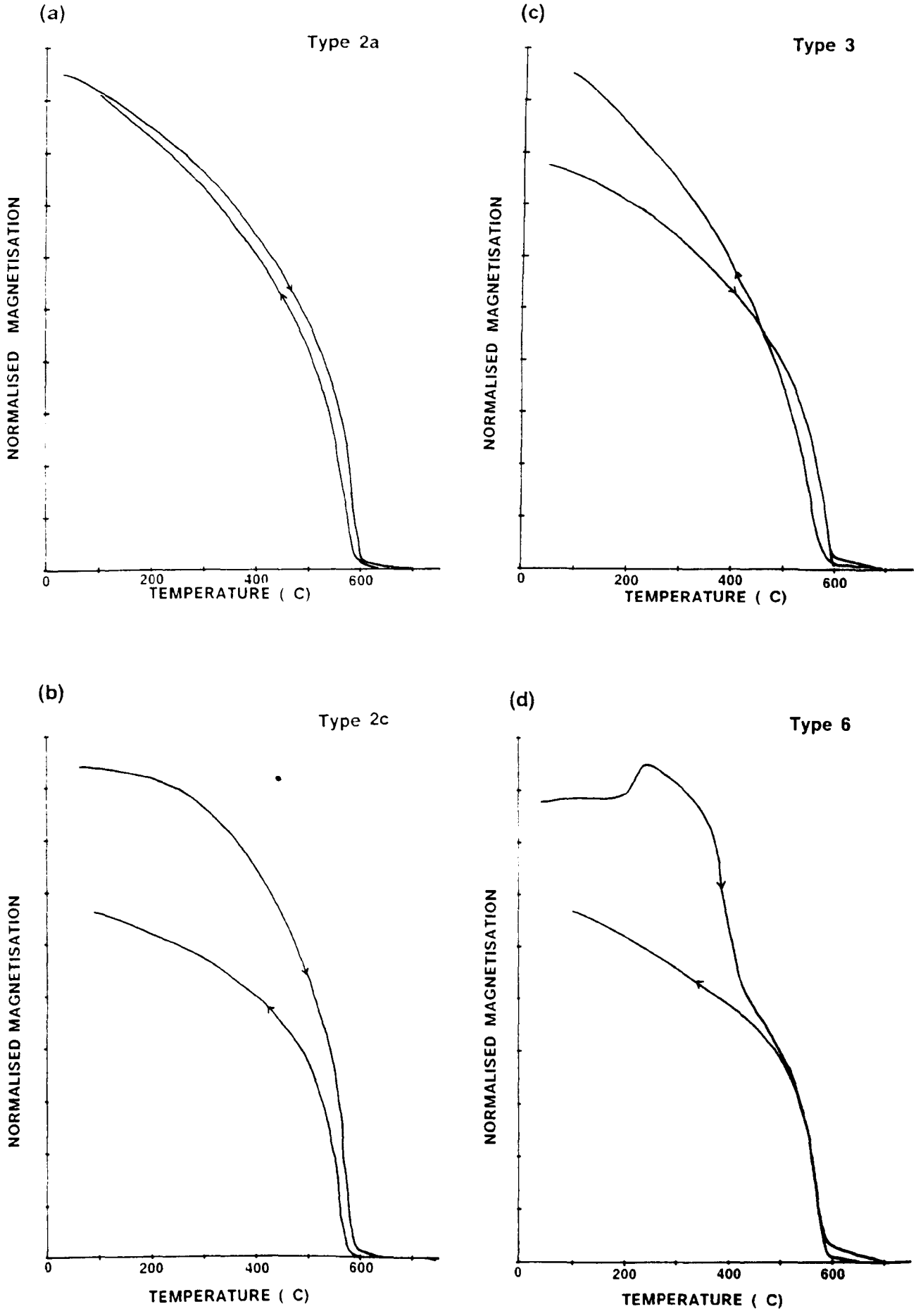

Figure 3.3 : Thermomagnetic curves exhibited by the flows of the Gardar lavas. See text for explanation of classification.

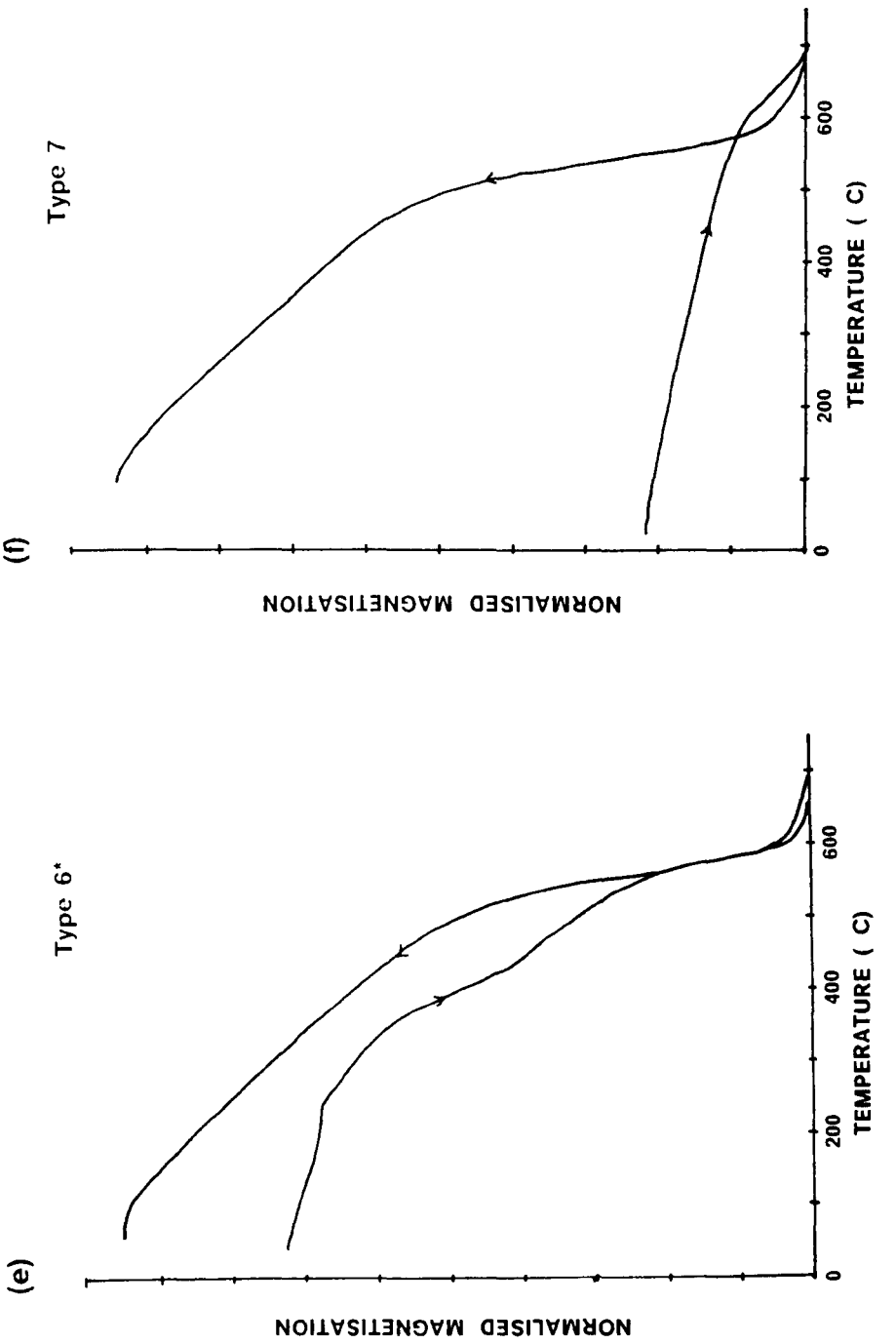
(f)
Type 7
NORMALISED MAGNETISATION
0
200
400
600
TEMPERATURE (C)
(e)
Type 6'
NORMALISED MAGNETISATION
0
200
400
600
TEMPERATURE (C)

400 – 480° C, with an average value for the break of slope at 430°C. The Curie temperature of the main mineral phase is between 580°C and 620°C. It is possible that the inflection represents a Curie temperature which, at 430°C, would correspond to a Ti-enriched titanomagnetite (TM30) phase (O'Reilly, 1984). The co-existence of TM0 and TM30 in a basalt of any age is, however, unlikely (D.J. Dunlop, pers. comm.), particularly in ancient basalts where titanomagnetites are generally absent. An alternative explanation is therefore necessary. Ade-Hall et al (1971) regard the type 6 curve, which they call an "e" type curve, as an expression of the highest degrees of regional hydrothermal alteration and deuteric oxidation, from their Zone I. They noticed that maghaemite is present in flows showing the inflection, an observation supported by separate studies by Larson et al (1969) and Readman and O'Reilly (1970). Some type 6 curves from the Gardar lavas show an increase in J_s on cooling (Fig. 3.3e), where the cooling curve returns above the heating curve. Readman and O'Reilly suggest that such samples may well possess a cation deficient phase, possibly a titanomaghaemite. One explanation is that on heating, the Ti-poor maghaemite (of the type 6 curve) inverts to haematite, which forms as a shell around the magnetite core of the grain. The haematite formed has a much lower saturation magnetisation than the magnetite and thus there is a decrease in J_s on cooling. If, however, the maghaemite is Ti-substituted, then it may invert to magnetite with an ilmenite rim, and this combination is stronger. This results in a small increase in J_s on cooling (the type 6* curve).

Further evidence for the presence of maghaemite (or a cation-deficient magnetite phase) in samples with type 6 thermomagnetic curves can be found in the results of high temperature susceptibility results (Section 3.5). The implications of maghaemitization for the palaeomagnetic study are

important. Maghaemite forms by low temperature oxidation sometime subsequent to the initial cooling of the lava, producing a chemical remanence (CRM). Consequently, the palaeomagnetic vector recorded by maghaemitized flows does not reflect the characteristics of the Earth's field at the time of formation of the rock. Thus, samples showing thermomagnetic curves which are characteristic of low temperature oxidation should be treated with caution for palaeomagnetic purposes.

Type 7 curves (Fig. 3.3f) are also an addition to the Mankinen et al (1985) classification. These are characterised by a single, high Curie temperature phase with a Curie temperature in the range 650 – 690° C, which has a magnetisation much weaker than seen in any other of the curve types. This, combined with the weak initial magnetisation, suggests that haematite is the magnetic mineral. A large increase in J_s occurs after heating, indicating the creation of a much stronger phase on the cooling cycle with a $T_c = 580°C$, suggesting magnetite.

3.2.5 Results from the Gardar lava succession

Between four and six samples from each lava flow were used for thermomagnetic analysis. The results are presented in Table 3.2 in the form of the Curie temperature for the heating and cooling cycles, and curve type for each flow. A breakdown of the results from each lava group is given in the following sections.

3.2.5.1 Lower (Mussartût) Lava Formation

Ninety samples were measured from twenty-three flows in this formation. Thirteen flows exhibited type 2a curves, and ten had type 3 curves (Fig.

3.4a). All of these curves record the presence of a single phase of Ti-poor titanomagnetite (magnetite), with varying degrees of alteration on heating. No haematite-bearing flows are observed. Also absent from this member are flows with type 6 curves, suggesting that severe low temperature oxidation is not an important factor in the lower group. However, three flows L8, L10 and L18) have Curie temperatures between 590° and 615°C suggesting the presence of a cation-deficient (CD) phase which may or may not be associated with slight low temperature oxidation.

3.2.5.2 Middle (Ulukasik) Lava Formation

Fig. 3.4b and Table 3.2 summarise the results of the thermomagnetic study, incorporating seventy-five samples from the eighteen flows in this stratigraphically-thin formation. The distribution of curve type shows far less variety than for the upper lavas (Fig. 3.4b); only type 2a (seven flows) and type 7 curves (eleven flows) are seen. A clear split is witnessed within the formation; flows M2-M8 have type 7 curves whereas flow M1 and most of the flows above M8 are characterised by type 2a curves. This split correlates almost exactly with the split of palaeomagnetic directions (Chapter 4), where flows M1-M8 have the 'A' direction and flows M9-M15 have the 'B' direction. The Curie temperatures for flows M9-M15 are slightly higher than expected for magnetite. It is possible that these flows carry a CD magnetite phase which may have arisen from slight low temperature oxidation.

3.2.5.3 Upper (Ilímaussaq) Lava Formation

One hundred and sixty thermomagnetic measurements were completed from the forty flows sampled in this formation. Fig. 3.4c shows the distribution of thermomagnetic curve type, indicating a variety of behaviour. The majority

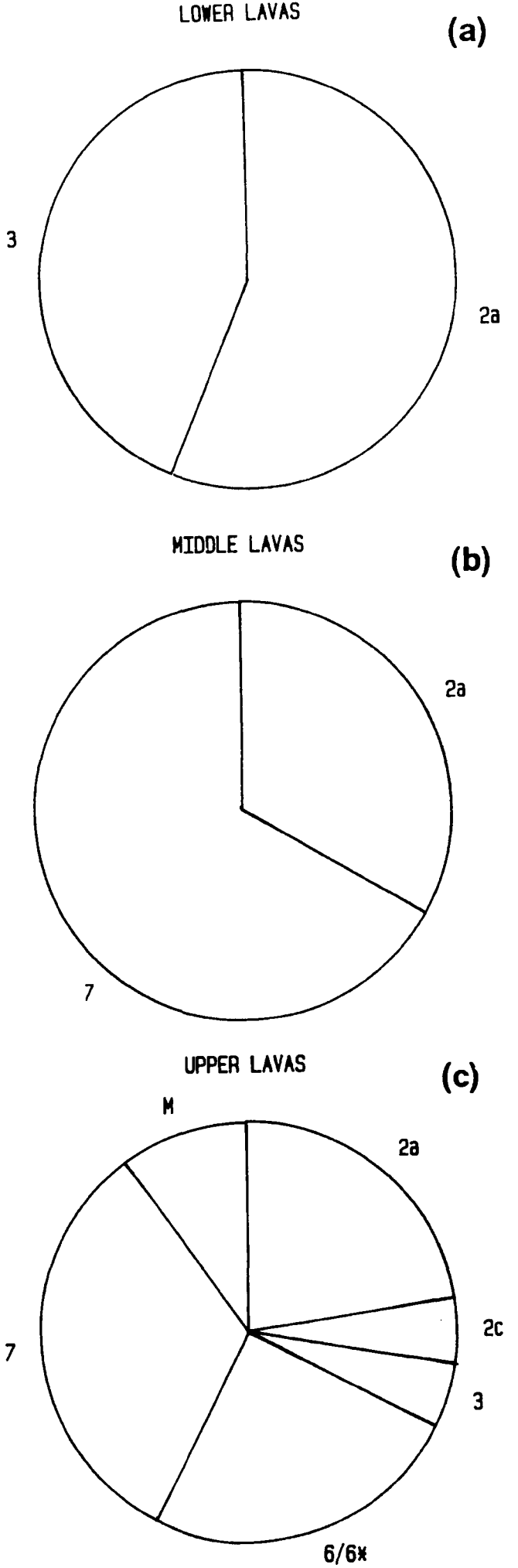

Figure 3.4 : Pie charts indicating the distribution of the thermomagnetic curve types for: (a) The Lower Lava Formation (b) The Middle Lava Formation (c) The Upper Lava Formation.

FLOW NUMBER	CURIE TEMPERATURE (°C) HEATING	COOLING	CURVE TYPE
L1	580	585	2a
L2	575	575	2a
L3	580	580	2a
L4	570	575	2a
L5	580x	575	2a
L6	580	575	3
L7	570	570	3
L8	600	590	3
L9	580	580	2a
L10	600	595	2a
L11	575	575	3
L12	575	575	3
L13	580	575	2a
L14	580	580	2a
L15	575	575	3
L16	580	580	3
L17	580	575	2a
L18	605	595	3
L19	580	575	2a
L20	585	580	2a
L21	580	580	2a
L22	580	575	3
L23	575	575	3
M1	575	575	2a
M2	680	580	7
M3	680	580	7
M4	690	600	7
M5	680	580	7
M6	680	580	7
M7	660	580	7
M8	680	580	7
M9	675	575	7
M10	600	580	2a
M11	615	580	2a
M12	615	580	2a
M13	590	580	2a
M14	680	680	7
M15	620,700	700,580	2a
M16	(610)680	670,590	2a
M17	680	580	7
M18	590	580	2a

Table 3.2 : Results of thermomagnetic measurements for the Lower and Middle Lava Formations (see text for explanation of curve types)

FLOW NUMBER	CURIE TEMPERATURE (°C)		CURVE TYPE
	HEATING	COOLING	
U1	580	580	2a
U2	590x	580	2a
U3	600#x	575	6
U4	575	575	2a/3î
U5	675	580	7
U6	680	580	7
U7	675	580	7
U8	580	575	3
U9	605	580	3
U10	650	575	7
U11	660	575	7
U12	670	580	7
U13	675	580	7
U14	600#x	575	6
U15	590x	575	2a
U16	580	575	2a/3î
U17	675	580	7
U18	675	580	7
U19	680	580	7
U20	600#x	575	6
U21	590	575	2a
U22	600	580	2a
U23	675	580	7
U24	600	575	2a
U25	660	580	7
U26	605#x	575	6
U27	600,680	580	7
U28	580	575	2a
U29	625#x	580	6
U30	600#x	580	6
U31	580	575	2c
U32	595#x	580	6
U33	610#x	580	6
U34	580#x	575	6/2aî
U35	610#x	580	6
U36	605#x	580	6
U37	630	580	7/4i
U38	600	580	2a
U39	640	580	7
U40	590	570	2c
U41	575	575	2a

Table 3.3 : Results of thermomagnetic measurements from the Upper Lava Formation (see text for explanation of curve types)

 # = Irreversible inflection present on heating curve between 300° and 400°C
x = Low temperature kink on heating curve
î = mixture of two types curve within the four measured samples for the flow.

of flows have type 2 (twelve flows) or type 7 (fourteen flows) curves, indicating single magnetic phases of magnetite and haematite respectively, both probably resulting from the deuteric oxidation of original Ti-rich titanomagnetites during cooling. Occasionally, flows having type 2a curves show Curie temperatures in excess of 575°C ($590° < T_c < 615°$). This may be due to the presence of CD magnetite which would indicate a degree of low temperature oxidation. Ten flows exhibited type 6 curves, indicating low temperature oxidation and the presence of maghaemite. Most of the flows showing type 6 curves occur in the middle to top part of the stratigraphic sequence, nearest to the younger, invading Ilímaussaq intrusive complex. Thus it is possible that the thermal effect of this intrusion was responsible for the low temperature oxidation (maghaemitization) of these flows.

3.2.5.4 Intra-flow variations

Considerable variations in the degree of deuteric oxidation within lava flows have been previously reported (Ade-Hall et al, 1968). Piper (1977) noticed that all stages of deuteric oxidation (from 700 – 500°C) occurred in the Gardar lavas but no investigation of intra-flow variation of thermomagnetic behaviour was made.

In terms of curve type, the results of the present study showed little or no intra-flow variation. Only four flows from forty in the upper lavas showed a variation in curve type between the four samples measured from the flows (Table 3.3). This variation usually took the form of either two different magnetite curves (types 2a, 2c or 3) in samples from the same flow or a mixture of magnetite and haematite curves (types 2,3 and 7) within the same site. Two of the four flows showing the variation occur in the top part of the group, nearest to the aureole of the Ilímaussaq intrusion. In the majority

of flows, all four measured samples show the same curve type, with occasional differences in the value of the Curie temperature, T_c. This is most noticeable in type 7 curves, where the value of T_c sometimes varies between 650° and 680°C within one flow. This could be a result of different amounts of Ti substitution in the titano- (ilmeno) haematite series, or it may be a result of thermal hysteresis since larger samples were used for the weakly-magnetic haematite-bearing rocks. For the magnetite-bearing flows, a maximum variation of 5 – 10° C in T_c was seen. No noticeable intra-flow variation was witnessed in the middle and lower groups.

3.2.5.6 Low temperature "kinks" in thermomagnetic curves

A number of flows, predominantly in the upper lava group and, to a lesser extent, in the lower group, exhibit a rise in saturation magnetisation (J_s) at temperatures between 100°C and 200°C, producing an irreversible "kink" in their thermomagnetic curves (e.g.Fig. 3.3d). These kinks only occur in the heating cycles of types 2a and 6 curves. The occurrence of such kinks has been witnessed in Tertiary lavas from Mull, Scotland, and is not uncommon in lavas of Proterozoic age; Ade-Hall et al (1971) recognised these curves in Keweenawan basalts and lavas from the Mull epidote metamorphic zone (Zone I), and observed that these kinks always occurred in lavas which had undergone regional hydrothermal alteration. Furthermore, they were frequently associated with samples indicating the "c" type thermomagnetic curves of their classification (type 6 in the present study).

Duff (1979) recognised similar kinks in the thermomagnetic curves of haematite-bearing granites from the Lower Palaeozoic Jersey volcanics. Those samples with magnetite as the main magnetic mineral showed no kinks. He performed experiments, using pure haematite samples (from a

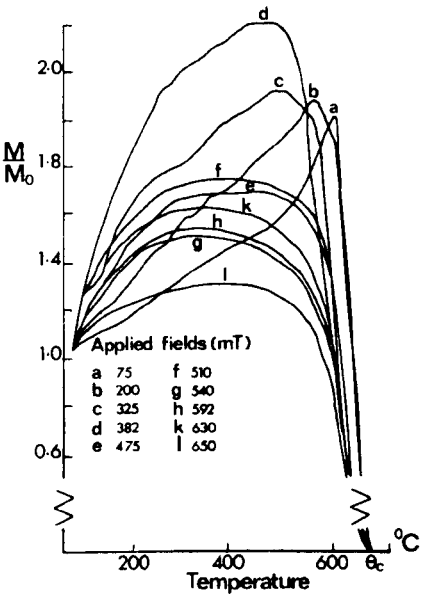

Figure 3.5 : Results of field-dependent thermomagnetic experiments performed on a haematite ore by Duff (1979).

TEXT CUT OFF IN THE ORIGINAL

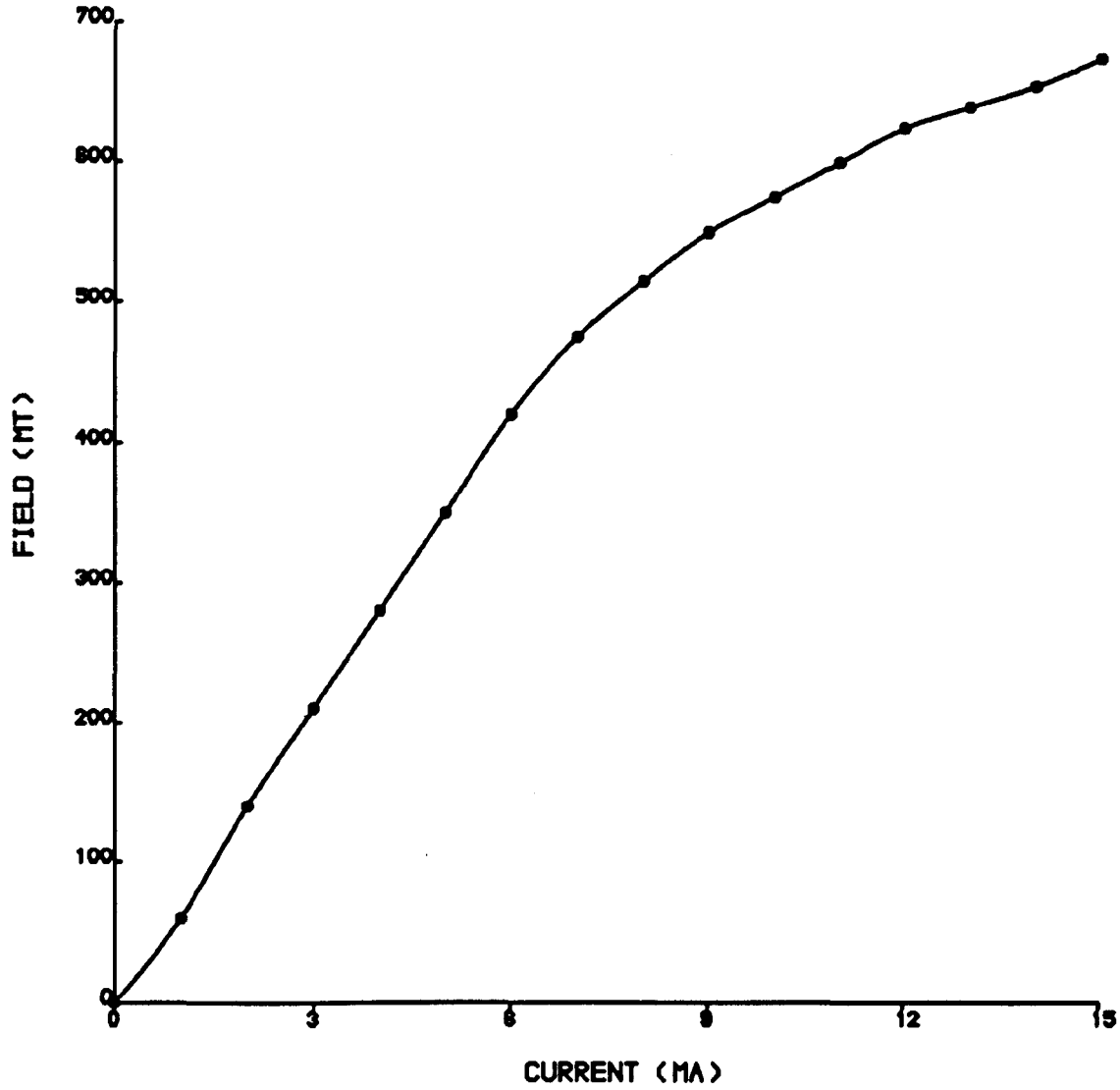

Figure 3.6 : (a) Results of the calibration of the Curie balance using a Hall prob

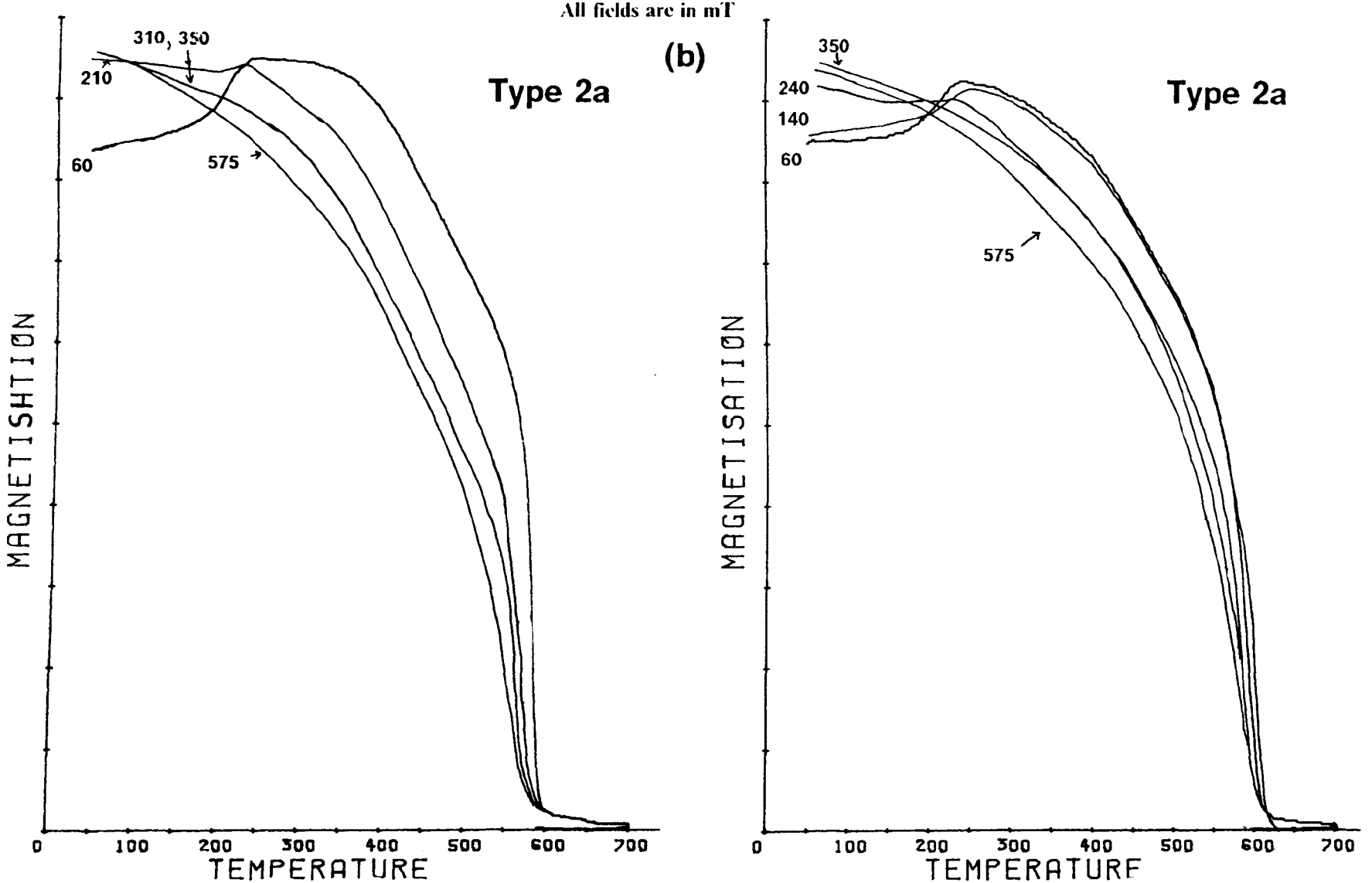

Figure 3.6 :
(b) Results of the field-dependent thermomagnetic experiment performed during the present study.

All fields are in mT

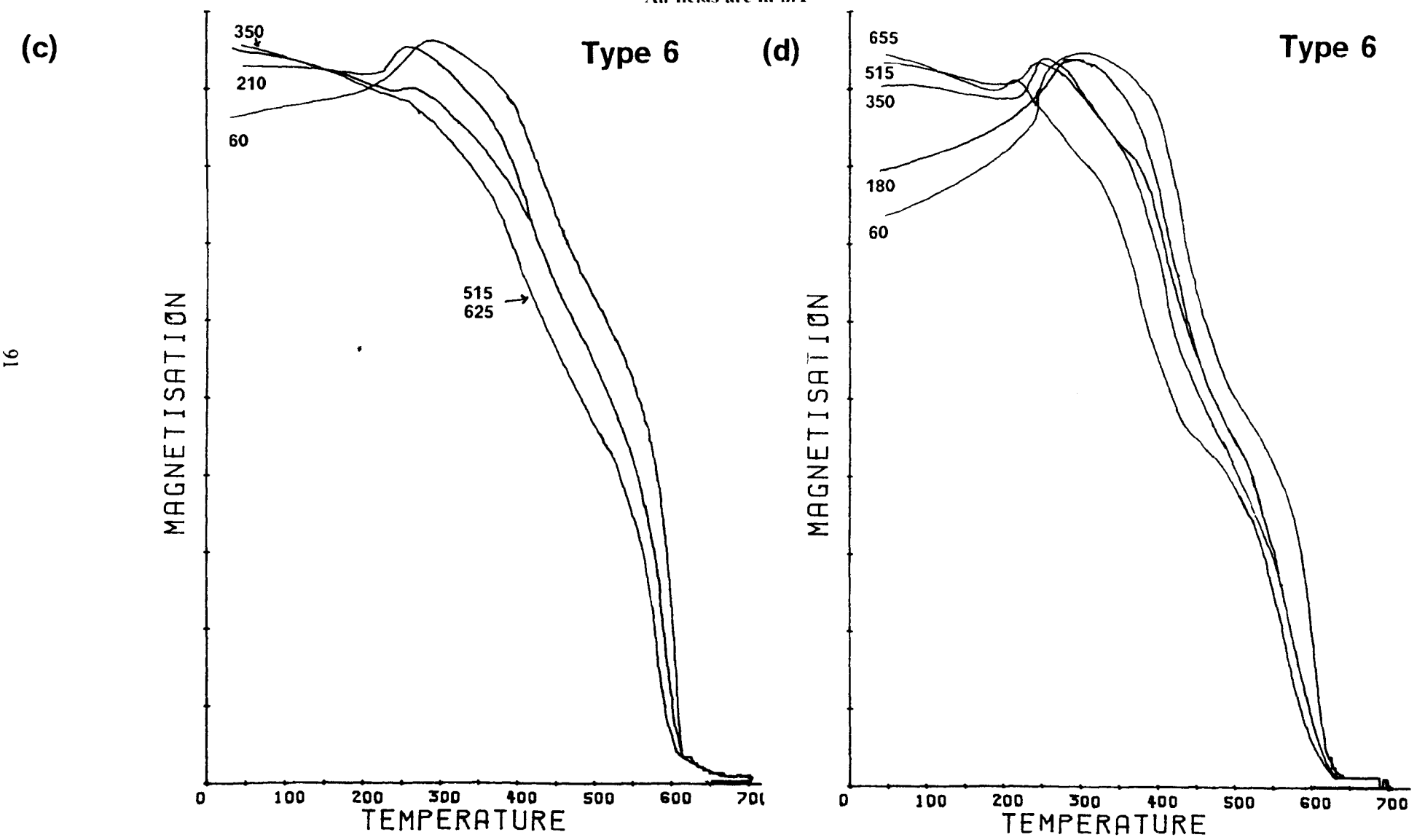

Cumberland hydrothermal deposit) to investigate whether or not the magnitude and shape of the kinks were dependent on the saturating field used in his Curie balance. Figure 3.5 shows his results for ten samples of the haematite ore. Clearly, the magnitude and shape of the kink is field dependent, suggesting that the feature is a direct result of an inability to saturate the haematite magnetisation at room temperature at lower fields. Unfortunately, Duff (1979) did not perform these field dependency tests on the volcanic rocks in which he discovered thermomagnetic kinks. Also, he stated that the kinks occur only in haematite bearing rocks and quotes the Gardar lavas results of Piper (1977) to reinforce this claim. However, close examination of Piper's results reveals that the kinks occur in magnetite-bearing samples, with Curie temperatures near 580°C, an observation which is unquestionably confirmed by the results of the present study (Section 3.2.5.5). Furthermore, Jim Hall has also observed these kinks in Troodos drill cores, which contain multi-domain (MD) magnetite (D.J. Dunlop, pers. comm.). This evidence suggests that the harder phase responsible for these kinks may not be haematite.

To investigate the occurrence of these thermomagnetic kinks in the Gardar lavas, a simple experiment was performed on four samples exhibiting kinks - two with type 2a curves and two with type 6 curves. Specimens from each sample were subjected to fields varying from 60mT-680mT, calibrated for the Curie balance using a Hall probe (Fig. 3.6a). Figure 3.6b shows the results of this experiment.

Clearly, for all four samples, the kink has its largest magnitude at the lowest field. As the field is increased the magnitude of the kink is reduced as the room temperature magnetisation gets closer to saturation. The kinks are

therefore Hopkinson peaks (Hopkinson, 1889). For type 2a curves, the kink disappears by 300mT - the theoretical maximum coercivity of SD magnetite (McElhinny, 1973). It is noticeable that the Curie temperatures for all type 2a curves showing kinks are between 590° and 615°C, suggesting the presence of CD magnetite. The kinks may therefore be due to the presence of CD magnetite which occurs as SSD grains. Perhaps, stress effects are important in CD magnetite, leading to high magnetostriction and therefore coercivity. Whatever the explanation, it is clear that the occurrence of kinks in the thermomagnetic curves of the Gardar lavas is a signature of some form of magnetite and not haematite as previously thought by Duff (1978). Samples which possess haematite as the magnetic mineral (type 7 curves) do not show low temperature kinks in their thermomagnetic curves.

The behaviour for type 6 curves is more difficult to explain. The size of the kink (which is larger than that seen in type 2a curves) decreases with increasing field but does not disappear completely by 680mT. The explanation for this behaviour is unclear.

3.2.5.7 Summary of thermomagnetic behaviour

The range of thermomagnetic behaviour witnessed in the flows of the Gardar lavas can be accounted for by the process of deuteric oxidation. Oxidation occurs in all three formations, resulting in the creation of a single, high Curie temperature magnetic phase of either magnetite ($T_c = 575°C$) or haematite ($T_c = 675°C$). In the Upper and Middle lavas, some flows have magnetite as the mineral and other flows have haematite. However, in the Lower Lavas, only magnetite is present. Partial deuteric oxidation, of the type witnessed by Mankinen et al (1985) and Wilson and Watkins (1967) in the Steens mountain basalts is absent. Low temperature oxidation (maghaemitization)

is an important factor in a number of flows near the top of the Upper Formation, as characterised by type 6 thermomagnetic curves. This may be a result of hydrothermal alteration by fluids from the Ilímaussaq igneous complex which intrudes this part of the succession. The occurrence of Curie temperatures between 590° and 615°C in certain flows suggests that these flows contain CD magnetite, possibly originating from slight low temperature alteration.

For magnetite-bearing samples, the degree of alteration on heating is low; the dominant magnetite curve is the type 2a curve, showing a decrease of less than 10% in J_s after heating. Even magnetite samples showing type 3 curves (where the cooling curve crosses the heating curve) show little or no alteration, with J_{sf} never more than 10% higher than J_{si}. These observations are encouraging regarding the potential suitability of the magnetite-bearing samples for use in palaeointensity experiments. This is discussed further in Chapters 6 and 7.

This section has highlighted the value of using the thermomagnetic behaviour witnessed in basalts to identify the extent of oxidation.

3.3 ROOM TEMPERATURE SUSCEPTIBILITY

3.3.1 Introduction

The susceptibility of a magnetic substance is a measure of the ease with which it becomes magnetised in an applied field. Magnetic susceptibility can be measured at either low or high applied fields and at different frequencies; in the present study only low fields were used.

This section describes the low-field mass susceptibility results for the Gardar lavas, obtained using a Bartington MS1 susceptibility meter.

3.3.2 Uses of room temperature susceptibility measurements

In the present study, four uses of room temperature susceptibility (K_{RT}) results were employed:

(1) Koenigsberger ratio, Q_n : Q_n is defined as the ratio of the remanent magnetisation to the induced magnetisation for a sample at the sampling locality (Koenigsberger, 1938) and is given by:

$$Q_n = \frac{J_n}{kH} \tag{3.1}$$

where: J_n = NRM intensity of the sample in Am^2kg^{-1}
k = mass susceptibility in m^3kg^{-1}
H = field strength at sampling site in Am^{-1}

For multi-domain samples, $Q_n \simeq 0.5$ whereas Q_n for SD material should be higher ($\simeq$5 to 10) so that samples with large Q_n values have mainly SD grains and samples with low Q_n values are MD rich Stacey (1963).

(2) Frequency dependent susceptibility (K_{FD}%) : Initial susceptibility falls with increasing frequency of applied field and the amount of change varies with grain size. Thus, K_{FD} can be used to give an estimate of grain size. The decrease in susceptibility of MD grains with frequency is virtually zero, the largest frequency effect is seen for grains which lie on the stable single-domain/superparamagnetic boundary (Thompson & Oldfield, 1986). This is because SP grains, which follow the applied field at low frequencies, cannot oscillate quickly enough to keep in phase with the field when the

frequency is increased. Consequently, the susceptibility is out of phase with the field and the measured susceptibility is lower than that observed at low frequencies.

The variation of susceptibility with frequency is usually represented as a percentage:

$$K_{FD}\% = \frac{K_{lf} - K_{hf}}{K_{lf}} \times 100 \qquad (3.2)$$

where K_{lf} and K_{hf} are the low and high field susceptibility values respectively.

Experimentally, Thompson and Oldfield (1986) have determined a range of 0-24% for K_{FD}, with the largest values occurring in samples with the largest SP fraction.

(3) Anisotropy of magnetic susceptibility (AMS) : As mentioned in Section 1.2, unless a sample is isotropic, its magnetic properties of samples vary with direction, with "easy" and "hard" axes of magnetisation. The susceptibility of a sample then varies according to the orientation of the applied field. If the magnetic grains have no preferred alignment (randomly oriented) then the susceptibility of the sample will be homogeneous (equal in all directions). However, if there is an anisotropy of alignment of magnetic grains in the sample, then it will have an associated AMS.

The AMS is normally represented in terms of three axes of reference, known as the principal susceptibility axes, which define the susceptibility ellipsoid. The orientation of these maximum (K_1), intermediate (K_2) and minimum (K_3) axes is determined using a susceptibility anisotropy delineator.

In AMS measurements, for palaeomagnetic purposes, four parameters are commonly used:

$$A = \text{anisotropy factor} = \frac{K_1}{K_3}$$

$$L = \text{lineation factor} = \frac{K_1}{K_2}$$

$$F = \text{foliation factor} = \frac{K_2}{K_3}$$

$$E = \text{eccentricity of ellipsoid} = \frac{F}{L} = \frac{K_2^2}{K_1 K_3}$$

If $E > 1$ and for $L \simeq 1$ the ellipsoid is oblate (disc) shaped.

If $E < 1$ and for $F \simeq 1$ the ellipsoid is prolate (cigar) shaped.

The value of A is particularly important to palaeomagnetism since it dictates the angle through which the magnetisation of a sample, for example a TRM in a basalt, is deflected by the anisotropy of the sample provided the AMS always indicates remanence anisotropy. McElhinny (1973) reported that for an applied field which lies in the plane of the maximum and minimum susceptibility axes, the TRM will be deflected, by the anisotropy, through a maximum angle β, where:

$$\beta = \tan^{-1}\left(\frac{A-1}{2\sqrt{A}}\right) \qquad (3.3)$$

Using equation 3.3, anisotropies of 10%, 20% and 50% (A = 1.1, 1.2 and 1.5) are able to deflect a TRM by only 2.7°, 5.2° and 11.6° respectively. McElhinny (1973) stated that an anisotropy of up to 20% can be tolerated without significantly deflecting the TRM. Basaltic rocks, such as those

witnessed in the Gardar lava succession, rarely have anisotropies in excess of a few percent. Therefore it is unlikely that the TRM in such rocks will be significantly affected by AMS. It is usually metamorphic rocks which show the greatest degree of AMS.

(4) Change in K_{RT} during thermal demagnetisation : The change in K_{RT} for selected samples was monitored after each step of the thermal demagnetisation studies described in Chapter 4. Changes in K_{RT} with temperature signify the occurrence of mineralogical changes in the sample on heating due to the creation of superparamagnetic (SP) grains, possibly as a result of the breakdown of ferrimagnetic material. Such changes can distinguish between samples containing magnetite from those containing haematite.

3.3.3 Results

The results of K_{RT} experiments are listed in Tables 3.4-3.5

3.3.3.1 Lower (Mussartût) Lava Formation

The combination of the various K_{RT} results illustrates that magnetite is the magnetic mineral present in the flows of this formation. The dramatic increase in susceptibility after 580°C reflects thermal alteration of the sample and the creation of SP grains (Fig. 3.8a). This is confirmed by an increase in frequency effect after 550° C. Low Q_n values suggest that multi-domain (MD) is the dominant domain state, supported by the absence of a significant room temperature frequency effect which suggests the absence of very small grains near to the SP/SSD boundary. The AMS results indicate low anisotropies (average 3.4% - Fig.3.7a) which imply that the remanence

FLOW	KRT_{LF} ($\times 10^{-8}m^3kg^{-1}$)	KRT_{HF}	Q_n	K_{FD}%	K1/3	K2/3	K1/2	β (°)	E
L1	8723	8723	0.67	0	1.031	1.013	1.018	0.9	1.01
L2	485	485	5.9	0	1.030	1.009	1.020	0.9	1.01
L3	2535	2519	0.48	0.63	1.021	1.003	1.019	0.6	1.02
L4	4048	4046	0.46	0.05	1.073	1.022	1.050	2.0	1.03
L5	8039	8033	0.61	0.07	1.033	1.017	1.016	0.9	1.00
L6	3141	3140	0.64	0.03	1.047	1.016	1.031	1.3	1.01
L7	1883	1881	0.66	0.11	1.039	1.005	1.034	1.1	1.03
L8	3398	3393	0.92	0.15	1.030	1.009	1.020	0.9	1.01
L9	2039	2039	1.04	0	1.022	1.006	1.016	0.6	1.01
L10	1963	1959	2.33	0.20	1.032	1.006	1.026	0.9	1.02
L11	1712	1711	0.76	0.06	1.026	1.018	1.008	0.7	0.99
L12	2958	2956	0.29	0.07	1.024	1.013	1.002	0.7	0.99
L13	7662	7660	0.87	0.03	1.035	1.031	1.004	1.0	0.98
L14	4123	4120	1.14	0.07	1.036	1.007	1.029	1.0	1.02
L15	1180	1180	3.47	0	1.033	1.007	1.026	0.9	1.02
L16	1585	1580	0.96	0.32	1.030	1.004	1.026	0.9	1.02
L17	3378	3376	0.71	0.06	1.053	1.023	1.030	1.5	1.01
L18	2100	2093	1.76	0.33	1.043	1.013	1.030	1.2	1.02
L19	5472	5470	0.51	0.04	1.042	1.008	1.033	1.2	1.02
L20	2552	2551	4.43	0.04	1.022	1.004	1.010	0.6	1.01
L21	2543	2542	0.75	0.04	1.027	1.013	1.014	0.8	1.00
L22	2171	2167	0.60	0.20	1.022	1.011	1.010	0.6	0.99
L23	6990	6988	3.06	0.03	1.022	1.008	1.014	0.6	1.01
M1	2158	2155	0.72	0.14	1.032	1.010	1.022	0.9	1.01
M2	87	87	2.86	0	1.033	1.006	1.026	0.9	1.02
M3	62	59	5.35	3.20	1.017	1.008	1.009	0.5	1.01
M4	36	35	9.42	2.80	1.009	1.003	1.006	0.3	1.00
M5	23	22	5.57	0	1.018	1.010	1.009	0.5	0.99
M6	30	29	8.04	0	1.007	1.002	1.005	0.2	0.99
M7	40	39	1.51	0	1.022	1.008	1.014	0.6	1.00
M8	50	50	4.67	0	1.015	1.005	1.010	0.4	1.00
M9	29	28	9.10	3.5	1.018	1.013	1.005	0.5	0.99
M10	4789	4779	0.46	0.20	1.013	1.011	1.002	0.4	0.99
M11	3974	3966	0.29	0.20	1.047	1.021	1.026	1.3	1.01
M12	3942	3936	0.33	0.15	1.010	1.009	1.001	0.3	0.99
M13	186	184	0.89	1.10	1.024	1.011	1.014	0.7	1.00
M14	56	54	2.29	1.80	1.028	1.023	1.005	0.8	0.98
M15	26	26	6.96	0	1.027	1.021	1.006	0.8	0.99
M16	57	56	0.66	1.80	1.045	1.017	1.028	1.4	1.01
M17	125	125	3.38	0	1.016	1.008	1.008	0.5	1.00
M18	19	18	5.95	0	1.028	1.015	1.013	0.8	1.00

Table 3.4 : Results of room temperature susceptibility measurements for the Lower and Middle Lava Formations. $KRT_{LF}$and KRT_{HF} are the room temperature susceptibility measurements at low and high frequency respectively. Q_n = Koenisberger ratio; K_{FD} = frequency dependent susceptibility; K1/3, K2/3 and K1/2 are the susceptibility ellipsoid axes ratios;β = the maximum angle of deflection of the TRM vector due to AMS in flows; E = the eccentricity of the susceptibility ellipsoid.

FLOW	KRT_{LF} ($\times 10^{-8} m^3 kg^{-1}$)	KRT_{HF}	Q_n	K_{FD}%	K1/3	K2/3	K1/2	β (°)	E
U1	5113	5100	1.26	0.25	1.120	1.028	1.082	3.2	1.10
U2	8340	8334	0.51	0.07	1.032	1.009	1.023	0.9	1.01
U3	1566	1560	0.6	0.40	1.007	1.001	1.006	0.2	1.00
U4	2492	2477	2.46	0.60	1.158	1.073	1.081	4.2	1.00
U5	41	40	11.1	2.40	1.019	1.008	1.012	0.5	1.00
U6	34	34	1.8	0	1.014	1.007	1.007	0.4	1.00
U7	43	42	1.74	2.30	1.003	1.001	1.001	0.1	1.00
U8	449	442	1.02	1.60	1.015	1.009	1.006	0.4	1.00
U9	73	73	4.53	0	1.012	1.009	1.002	0.3	0.99
U10	48	48	31.5	0	1.015	1.002	1.012	0.4	1.01
U11	69	69	26.22	0	1.052	1.019	1.032	1.5	1.01
U12	59	59	11.49	0	1.030	1.013	1.017	0.9	1.00
U13	73	73	35.1	0	1.035	1.024	1.010	1.0	0.99
U14	777	772	1.08	0.60	1.026	1.003	1.023	0.7	1.02
U15	3764	3760	0.87	0.10	1.023	1.009	1.014	0.7	1.01
U16	2925	2914	0.96	0.40	1.077	1.017	1.058	2.1	1.04
U17	68	68	1.65	0	1.009	1.003	1.006	0.3	1.00
U18	59	58	24.3	1.70	1.009	1.005	1.004	0.3	1.00
U19	50	50	28.65	0	1.011	1.003	1.008	0.3	1.01
U20	940	940	1.05	0	1.031	1.007	1.024	0.9	1.02
U21	1185	1184	0.67	0.08	1.033	1.007	1.026	0.9	1.02
U22	3603	3593	0.54	0.30	1.045	1.031	1.013	1.3	0.98
U23	80	80	1.89	0	1.009	1.004	1.005	0.3	1.00
U24	4668	4650	1.02	0.40	1.038	1.035	1.003	1.1	0.97
U25	64	64	3.81	0	1.009	1.006	1.003	0.3	0.99
U26	1114	1111	0.42	0.30					
U27	89	89	3.81	0	1.014	1.007	1.007	0.4	1.00
U28	6930	6920	0.69	0.10	1.035	1.009	1.025	1.0	1.02
U29	814	813	0.45	0.10					
U30	642	640	1.41	0.30	1.027	1.011	1.016	0.8	1.01
U31	1743	1741	1.68	0.10	1.030	1.009	1.021	0.9	1.02
U32	305	304	2.97	0.30	1.017	1.012	1.005	0.5	0.99
U33	3951	3940	0.39	0.30	1.025	1.009	1.016	0.7	1.00
U34	197	196	2.67	0.50					
U35	35	35	36.6	0	1.029	1.010	1.019	0.8	1.00
U36	38	38	47.61	0					
U37	222	220	3.75	0.90	1.017	1.003	1.015	0.5	1.01
U38	49	49	32.31	0					
U39	1733	1724	1.26	0.50	1.026	1.010	1.015	0.7	1.01
U40	3794	3782	1.29	0.30	1.029	1.014	1.015	0.8	1.00

Table 3.5 : Results of room temperature susceptibility experiments for the Upper Lava Formation (See legend to Table 3.4 for explanation of symbols).

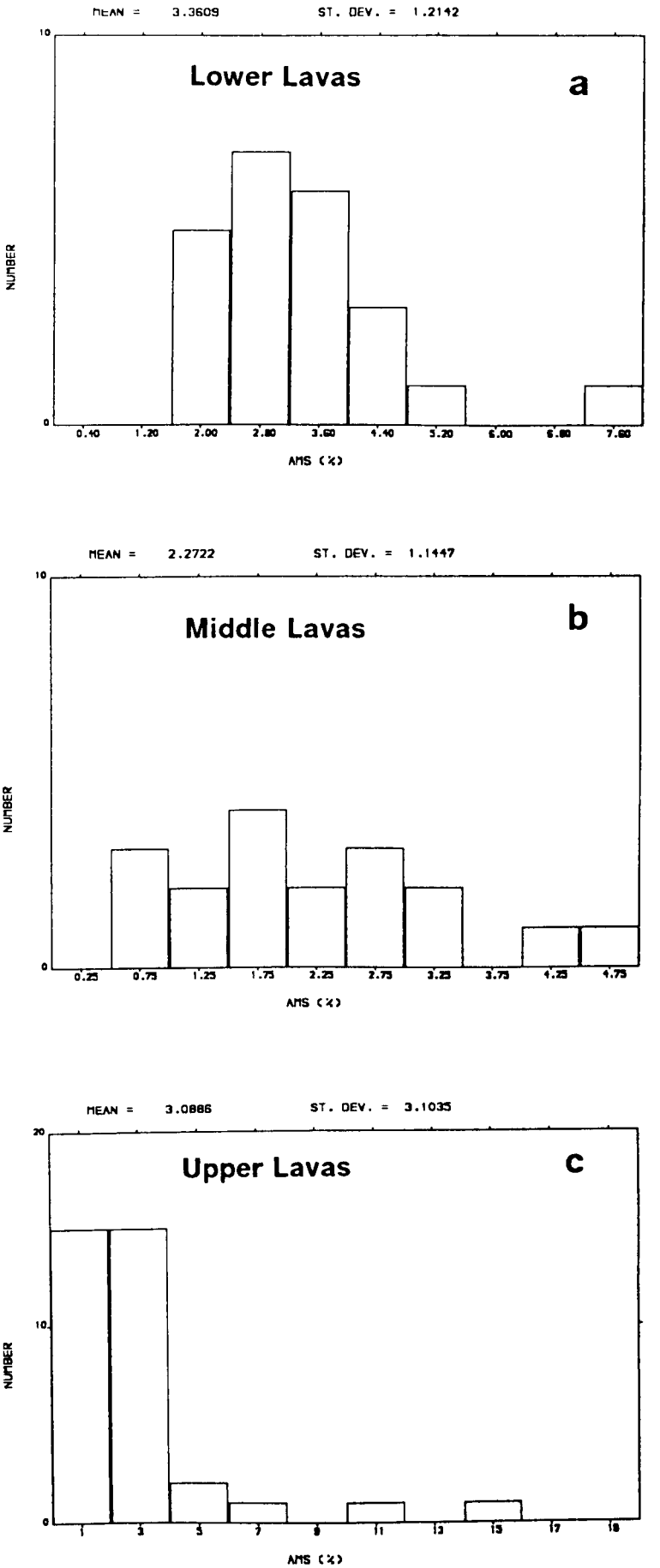

Figure 3.7 : Histograms of anisotropy (K1/K3) values for: (a) The Lower Lava Formation (b)The Middle Lava Formation (c) The Upper Lava Formation.

TEXT CUT OFF IN THE ORIGINAL

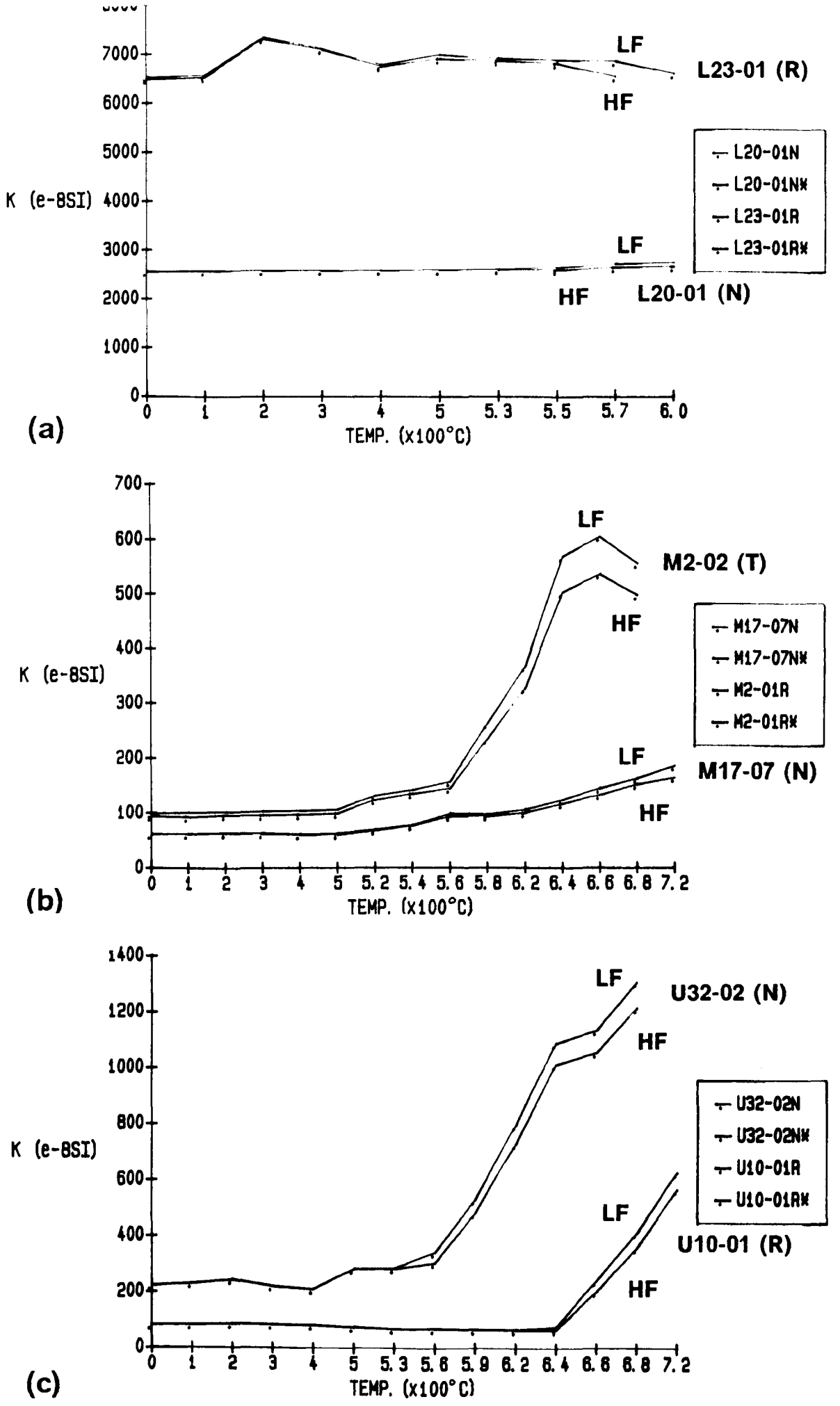

Figure 3.8 : Graphs illustrating the change in KRT measured after each demagnetisation step in the thermal demagnetisation study. LF and HF are the low frequency and high frequency room temperature susceptibility curves respectively.

directions within the flows of the lower lavas will not be significantly deflected (Section 3.3.2 and Table 3.4). The E values suggest that the majority of flows have oblate susceptibility ellipsoids, which are disc-shaped.

3.3.3.2 Middle (Ulukasik) Lava Formation

The K_{RT} results indicate a variety of magnetic behaviour within this formation. Large and small K_{RT} values, corresponding to MD magnetite and haematite, respectively, are witnessed. The largest frequency effect is observed for samples with low K_{RT} values. AMS results again show the lack of a significant anisotropy and the susceptibility ellipsoid is oblate and dominantly disc-shaped. A rise in susceptibility is usually seen between 640° C and 680°C, indicating thermal alteration of samples at these high temperatures and the creation of SP grains (Fig 3.8b).

3.3.3.3 Upper (Ilimaussaq) Lava Formation

The degree of anisotropy is generally higher in this formation than the other two but is still too low to significantly affect the remanence directions. The largest anisotropy is exhibited by feldspar-phyric flows in the bottom half of the formation within the "star basalt" and "platy basalt" units (Table 3.5). Q_n values are smaller than those seen in the lower formation suggesting that MD grains are more abundant in the upper lavas. E values indicate oblate shapes of the susceptibility ellipsoid for most flows. An increase in susceptibility is seen after 580°C for some flows and after 680°C for others, indicating thermal alteration and the creation of SP grains.

3.3.4 Summary

The K_{RT} results indicate that multi-domain magnetite and haematite are probably the dominant magnetic mineral phases within the flows of the Gardar lavas. All flows show low degrees of anisotropy of magnetic susceptibility, suggesting that the remanence directions will not be significantly affected by magnetic fabric. This is an important result in the context of the palaeomagnetic study (Chapter 4). Studies of the change in low-field K_{RT} with temperature indicate that most flows show little alteration until the blocking temperature is reached, when large increases in susceptibility were observed. This is useful in the identification of thermally-induced changes in magnetic mineralogy.

The K_{RT} results give a broad idea of the magnetic mineralogy of the flows of the Gardar lavas succession. The following rock magnetic studies give a more detailed account of the composition, domain states and extent of oxidation witnessed in these flows.

3.4 LOW TEMPERATURE SUSCEPTIBILITY (KLT)

3.4.1 Introduction

During the past twenty-five years, many workers have reported results of temperature dependent susceptibility experiments on synthetic magnetic materials (Parry, 1965; Day, 1973; Dunlop 1972). However, it is only within the last ten years or so that such studies have been extended to the much more complex situation that exists in naturally occurring rocks (Radhakrishnamurty et al, 1977, 1978, 1981; Senanayake and McElhinny, 1981, 1982; Sherwood, 1986, 1988). This section describes the theory and

different interpretations of low temperature susceptibility behaviour in basalts and applies these interpretations to results of low temperature susceptibility measurements on the Gardar lavas.

3.4.2 Theory and diagnostic models

A large number of magnetic measurements have been made on basalts by the rock magnetism group at the Tata Institute of Fundamental Research (TIFR) in Bombay. The importance of this work is that results from synthetic materials (referenced above) have been applied to natural rock samples, whilst acknowledging that there are important differences in the behaviour shown by synthetics and basaltic rocks which have a complex magnetic mineralogy.

Several different types of magnetic grain are found in basalts. The susceptibility behaviour of each of these grain types when cooled to liquid nitrogen temperatures is now summarised.

1. **Multi-domain (MD) grains.**

It is generally accepted that in large magnetic (MD) grains, magnetocrystalline anisotropy is more significant than shape anisotropy in controlling the susceptibility behaviour. The magnetocrystalline anisotropy constants K_1 and K_2 are strongly temperature dependent. It has been shown (Bickford, 1950; Syono and Ishikawa, 1963) that for magnetite the sign of K_1 changes from negative to positive at -150°C (130K). This temperature signifies the isotropic point of magnetite, where $K_1 \rightarrow 0$. At this low temperature transition, known as the Verwey transition, a peak in

susceptibility occurs for MD magnetite. The presence of this peak in any sample is a clear indication of the presence of MD magnetite.

2. **Single domain (SD) grains.**

The susceptibility of single domain grains, where elongation exceeds 10% is dominated by shape anisotropy, as opposed to magnetocrystalline anisotropy (Pullaiah et al, 1975). Shape anisotropy is not strongly temperature dependent, since the shape of the crystal will not change with decreasing temperatures down to -196°C. Hence, only small changes in susceptibility are expected down to liquid nitrogen temperatures. Consequently, the peak in susceptibility seen for MD grains is not observed for SD grains.

3. **Superparamagnetic (SP) grains.**

Superparamagnetic grains (Néel, 1955) can be regarded as very small single domain grains. The susceptibility of SP grains should fall with temperature as the thermal energy of the system decreases and the blocking volume decreases. Once all of the SP grains have been blocked in then the susceptibility should stabilise (Maher, 1988). Consequently, the susceptibility drops steadily to a temperature in the region of -150°C, after which there is little or no change down to -196°C.

4. **Paramagnetic (PM) grains.**

The susceptibility of paramagnetic grains follows the Curie Law (Equation 3.4), which dictates that the susceptibility of PM grains (which is very weak) should rise with decreasing temperature.

$$K = \frac{C}{T} \qquad (3.4)$$

where C = Curie constant and T = absolute temperature.

5. **Cation deficient (CD) grains.**

Radhakrishnamurty et al (1977) believe that CD magnetite is very common in basalts and its presence suppresses the low temperature Verwey transition. Radhakrishnamurty (1989) considers that CD magnetite shows essentially SD behaviour. Senanayake (1981), however, suggests that although CD titanomagnetites have been identified in nature (eg. Akimoto and Katsura, 1959; Creer and Ibbetson, 1970; Sanver and O'Reilly, 1970), investigations of non-stoichiometric (CD) titanomagnetites (Rahman and Parry, 1978; Senanayake and McElhinny, 1981) have concluded that the low temperature characteristics of these materials cannot differ greatly from those of the stoichiometric form. Consequently, Senanayake (1981) believes that the presence of CD grains cannot explain large increases of susceptibility down to -196°C, as suggested by Radhakrishnamurty et al (1977). The effect of CD grains in basalts on their KLT behaviour is still uncertain, although the results of the present study provide some idea of this behaviour.

The first classification of KLT behaviour for basalts was made by Radhakrishnamurty et al (1977) and the following discussion outlines the basic ideas and assumptions behind the classification. The basis of this classification is the assumption that Ti-rich titanomagnetites occur rarely in natural rocks, being chiefly found in pillow lavas younger than 30,000 years and absent from basalts older than several million years. Thus, Radhakrishnamurty et al (1977) believe that most basalts, older than a few

million years in age contain either SD, MD or SP grains of magnetite, CD magnetite or a combination of these. Each of the four types of grain (SD, MD, SP, CD) show a characteristic variation in susceptibility down to -196°C (Fig. 3.9a). They define the parameter RS (relative susceptibility) as the ratio K_{196}/K_{30} and believe that the value of this parameter can be used to recognise the dominant kind of magnetic grain present in a basalt. They also recognise that the magnetic mineralogy of basalts is very rarely composed entirely of a single grain size and mixed grain sizes frequently occur, with most basalts containing three of the above grain types, one of which plays a minor role compared with the other two. Fig. 3.9b shows the KLT behaviour of samples showing various mixed grain sizes of pure magnetite and Table 3.7 gives RS values of both the pure and hybrid magnetic grain states.

Senanayake and McElhinny (1981) recognised that the major assumption of Radhakrishnamurty et al. (1977), namely that titanomagnetites did not exist in old basalts, was in conflict to the view of petrologists (e.g. Haggerty, 1976). They used KLT results from over 1000 Tertiary basalts from various localities to compile a classification based on the presence of pure magnetite and Ti-rich titanomagnetites. They discovered that 95% of their samples fell into one of three categories (Fig 3.10):

Group 1 : K decreases to an average RS value of 0.28

Group 2 : K increases to an average RS value of 1.26

Group 3 : A peak in K occurs near -150°C, averaging 1.24 times the room temperature value. Samples show an average RS value of 1.03.

The interpretation of the behaviour characteristic of each group is given in Table 3.6.

GROUP	INTERPRETATION OF BEHAVIOUR
1	Mainly MD Ti-rich titanomagnetites
2	Ti-rich titanomagnetites with exsolved ilmenite lamellae, resulting from deuteric oxidation, which effectively subdivide the grains into magnetically distinct regions which behave as SD grains.
3	MD Ti-poor titanomagnetites (pure magnetite)

Table 3.6 : The classification and interpretation of KLT behaviour according to Senanayake & McElhinny (1981).

Subsequently, Radhakrishnamurty (1985) added to his earlier classification by explaining that KLT behaviour can also be attributed to different compositions of titanomagnetites (Fig. 3.11). This interpretation is closer to that of Senanayake and McElhinny (1981) than was his original version. However, Radhakrishnamurty (1990) explains that titanomagnetite-bearing basalts (with $x > 0.3$) show complex magnetic behaviour, requiring the invocation of mixed domain states even when only one member of the TM series is present. Quite often, though, more than one member is present (Radhakrishnamurty, 1985) which further complicates the issue.

It has been previously mentioned that the susceptibility of SD grains should not change much down to -196°C and hence should have an RS value close to unity. In view of this, the interpretation of SD behaviour presented by

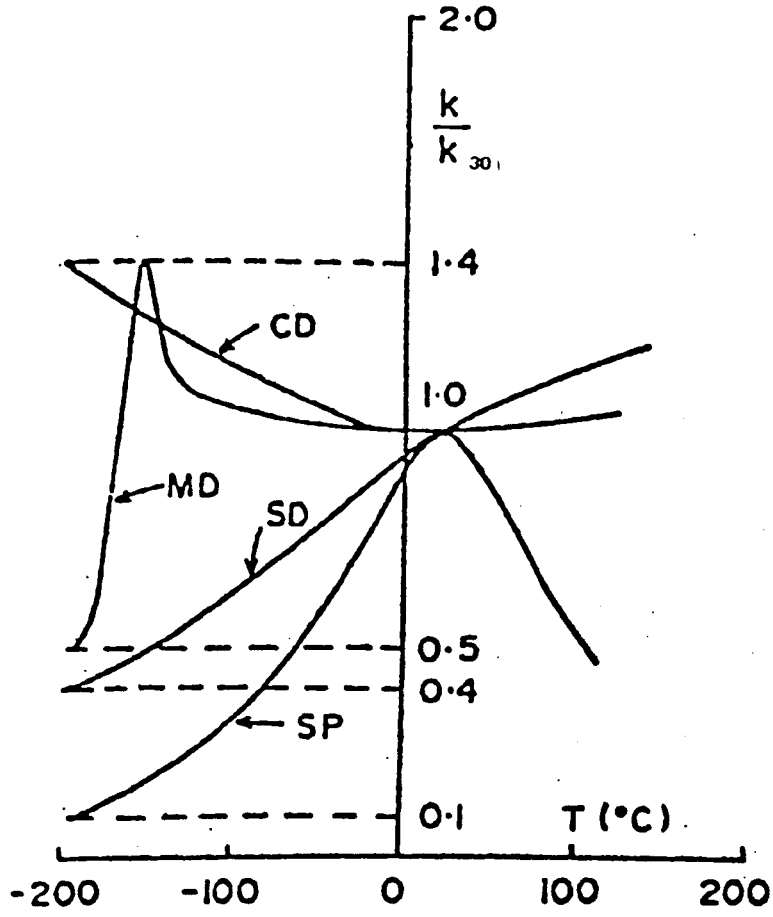

Figure 3.9a : Interpretation of low temperature susceptibility behaviour for pure magnetite (from Radhakrishnamurty et al, 1977)

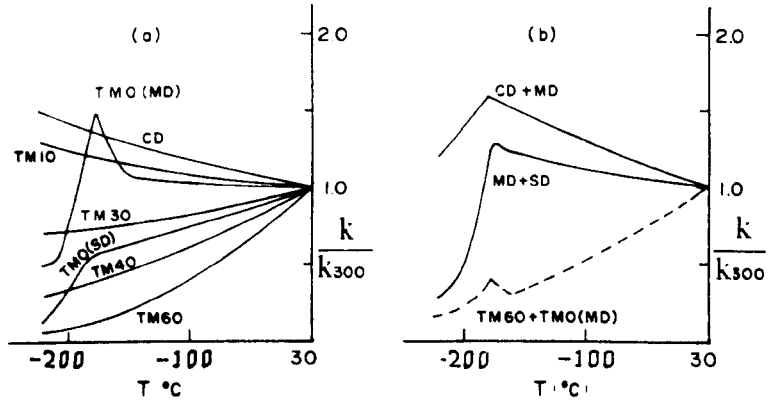

Figure 3.9b : Examples of low temperature susceptibility curves for basalts with mixed domain states (from Radhakrishnamurty, 1990).

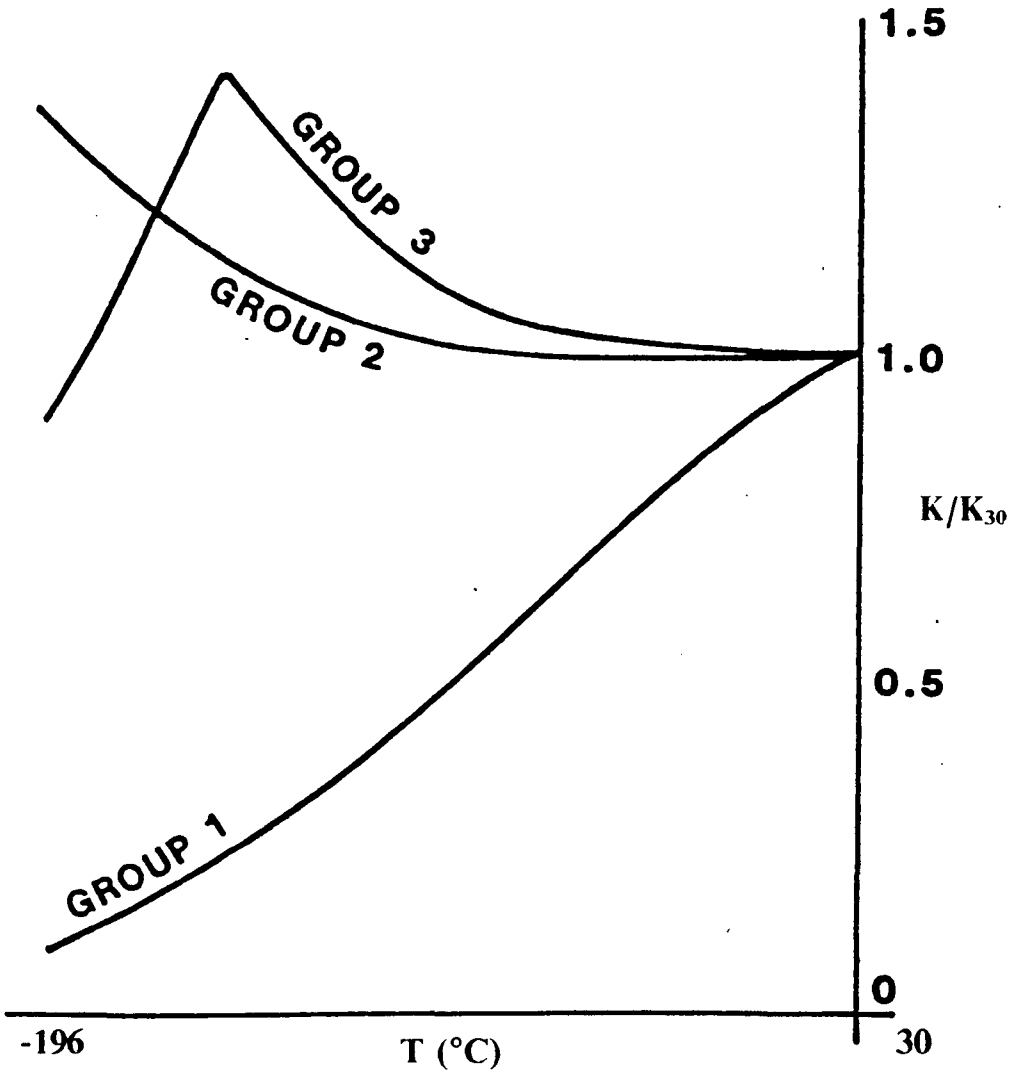

Figure 3.10 : Interpretation of low temperature susceptibility behaviour for titanomagnetites, according to Senanayake and McElhinny (1981).

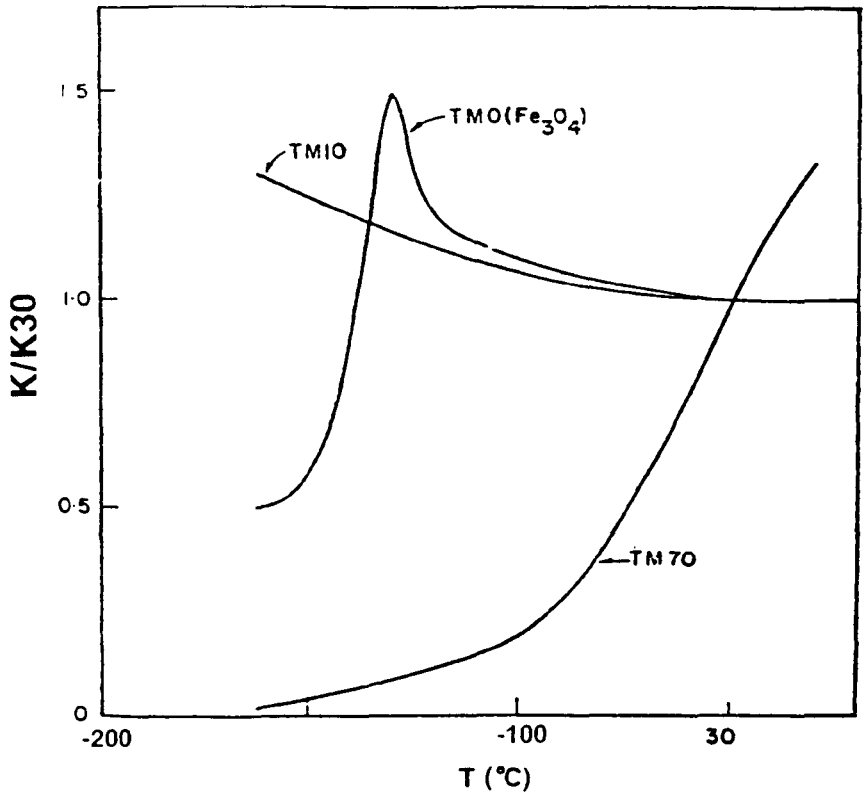

Figure 3.11 : Classification of low temperature susceptibility behaviour for the titanomagnetites TM0, TM10, and TM70 (from Radhakrishnamurty, 1985).

MAGNETIC STATE	RS VALUE
MD	0.50
SD	0.40
SP	0.10
CD	1.40
MD + SD	0.41-0.49
MD + CD	0.59-1.31
MD + SP	0.14-0.46
SD + SP	0.13-0.37
SD + CD	0.50-1.30
SP + CD	0.23-1.27
SP + SD + MD	0.17-0.45
SD + CD + MD	0.51-1.21
SP + SD + CD	0.26-1.17
SP + CD + MD	0.27-1.18

Table 3.7 : RS values ($k_{-1\%}/k_{10}$) for pure and mixed magnetic grain states. SP = superparamagnetic, SD = single domain, MD = multi-domain, CD = cation deficient magnetite grains.

Radhakrishnamurty et al (1977) (Fig. 3.9a) must be questioned; they quote an RS value for SD grains of 0.4. The interpretation of SD behaviour by Senanayake and McElhinny (1981) also contradicts theory. Their Group 2 behaviour, where the RS value averages 1.26, is interpreted as being due to deuterically oxidised samples with crowding of ilmenite lamellae causing the subdivision of titanomagnetite grains into magnetically distinct regions which behave as elongate SD grains. Again, the RS value is too high to be accounted for by the presence of SD grains. However, stress anisotropy may be important for such grains and the decrease in temperature may affect the stress of the grain and hence cause an increase in susceptibility. Consequently, RS values of $\simeq 1.0$ may only be true for discrete SD grains in which shape is the only factor.

The major problem with the classification of Senanayake and McElhinny is that they do not consider mixed magnetic grain sizes, which are frequently observed in basalts (Radhakrishnamurty et al, 1991). The importance of mixed grain sizes in the context of the present study will become clear later in this section.

3.4.3 The uses of low temperature susceptibility

The technique of measuring susceptibility down to liquid nitrogen temperature (-196°C) can provide valuable information on both the composition and domain state (size) of the magnetic minerals present in a sample. There are three important parameters to consider when interpreting Group 3 behaviour:

1. **The RS value** : This is the ratio of susceptibility at liquid nitrogen temperature to that at room temperature K_{-196}/K_{30}).

2. **The PS value** : This is the ratio of susceptibility at the isotropic point (-150°C) of magnetite to that at room temperature (K_{peak}/K_{30}).

3. **The ΔS value** : This is the difference between the PS and RS values, i.e. ΔS = PS-RS.

The values of these parameters indicate the relative amounts of SD and MD material present in a sample and neglect the effect of SP grains which appear to be unimportant in the present study (Section 3.3.3).

KLT results can identify the following mineral phases unambiguously (Radhakrishnamurty et al, 1991):

1. MD grains of magnetite, by the presence of a peak in susceptibility at -150°C.

2. TM60 grains (Radhakrishnamurty, 1990), regardless of the domain state in which they are present. Such grains have an RS value of 0.1.

3.4.4 Results from the Gardar lavas

One sample from each of the eighty-one flows in the Gardar lava succession was used for KLT experiments, the results of which are presented in Tables 3.8-3.9. The group number of Senanayake and McElhinny (1981) is quoted, along with the RS value, the PS value and the ΔS value. Figure 3.12 shows the different types of KLT behaviour witnessed in the Gardar lavas collection. It should be noted here that the classification of Groups 1, 2 and 3 is used only for convenience. The interpretation of behaviour characterised by these groups in the present study is not necessarily equivalent to that proposed by Senanayake and McElhinny (1981).

The samples showing "Group 2" behaviour, in the present study, exhibit type 7 thermomagnetic curves and are thus haematite bearing. Additional rock magnetic experiments, described elsewhere in this chapter, corroborate this conclusion. In this case, the classification of Senanayake and McElhinny (1981) is not relevant since it applies only to titanomagnetites. The magnetic phase responsible for the "Group 2" curves seen in the present study can be explained quite simply. Haematite itself has a very weak susceptibility and, consequently, it is completely overshadowed by the presence of paramagnetic grains within the basaltic samples (silicates etc..), for which the susceptibility should increase down to -196°C by the Curie law (equation 3.4), and give rise to the "group 2" curve.

By far the most frequently occurring type of KLT behaviour in the collection is that which is characterised by a peak in susceptibility at $\simeq$-150°C - namely Group 3 of Senanayake and McElhinny (1981), indicative of samples containing multi-domain grains of magnetite. Careful examination of the Group 3 samples identifies two different curves which show isotropic peaks. These are labelled Group 3a and 3b in Fig. 3.12. The major difference between the two is that for Group 3a the RS value is always less than 0.5 (average = 0.4), whereas for Group 3b samples the RS value is always greater than 0.5 (average = 0.8). Radhakrishnamurty et al (1977) describe the Group 3a behaviour as being indicative of almost pure MD magnetite (Fe_3O_4), with effectively no Ti substitution ($x < 0.15$). Results from other rock magnetic tests, described later in this chapter, corroborate this suggestion. The Group 3b curve, observed by both Senanayake and McElhinny (1981) and the TIFR group, is interpreted by Senanayake and McElhinny to reflect the presence of only MD magnetite. The TIFR group, however, suggest that the higher RS value may be due to contamination of the MD-dominant sample by either

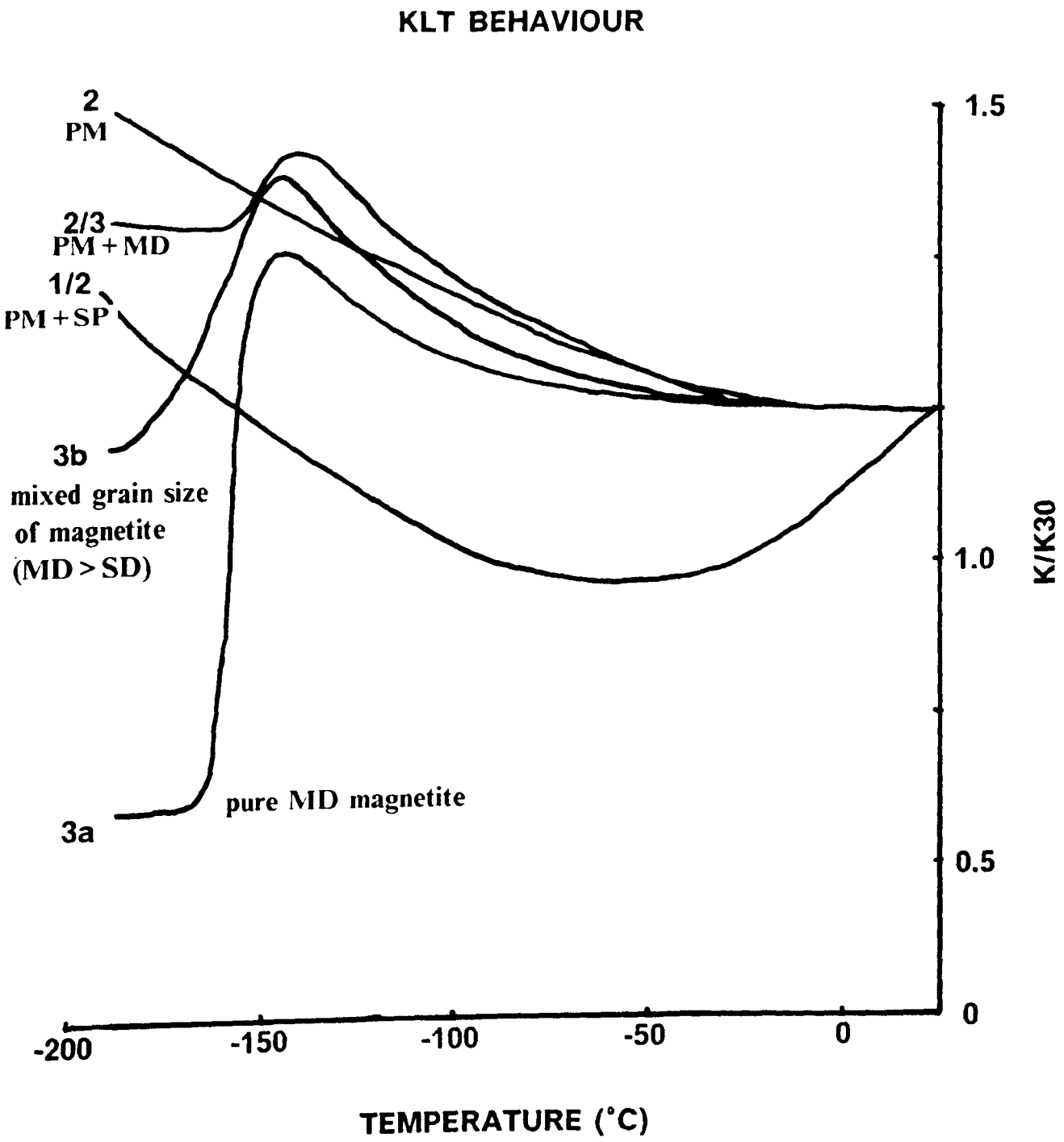

Figure 3.12 : Low temperature susceptibility curves exhibited by the Gardar lavas. SP = superparamagnetic, SD = single domain, MD = multi-domain, PM = paramagnetic (see text for explanation of behaviour).

FLOW	Grp	KLT RS	HYSTERESIS Peak	ΔS	Ms	Mrs/Ms	Hc	X_{MD}	AFD Curve	MDF (mT)
					$\times 10^3 Am^2kg^{-1}$		A/m			
L1	3b	0.62	1.37	0.75	2.9	0.28	24.3	45.8	H	11
L2	3b	0.66	1.34	0.68	0.7	0.18	12.9	66.7	S	9
L3	3b	0.76	1.15	0.39	1.1	0.17	11.7	68.7	H	11
L4	3a	0.46	1.37	0.91	4.0	0.19	8.3	64.6	S	7
L5	3b	0.56	1.37	0.81	2.1	0.16	11.3	70.8	H	22
L6	3b	0.89	1.51	0.62	3.6	0.21	11.9	60.4	H	11
L7	3b	0.85	1.43	0.58	1.0	0.12	7.8	79.2	S	5
L8	3b	0.75	1.33	0.58	0.9	0.29	11.4	43.7	H	12
L9	3b	0.82	1.52	0.70	1.2	0.17	12.9	68.7	H	34
L10	3a	0.53	1.24	0.71	1.5	0.16	10.7	70.8	H	15
L11	3b	0.93	1.46	0.53	0.6	0.20	15.8	62.5	H	17
L12	3b	0.88	1.51	0.63	1.1	0.14	10.2	75.0	H	14
L13	3a	0.42	1.20	0.78	2.6	0.31	34.6	39.6	S	9
L14	3a	0.56	1.35	0.79	1.8	0.10	7.8	83.3	H	15
L15	3b	0.87	1.48	0.61	0.6	0.22	16.6	58.3	H	19
L16	3b	1.00	1.63	0.63	0.8	0.22	11.9	58.3	H	17
L17	3b	0.57	1.32	0.75	1.0	0.09	4.7	85.4	S	7
L18	3b	0.68	1.14	0.46	0.4	0.21	18.7	60.4	H	36
L19	3a	0.45	1.39	0.94	2.1	0.10	6.7	83.3	H	11
L20	3b	0.61	1.16	0.55	0.4	0.14	15.9	75.0	H	18
L21	3b	0.80	1.68	0.88	0.9	0.08	5.1	87.5	S	7
L22	3b	0.75	1.52	0.77	1.2	0.18	13.1	66.7	S	7
L23	3b	0.81	1.33	0.52	3.7	0.22	18.4	58.3	H	30
M1	3a	0.62	1.40	0.78	1.0	0.09	7.8	85.4	S	6
M2	2/3	1.07	1.24	0.17	-	-	-	-	H +	-
M3	1	0.63	-		-	-	-	-	H +	-
M4	2	1.49	-		-	-	-	-	H +	-
M5	1/2	2.32	-		-	-	-	-	H +	-
M6	1/2	1.91	-		-	-	-	-	H +	-
M7	2	1.35	-		-	-	-	-	H +	-
M8	2	1.83	-		-	-	-	-	H +	-
M9	2/1	2.00	-		-	-	-	-	H +	-
M10	3a	0.47	1.32	0.85	4.4	0.08	6.1	87.5	S	7
M11	3b	0.60	1.35	0.75	3.3	0.26	22.2	50.0	H	11
M12	3a	0.55	1.36	0.81	1.3	0.13	8.9	77.1	S	9
M13	2/3	1.51	1.50	-	-	-	-	-	SH +	-
M14	2	1.84	-	-	-	-	-	-	H	10
M15	2/3	1.29	1.31	0.02	-	-	-	-	SH +	-
M16	3a	0.50	1.31	0.81	-	-	-	-	S	7
M17	2/3	0.81	1.01	0.20	-	-	-		H	16
M18	2	1.68	-	-	-	-	-		H +	-

Table 3.8 : Results of non-thermal rock magnetic tests for the Lower and Middle Lava Formations. KLT = Low temperature susceptibility, RS = k_{-196}/k_{30}; Peak = k_{peak}/k_{30}; ΔS = Peak-RS; Ms = saturation magnetisation; Mrs = saturation remanence; Hc = coercivity X_{MD} = percentage of multi-domain material in a mixed grain size of pure magnetite; MDF = median destructive field.

FLOW	Grp	KLT RS	HYSTERESIS Peak	ΔS	Ms $\times 10^3 Am^2kg^{-1}$	Mrs/Ms	Hc A/m	X_{MD}	AFD Curve	MDF (mT)
U40	3a	0.38	1.30	0.92	2.6	0.08	5.3	87.5	S	8
U39	3a	0.40	1.22	0.82	2.3	0.07	4.7	89.6	S	6
U38	2	1.48	-	-	-	-	-	-	-	-
U37	2/3	1.01	1.26	0.25	-	-	-	-	-	-
U36	2	1.57	-	-	-	-	-	-	H+	-
U35	3a	0.47	1.21	0.74	-	-	-	-	H+	-
U34	3b	0.82	1.16	0.34	-	-	-	-	-	-
U33	3a	0.50	1.28	0.78	4.3	0.33	24.0	35.4	H+	-
U32	3b	0.75	1.29	0.54					SH	+109
U31	3b	0.72	1.31	0.59					S	9
U30	3b	0.66	1.05	0.39	-	-	-	-	H+	-
U29	3b	0.76	1.20	0.44	-	-	-	-	-	-
U28	3a	0.39	1.22	0.83	3.0	0.15	10.2	72.9	H	12
U27	2/3	1.46	1.53	0.07	-	-	-	-	SH	2
U26	3b	0.55	1.03	0.48					-	-
U25	2	1.42	-	-	-	-	-	-	-	-
U24	3a	0.35	1.17	0.82	2.3	0.15	9.4	72.9	H+	-
U23	2	1.62	-	-	-	-	-	-	SH	+165
U22	3a	0.42	1.25	0.83	3.9	0.09	5.8	85.4	S	3
U21	3a	0.43	1.25	0.82	1.3	0.07	4.9	89.6	S	5
U20	3b	0.59	1.17	0.58	-	-	-	-	H	17
U19	2	1.87	-	-	-	-	-	-	H+	-
U18	2	1.23	-	-	-	-	-	-	H+	-
U17	2	1.46	-	-	-	-	-	-	-	-
U16	3a	0.45	1.10	0.65	2.5	0.07	4.4	89.6	H+	-
U15	3a	0.38	1.15	0.77	1.2	0.14	12.7	75.0	S	7
U14	3a	0.48	1.37	0.89	2.2	0.26	19.8	50.0	H+	-
U13	2	1.32	-	-	-	-	-	-	H+	-
U12	2	1.41	-	-	-	-	-	-	H+	-
U11	2/1	1.22	-	-	-	-	-	-	H+	-
U10	2	1.15	-	-	-	-	-	-	H+	110
U9	1/3	0.73	0.92	0.19	-	-	-	-	-	-
U8	3b	0.76	1.37	0.61	-	-	-	-	S	11
U7	2	1.84	-	-	-	-	-	-	H	12
U6	2	1.83	-	-	-	-	-	-	H+	109
U5	2	1.87	-	-	-	-	-	-	H+	92
U4	3a	0.40	1.34	0.94	9.1	0.09	5.7	85.4	S	7
U3	3b	0.99	1.23	0.24	0.7	0.17	11.1	68.7	-	-
U2	3a	0.40	1.26	0.86	5.2	0.15	11.3	72.9	H	13
U1	3a	0.40	1.38	0.98	7.4	0.09	5.0	85.4	S	8

Table 3.9 : Results of non-thermal rock magnetic tests for the Upper Lava Formation (See legend to Table 3.8 for explanation of symbols).

SD or CD grains (or a combination of both) as a mixed grain size of magnetite (Radhakrishnamurty et al, 1977; Radhakrishnamurty, 1990). Senanayake and McElhinny (1981) do not consider the presence of mixed grain sizes which are undoubtedly present in basalts. Since the susceptibility of pure SD grains should not vary much with temperature, the presence of SD grains in an MD dominant sample may have the effect of raising the RS value closer to 1. Pure MD grains have an RS value of $\simeq$0.5 (Radhakrishnamurty et al, 1977). Thus, the Group 3b curve is interpreted as being the signature of a mixed grain size of magnetite where MD dominates, probably over SD. The larger the SD fraction, the larger the RS value. In such situations, the isotropic peak may also be suppressed, resulting in a lower PS value. It is proposed that the difference, ΔS, between the PS and RS values is a semi-quantitative method of assessing the relative proportions of MD and SD material present in a mixed grain size of magnetite. Larger values of ΔS correspond to the presence of only small amounts of SD material, whereas smaller values of Δ S reflect the presence of more SD material. For Δ S$\simeq$0.9, the sample will have effectively only MD grains and for ΔS$\simeq$0, only SD grains will be present.

Both composite KLT curves in Fig. 3.12 - namely the Hybrid 1/2 and Hybrid 2/3 - show a weak initial susceptibility, suggesting that haematite is the dominant mineral in both cases. The Hybrid 1/2 curve shows an initial decrease in K on cooling from room temperature, followed by an increase so that the RS value is >1, resulting in a saucer-shaped curve. It has already been established (Section 3.4.3) that the susceptibility of SP grains decreases down to $\simeq$-150°C and that the susceptibility of PM grains increases with decreasing temperature. Thus, the shape of the Hybrid 1/2 curve may be explained by the contribution to susceptibility of a combination of

paramagnetic and superparamagnetic grains. Sherwood (1990) has found that saucer-shaped KLT curves are exhibited by samples with large amounts of ilmenite, which behaves paramagnetically.

The Hybrid 2/3 curve shows an increase in susceptibility down to -196°C but also has a peak in susceptibility at -150°C, corresponding to the isotropic point of magnetite and confirming the presence of some MD grains of magnetite. Since all other rock magnetic evidence points to haematite as the magnetic mineral, with no evidence of magnetite (Tables 3.2 and 3.8), the Hybrid 2/3 curve can be explained by the contribution to susceptibility of a combination of paramagnetic grains and MD magnetite. The latter apparently contribute to the susceptibility but not to the remanence (Chapter 4).

The results from each of the three lava formations within the Eriksfjord Group will now be considered separately.

3.4.4.1 The Lower (Mussartût) Lava Formation

In contrast to the other two lava formations, only Group 3 KLT behaviour is seen. Samples from five flows have Group 3a curves and samples from the remaining eighteen flows exhibit Group 3b curves, suggesting the presence of a significant amount of SD material in a mixed grain size of magnetite. The results are summarised in Table 3.8.

For Group 3a samples, the average RS value is 0.48 and for Group 3b samples, it is 0.77. These values are close to the corresponding values of Radhakrishnamurty et al (1977). Figure 3.13 shows histograms of the RS and PS values for the Group 3a and 3b samples from both the Lower and

Upper formations. From these data, it is clear that a difference exists in the Group 3 behaviour witnessed in the two formations. The Group 3b samples of the Lower Lavas have a higher mean RS value than those from the Upper Lavas. Conversely, the mean RS value for the Group 3a samples from the Lower Lavas is higher than that of the upper lavas. These observations show that true MD magnetite behaviour (Group 3a with $RS \leq 0.5$) is more apparent in the Upper Lavas than the Lower Lavas. Also, the SD fractions in a mixed grain size (Group 3b with $0.5 < RS < 1.0$) seen in the Lower Lavas are larger than for the Upper Lavas. For Group 3a samples, the mean PS values are 1.25 and 1.31 for samples in the Upper Lavas and the Lower Lavas respectively. For Group 3b samples, the mean PS values are 1.2 and 1.4 for the Upper and Lower lavas respectively. These values are close to the values of 1.3 and 1.24 quoted by Radhakrishnamurty (1990) and Senanayake and McElhinny (1981) respectively for all Group 3 samples.

Δ S results for the Gardar lavas are presented in Tables 3.8-3.9 for all Group 3 KLT samples and have considerable importance when choosing samples for use in palaeointensity experiments (Chapter 7).

3.4.4.2 The Middle (Ulukasik) Lava Formation

A variety of KLT behaviour was witnessed in the samples from this formation. Five flows exhibit Group 3 behaviour, indicating the presence of MD magnetite, four of which have Group 3a curves, the other has a Group 3b curve, suggesting that SD material is not so abundant as in the lower formation. Five flows show Group 2 characteristics, interpreted in this study as due to the presence of paramagnetic grains. Both of the hybrid curves described earlier in this section are evident, with three flows having hybrid 1/2 curves showing a combination of paramagnetic (possibly ilmenite) and a

(a)

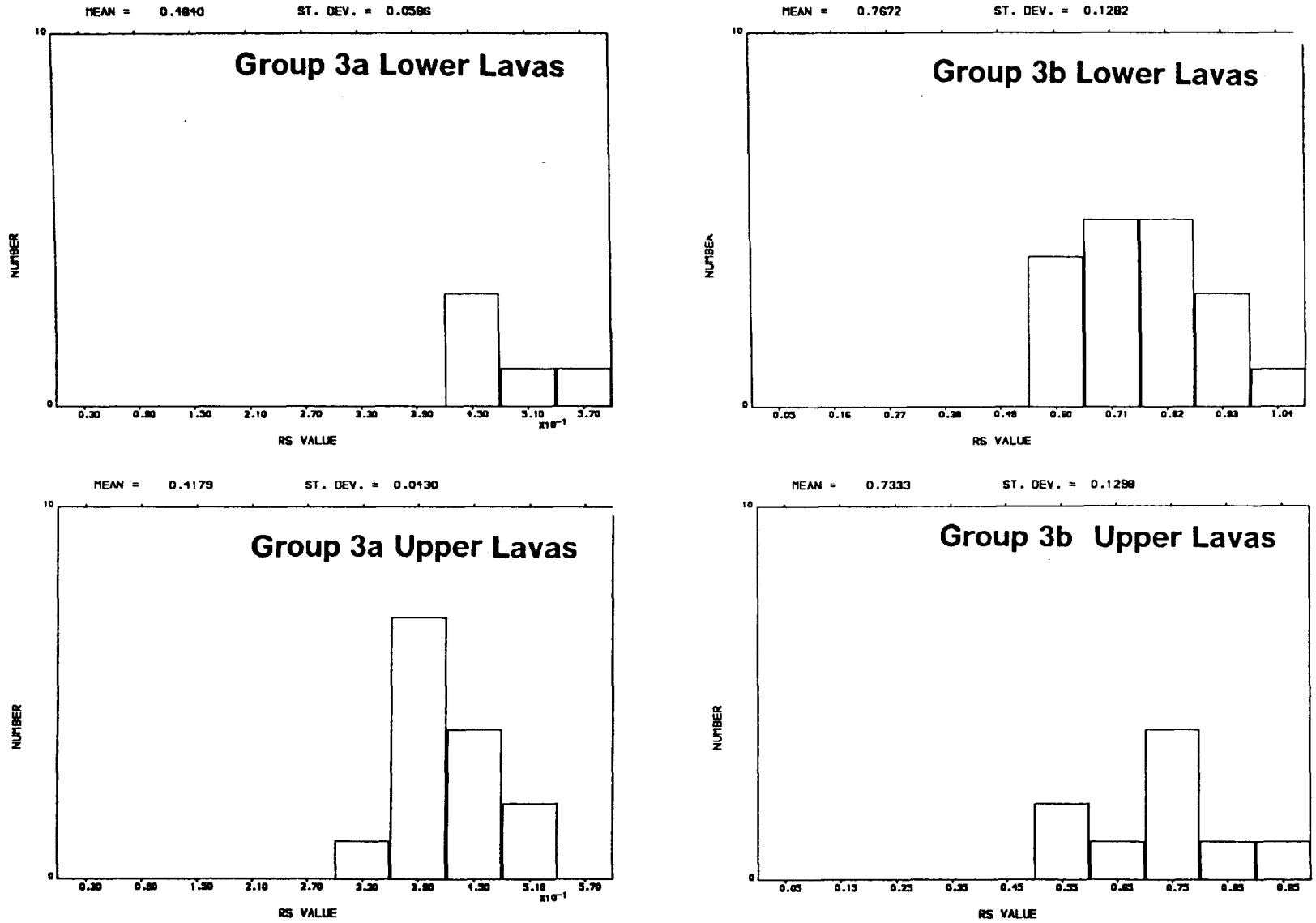

Figure 3.13 : Histograms indicating the values of the low temperature susceptibility parameters (a) RS and (b) PS for Group 3 samples from the Lower and Upper Lava Formations.

(b)

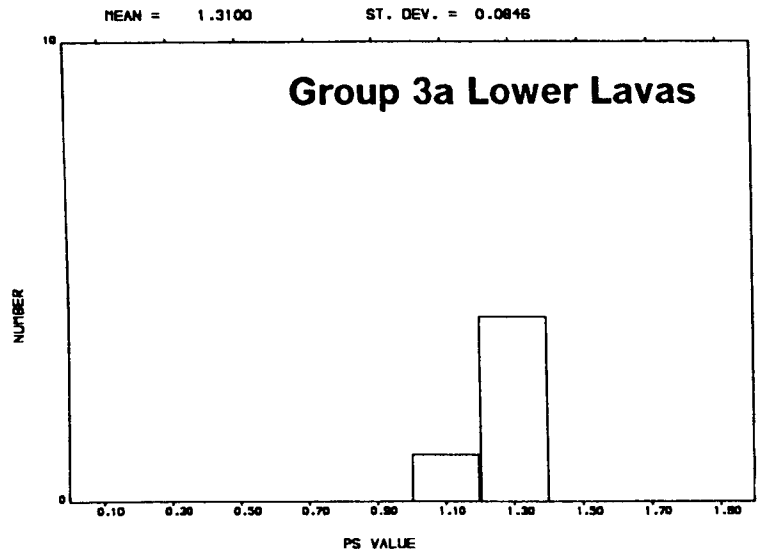
MEAN = 1.3100
ST. DEV. = 0.0846
Group 3a Lower Lavas
NUMBER
PS VALUE

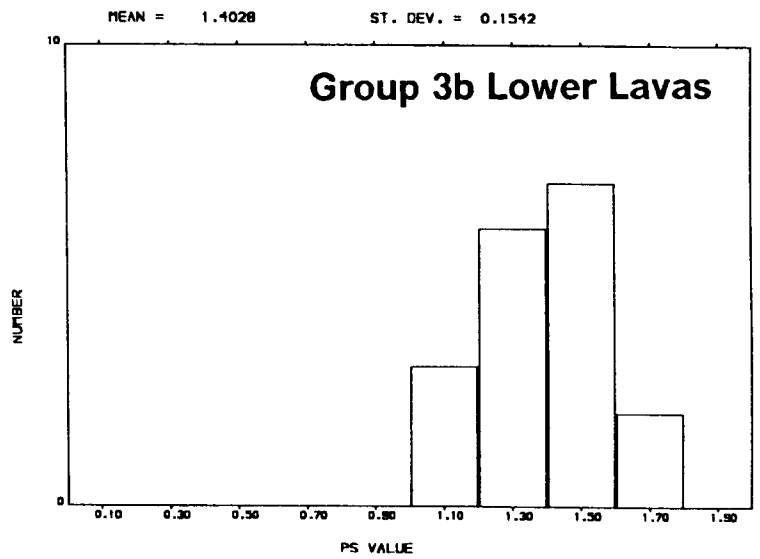
MEAN = 1.4028
ST. DEV. = 0.1542
Group 3b Lower Lavas
NUMBER
PS VALUE

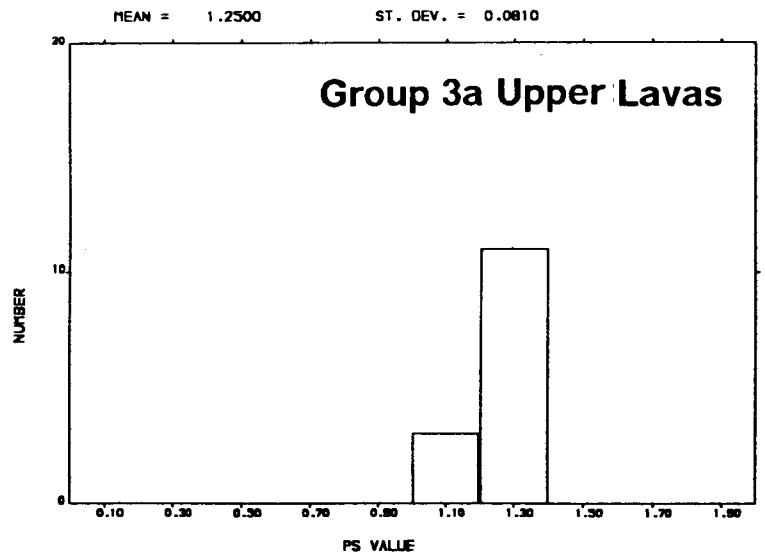
MEAN = 1.2500
ST. DEV. = 0.0810
Group 3a Upper Lavas
NUMBER
PS VALUE

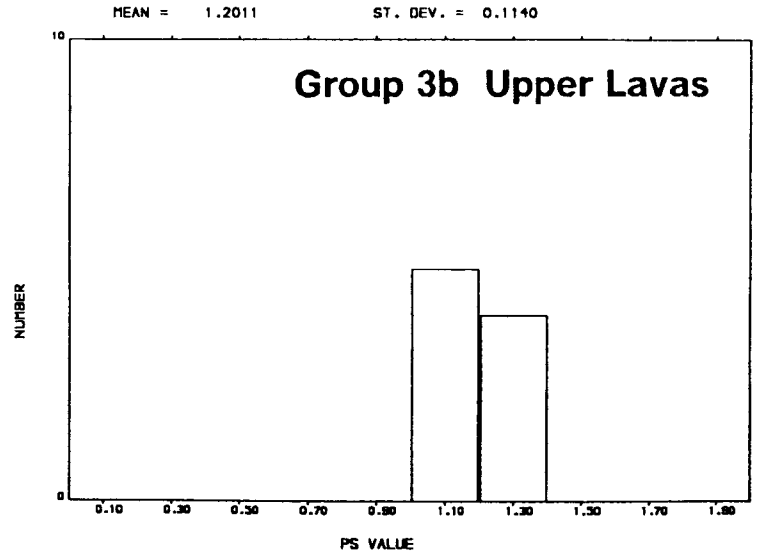
MEAN = 1.2011
ST. DEV. = 0.1140
Group 3b Upper Lavas
NUMBER
PS VALUE

small amount of SP grains; four samples have hybrid 2/3 curves, indicating the presence of a small amount of MD magnetite in addition to paramagnetic grains.

3.4.4.3 The Upper (Ilímaussaq) Lava Formation

Eighty measurements were completed on the forty flows from this formation. Table 3.9 summarises the results and Fig. 3.14c shows the distribution of behaviour seen. All types of behaviour shown in Fig. 3.12 are witnessed in the upper lava formation. Groups 2 and 3 behaviour are dominant, with fifteen flows exhibiting Group 3a behaviour, eight showing Group 3b curves and thirteen showing Group 2 characteristics. These results suggest that MD grains dominate in the mixed grain size for magnetite-bearing flows and that haematite (weak susceptibility-Group 2) is an important remanence carrier in this group. The remaining 4 flows possess exhibiting showing either one of the hybrid curves.

3.4.4.4 The effect of heating on KLT behaviour

Senanayake and McElhinny (1982) performed KLT measurements on samples from each of their three KLT groups before and after heating the samples to 615°C. Figure 3.15 illustrates their results. For Group 1 samples (RU33, NF80 and RU107) the RS value rose considerably after heating and the curve shapes also changed, with RU33 and RU107 developing some Group 2 characteristics. The Group 2 sample (AV175) and the Group 3 sample (RU89), however, show very little change in RS value or curve shape after heating. Consequently, Senanayake and McElhinny concluded that Group 2, and possibly Group 3, samples may prove satisfactory for use in palaeointensity experiments since their KLT characteristics do not alter on

heating. The Group 3 sample used in the study is, in fact, a Hybrid 2/3 specimen. Considering that this is the only sample in that study with a Verwey transition, their conclusion that Group 3 samples may prove satisfactory for palaeointensity studies must be questioned. It was therefore decided to perform the test on some true Group 3 samples from the Gardar collection.

KLT experiments were performed on nine samples (four with Group 3a curves, 4 with Group 3b curves and one which is on the borderline between the two groups) at room temperature, and after heating each sample to 150°C, 300°, 450°C and 700°C. The results are listed in Table 3.10 and examples are illustrated in Figure 3.16. Generally, no dramatic changes in KLT behaviour were observed and all samples retained their overall Group 3 characteristics throughout the experiment. However, it was noticeable that eight samples showed an increase in the RS value at 300°C but this increase did not intensify at higher temperatures. The PS values showed only a small corresponding decrease, with the result that ΔS decreased. These observations suggest that there was some reordering of grain sizes at 300° C with more SD material apparently being created at this temperature. At 700°C, most samples show changes in susceptibility and some develop curves which are a combination of Groups 2 and 3 of Senanayake and McElhinny (1981) (Fig. 3.16b). The susceptibility changes also appear to be more pronounced in Group 3b curves, which is also witnessed from high temperature susceptibility results (Section 3.5). The results of this experiment suggest that, although changes do occur at 300°C, Group 3 samples show no drastic changes in KLT behaviour below their Curie temperatures. This confirms the findings of the study by Senanayake and McElhinny (1982).

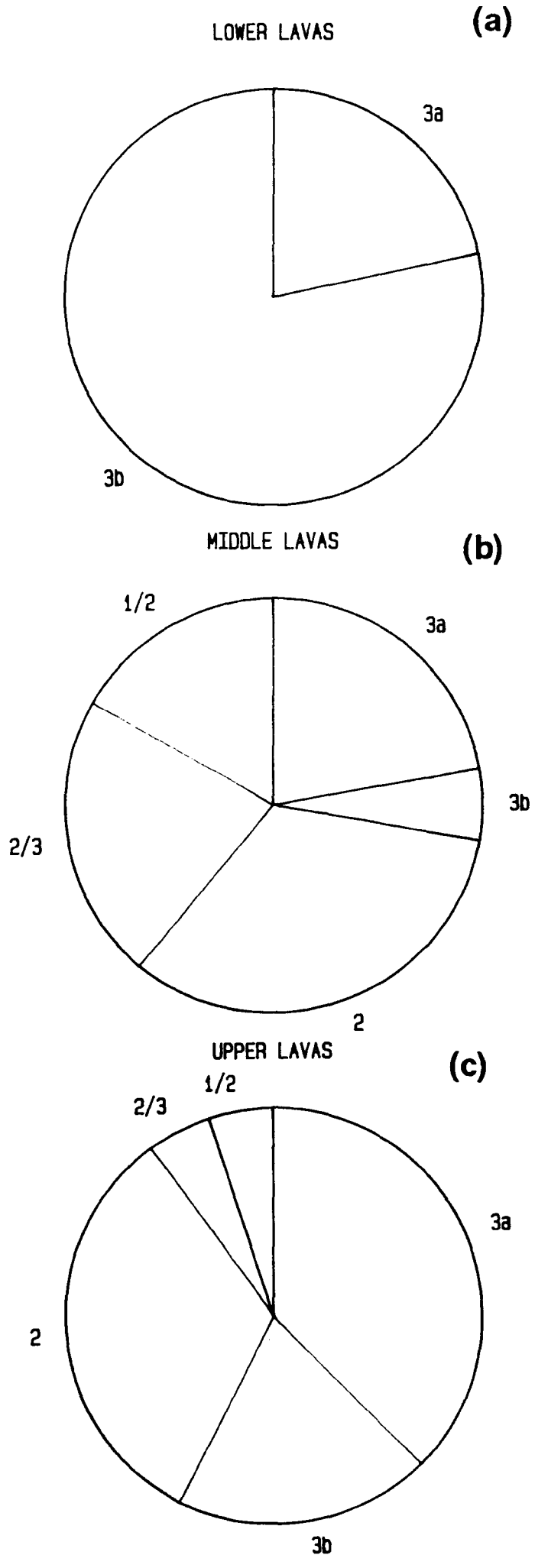

Figure 3.14 : Pie charts showing the distribution of low temperature susceptibility curves for (a) The Lower Lava Formation (b) The Middle Lava Formation (c) The Upper Lava Formation.

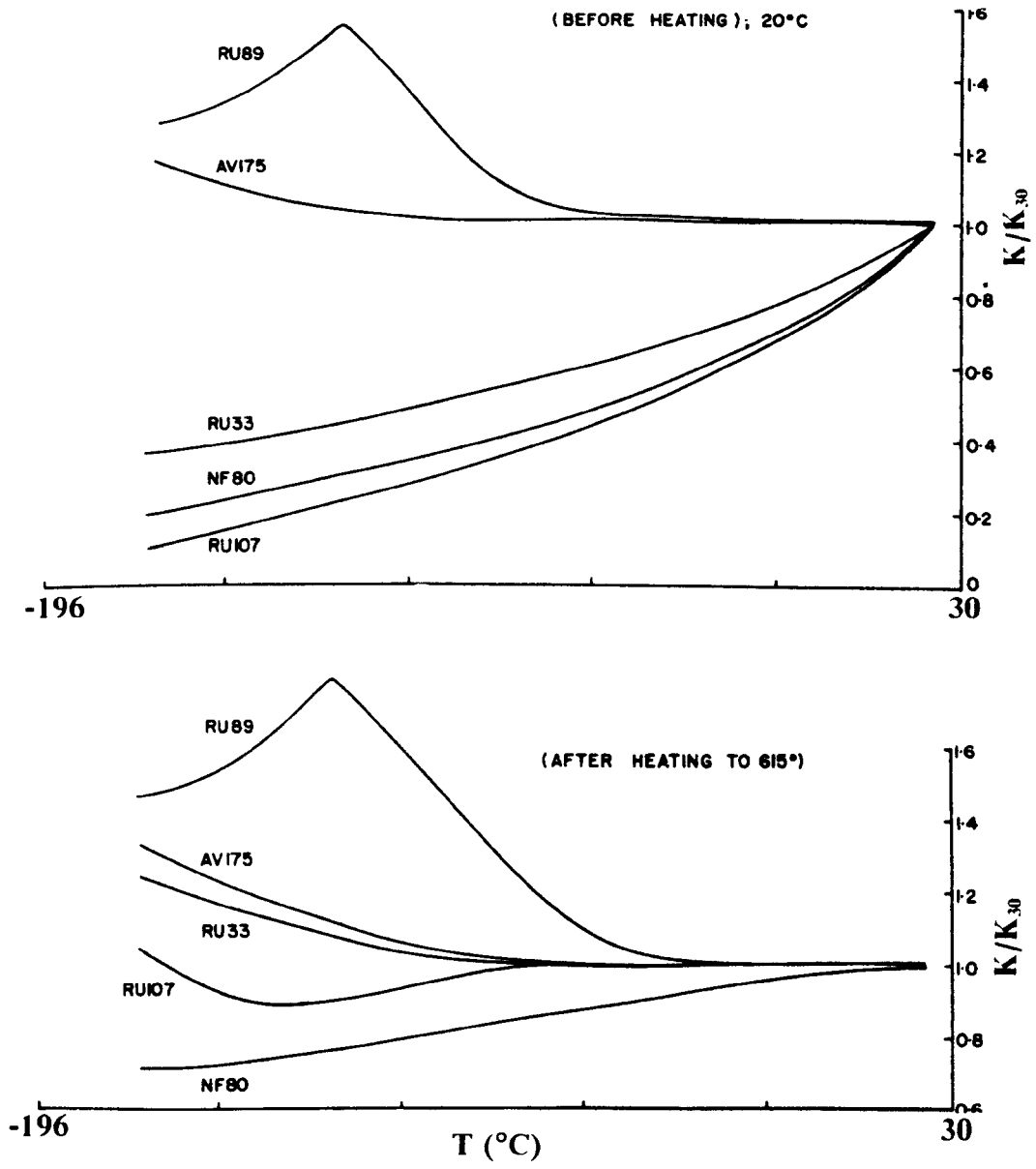

Figure 3.15 : Results from a study into the effect of heating on the low temperature susceptibility behaviour of basalts (from Senanayake and McElhinny, 1982).

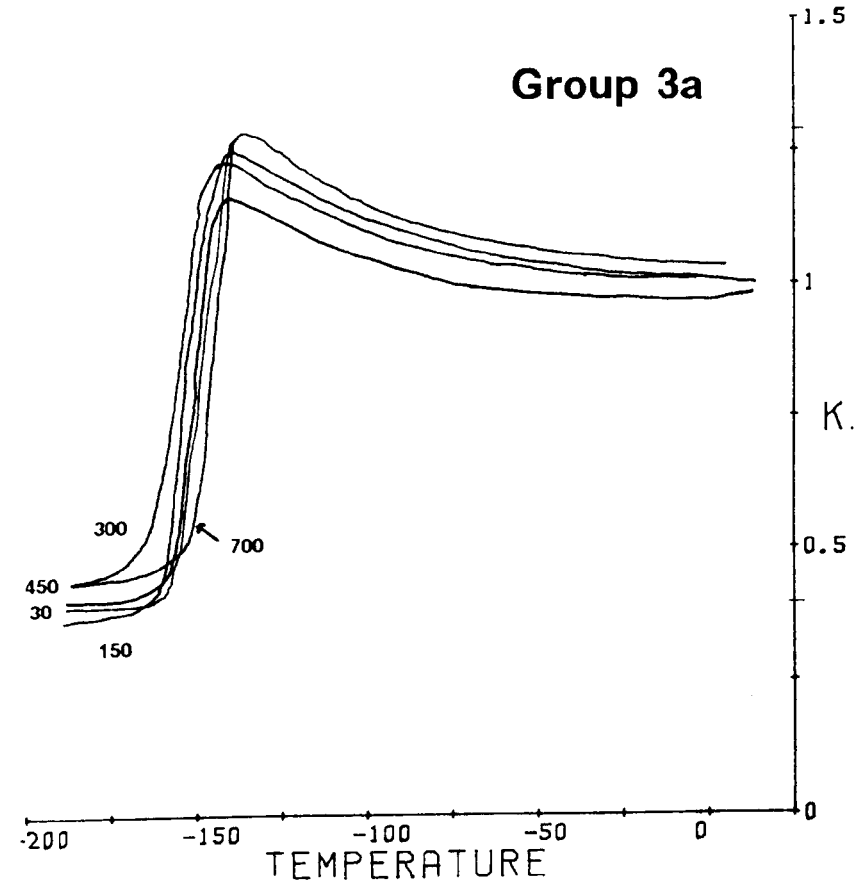

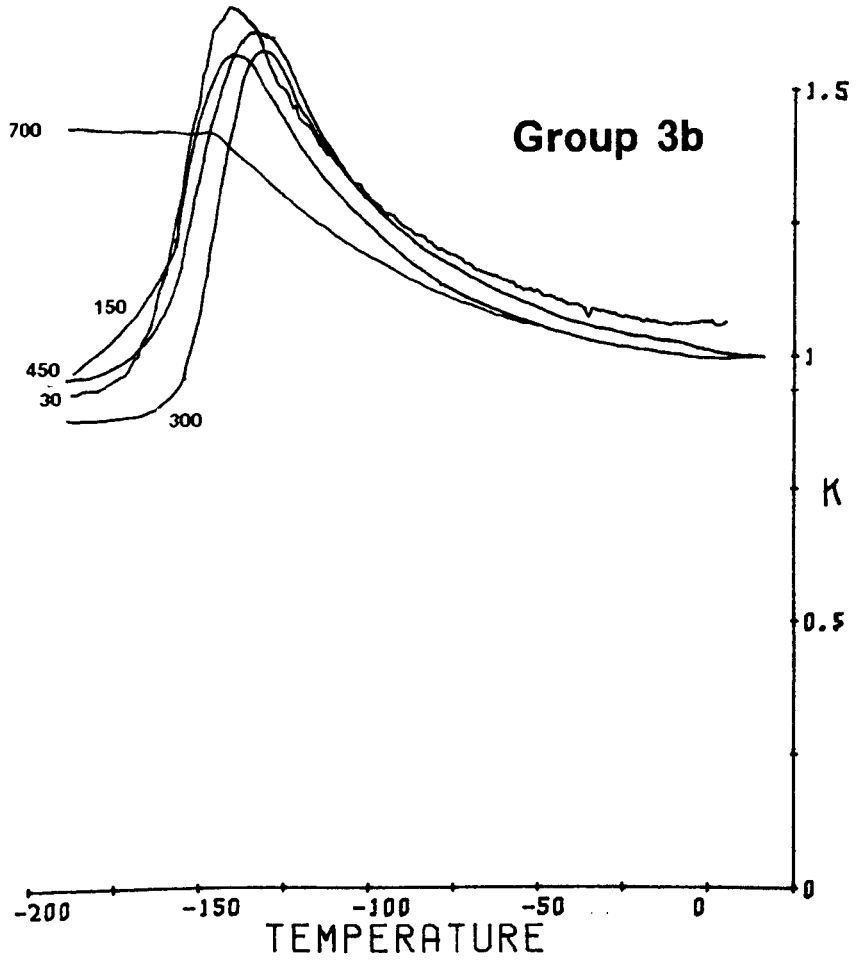

Figure 3.16 : Results from a study into the effect of heating on the low temperature susceptibility behaviour of Group 3 samples.

SAMPLE	KLT GROUP	TEMPERATURE (°C)	RS	PS	ΔS
L5-03	3b(a)	30	0.51	1.31	0.80
		150	0.52	1.29	0.77
		300	0.52	1.31	0.79
		450	0.53	1.31	0.78
		700	0.73	1.32	0.59
L8-03	3b	30	0.69	1.22	0.53
		150	0.73	1.23	0.50
		300	0.91	1.34	0.43
		450	0.72	1.31	0.59
		700	0.93	1.14	0.31
L10-03	3b	30	0.63	1.41	0.78
		150	0.57	1.26	0.69
		300	0.75	1.29	0.54
		450	0.62	1.35	0.73
		700	0.78	1.27	0.49
L13-06	3a	30	0.45	1.12	0.67
		150	0.48	1.13	0.65
		300	0.80	0.98	0.18
		450	0.66	1.19	0.53
		700	0.80	1.37	0.57
L16-04	3b	30	0.94	1.66	0.72
		150	0.94	1.58	0.64
		300	0.89	1.58	0.69
		450	0.96	1.59	0.63
		700	1.43	1.41	-0.02
L20-07	3b	30	0.59	1.40	0.81
		150	0.55	1.35	0.80
		300	0.61	1.33	0.72
		450	0.65	1.38	0.73
		700	0.86	1.45	0.59
U2-06	3a	30	0.38	1.30	0.92
		150	0.38	1.29	0.91
		300	0.44	1.28	0.84
		450	0.42	1.20	0.78
		700	0.44	1.19	0.77
U4-06	3a	30	0.40	1.29	0.89
		150	0.37	1.25	0.88
		300	0.43	1.23	0.80
		450	0.38	1.17	0.79
		700	0.40	1.15	0.75
U40-01	3a	30	0.40	1.29	0.89
		150	0.37	1.25	0.88
		300	0.43	1.23	0.80
		450	0.38	1.17	0.79
		700	0.40	1.15	0.75

Table 3.10 : Results of the study on the temperature dependence of KLT characteristics for some Group 3 samples.

3.4.5 Summary of KLT results

The results of the low temperature susceptibility studies indicate that the dominant magnetic mineral state present in the flows of the Gardar lava succession is MD magnetite, confirmed by the presence of a peak in susceptibility at the isotropic point of magnetite ($\simeq$-150°C). Two different MD magnetite curves were observed, having RS values of $\leq$0.5 and $>$0.5-1.0 respectively. The former, particularly abundant in the upper lava formation, characterises nearly pure MD magnetite with very little SD contamination. The latter, most abundant in the lower lava formation, is indicative of a mixed magnetic grain size with MD and SD magnetite present in varying proportions within a single magnetic phase. The relative amounts of MD and SD material can be estimated, in a semi-quantitative manner, by the parameter ΔS which is defined as the difference in the PS and RS values. For large ΔS, the SD fraction is small and for small ΔS the SD fraction is larger.

The low temperature susceptibility technique has been employed here to indicate magnetic composition and grain size. The technique is also useful, when considered in conjunction with the other non-thermal RM techniques, for identifying suitable samples for palaeointensity work. It is stressed, however, that KLT data alone has limited use in this respect. This is discussed in detail in Chapter 7.

3.5 HIGH TEMPERATURE SUSCEPTIBILITY (KHT)

3.5.1 Introduction

Although the method of measuring susceptibility down to -196°C has received a great deal of attention over the last few years, the extension of the susceptibility curve to temperatures in excess of the Curie point of samples has received limited coverage by comparison. However, the susceptibility behaviour of magnetic materials at high temperatures is an established subject. Hopkinson (1889) first observed the "ideal" K(T) curve for iron which was subsequently assumed to be shown by all magnetic substances. This behaviour, shown in Fig. 3.17a, indicates a steady increase in K which reaches a peak (where $K \simeq 1.8K_{RT}$), just before the Curie point. This is known as a Hopkinson peak. After this peak, the susceptibility rapidly falls to zero at the Curie temperature of the material. This classical Hopkinson curve is reversible on cooling back to room temperature.

This section describes the application of the high temperature susceptibility technique, the second so-called thermal rock magnetic method, to whole rock basalt samples. The various interpretation models are discussed and the results from the Gardar lavas analysed.

3.5.2 Theory and interpretation

Radhakrishnamurty and Likhite (1970) performed a study of the Hopkinson effect in basalts. They considered that the many curious magnetic properties of basalts, such as origin of TRM (Dickson et al, 1966), variation in Koenigsberger ratio value (Stacey, 1967) and susceptibility (Radhakrishnamurty et al, 1970) were the result of the grain size distribution

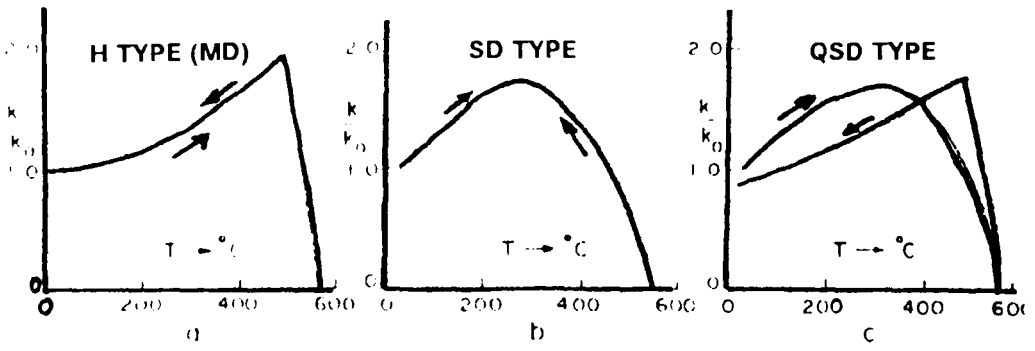

Figure 3.17 : Classification of high temperature susceptibility behaviour for basalts (from Radhakrishnamurty and Likhite, 1970).

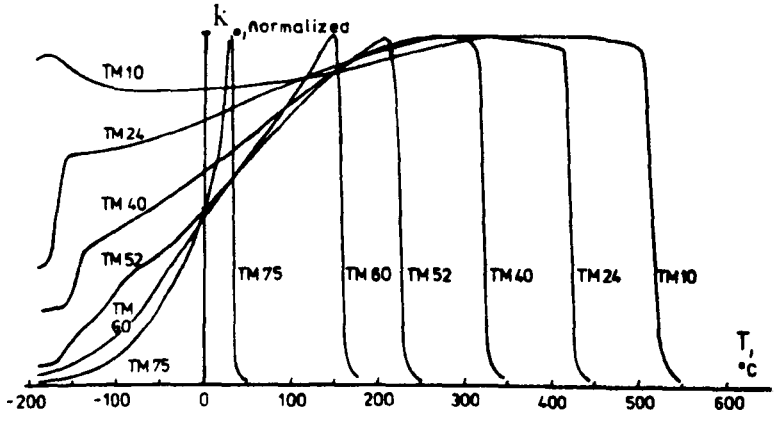

Figure 3.18 : High temperature susceptibility behaviour for titanomagnetites with varying Ti substitution (from Appel and Soffel, 1985).

of the magnetic minerals present in a rock. Thus, they performed experiments on whole rock basalt samples, since results from magnetic separates may not give all the finer details shown by whole rock samples, eg. for separates, the relative configuration of grains would be lost, along with some very fine grains. Their studies show that basalt samples can show KHT behaviour which is either purely one of three types, or a combination of them. The three "pure" states are:

1. **H Type** (Fig. 3.17a) : This behaviour reflects that observed for iron by Hopkinson (1889). Since most magnetic materials contain grains sufficiently large to be considered as MD, this curve is regarded as characteristic of the behaviour shown by MD grains. Thus, for a purely MD sample, a Hopkinson peak should be observed immediately below the Curie temperature.

2. **SD Type** (Fig. 3.17b) : For a sample containing purely SD grains which are too large to be superparamagnetic at room temperature, a maximum susceptibility will be seen at the higher temperatures at which the grains become SP. The result is that the Hopkinson peak will be much broader than the one observed for MD grains.

3. **QSD Type** (Fig.3.17c) : SD behaviour is very sensitive to the size, shape and internal strains in a grain and to the material itself. Consequently, on heating, irreversible changes may occur due to these factors and the character of the sample changes. After heating to a temperature above the Curie point, a sample showing an SD type heating curve can conceivably show an H type (MD) curve on the cooling cycle. This reflects the irreversible changes resulting from the redistribution of

magnetic grain sizes on heating. Such curves are referred to as quasi single-domain (QSD) types.

Dunlop (1974) reported KHT results for both magnetic separates and rocks. He discussed the factors which control the characteristics of the Hopkinson peak in magnetic samples. The magnitude (height) of the peak, K_p, which determines the enhancement of susceptibility with temperature, is controlled by both the coercivity of remanence, H_{cr} (see Section 3.6.2), at room temperature and the minimum blocking temperature, $(T_b)_{min}$, of a sample. The larger these values are, the larger is the enhancement factor in susceptibility and consequently, the height of the Hopkinson peak increases. The width of the Hopkinson peak, which controls the temperature range over which susceptibility is enhanced, is entirely controlled by the width of the blocking temperature spectrum of the sample. For large MD grains, the T_b spectrum is narrow just below the Curie point and susceptibility does not increase below $(T_b)_{min}$. Thus, a narrow and rather low Hopkinson peak is anticipated for large MD grains. Smaller MD grains may show a greater enhancement in susceptibility resulting from a higher, but still narrow, Hopkinson peak.

Single domain grains have a broader range of blocking temperatures and hence a broader Hopkinson peak. Dunlop (1974) notes that, in instances where SD grains are needle-like (0.2-0.3μm long), the T_b spectrum resembles that of MD grains and a narrow Hopkinson peak with a lower enhancement factor is observed. The net result is that SD grains, in special cases, can also show the H type curve of Radhakrishnamurty and Likhite (1970).

Appel and Soffel (1985) describe the KHT behaviour of natural and synthetic titanomagnetites of varying composition; Fig. 3.18 summarises their results.

The Hopkinson peak is suppressed for samples with lower Ti content ($x \leq 0.5$), where little enhancement in susceptibility is observed. However, for samples with higher Ti content ($x > 0.5$) the Hopkinson peak is more apparent. For the largest Ti content, the blocking temperature approaches room temperature.

The existence of mixed grain sizes in basalts complicates the KHT curves of samples. In some cases, this complication becomes so great that it may not be possible to interpret the behaviour in terms of the three "pure" states described by Radhakrishnamurty and Likhite (1970). However, as they show, most samples can be explained by the combination of these three states. In Section 3.5.4, the results of KHT experiments on the Gardar lavas are discussed, where the behaviour of mixed grain sizes is important

3.5.3 The uses of high temperature susceptibility

The maximum benefit of KHT results is seen when they are used in conjunction with the results of thermomagnetic studies (Chapter 7). High temperature susceptibility studies can not only provide information on the composition of magnetic minerals but also on their grain sizes, recognising the presence of mixed magnetic grain sizes. In addition, the Curie temperature can be estimated and the blocking temperature spectrum identified (Radhakrishnamurty and Likhite, 1970; Dunlop, 1974).

3.5.4 Results from the Gardar lavas

Eighty measurements (one per flow) of KHT were made. The results are presented in three ways (Tables 3.10-3.11): curve type (Fig. 3.19), degree of

alteration and the ratio HS (K_p/K_{30}) for the heating cycle. The degree of alteration is classified A, B or C, as follows:

A : Sample effectively unaltered, with the value of K_{RT} after cooling ($K_{RT}f$) within 10% of that before heating ($K_{RT}i$).

B : Sample suffers moderate alteration, with $K_{RT}f$ being between 10 and 40% higher or lower than $K_{RT}i$.

C : Sample suffers considerable alteration, with $K_{RT}f$ over 40% higher or lower than $K_{RT}i$.

The HS value for the heating cycle gives an indication of the enhancement of susceptibility at the Hopkinson peak and, consequently, magnetic grain size (Dunlop, 1974).

Figure 3.19 shows the different types of KHT curve exhibited by the flows of the Gardar succession. The classification of curve type is based on, and is an extension of, that of Radhakrishnamurty and Likhite (1970).

H Type (Fig.3.19a) : Represents the closest approximation to the classical Hopkinson curve and indicates the presence of MD grains.

MD/SD Type (Fig.3.19b) This curve is dominated by H type behaviour (MD) but has a broad, low amplitude "hump" superimposed on the heating curve between 200° and 300°C. This feature is absent on the cooling

curve, which is of H type.

H′ Type (Fig.3.19c) : Essentially, a H Type curve, with a HS value of close to 1 (low susceptibility enhancement), which has a narrow, high amplitude peak between 250°C and 300°C on the heating curve. This feature is absent on the cooling curve, which is of H type.

He Type (Fig.3.19d) : Susceptibility increases gradually up to 700°C, with an HS value of 1.5 -2.0. On cooling, magnetite is formed resulting in a large increase in susceptibility. This curve reflects the presence of haematite grains.

He′ Type (Fig.3.19e) : This curve type is similar to the He type, differing only on the heating cycle, where the unblocking of magnetite is seen. This curve reflects the presence of both magnetite and haematite.

The interpretation of the H Type curve is the same as that of Radhakrishnamurty and Likhite (1970). The MD/SD and H′ type curves are more intriguing. Samples which possess MD/SD type curves are shown, by other rock magnetic techniques, to have mixed grain sizes with MD

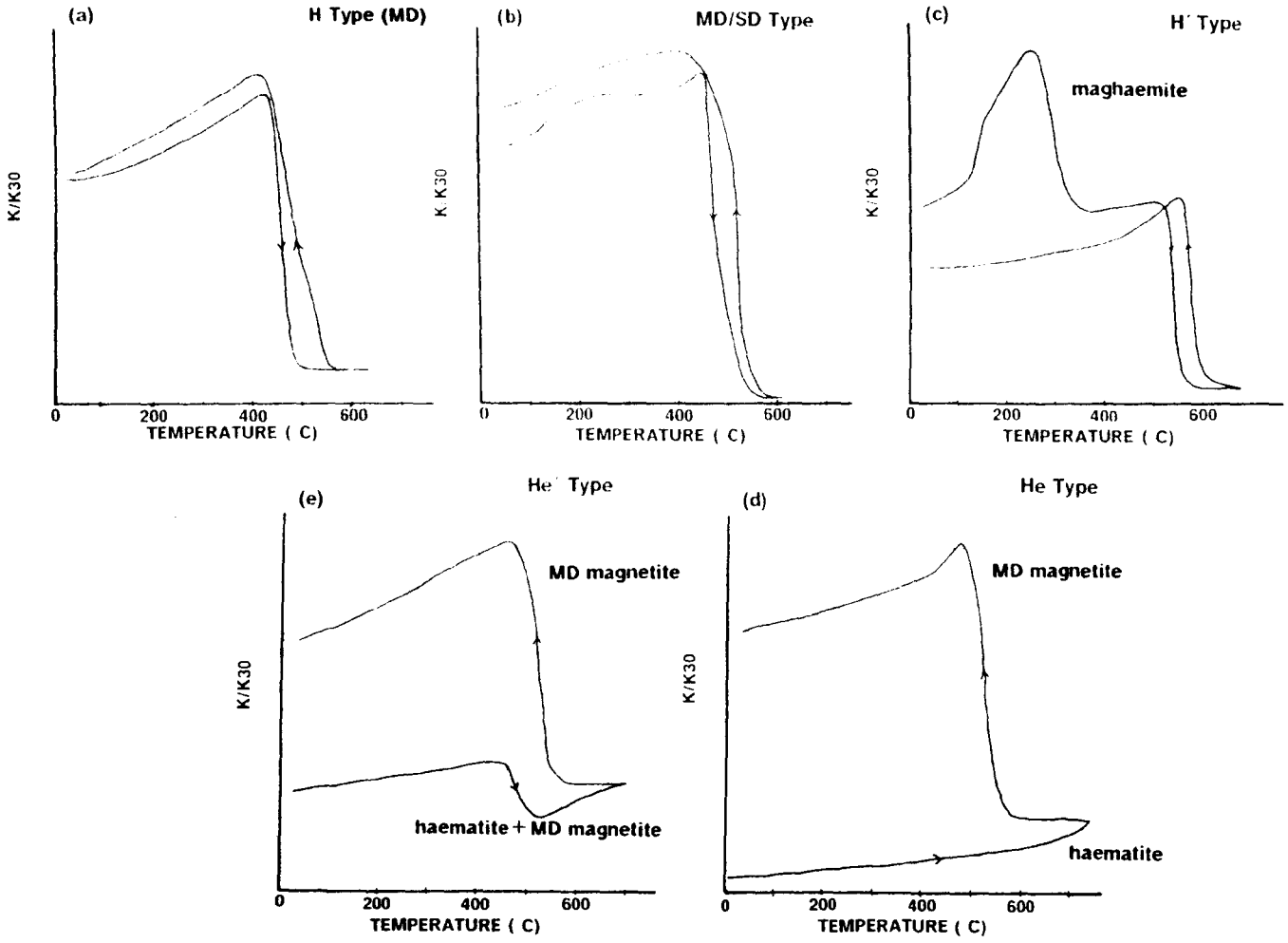

Figure 3.19 : High temperature susceptibility curves exhibited by the Gardar lavas (see text for explanation of behaviour).

dominating over SD, which is present in varying amounts. Thus, a possible explanation for the occurrence of the hump on the heating curve is the re-ordering of a SD, and possibly CD, fraction with a wide range of grain sizes. This would cause the observed rise in susceptibility superimposed on the dominant H type trend which reflects the presence of MD grains of magnetite as the main carrier.

The interesting feature of the H′ type curve is the existence of a high amplitude, narrow peak on the heating curve between 200° and 300°C. All samples which show a type H′ curve possess type 6 thermomagnetic curves, having a inflection on the heating curve between 400° and 450°C. The possibility of these two features indicating the presence of a TM30 phase has no support from experimental evidence. Appel and Soffel (1985) show that TM30 would have a KHT curve shape very similar to a H type, with a very low enhancement of susceptibility. From their results, a composition of $\simeq$ TM50 ($x \simeq 0.5$) would have a KHT curve similar to the peak seen in the H′ type curves from the Gardar lavas. However, titanomagnetites with $x \geq 0.5$ show a steady reduction in susceptibility down to -196°C, with an RS value of $\simeq 0.3$. Continuation of the K(T) curve for H′ type samples down to -196°C (Fig. 3.20) reveals that all show a MD magnetite peak at $\simeq -150$°C and have an RS value close to 1.0. This evidence suggests that there is no Ti-enriched titanomagnetite present in these samples. A more likely explanation is that the peak in the KHT curve represents the re-ordering of a SD or CD phase which has a narrow range of grain sizes. The thermomagnetic results suggest that this phase is maghaemite, a theory supported by Phil Schmidt (pers. comm.) who has witnessed KHT curves identical to the H′ type described here. Transmission Electron Microscopy (TEM) images indicated the presence of maghaemite in all of his samples.

Flows showing the presence of maghaemite have evidently been affected by low temperature oxidation (maghaemitization), producing a CRM which contaminates the primary TRM of the flows. Samples showing type H′ KHT curves all have Group 3b KLT curves, which further supports the presence of SD grains in a mixed grain size.

Samples which possess Type 7 thermomagnetic curves, indicating a haematite Curie temperature, have He or He′ type curves. Those with He′ type curves, characterised by a sharp drop in susceptibility near 580° C, show Hybrid 2/3 KLT curves (Table 3.8), with the small isotropic peak of MD magnetite. Thus, the He′ type curves identify the presence of a small amount of MD magnetite in a haematite dominated sample. He type samples just show a steady increase in susceptibility on heating to 700°C, followed by a massive increase in susceptibility on cooling, indicating reduction to magnetite.

Having described and explained the different types of KHT behaviour witnessed in the Gardar lavas collection, an account of their occurrence in each of the three lava formations will now be discussed.

3.5.4.1 The Lower (Mussartût) Lava Formation

The thermomagnetic and KLT results from this formation (Sections 3.2 and 3.4 respectively) suggests that the magnetic mineralogy for the majority of flows comprises a mixed grain size of magnetite with MD dominating over varying amounts of SD material. These results are confirmed by the presence of H and MD/SD type curves for KHT Most flows show a low or moderate degree of alteration (Class A or B, Section 3.5.4) and a low enhancement of susceptibility. Some flows (Fig. 3.21) give curious results, with the shape of the heating and cooling curves differing markedly. On heating, sample L8

has created a mineral with a much higher susceptibility and a lower blocking temperature than the original phase. Sample L13 has an identical curve shape on cooling but a massive increase in susceptibility. The occurrence of the MD/SD "hump" is quite frequent in the flows of the lower lavas, with the size of the hump varying between flows, suggesting a varying amount of SD material. However, the H′ type curve is absent, suggesting that the SD grains present cover a large range of sizes and also that the flows are not affected by severe low temperature oxidation to produce maghaemite.

3.5.4.2 The Middle (Ulukasik) Lava Formation

Types H, MD/SD, He and He′ curves were witnessed in this member, indicating the presence of MD magnetite, haematite and a mixture of magnetite and haematite respectively as the magnetic minerals. No H′ type curves were observed, suggesting that severe low temperature oxidation has not occurred. Unfortunately, a more comprehensive investigation of the KHT behaviour for flows from this formation was not possible due to an apparatus failure.

3.5.4.3 The Upper (Ilímaussaq) Lava Formation

As for the thermomagnetic results, it is in this largest formation of the Eriskfjord Group that the most varied KHT behaviour was found. Table 3.11 summarises the results. The majority of samples show one of three types of curve - the H, MD/SD or He type. Those with H type curves never show totally reversible behaviour, some change in character is always seen, probably as a result of the redistribution of grain sizes and internal strains.

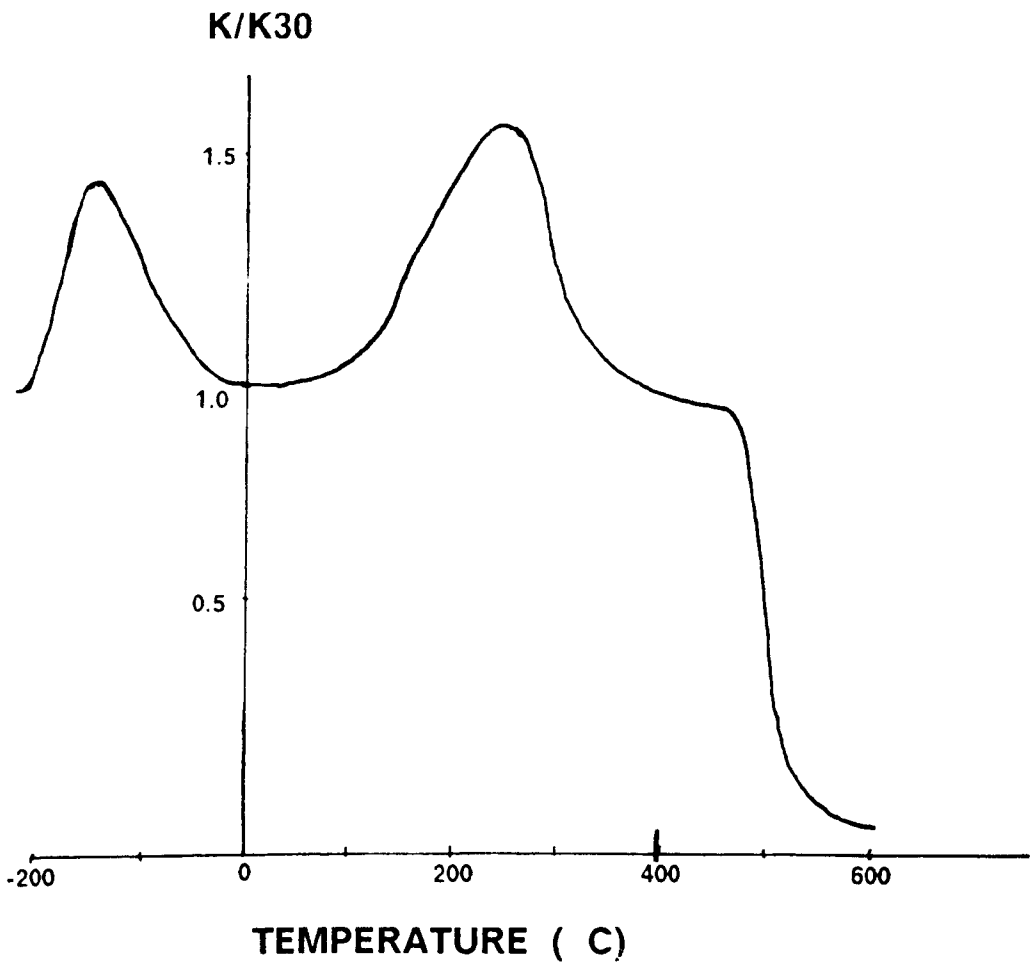

Figure 3.20 : Complete temperature dependent susceptibility curve (-196°C to +700°C) for samples exhibiting the H′ type of KHT curve.

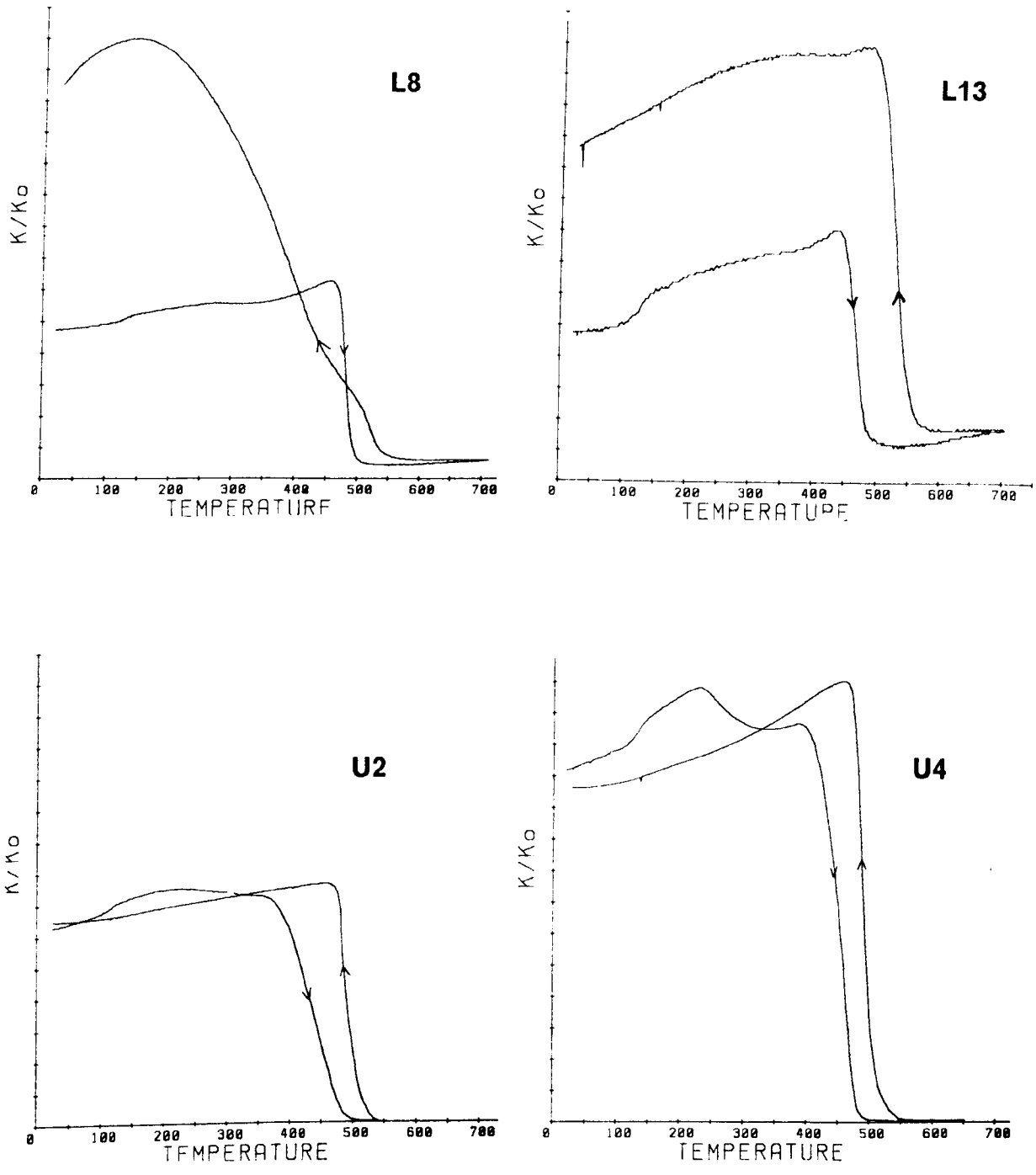

Figure 3.21 : Examples of high temperature susceptibility curves witnessed

FLOW NO.	CURVE TYPE	DEGREE OF ALTERATION	H_S VALUE
L1	-	-	-
L2	-	-	-
L3	-	-	-
L4	H	A	1.4
L5	MD/SD	A	1.3
L6	-	-	-
L7	H	B	1.3
L8	MD/SD	C	1.3
L9	H	A	1.3
L10	MD/SD	A	1.2
L11	MD/SD	A	1.3
L12	-	-	-
L13	MD/SD	B	1.0
L14	-	-	-
L15	MD/SD	A	1.3
L16	MD/SD	B	1.2
L17	MD/SD	B	1.3
L18	MD/SD	B	1.7
L19	-	-	-
L20	MD/SD	B	1.4
L21	-	-	-
L22	-	-	-
L23	-	-	-
M1	H	A	1.2
M2	He′	C	1.1
M3	He	C	2.6
M4	He	C	1.9
M5	He	C	1.7
M6	He′	B	1.3
M7	He	B	1.7
M8	He	C	2.1
M9	He	C	2.4
M10	-	-	-
M11	-	-	-
M12	-	-	-
M13	-	-	-
M14	-	-	-
M15	-	-	-
M16	MD/SD	A	1.3
M17	He′	B	2.0
M18	He	C	1.5

Table 3.10 : Results of high temperature susceptibility measurements on the Lower and Middle Lava Formations (see text for explanation of abbreviations).

FLOW NO.	CURVE TYPE	DEGREE OF ALTERATION	H_S VALUE
U1	MD/SD	A	1.0
U2	MD/SD	A	1.0
U3	H′	A	1.1
U4	MD/SD	A	1.1
U5	He	C	2.1
U6	He	C	6.0
U7	He	C	2.0
U8	H	B	1.3
U9	He′	C	1.4
U10	H	C	2.3
U11	H	C	2.0
U12	H	C	2.9
U13	H	C	2.8
U14	H′	B	1.2
U15	MD/SD	A	1.1
U16	MD/SD	C	1.3
U17	He	C	2.4
U18	He	C	2.0
U19	He	B	1.7
U20	H′	B	1.0
U21	MD/SD	B	1.0
U22	MD/SD	A	1.2
U23	He′	C	1.0
U24	H′	A	1.3
U25	He′	C	2.2
U26	H′	A	1.1
U27	He′	C	1.6
U28	MD/SD	A	1.3
U29	H′	B	1.0
U30	H′	B	1.0
U31	MD/SD	A	1.4
U32	H′	A	1.0
U33	H′	A	1.1
U34	H′	A	1.0
U35	H′	B	1.0
U36	He	B	3.9
U37	H	A	1.3
U38	He	C	3.5
U39	MD/SD	A	1.3
U40	MD/SD	A	1.4

Table 3.11 : Results of high temperature susceptibility experiments on the Upper Lava Formation (see text for explanation of abbreviations).

Varying degrees of alteration are seen with $K_{RT}f$ differing from $K_{RT}i$ sometimes by less than 5% and at other times by up to 30%. The enhancement of susceptibility at the Hopkinson peak is generally low, suggesting the presence of large MD grains of magnetite (Dunlop, 1974).

For flows which have the MD/SD type curve, the magnitude of the low temperature hump varies. In some samples, it is almost indistinguishable and the curve is almost H type (Fig. 3.21) These samples probably have only very small amounts of SD material in the mixed grain size. For other samples, the hump is large (Fig. 3.21) and approaches an H′ type curve. Such samples may possess CD magnetite, which is supported by the thermomagnetic evidence (Section 3.2). In this way, the magnitude of the hump can be used as a qualitative estimate of the amount of SD material present in a mixed magnetite grain size. Comparison of the KHT results with the KLT results confirms that samples having small humps possess lower RS values than those with larger humps and therefore have more SD material.

From Table 3.11, it can be seen that samples possessing H′ type curves (eleven flows from this formation) predominantly occur near the top of the lava stratigraphy, closest to the Ilímaussaq intrusion. This is further evidence to support the claim, made in Section 3.2, that these flows have suffered low temperature oxidation (maghaemitization) as a result of their proximity to the hydrothermally active intrusion.

Finally, twelve flows from the upper group have He or He′ type curves, indicating the presence of haematite as the dominant magnetic mineral.

3.5.5 Summary of high temperature susceptibility behaviour

The high temperature susceptibility behaviour of the basalts from the Gardar lavas is quite complex. The upper lavas, as predicted by other RM results in this chapter, show a mixture of MD and SD grains or possibly SD grains of CD magnetite (SDCD grains) in seventeen flows, maghaemite in eleven flows and haematite in twelve of the flows. In at least three flows from the incomplete data set for the middle lavas, which show He' type curves, magnetite contributes to the susceptibility (confirming the KLT results) but apparently not to the remanence (Chapter 4). The lower lavas show only magnetite with mixed grain sizes of MD and SD material, with MD dominating.

The interpretation of KHT results is not always as easy as that for KLT results. However, a good correlation exists between the presence of SD grains (in a mixed grain size) and the existence of a "hump" feature on the heating curves of Type MD/SD samples. If the range of SD grain sizes is sufficiently narrow, the hump becomes a more sharply defined peak. The Curie temperature values obtained from the KHT curves are systematically lower than those obtained from the thermomagnetic curves (Section 3.2). This is probably a result of thermal hysteresis in the susceptibility apparatus, where the temperature of the sample lags the temperature of the thermocouple on the heating cycle. This effect is more important in KHT experiments because the samples used are much larger than those for thermomagnetic analysis. The combined results from the two so-called thermal rock magnetic techniques give a complete record of the magnetic response of a sample to heating above its Curie temperature and subsequent cooling to room temperature.

An important new diagnostic rock magnetic property has been identified in this section. Previously, the susceptibility behaviour of maghaemite-bearing samples has received little attention. The identification of maghaemite, characterised by type H′ curves, is a very important rock magnetic result.

3.6 MAGNETIC HYSTERESIS

3.6.1 Introduction

As for the susceptibility behaviour, it has been predicted that the hysteresis properties of basalts will be dependent on the magnetic minerals present, their domain states (grain sizes) and shapes (Stoner and Wohlfarth, 1948; Stacey, 1963; Stacey and Banerjee, 1974). Many rock magnetists have obtained experimental results for synthetic materials which confirm these predictions (Dunlop, 1969, 1972; Day et al, 1976, 1977). In recent years, these studies have been extended to natural rocks, which have a far more complex magnetic mineralogy (Radhakrishnamurty et al, 1977, 1978; Pesonen, 1978; Senanayake and McElhinny, 1981, 1982). In this section, the hysteresis properties of the Gardar lavas are studied in an attempt to confirm results concerning their magnetic composition and grain size, obtained from other rock magnetic techniques described in this chapter.

3.6.2 Theory of magnetic hysteresis

When a demagnetised ferromagnetic sample is placed in an applied field H, which is cycled between peak fields $-H_{max}$ and $+H_{max}$, the magnetisation M induced in the sample lags behind the field, resulting in a hysteresis curve or loop (Figure 3.22).

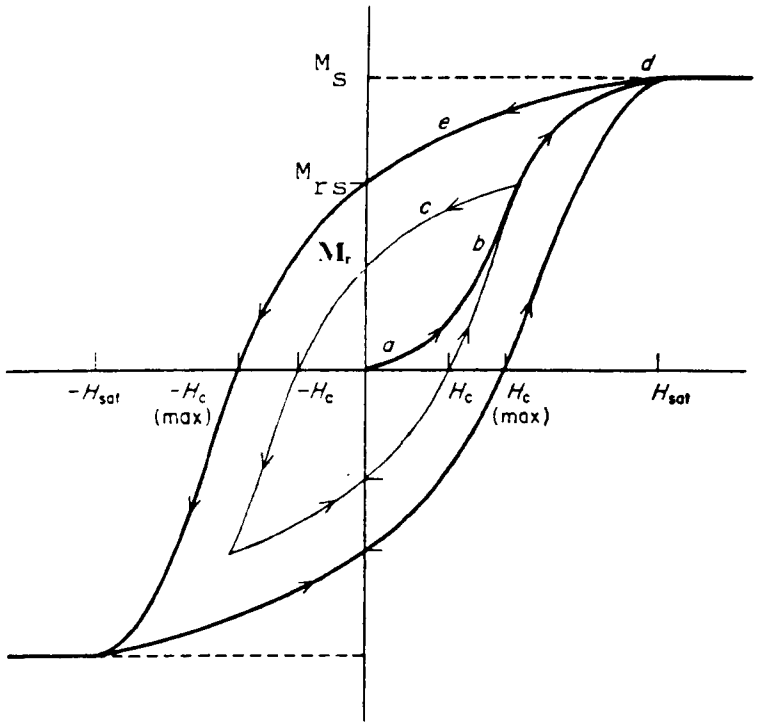

Figure 3.22 : Saturated hysteresis loop and parameters (from McElhinny, 1973). See text for explanation of parameters.

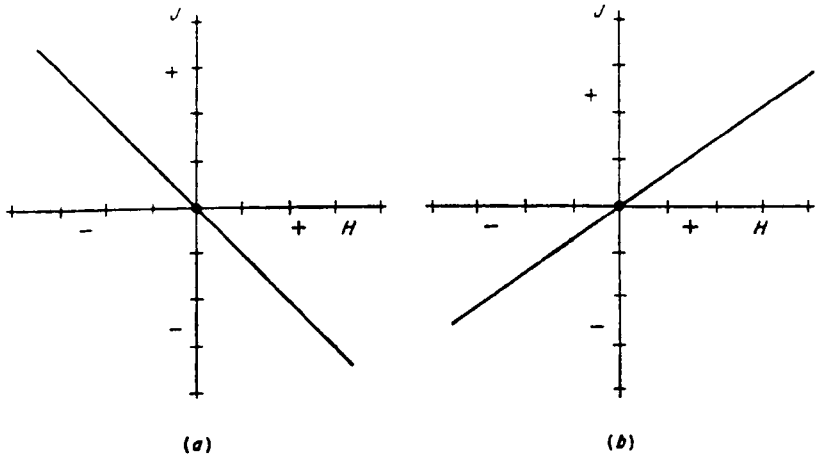

Figure 3.23 : Variation of magnetisation with applied field for (a) diamagnetic materials (b) paramagnetic materials (from McElhinny, 1973).

Initially, as the field, H, is increased from zero, the magnetisation, M, rises linearly with H along the portion of the curve a in Fig. 3.22. In this region, known as the Rayleigh region, the sample's magnetisation is reversible. If H is removed in this region, M will reduce to zero. The slope of the M-H curve over this low field region gives the initial susceptibility of the sample. On increasing the applied field, the slope of the curve increases (portion b) and the curve becomes irreversible. If H is now reduced to zero, the magnetisation will not fall to zero but follows the path c, with the result that the sample acquires an isothermal remanence (IRM), given by M_R. A characteristic of ferro- and ferri- magnetic materials is that when the applied field reaches some finite value, H_{sat} , the magnetisation shows no further increase with increasing field, i.e. its magnetisation becomes saturated. This is known as the saturation magnetisation, M_s. When the field is reduced from H_{sat} to zero, along portion e, the curve intercepts the M axis ($H = 0$) at a value known as the saturation IRM, M_{rs} . If a field is now applied in the opposite direction at some field, H_c, the IRM is overcome and M is reduced to zero. This field, H_c, is called the coercivity or coercive force of the sample. Further increases in H in the negative direction result in saturation in this direction. Repeated cycling of the field in this way causes the magnetisation to trace out the hysteresis loop seen in Fig. 3.22. The largest loop is seen when the magnetisation is saturated. For an unsaturated sample, the hysteresis loop is smaller and neither M_{rs} nor M_s can be obtained.

Paramagnetic and diamagnetic substances do not exhibit hysteresis, since the variation of M with H for such substances is linear (Figure 3.23). Superparamagnetic (SP) ferromagnetic substances also do not exhibit hysteresis; their magnetisation increases steeply at first and saturates at low fields (Thompson and Oldfield, 1986).

3.6.3 Hysteresis parameters for various magnetic states

For a saturated sample, the parameters H_c, M_{rs}, M_s and the ratio M_{rs}/M_s are of interest in determining the magnetic composition and magnetic grain size of the sample. Table 3.13 lists the value of these important hysteresis parameters for various magnetic minerals. For a given sample, M_{rs} and M_s depend on both the type and concentration of the constituent magnetic minerals. M_{rs} further varies according to the domain state of the magnetic minerals, whereas M_s is independent of grain size. Consequently, the ratio M_{rs}/M_s gives an indication of the domain state (grain size) of the magnetic mineral present in a sample. In the context of the present study, the values of M_{rs}/M_s for various domain states of magnetite are important.

MINERAL	M_s Am^2kg^{-1}	M_{rs}/M_s	H_c $\times 10^3 Am^{-1}$	H_{sat} (T)
Stable SD magnetite	92	0.5	8.0	0.3
MD magnetite	92	0.02	1.7	$\simeq$0.1
Haematite	0.5	$\simeq$0.5	140.0	1.5-6.0

Table 3.13 : Hysteresis parameters for minerals relevant to the present study. Sources : O'Reilly (1984); Thompson & Oldfield (1986).

For a random assemblage of uniaxial single-domain (SD) particles, $M_{rs}/M_s = 0.5$ (Stoner and Wohlfarth, 1948). This theoretical value is independent of magnetic composition. For multi-domain (MD) magnetite (100 μm particles), $M_{rs}/M_s = 0.02$ (Day et al, 1977). Thus, for samples with a mixed grain size of only magnetite, which is the case for many basalts (Radhakrishnamurty et al 1991), the M_{rs}/M_s value should lie between 0.02 and 0.5. Using this assumption, a crude estimation of the relative

proportions of SD and MD grains, in a purely magnetite-bearing sample, can be made. Assuming that the total M_{rs}/M_s ratio for the sample is a result of the sum of the M_{rs}/M_s ratios for SD and MD grains only, then:

$$\left(\frac{M_{rs}}{M_s}\right)\text{sample} = X_{MD}\left(\frac{M_{rs}}{M_s}\right)_{MD} + (1 - X_{MD})\left(\frac{M_{rs}}{M_s}\right)_{SD} \qquad (3.5)$$

where X_{MD} = fraction of MD grains in the sample.

Using the M_{rs}/M_s ratios for SD and MD grains given in Table 3.13,

$$\left(\frac{M_{rs}}{M_s}\right)\text{sample} = 0.02X_{MD} + 0.5(1 - X_{MD})$$

Hence,

$$\left(\frac{M_{rs}}{M_s}\right)\text{sample} = 0.5 - 0.48X_{MD}$$

or,

$$X_{MD} = \frac{0.5 - \left(\frac{M_{rs}}{M_s}\right)\text{sample}}{0.48} \qquad (3.6)$$

In some instances, M_{rs}/M_s may be greater than 0.5. This could be due to either the presence of grains with multi-axial anisotropy (Dunlop, 1971) or could be a result of the erroneous selection of M_{rs} and M_s from unsaturated hysteresis loops, where M_s cannot be accurately obtained. Superparamagnetic grains, if present in a sample, could decrease the value of M_{rs}/M_s since SP grains contribute only to M_s. For Ti-rich

titanomagnetites, M_{rs}/M_s will increase with increasing Ti substitution compared with magnetite grains of the same size and shape (O'Reilly, 1984).

By substituting M_{rs}/M_s values obtained from the hysteresis results, equation 3.6 can be used to estimate the percentage of MD, and hence SD, material present in basalts with a mixed grain size of pure magnetite (Tables 3.8-3.9). The implications of this are discussed at length in Section 3.6.4 and Chapter 7.

The coercivity, H_c, varies with grain size and domain state. Table 3.13 shows that H_c is larger for SD than MD magnetite so that hysteresis loops for SD magnetite are wider than those for MD magnetite. Haematite has a much larger coercivity than magnetite. Like M_{rs}/M_s, H_c also increases with increased Ti substitution in Ti-rich titanomagnetites (O'Reilly, 1984).

3.6.4 The uses of hysteresis results

For magnetite-bearing samples, the values of hysteresis parameters, particularly M_{rs}/M_s, can be used to give a speedy indication of the magnetic grain size when calculated from saturated hysteresis loops on the Molspin Vibrating Sample Magnetometer (VSM). This magnetometer supplies a maximum applied field of 1.0T and can thus only saturate magnetite (Table 3.13).

This method of estimating the grain size distribution in basalts can be compared with that used in the other two so-called non-thermal rock magnetic techniques.

3.6.5 The Molspin Vibrating Sample Magnetometer (VSM)

In the Molspin VSM, a sample is vibrated at a fixed frequency of 50 Hz in a uniform magnetic field produced by an electromagnet. The magnetisation induced in the sample by this field induces an alternating voltage in the pick-up coils of the instrument. The magnetic field is cycled in a stepwise fashion, from 0 to $+H_{max}$, back through zero to $-H_{max}$ and then back to $+H_{max}$. The values of magnetisation for each applied field are processed by a BBC microcomputer and subsequently stored on disk and displayed graphically. The VSM is calibrated against a standard hydrated copper sulphate sample of known mass and susceptibility. The hysteresis parameters for a sample are calculated using an interpretation program, called HISTER, developed by Dr. D.J. Robertson of the Geography Department, University of Liverpool and modified by Dr. T.C. Rolph of the Geomagnetism Laboratory, University of Liverpool.

3.6.6 Results from the Gardar lavas

One sample per flow was measured on the VSM. The results, in the form of M_s, M_{rs}/M_s and H_c, are presented in Tables 3.8-3.9 along with an estimate of the amount of MD material (X_{MD}) present in the sample, calculated using equation 3.6. Fifty-five percent of the flows in the entire succession have haematite as the only magnetic mineral (Section 3.3) and are therefore not saturated in the VSM maximum field of 1.0T. All such samples show the unsaturated hysteresis loops indicated in Figure 3.24b. Consequently, only flows having magnetite as the sole magnetic mineral exhibit the saturated hysteresis loops necessary to define M_{rs} and M_s. Examples of hysteresis loops from such samples are given in Figure 3.24a.

For the purposes of the present study, samples were assigned to one of three classes, based on their M_{rs}/M_s values:

Class 1 : $M_{rs}/M_s < 0.1$ (MD rich)

Class 2 : $0.1 < M_{rs}/M_s < 0.15$ (MD dominated, small SD fraction).

Class 3 : $M_{rs}/M_s > 0.15$ (MD dominated, larger SD fraction).

3.6.6.1 The Lower (Mussartût) Lava Formation

As with the K(T) results (Sections 3.4 and 3.5), the hysteresis results (Table 3.8) from this oldest lava formation are the most interesting in the succession. M_{rs}/M_s values range from 0.06-0.31, suggesting that, as expected from the results of the K(T) experiments, these flows possess a mixed grain size of magnetite with MD dominating over SD, which is present in varying amounts. Only two samples (from flows L17 and L21) have M_{rs}/M_s values less than 0.1. Samples from five flows have M_{rs}/M_s values between 0.1 and 0.15 and fourteen flows have values above 0.15. The highest M_{rs}/M_s values indicate flows which have the largest SD fraction.

Coercivities range from $4.7\times 10^3 Am^{-1}$ to $34.6\times 10^3 Am^{-1}$. These extreme values are shown by samples from flows L17 and L13 respectively. The former has the smallest M_{rs}/M_s value and the latter has the largest which confirms that samples with a larger SD fraction show higher coercivities than those with a smaller SD fraction.

Figure 3.25 shows histograms of the M_{rs}/M_s and H_c results.

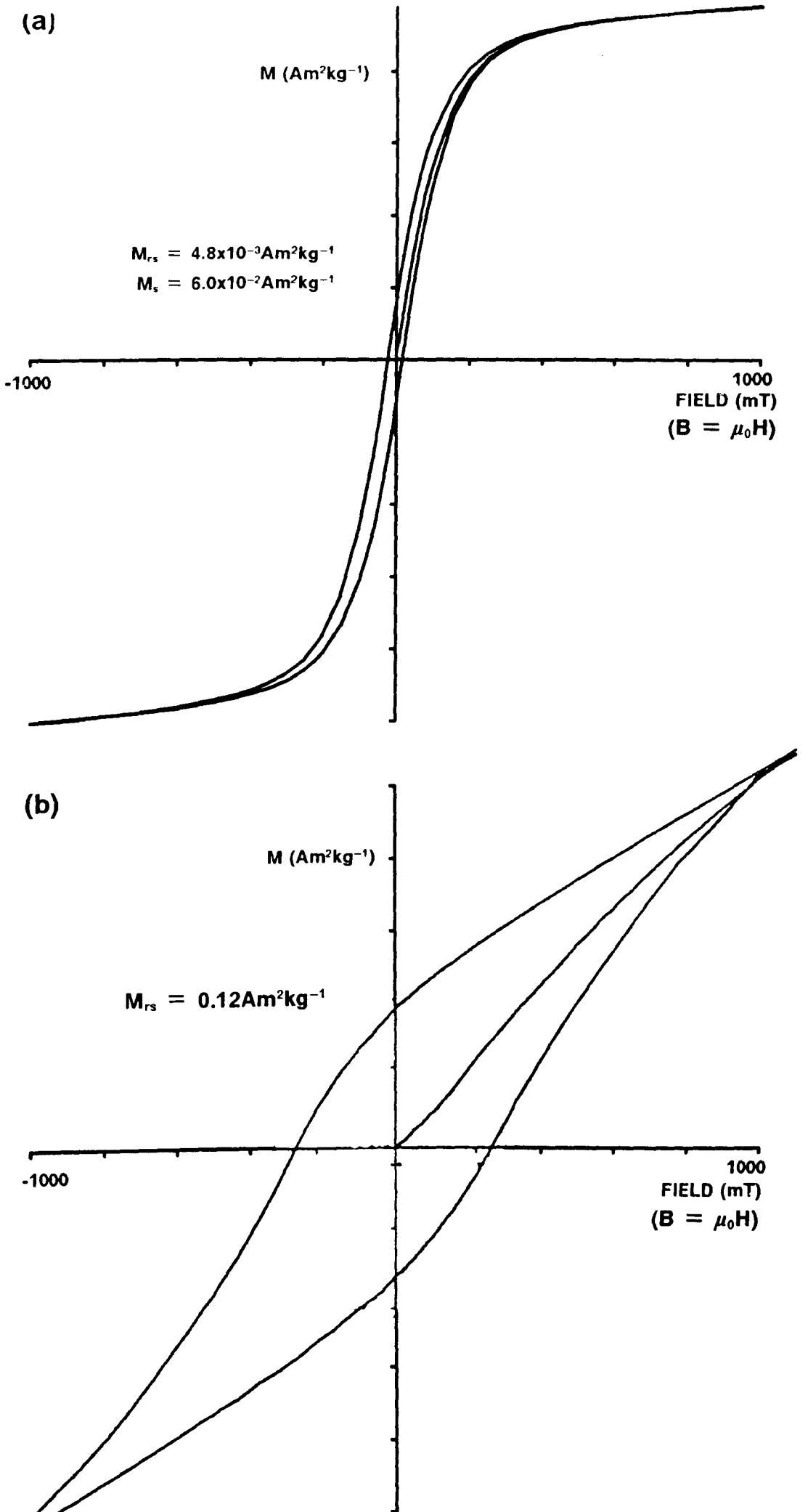

Figure 3.24 : Examples of hysteresis loops exhibited by the Gardar lavas (a) saturated (b) unsaturated.

(a)

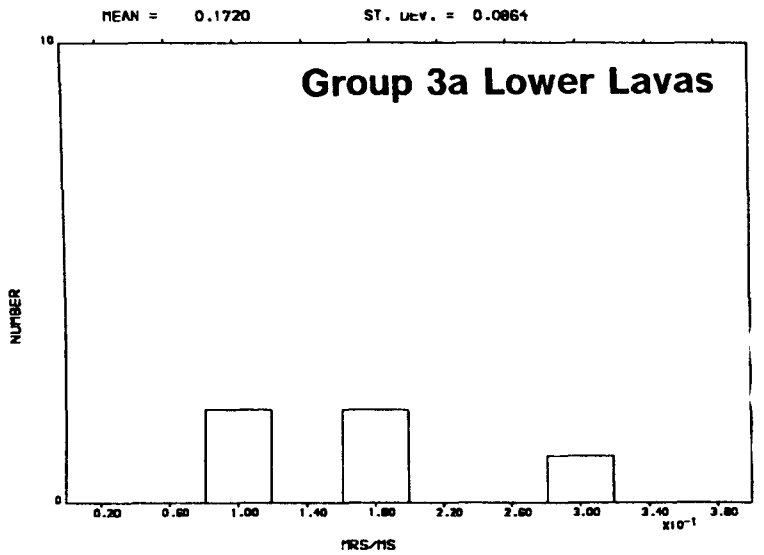

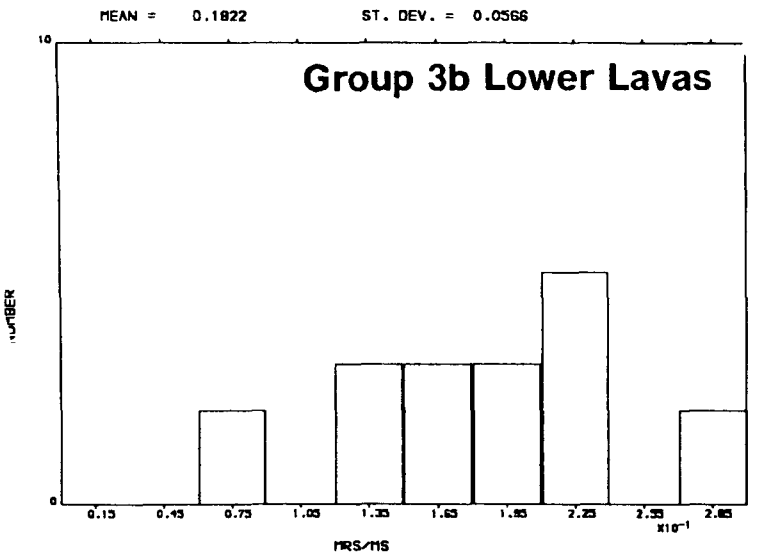

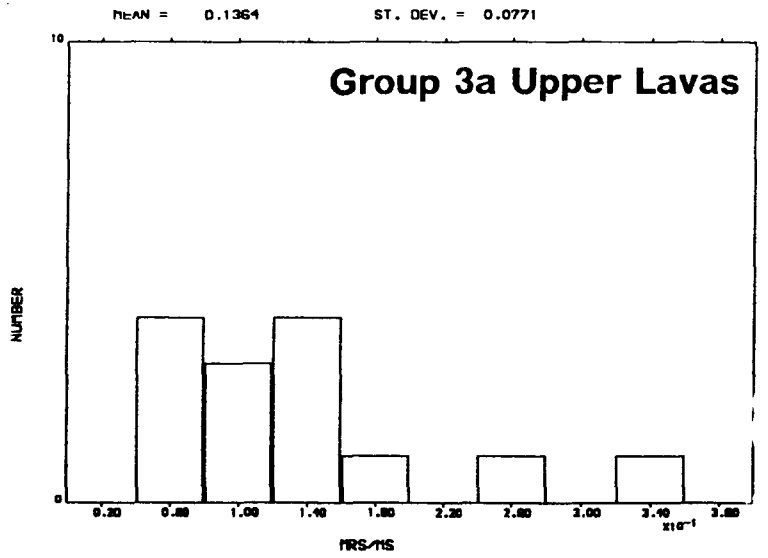

Figure 3.25 : Histograms of hysteresis parameters for the Lower Lava Formation and the Upper Lava Formation.

(b)

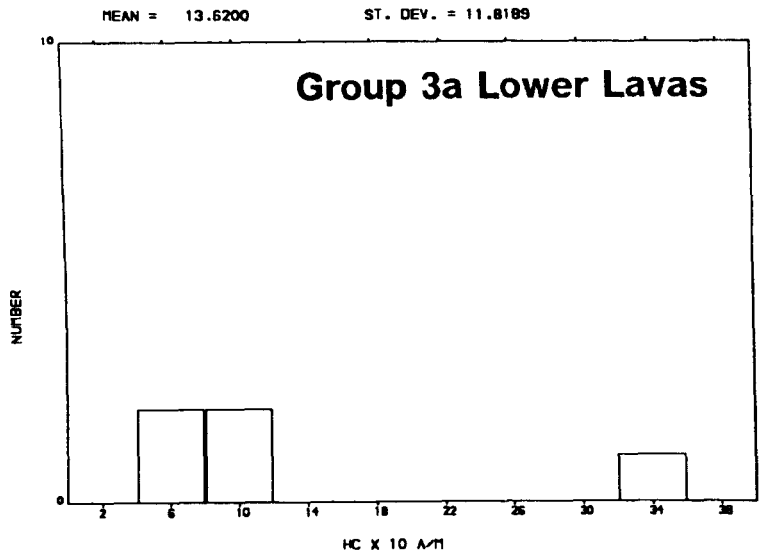
MEAN = 13.6200
ST. DEV. = 11.8189
Group 3a Lower Lavas
NUMBER
HC X 10 A/M

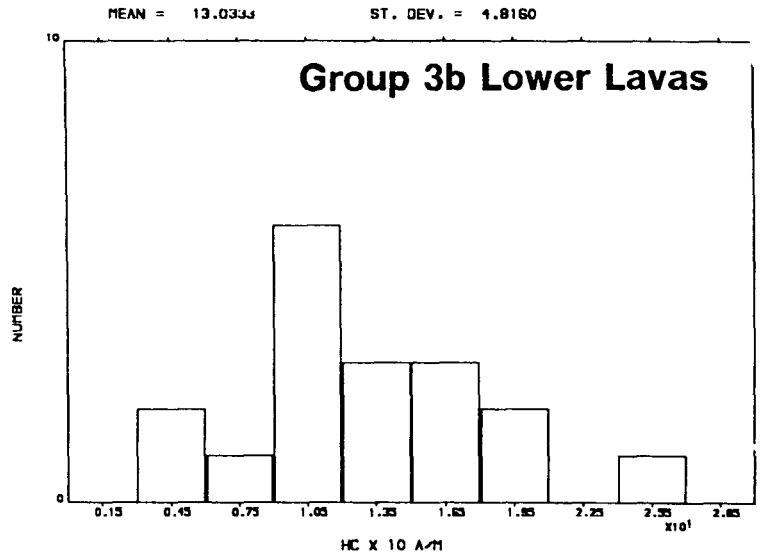
MEAN = 13.0333
ST. DEV. = 4.8160
Group 3b Lower Lavas
NUMBER
HC X 10 A/M

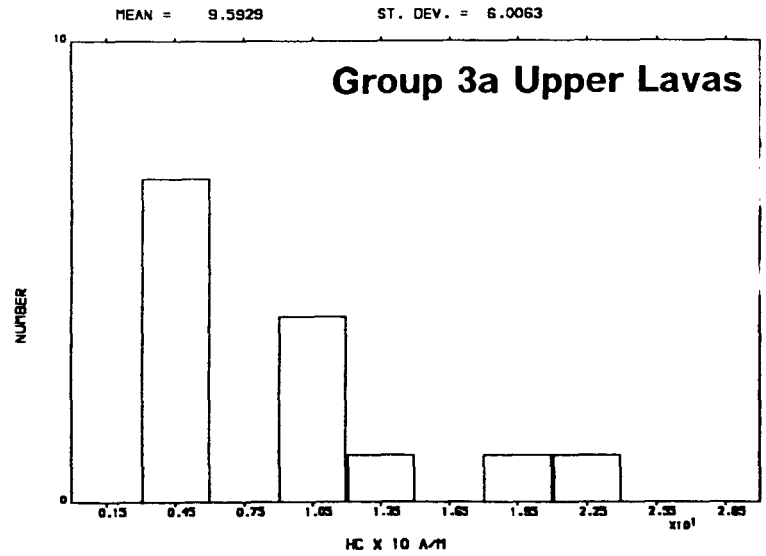
MEAN = 9.5929
ST. DEV. = 6.0063
Group 3a Upper Lavas
NUMBER
HC X 10 A/M

3.6.6.2 The Middle (Ulukasik) Lava Formation

Samples from four flows of this formation exhibited saturated hysteresis loops. Two (from flows M1 and M10) Class 1 M_{rs}/M_s values characteristic of MD rich samples, the other two (flows M11 and M12) showed values suggesting the existence of more SD material. Flows exhibiting the hybrid 2/3 KLT curve did not saturate in the 1T field, suggesting that the multi-domain magnetite in these flows is not dominant. The remainder of flows from this group, being haematite-bearing, were not saturated in the 1T field.

3.6.6.3 The Upper (Ilímaussaq) Lava Formation

Table 3.9 shows that only fifteen flows from this member show saturated hysteresis loops on the VSM. The remaining twenty-five flows were not saturated, having haematite as the magnetic mineral, as identified in Section 3.3.

Figure 3.25a shows a histogram of M_{rs}/M_s results for the Group 3a samples. Group 3b samples do not saturate, which is surprising since other rock magnetic results suggest that a SD fraction is present in these samples. The reason for this may be related to the fact that all Group 3b samples in the Upper Lavas have thermal rock magnetic results consistent with the existence of maghaemite, which is CDSD magnetite. Most of the samples which saturated are MD rich or MD dominated, characterised by M_{rs}/M_s ratios of <0.1 and 0.1-0.15 respectively. Only five of the flows showing saturated hysteresis loops have M_{rs}/M_s values > 0.15, indicating the presence of a larger SD fraction. Coercivity values range from 4.4×10^3 to 2.4×10^3 Am^{-1}.

3.6.7 Summary

This section has shown that the hysteresis ratio M_{rs}/M_s can be used in both a qualitative manner (Classes 1-3) and a crudely quantitative manner (equation 3.6) to determine the relative amounts of multi-domain and single-domain material in a mixed grain size of magnetite. These, when combined with results from KLT and a.f. demagnetisation studies, have considerable use in the selection of samples for palaeointensity studies (Chapter 7).

The hysteresis results for the Gardar lavas show that the Upper (Ilímaussaq) Lava Formation is characterised by MD rich and MD dominated flows with very little evidence of larger SD fractions. The majority of flows in the Middle (Ulukasik) Lava Formation do not show saturated hysteresis loops in a maximum applied field of 1.0T because they have haematite as the magnetic mineral. The Lower (Mussartût) Lava Formation shows the most varied hysteresis behaviour. Samples from all flows in this group are saturated in the 1.0T field, confirming the presence of magnetite as the predominant magnetic mineral, as suggested by all the other rock magnetic results documented in this chapter.

It is worth mentioning, at this stage, that although the M_{rs}/M_s ratio is useful for diagnosing the grain sizes present in a sample, caution should be exercised in its application. If used without supporting rock magnetic evidence, the M_{rs}/M_s ratio can be misleading. For example, in the present study, many samples have M_{rs}/M_s values between 0.15 and 0.3. If no other rock magnetic data were available, these values could well be interpreted as being large enough to suggest PSD/SD magnetite as the magnetic mineral phase (e.g. Pesonen, 1978). However, K(T) and a.f. demagnetisation results clearly show

that all samples contain MD magnetite as the characteristic mineral phase, with SD grains present only as a minor member in the mixed grain size. This highlights one of the disadvantages of using only one rock magnetic technique to obtain an estimate of magnetic mineralogy.

3.7 ALTERNATING FIELD (A.F.) DEMAGNETISATION

3.7.1 Introduction

The technique of a.f. demagnetisation (As & Zijderveld, 1955), was used extensively in the early palaeomagnetic studies which first employed the magnetic cleaning of samples. A.F. demagnetisation is, however, not merely a palaeomagnetic technique; the decay of NRM intensity with progressively increasing peak alternating field is recognised as an important method of diagnosing the grain sizes and composition of magnetic minerals in rocks. Various authors (Parry, 1965; Dunlop, 1969, 1973; Lowrie and Fuller, 1971) have attempted to define median destructive field (MDF) values of TRM as a function of magnetic grain size. The MDF of a sample is defined as the demagnetisation field at which 50% of the original moment of the sample is lost. Qualitatively, in magnetite-bearing samples, large values of MDF indicate the presence of grains which are resistant to a.f. demagnetisation and low MDF values indicate grains which show little resistance to a.f. demagnetisation. The former are usually smaller magnetic grains (SD) and the latter are larger (MD) grains. Therefore, the a.f. demagnetisation spectrum provides an indication of a sample's magnetite grain size distribution and is thus a powerful and speedy diagnostic rock magnetic technique. The technique of a.f. demagnetisation is the third non-thermal rock magnetic technique employed in the present study.

This section reports the results of a.f. demagnetisation, used as a rock magnetic technique, for the Gardar lavas.

3.7.2 Theory of a.f. demagnetisation

Consider an assemblage of magnetic grains in a zero d.c. field environment. If this assemblage is subjected to a peak alternating field (H) and is tumbled about two orthogonal axes, then as H is slowly reduced to zero, the magnetic moments of all SD magnetic grains with coercivities less than H will become randomly oriented, and all MD grains with coercivities less than H will be effectively demagnetised. The net result is that the portion of the coercive force spectrum of the magnetic assemblage with a coercivity less than H will become demagnetised. This is repeated for successively higher alternating fields until the coercivity spectrum of the sample is exceeded or the maximum demagnetising field available is reached.

As and Zijderveld (1958) demagnetised samples along their three mutually perpendicular axes at progressively higher fields. Creer (1959) recognised that in this technique, all directions are not exposed to the same peak alternating field. He introduced the technique of tumbling the sample about two orthogonal axes perpendicular to the axis of the demagnetising coil. This tumbling aligns the magnetic 'easy' axes of all grains with the alternating field so that demagnetisation of all grains with coercivities below the peak a.f. occurs.

For single domain (SD) grains, the relaxation time, τ , is directly related to coercivity, H_c (equation 1.8)

Thus, progressive demagnetisation of a rock initially randomises the moments of grains with the lowest coercivities which, for any given volume, are also those with the shortest relaxation times. So, a rock capable of withstanding high alternating fields must have grains with long relaxation times which are capable of retaining their magnetisation for longer than the age of the rock. Since the coercivity of stable SD grains is controlled by shape anisotropy, it is directly related to the length to breadth ratio of the grains (Evans and McElhinny, 1969). The more elongate the SD grain is, the higher is its coercivity. The maximum theoretical coercivity for SD magnetite grains, and hence the maximum peak alternating field which they can survive without being demagnetised, is 300 mT (Stacey, 1961). This is a theoretical result for infinitely long needles, and in practice, the maximum coercivity of SD grains is smaller. Multi-domain (MD) grains are less resistant to a.f. demagnetisation and are unlikely to have coercivities greater than a few tens of milliTeslas (Stacey, 1961) and never greater than 100 mT (McElhinny, 1973). This low resistance to a.f. demagnetisation is a characteristic feature of MD grains which can be used as a diagnostic rock magnetic property.

Haematite has much larger coercivities than magnetite (Table 3.13). Few available a.f. demagnetisers are able to produce peak fields large enough to demagnetise haematite. Thus, the use of a.f. demagnetisation is more relevant to magnetite-bearing samples than to haematite rich ones. For palaeomagnetic purposes, the technique of thermal demagnetisation (Section 4.4.1.) is more practical for haematite-rich samples.

3.7.3 The uses of a.f. demagnetisation

The uses of a.f. demagnetisation, as employed in the present study, were :

1. To distinguish between magnetite and haematite bearing samples.

2. To identify the presence of MD grains of magnetite within a sample. Such grains have low coercivities and are thus demagnetised by low peak alternating fields, certainly below 100 mT (Evans and McElhinny, 1969) and, in many cases, probably below about 50 mT. This low resistance of MD grains to a.f. demagnetisation can be used in conjunction with other non-thermal rock magnetic techniques during the assessment of the suitability of a sample for use in palaeointensity experiments, since the most suitable samples are generally those with the smallest amount of MD material (Chapter 7).

3.7.4 Results

Samples from each flow were a.f. demagnetised to a maximum peak field of 180 mT, and the results are presented in Tables 3.8-3.9. Two parameters are listed, namely the median destructive field (MDF) and the resistance category, which is a classification of the sample's response to a.f. demagnetisation. The categories seen are:

S : Magnetite samples which show very little resistance
(Soft) to a.f. demagnetisation. Between 75 and 90% of the original moment is lost on demagnetisation to 10 mT. No stable, higher coercivity component exists. MDF < 10 mT (Fig. 3.26a).

SH : Magnetite samples showing little initial resistance to a.f. demagnetisation and which have MDFs < 10 mT but also have a stable, higher coercivity component (Fig. 3.26b).

H : **(Hard)** Magnetite samples showing greater resistance to a.f. demagnetisation. MDF > 10 mT (Fig. 3.26c).

H+ : Haematite samples showing maximum resistance to a.f. demagnetisation, with 90-100% of the original moment remaining after demagnetisation to 180 mT (Fig. 3.26d).

SH+ : Samples showing two parts to the coercivity spectrum. Up to 30% of the original moment is lost by demagnetisation to 20 mT but no further loss of moment is observed on demagnetisation to 180 mT. These samples contain both MD magnetite and haematite (Figure 3.26e).

3.7.4.1 The Lower (Mussartût) Lava Formation

The lower formation is dominated by flows showing H type behaviour, indicating a mixed grain size of MD and SD magnetite. Figure 3.27a shows the distribution of MDF values for this group, which show a peak at 14 mT, with a range of 8-30 mT. The MDF values are higher than those of the Upper Lava Formation, indicating the presence of more SD material in the Mussartût flows.

3.7.4.2 The Middle (Ulukasik) Lava Formation

This formation is dominated by samples which have H+ type demagnetisation curves (flows M3-M9, M14-M15 and M18), indicating the presence of haematite. Samples from five flows (M1, M10-12 and M16) have S type curves, indicating the presence of MD magnetite. The remaining three flows are characterised by SH+ type curves, indicating the presence of both multi-domain magnetite and haematite. The occurrence of SH+ curves is coincident, in three flows, with the Group 2/3 hybrid KLT curve, which also suggests the presence of MD magnetite.

3.7.4.3 The Upper (Ilimaussaq) Lava Formation

This formation is characterised by S (15 flows) and H+ (17 flows) behaviour, confirming that MD magnetite and haematite are the predominant magnetic minerals present. Four flows show type SH behaviour, indicating that MD magnetite may be present as the magnetic mineral in a viscous component of magnetisation, which is removed by a.f. demagnetisation to about 10 mT. The stable component of magnetisation is carried by a mixed grain size of MD and SD magnetite. Two flows show type H behaviour where the remanence is single component and is carried by a mixed grain size of MD and SD magnetite. Two flows have the rare type SH+ behaviour, indicating the presence of both MD magnetite and haematite.

3.7.5 Summary

The response of the Gardar lavas to a.f. demagnetisation is a range of behaviour which confirms that MD magnetite, with varying amounts of SD magnetite and haematite, are the magnetic minerals present in the flows. A

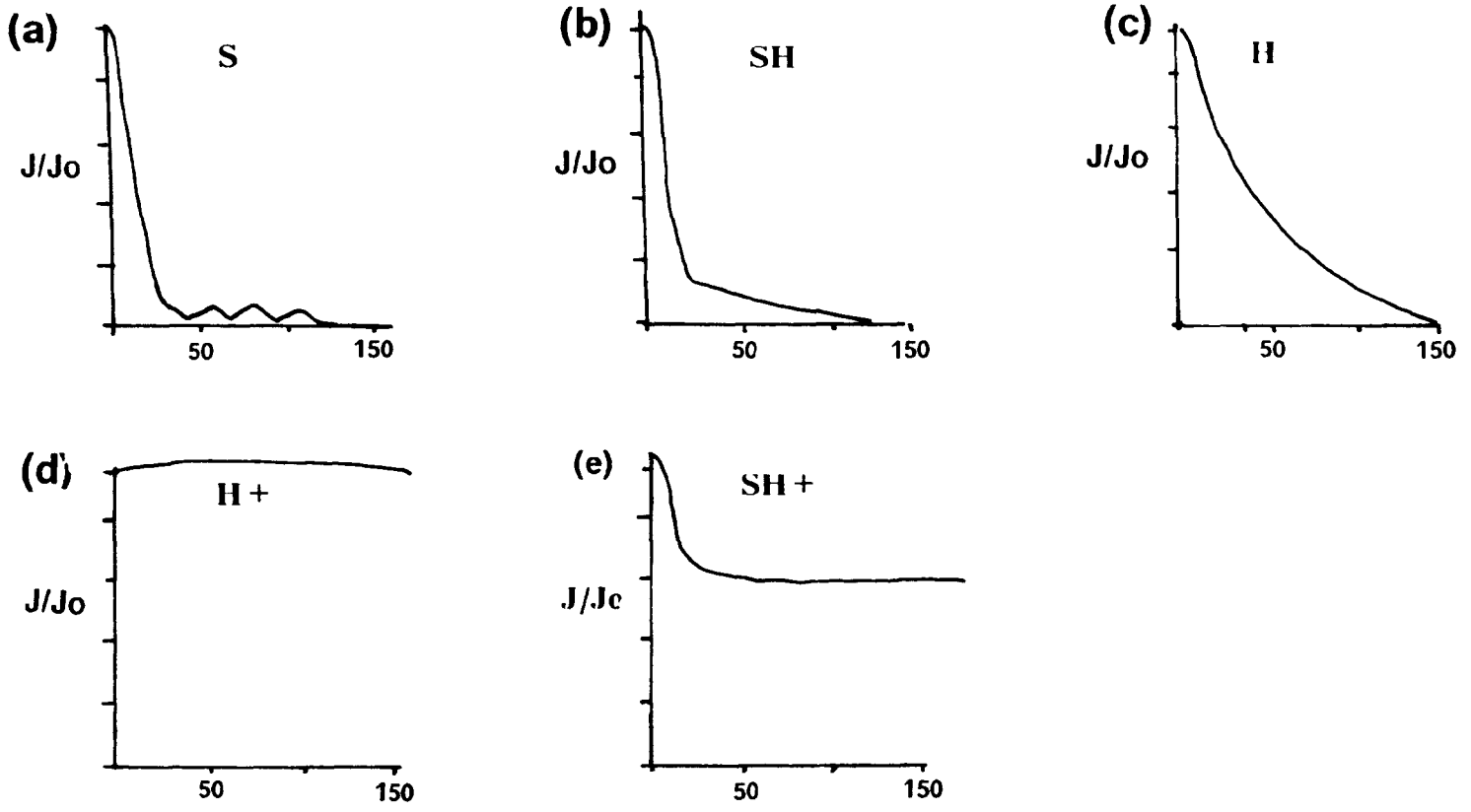

Figure 3.26 : Classification of the response to a.f. demagnetisation exhibited by the Gardar lavas (a) S type (b) SH type (c) H type (d) H + type, and (e) SH + type. (See text for explanation of behaviour).

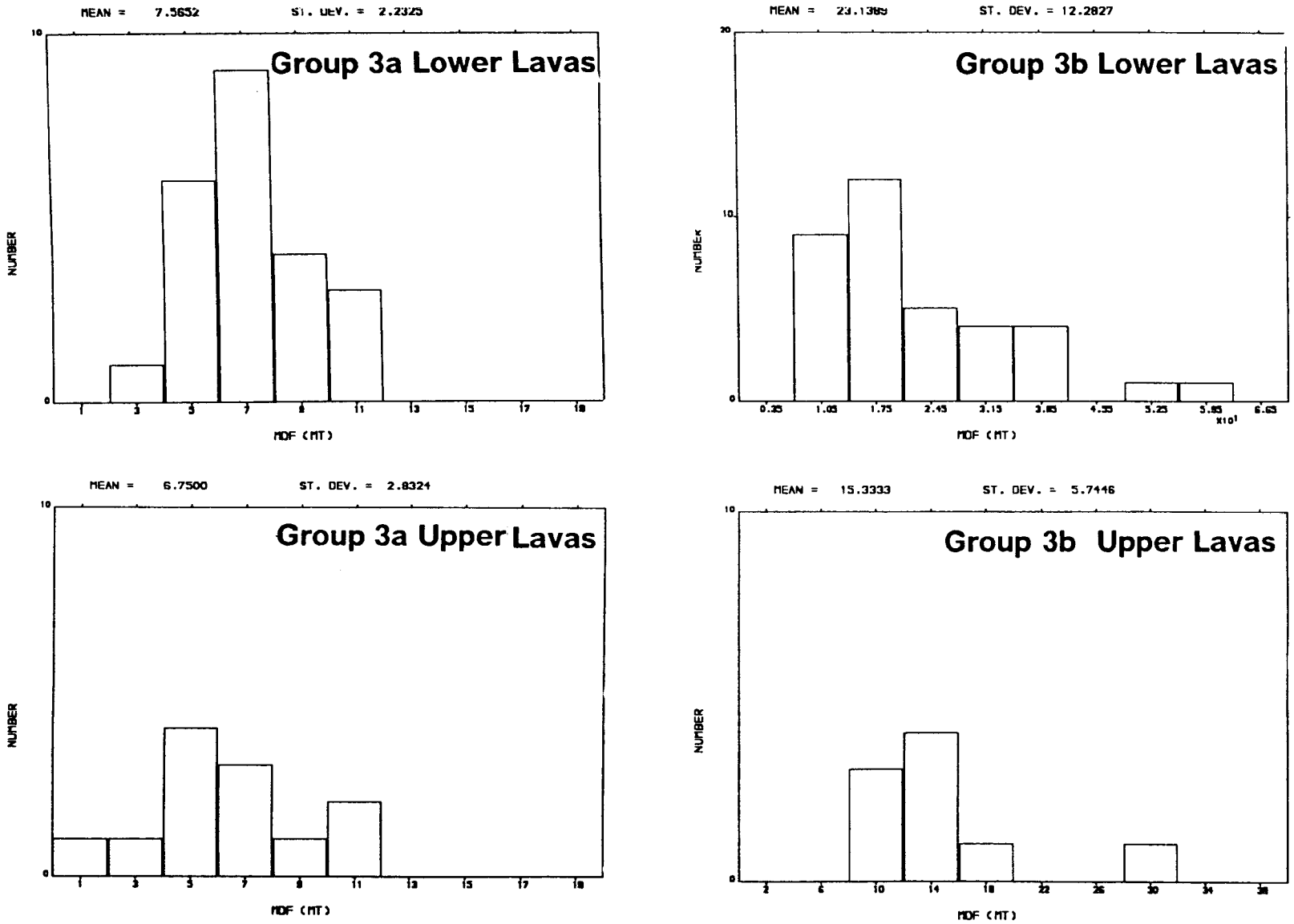

Figure 3.27 : Histograms of MDF values for flows from the Lower and the Upper Lava Formations.

range of MDF values is seen between 4 mT and 30 mT, with the lowest values shown by the most MD rich samples in the upper lava group.

These results confirm the interpretations based on the analysis of the other non-thermal rock magnetic results in this chapter.

3.8 SUMMARY AND DISCUSSION OF ROCK MAGNETIC RESULTS

The combination of results from thermal and non-thermal rock magnetic techniques has given a detailed account of the composition and grain size of the magnetic minerals in the flows of the Gardar lavas. This is summarised in Figure 3.28.

The thermal rock magnetic techniques show that the majority of flows, from all three lava groups, have a single magnetic mineral phase. This phase invariably has a high Curie temperature, of either 575° C - representing pure magnetite, or 680°C - representing haematite. The use of high temperature susceptibility, in conjunction with thermomagnetic behaviour, provides invaluable information on the domain state of the dominant magnetic mineral phase and the blocking temperature spectrum. The combined results from thermal rock magnetic techniques can indicate the likely degree of sample alteration during heating, which is an important consideration for palaeointensity work (Chapters 6 and 7). Also, the nature of the thermomagnetic curve reflects the extent of oxidation of a sample. Samples with a magnetic mineralogy defined by single, high Curie temperatures in this study (types 2, 3 and 7) have all undergone high temperature (deuteric) alteration, during or shortly after initial cooling and consequently are believed to carry a primary thermoremanent magnetisation (TRM) or

thermochemical remanence (TCRM). However, samples which possess type 6 thermomagnetic curves have been demonstrated to possess maghaemite which develops as a result of low temperature oxidation (maghaemitization). These samples are believed to carry a secondary chemical remanent magnetisation (CRM), which normally totally overprints the primary, and is not a TRM. This precludes their use in palaeointensity studies.

A strong indication of magnetic grain size is given by a combination of results from the non-thermal rock magnetic techniques. When used together, these results can indicate the relative amounts of MD and PSD/SD material present in a mixed grain size of magnetite. The potential hazards of using a single rock magnetic technique to indicate magnetic grain sizes has been stressed. The results from the Gardar lavas show that it is important to use as many rock magnetic techniques as possible before reaching conclusions regarding the composition and domain states of magnetic minerals present in basalts.

The non-thermal RM results indicate that some flows which possess magnetite as the magnetic mineral have predominantly MD grains; this is particularly obvious in the Upper (Ilímaussaq) Lava Formation. Other flows, especially those in the Lower (Mussartût) Lava Formation, have a mixed grain size comprising multi-domain and pseudo-single/single domain grains of magnetite. These observations are supported by detailed opaque petrological investigations (using reflected light microscopy) on the Gardar lavas (Piper, 1977), listed in Table 3.14. The origin of the MD and SD grains is unclear although the larger (MD) grains could possibly be due to granular (composite) type or sandwich type exsolution. This process forms large laths with enclosed regions which cause the grains to behave as MD grains of

magnetite (see Buddington & Lindsley, 1974; Haggerty, 1976). This process occurs during deuteric oxidation (Senanayake, 1981) and would therefore suggest that the MD grains do carry a primary TRM. MD magnetite could also be primary in lavas which have undergone slow cooling or annealing (Radhakrishnamurty et al, 1977) but geological evidence (Chapter 2) suggests that this was not the case for the Gardar lavas. Radhakrishnamurty (1990) suggested that the monotonous appearance of MD magnetite as the main magnetic mineral in Precambrian basalts may be the result of the evolution of the original magnetic minerals with time and that the palaeomagnetic directions obtained from such samples may not be primary magnetisations. He supports this claim with documentation of highly inconsistent NRM and cleaned directions from various Precambrian basalts. However, the results of Chapter 4 show that the palaeomagnetic directions for the Gardar lavas are highly consistent and stable. The most likely explanation for the occurrence of SD grains in the Gardar lavas samples is the subdivision of MD grains by ilmenite lamellae into regions which are magnetically distinct and behave as SD grains. This effect is observed from opaque petrological studies of the lavas (Piper, 1977).

The positive identification of maghaemite from its characteristic thermal RM behaviour is a new and extremely important result in Precambrian basalts because it indicates the effects of low temperature oxidation. Also, the low temperature susceptibility behaviour of maghaemite has been described for the first time.

The comprehensive set of RM results reported in this chapter will be used in Chapter 7, along with the palaeointensity data presented Chapter 6, to describe a new method for assessing the suitability of basalts with mixed

grain sizes (MD and SD ± CD) of magnetite for use in palaeointensity experiments.

LAVA GROUP	OXIDATION NO		MAGNETITE GRAIN SIZE (μm)	
	Mean	Range	Mean	Range
LOWER	1.8	1.0-3.2	10.7	5.2-19.3
MIDDLE	3.2	1.6-4.3	26.1	11.3-58.8
UPPER	3.7	1.2-5.3	32.9	8.8-58.9

Table 3.14 : Summary of detailed opaque petrological results for the Gardar lavas (from Piper, 1977).

Oxidation number = $\sum_{n=1}^{6} (n \times F_n)$

where n = any magnetite oxidation class from 1 to 6 (Watkins & Haggerty, 1968) and

F_n is the % of total magnetite in sample represented by class n.

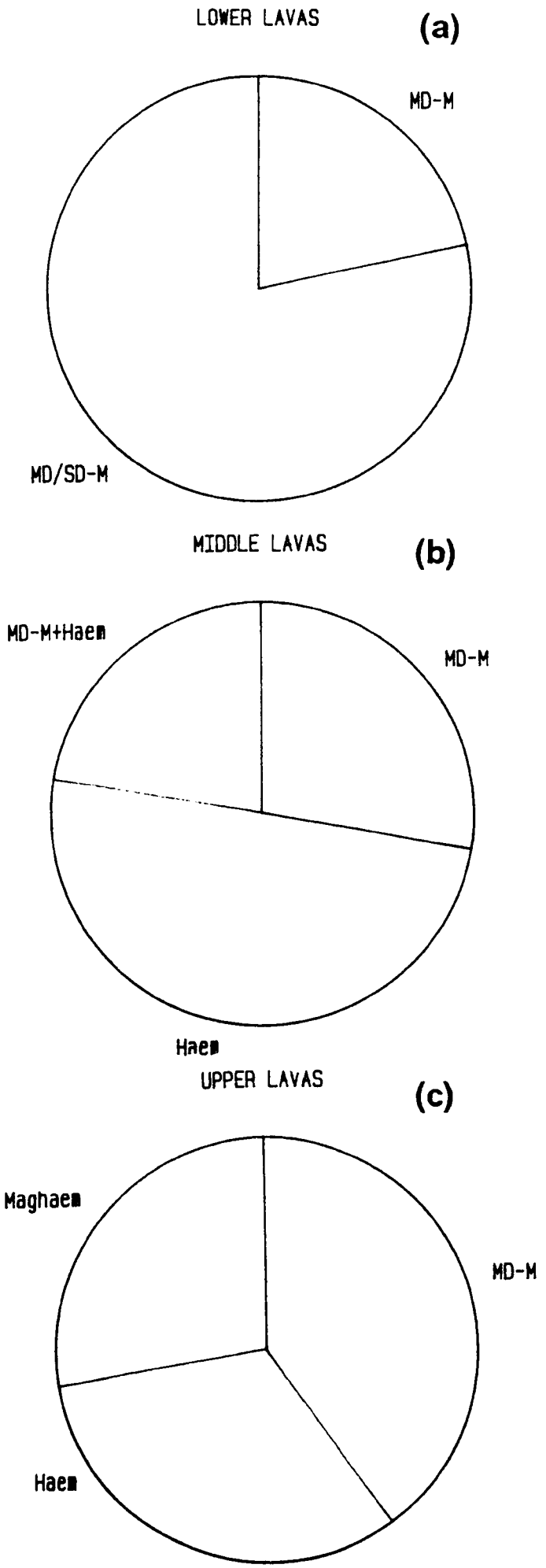

Figure 3.28 : Summary of the distribution of various magnetic minerals and domain states throughout the three lava formations of the Eriksfjord Group. MD-M = Multi-domain magnetite, MD/SD-M = Mixed grain size comprising multi- and single-domain magnetite, Haem = Haematite, Maghaem = Maghaemite, MD-M + Haem = Multi-domain magnetite and haematite.

CHAPTER 4 : PALAEOMAGNETIC STUDY OF THE GARDAR LAVAS

4.1 INTRODUCTION

The definition of a magnetic stratigraphy for the Mid-Proterozoic (ca.1300Ma) Gardar lava succession was the subject of a previous study by Piper (1977). That study resolved stable remanence directions chiefly by alternating field (a.f.) demagnetisation and identified five polarity reversals throughout the lower three quarters of the ca.1500m thick lava stratigraphy. Four of these reversals, within the Upper Lava Formation, showed an asymmetry of ca.20° in inclination which suggested that the geomagnetic field source at the time that these lavas were erupted may have been more complex than a geocentric axial dipole.

Stimulated by this original work, the present study has aimed to investigate the significance of this reversal asymmetry by resolving the detailed component structure of remanence in the lavas using thermal demagnetisation and modern techniques of component analysis (Kirschvink, 1980), which were not employed in the previous study. The entire Gardar lava succession was resampled during two field seasons (Section 4.3) thus extending the section sampled by Piper (1977) to cover the complete 1500m of lava stratigraphy, in order to investigate the geomagnetic field directions recorded in the previously unsampled upper 200m of the lava pile. It has also aimed to clarify the significance of anomalous results obtained by Piper, mainly in the middle of the three Lava Formations.

4.2 PREVIOUS WORK

4.2.1 Sampling

Piper (1977) sampled a total of forty-eight lava flows from the Eriksfjord Group, covering approximately the lower 1300m of the lava stratigraphy exposed on the Ilímaussaq Peninsula. The collection comprised nine flows from the Lower Formation, thirteen from the Middle Formation and twenty-six from the lower part of the Upper Formation. Figure 4.1 shows the sampling localities for that study.

Due to the lack of time, the Lower Formation was sampled in much less detail than in the present study. The Middle Formation and the basal part of the Upper Formation were collected from similar localities to those in the present study. The major difference between the two collections is for the middle and top parts of the Upper Formation. The sampling route followed in the previous study for this section was situated approximately 3-4 km. to the NE of that in the present study and terminates just above the "platy-basalt" flows some three quarters of the way up the lava pile (Figure 4.3c). These flows were a valuable stratigraphic marker for the present study.

4.2.2 Laboratory techniques

Progressive alternating field (a.f.) demagnetisation (Section 3.7) was employed, with steps of 5 mT (50 Oe) used up to peak demagnetising fields of between 50 and 140 mT (500 and 1400 Oe). Magnetisations were measured using a parastatic magnetometer situated in the ambient laboratory field. The demagnetisation data were analysed using only stereographic

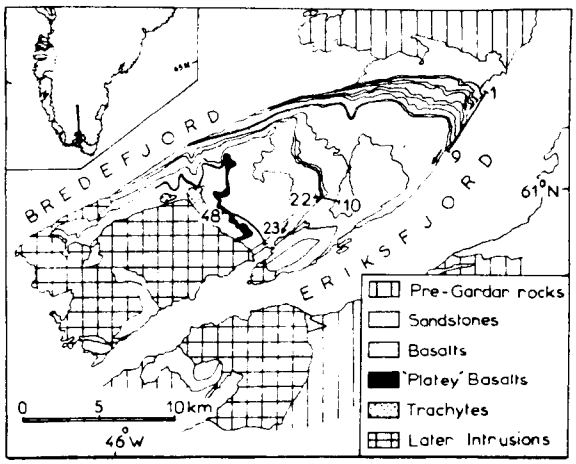

Figure 4.1 : Sketch map showing sampling localities used in the previous palaeomagnetic study of the Gardar lavas (from Piper, 1977).

projections and normalised intensity (J/J_o) plots; no modern techniques of component analysis (e.g. Kirschvink, 1980) were employed.

4.2.3 Results

The flows of the Lower and Middle Lava Formations generally showed the greatest resistance and stability to a.f. demagnetisation, whereas the Upper Lavas exhibited varying degrees of resistance and stability, with many flows losing as much as 90% of their moment on demagnetisation to fields as low as 60 mT (600 Oe). Figure 4.17b illustrates the variation in declination (D) and inclination (I) throughout the succession. Four asymmetric reversals were seen in the Upper Lava Formation (N→R→N→R→N), showing a difference of 20 – 25° between the normal and reversed field axes, with the normal (westerly) directions always being steeper than the reversed (easterly) ones. The single reversal found in the Lower Formation does not appear to be asymmetric. No reversals were found in the Middle Formation where two group mean directions were seen. The 'A' direction (SE intermediate positive) bears no resemblance to the directions from the other formations and is thus considered anomalous. The 'B' direction (SE shallow negative) has a slightly more southerly declination than the reversed directions seen in the Upper Formations. The 'A' direction was interpreted to be due either to a secondary chemical remanence (CRM) or a "polarity excursion of uncertain significance". The arguments are, however, not entirely convincing and further evidence such as palaeointensity data from the 'A' direction flows is required to clarify the situation.

The pole positions calculated by Piper (1977) for the Gardar lavas are listed, along with those derived from the results of the present study, in Table 4.3.

4.2.4 Points arising from the previous work

The study of Piper (1977) raised some interesting issues and, as a consequence of that work, the following aims were targeted for the palaeomagnetic part of the present study:

1. Extension of the sample collection to incorporate the top 200m of the Upper Lava Formation, and subsequent palaeomagnetic analysis of the flows in this interval, with the objective of completely evaluating the magnetostratigraphy of the lava sequence.

2. Extensive re-sampling of the Middle Lava Formation to investigate the geomagnetic significance of the anomalous results found for this formation in the previous study.

3. Detailed sampling and measurement of the flows from the Lower Lava Formation, for which only limited sampling was possible in the previous study, to fully determine the magnetostratigraphy of this formation.

4. Investigation of the reality and significance of the field asymmetry found in the previous study. This is discussed in Chapter 8, where the palaeomagnetic results are analysed in conjunction with the palaeointensity data.

4.3 PALAEOMAGNETIC SAMPLING

Eighty-one lava flows were sampled within the three lava formations of the Eriksfjord Group exposed on the Ilímaussaq Peninsula. (Figure 4.2). These sections cover the entire 1500m of lava stratigraphy and comprise

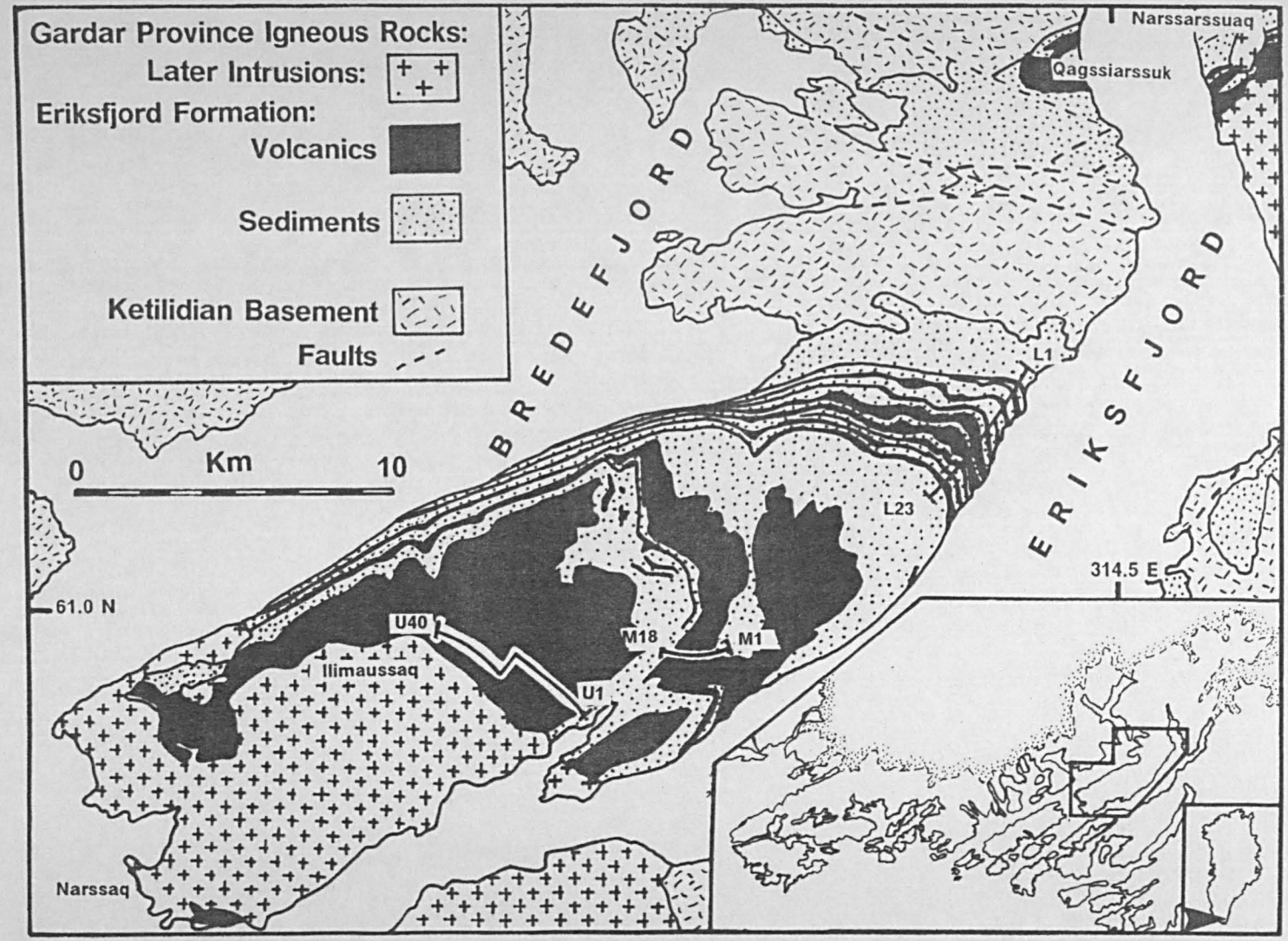

Figure 4.2 : Sketch map showing sampling localities used in the present study. Inset indicates the geographic position of the area. Flow numbers are indicated on the map.

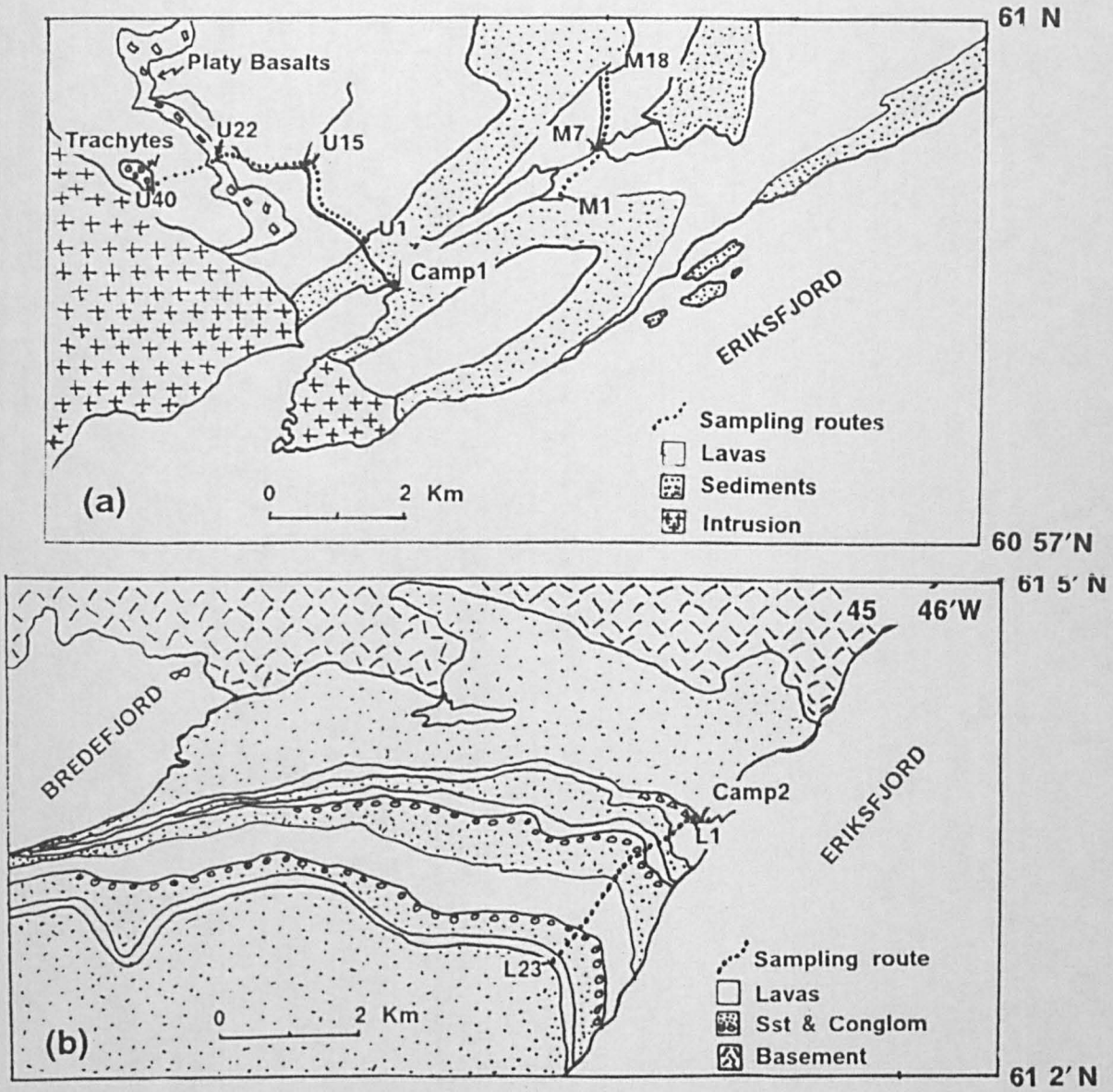

Figure 4.3 : Sketch maps showing the routes followed during palaeomagnetic sampling in the present study, for: (a) The Upper and Middle Lava Formations, and (b) The Lower Lava Formation

LAVA FORMATION	FLOW NUMBERS	PETROGRAPHIC DESCRIPTION
LOWER	L1-L3	COLUMNAR BASALTS
	L4	SILL
	L5-L23	BASALTS
MIDDLE	M1-M18	OLIVINE BASALTS
UPPER	U1-U10	STAR BASALTS
	U11-U16	AMYGDALOIDAL BASALTS
	U17-U20	PORPHYRITIC BASALTS
	U21-U22	PLATY BASALTS
	U23-U38	TRACHYBASALTS, TRACHYANDESITES,
	U39-U40	TRACHYTES

Table 4.1 : Summary of the petrographic characteristics of the flows in each of the three Lava Formations of the Eriksfjord Group, sampled for palaeomagnetic purposes during the present study.

twenty-three flows from the lower formation, eighteen flows from the middle formation and forty flows from the upper formation. Table 4.1 gives the details of the sampling sites and Figure 4.3 shows the detailed routes taken during the collection of samples from each of the three lava formations.

Between four and eight three inch cores (each one inch in diameter) were drilled from each flow using a water cooled diamond drill bit attached to a portable two stroke motor. The cores were oriented in situ, using a sun compass in conjunction with a magnetic compass. A scribe line was scratched on the top of each core using a strip of brass wire. The cores were then removed from the outcrop and labelled with the site and sample numbers. Care was taken to avoid drilling samples from the tops of lava flows where the baking effect of the flow above might be important. The tectonic dips of the lower, middle and upper lava formations, determined

from flow surfaces and interleaved sediments were 9° towards 180°E, 10° towards 220°E and 10° towards 220°E respectively. Four one inch long cores were cut from each site in the laboratory, for palaeomagnetic measurements.

The 1989 Field Season

This first field season, completed during June and July of 1989, concentrated on the collection of samples from the three Lava Formations. Two camp sites were utilised during the fieldwork (Figure 4.2), the first was situated on the Nunasarnaq inlet (Camp 1) and the second (Camp 2) was situated approximately 17km to the northeast at Mâjût bay.

Camp 1 was used as a base for the sampling of the Upper and Middle Lava Formations. The former was completed in four uninterrupted days' sampling and the latter was completed in two days' sampling along the stream sections illustrated in Figure 4.3a.

The flows of the Lower Lava Formation were sampled in three days from the base at Camp 2 (Fig. 4.3b). This base was also used for the sampling of the NE-trending Late Gardar dykes and contact rocks along the shoreline at M âjût and across the Ilímaussaq Peninsula at Isafjord (described in Chapter 5).

The 1990 Field Season

The main objective of this second field season, completed during July 1990, was to collect further samples from the three Lava Formations for palaeointensity work and to sample the marginal syenites of the Ilímaussaq intrusive complex. Both of the camp sites established in the 1989 field season

were again used, in addition to a base in the town of Narssaq, which was used for sampling the Ilímaussaq intrusion (Chapter 5).

4.4 LABORATORY TECHNIQUES

4.4.1 Thermal demagnetisation

It is quite common for the natural remanent magnetisation (NRM) of very old rocks to be composed of more than one component of magnetisation; over its long geological history a rock may have acquired one or more secondary components as a result of a variety of processes, summarised in Section 1.2. In favourable situations, these secondary components may be superimposed on a primary component of magnetisation acquired by the rock during, or shortly after, its formation. For the purposes of most palaeomagnetic studies, it is essential to isolate the component structure by demagnetising the NRM. The principle of demagnetisation is to remove components of magnetisation in order of their increasing resistance to the demagnetising process, which in the case of thermal demagnetisation, is heating.

Two approaches of thermal demagnetisation have been applied. Wilson (1962b) developed a method in which a rock sample is heated continuously and its magnetisation measured at selected temperatures whilst the sample is still hot. In the alternative method, a sample is heated to successively higher temperatures and allowed to cool in zero field before its magnetisation is measured. This stepwise thermal demagnetisation method (Thellier, 1938; Irving et al, 1961) is commonly preferred to the continuous method because it presents fewer technical problems and was employed in the present study.

The magnetic grains within a rock sample have different relaxation times and hence, different blocking temperatures (Section 1.2). If the rock is heated to a temperature, T, below its Curie temperature, and cooled in zero magnetic field, only the magnetic grains with blocking temperatures lower than T will be demagnetised, i.e. their magnetisation is 'unblocked' and their contribution to the NRM of the sample is eliminated. Repetition of this process up to the Curie temperature, or the temperature at which all of the magnetic moment is destroyed, results in complete demagnetisation of the sample and allows the blocking temperature spectrum of the rock to be investigated. Magnetic grains with low blocking temperatures have short relaxation times and are generally magnetically unstable because they are most susceptible to acquiring secondary components of magnetisation. Partial thermal demagnetisation of the rock removes these secondary components to leave the stable primary component which is held in grains with higher blocking temperatures having longer relaxation times.

4.4.2 The Spinner Magnetometer

The magnetisation of all samples was measured using a "Molspin" Spinner Magnetometer (Molyneux, 1971). This commercial magnetometer is able to rapidly and accurately measure both the intensity and direction of magnetisation for samples whose NRM intensities are $\geq 10^{-5}Am^2kg^{-1}$. The noise level of the magnetometer, for the ca. 30 g one-inch cores used in this study, is approximately $0.01 \times 10^{-5}Am^2kg^{-1}$.

The "Molspin" magnetometer determines the magnetisation of a sample following spinning operations in six orthogonal positions in a circular fluxgate sensor (Figure 4.4) to derive three orthogonal components of magnetisation. As the sample spins a voltage is induced in this sensor, with an amplitude

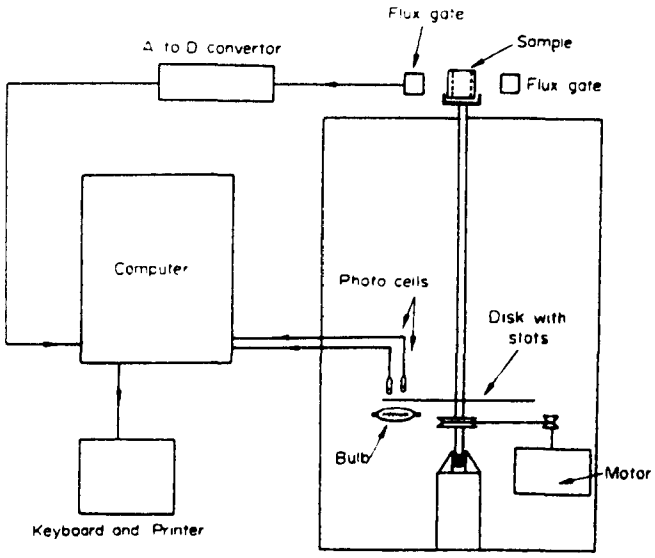

Figure 4.4 : Schematic diagram of the "Molspin" spinner magnetometer which was routinely used for measurement of magnetisations in the present study (from Molyneux, 1971).

proportional to the intensity of magnetisation and a phase proportional to the direction of magnetisation. The fluxgate signals are digitised and resolved by Fourier analysis. The processed results are displayed on a VDU and output on a line printer and are stored on disk for addition to the database on the University Mainframe computer for further analysis.

4.4.3 Experimental details

The following experimental procedures were followed in the thermal demagnetisation and measurement of all the palaeomagnetic samples:

1. Samples were demagnetised in a Magnetic Measurements Thermal Demagnetiser. The ambient field within the oven of the demagnetiser is kept to a minimum to reduce the possibility of samples acquiring a laboratory PTRM on cooling.

2. Both the demagnetiser and the spinner magnetometer were situated inside a $2m^3$ Rubens coil arrangement (Rubens, 1945), known here as the 'cage', which is designed to further minimise the ambient geomagnetic field in the laboratory. During the experiments, periodic fluxgate magnetometer measurements of the field in the cage and the oven were conducted. These showed that the field inside the cage was as low as 0.1 μT and that inside the oven of the demagnetiser 0.01 μT (0.2% and 0.02% of the earth's field respectively).

3. Demagnetisation steps of 50° or 100°C were used up to a temperature of 500°C, followed by 10°, 20° or 30°C steps up to the maximum unblocking temperature of the sample.

4. Four samples from each flow in the lava succession (i.e. four per site) were used in the palaeomagnetic study.

4.4.4 Data analysis and presentation

All demagnetisation data were plotted as orthogonal vector plots (OVPs) (Wilson, 1961; Zijderveld, 1967). These plots indicate the change in the magnitude and direction of the sample's remanence vector during progressive stepwise demagnetisation. These changes are displayed as two vector projections, one onto the horizontal (x,y) plane, the other onto the vertical (x,z or y,z) plane. The vertical projection is chosen by the computer program to provide the best visual presentation of the remanence vector. For example, if the vector lies mainly in the x,z plane then this plane will be used for all projections. The horizontal plane is labelled with respect to the geographic axes N, S, E and W respectively on all OVPs in this study. This plane contains the point (x,y) and is marked by a '+'. The vertical projection, labelled UP and DOWN, contains the point (x,z or y,z) which is marked by a 'x'. The distance of any point from the origin of the OVP is proportional to the magnitude (i.e. the intensity) of the magnetic vector.

A single component of magnetisation will then be represented by a pair of straight lines which converge to the origin of the OVP. The magnetic declination, D, is given by the angle between the straight line in the horizontal projection and the north axis. A measure of the magnetic inclination, I, is given by the angle between the straight line in the vertical projection and the horizontal axis.

OVPs are very useful for isolating the components of a multi-component NRM, provided that the blocking temperature or coercivity spectra have only

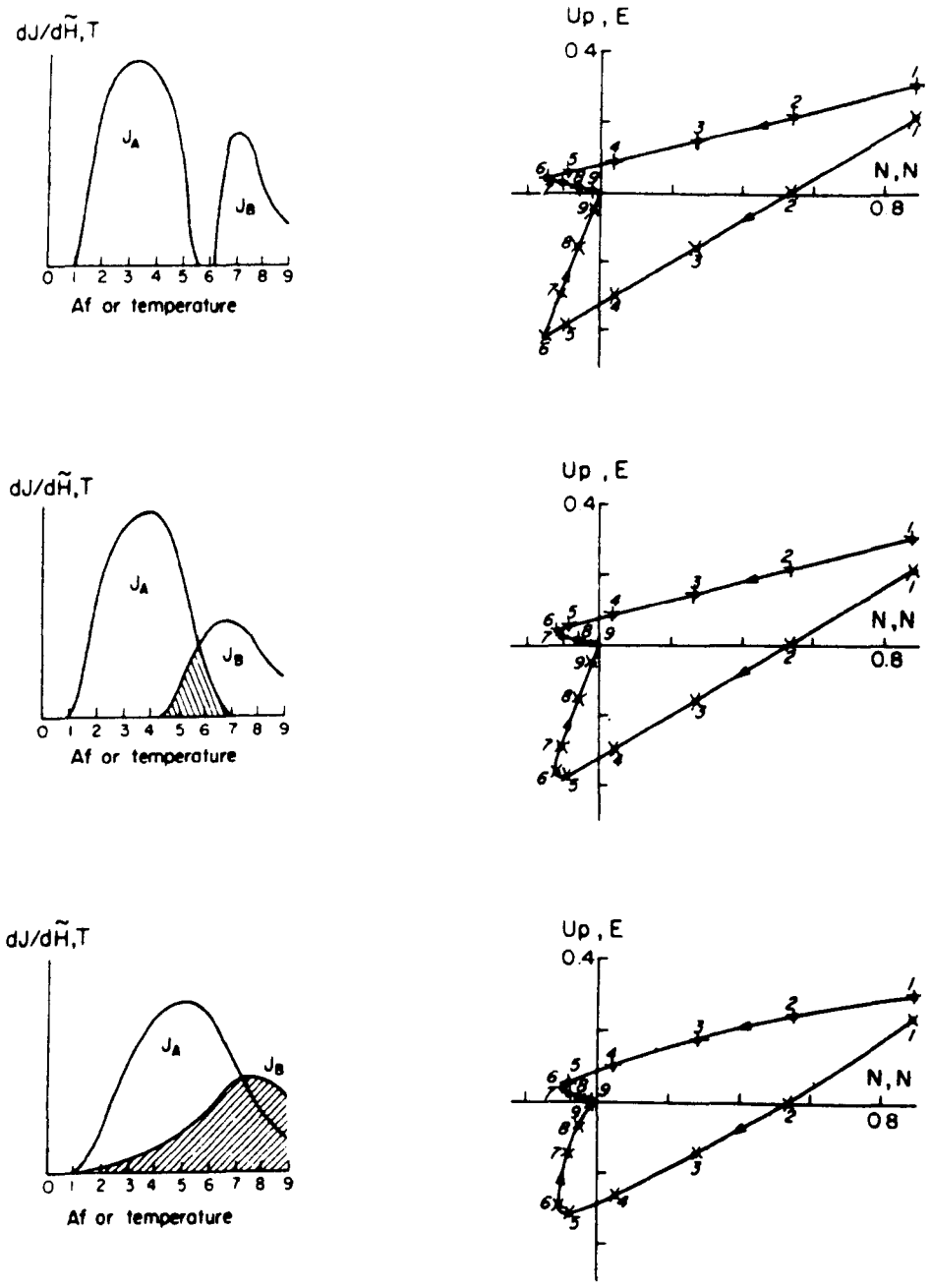

Figure 4.5 : Orthogonal Vector Plots (OVPs) for three samples, each having two components of magnetisation. Varying degrees of overlap of the blocking temperature (or coercivity) spectra are shown. '+' ('x') symbols represent horizontal (vertical) components (from Dunlop, 1979).

limited overlap. For example, Figure 4.5 shows a sample possessing a two-component NRM. The vectors for each magnetisation component are no longer defined as discrete linear segments as their blocking temperature spectra (or coercivity spectra) show a greater degree of overlap.

In reality, very few samples give perfect converging straight lines on OVPs due to the tendency of samples to acquire laboratory VRMs or PTRMs when the residual component is small. The operator first isolates the components constituting the NRM by an interactive graphics procedure and a best fit is determined for the data points using the method of Principal Component Analysis (PCA), as described by Sherwood (1989). A measure of the precision of the fitted direction is given by the maximum angular deviation (MAD) about the best fit straight line (Kirschvink, 1980). For each sample, a minimum of three consecutive data points which form a vector that converges on the origin were used to define the direction of the characteristic (highest blocking temperature) component of magnetisation. This part of the data analysis was completed using the PLOTCORE program developed at the Earth Sciences Department, Liverpool University for use on the university mainframe and based on the MATZIJ program written for a BBC microcomputer (Sherwood, 1989). After this vector was identified for each sample, a tilt corrected flow mean direction was calculated with a precision defined by Fisher statistics (Fisher, 1953). Likewise, group mean directions for each of the three lava formations were calculated and palaeomagnetic poles derived. All software used to calculate mean directions and pole positions was developed at the Geomagnetism laboratory by Drs. T.C. Rolph and G.J. Sherwood or by Mr. A.G. McCormack of the Dept. of Earth Sciences, University of Liverpool and has been routinely applied during the present study.

The statistical system generally used for analysing palaeomagnetic data is that developed by Fisher (1953). Fisher statistics regard palaeomagnetic directions as distributions of points on the surface of a sphere. The two parameters most widely quoted in palaeomagnetic analysis are the precision parameter, k and the α_{95} value. The precision parameter is a measure of how well the directions are grouped and ranges from zero for random grouping (R = 0) to infinity (N = R) for no dispersion. The α_{95} value is the semi-angle of the cone of 95% confidence centred on the mean direction, i.e. there is a 95% probability that the mean direction lies within $\alpha°$ of the calculated mean.

To calculate the mean of N palaeomagnetic directions, the declination (D) and the inclination (I) of each direction are transformed into their direction cosines, x_i, y_i and z_i, where:

$$\begin{aligned} x_i &= \cos D_i \cos I_i \\ y_i &= \sin D_i \cos I_i \\ \text{and,}\quad z_i &= \sin I_i \end{aligned}$$

The resultant of these direction cosines, R, is then calculated where:

$$R^2 = \left(\sum x_i\right)^2 + \left(\sum y_i\right)^2 + \left(\sum z_i\right)^2$$

For k > 3, the precision parameter is of the form

$$k = \frac{(N-1)}{(N-R)}$$

the mean declination (D_m) and inclination (I_m) are given by:

$$\tan D_m = \frac{\sum y_i}{\sum x_i}$$

$$\text{and,} \quad \sin I_m = \frac{\sum z_i}{R}$$

The corresponding α_{95} value is given by:

$$\alpha_{95} = 1 - \left[\frac{(N-R)}{R} \right] \left[(20)^{1/(N-1)} - 1 \right]$$

4.5 THERMAL DEMAGNETISATION RESULTS

Tables 4.2-4.4 and Appendices 1-3 show the results of the thermal demagnetisation study. The remanence of each sample was categorised (A-E) according to the number of components of magnetisation isolated by analysis of OVPs. The categories were defined as follows:

Category A : The NRM is a single component, converging directly to the origin of the OVP, with no evidence of a component in the present field distributed in the lower part of the blocking temperature spectrum.

Category B : NRM shows evidence of low temperature ($<200°C$) contamination with a steep positive component probably in the present field, subtracted in the first few steps of demagnetisation. Otherwise, as for Category A, one high blocking temperature

component exists.

Category C : NRM has two components of magnetisation, both remote from the present Earth's field (P.E.F.). One component resides in the lower part of the blocking temperature spectrum and the other resides in the higher part (> 450°C).

Category D : NRM shows evidence of low temperature (< 200°C) contamination with a steep positive component, probably in the P.E.F., subtracted in the first few steps of demagnetisation. Otherwise, as for Category C, two higher blocking temperature components exist.

4.5.1 The Lower (Mussartût) Lava Formation

The flows from the lower lavas show high stability to thermal demagnetisation. All flows have either Category A or B remanences, and examples are shown in Figures 4.6-4.7. Those with Category B normally have a low temperature component (between room temperature and 150 or 200°C) superimposed on the primary component. This low temperature component (a viscous partial thermoremanence - VPTRM or a TCRM) may be a signature of burial remagnetisation, such as is witnessed in the lavas from the Keweenawan Province (Pullaiah et al, 1975; Merrill, 1975; Dunlop and Buchan, 1977; Pesonen, 1978). The majority of flows have narrow blocking temperature spectra with high unblocking temperatures (Figure 4.6), often exhibiting the type of intensity decay curve illustrated in Figure 4.16d,

with up to 90% of the remanence being subtracted in a 20 – 30°C interval just below 580°C. Some flows show distributed blocking temperature spectra (Figure 4.16a). Only two flows with easterly, negative directions were found in the lower lavas (Figure 4.7). These are located at the top and bottom of the formation. This direction is hereafter referred to as "reversed" although it should be noted that the normal or reversed sense with respect to the P.E.F. cannot be resolved with certainty at present. Both reversals appear to be symmetrical, in contrast to those witnessed in the upper formation. Most of the remaining flows are normally magnetised (westerly positive) and those which show directions unrepresentative of the remainder of the group tend to have at least one unstable sample per flow (Appendix 3). One flow (flow L13) has an anomalous NE positive direction. This direction was found using both thermal and a.f. demagnetisation methods on several samples from the flow and no appreciable magnetic fabric ($K_1/K_3 = 1.03$) was identified during magnetic anisotropy experiments on four samples from the flow (Section 3.3). Thus, the direction must be considered to be real. The existence of a 4m thick shaley horizon immediately below flow L13 in the stratigraphic sequence is indicative of a sizable time gap between the extrusion of flows L12 and L13, probably long enough to record a brief excursion of the geomagnetic field. Unfortunately, this shaley horizon was too fissile to be drilled, thus precluding a test of this explanation. This flow, along with those with one or more unstable samples, was excluded from the group mean direction calculation. The flow mean directions show a close grouping (Fig. 4.14a) with a tilt-corrected formation mean direction of D = 293.8°, I = 25.4°.

4.5.2 The Middle (Ulukasik) Lava Formation

Two groups of characteristic remanence directions were isolated in this formation - almost identical to the 'A' and 'B' directions recognised by Piper (1977). Seven flows possess the 'A' direction and six record the 'B' direction. Figures 4.8-4.10 illustrate typical palaeomagnetic behaviours exhibited by flows of this formation. The stereographic projections show the direction of magnetisation remaining constant throughout stepwise thermal demagnetisation. In general, samples showing the 'A' direction have discrete, high unblocking temperatures associated with the type of demagnetisation curve illustrated in Figure 4.16c and subtraction of the NRM does not commence until demagnetisation temperatures well in excess of 400°C are employed. The samples which carry the 'B' direction tend to show lower blocking temperatures, indicating the presence of magnetite. It was suggested (Piper, 1977) that the samples showing the 'A' direction may have suffered low temperature alteration, resulting in acquisition of a secondary magnetisation. However, the stability of the remanence direction and the OVPs show no sign of a secondary component different from the characteristic component which is always recovered from the higher temperature portion of the blocking temperature spectrum. This suggests that any secondary component could only have been acquired shortly after initial cooling of the lava at a time when the geomagnetic field had the same direction. Figures 4.8 - 4.9 clearly show that there is no secondary component superimposed on two different primary ('A' or 'B') directions. The thermal demagnetisation results strongly suggest that the magnetisation of most of the flows in the middle lava formation comprise a single, high blocking temperature component.

FLOW	MEAN DIRECTION						CAT	POLARITY
	N	J_n	D	I	α_{95}	k		
L1 *	2	75.8	27.8	39.0	-	-	A	N
L2 *	2	38.3	308.3	24.1	69.0	15.3	A	N
L3	2	16.2	303.7	11.1	24.0	110.6	A	N
L4 *	4	24.9	3.6	55.9	42.7	5.6	A	N
L5	4	65.5	302.8	22.5	4.8	373.7	C	N
L6	4	26.7	295.4	26.3	20.4	37.4	A	N
L7 *	4	16.4	-	-	-	-	A	N
L8 *	4	41.3	-	-	-	-	M	M
L9	3	28.2	291.6	26.0	8.3	224.0	A	N
L10 *	4	60.6	288.2	-3.0	16.1	33.6	M	M
L11 *	4	17.2	-	-	-	-	C	N
L12 *	2	11.5	342.1	73.4	8.3	907.6	A	N
L13 *	4	88.1	89.1	5.2	8.9	107.1	A	I
L14	1	62.1	297.0	16.0	-	-	A	N
L15	4	54.3	296.2	15.9	1.9	231.6	A	N
L16	4	20.2	296.7	31.4	3.3	771.0	A	N
L17	4	31.8	296.8	26.6	7.8	141.2	C	N
L18	3	41.9	288.4	15.7	5.7	464.2	A	N
L19	2	36.8	310.9	40.7	14.4	302.8	A	N
L20	4	150.0	290.2	8.6	5.9	248.0	A	N
L21 *	1	25.2	83.2	71.0	-	-	C	I
L22 *	1	17.3	305.6	72.3	-	-	B	N
L23 *	3	283.5	104.6	-11.7	25.4	24.6	A	R

Table 4.2 : Flow mean directions for the Lower (Mussartût) Lava Formation. Flows marked with an asterisk * were omitted from calculation of the formation mean direction. Remanence categories are defined in the text. M denotes the presence of mixed remanence categories or mixed polarities. See text for explanation of standard Fisher statistics parameters N, α_{95} and k. J_n is the mean NRM intensity of the N flows in the site.

FLOW	MEAN DIRECTION						CAT	POLARITY
	N	Jn	D	I	α_{95}	k		
M1	4	20.5	162.4	57.1	4.6	397.4	A	I
M2	4	3.3	148.0	41.6	6.2	221.4	A	I
M3	4	4.4	149.4	47.4	4.0	518.4	A	I
M4	4	4.5	153.3	49.5	11.1	69.2	A	I
M5	4	1.7	156.1	43.9	4.8	370.1	A	I
M6	4	3.2	157.2	46.4	6.7	187.4	A	I
M7	4	0.8	148.1	39.5	12.1	58.9	A	I
M8 *	2	3.1	306.5	-25.1	17.2	214.1	A	I
M9	2	3.5	141.6	-16.2	3.1	6668.3	A	R
M10	2	29.3	158.7	-9.6	13.6	339.4	A	R
M11 *	2	15.1	264.7	15.2	69.7	7.5	C	I
M12	2	17.3	138.3	-12.2	18.1	192.9	A	R
M13	2	2.2	140.9	-12.4	16.1	242.1	A	R
M14	2	1.7	135.9	-16.0	7.6	1078.0	A	R
M15	2	2.4	138.3	-17.7	12.1	431.2	A	R
M16 *	2	0.5	292.2	27.3	9.3	720.9	A	N
M17 *	4	5.6	316.1	-8.5	4.4	447.9	A	I
M18 *	4	1.5	328.5	31.1	22.4	17.8	A	N

Table 4.3 : Flow mean directions for the Middle (Ulukasik) Lava Formation. Symbols are as for Table 4.2.

FLOW	MEAN DIRECTION						CAT	POLARITY
	N	Jn (°)	D (°)	I	α95	k		
U1	4	85.0	332.0	54.9	19.9	22.1	B	N
U2	4	55.0	326.8	42.3	17.7	27.9	B	N
U3 *	4	12.4	314.0	36.0	30.6	10.0	C	N
U4	4	81.0	337.0	64.4	8.5	116.8	A/C	N
U5	4	6.0	311.6	27.4	9.7	91.3	A	N
U6	3	0.8	317.7	30.9	5.0	341.3	A	N
U7	4	1.0	305.8	30.9	7.7	144.8	A	N
U8	4	6.0	294.4	64.2	19.5	23.3	C	N
U9	4	4.4	93.5	-20.8	3.8	602.7	A	R
U10	4	20.0	97.5	-15.1	4.2	475.6	A	R
U11	4	24.0	105.9	-34.2	19.0	24.3	A	R
U12	4	9.0	99.4	-22.5	5.0	340.3	A	R
U13	4	34.0	102.0	-27.6	4.5	425.6	A	R
U14	4	11.0	104.5	-15.1	12.9	52.0	C	R
U15 *	3	43.0	93.9	4.9	-	1.7	C	I
U16 *	4	37.0	329.0	79.1	11.7	63.3	A	R
U17	4	1.5	305.7	20.6	7.7	143.9	C	N
U18	4	10.0	280.7	21.9	8.5	116.7	A	N
U19	4	19.0	275.9	22.8	13.0	51.9	A	N
U20	4	13.0	276.4	29.5	8.1	130.9	C	N
U21 *	4	18.0	52.6	78.6	-	2.6	A	I
U22 *	4	157.0	278.9	56.5	-	1.6	A	N
U23	4	2.0	334.2	43.2	7.8	139.8	A	N
U24 *	4	64.0	30.9	65.2	-	1.3	A	I
U25 *	4	2.0	326.6	37.4	13.2	49.4	A	N
U26 *	4	6.0	318.9	67.8	43.5	5.4	C	N
U27 *	4	4.5	340.3	54.1	31.6	9.4	A	N
U28	4	63.0	295.4	38.3	-	2.7	A	N
U29 *	4	5.0	47.8	62.0	12.5	55.2	C	I
U30 *	3	12.0	344.1	-36.3	-	1.2	C	I
U31	4	39.0	291.2	59.4	14.2	43.1	C	N
U32	3	12.0	276.3	38.9	8.2	229.2	A	N
U33 *	4	20.0	257.7	58.1	-	1.7	B	N
U34 *	4	7.0	329.3	76.8	17.9	27.4	M	N
U35 *	4	17.0	338.9	79.8	7.3	158.2	A	N
U36 *	4	24.0	345.6	77.5	25.4	14.1	C	N
U37	3	11.0	293.0	60.0	20.4	37.5	M	N
U38 *	3	21.0	264.9	85.1	8.4	217.9	A	N
U39	3	29.0	277.4	45.2	30.8	17.1	C	N
U40	1	65.0	285.5	19.4	-	-	C	N

Table 4.4 : Flow (site) mean directions for the Upper (Ilimaussaq) Lava Formation. (Flows marked with an asterisk * are omitted from calculation of the mean directions for the formation listed in Table 4.5)

Figure 4.6 : Palaeomagnetic plots for flows with normal (westerly, positive) magnetisation directions in the Lower (Mussartût) Lava Formation. D/I = Declination/Inclination values for the magnetisation vector. Units of J are $\times 10^{-5}Am^2kg^{-1}$. The alpha95 value given in all diagrams refers is the maximum angular deviation (MAD) of the best fit direction (Kirschvink, 1980) and not to the Fisher parameter α_{95} See text for explanation of other symbols.

(a)

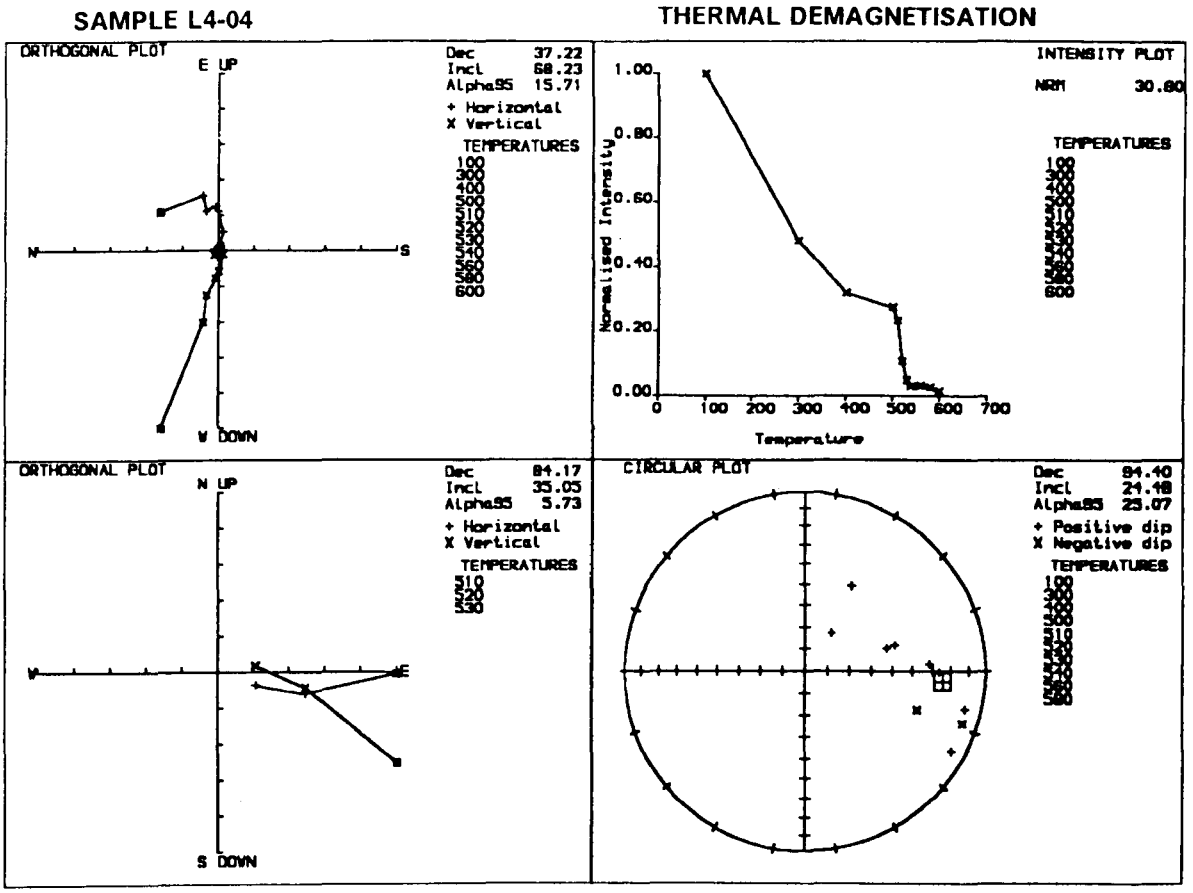
SAMPLE L4-04
THERMAL DEMAGNETISATION
ORTHOGONAL PLOT
E UP
N
S
W DOWN
Dec 37.22
Incl 68.23
Alpha95 15.71
+ Horizontal
X Vertical
TEMPERATURES
100
300
400
500
510
520
530
540
560
580
600
INTENSITY PLOT
NRM 30.80
TEMPERATURES
Normalised Intensity
1.00
0.80
0.60
0.40
0.20
0.00
0 100 200 300 400 500 600 700
Temperature
ORTHOGONAL PLOT
N UP
W
E
S DOWN
Dec 84.17
Incl 35.05
Alpha95 5.73
+ Horizontal
X Vertical
TEMPERATURES
510
520
530
CIRCULAR PLOT
Dec 84.40
Incl 24.48
Alpha95 23.07
+ Positive dip
X Negative dip
TEMPERATURES

(b)

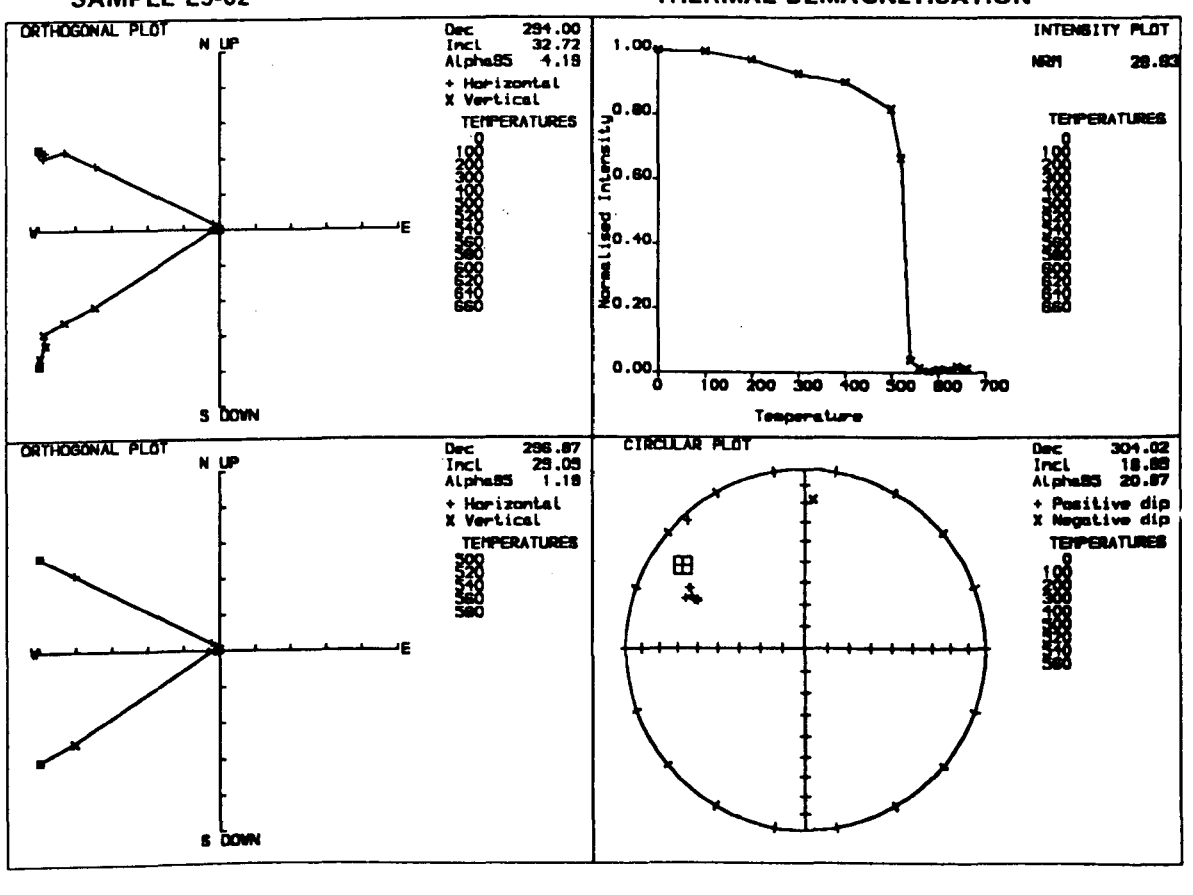
SAMPLE L9-02
THERMAL DEMAGNETISATION
ORTHOGONAL PLOT
N UP
W
E
S DOWN
Dec 294.00
Incl 32.72
Alpha95 4.19
+ Horizontal
X Vertical
TEMPERATURES
0
100
660
INTENSITY PLOT
NRM 28.83
TEMPERATURES
Normalised Intensity
1.00
0.80
0.60
0.40
0.20
0.00
0 100 200 300 400 500 600 700
Temperature
ORTHOGONAL PLOT
N UP
W
E
S DOWN
Dec 296.87
Incl 29.05
Alpha95 1.19
+ Horizontal
X Vertical
TEMPERATURES
500
520
540
560
580
CIRCULAR PLOT
Dec 304.02
Incl 18.88
Alpha95 20.87
+ Positive dip
X Negative dip
TEMPERATURES
0
100
580

(c) SAMPLE L11-03 THERMAL DEMAGNETISATION

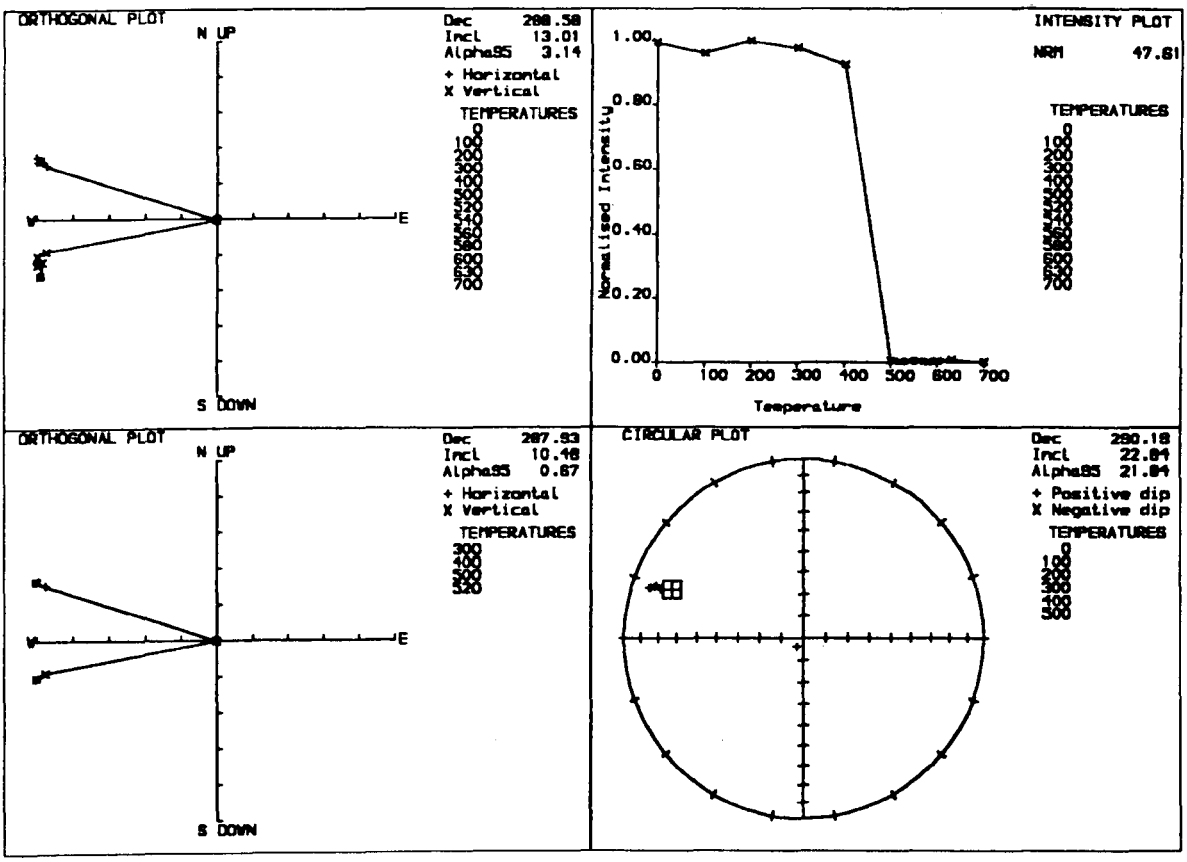

(d) SAMPLE L11-07 THERMAL DEMAGNETISATION

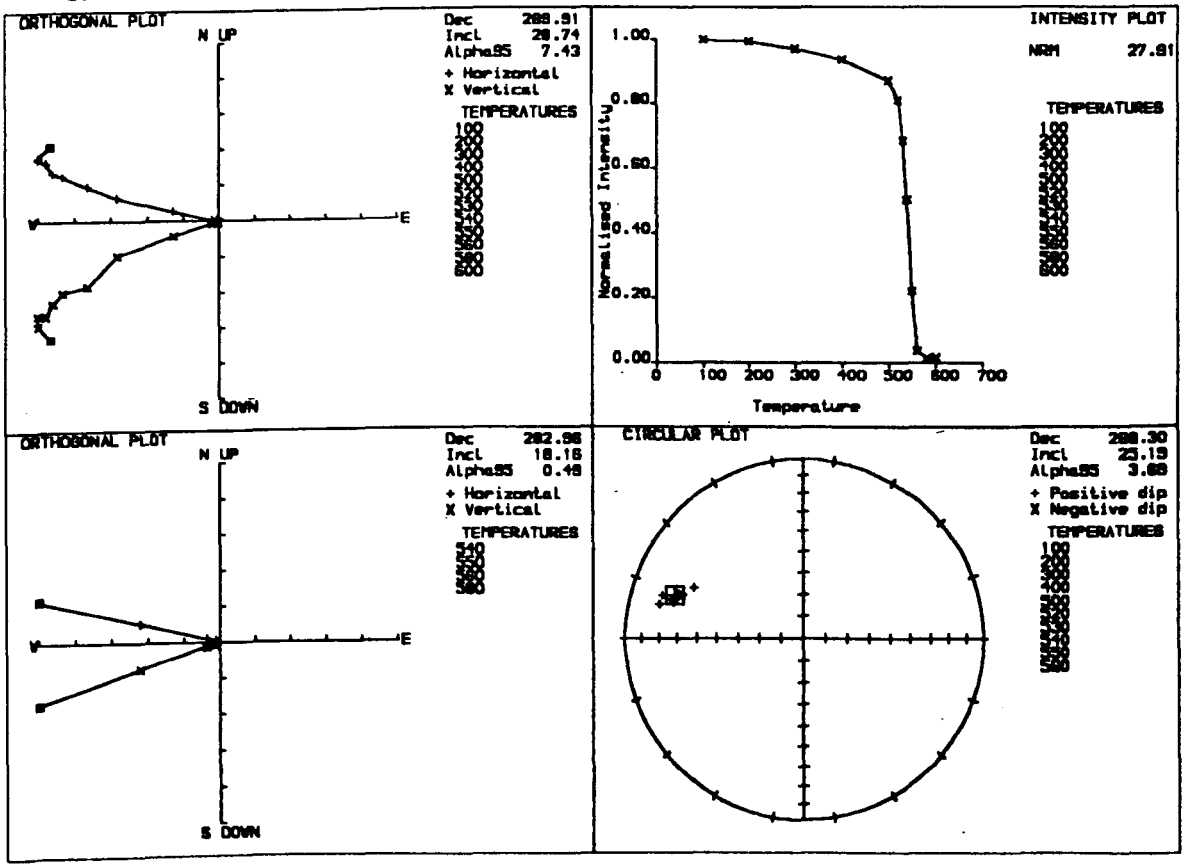

(e) SAMPLE L13-01 THERMAL DEMAGNETISATION

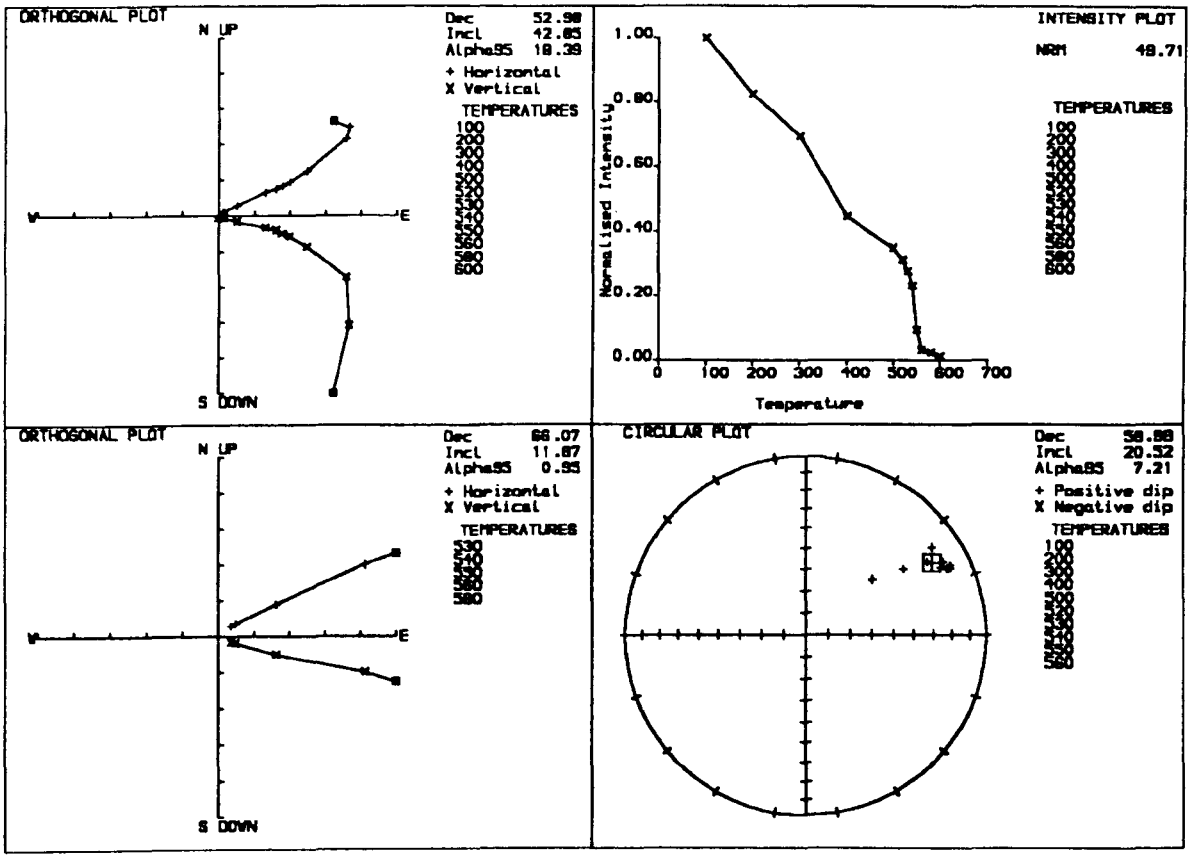

(f) SAMPLE L18-03 THERMAL DEMAGNETISATION

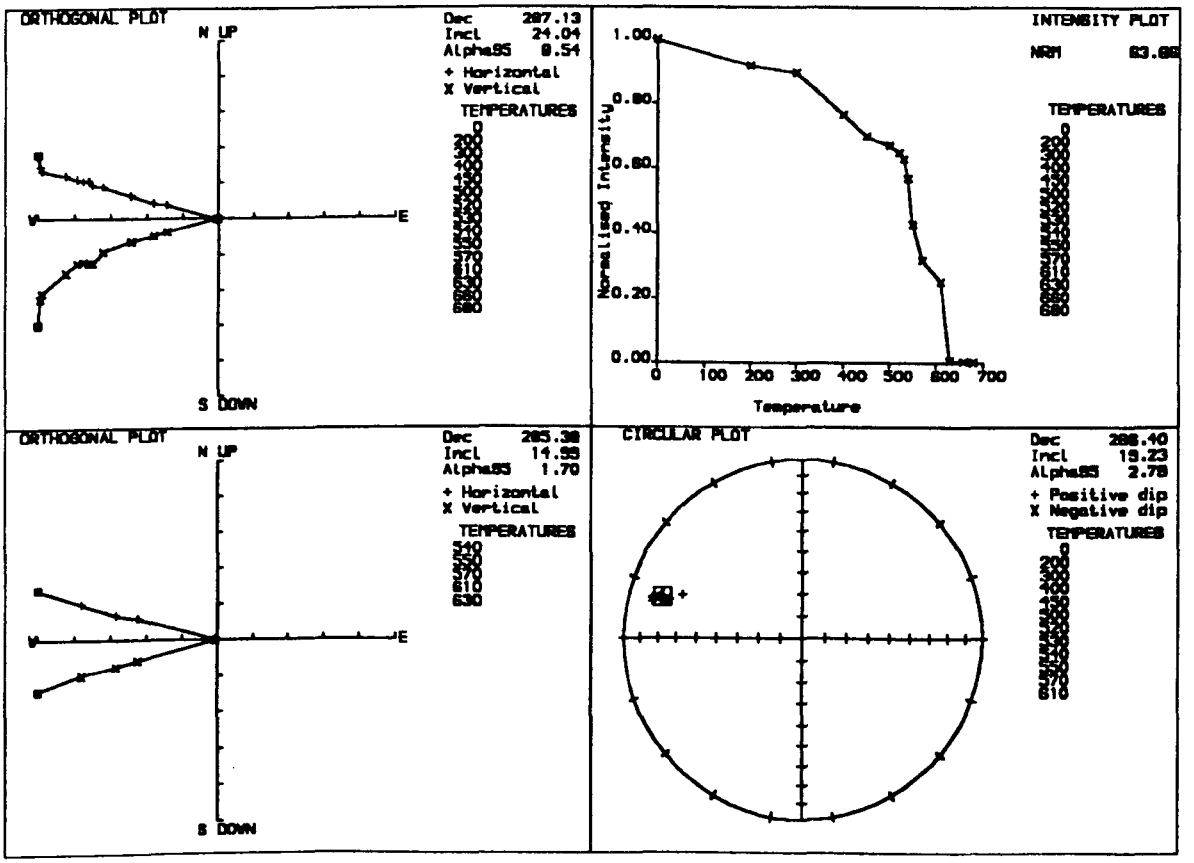

(g) SAMPLE L18-07 THERMAL DEMAGNETISATION

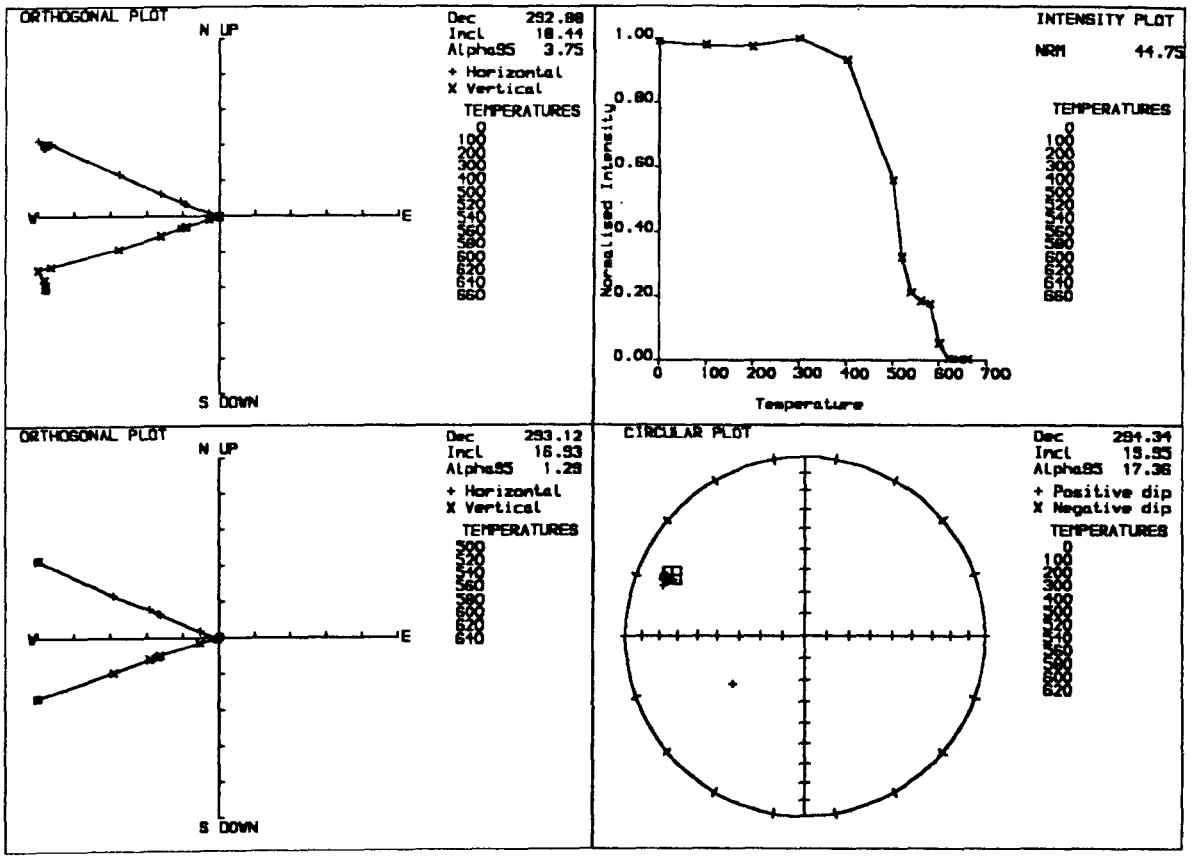

(h) SAMPLE L20-02 THERMAL DEMAGNETISATION

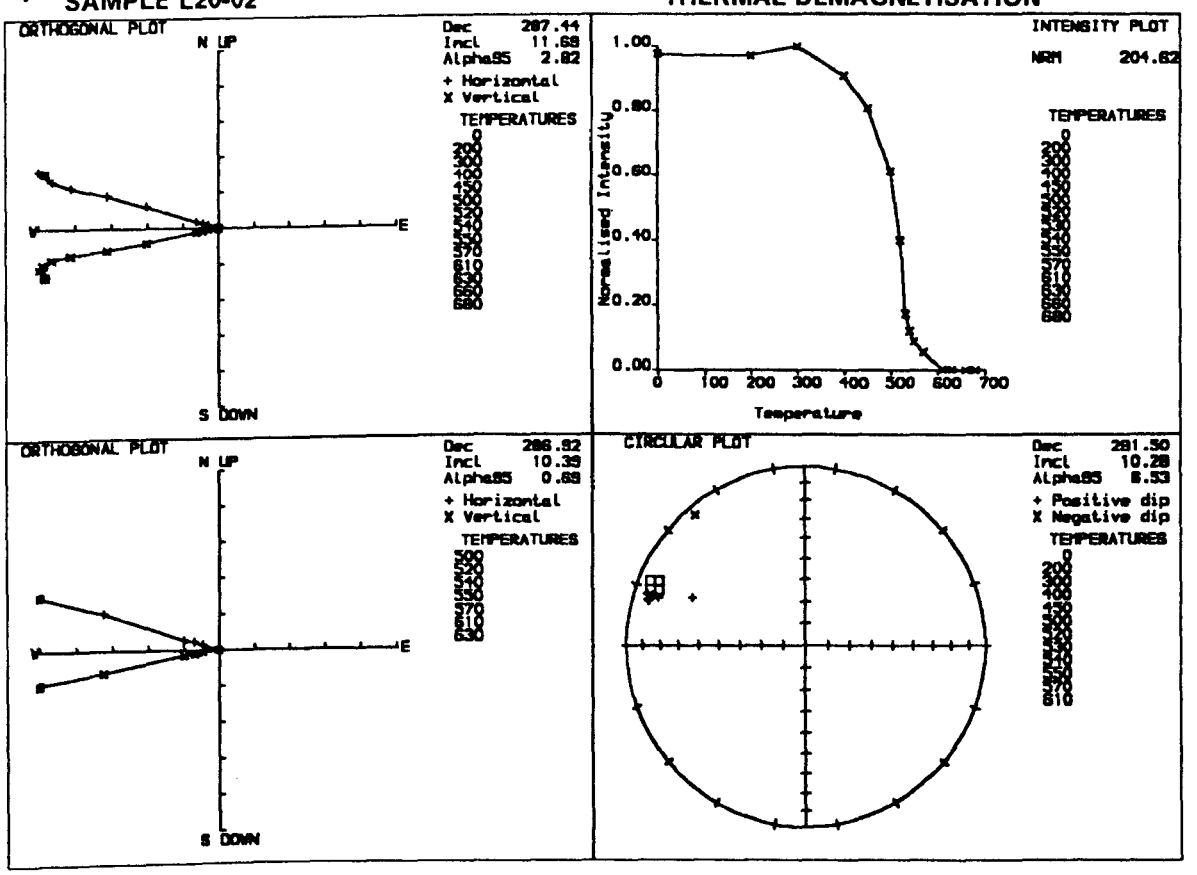

Figure 4.7 : Palaeomagnetic plots for flows with reversed (easterly, negative) magnetisation directions in the Lower (Mussartût) Lava Formation. Symbols as in Figure 4.6.

(a) SAMPLE L1-02 THERMAL DEMAGNETISATION

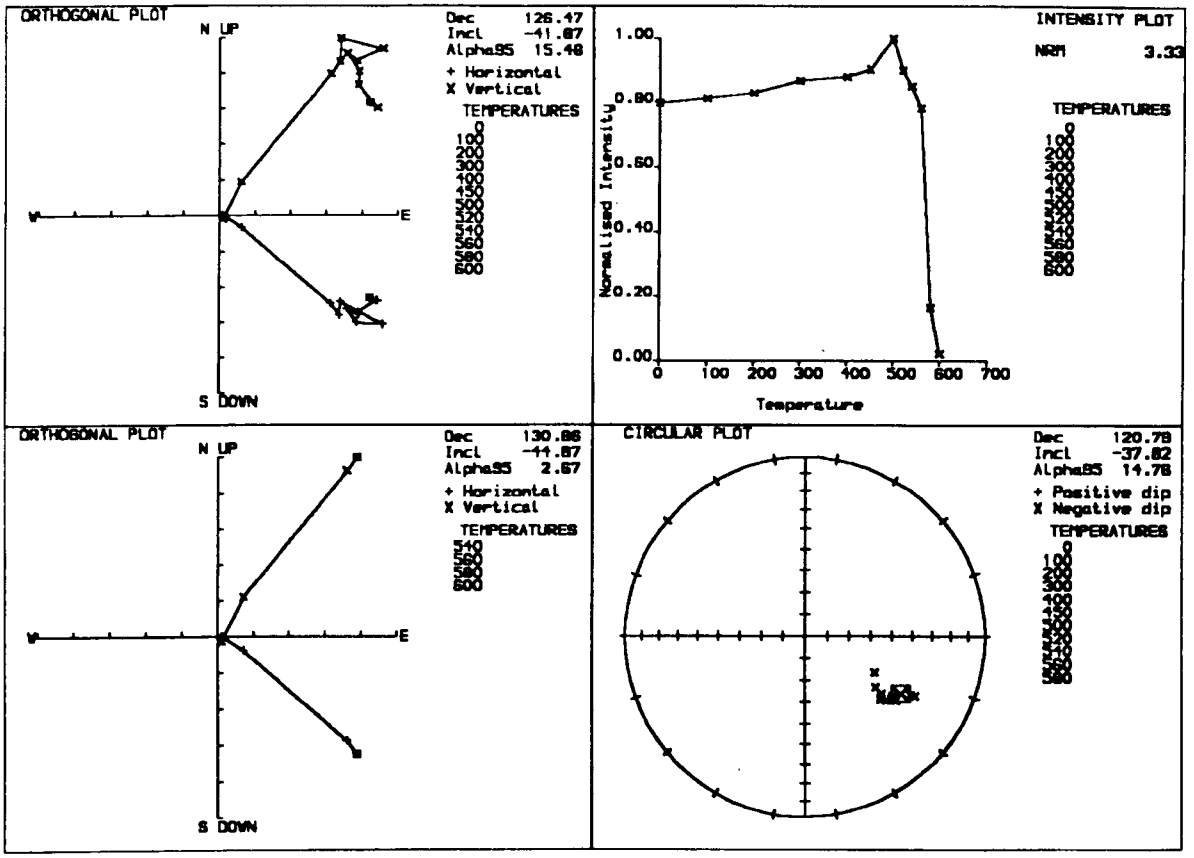

(b) SAMPLE L23-03 THERMAL DEMAGNETISATION

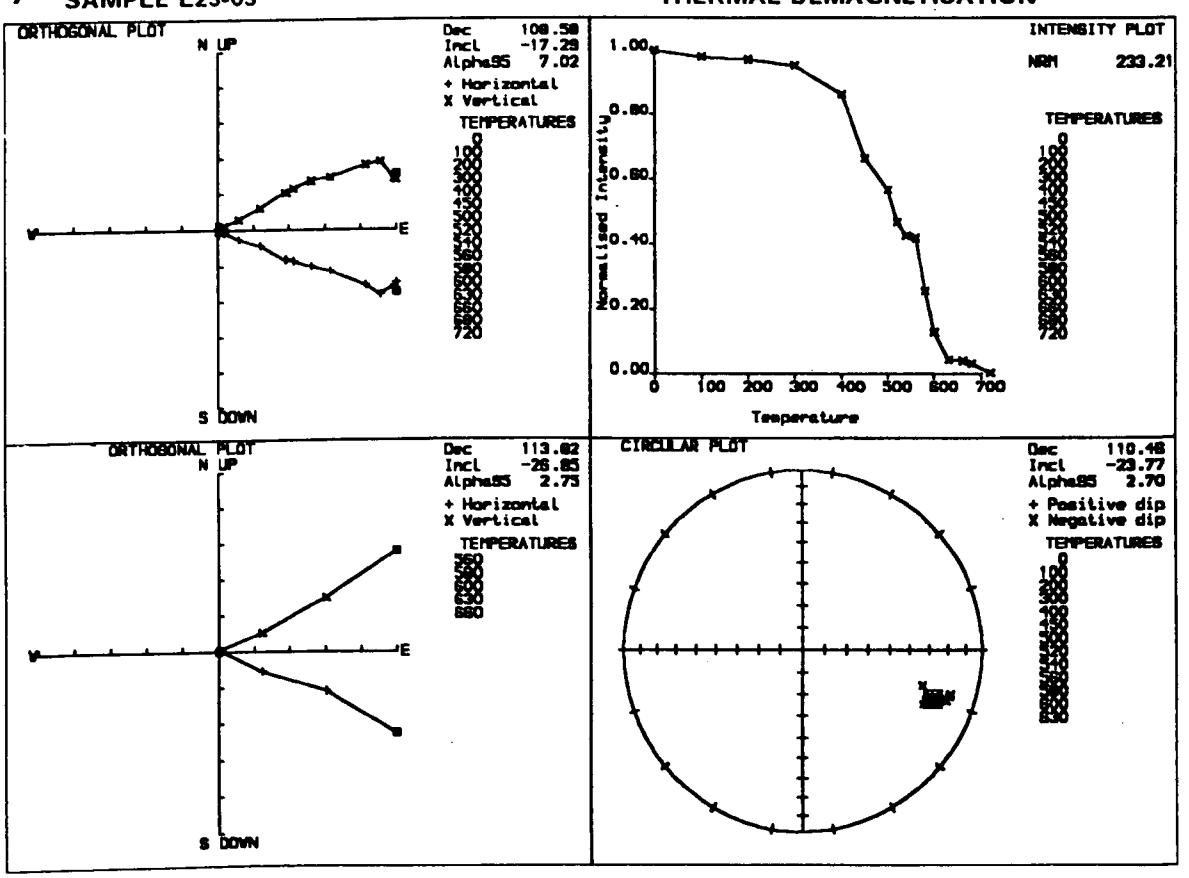

Figure 4.8 : Palaeomagnetic plots for flows from the Middle (Ulukasik) Lava Formation showing the anomalous 'A' direction of magnetisation. Symbols as in Figure 4.6.

(a) SAMPLE M2-01

THERMAL DEMAGNETISATION

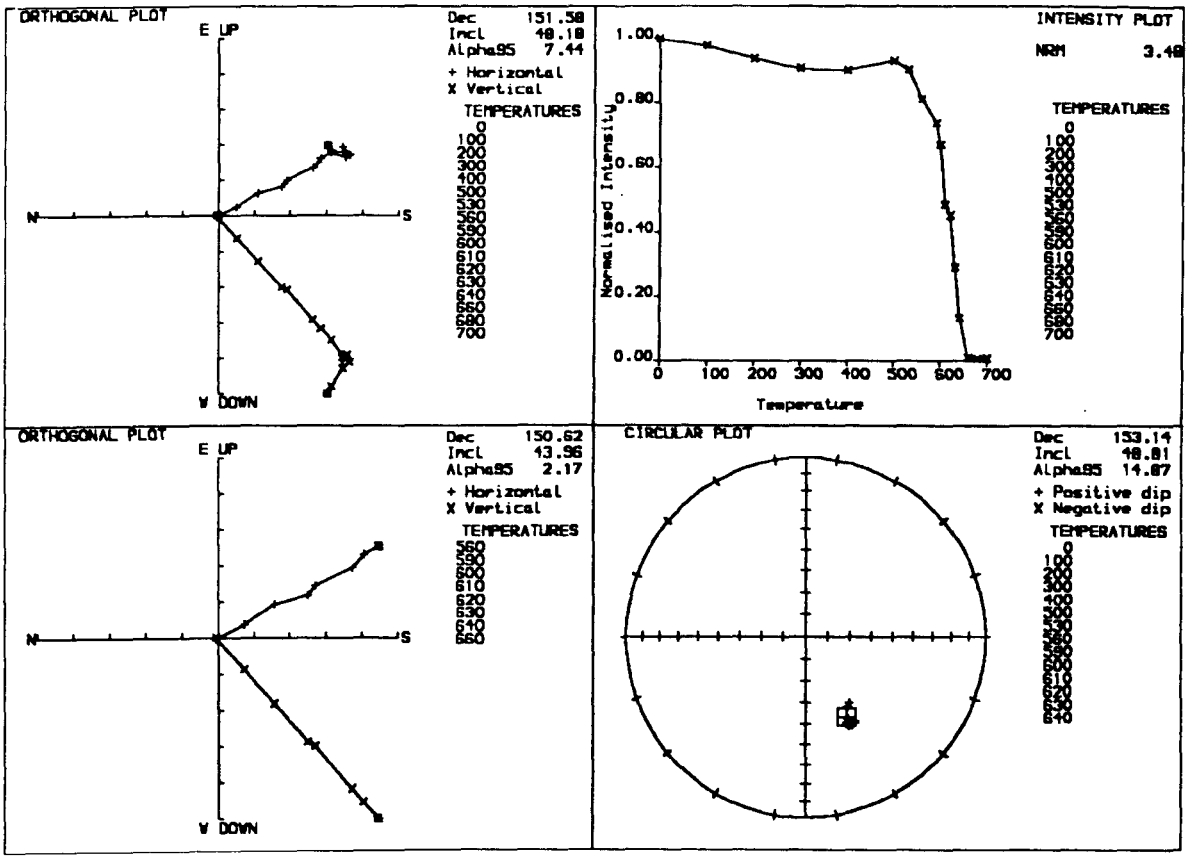

(b) SAMPLE M3-02

THERMAL DEMAGNETISATION

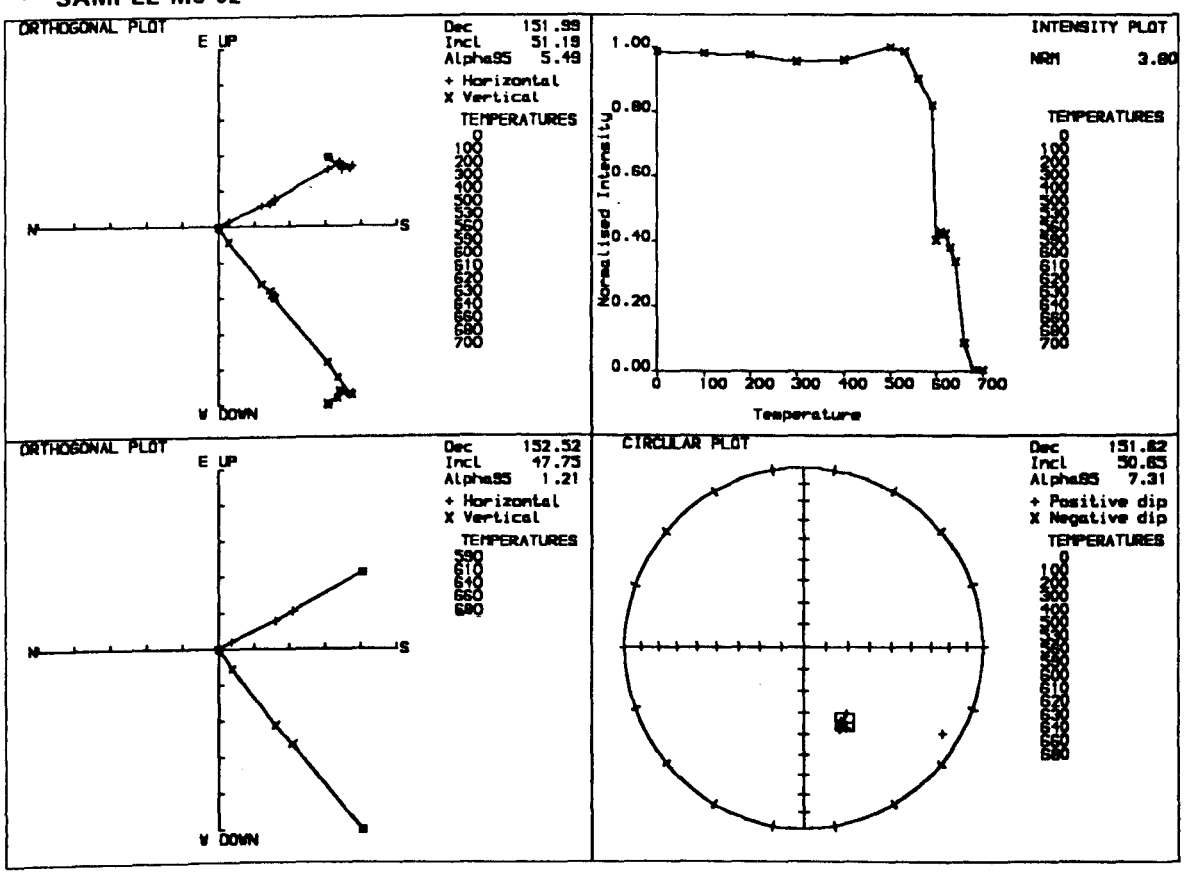

(c) SAMPLE M4-06 THERMAL DEMAGNETISATION

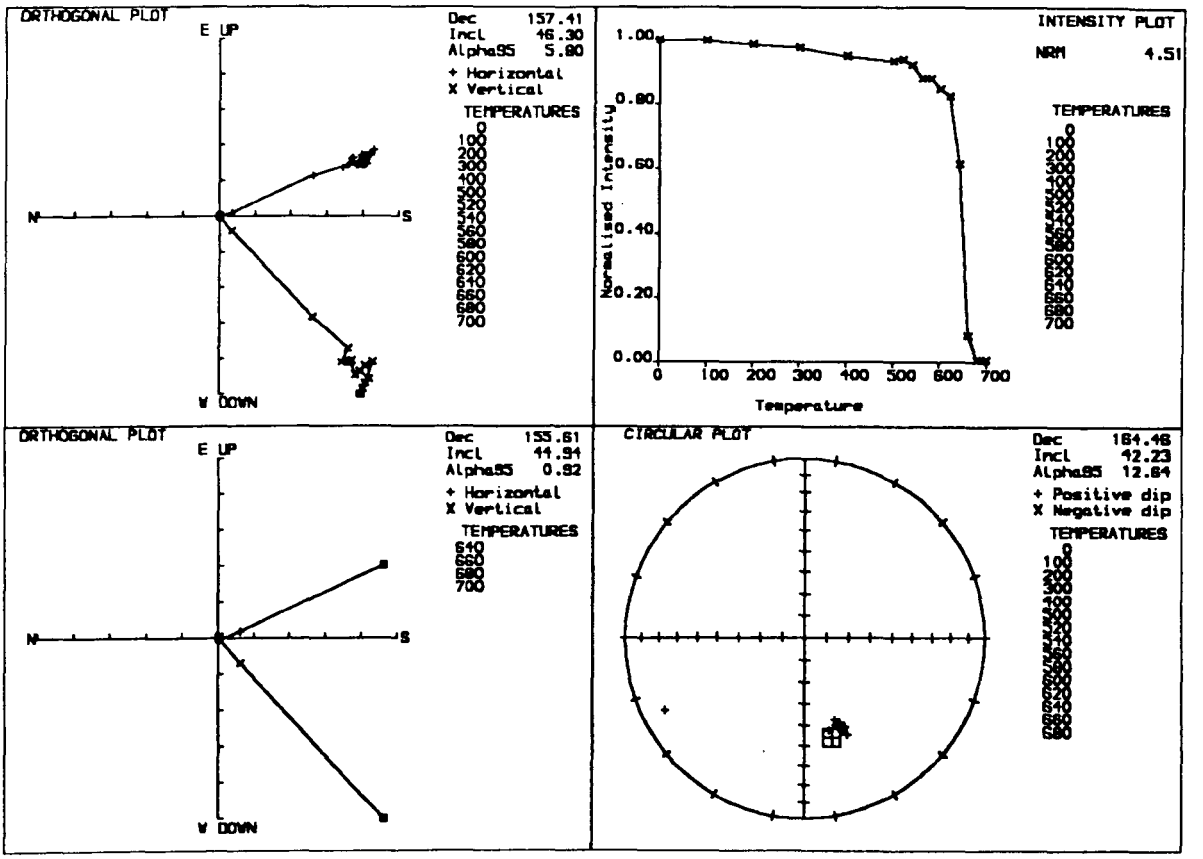

(d) SAMPLE M6-02 THERMAL DEMAGNETISATION

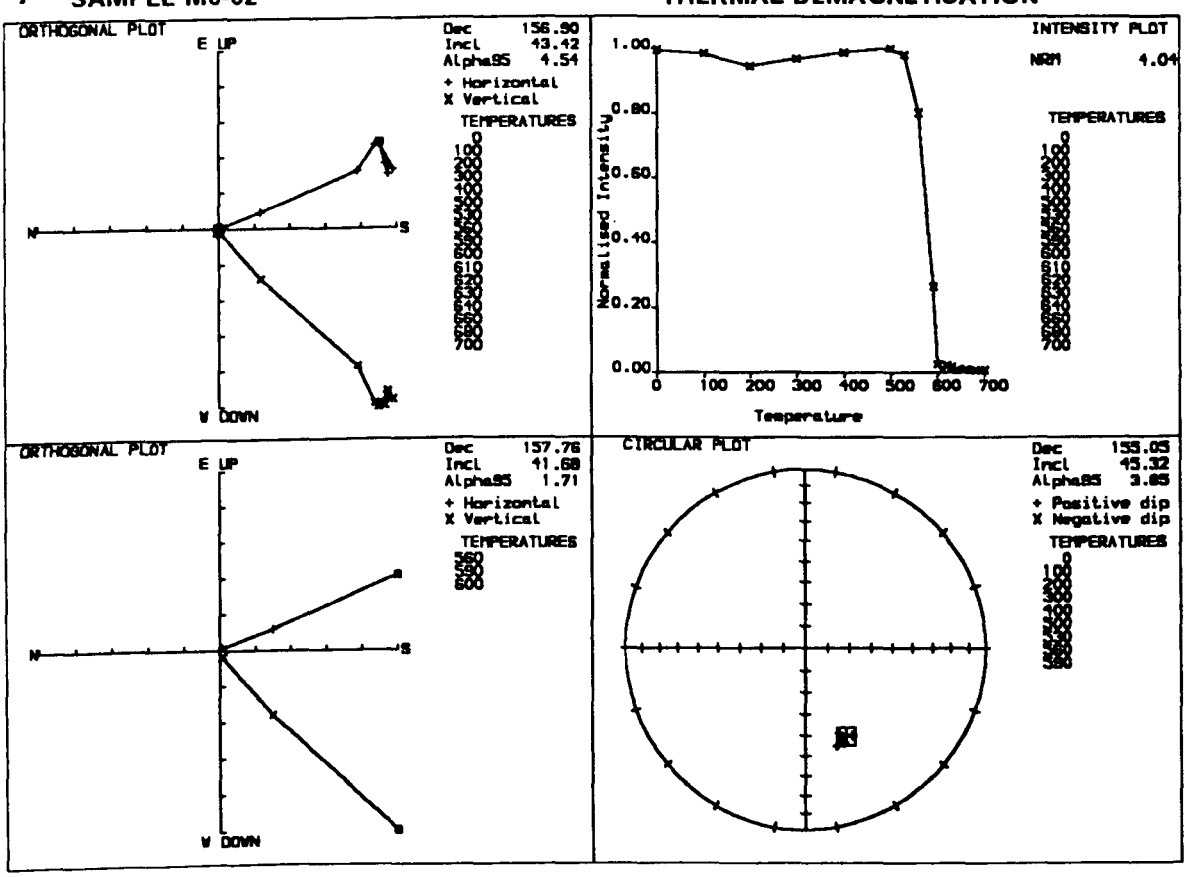

Figure 4.9 : Palaeomagnetic plots for flows from the Middle (Ulukasik) Lava Formation showing the 'B' direction of magnetisation. Symbols as in Figure 4.6.

(a) SAMPLE M14-02 THERMAL DEMAGNETISATION

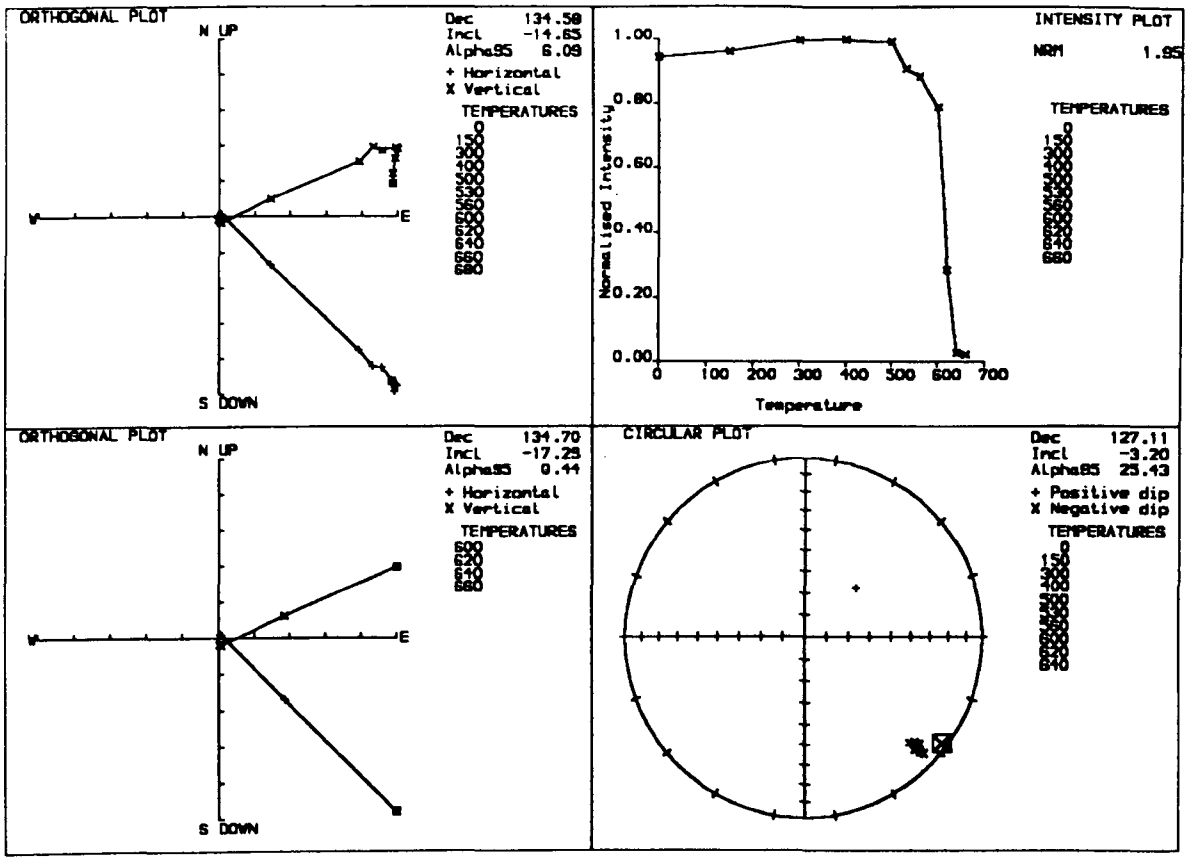

(b) SAMPLE M15-01 THERMAL DEMAGNETISATION

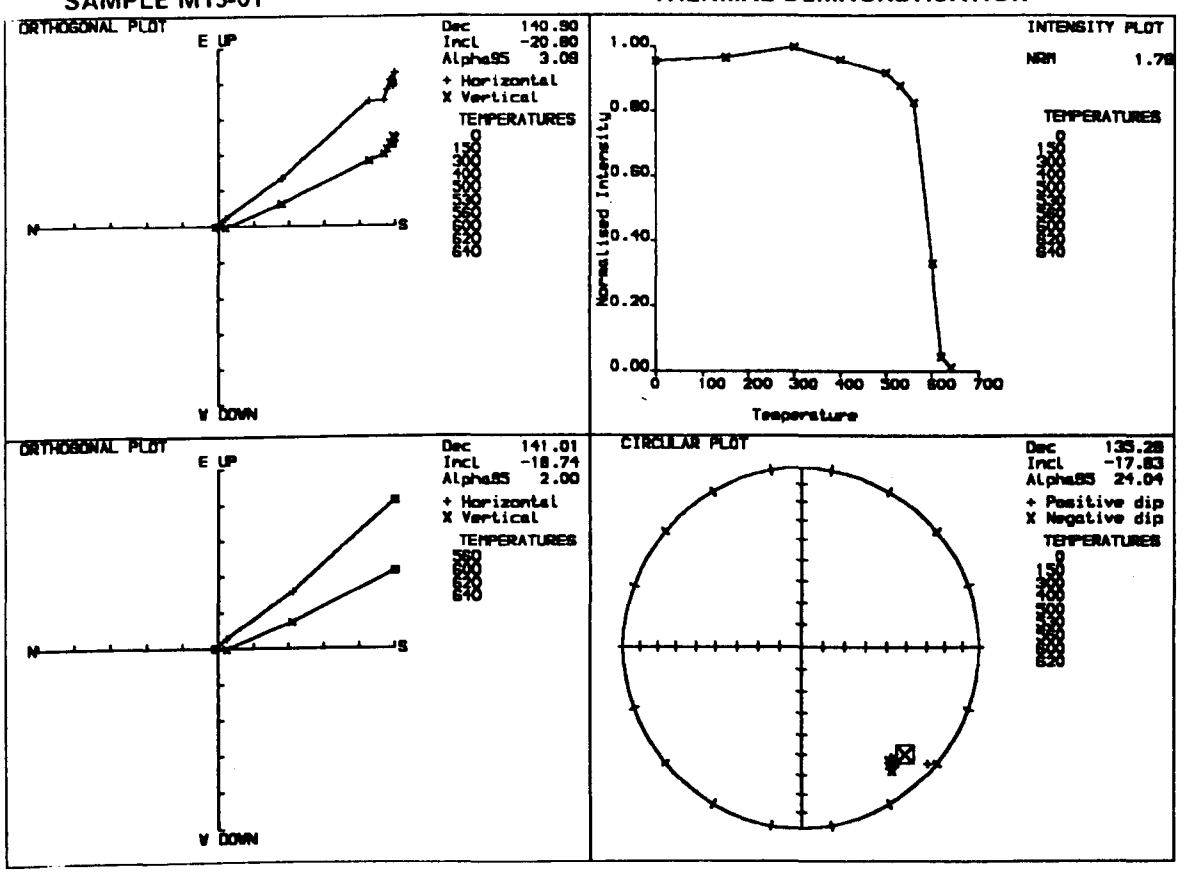

(c) SAMPLE M13-02 THERMAL DEMAGNETISATION

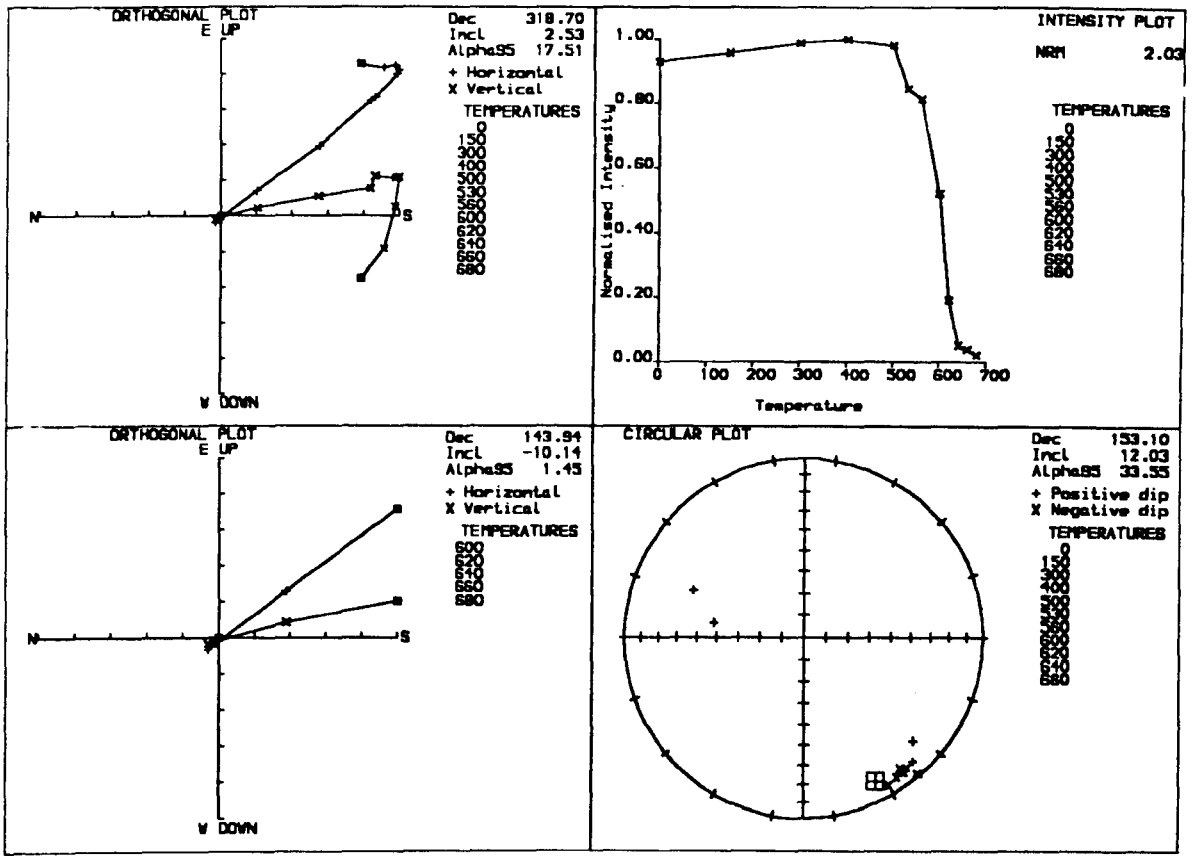

(d) SAMPLE M10-01 THERMAL DEMAGNETISATION

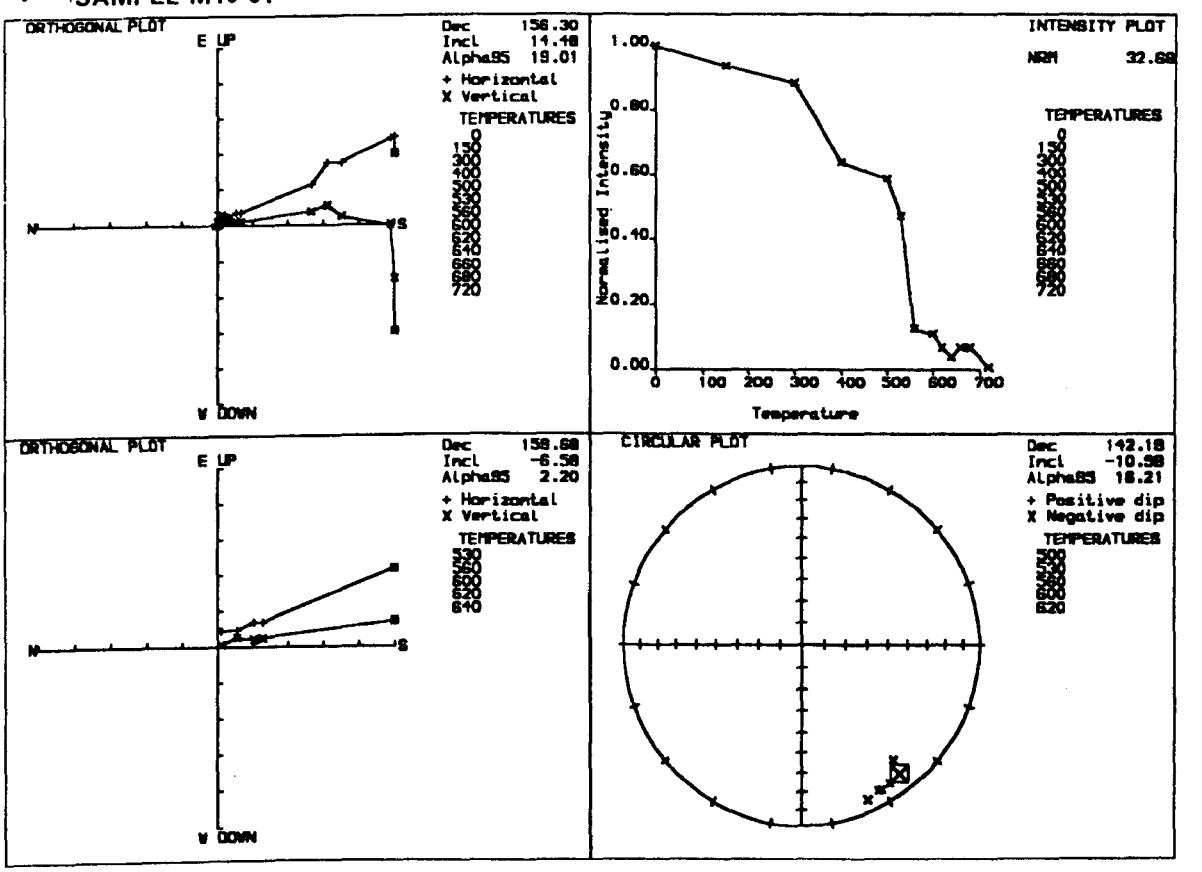

Figure 4.10 : Palaeomagnetic plots for flows from the Middle Lava Formation which have westerly directions.

(a) SAMPLE M17-03 THERMAL DEMAGNETISATION

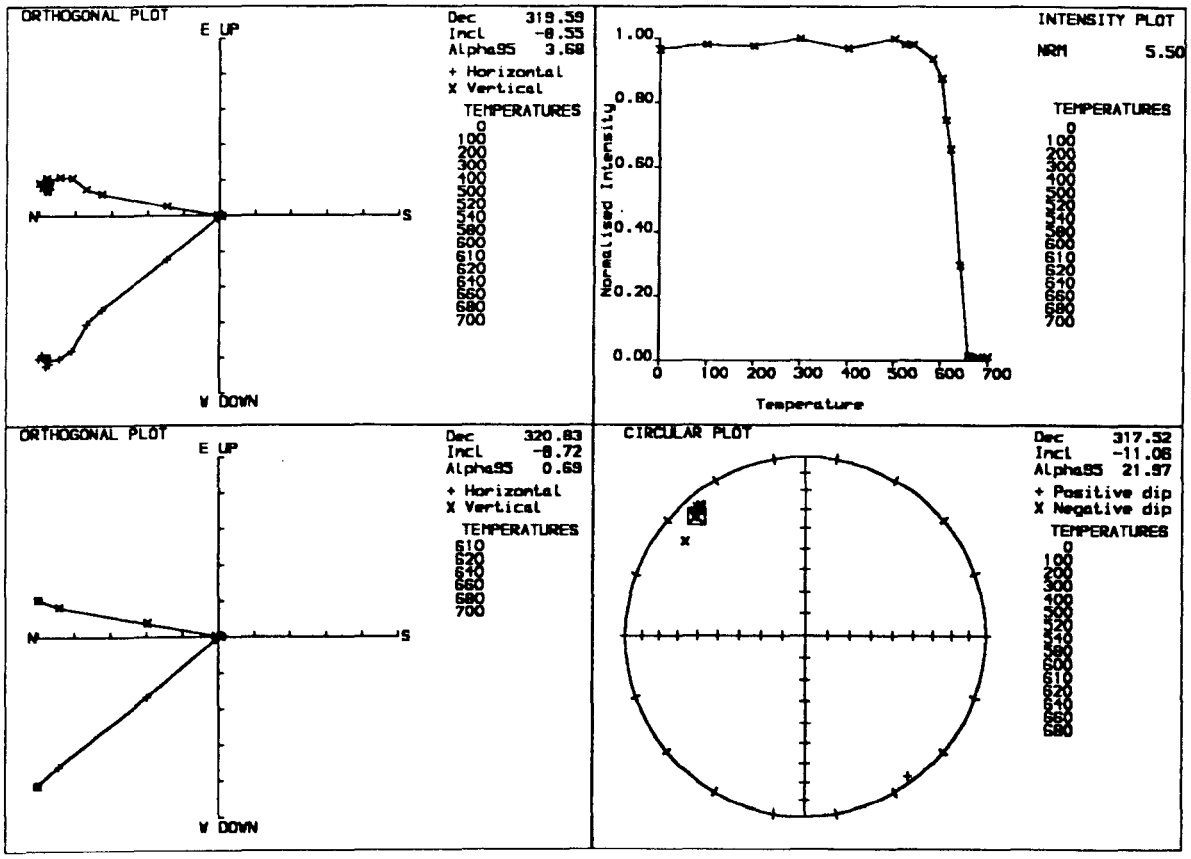

(b) SAMPLE M18-02 THERMAL DEMAGNETISATION

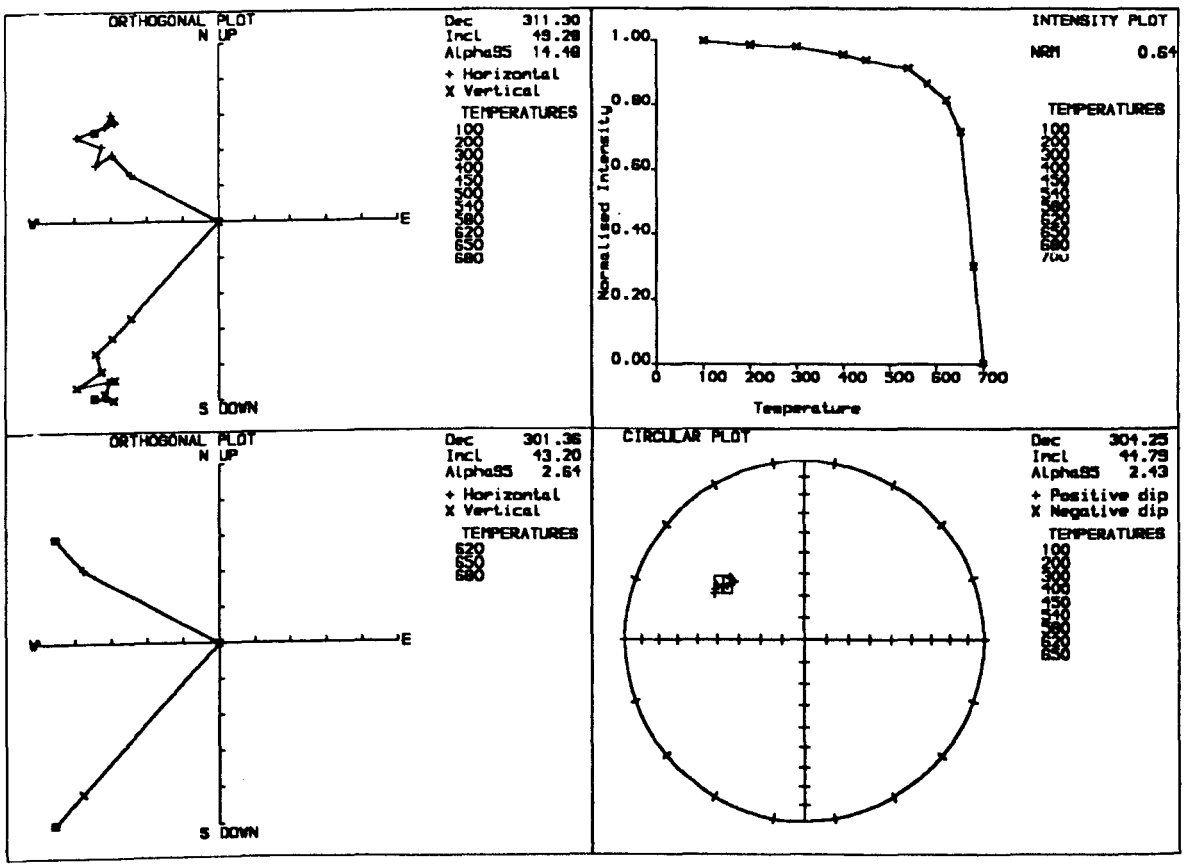

Figure 4.11 : Palaeomagnetic plots for flows with normal (westerly, positive) magnetisation directions in the Upper (Ilímaussaq) Lava Formation. Symbols as in Figure 4.6.

(a) SAMPLE U3-01 THERMAL DEMAGNETISATION

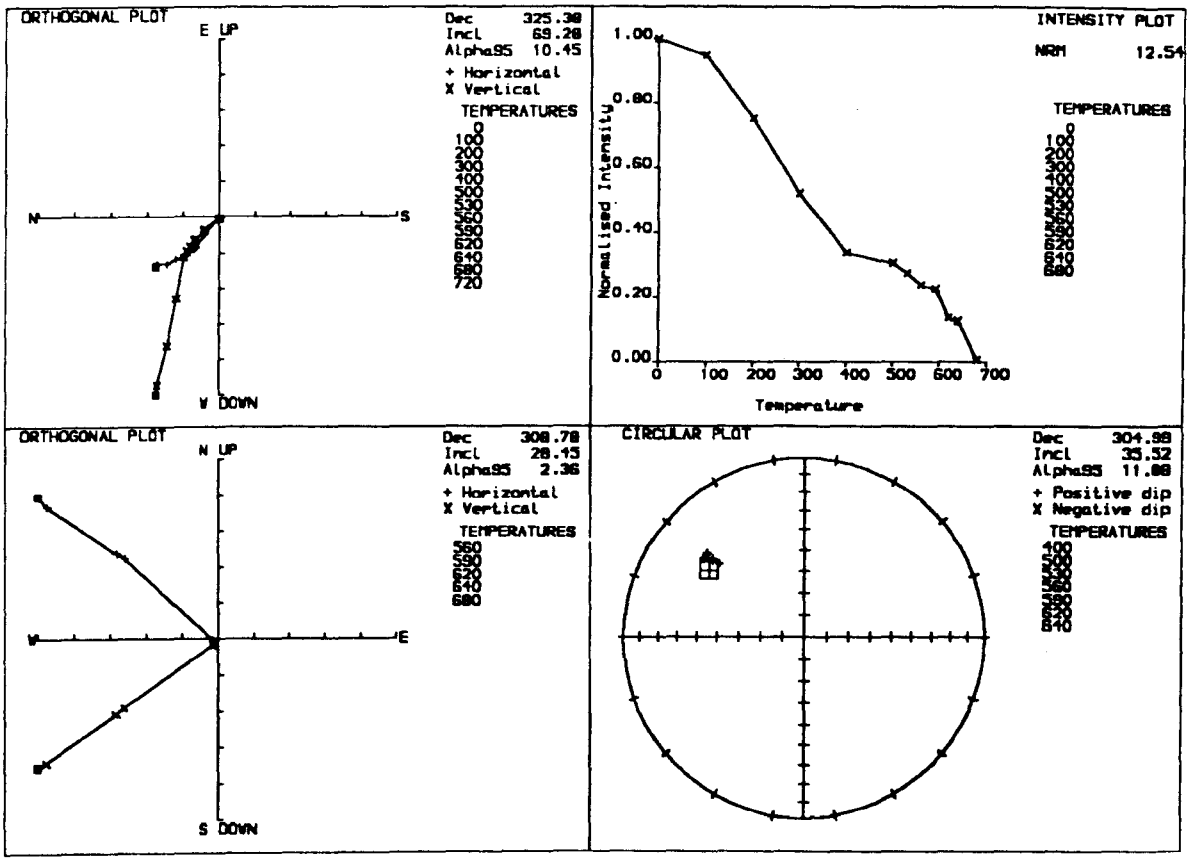

(b) SAMPLE U5-01 THERMAL DEMAGNETISATION

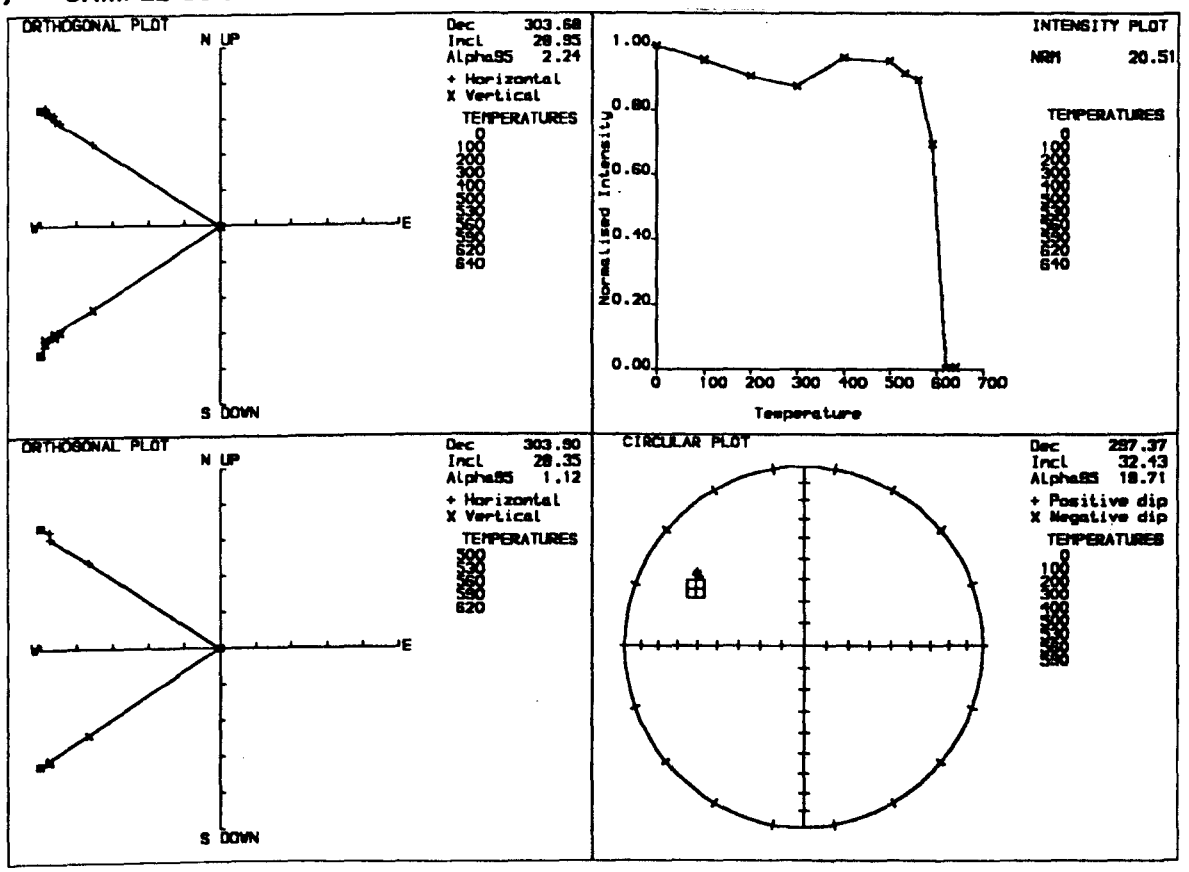

(c) SAMPLE U18-06 THERMAL DEMAGNETISATION

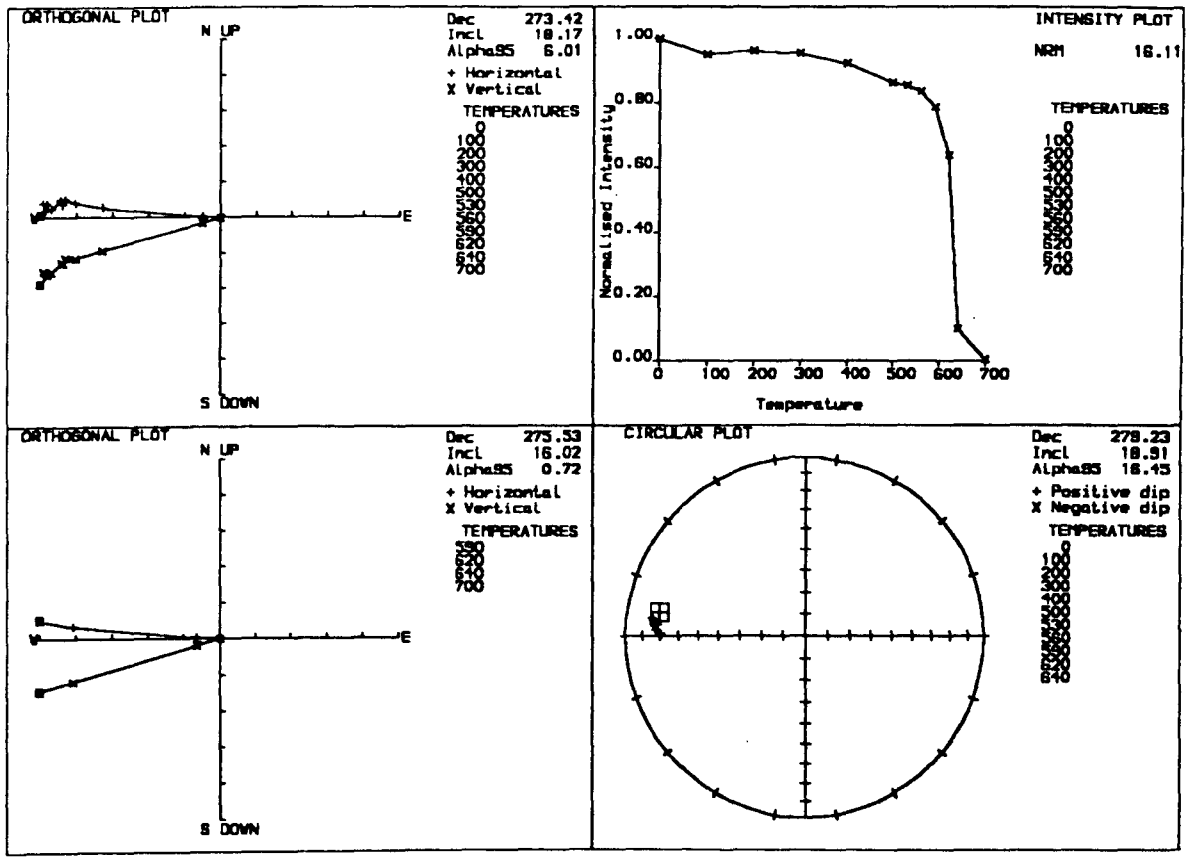

(d) SAMPLE U19-04 THERMAL DEMAGNETISATION

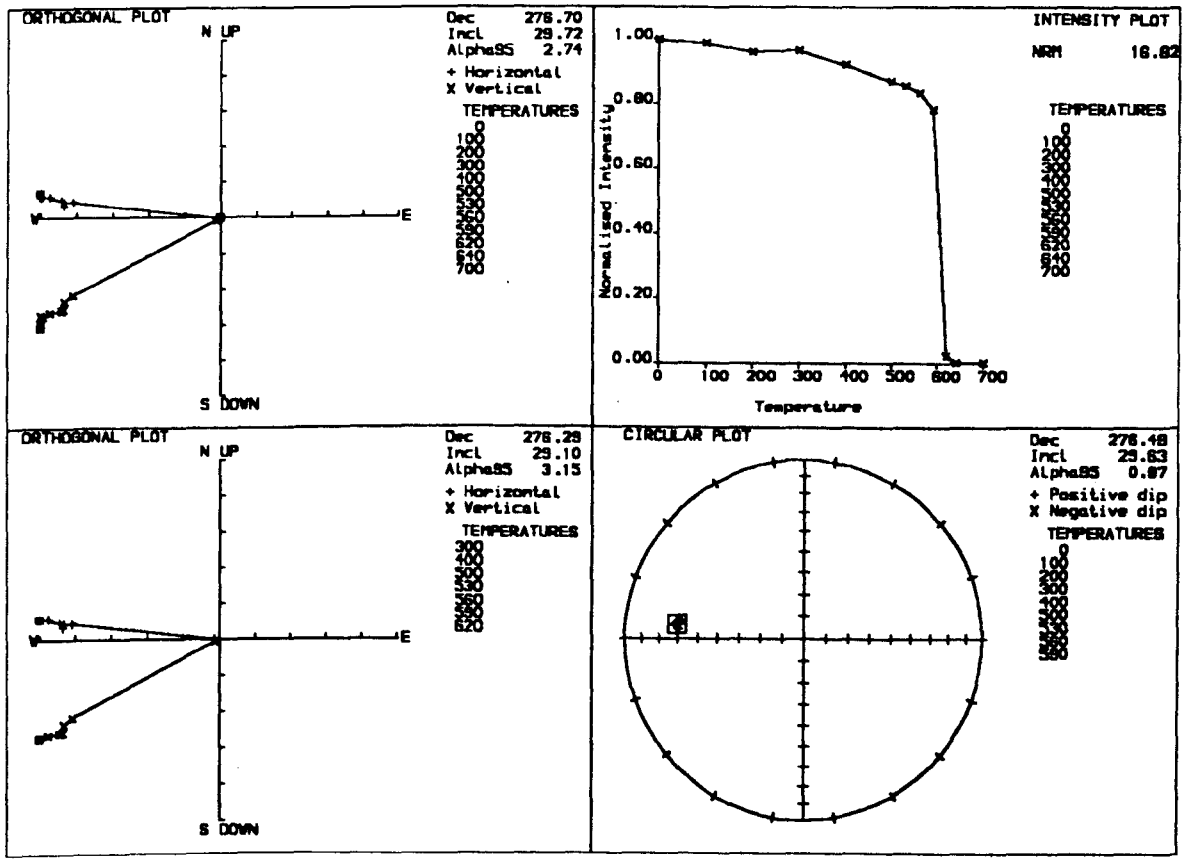

(e) SAMPLE U23-06 THERMAL DEMAGNETISATION

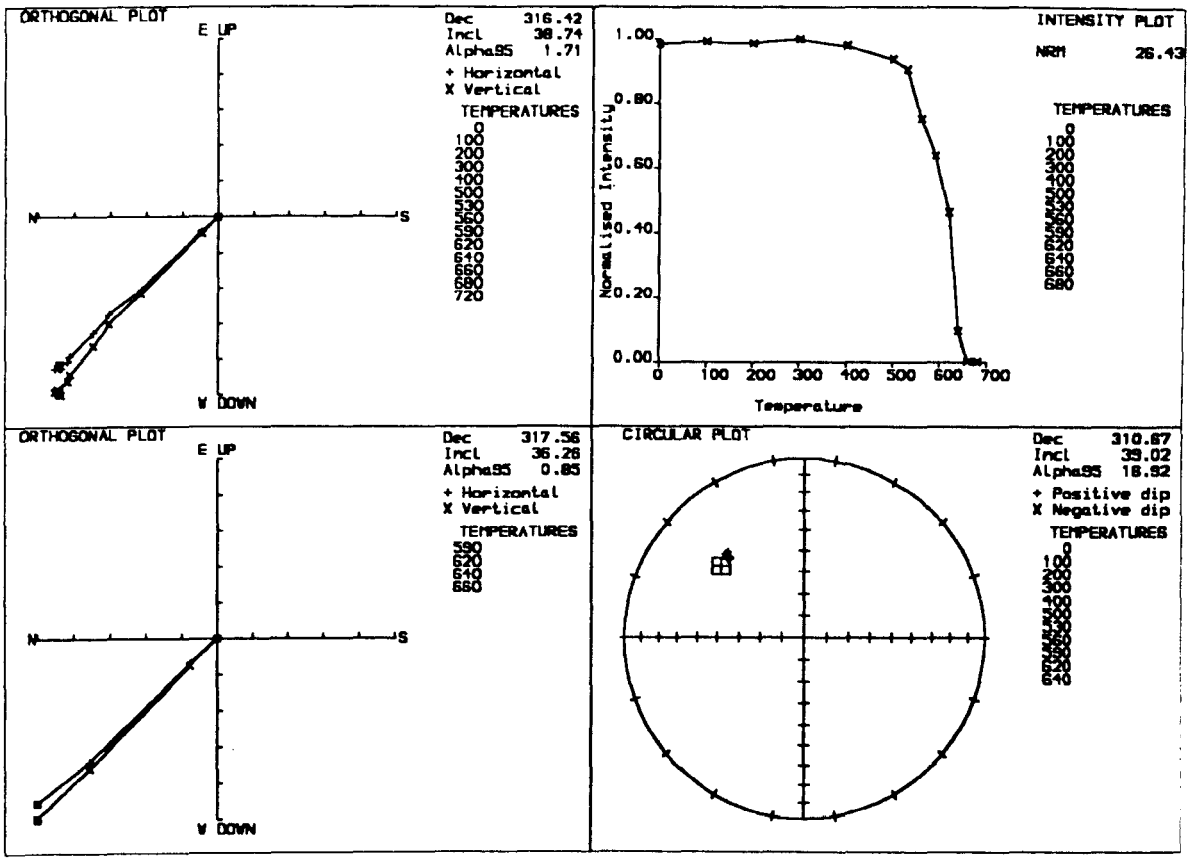

(f) SAMPLE U25-04 THERMAL DEMAGNETISATION

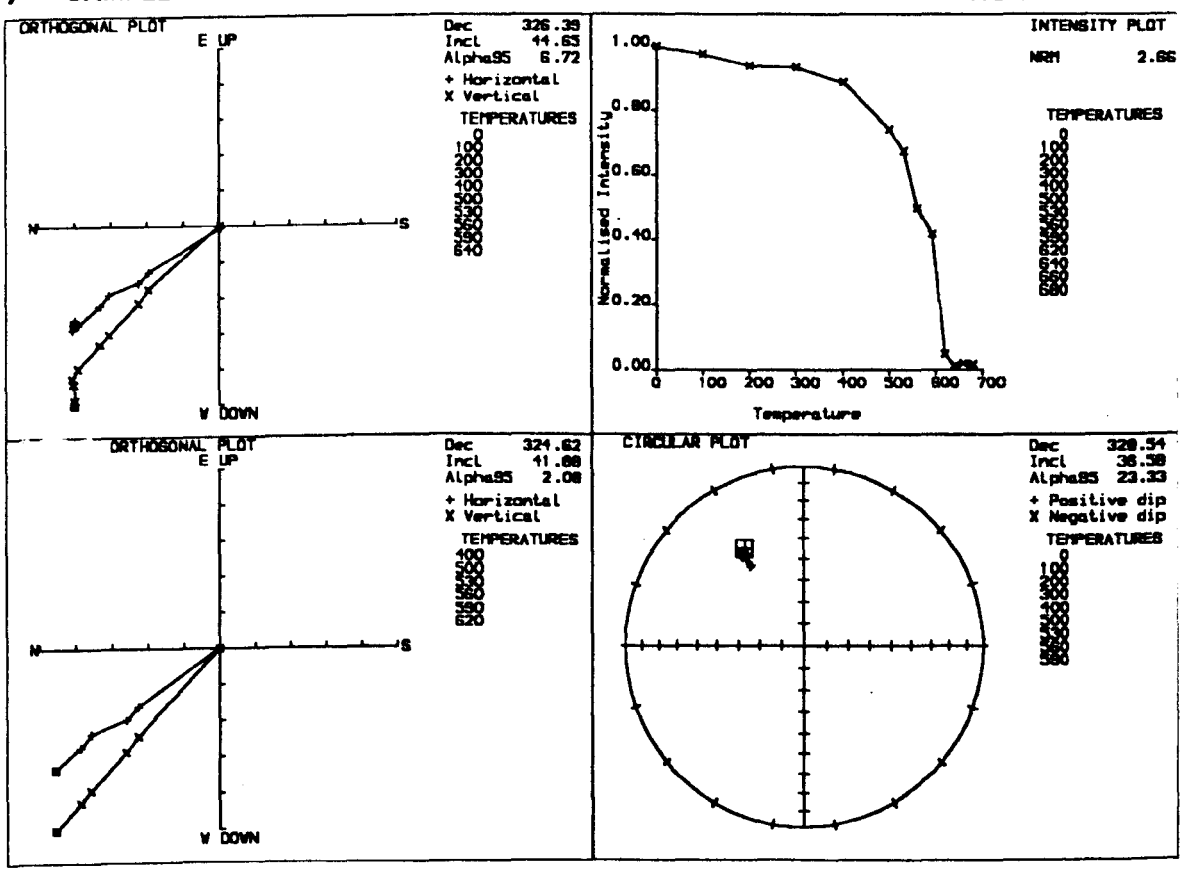

Figure 4.12 : Palaeomagnetic plots for flows with reversed (easterly, negative) magnetisation directions in the Upper (Ilímaussaq) Lava Formation. Symbols as in Figure 4.6.

(a) SAMPLE U10-01 THERMAL DEMAGNETISATION

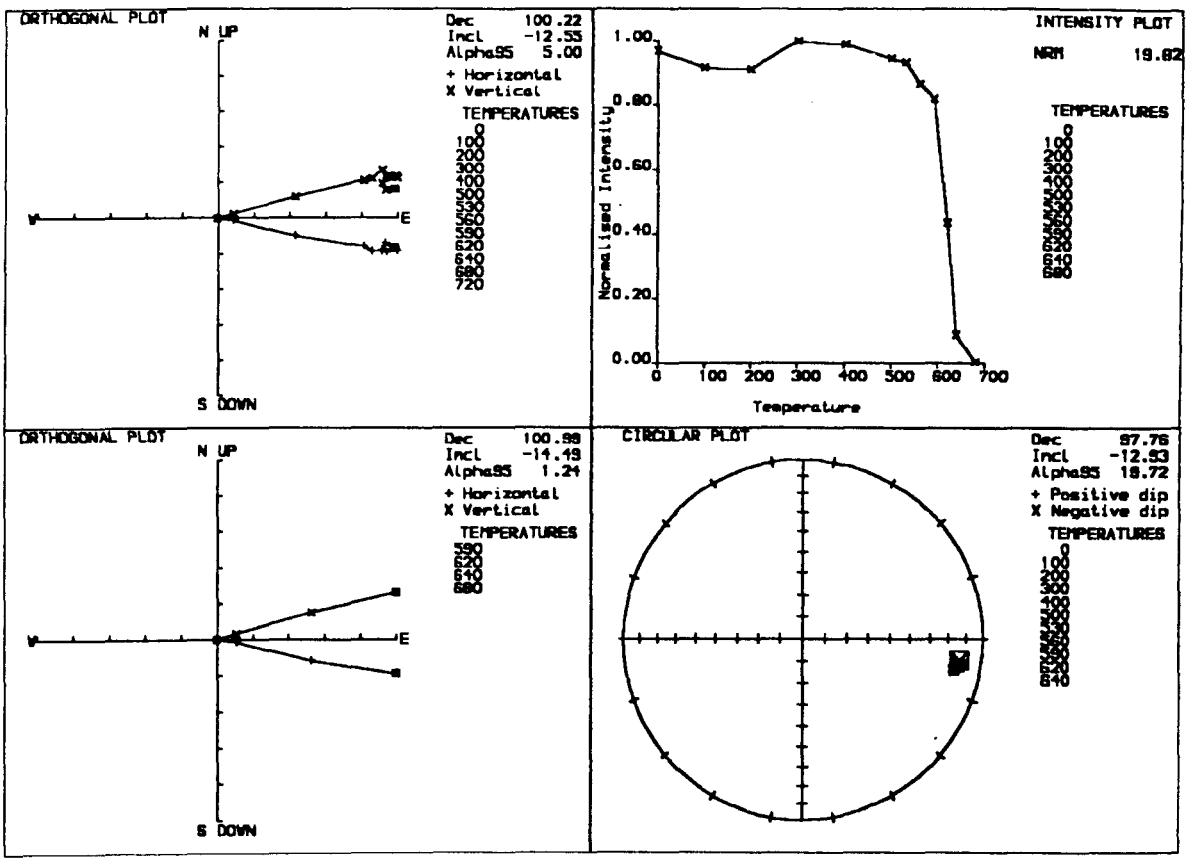

(b) SAMPLE U10-05 THERMAL DEMAGNETISATION

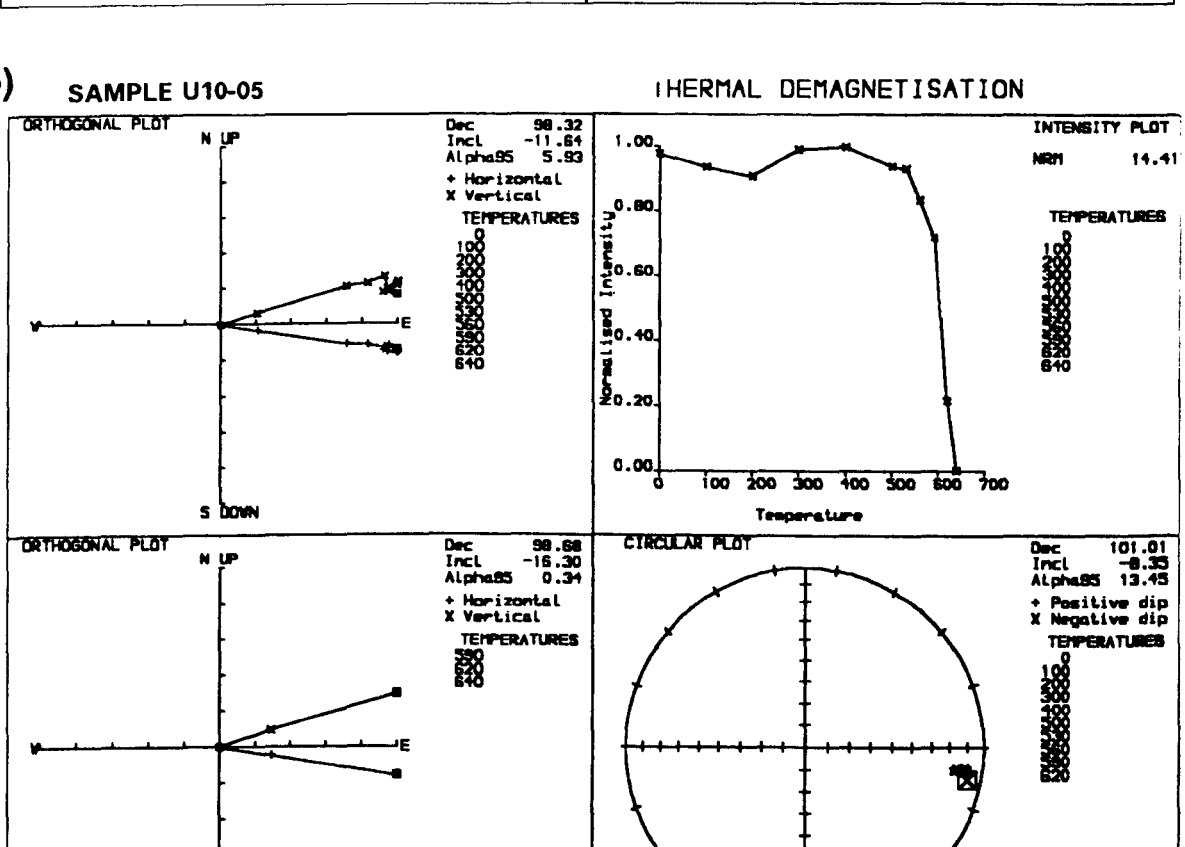

(c) SAMPLE U12-02 THERMAL DEMAGNETISATION

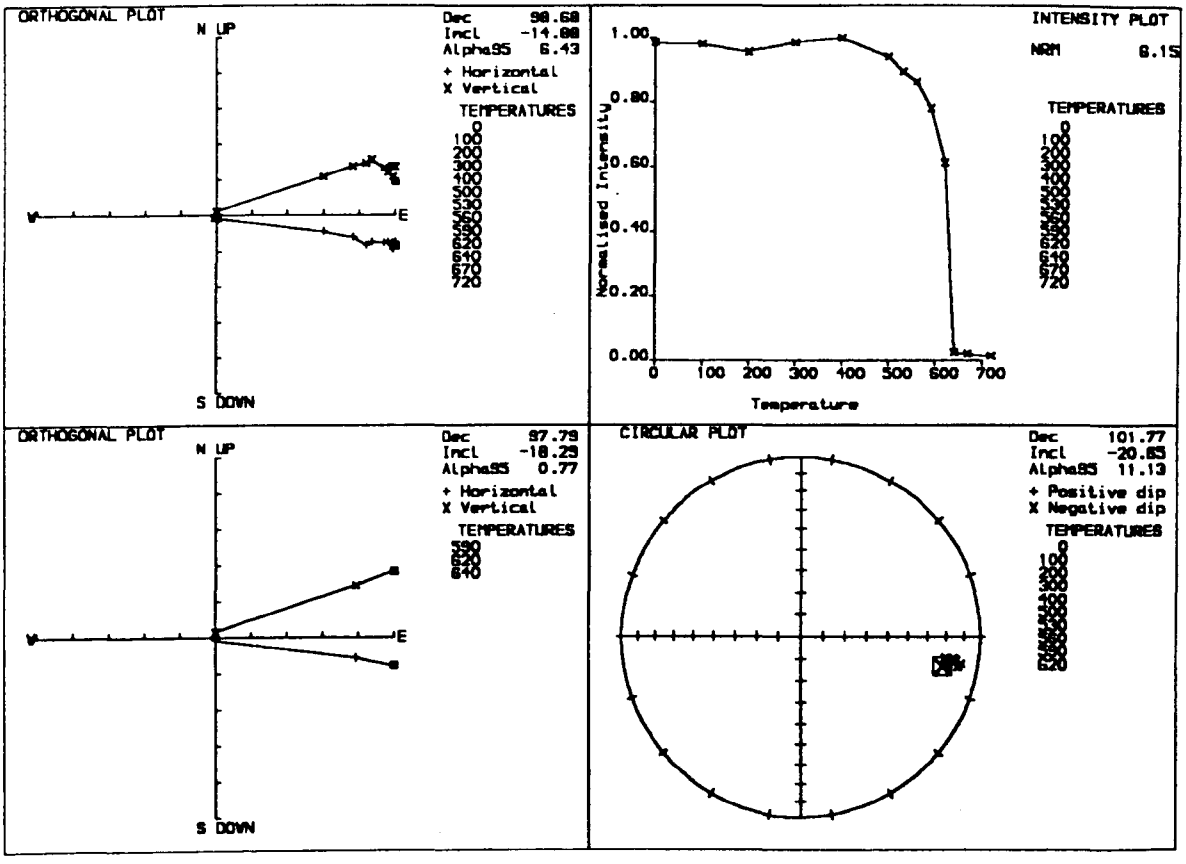

(d) SAMPLE U13-03 THERMAL DEMAGNETISATION

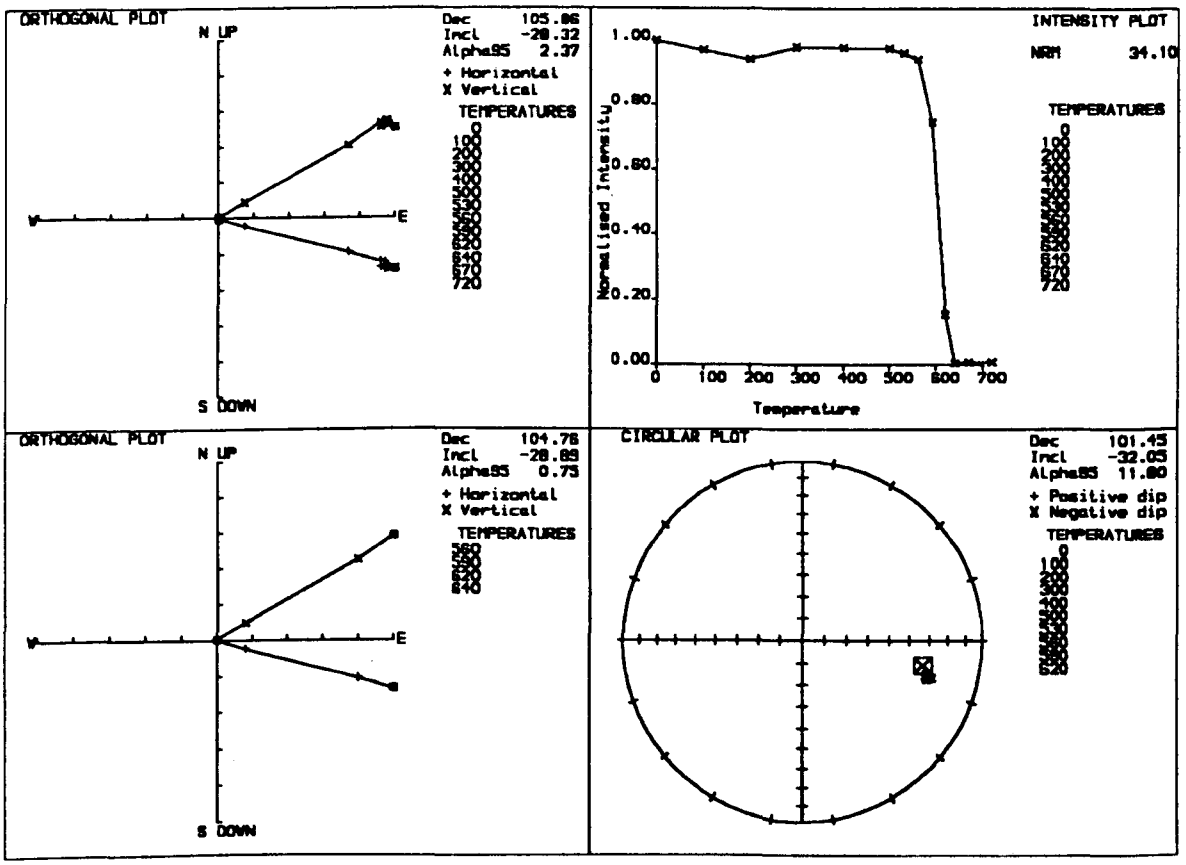

(e) SAMPLE U14-02 THERMAL DEMAGNETISATION

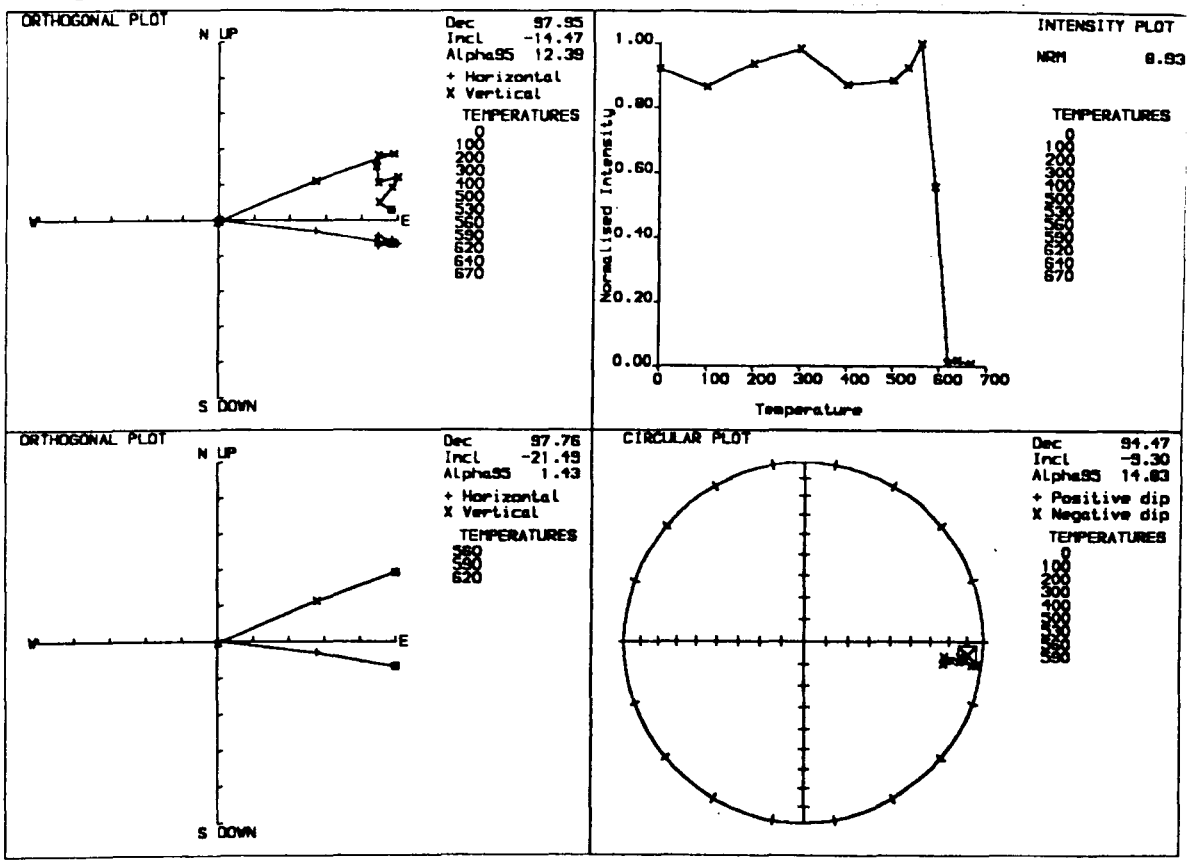

(f) SAMPLE U21-01 THERMAL DEMAGNETISATION

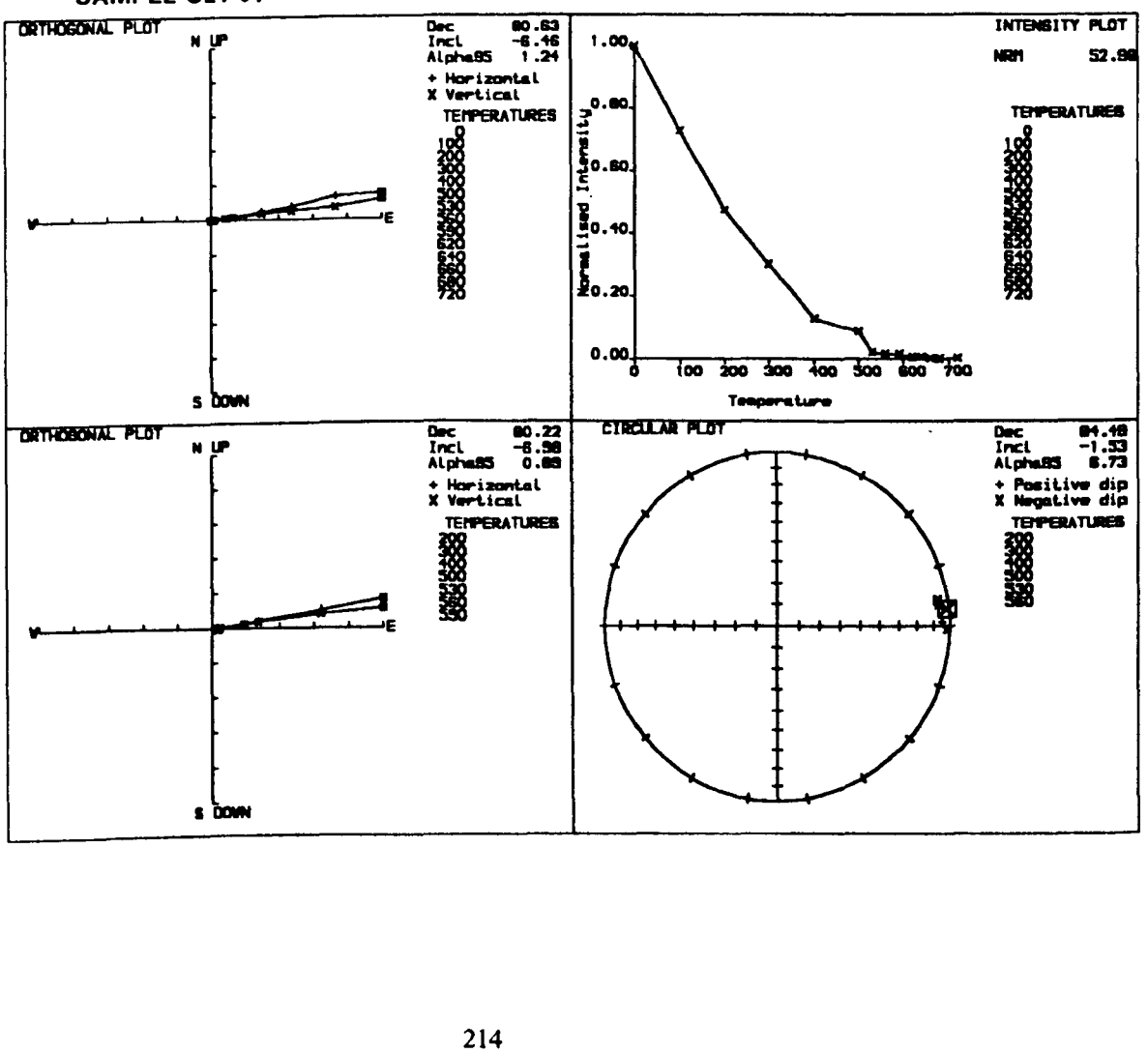

Figure 4.13 : Palaeomagnetic plots indicating (a) and (b) multi-component magnetisations and (c) and (d) completely overprinted magnetisation directions in flows from the Upper Lava Formation adjacent to the Ilímaussaq intrusion. Symbols as in Figure 4.6.

(a) SAMPLE U15-03 THERMAL DEMAGNETISATION

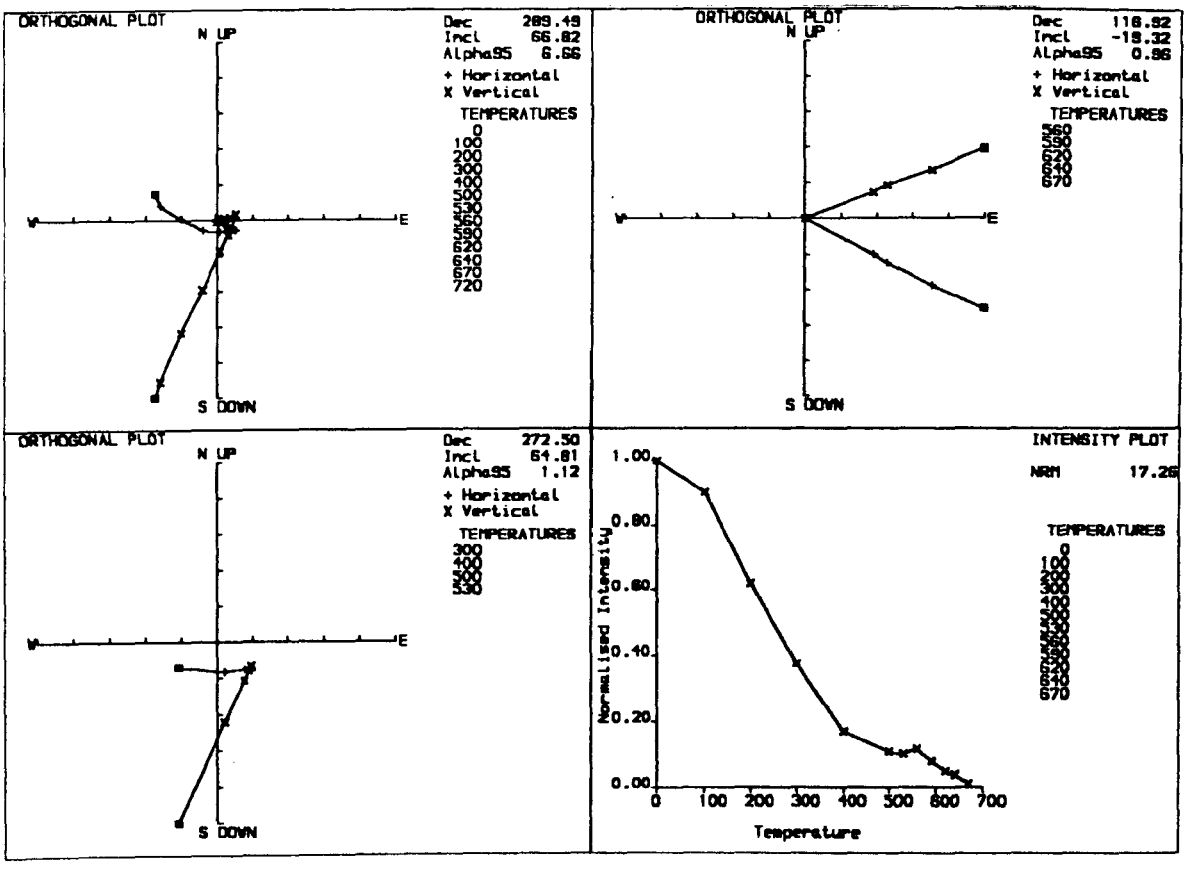

(b) SAMPLE U31-03 THERMAL DEMAGNETISATION

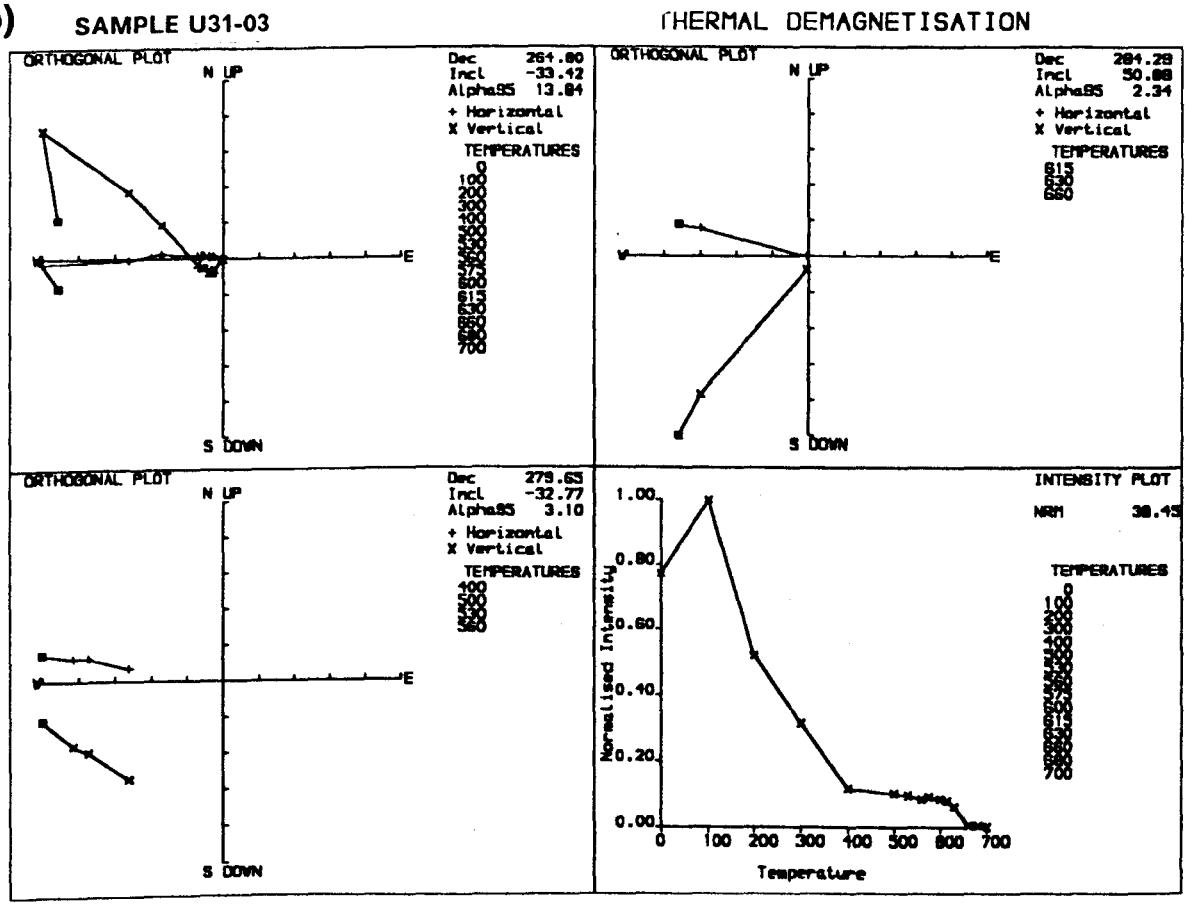

(c) SAMPLE U29-02

THERMAL DEMAGNETISATION

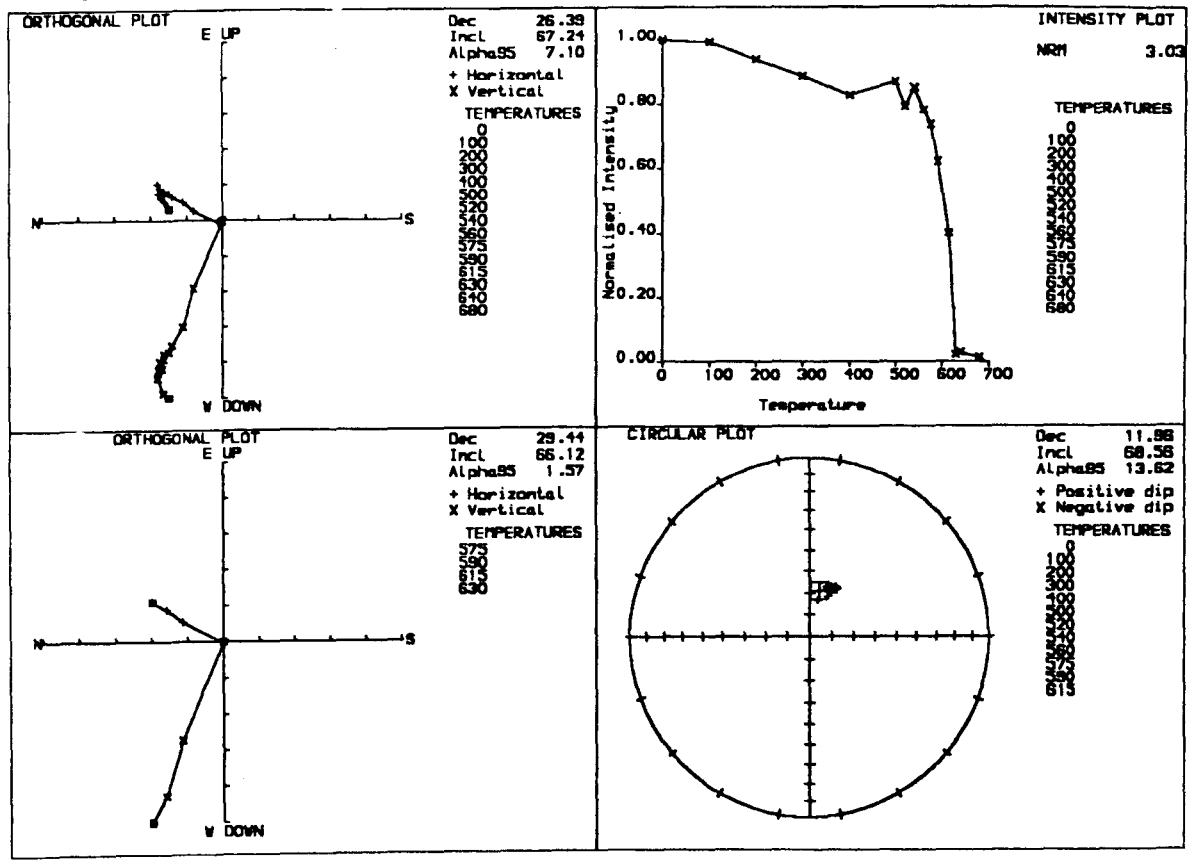

(d) SAMPLE U36-02

THERMAL DEMAGNETISATION

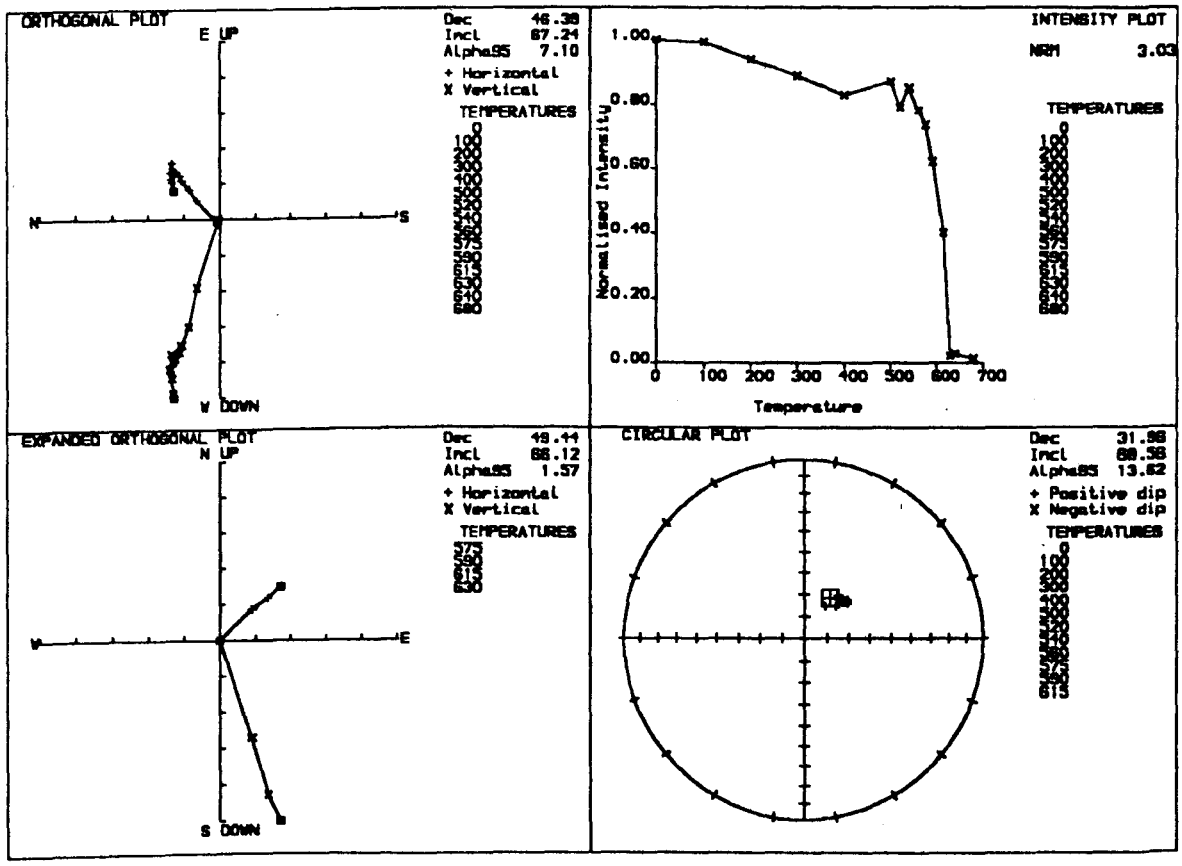

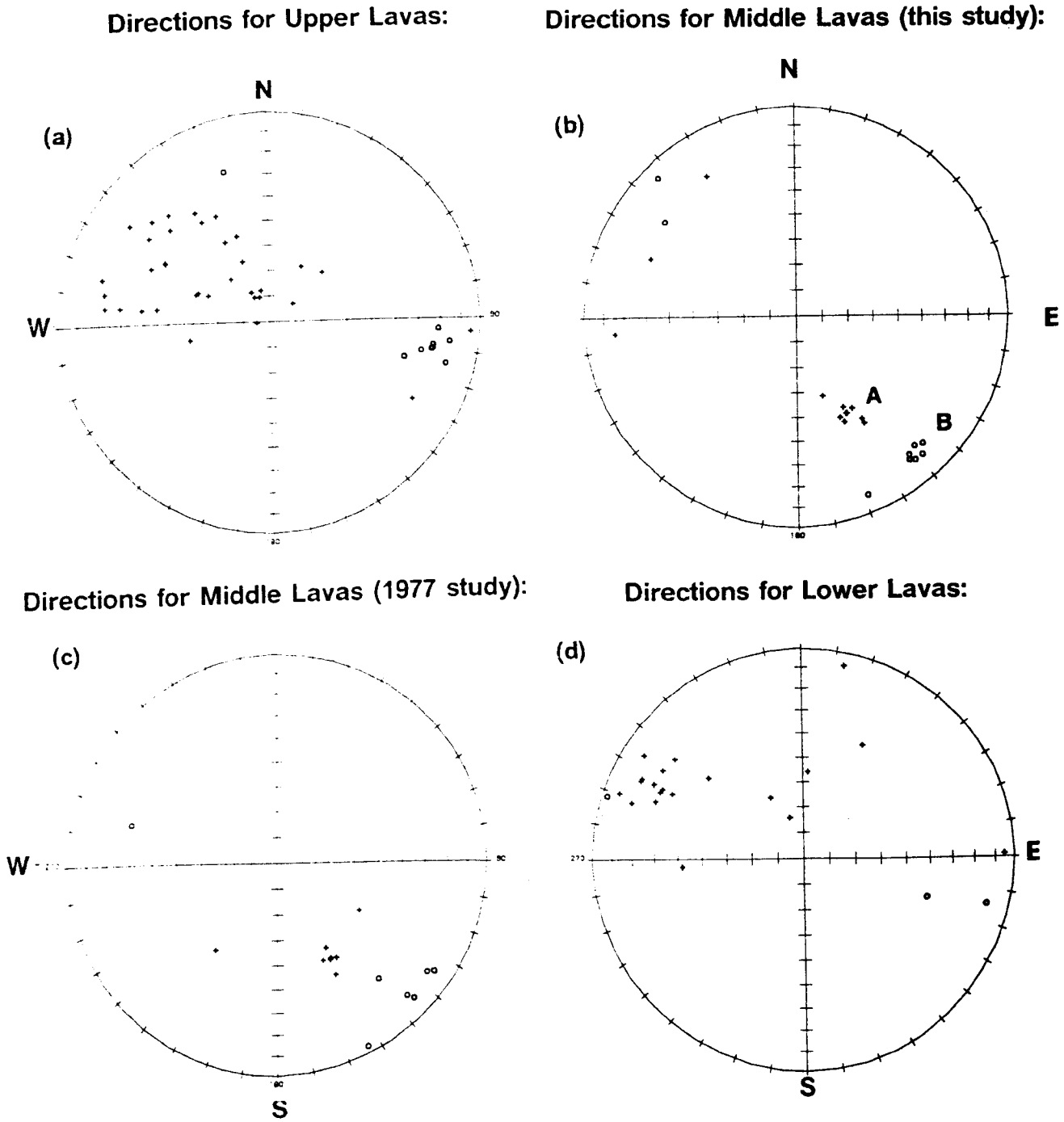

Figure 4.14 : Thermally cleaned flow mean characteristic magnetisation directions for:

(a) The Lower Lava Formation, (b) The Middle Lava Formation, and (c) The Upper Lava Formation

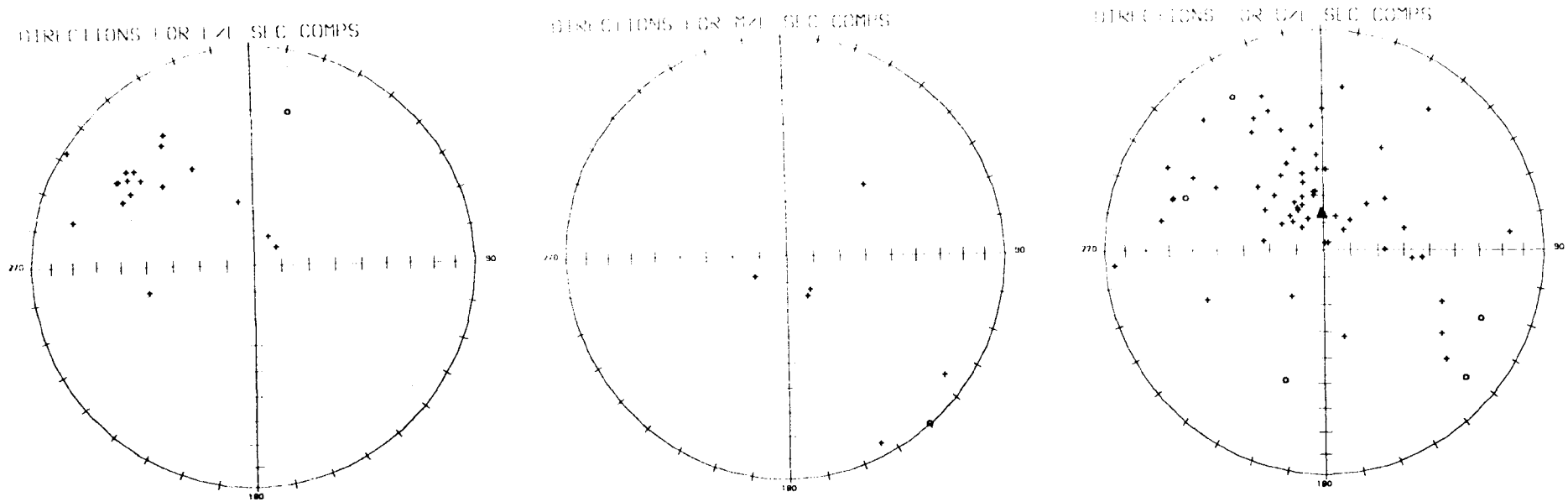

Figure 4.15 : Secondary component magnetisation directions for:

(a) The Lower Lava Formation, (b) The Middle Lava Formation, and (c) The Upper Lava Formation

Triangle illustrates the Present Earth Field (P.E.F.) direction (D/I = 0/78) at the sampling locality.

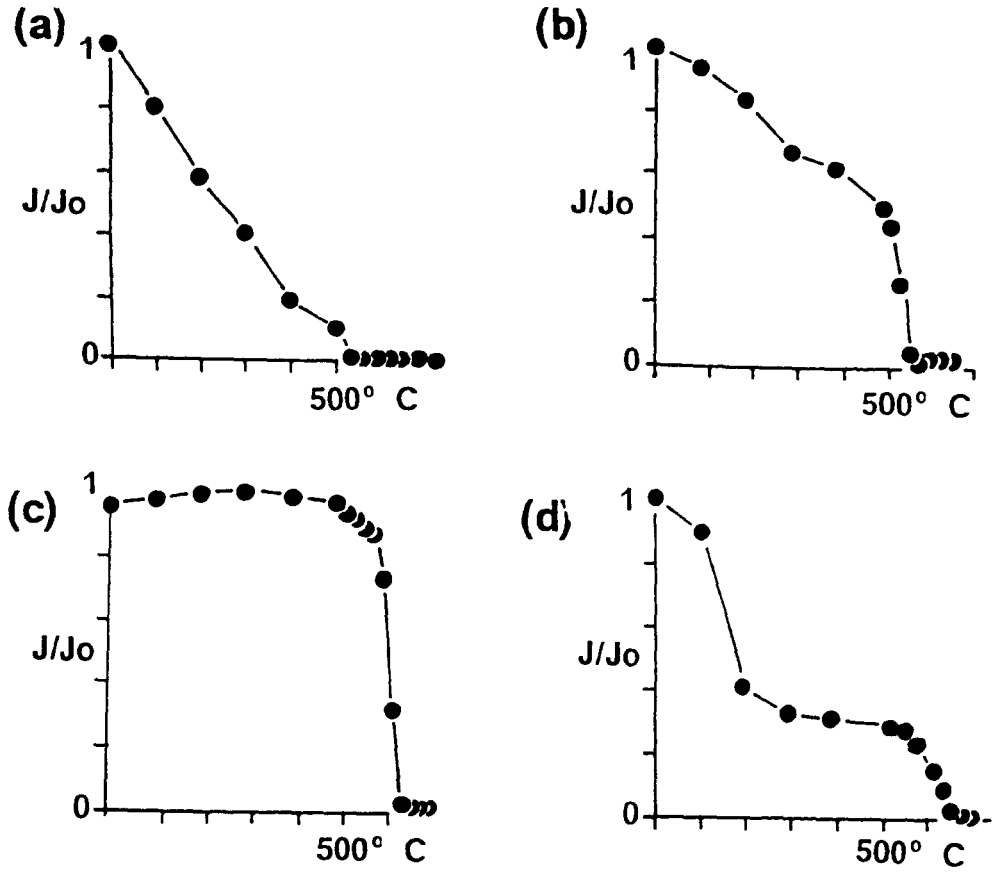

Figure 4.16 : Intensity decay (J/Jo) curves witnessed in the Gardar lavas. Units of J are $\times 10^{-5} Am^2kg^{-1}$

The flow (site) mean directions for the middle lava formation are shown in Figure 4.14b. The mean directions calculated in the present study are very similar to those of the previous study (Table 4.3). The 'A' direction (tilt-corrected mean = 161.8°, 42.0°, $\alpha_{95} = 5.1°$, k = 141.1) bears no similarity to the directions observed in any other part of the lava succession, whereas the 'B' direction (tilt-corrected mean = 139.7, -16.0, $\alpha_{95} = 7.2°$, k = 87.9) resembles the reversed polarity directions witnessed in the flows of the upper lava formation (Figure 4.14c).

4.5.3 The Upper (Ilímaussaq) Lava Formation

Approximately half of the lava flows (52%) in the upper (Ilímaussaq) formation possess a single component of magnetisation. Figures 4.11 and 4.12 show orthogonal vector plots of several typical normal and reversed flows respectively from the upper formation which reflect the single component nature of the majority of flows within the formation. This behaviour is preferentially seen in the flows towards the base of the formation. It is only in the top and, to a certain extent, the middle of the formation that multi-component behaviour is witnessed (Figs.4.13a-b). The sampled upper part of the of the lava pile lies adjacent to the Ilímaussaq intrusion (Figure 4.2), dated at 1143 Ma (Section 2.2.3) and the flows in this section (all flows above flow U29) are close to, or within, metamorphic Zone 1 of the intrusion as defined by Larsen (1977) (Section 2.4). The multi-component magnetisations possessed by flows in this section are a possible consequence of the thermal effect and hydrothermal systems adjacent to this intrusion which may have both heated the flows and altered their magnetic mineralogy. This can possibly be addressed by a palaeomagnetic contact test, which is described fully in Chapter 5 but warrants brief discussion here. Figures 4.13c

and d show the stable directions of magnetisation obtained from a flow close to the top of the pile (c) and from a marginal syenite of the Ilímaussaq intrusion (d). The two directions are comparable with each other and different from the directions seen in the other samples. These results, in themselves, constitute a palaeomagnetic baked contact test which is positive. It demonstrates that the characteristic remanence of the flows in the upper group is older than the 1143 Ma Ilímaussaq intrusion (See Section 5.3.3 for details). All flows which show the totally overprinted direction as a single component of stable remanence were omitted from calculation of the group mean direction for the upper lavas (Table 4.2).

Flow (site) mean directions for the upper lava group are shown in Figure 4.14a. A wide range of inclinations were recorded by flows with normal (westerly) polarity; some with shallow to intermediate (0 – 60°) inclinations and others with steep (>70°) inclinations. The latter have inclinations close to the present Earth field (P.E.F.) direction at this locality (I=78°). It is therefore plausible that these sites have become totally remagnetised in the P.E.F. Alternatively, they may have been overprinted by an event, such as the emplacement of the Ilímaussaq intrusion in Late Gardar times, which was also characterised by steep positive field directions; the Ilímaussaq pluton shows a steep E to NE direction compatible with this population (Piper, 1976). The tilt-corrected mean direction for normally magnetised flows in this Formation is D=284.6°, I=36.9°, α_{95}=8.6°, k=17.2° and that for the reversely magnetised flows is D=97.3°, I=-17.4°, α_{95}=7.1°, k=90.1. The reversed (easterly) directions are therefore more closely grouped than the normal directions, in a shallow E to ESE direction and have shallower inclinations than the normal mean directions, suggesting that the reversals

seen in the upper formation may be asymmetric, confirming the findings of Piper (1977).

It is possible that the self-demagnetising field within the lavas may be responsible for deflecting the inclination of the field within the flow. This refraction effect was studied by Aitken and Hawley (1971) in kiln walls. They derived the following equation which expresses the angle of deviation (in radians) caused by the self-demagnetising field:

$$\text{Deviation} = (2\pi M/F)\sin(2I)$$

where M is the magnetisation intensity at the maximum blocking temperature of the sample, measured in emu/cc (1 emu/cc = 1 emu/g$\times \rho$, where ρ is the density of the lavas (=2.70g/cc; Upton and Blundell, 1978) and 1 emu/g = $1 Am^2kg^{-1}$). F is the ancient field intensity in Oersteds (1 Oersted = $10^3/4\pi Am^{-1}$) and I is the inclination of the field at the site.

If the deviation is more than a few degrees, then the self-demagnetising field is considered important. Using the mean N and R inclinations, the mean N and R effective intensities (which approximate to the NRM intensities for the high blocking temperatures seen here), and the mean N and R palaeointensities (Chapter 6) in the above equation, the deviations are 1.5° and 1.2° for the normal and reversed fields respectively. This value is well within the error limits of the inclination anomaly and thus the self-demagnetising effect is not important in the context of the anomaly witnessed here.

Half of the flows in the upper formation have distributed blocking temperature spectra (Fig. 4.16a) and the other half have discrete spectra with

single, high, blocking temperatures (Fig. 4.16c). In extreme cases of the latter type, up to 90% of the remanence can be lost in a 20° interval, just below the maximum unblocking temperature. Figure 4.15c shows the directions for the secondary (low temperature) components of magnetisation. They show a clear grouping close to the P.E.F. direction.

4.6 MAGNETOSTRATIGRAPHY

Studies of the variation in magnetic polarity within well dated sedimentary sequences or lava flows has been a subject of great interest since the development of palaeomagnetism in the 1950s and especially since its application to the study of sea floor spreading (e.g. McElhinny, 1973; Hailwood, 1989). Such studies have enabled the determination of the Geomagnetic Polarity Time Scale (GPTS). The documentation of the polarity changes in the geomagnetic field for rocks older than 5 Ma is less well understood because errors associated with age determinations are comparable to the duration of short reversal events. The absence of sea floor able to record the reversal history prior to 200 Ma places a further constraint on recovery of the GPTS. The problem of a duration of a polarity sequence cannot be effectively addressed in a very old lava sequence such as the Eriksfjord Group. Only use of the geological relationships with well dated intrusive complexes can be used to obtain broad limits on the age of the succession and the error limits of say 5-10% on these ages are longer than the likely duration of the volcanic episode.

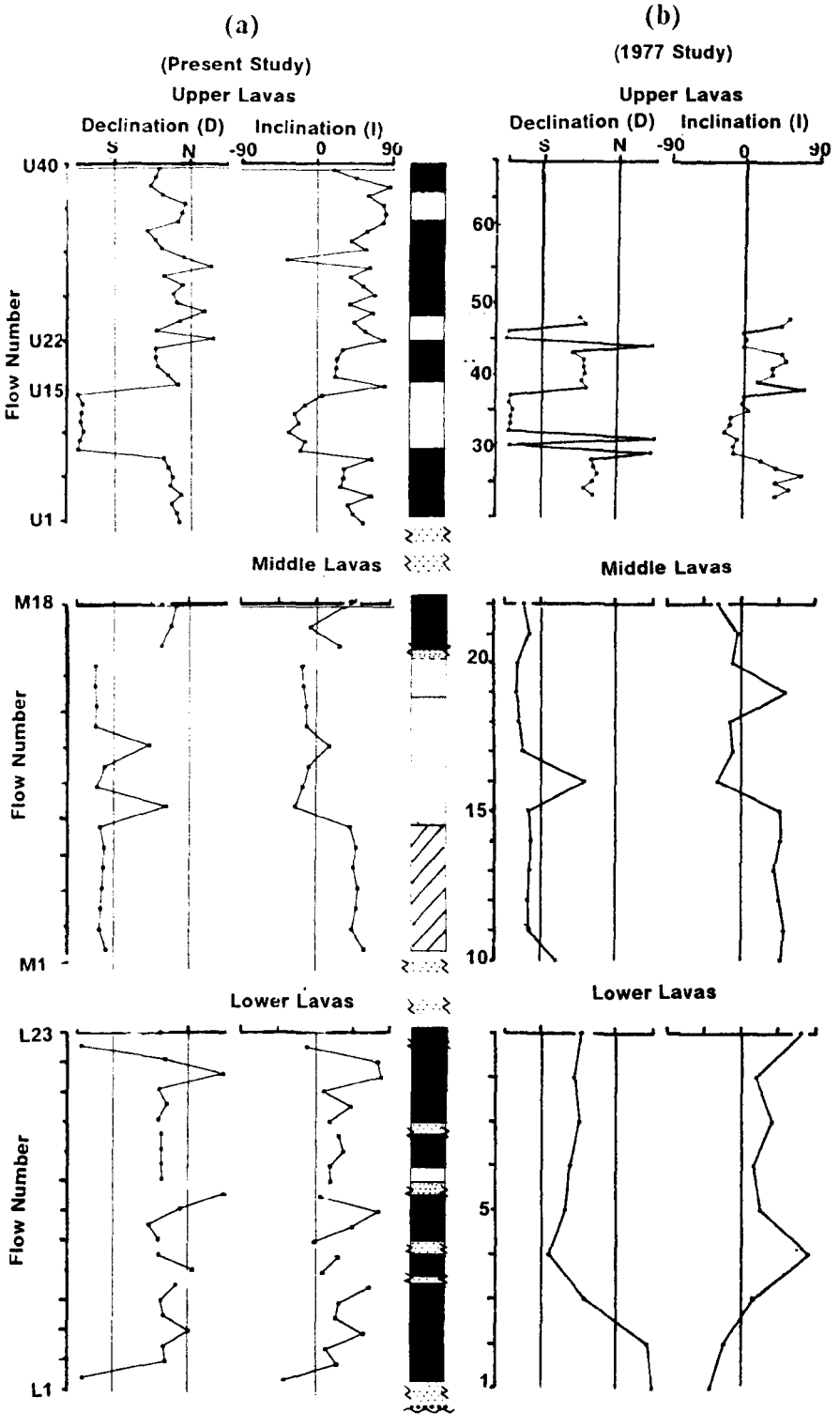

Figure 4.17 : Magnetostratigraphy for the Gardar lavas (a) Results from the present study, and (b) Results from the previous study (Piper, 1977).

Each point on the diagrams represents a flow mean characteristic magnetisation direction. Vertical axes figures indicate the flow number. Black shading indicates normal polarity, white indicates reversed polarity, hashed area indicates polarity transition. Dotted areas indicate positions of sandstone horizons in the sequence.

The Eriksfjord Group is one of the very few geological settings which offer a suitable section for defining a polarity stratigraphy of Proterozoic age. Continuous lava sequences with interleaved sediments having a total thickness of 3 km are otherwise rare. The magnetic stratigraphy defined by Piper (1977), shown in Figure 4.17b covers only the bottom three quarters of the lava stratigraphy. There are some 200m, comprising nineteen flows, above the "platy basalts". Results from these nineteen flows, in addition to the remainder of the lava pile, together totalling eighty-one flows, define a new magnetostratigraphy shown in Figure 4.17a.

The old and new polarity stratigraphy plots show critical differences. In the Upper Lava Formation, four complete inversions of the palaeofield are observed in the previous study, whereas only two complete inversions are identified by the present study. Two flows (U29 and U30), within the division of "platy basalts", record easterly directions which appear to correlate with the upper inversions identified in the previous study (Figure 4.17b). In the new study, these flows record directions which show characteristic reversed (easterly) declinations but the inclinations are positive, hence no complete inversion of the field has been recognised. There are no further inversions seen in the top part of the Upper Formation, which was not sampled by Piper (1977). Figure 4.17a shows that in this section, certain flows exhibit directions which are close to the P.E.F. direction and others record directions similar to that of the Ilimaussaq intrusion.

The Middle (Ulukasik) Lava Formation shows a polarity stratigraphy which can be regarded as the most intriguing of the entire succession. The top two flows (M17 and M18) have recorded westerly directions. Below these two flows, a flow yielding a single intermediate direction (M16) is underlain by a

sequence of seven flows yielding reversely magnetised directions (M9-M15). The seven flows at the base of the formation (M1-M7) exhibit anomalous SE, intermediate positive directions, corresponding to the 'A' direction. It is possible that these flows were erupted during a transitional phase of the geomagnetic field, where the field was changing from normal polarity, which presumably existed prior to the extrusion of the middle lavas, to the reversed polarity interval recorded by flows M9-M15. This, and alternative explanations for this anomalous direction are discussed later (Section 4.8).

The polarity stratigraphy for the Lower (Mussartût) Lava Formation is much better defined than in the previous study, where samples were collected from isolated localities only and not as part of a continuous traverse through the lava formation, as was the case during sampling for the present study. Thus, results reported here are in stratigraphical order whereas there was some ambiguity regarding the stratigraphical position of some of the flows collected from the Lower Lavas for the previous study. Furthermore, at the base of the Mussartût Formation, in a formation thickness of 200m only two flows were sampled in the previous study and only nine were sampled in the whole of the formation, compared to the twenty-three in the present study.

The polarity stratigraphy itself provides a limited temporal coverage; the total thickness of interleaved lava flows, sediments and conglomerates which comprise this formation is some 745m, to which the lavas contribute only some 400m (Table 2.1, Chapter 2). At first glance, the Mussartût Formation appears to reflect a constant normal polarity interval (flows L2-L21), bracketed by two reversely magnetised flows at the top and bottom of the formation (flows L22 and L1 respectively). This may be misleading, however, because the lack of results from interleaved shales and sandstones,

totalling a formation thickness of 300m, means that the magnetostratigraphy resolved from this formation is incomplete. Unfortunately, most of the fissile and crumbly sediments were unsuitable for palaeomagnetic sampling and shattered as soon as the rock drill penetrated the surface of the outcrop.

It must be stressed that the polarity stratigraphy documented here is only a record from the lava flows of the Eriksfjord Group. The disappointing aspect of this study was that sediments of the Mussartût, Naujarssuit and Nunasarnaq sandstones were not suitable for palaeomagnetic sampling. The reasons for this are firstly that they are either massive, cemented quartzites and consequently very hard, or alternatively they are very fissile or crumbly; in either case, sampling was ineffective. Also, unlike the lava flows, much of the sandstone outcrop is exposed as inaccessible cliff sections. Consequently, although the results from this study define a detailed polarity stratigraphy for the Gardar lava succession, the polarities represented by the intervening intervals of sediment deposition have not been resolved.

4.7 POLE POSITIONS

Five new pole positions were calculated for the Gardar lavas; two for the Upper Lava Formation, two for the Middle Lava Formation and one for the Lower Lava Formation (Table 4.5). The Upper Formation was split into normal and reversed flows and a separate pole position calculated for each polarity. This approach follows that of Pesonen (1978) and differs from that of Piper (1977) who calculated a single pole position for the Upper Lavas from a mean magnetisation direction derived from flows of both polarities. Table 4.5 shows that there is little difference between the pole positions calculated in the present study and Piper's study. The relative positions of

the two poles on the contemporaneous apparent polar wander path (APWP) for the Laurentian shield incorporating the Logan and Keweenawan loops are shown in Figure 4.18. The new poles were plotted on the APWP after reconstruction of the Laurentian shield by closing the Davis Strait between Greenland and Labrador and using a combined rotation of Greenland to Europe, and then Europe and Greenland to North America as defined by Bullard et al (1965); these operations are detailed in the legend of Table 4.5. Three sets of poles are shown for the Gardar lavas on Figure 4.18 - those of Piper (1977), the reinterpretation of these data by Pesonen (1978), and the new data. Pesonen's recalculated pole for the Upper Lavas normal flows (ULN) has a higher latitude than the new UNL pole. This difference probable arises because Pesonen used all of Piper's normally magnetised flows to calculate his pole, including those which record a direction close to the Present Earth's Field. These were ommited by Piper and in the present study and consequently the mean inclination and pole latitude are higher for Pesonen's pole. Pesonen's pole plots on the 1120-1150 Ma section of the APWP, which is a time interval appreciably younger than the inferred age of the Eriksfjord Group ($\simeq$1320 Ma). The previous and present ULN poles plot nearer to the 1200-1300 Ma section which is closer to, but still younger than, the inferred age.

The poles for the Middle Lava Formation plot remote from the section of the APWP which their stratigraphic relationship to the Upper and Lower Formations predicts. Geological evidence, described in Chapter 2, suggests that this formation erupted and cooled quicker than either the Upper or Lower Lava Formations and it is possible that the volcanic event responsible for the Middle Lavas lasted for a period of only

LAVA FORMATION	STUDY	MEAN DIRECTION D	I	POLE DETAILS** Lat,	Long	N	STATISTICS α95	k
UPPER (NORMAL)	This study	284.6	36.9	29.7N (dp=5.2,dm=10.4)	207.0E	17	9.9	14.1
	Pesonen (1978)	-	-	42.0N	197.0E	-	-	-
(COMBINED N AND R)	Piper(1977)	279.5	24.0	20.3N (dp=4.8,dm=9.0)	206.3E	24*	8.4	13.0
UPPER (REVERSED)	This study	97.3	-17.4	16.0N (dp=4.3,dm=7.2)	206.1E	6	7.1	90.1
	Pesonen (1978)	-	-	13.0N	203.0E	-	-	-
MIDDLE (INTER-MEDIATE)	This study A	161.8	42.0	8.6N (dp=3.1,dm=6.6)	313.5E	7	5.1	141.1
	B	139.7	-16.0	35.4N (dp=4.3,dm=7.2)	344.3E	6	7.2	87.9
	Piper(1977) A	151.0	46.4	3.7S (dp=3.6,dm=5.5)	322.7E	5	4.3	317.0
	B	135.5	-12.8	32.3S (dp=7.2.dm=14.2)	348.4E	5	13.9	31.0
LOWER (NORMAL)	This study	293.0	25.4	28.1N (dp=3.8,dm=6.7)	194.7E	11	6.3	52.9
	Piper(1977)	260.0	25.0	10.5N (dp=7.6,dm=14.1)	222.8E	7	13.1	22.0

Table 4.5 : Site mean directions and rotate pole positions for the Gardar lavas.

D, I = Mean declination and inclination values

N = Number of sites α95 = semi-angle of 95% confidence cone

k = precision parameter; dp, dm are the semi axes of the oval of confidence about the palaeomagnetic pole at the 95% confidence level in the direction of the colatitude and perpendicular to it.

*** Calculation of pole position includes 12 reversed flows in addition to 12 normal flows (Combined N and R pole).**

**** Rotated poles calculated after closure of the Davis Strait by a combined rotation of Greenland to Europe and Europe/Greenland to North America amounting to 18° clockwise rotation about an Euler pole at 265.6E, 70.5N, according to the Bullard et al (1965) fit.**

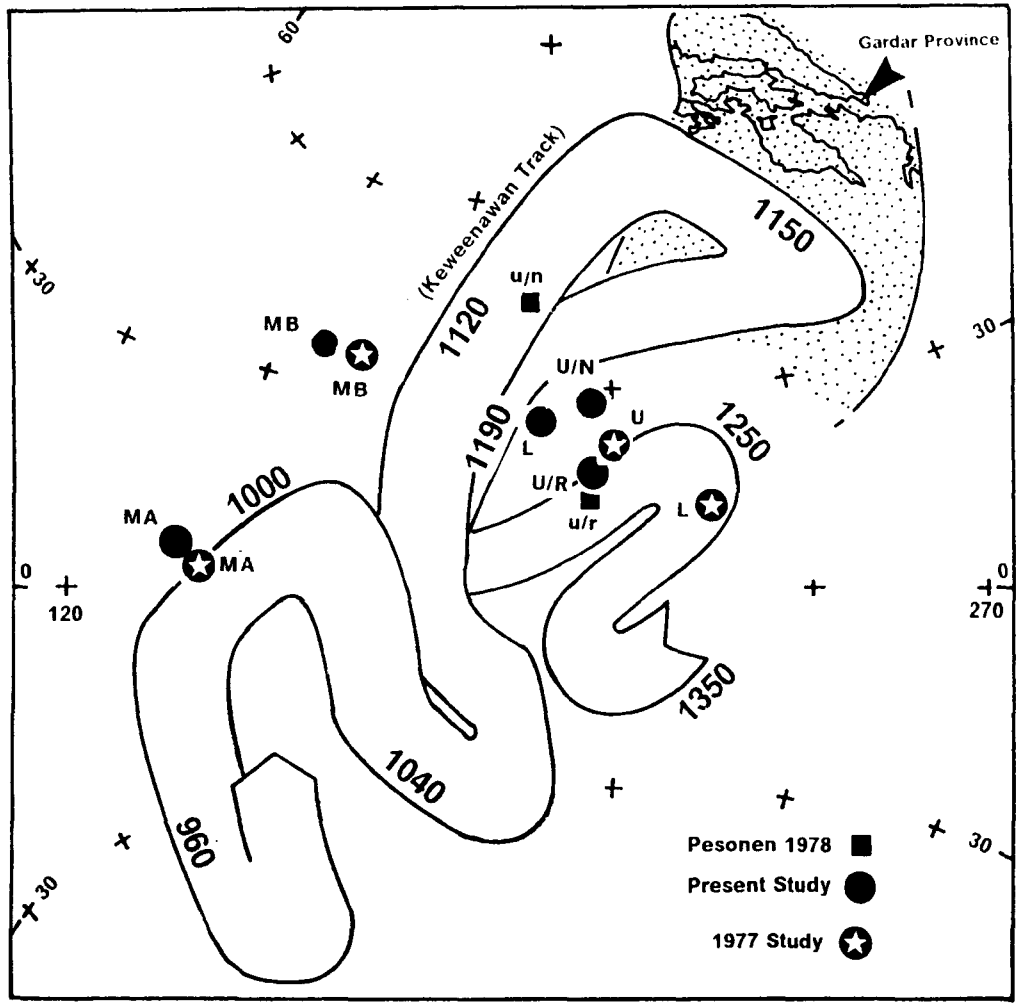

Figure 4.18 : Apparent Polar Wander Path for the Laurentian craton, showing the palaeomagnetic pole positions for the Gardar lavas. Poles were calculated after closure of the Davis Strait by rotating Greenland and Europe back to North America in the manner described by Bullard et al, (1965). The projection is a Lambert equal area projection centred on 200°E, 0°N.

Poles labelled U are for the Upper Lava Formation (normal (N), reversed (R)). Poles labelled M are for the Middle Lava Formation (A and B directions). Poles labelled L are for the Lower Lava Formation Figures on the APWP represent the age of a particular section of the path.

tens or hundreds of years (B.G.J. Upton, pers. comm.). This length of time would probably not be long enough to successfully average-out secular variation of the geomagnetic field. Consequently the calculated pole positions are Virtual Geomagnetic Poles rather than true palaeomagnetic poles (Section 1.2). The pole position for the Lower Lavas plots on a younger section of the APWP than the corresponding pole given by Piper (1977) but does not differ greatly from the ULN pole positions. This supports geological evidence which suggests that the entire Gardar lava succession was erupted over a short period of time (see Section 4.8).

4.8 DISCUSSION

The new polarity stratigraphy is a more complete record of the behaviour of the geomagnetic field during Early Gardar times than that previously presented by Piper (1977). The new data suggest that the reversal frequency during the eruption of the Gardar lavas may not be as high as previously suspected (Piper, 1977). Two complete reversals (N→R and R→N) are found in the Upper (Ilímaussaq) Formation as opposed to the four identified by Piper (1977). The thermal demagnetisation method was unable to completely isolate the two reversals seen in the "platy basalts" in the previous (a.f. demagnetisation) study. This may be because the present study sampled a different section, some 3-4 km to the SW of the previous study, which may not have fully recorded this event (Section 4.3). In the top 200m of the lava pile no further reversals were isolated. However, it is believed that the characteristic remanence directions exhibited by certain flows in this section may record the field direction which prevailed during the emplacement of the nearby Ilímaussaq intrusion. This observation is of great importance in

identifying the age of the lava remanence. Consequently, a separate section (Section 5.3.3) is devoted to its discussion.

Two reversals of magnetisation (R→N and N→R) were found in the Lower Lava Formation, one of which probably corresponds to that identified by Piper (1977) where the two isolated lowest flows of reversed polarity correlate with the single lowest lava of reversed polarity sampled in the present study. The other reversal, at the top of the Formation, was not identified in the previous study because this part of the succession was not sampled. The evidence from the single flow L13 suggests that it may record a brief palaeoexcursion of the geomagnetic field although there is no evidence that the field attained a reversed state here.

Both complete reversals recorded in the Upper Formation show inclination asymmetries of $\simeq 20°$, which support the findings of Piper (1977). The two reversals in the Lower Formation, however, appear to be symmetrical, although this is difficult to confirm since only a single flow possesses the reversed polarity in each case. If these reversals are symmetrical, the field source that existed during Mussartût times may have been quite different to that which prevailed during the volcanic event responsible for the extrusion of the Upper Lava Formation. The existence of a reversal asymmetry has important consequences to the nature of the geomagnetic field source during these times and a whole chapter is devoted to its investigation (Chapter 8), in which the geomagnetic significance of the palaeomagnetic and palaeointensity results of this study is analysed.

Results from the Middle (Ulukasik) Lava Formation continue to be enigmatic and are a major discussion point arising from this work. Several possible explanations can account for the anomalous 'A' direction. It is

possible that burial metamorphism or regional hydrothermal alteration has caused total remagnetisation of the Middle Lava Formation. However, the palaeomagnetic evidence from both this new study and the previous work suggests that the former explanation is unlikely. It is difficult to explain why such a mechanism should selectively remagnetise a series of lavas at the base of the formation. Furthermore, magnetite unblocking relationships calculated by Pullaiah et al (1975) suggest that temperatures of 520°C persisting for a period of 1 Ma would be necessary to unblock a remanence with blocking temperatures of the order of 550°C and lower temperatures, of the order of 350°C would need to persist for 100 Ma in order to unblock remanences with blocking temperatures below 490°C. There is no geological evidence to suggest that such temperatures selectively persisted at this location for these lengths of time. Indeed, absence of any such profound unblocking influence is evidently the reason why the flows of the Upper and Lower formations retain a detailed and probably complete record of N and R polarities. Burial remagnetisation is therefore unlikely to be the cause of significant overprinting in the Eriksfjord Group.

The existence of a secondary chemical remanence (CRM) to explain the 'A' direction is more difficult to disprove in this case. However, thermal demagnetisation isolates only a single, high temperature component of magnetisation. The characteristic direction has a single blocking temperature in excess of 600°C. It is therefore likely to reside in a titanohaematite phase but was probably not acquired below deuteric temperatures. There is no evidence of maghaemite in the thermomagnetic curves of the Middle Lavas (Section 3.2) which would appear to eliminate the possibility of significant low temperature oxidation, evident in the top part of the lava pile and associated with epidote-grade hydrothermal metamorphism. The existence

of haematite (Curie temperatures ≃680°C) as the remanence carrier and the high oxidation states exhibited by the flows (Piper, 1977) shows that they have suffered a high degree of deuteric oxidation. Moreover, there is no obvious geological reason why only the middle of the three lava formations should be remagnetised as a result of hydrothermal alteration and further, there is no obvious reason why only seven of the eighteen flows in this rapidly-extruded Middle Formation should be affected. Although these arguments are not conclusive, the evidence strongly suggests that the anomalous 'A' direction is not a secondary chemical remanence, but a primary TCRM acquired at an advanced stage of deuteric oxidation.

Recognising that the 'A' direction was most probably acquired at the time of initial cooling of the lavas, it is interpreted as being representative of the geomagnetic field at this time. It follows, then, that the flows possessing the 'A' direction, which bears no resemblance to either the normal or reversed directions, may have acquired their magnetisation at a time when the geomagnetic field was in a transitional state during a reversal. Hoffman (1984) has described a method for distinguishing transitional field directions from those which have N or R polarities. He converts geomagnetic field directions into a D',I' plot (transformed D,I plot), with an axis corresponding to the geocentric axial dipole direction as defined by the mean N-R axis for the particular data set. The declination, D, and inclination, I, of all data points are then transformed onto this plot. Any points lying outside a circle of radius 30°, centred on the pole of the plot, are defined as transitional field directions. Figure 4.19 shows a D',I' plot for the Middle Lava Formation. Clearly, the flows showing the 'A' direction lie well outside the 30° circle, whereas those showing the 'B' direction lie within it. This supports the interpretation that the flows exhibiting the 'A' direction were erupted during

a period when the geomagnetic field was in a transitional phase, between a normal polarity interval prior to the eruption of the flows, and before the reversed polarity interval (characterised by the 'B' direction) defined by the higher flows. Geological evidence also provides general support for this interpretation; the absence of vesicular flow tops and intervening clastics and the presence of pahoehoe surfaces indicate a lack of erosion and a small time gaps between the eruption of successive flows. The whole of the Middle Formation (including the sedimentary layers at the top) is only 250m thick (Upton et al, 1974). This undoubtedly constitutes the shortest eruption time period of all three Lava Formations and could be of the order of a few hundred years, or less. It is therefore conceivable that during the time period represented by this brief volcanic episode, the geomagnetic field was executing a transitional phase. This interpretation is further supported by the palaeointensity results (Chapter 6). It is well documented (e.g. Dagley and Wilson, 1971; Bogue and Coe, 1981; Prévot et al, 1985; Roberts and Shaw, 1984) that the field intensity decreases substantially during a field reversal. The results of Thellier palaeointensity experiments, presented in Chapter 6, indicate that the lowest palaeointensity values in the entire lava succession are recorded by flows exhibiting the 'A' direction.

In summary, the palaeomagnetic evidence, strongly supported by the geological evidence, suggests that the sequence of flows with SE, positive directions (constituting the anomalous 'A' mean direction) acquired their magnetisation during, or shortly after initial cooling and were erupted during a transitional phase of the geomagnetic field. Furthermore, hydrothermal alteration does not appear to have produced a secondary CRM.

Geochemical evidence (Upton and Emeleus, 1987) indicates a generalised increase in differentiation from the Lower to the Upper lava formations, suggesting that the lava source was a single magma chamber, or a closely related nest of chambers, which cooled and evolved compositionally with time (B.G.J. Upton, pers. comm.). This evidence is important for estimating the time span of the geomagnetic changes identified here because single volcanic systems rarely have lifespans in excess of 5 Ma. This implies that the entire Eriksfjord Group was formed within this time, and the Gardar lavas themselves, in about 0.75 - 1 million years. Thus, the polarity stratigraphy documented here probably records the behaviour of the geomagnetic field over only a very short interval of geological time. During this short time, the field direction changed rapidly in the Upper Lava Formation, where no prolonged transitional directions are recognised, but remained locked in a transitional direction during the eruption of the Middle Lava Formation.

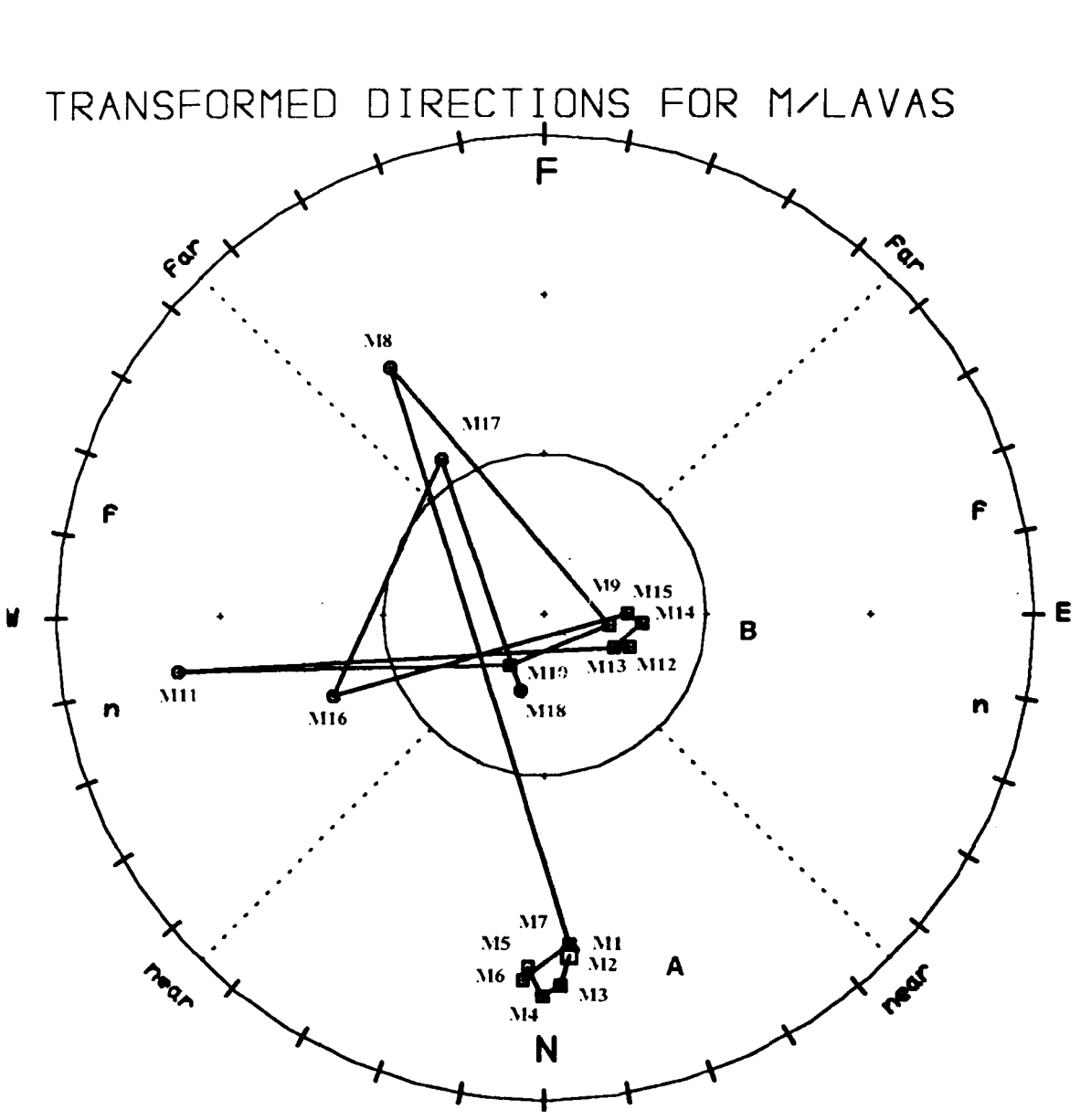

Figure 4.19 : Transformed directions (D′,I′) for the Middle Lava Formation (See text for explanation of the plot). Directions are labelled with corresponding flow numbers. 'A' and 'B' indicate the flows with the A and B directions (Section 4.5.2) respectively.

CHAPTER 5 : THE ORIGIN OF THE LAVA REMANENCE

5.1 INTRODUCTION

The major aims of this project as a whole were to investigate the strength and direction of the geomagnetic field during Early Gardar times by obtaining palaeointensity and palaeomagnetic results from the Gardar lavas (Chapters 6 and 4 repectively). As with all palaeomagnetic studies, the data are only of interpretive value if the age of these results can be constrained. In the case of palaeointensity information, it is necessary to establish a primary origin and furthermore, this primary remanence should be a TRM (or a TCRM resulting from deuteric oxidation).

This chapter describes the results of a series of tests performed in an attempt to identify the age and the nature of the remanence held by the Gardar lava flows. These tests include palaeomagnetic contact tests (Everitt and Clegg, 1962; Wilson, 1962a), performed on lavas and red beds of the Eriksfjord Group where they are baked by Late Gardar trachytic and basaltic dykes, a large scale contact test where the lavas are baked by a syenitic intrusive complex, and an agglomerate test where basic clasts emplaced by an explosive volcanic event are analysed using the same principal as that employed in the standard palaeomagnetic conglomerate test (Graham, 1949).

Before considering the results of these tests and their implications to the project, it is appropriate to describe the methodology of the tests themselves.

5.2 DESCRIPTION OF FIELD TESTS

5.2.1 The baked contact test (BCT)

When an igneous intrusion is emplaced it will heat the surrounding country rock and partially or completely unblock any remanence in the latter. After cooling, a partial or complete overprint with a component of magnetisation in the same direction as that of the intrusion may be observed in the adjacent country rock. Agreement between the direction of magnetisation held by the intrusion and that of the baked country rock, and disparity of this common direction with that held by the unbaked country rock, remote from the intrusion, is positive evidence that the remanence in the intrusion is a primary, cooling related, phenomenon. It may also indicate that any remanence in the unbaked country rock has been stable at least since the emplacement of the intrusion. This is the principle of the baked contact test described by Everitt and Clegg (1962) and Wilson (1962a). The value of the test is much enhanced if the magnetic properties of the country rock are demonstrated to change with distance away from the intrusion, corresponding to the diminishing thermal effect of the intrusion (Everitt and Clegg, 1962) and Figure 5.1. Thus for a contact test of maximum benefit, palaeomagnetic samples should be taken at increasing distances from the intrusion.

Five regions can be defined in a baked contact scenario (Fig. 5.1): the intrusion, the metamorphic zone, the heated zone, the warmed zone and the unheated country rocks. In the metamorphic zone, temperatures in excess of the Curie temperature, T_c, of the country rock will be expected and consequently, there will be extensive changes in the magnetic minerals. The

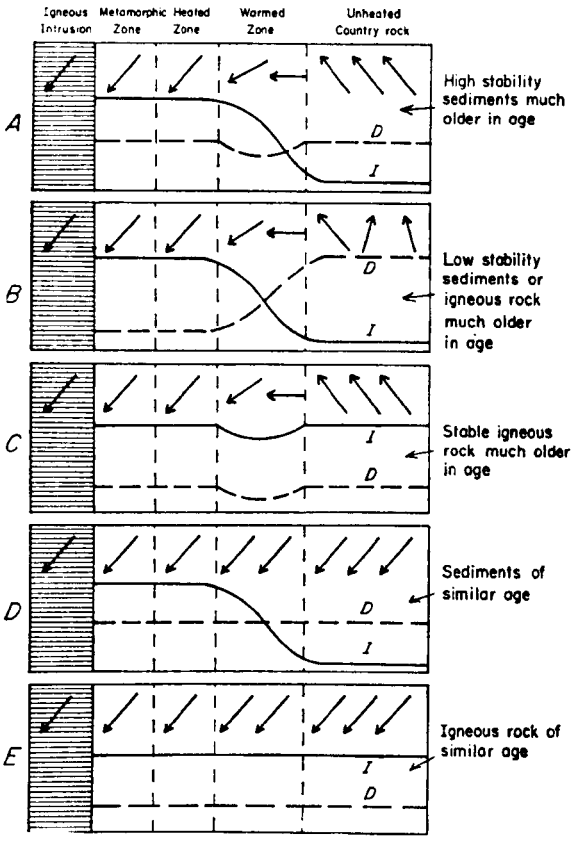

Figure 5.1 : The palaeomagnetic baked contact test. The variation in direction of magnetisation (arrows), intensity (I) and dispersion (D) with distance from an igneous intrusion in five possible situations is indicated schematically (from McElhinny, 1973).

rocks in this zone will be totally remagnetised. Similar directions of magnetisation in the intrusion and the country rock are a record of the magnetic field at the time of cooling. In the adjacent heated zone, chemical changes may not be obvious and it is in this zone that the new NRM is most likely to be a TRM. Temperatures in the warmed zone never reach the Curie temperature of the magnetic minerals and consequently, a partial thermoremanence (PTRM) is acquired which may combine with any stable, high temperature remanence of the country rock. In principle, these two remanences can be separated by thermal demagnetisation. In the unheated country rock, the original direction of magnetisation will be unaffected by the thermal effect of the intrusion. The possible situations illustrated in Figure 5.1 are:

Case A : The country rock is much older than the intrusion and consists of sedimentary material of high magnetic stability. The NRM intensity at the contact is high but falls to low values further from the intrusion. The change in intensity may be an order of magnitude, since a remanence of the sediments is likely to be a CRM whereas that of the baked rock is a TRM. This change in intensity, coupled with the similarity of directions in the intrusion and contact zone, indicates that both the intrusion and the contact rock are stable and that their magnetisation was acquired when the intrusion cooled.

Case B : The age of the country rock is the same as in A but is sedimentary or igneous material of low magnetic stability. The NRM intensity decreases away from the contact but the dispersion increases and directions are scattered.

Case C : In this scenario, the country rock is older than the intrusion but is composed of igneous material of similar composition. Hence, no great change in NRM intensity (J_o) may be seen since the remanence held by both rock types is of similar origin.

Case D : The country rock is sedimentary and of comparable age or a little older than the intrusion. Here, the only change seen is a decrease in J_o away from the contact.

Case E : The situation is the same as Case D but this time the country rock is igneous. Little or no change in J_o or D may be seen. This is the least favourable baked contact scenario.

The behaviour of J_o and D that would occur in Case E could be mistaken for that arising as a result of heating during a period of regional metamorphism or deep burial. The presence, or otherwise, of systematic changes in J_o or susceptibility away from the contact, however, may allow discrimination between the two possibilities.

5.2.2 The agglomerate test

This test is an adaptation of the original palaeomagnetic conglomerate test proposed by Graham (1949). In that test, pebbles of a suitable rock type from one formation, whose stability of remanence is being tested, are sampled as clasts in a later formation. If the directions of magnetisation isolated from the pebbles are completely random, it is likely that the remanence of the parent formation has been stable since the formation of the conglomerate. Uniform magnetisation directions from the pebbles implies the possibility of

magnetic overprinting by an event subsequent to the formation of the conglomerate.

The conglomerate test may be the least definitive of the palaeomagnetic field tests because uniform directions in pebbles does not unequivocally prove that the magnetisation in the parent formation is secondary. It is possible, but unlikely, that the formation process of the conglomerate itself may have affected that magnetisation. Also, if the clasts have a shape anisotropy inherited from the parent formation, it is conceivable that this may be preserved as a fabric within the conglomerate. Furthermore, secondary overprints may be difficult to detect in small sample collections, depending on the size of the secondary component compared with the primary (Starkey and Palmer, 1971) and it is often necessary to conduct statistical tests to evaluate whether the magnetisations are coherent or random. Random magnetisations may be produced by lightning strikes (Cox, 1961; Graham, 1961) although this is unlikely to affect every pebble in the conglomerate and could, in any case, be detected by abnormally high NRM intensities and very low resistance to a.f. demagnetisation. The value of the test is greatly enhanced if paired cores are taken from the same clast because this provides a comparison of the within-clast and between-clast dispersions.

An application of this basic test to clasts in an agglomerate band has been described by Briden and Mullan (1984) and Trench et al (1991).

5.3 BAKED CONTACT TESTS

5.3.1 Baked Contact tests A and B (country rock:lava)

(a) Geological setting and sampling

Figure 5.2 shows the sampling localities for the baked contact study (sites A and B) on the Mussartût lavas. Two NE-trending Late Gardar dykes, one basaltic (Dyke A = 5.5m wide) and one trachytic (Dyke B = 4m wide), were sampled on the top of the cliff at Mâjût Bay. Both dykes intrude the basal flows of the Mussartût Lava Formation. The positions of the samples in the baked and unbaked lava with respect to the western and eastern margins of the dyke are listed in Table 5.1. The situation in contact sites A and B represents that described by Case C in Section 5.2.1 (Figure 5.1), because the Late Gardar dykes intrude lavas which are at least 150 Ma older.

(b) NRM measurements

Figure 5.3a illustrates the NRM directions for the dyke samples and the baked and unbaked lava samples for both contact sites A and B. Samples from the interior of the dykes have normal polarities but those from the chilled margins of the dykes have negative inclinations with northerly declinations. Figure 5.3b shows the variation of NRM intensity with increasing distance away from both margins of the dykes. This variations shows an increase in intensity away from the dyke margins.

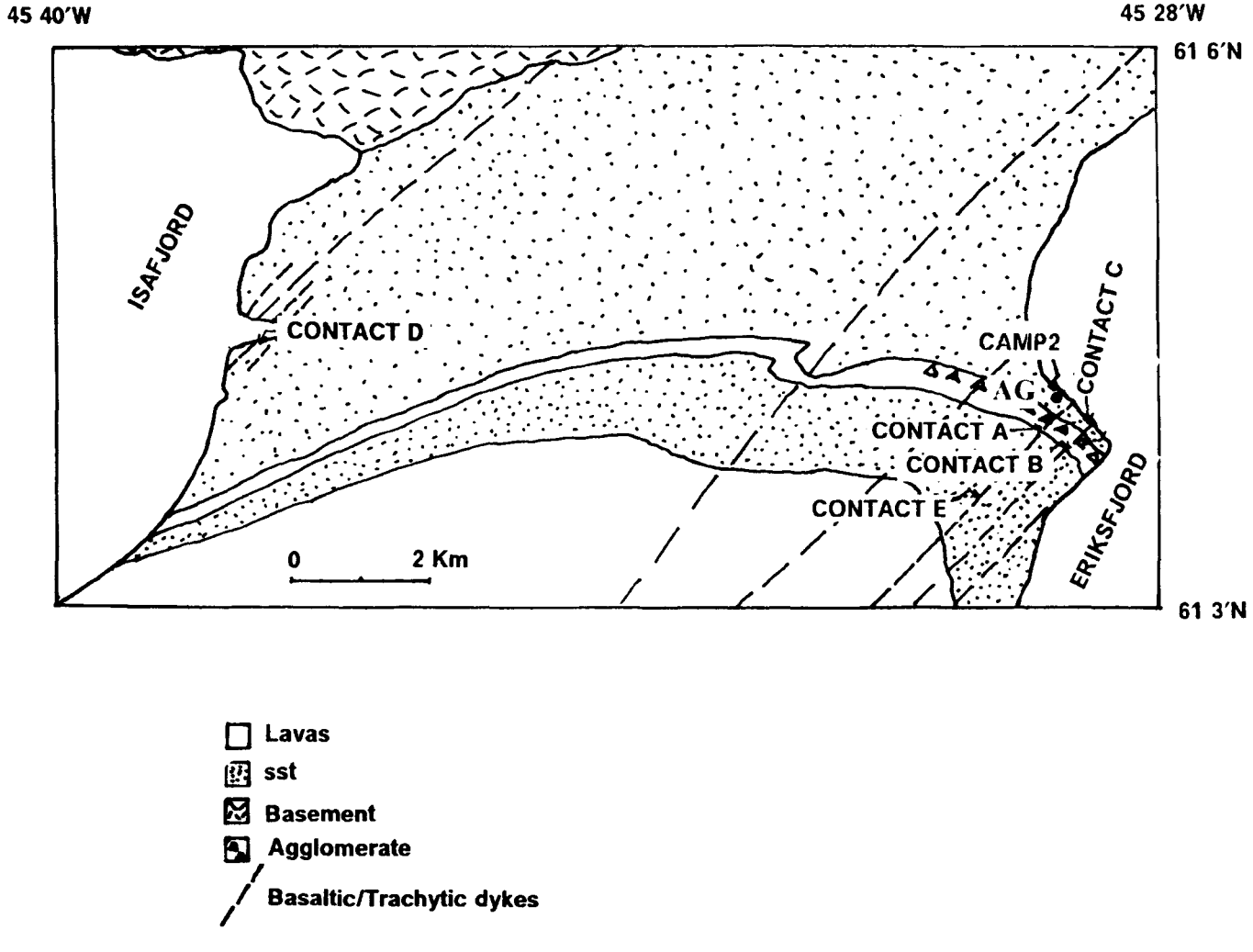

Figure 5.2 : Sketch map indicating sampling localities for baked contact tests A-E and the agglomerate test, AG.

(c) Thermal demagnetisation results

Stepwise thermal demagnetisation of all samples in each site was employed to investigate the component structure of the remanence and isolate any component of magnetisation (TRM) resulting from the thermal effect of dyke emplacement. Samples were demagnetised in steps of 50° or 100°C steps to 450°C and subsequently in 20°C or 30° C steps to the maximum unblocking temperature.

The results of the thermal demagnetisation study are listed in Table 5.1 and illustrated in Figures 5.4-5.6. Figure 5.4 shows the thermally cleaned directions obtained from all samples. The component structure of the remanence is illustrated in Figure 5.5-5.6.

Five observations were made from the results:

1. Samples from the interior of the dykes show high temperature components (>200°C) of magnetisation with N-NNE steep positive directions.

2. Samples from the chilled margins of the dykes show high temperature components (>200°C) with N-NNW declinations and negative inclinations.

3. Samples from the lava closest to the dyke (0-0.5m- metamorphic and heated zones) showed single, high temperature components of magnetisation (>500°C) with directions similar to that of the dyke margins but show no evidence of the characteristic lava direction.

4. Samples further away (0.5-1.0m) from the dyke show two components of magnetisation. The lower temperatures (<400°C) component is characterised by a N-NNE steep positive direction similar to that of the dyke and the higher temperature component at higher temperatures (> 500°C) is characterised by a shallow westerly positive direction similar to the characteristic remanence direction residing in the unbaked lava.

5. Samples remote from the dyke (> 1m away) show single components of magnetisation with a shallow westerly positive direction similar to that isolated from the lower flows of the Mussartût Formation in the palaeomagnetic study (Chapter 4).

These observations are indicative of a positive baked contact test for both sites A and B, where samples closest to the dyke have been totally overprinted and have acquired a total TRM or a TCRM with a direction similar to that observed in the dykes, which is therefore contemporaneous with the intrusion and subsequent cooling of the dyke. Samples further away from the dyke were partially overprinted during the intrusion and cooling of the dyke and acquired a partial thermoremanence (PTRM) below ca. 400° C which has a direction close to that held by the dyke. Above 500°C, a component of magnetisation is isolated in these samples which has a direction similar to that observed in the unbaked lava samples. This direction was observed on the stereoplot for temperatures in excess of 500° C but no vector for these points was defined on the OVP because the intensity was rather weak. The unbaked lava samples are therefore interpreted to have a single high temperature component of TRM acquired during the initial cooling of the lava which is unaffected by the intrusion of the dyke.

SAMPLE				HIGH TEMP COMPONENT (T≥ 500°C)			LOW TEMP COMPONENT (T≤ 400°C)		
		DIST	Jnrm	D	I	α_{95}	D	I	α_{95}
A-1	Dyke I	0	20.1	342.6	52.8	2.2	-	-	
-2	Dyke I	0	16.6	339.7	37.4	2.3	-	-	
-3	Dyke MW	0	3.9	309.2	-25.7	4.3	-	-	
-4	Dyke ME	0	6.2	337.2	-31.3	2.9	-	-	
-5	MetamW	0.06	8.4	2.6	35.1	2.8	-	-	
-6	MetamW	0.04	6.6	28.7	30.8	6.6	-	-	
-7	MetamE	0.1	6.2	336.7	-28.5	7.5	-	-	
-8	MetamE	0.03	0.6	235.3	-0.3	6.3	-	-	
-9	WarmedW	0.1	4.5	266.7	28.4	4.6	5.2	44.4	8.2
-10	WarmedW	0.2	6.7	270.0	16.0	7.4	21.2	45.1	6.2
-11	WarmedE	0.34	12.7	252.7	19.5	7.4	28.5	47.8	2.7
-12	Unbak	3.0	77.2	300.7	15.6	1.4	-	-	
-13	Unbak	2.95	76.9	302.2	15.8	2.3	-	-	
B-1	Dyke I	0	24.4	7.3	65.0	3.3	-	-	
-2	Dyke I	0	25.6	358.8	41.4	4.8	-	-	
-3	Dyke M	0	7.7	346.1	-18.4	5.0	-	-	
-5	Dyke M	0	5.9	349.9	-28.6	7.5	-	-	
-6	Metam	0.05	8.0	343.5	-17.1	2.1	-	-	
-7	Metam	0.03	7.8	5.0	-26.4	4.9	-	-	
-8	Heated	0.25	19.3	65.7	38.3	5.4	-	-	
-9	Heated	0.15	3.9	51.3	31.5	1.0	-	-	
-10	Warmed	0.3	14.6	298.4	21.7	18.5	67.8	32.2	2.2
-11	Warmed	0.78	94.4	274.7	33.2	11.9	56.2	41.2	2.4
-12	Unbaked	1.3	133.6	316.6	1.1	1.5	-	-	

Table 5.1 : Results of the baked contact tests on sites A-B within the Lower Lava Formation Dyke I/M = Dyke interior/margin; Metam = metamorphic zone; Heated = heated zone; Warmed = warmed zone; Unbak = Unbaked country rock; W = western contact, E = eastern contact. DIST = distance of country rock sample from the dyke margin in metres.

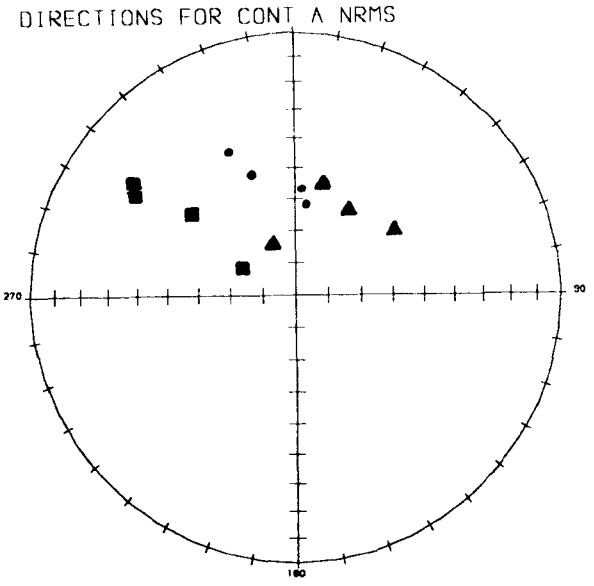

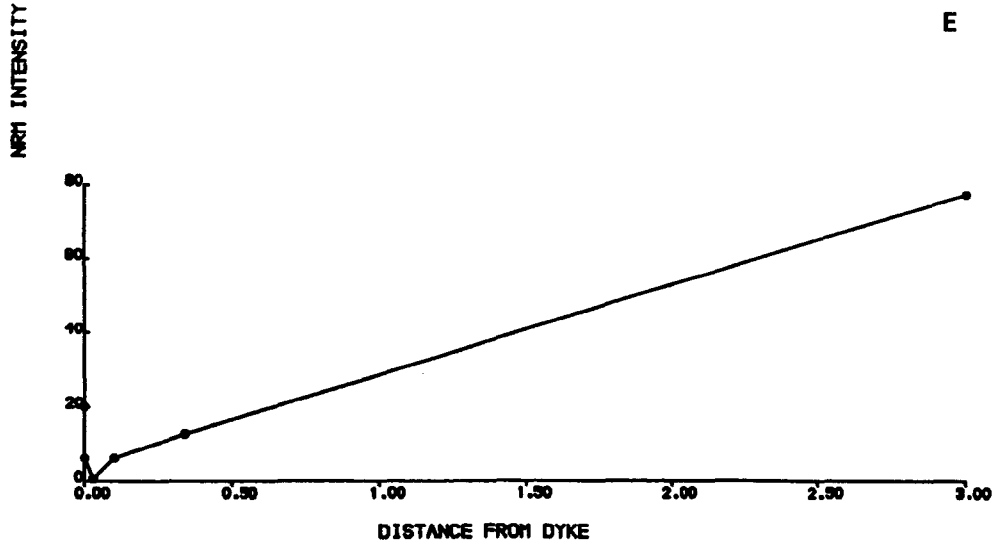

Figure 5.3a : NRM directions for dyke samples (o), baked lavas (Δ) and unbaked lavas (□) and the variation of NRM intensity with distance from western and eastern dyke margins for contact site A. Closed (open) symbols indicate positive (negative) inclinations. Units of NRM intensity are $\times 10^{-5}Am^2kg^{-1}$ and distance is in metres.

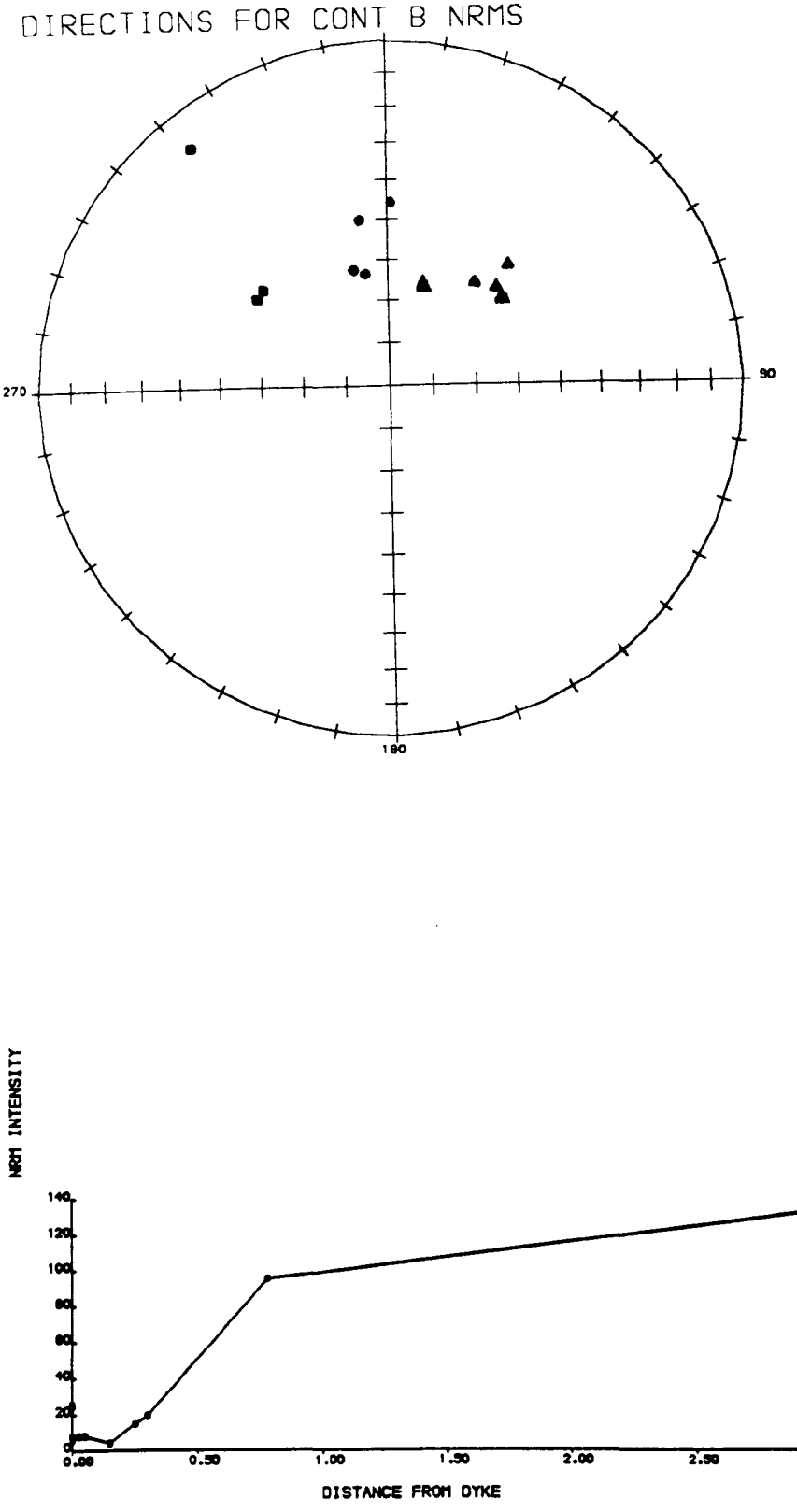

Figure 5.3b : NRM directions for dyke samples (o), baked lavas (▵) and unbaked lavas (□) and the variation of NRM intensity with distance from the dyke margins for contact site B. Labels as for Fig. 5.3a

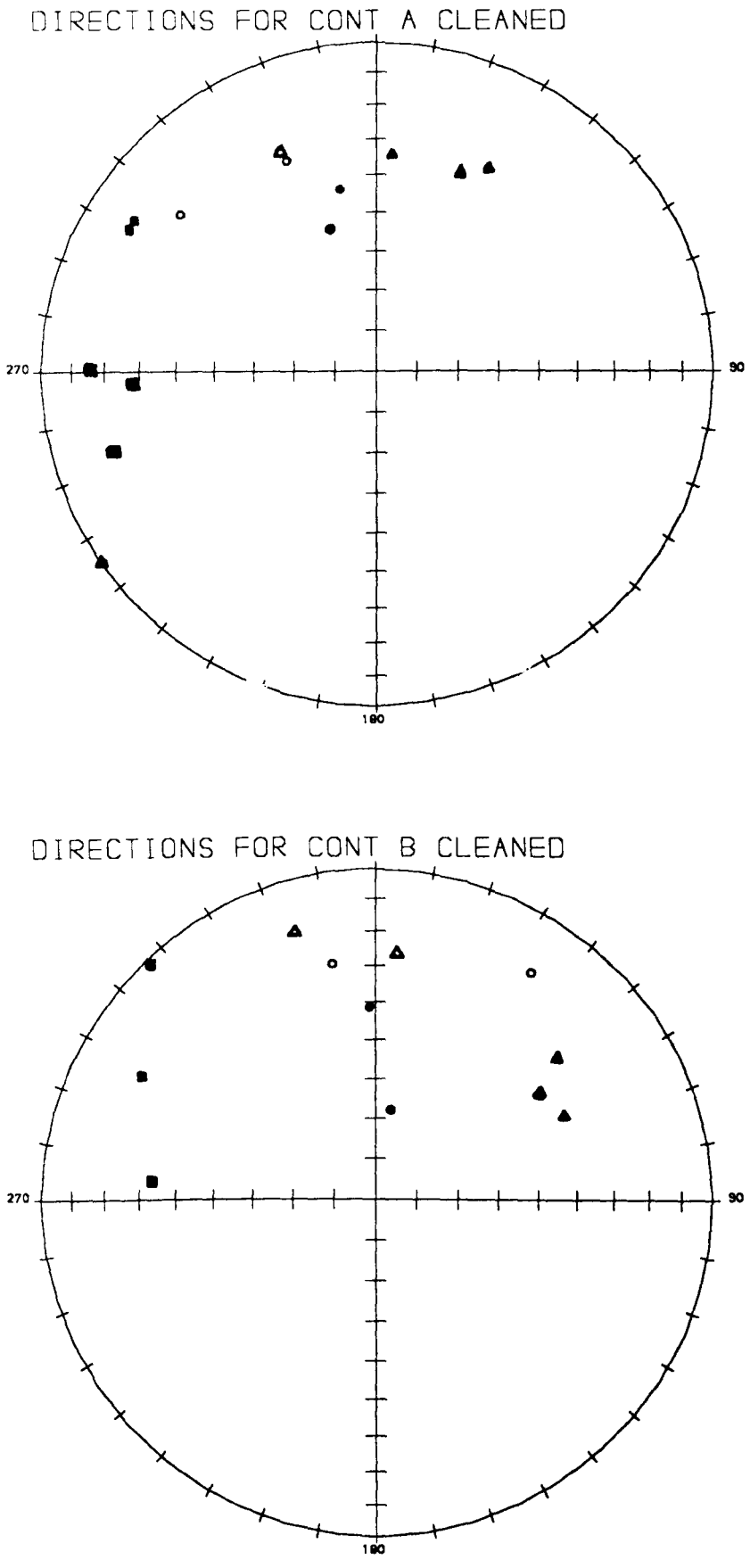

Figure 5.4 : Thermally demagnetised (characteristic remanence) directions for samples from the dyke (o), baked lavas (△) and unbaked lavas (□) for (a) contact site A, and (b) contact site B.

Figure 5.5 : Palaeomagnetic plots illustrating the component structure of remanence for typical samples from contact site A. Labels as for Figure 4.6.

DYKE INTERIOR

THERMAL DEMAGNETISATION

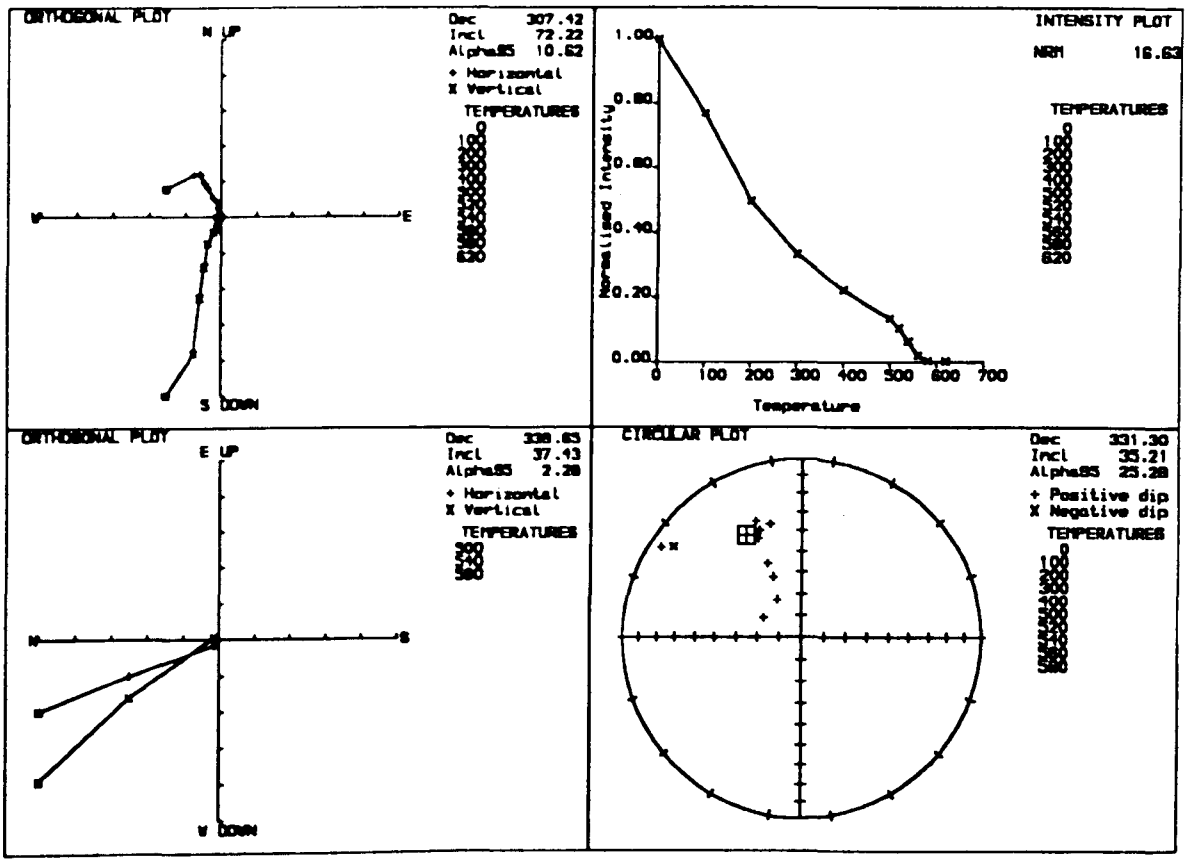

DYKE MARGIN

THERMAL DEMAGNETISATION

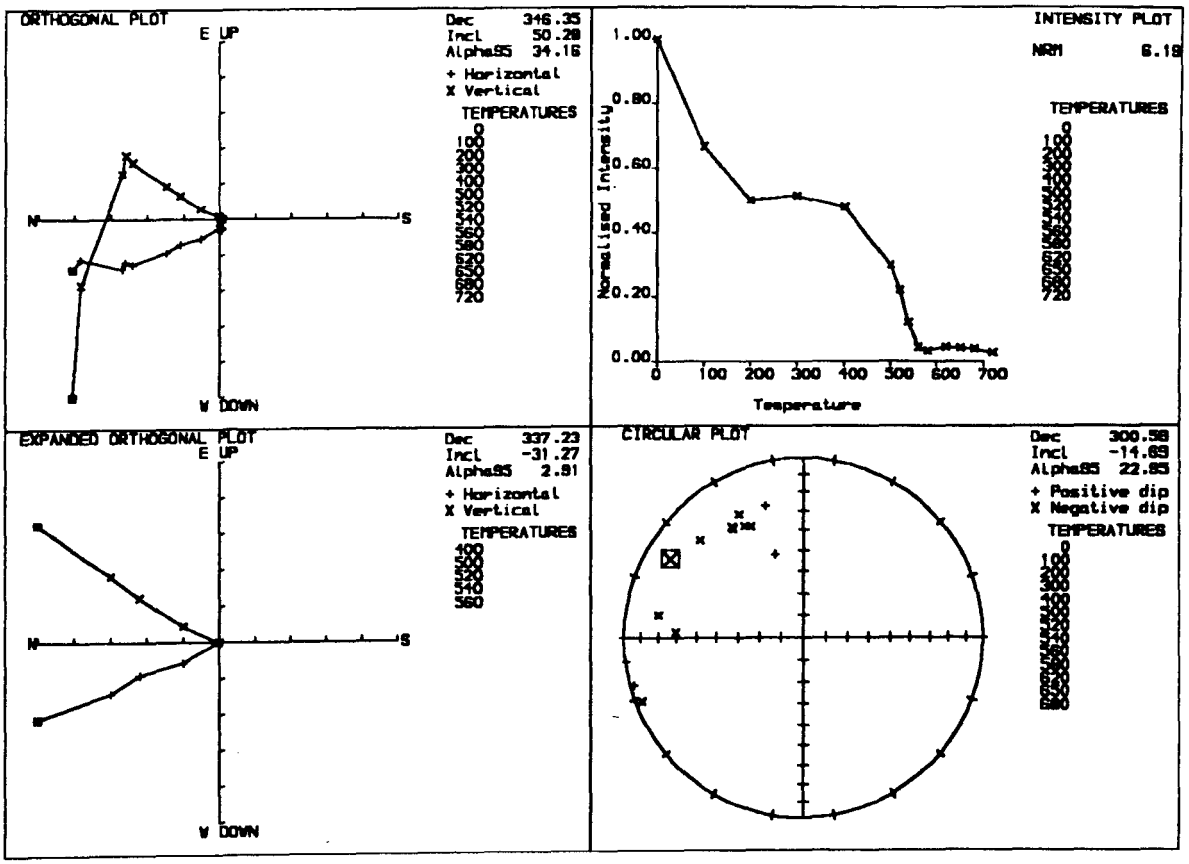

METAMORPHIC ZONE

THERMAL DEMAGNETISATION

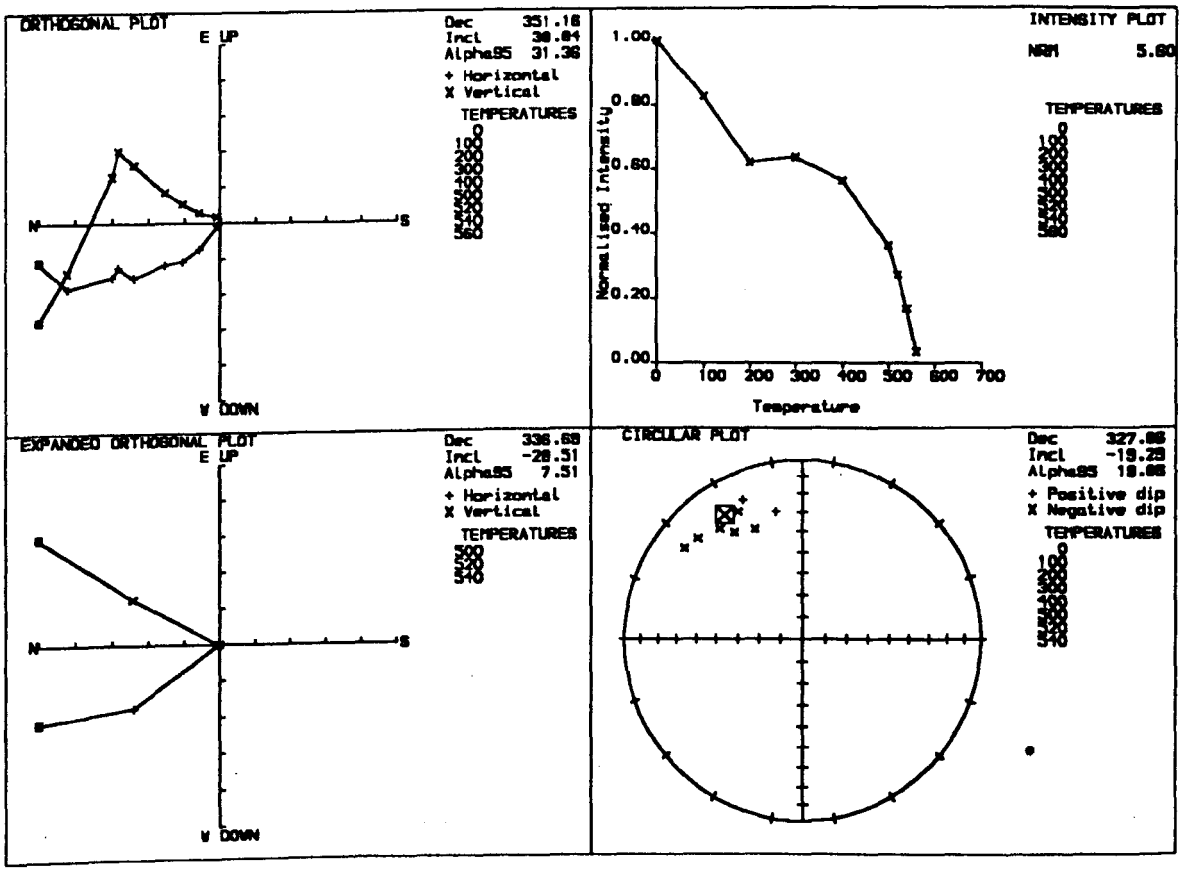

WARMED ZONE

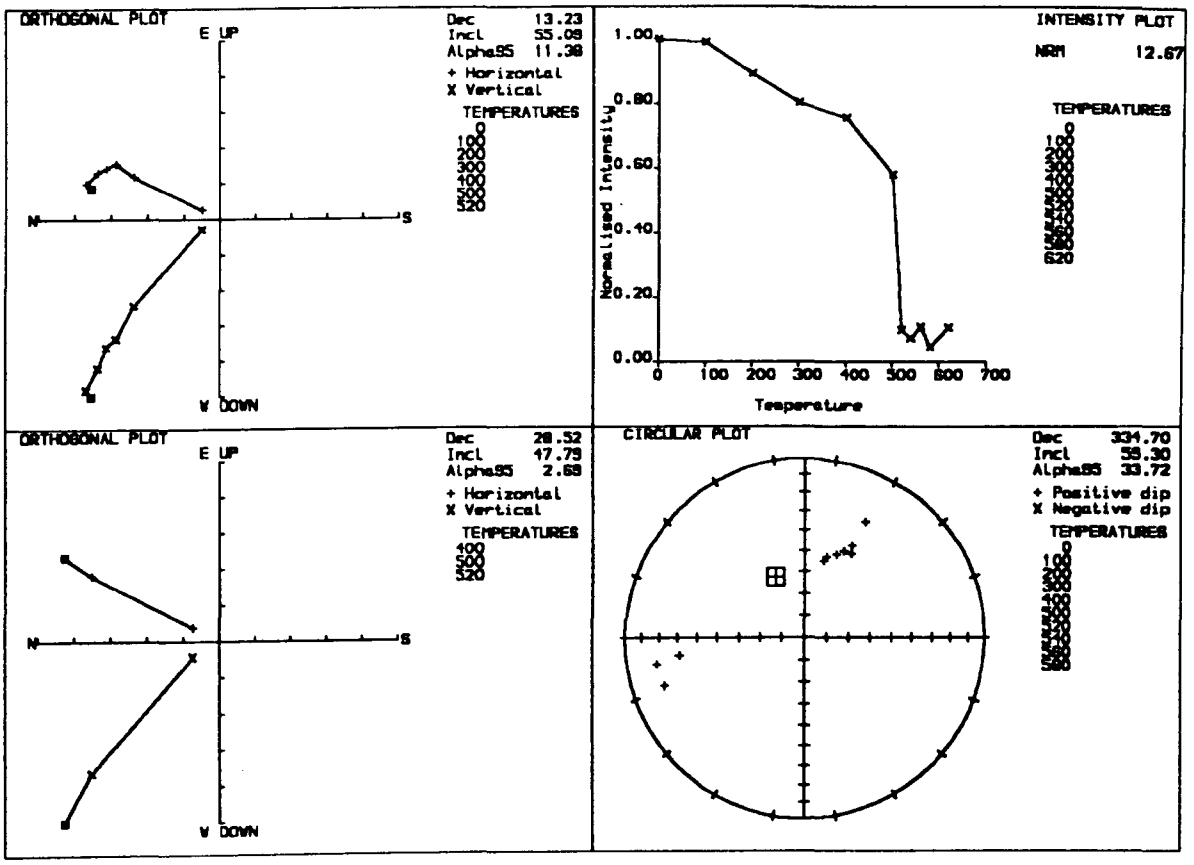

UNBAKED ROCK

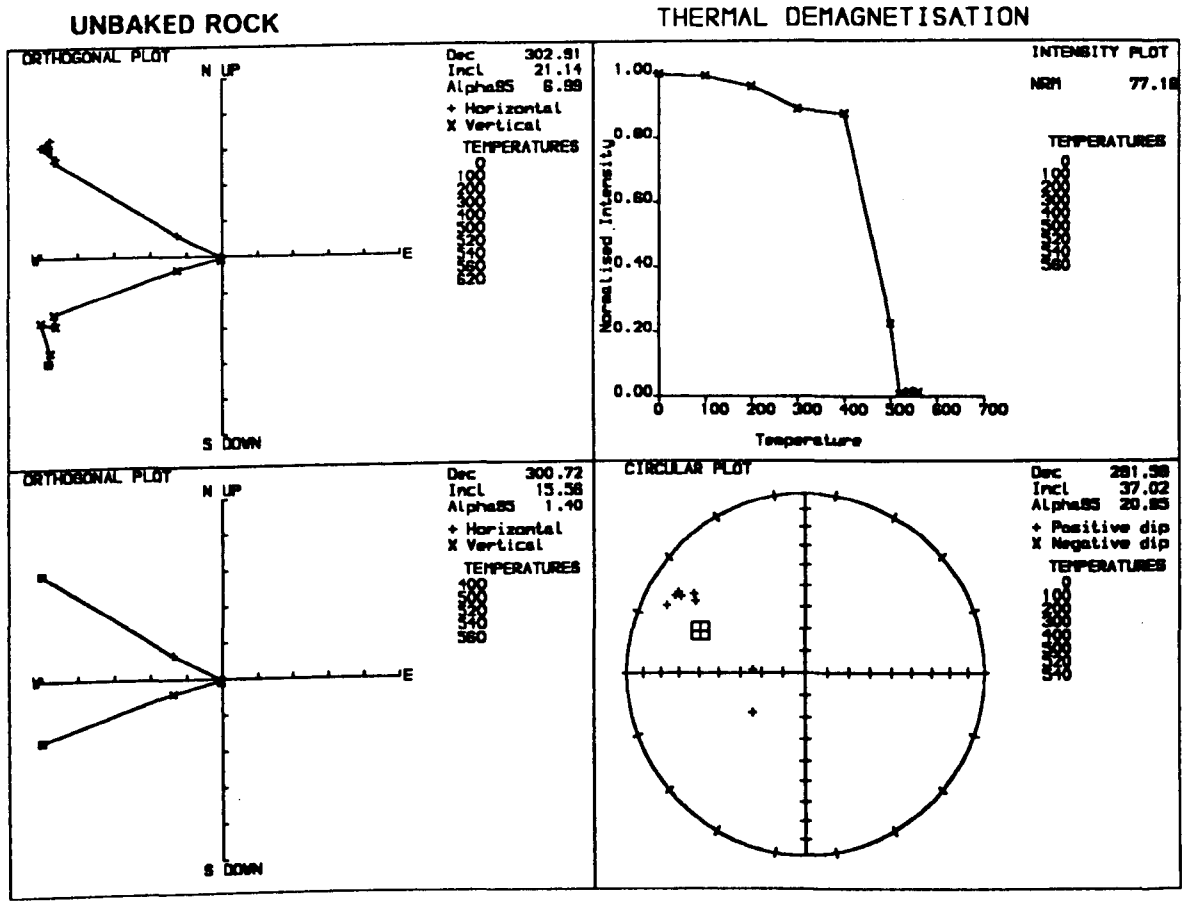

Figure 5.6 : Palaeomagnetic plots illustrating the component structure of remanence for typical samples from contact site B. Labels as for Figure 4.6.

DYKE INTERIOR

THERMAL DEMAGNETISATION

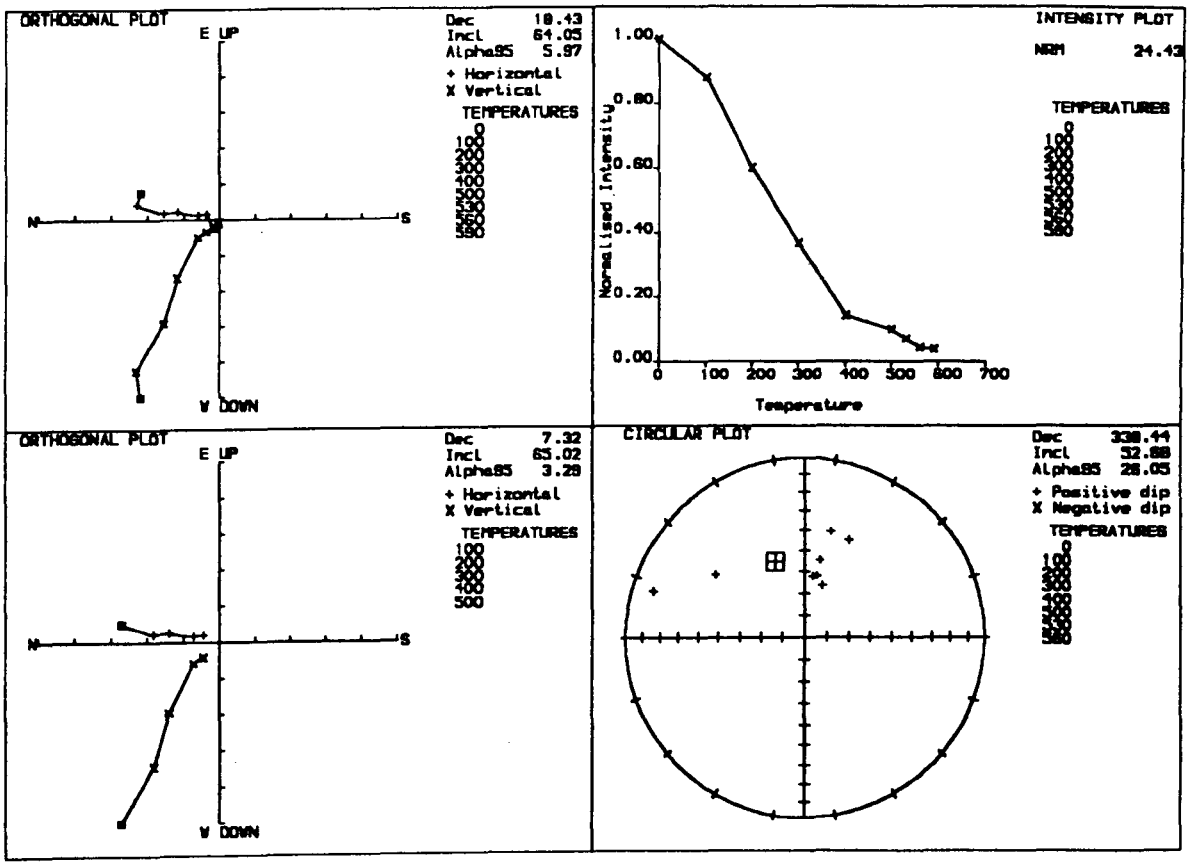

DYKE MARGIN

THERMAL DEMAGNETISATION

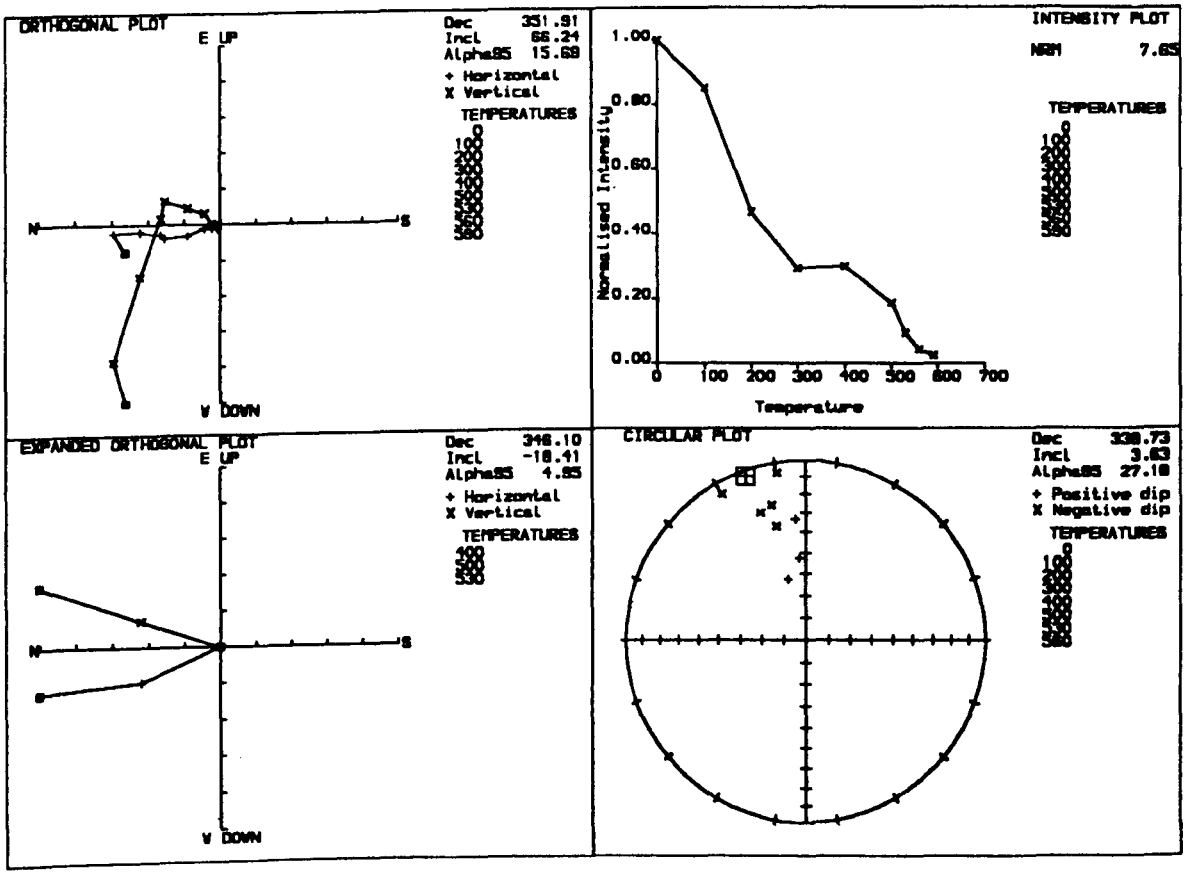

METAMORPHIC ZONE

THERMAL DEMAGNETISATION

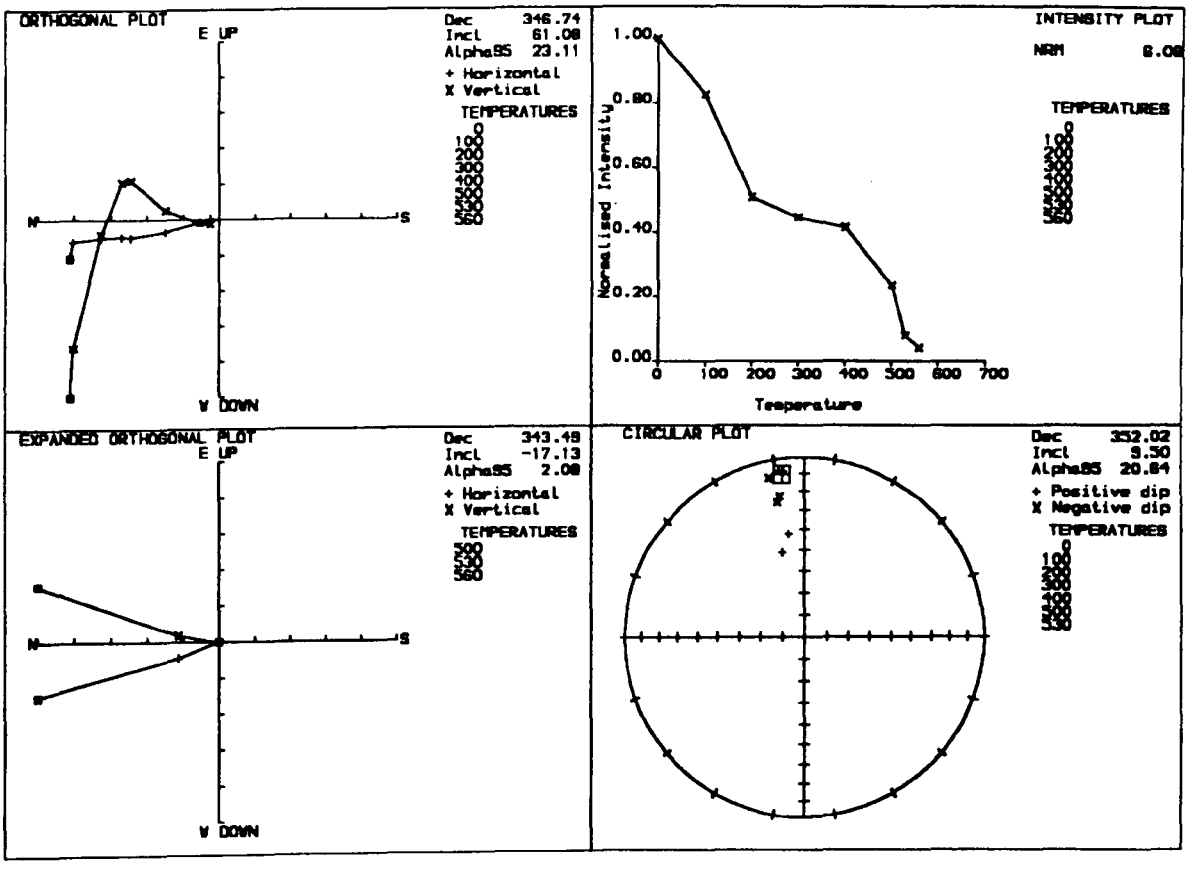

HEATED ZONE

THERMAL DEMAGNETISATION

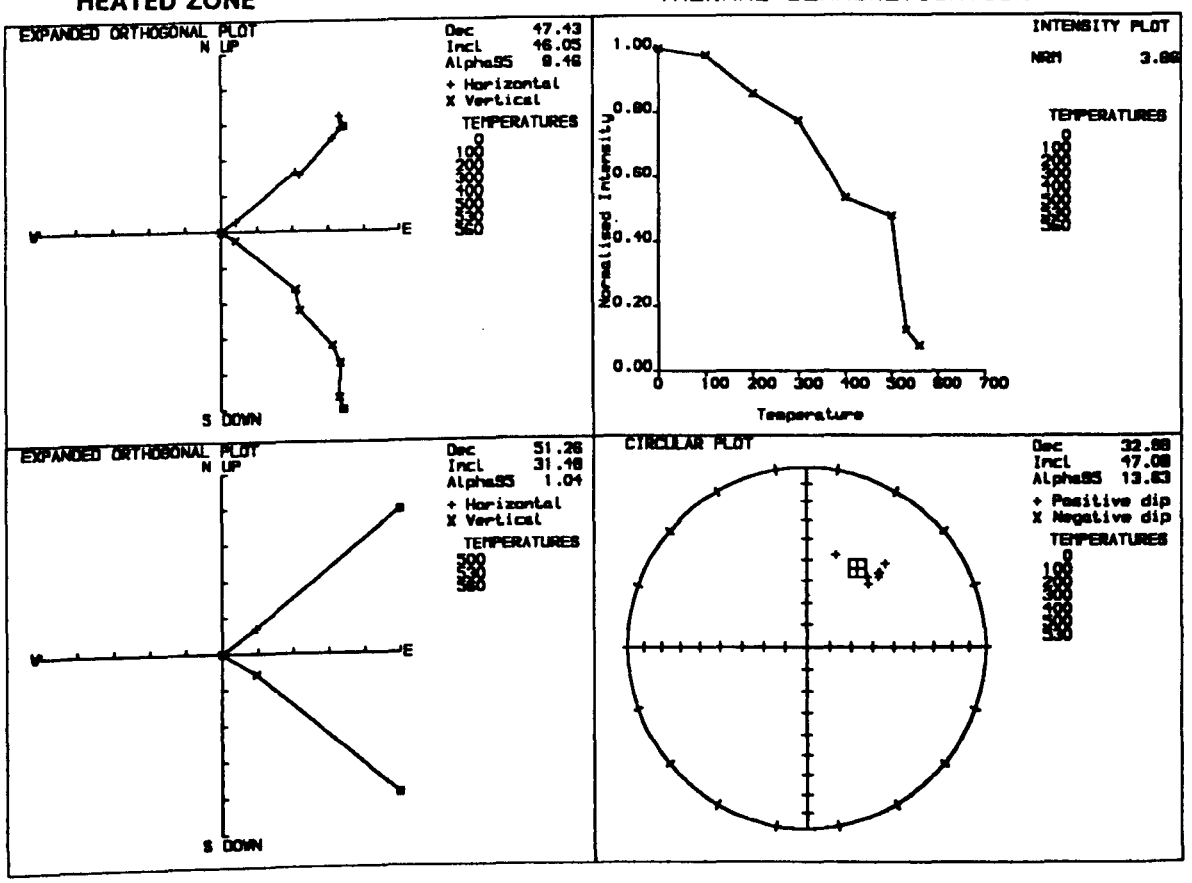

WARMED ZONE

THERMAL DEMAGNETISATION

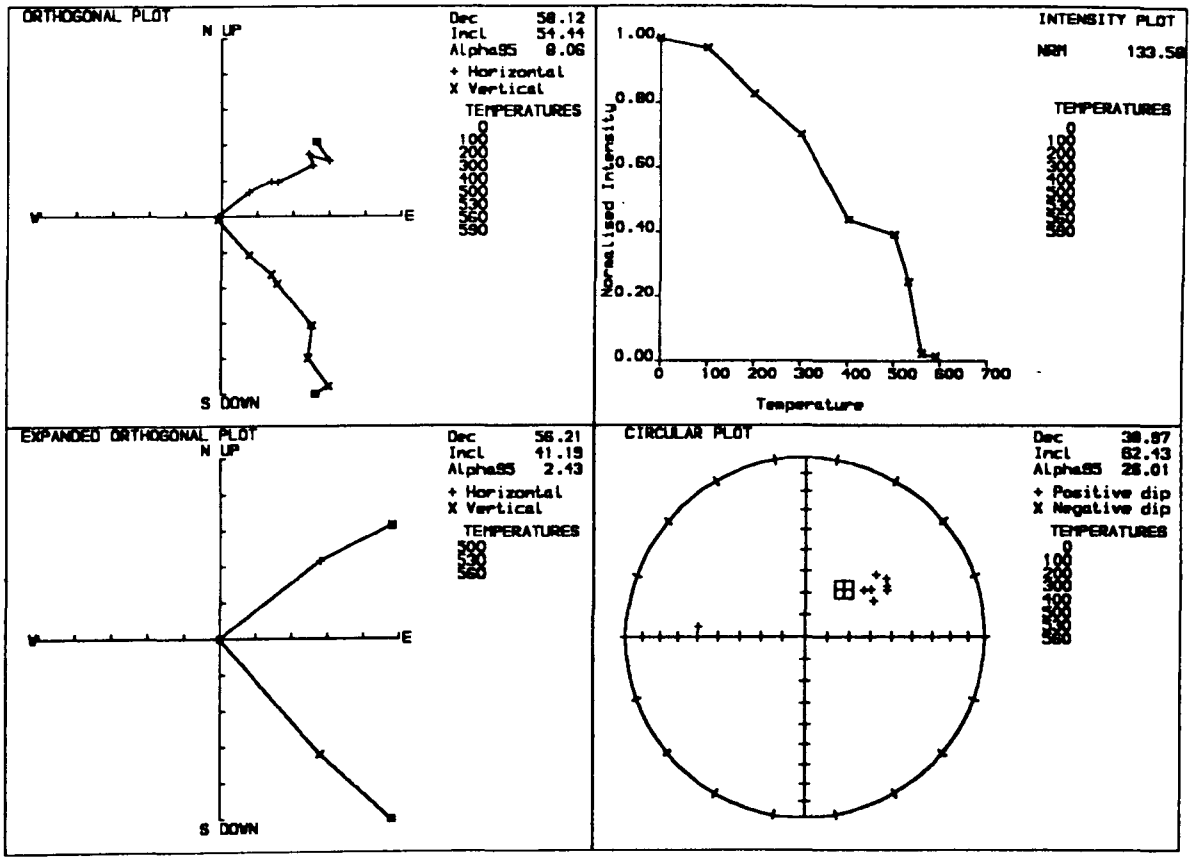

UNBAKED ROCK

THERMAL DEMAGNETISATION

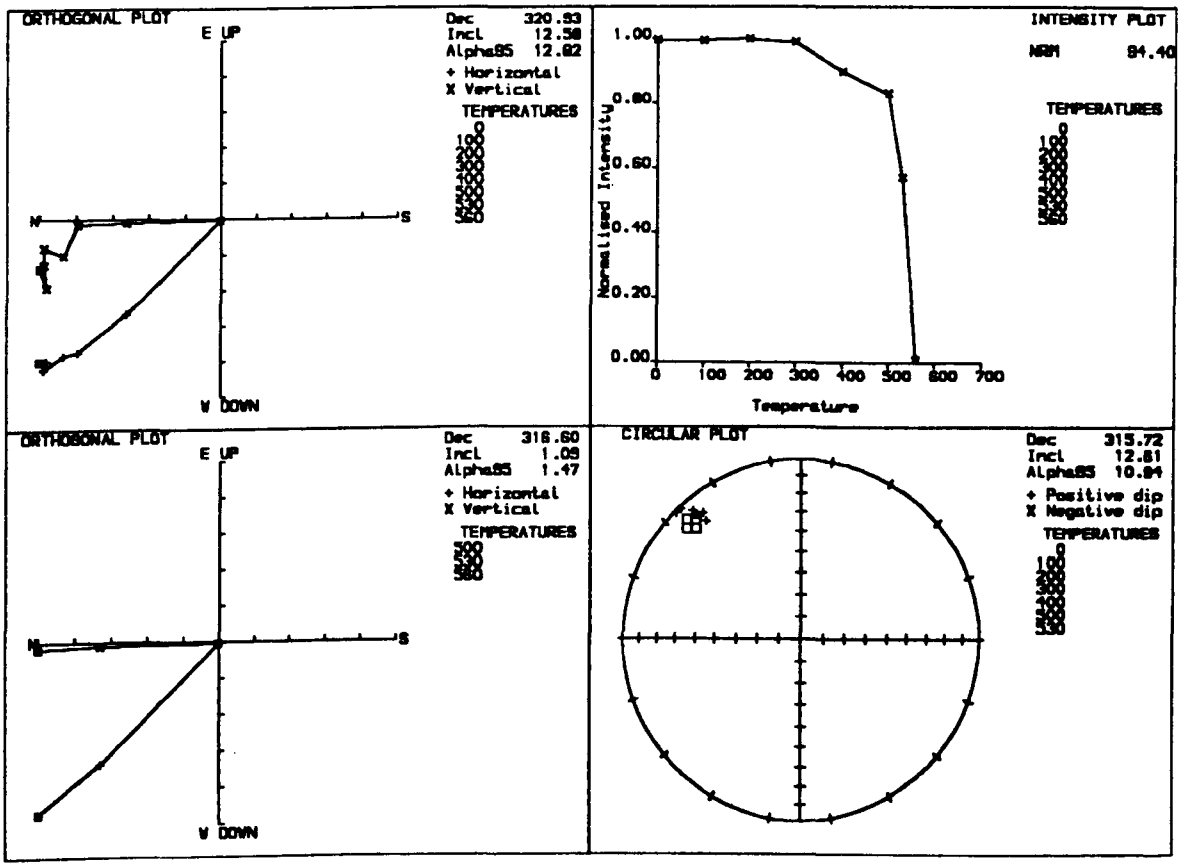

5.3.2 Baked Contact tests C-E (country rock : red beds)

(a) Geological setting and sampling

Figure 5.2 shows the sampling localities for baked contact tests C-E. Test C was performed on samples from Mâjût Bay on the shore of Eriksfjord. Samples for site D were collected from three dykes and contacts in the Mâjût sandstone on the shoreline of Isafjord on the western side of the Ilímaussaq Peninsula (Figure 5.2). The dykes in the Isafjord area are intruded very close together, separated by only a few metres of country rock and therefore samples were collected only from the metamorphic zone of each dyke to avoid complications in the remanence record caused by the effects of neighbouring dykes. The samples for site E were collected from a 4m wide trachytic dyke intruded into silty sandstones deposited between flows L8 and L9 of the Mussartût Lava Formation. The positions of samples with respect to the dykes are listed in Table 5.2.

(b) NRM measurements

Figure 5.7a illustrates the NRM directions for all samples from sites C-E and Figure 5.7b shows the variation in NRM intensity with increasing distance from the dykes. The NRM intensities of all unbaked sandstone samples and the majority of baked sandstones are very weak ($< 0.05 \times 10^{-5} Am^2kg^{-1}$) and are therefore close to, or below, the noise level ($\simeq 0.01 \times 10^{-5} Am^2kg^{-1}$) of the spinner magnetometer. Due to time constraints it was only possible to measure a limited number of unbaked red bed samples on the cryogenic magnetometer . However, these results showed that future work should be carried out using this more sensitive magnetometer since the weak samples proved to define stable remanence vectors.

(c) Thermal demagnetisation results

The thermal demagnetisation results are listed in Table 5.2 and illustrated in Figures 5.8-5.11. Unfortunately, the majority of samples fail to define remanence vectors over any temperature interval, since their NRM intensities are so close to the noise level that they fail to converge on the origin. Most samples show consistent directions on the stereoplot during demagnetisation and a mean can be calculated for the characteristic remanence directions from the sandstones by applying Fisher statistics to the directional distribution. However, the component structure of this remanence was not resolved and is is not possible to be certain that it is single component.

Most samples from site C show only one magnetisation direction, usually at low temperatures ($<400°C$), which has a steep inclination and a N-NW declination. The directions of magnetisation illustrated by the dyke itself do not form a coherent group and this makes it difficult to compare them with those from the sandstones. Figures 5.8a and 5.9 indicate that very little can be deduced from the results of this detailed contact study.

The contact site at Isafjord (site D) also shows poor thermal demagnetisation results; the NRM intensity of the baked sediments is very low and consequently no vectors can be isolated in these samples (Fig. 5.10).

The low NRM intensities of the baked sediments from sites C and D suggest that the baking effect of the Late Gardar dykes, which intrude the Mâjût Sandstone on both sides of the Ilímaussaq Peninsula has not been to create new minerals and impart a total TRM although these sediments are visibly bleached. The related hydrothermal activity may have removed any magnetic component. This inference receives support from a palaeomagnetic

SAMPLE	DIST	J_{nrm}	HIGH TEMP COMPONENT D (°)	I (°)	α95	LOW TEMP COMPONENT D (°)	I (°)	α95
			(>450°C)			(<450°C)		
C-1 DykeM	0	3.4	282.2	-62.3	3.8	-	-	
C-2 DykeI	0	2.5	18.8	-13.4	1.6	29.3	4.5	4.1
C-3 DykeM	0	2.1	330.1	-60.2	3.6	-	-	
C-4 Metam	0.03	0.04	-	-	-	358.5	69.9	1.9+
C-5 Heated	0.1	0.04	-	-	-	26.6	50.9	20.0+
C-6 Heated	0.12	0.04	-	-	-	314.7	-57.5	8.9+
C-7 Warmed	1.5	0.02	-	-	-	306.0	44.3	22.6+
C-8 Warmed	1.8	0.05	-	-	-	67.9	41.3	9.6+
C-9 Unbak	2.0	0.04	-	-	-	87.7	12.4	11.2+
C-10Unbak	2.2	0.04	-	-	-	69.8	21.9	4.2+
C-11Unbak	3.0	72.9	-	-	-	61.6	56.1	1.8
D-1 Dyke	0	48.0	304.5	66.3	4.2	-	-	-
D-2 Metam	0.03	0.1	189.0	25.8	53.2	-	-	-
D-3 Dyke	0	27.8	298.2	82.5	2.6	-	-	-
D-4 Metam	0.03	0.02	-	-	-	253.0	16.0	15.2
D-5 Dyke	0	10.8	49.3	75.1	2.2	-	-	-
D-6 Metam	0.03	Unstable		-	-	-	-	-
E-1 DykeM	0	25.9	8.5	-31.1	0.7	-	-	-
E-2 DykeI	0	10.4	248.8	24.5	17.5	27.7	-52.2	12.2
E-3 Unbak	1.5	1.3	87.1	-22.4	2.5	-	-	-
E-4 Unbak	1.7	0.9	86.7	-10.9	1.9	-	-	-
E-5 Unbak	2.0	2.2	92.2	-2.5	5.4	-	-	-
E-6 Unbak	2.2	2.8	95.1	-15.2	2.6	-	-	-

Table 5.2 : Results of baked contact tests on sites C-D within the Mâjût sandstone formation. Symbols as in Table 5.1. + Denotes sample for which no vector was defined and the mean direction was calculated by applying Fisher statistics to points which define consistent directions throughout demagnetisation.

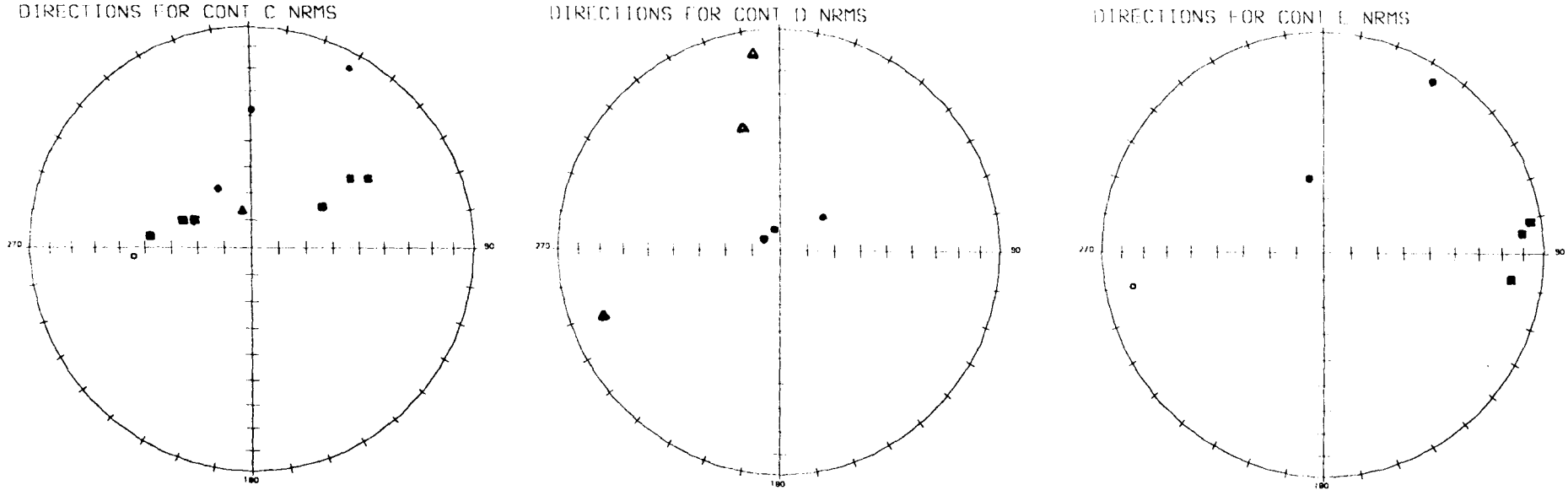

Figure 5.7a : NRM directions for dyke samples (o), baked lavas (Δ) and unbaked lavas (□) for contact sites C-E.

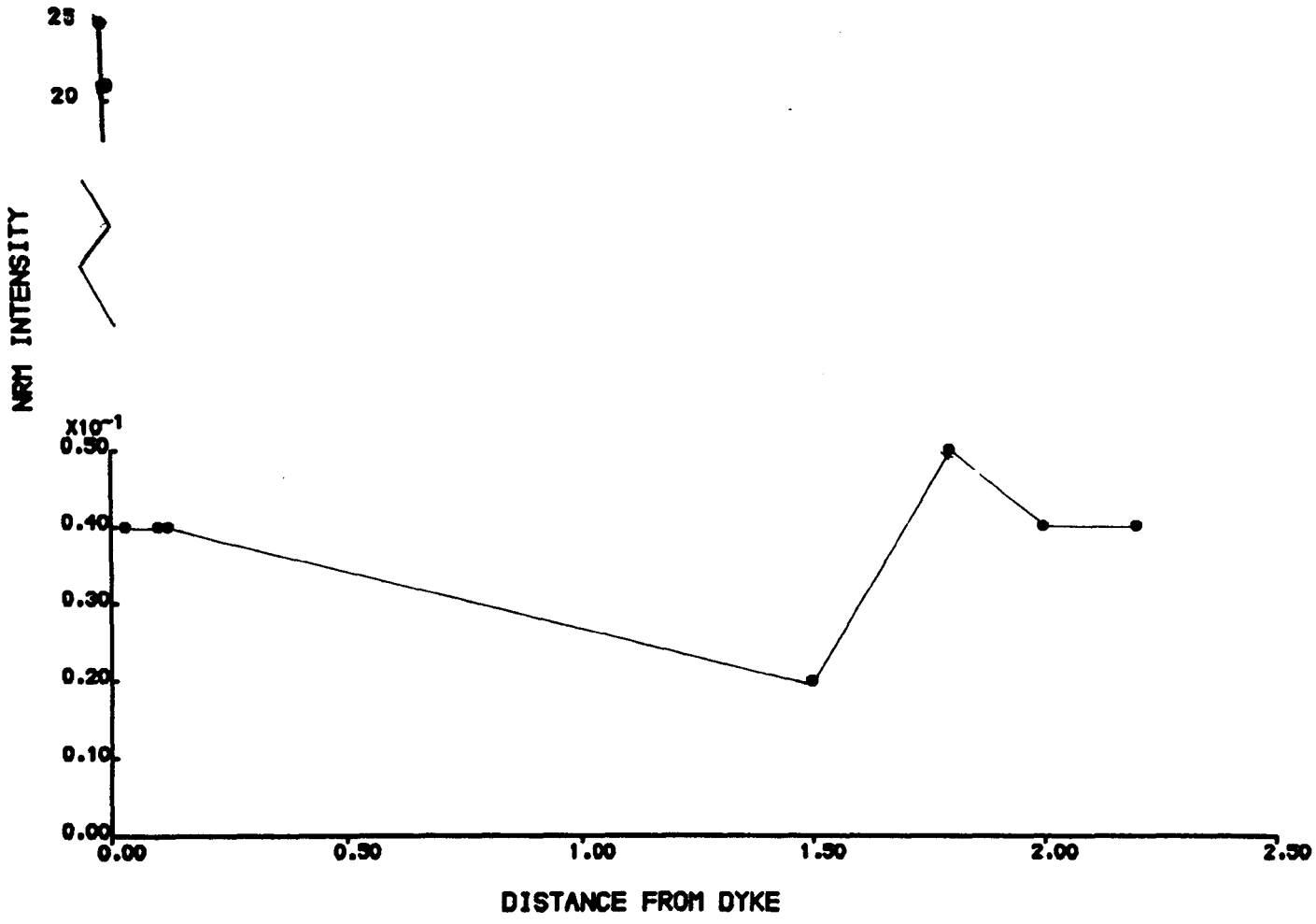

Figure 5.7b : Graph indicating the variation in NRM intensity with distance away from the dyke margins for contact sites C. Labels as for Fig. 5.3a.

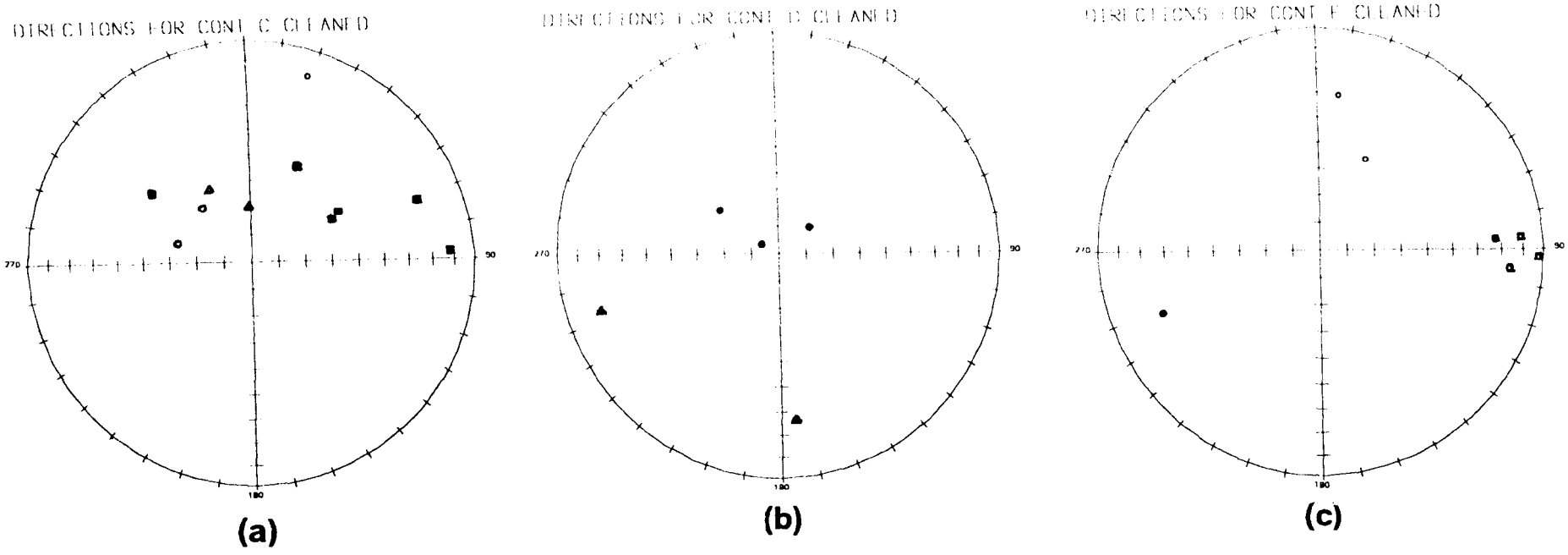

Figure 5.8 : Thermally demagnetised (characteristic remanence) directions for samples from the dyke (o), baked lavas (▵) and unbaked lavas (▫) for (a) contact site C, (b) contact site D and (c) contact site E.

Figure 5.9 : Palaeomagnetic plots illustrating the component structure of remanence for typical samples from contact site C. Labels as for Figure 4.6.

DYKE INTERIOR

THERMAL DEMAGNETISATION

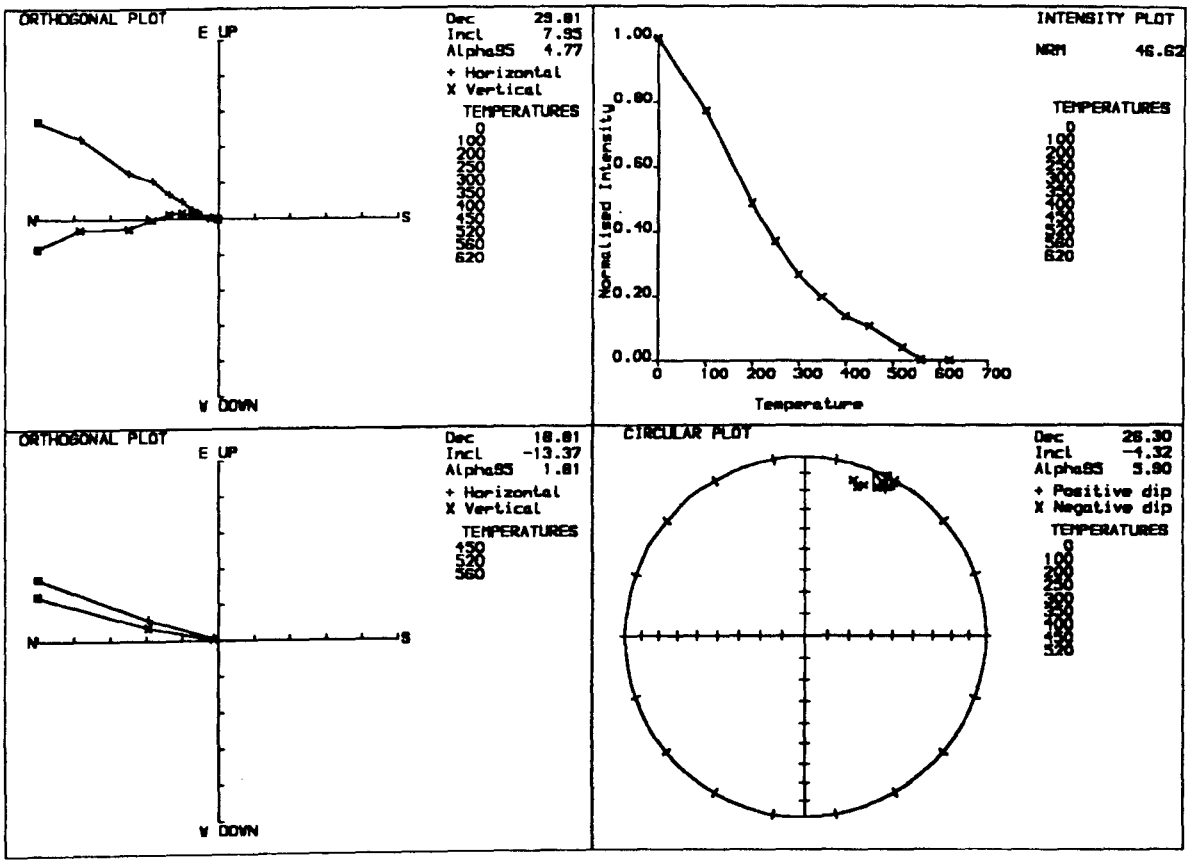

DYKE MARGIN

THERMAL DEMAGNETISATION

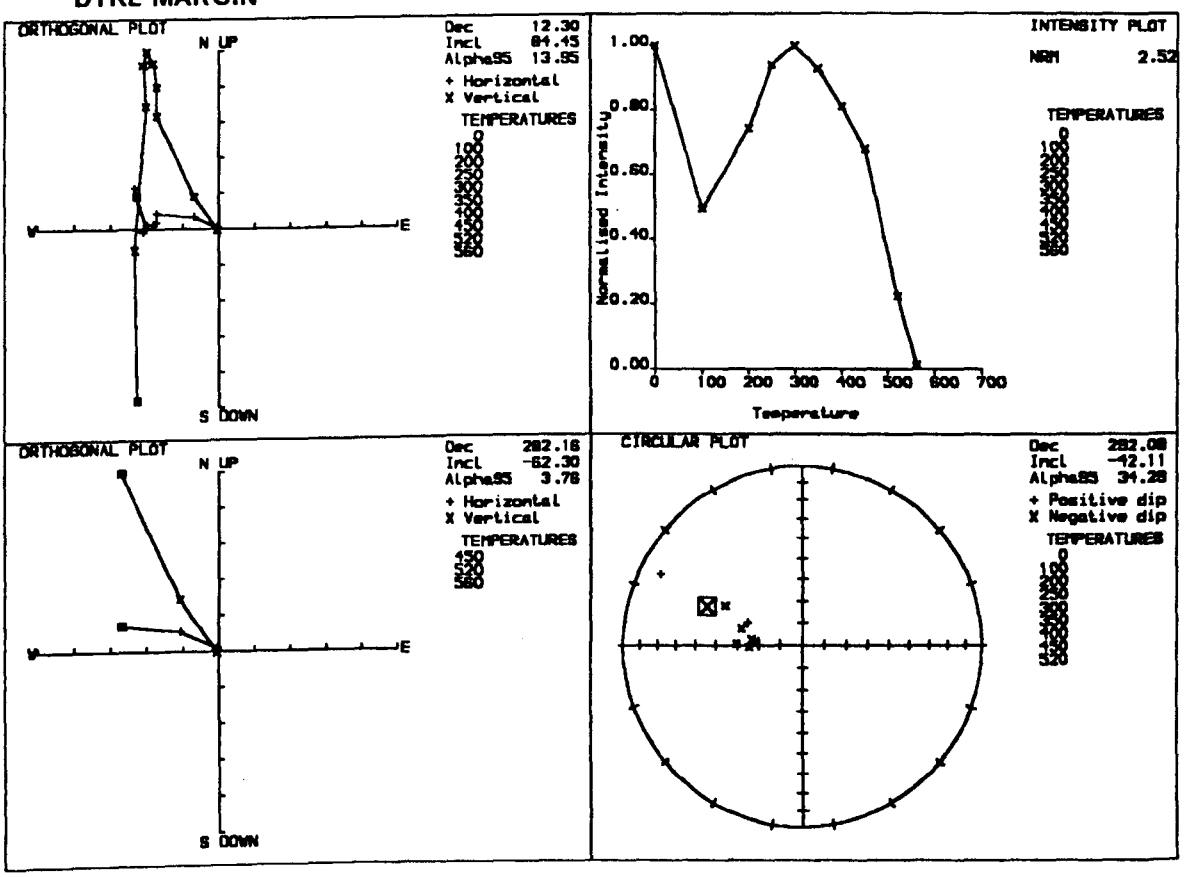

METAMORPHIC ZONE

THERMAL DEMAGNETISATION

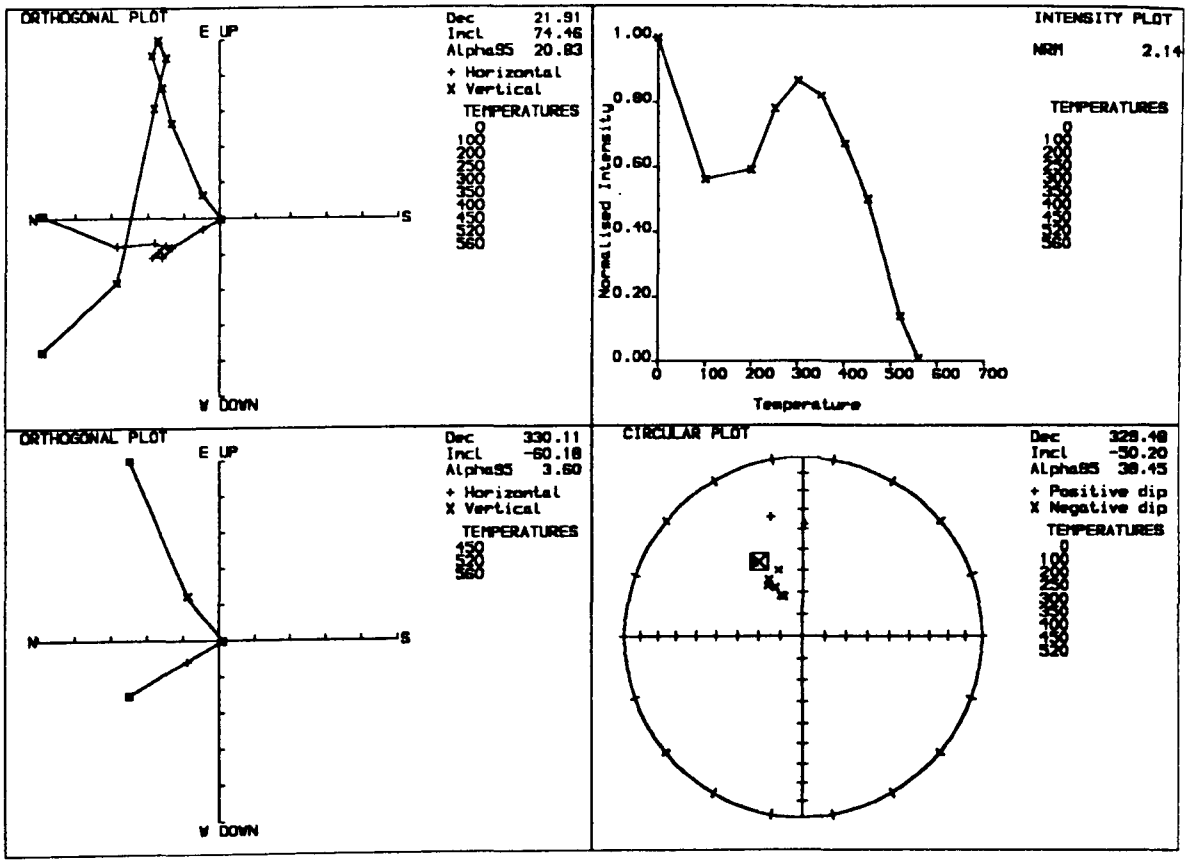

HEATED ZONE

THERMAL DEMAGNETISATION

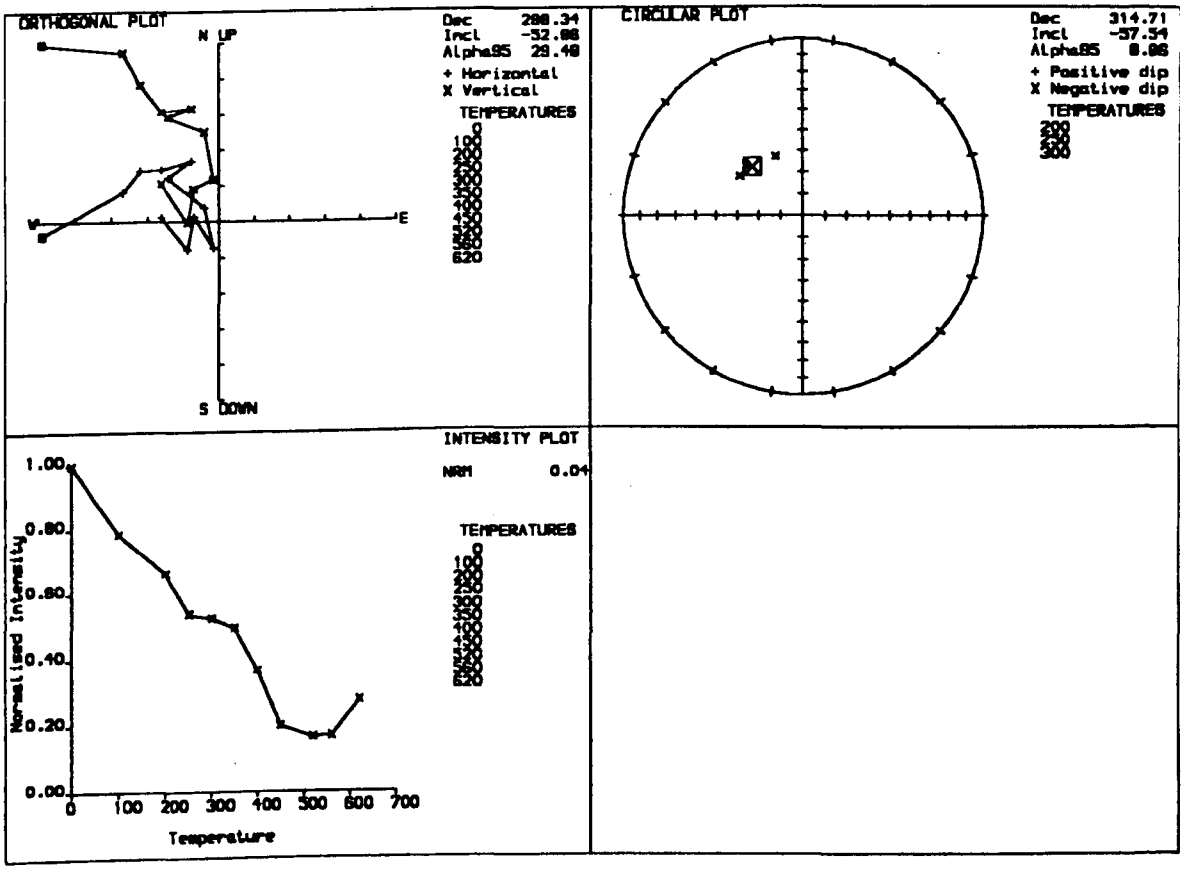

WARMED ZONE

THERMAL DEMAGNETISATION

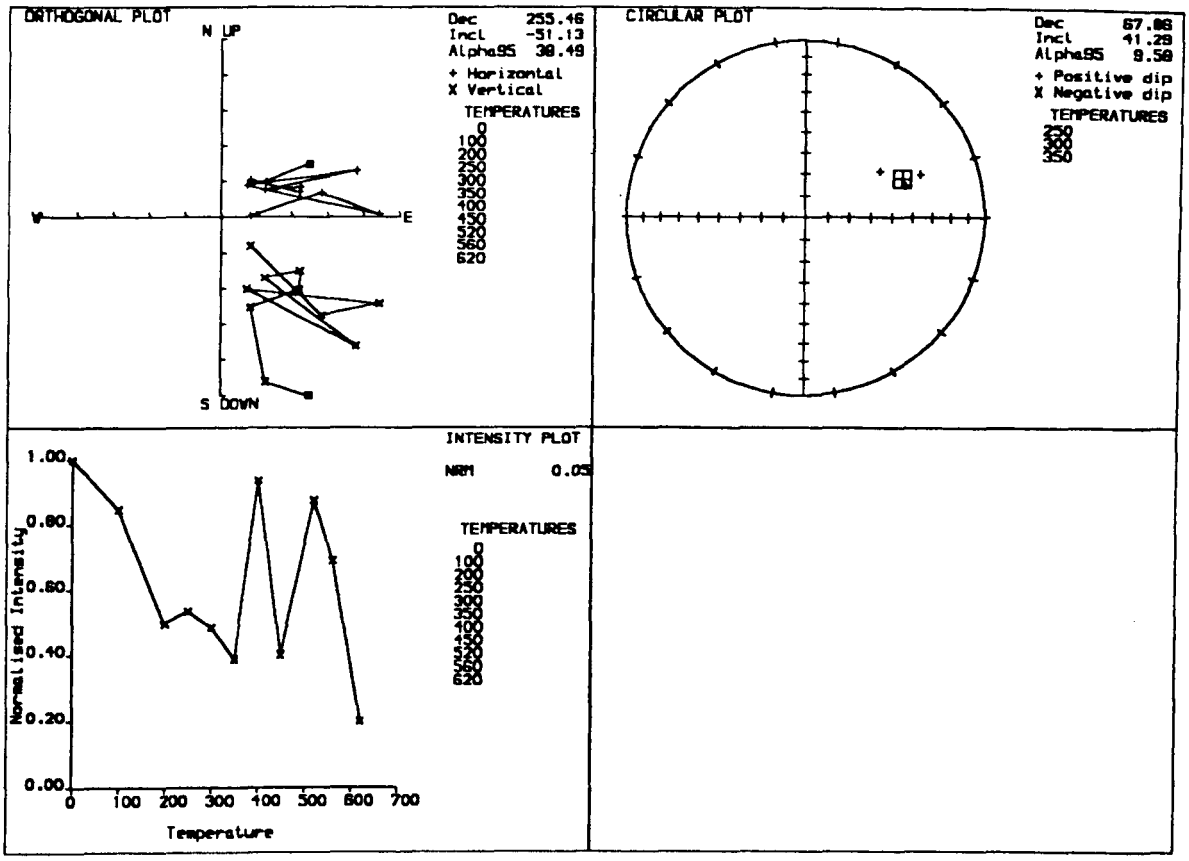

UNBAKED ROCK

THERMAL DEMAGNETISATION

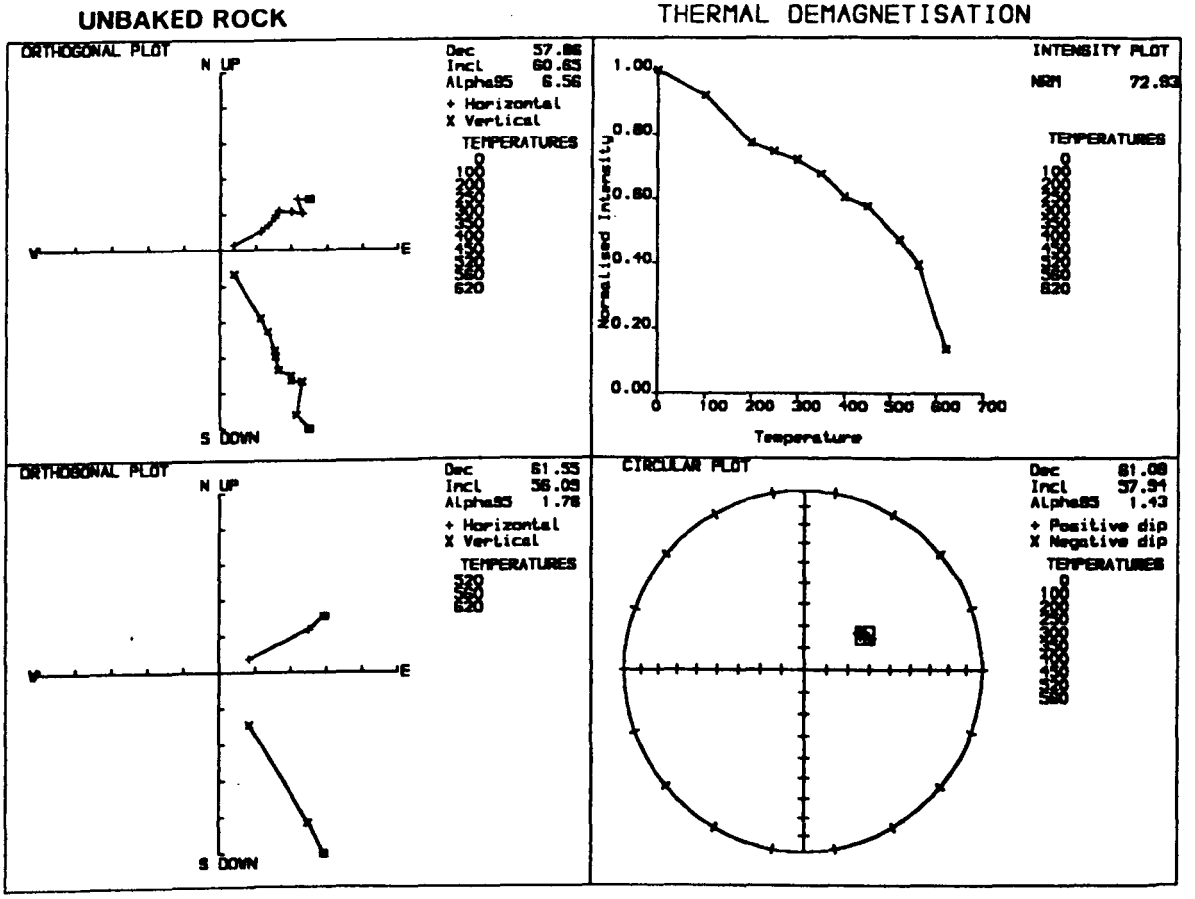

Figure 5.10 : Palaeomagnetic plots illustrating the component structure of remanence for typical samples from contact site D. Labels as for Figure 4.6.

DYKE INTERIOR

THERMAL DEMAGNETISATION

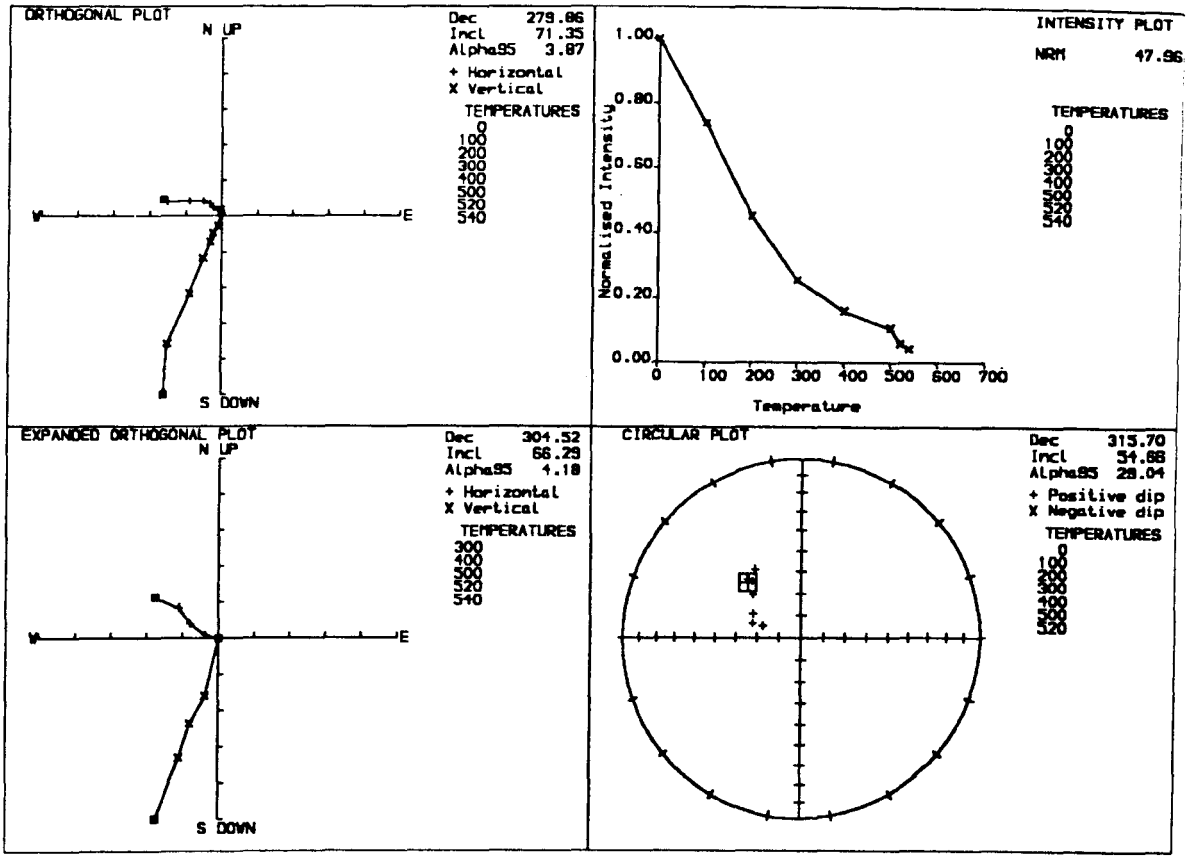

METAMORPHIC ZONE

THERMAL DEMAGNETISATION

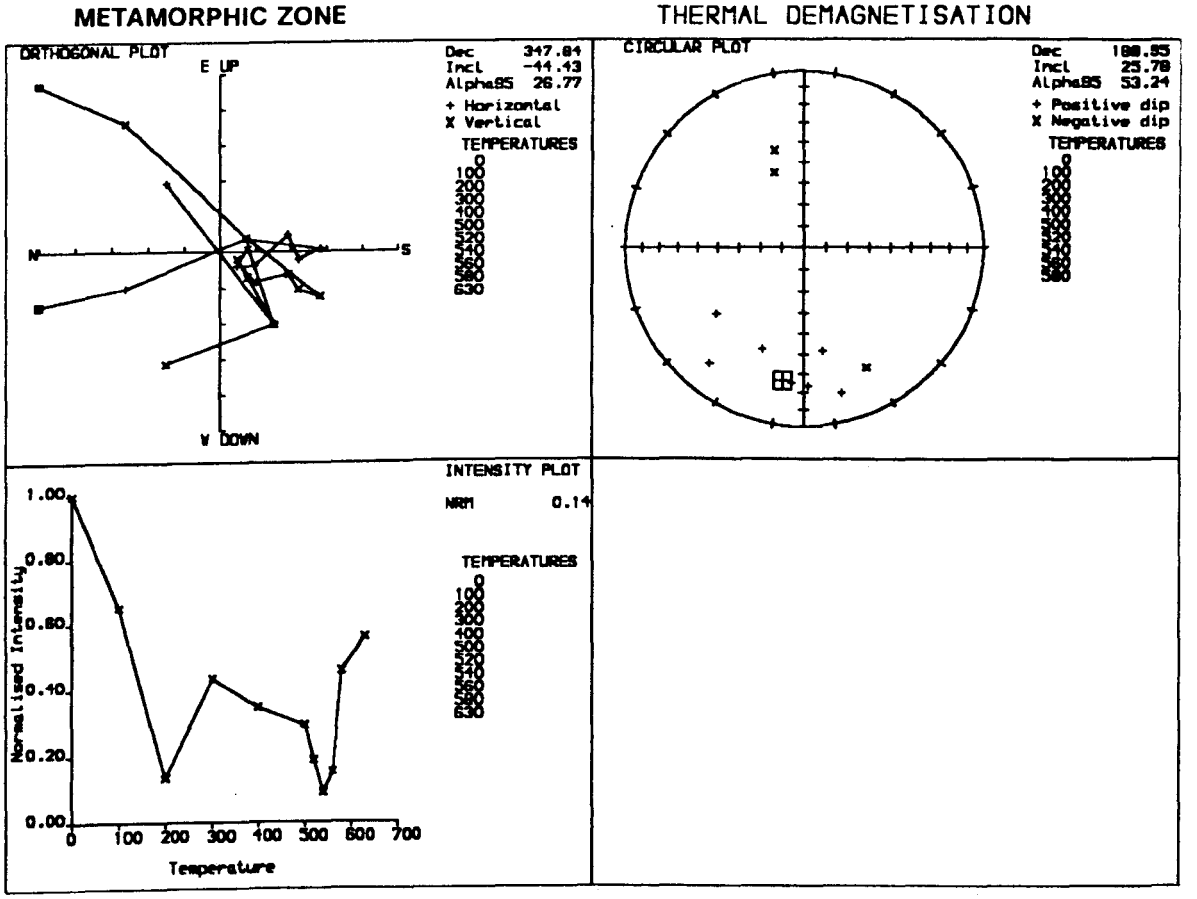

Figure 5.11 : Palaeomagnetic plots illustrating the component structure of remanence for typical samples from contact site E. Labels as for Figure 4.6.

DYKE MARGIN

THERMAL DEMAGNETISATION

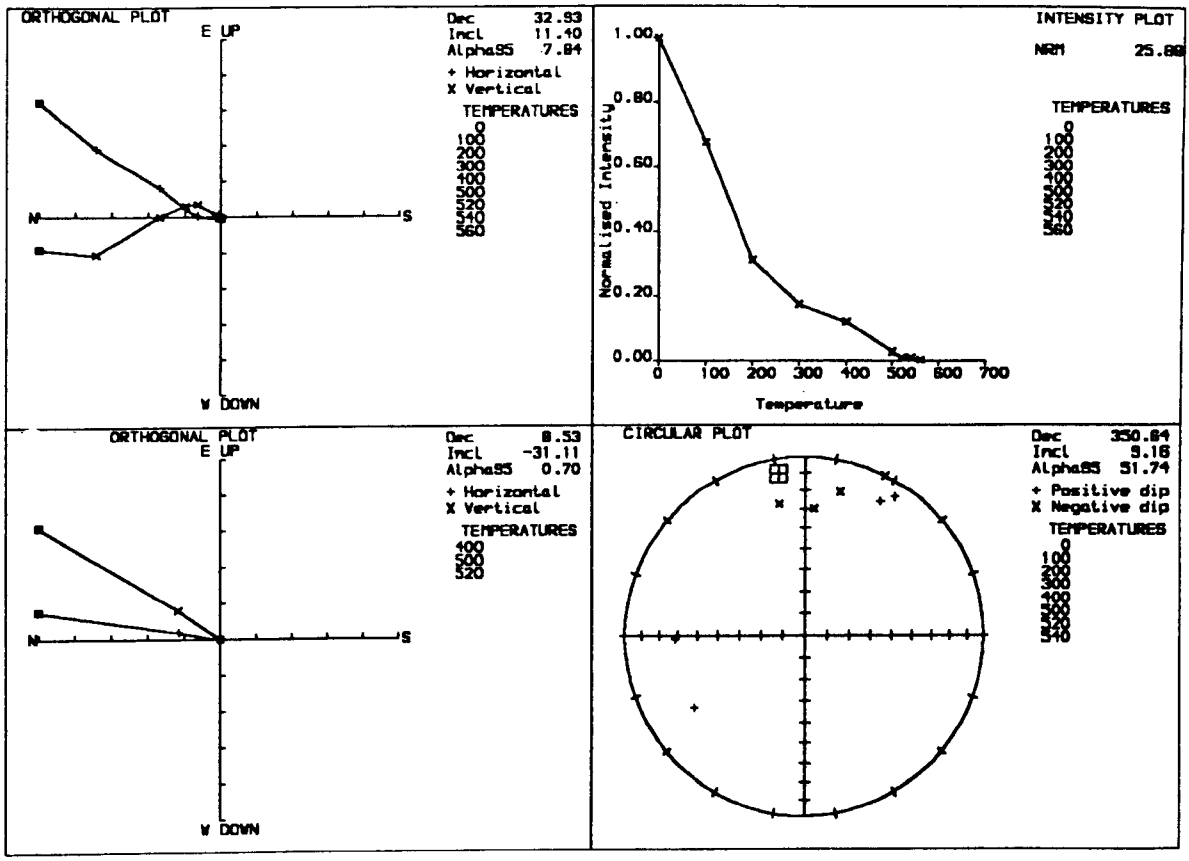

UNBAKED ROCK

THERMAL DEMAGNETISATION

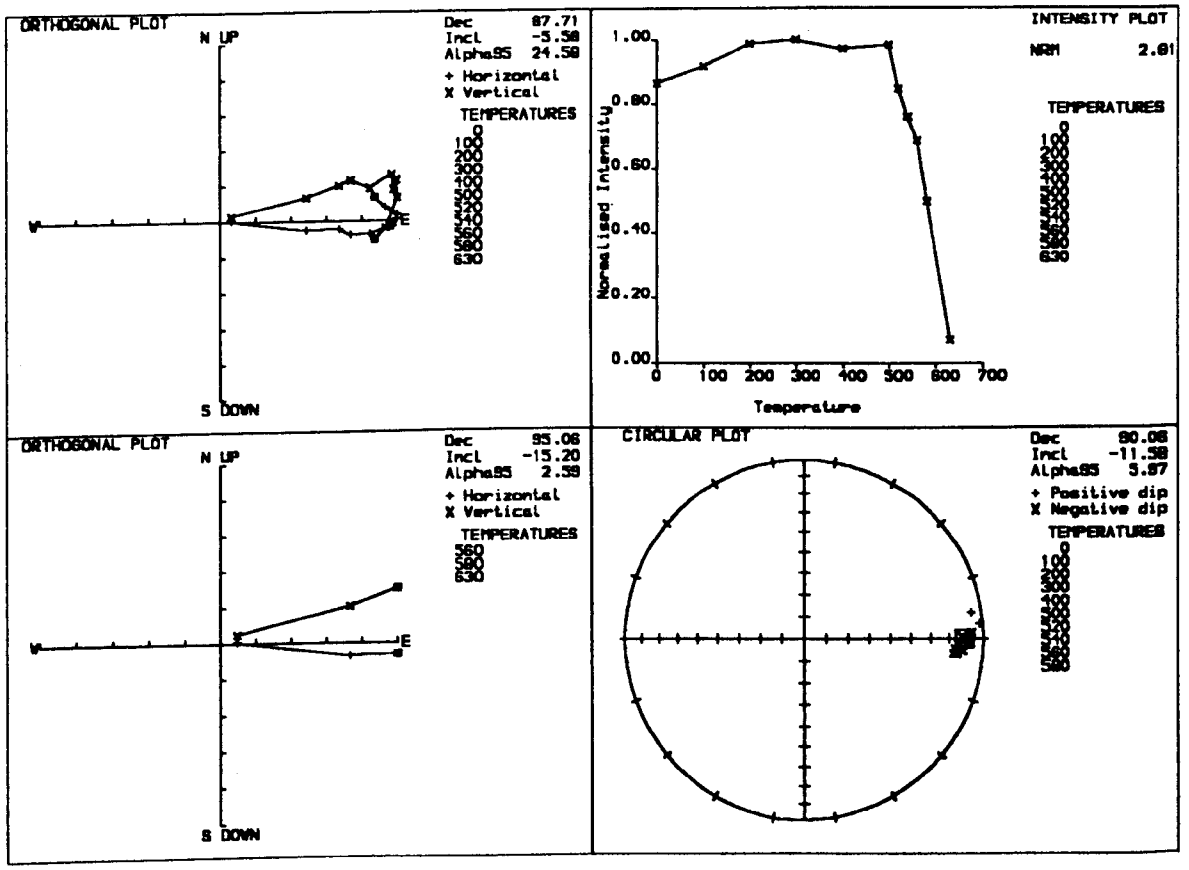

study on the Mâjût Sandstone Formation, performed as an honours project at Liverpool by Jim Parsons (Parsons, 1989). He found that sandstone samples adjacent to NE-trending fractures, associated with the Late Gardar activity, which were white in colour, had lower NRM intensities than the red sandstones which characterise the bulk of the Mâjût Formation. He concluded that the pale samples had been bleached by hydrothermal fluids permeating these fractures in Late Gardar times. Dyke intrusion in Late Gardar times may be linked to this event. The Mâjût Sandstone therefore appears to be unsuitable for a palaeomagnetic baked contact test.

The samples from site E give curious results. No samples were collected from the metamorphic and heated zones adjacent to the 3m thick trachyte dyke, since the rocks were highly fractured in these regions and accurate orientation was not possible. The nearest sample was 1.5 m away from the dyke margin (Table 5.2) which means that this site is unlikely to give any useful contact information. However, the results are interesting since it appears that the unbaked sandstone unit sampled here records a reversely magnetised field direction (Figure 5.11). This direction may represent a reversed magnetozone occuring between lava flows L8 and L9 of the Mussartût formation, or else this sediment possesses a PDRM, younger than the remanence in both lava flows, acquired during a later period of reversed polarity.

5.3.3 Baked Contact test F (country rock : upper lavas)

The palaeomagnetic study of the upper (Ilímaussaq) lava formation (Chapter 4) was, in effect, a large scale baked contact test. The Ilímaussaq alkaline complex intrudes the top of the lava pile and it has been suggested (Chapter 4) that the thermomagnetic effect of the intrusion has contaminated the original remanence of the flows in this part of the stratigraphy. The NE,

steep positive directions obtained from the flows in question were thought to reflect the geomagnetic field direction at the time of cooling of the intrusion.

The results reported in this section are the outcome of a palaeomagnetic investigation of several different facies from this intrusion which has attempted to isolate the characteristic remanence direction for the body and compare this direction with the components of remanence isolated in the highest flows of the Ilímaussaq Lava Formation.

(a) Geological setting and sampling

Detailed descriptions of the geology of the Ilímaussaq intrusion are given in by Ussing (1912), Ferguson (1964, 1970), Hamilton (1964) and Sørensen et al (1969). The intrusion is the most intensively studied, and constitutes one of the most petrologically-varied, peralkaline complexes anywhere in the world. The earliest phase is an augite-syenite which is effectvely a chilled facies forming a marginal envelope around the intrusion and it also comprises the surviving roof zone of the complex. The bulk of this unit is medium-coarse grained but includes a chilled marginal facies; nepheline occurs further from the contact with the country rock. Within the intrusion, rhythmically-layered, eudialyte-bearing nepheline syenites (kakortokites) represent the deepest exposed part of the intrusion and twenty-nine layered horizons are recognised (Bohse et al, 1971). Overlying the kakortokites, a 600-800m thick unit of coarse grained poikilitic rocks called naujaites occur, comprising arfvedsonite, aegirine, feldspar and eudialyte enclosing sodalite crystals. These have the widest distribution of all rocks in the intrusion and form a sheet-like unit underlying sodalite foyaite (undersaturated syenite). The naujaites crystallised contemporaneously with the kakortokites but in a different part of the intrusion. Lujavrites (arfvedsonite and aegirine-bearing

nepheline syenites) intrude and brecciate the lower part of the naujaites. The kakortokites, naujaites and lujavrites collectively comprise the agpaitic rocks, within which xenoliths of the marginal syenite are found. Consequently, it is inferred that the marginal syenite solidified before the intrusion of the agpaitic rocks. Hamilton (1964) regards the two rock types as separate intrusive events with differentiation at depth from an augite syenite magma forming the agpaites.

Blaxland et al (1978) derived a Rb-Sr isochron age for the emplacement of the marginal syenites of 1143 $\pm$ 21 Ma. Consolidation of the remainder of the pluton may have been protracted. It is believed that the intrusion of the agpaites marks the termination of Gardar magmatism in this part of the Province.

Sixty-seven palaeomagnetic samples were collected from ten sites within the intrusion from an area 5 km north of the town of Narssaq (Figure 5.12). Three sites were located within the agpaitic facies and seven within the marginal syenites.

(b) NRM measurements

Figure 5.13 shows the NRM directions and histograms of NRM intensity for the marginal syenite and agpaitic samples. The syenites have considerably higher NRM intensities than the agpaites and their NRM directions are less scattered.

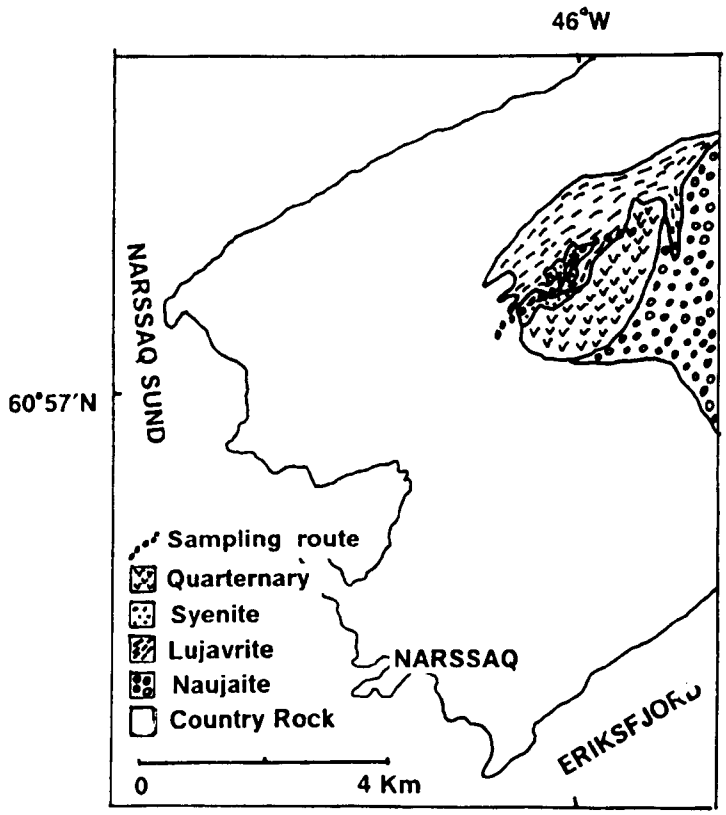

Figure 5.12 : Sketch map indicating the sampling localities for baked contact test F.

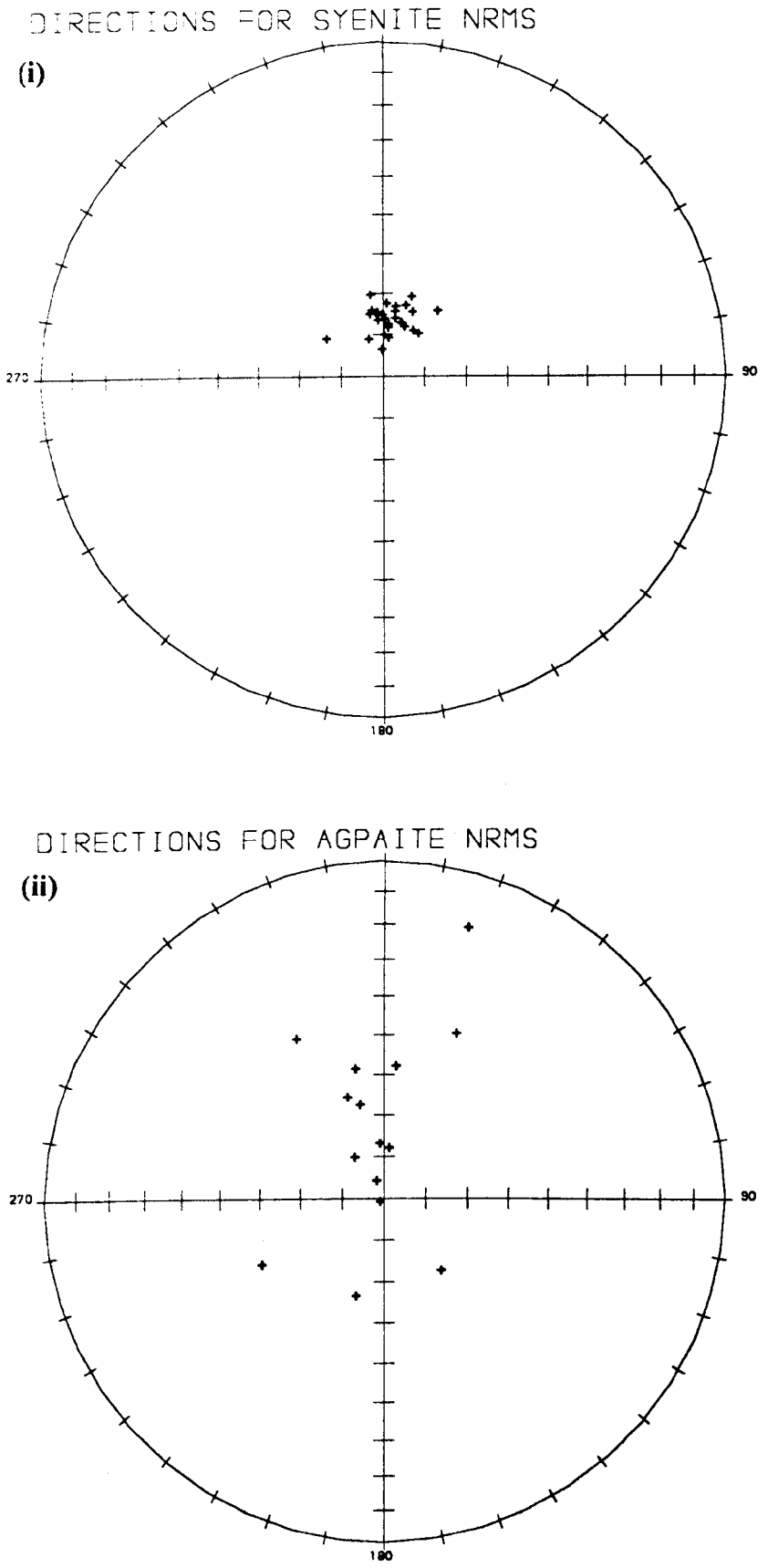

Figure 5.13a : NRM directions for samples from (i) the marginal syenite facies, and (ii) the agpaitic facies of the Ilímaussaq intrusion.

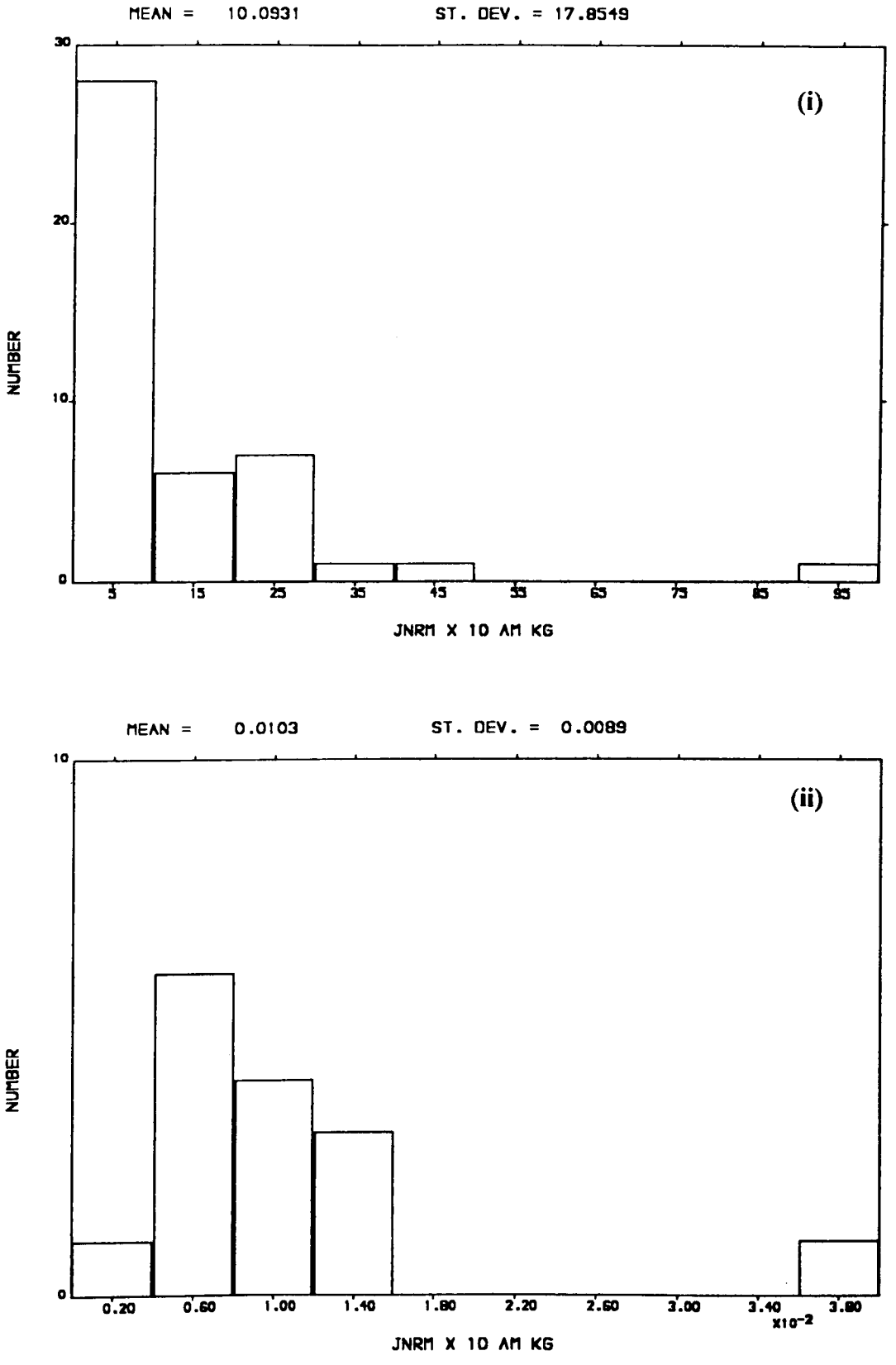

Figure 5.13b : Histograms for NRM intensities for samples from (i) the marginal syenite facies, and (ii) the agpaitic facies of the Ilímaussaq intrusion.

(c) Thermal demagnetisation results

Figures 5.14-5.16 illustrate the characteristic remanence directions isolated by thermal demagnetisation for the marginal syenites and agpaites. The demagnetisation steps used were similar to those used in baked contact sites A-E. Table 5.3 lists the results of thermal demagnetisation and the site means and the overall mean data for the intrusion.

The agpaitic rocks, which were unstable to a.f. demagnetisation (Piper, 1976), also proved to be unstable to thermal demagnetisation; they failed to define any vectors (Figure 5.16) and yielded no consistent directions throughout demagnetisation. This may be because the iron content in the agpaitic facies is incorporated in silicate phases which behave paramagnetically, and there is a general absence of ferrimagnetic minerals, resulting in a very weak NRM intensity. Consequently, no remanence vectors are isolated for these rocks. The marginal syenites, however, were stable to thermal demagnetisation and gave well defined vectors (Figure 5.15). The agpaitic rocks were discarded and the mean direction of magnetisation for the intrusion (Table 5.3) was calculated using the results from the marginal syenites only.

(d) Comparison with results from the Upper Lavas

Figures 5.15 h-i show OVPs for two flows near the top of the upper (Ilímaussaq) lava formation. In this collection, these flows lie closest to the margins of the Ilímaussaq intrusion and can be considered to lie within the contact aureole of the intrusion (which is oval shaped and is about 17 km long by 8km wide). The remanence directions isolated from these flows are almost identical to those isolated from the marginal syenites of the Ilímaussaq intrusion (Figs. 5.15 a-g). The steep N-NE positive directions are also totally

SAMPLE	Jnrm	D	I	α95	T
IL1-1	0.003	Unstable			
-2	0.004	Unstable			
-3	16.0	304.6	70.8	3.1	200-560
-4	0.011	58.9	75.1	1.1	200-560
-5	1.8	63.2	68.8	2.0	300-560
-6	37.7	99.4	-73.3	1.2	300-590
-7	99.4	143.4	-64.2	1.2	200-590
-8	5.5	310.2	76.0	1.2	200-400
Site mean	(N = 5)	75.0	66.8	-	k = 1.02
IL2-1	41.9	9.2	83.6	2.6	200-530
-2	16.0	325.5	73.1	3.0	300-560
-3	23.5	12.5	74.2	1.0	400-530
-4	26.6	9.2	78.4	2.4	300-590
-5	20.5	253.7	80.1	2.6	50-500
-6	25.1	18.6	78.8	1.2	300-560
-7	21.2	35.8	73.3	0.3	300-560
Site mean	(N = 6)	5.3	77.7	5.5	k = 152.1
IL3-1	0.5	14.6	74.4	2.0	0-450
-2	0.6	35.2	67.0	2.7	200-400
-3	0.9	38.7	75.9	0.2	0-200
-4	0.5	30.3	80.0	7.3	0-500
-5	0.6	15.6	68.6	1.5	100-300
Site mean	(N = 5)	31.5	73.4	5.7	k = 183.1
IL4-1	0.5	359.8	52.5	7.0	400-525
-2	0.3	66.1	73.2	2.4	100-400
-3	0.5	21.8	72.7	2.5	100-450
-4	0.4	40.3	72.7	1.3	100-350
-5	0.4	36.9	72.2	1.9	200-400
-6	0.023	Unstable			
Site mean	(N = 5)	25.2	72.0	13.3	k = 33.9
IL5-1	0.4	38.5	77.9	3.3	200-500
-2	0.4	54.5	66.9	14.4	500-620
-3	0.4	51.7	77.1	4.3	200-500
-4	0.4	3.8	73.1	2.4	400-550
-5	0.5	36.0	68.9	0.9	200-450
Site mean	(N = 5)	41.2	73.1	5.8	k = 173.6
IL6-1	0.04	322.6	60.8	1.9	200-400
-2	0.04	44.7	69.8	3.4	0-300
-3	20.5	60.4	69.8	2.8	0-550
-4	25.1	49.0	76.0	1.8	200-550
-6	12.2	30.7	82.0	2.3	100-525
-7	14.9	55.9	78.6	1.9	100-525
-8	12.9	33.8	74.9	2.8	100-525
-9	15.4	30.9	80.4	1.6	0-525
Site mean	(N = 7)	45.6	76.2	4.2	k = 208.7
IL7-1	0.1	37.1	80.9	7.7	100-400
-2	0.1	22.9	70.8	2.8	200-500
-3	0.09	20.7	67.3	0.6	200-500
-4	0.1	15.7	71.2	3.8	0-400
-5	0.09	37.0	73.7	2.4	0-400
Site mean	(N = 5)	25.0	72.9	5.4	k = 202.8
Intrusion mean		38.1	74.2	5.5	k = 123.8

Table 5.3 : Thermal demagnetisation results from the Ilímaussaq alkaline intrusive complex. (Symbols as for Table 5.1).

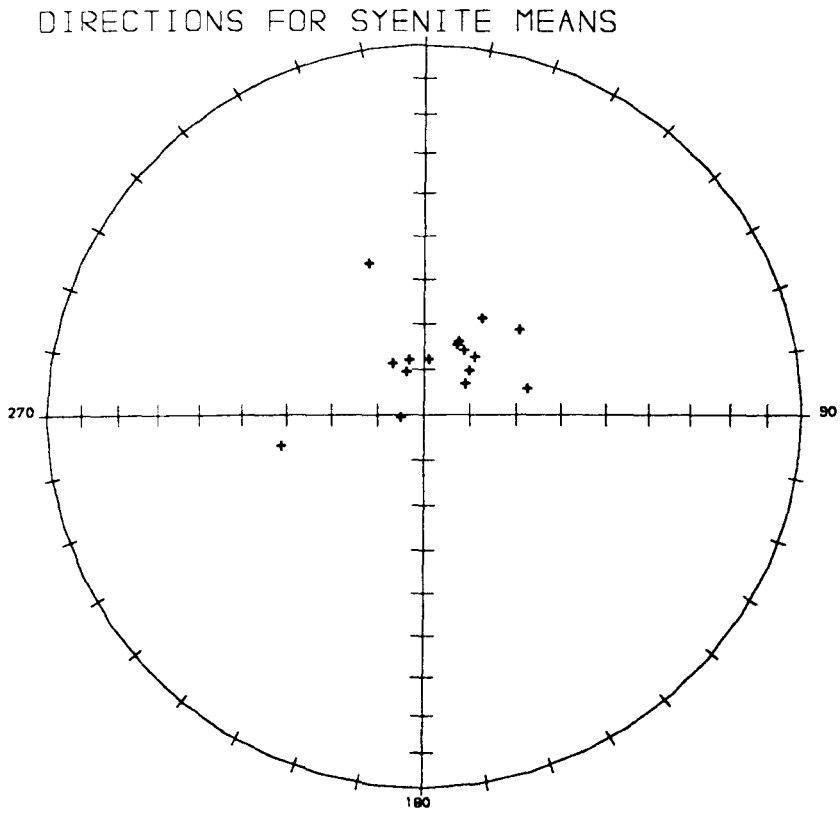

Figure 5.14 : Thermally demagnetised (characteristic remanence) directions for samples from the marginal syenite facies.

Figure 5.15 : Palaeomagnetic plots illustrating the component structure of remanence for typical samples from (a-c) the marginal syenite facies, and (d-e) two flows from the top part of the Upper Lava Formation nearest to the margin of the intrusion. Labels as for Figure 4.6.

(a) SAMPLE I1-05

THERMAL DEMAGNETISATION

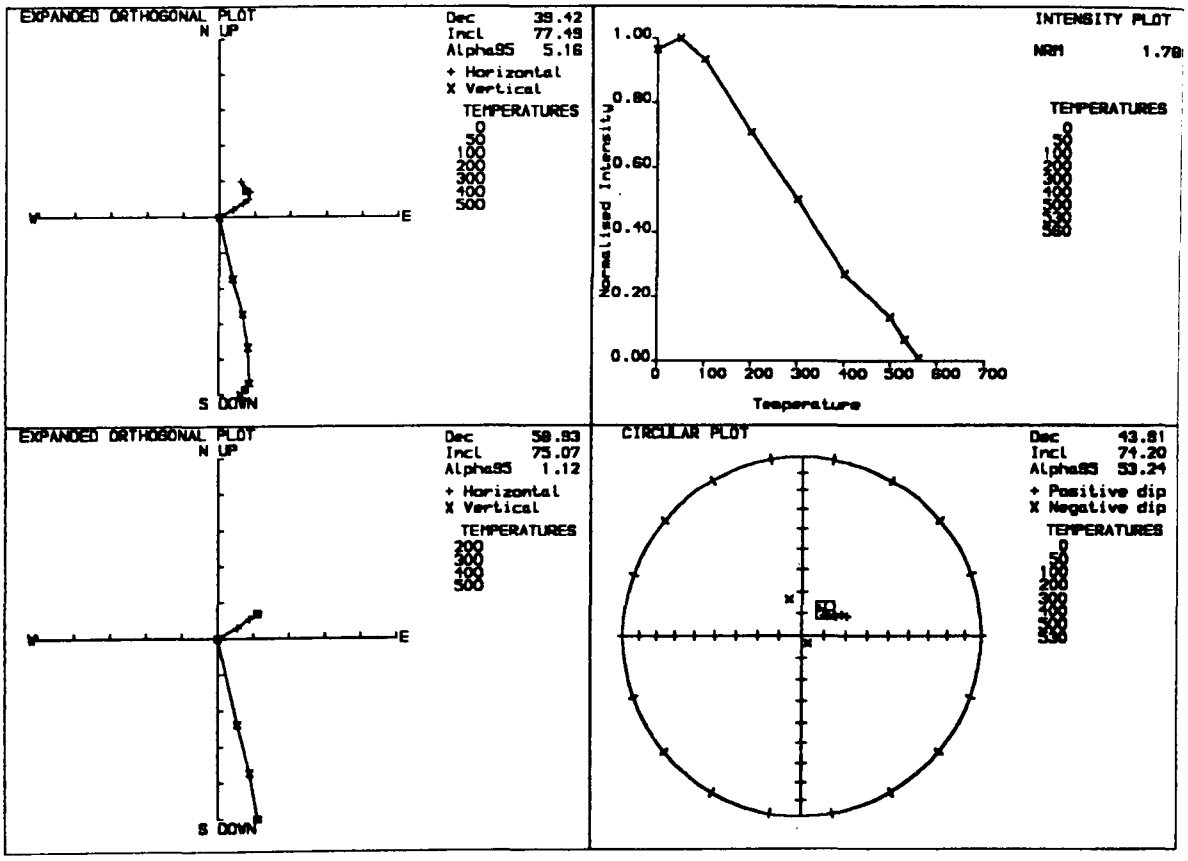

(b) SAMPLE I2-07

THERMAL DEMAGNETISATION

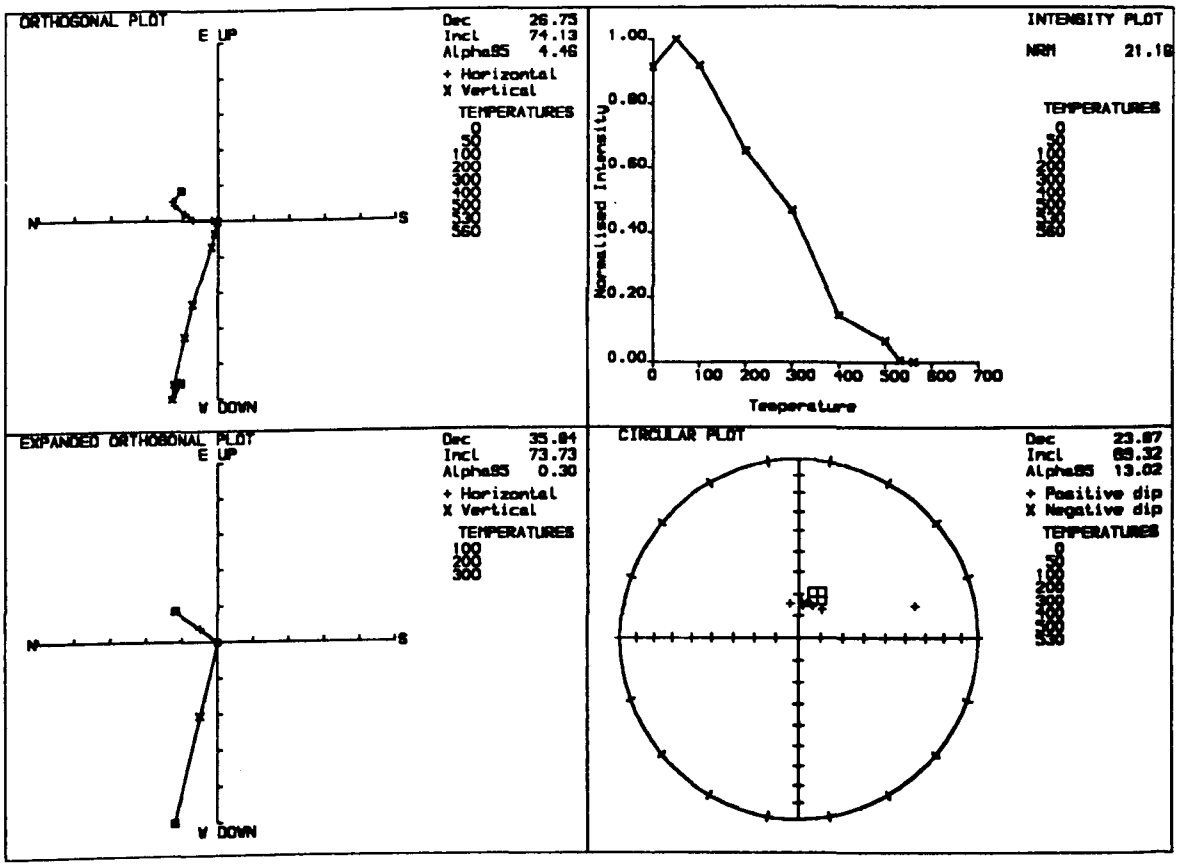

(c) SAMPLE I3-05 THERMAL DEMAGNETISATION

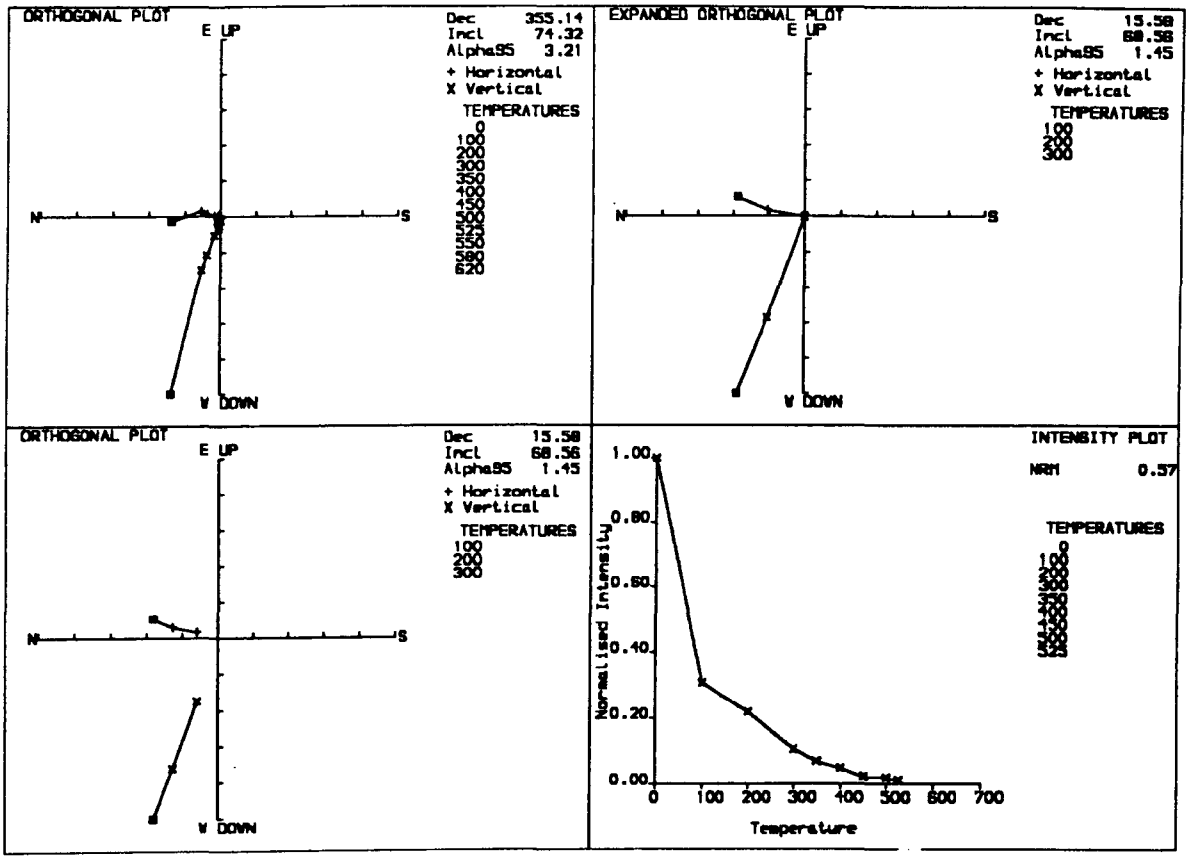

(d) SAMPLE U29-02

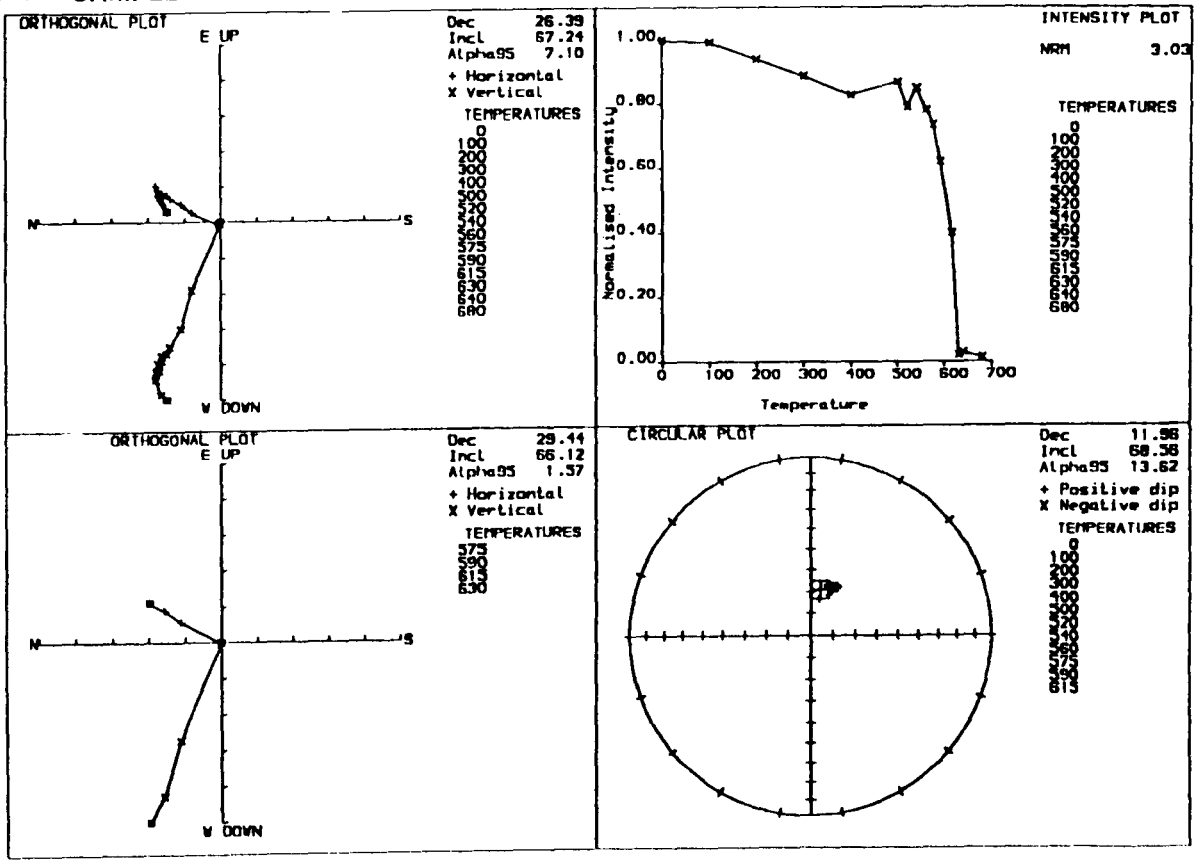

(e) SAMPLE U36-02

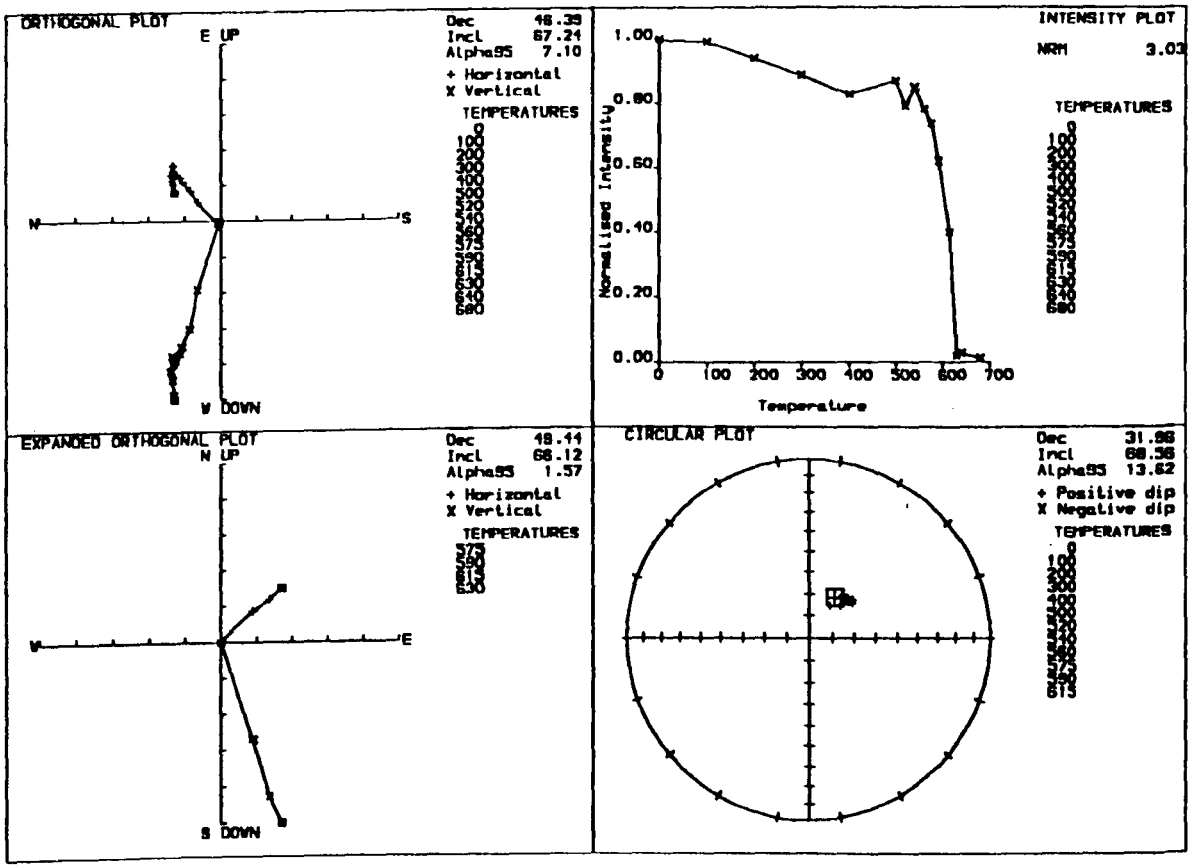

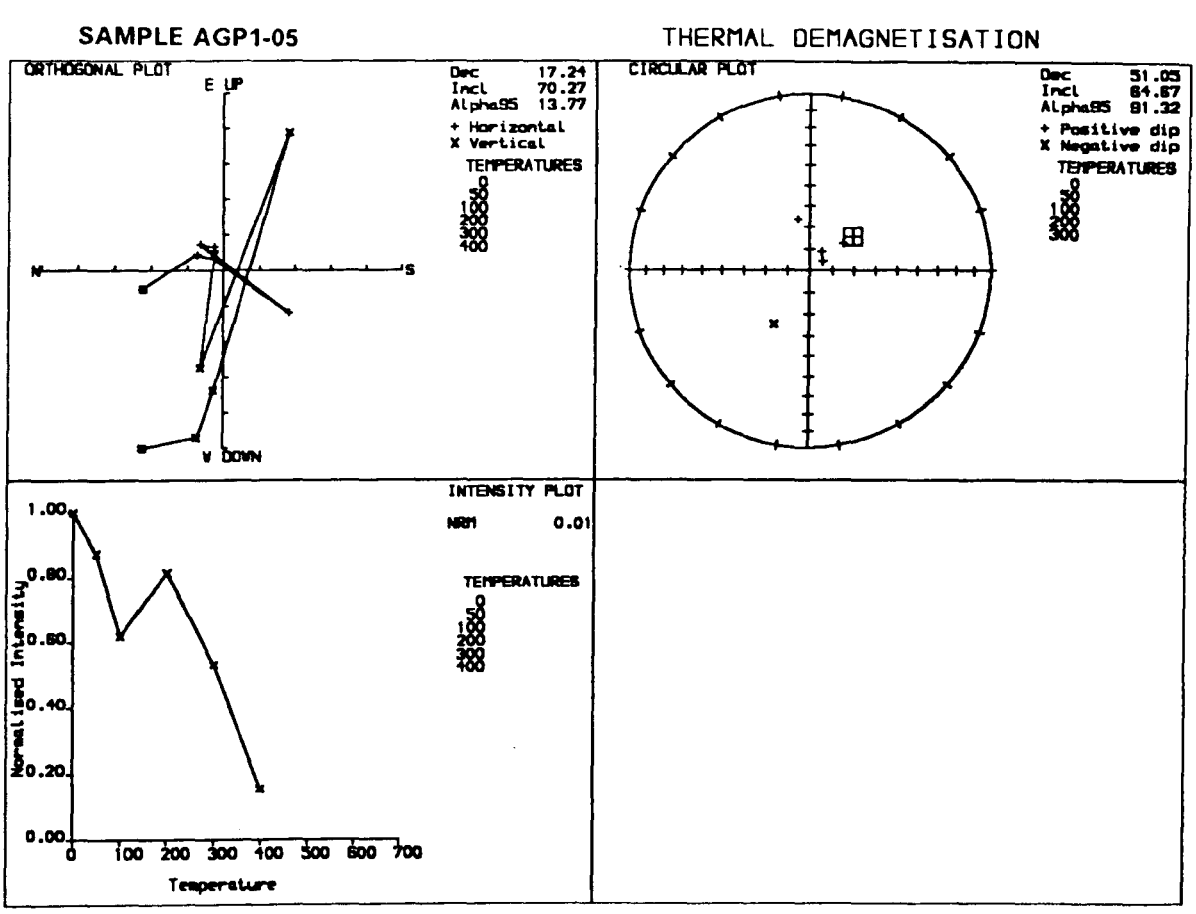

Figure 5.16 : Palaeomagnetic plots showing the instability of remanence for sample from the agpaites. No components of remanence were isolated from these facies. Labels as for Figure 4.6.

different to those exhibited by the majority of flows from the Upper Lava Formation remote from the intrusion and in zones (2) and (3) defined by Larsen (1977) (Section 2.4). These unbaked flows are characterised by shallow-intermediate directions, of both polarities, on an approximately east-west axis.

These results constitute a positive baked contact test for the Upper lava formation with the Ilímaussaq intrusion and further suggest that the remanence held by the lava flows remote from the intrusion (those below flow U29 in the stratigraphic sequence) pre-dates the emplacement and cooling of this body.

5.4 AGGLOMERATE TEST

(a) Geological setting and sampling

Figure 5.2 indicates the presence of three thick conglomerate horizons within the top part of the Mussartût Formation. On inspection of these horizons during fieldwork, all clasts were found to be composed of basement rock (Julianehåb granite) and acid gneisses and were unsuitable for palaeomagnetic purposes. No basaltic clasts from the lava flows of the Mussartût Formation were found. Consequently, no standard conglomerate test could be performed to assess the palaeomagnetic stability of the Mussart ût lavas. There is, however, an agglomerate band at the base of the Mussart ût Formation, which is believed to mark an explosive opening phase of this volcanism (Upton et al, 1974). Sub-angular clasts of basaltic material within this agglomerate band were sampled to perform a palaeomagnetic agglomerate test.

Paired samples were collected from eleven clasts. The total collection of 22 cores were thermally demagnetised in steps of 50° or 100°C up to 500°C and subsequently in steps of 30°C up to the maximum unblocking temperature. The component structure of the remanence residing in each sample was analysed in the way described in Section 4.4.4.

(b) Thermal demagnetisation results

Figures 5.17-5.18 and Table 5.4 illustrate the results of the agglomerate test. The majority of clasts possess a single component of magnetisation with a shallow- intermediate westerly positive direction (Fig. 5.17a). This is similar to the remanence which characterises the lower flows of the Mussartût formation. Figure 5.17b shows the mean characteristic directions for all samples with envelopes around those from the same clast. Two observations can be made from the results:

1. The magnetisation directions from sister samples from the same clast are often dissimilar (Fig. 5.17b) although each sample shows a stable, single component vector. This suggests that the clasts themselves may not be entirely suitable for palaeomagnetic study.

2. The magnetisation directions for separate clasts are not significantly random; the mean direction for all cores (without meaning the samples from each clast) is D=313.3°, I=46.4°, α_{95} = 10.5°, k=11.9°, N=18, R=16.6. The α_{95} and k values illustrate that the scatter of directions is low. R is above the value of 6.79 (Watson, 1956) for the corresponding value of N, required to demonstrate significance at the 95% confidence level. Hence, the directions are not random at this level of confidence.

The second point is crucial. For example, Briden and Mullan (1984) studied clasts from an agglomerate band within the 400m thick Ordovician Builth Volcanic sequence from Mid Wales. They identified three components in samples from the main volcanic sequence (their P, S and R components), corresponding to a primary TCRM of Ordovician age, a secondary CRM of Permo-Carboniferous origin and a recent viscous remanent magnetisation (VRM) respectively. Two of these components - the S and R vectors - were identified in the agglomerate clasts but the P component was not significantly grouped in the clasts. Consequently, they were able to postulate that the P component originated prior to agglomerate formation, whereas the S and R components were later overprints.

By a similar reasoning, the non-random westerly positive remanence component isolated in the majority of clasts in the present study could conceivably post-date the formation of the Mussartût agglomerate. Alternatively, the direction of magnetisation recorded in the clasts may reflect the Earth's field at the time of formation of the agglomerate, if the clasts were emplaced at temperatures above the Curie points, i.e. the remanence is a TRM acquired at the opening phase of Mussartût volcanism. Geological evidence (Upton et al, 1974) suggests that the temperatures during the explosive opening to the Mussartût event could have exceeded the Curie temperatures of magnetite (the magnetic mineral within the clasts), and this would support the interpretation that the clasts acquired their magnetisation during emplacement.

In the absence of information which unequivocally defines the temperature of the suspension responsible for emplacing this deposit, the significance of this palaeomagnetic result is unclear.

SAMPLE NUMBER	CHARACTERISTIC REMANENCE VECTOR				
	J_{nrm}	D	I	α_{95}	T
A1-1	130.7	318.9	57.3	3.2	520-620
-2	105.4	331.8	36.2	2.0	520-580
A2-1	67.9	302.9	29.0	5.9	550-620
-2	60.5	306.0	32.7	4.3	550-620
A3-1	55.2	318.0	40.9	6.7	200-500
-2	81.7	228.8	50.4	5.3	300-500
A4-1	84.0	315.9	65.0	4.5	200-500
-2	55.0	344.2	60.0	2.3	200-500
A5-1	110.7	305.2	27.2	1.0	520-620
-2	122.9	357.9	85.4	4.1	0-300*
A6-1	---------- +				
-2	52.1	311.2	46.3	18.5	0-580+
A7-1	---------- +				
-2	49.1	317.4	49.3	6.6	500-580+
A8-1	60.8	347.4	49.0	12.8	0-620+
-2	---------- +				
A9-1	94.0	293.3	17.9	9.0	550-620
-2	90.7	286.2	31.1	4.2	550-620
A10-1	97.3	307.8	32.4	9.8	550-620
-2	112.7	311.6	51.2	1.7	400-620
A11-1	117.1	311.3	40.2	5.0	400-550
-2	39.8	337.8	19.8	7.9	400-550

Table 5.4 : Results of thermal demagnetisation studies on clasts from the basal agglomerate of the Mussartût Formation. (* denotes possible P.E.F. contamination + denotes unstable remanence)

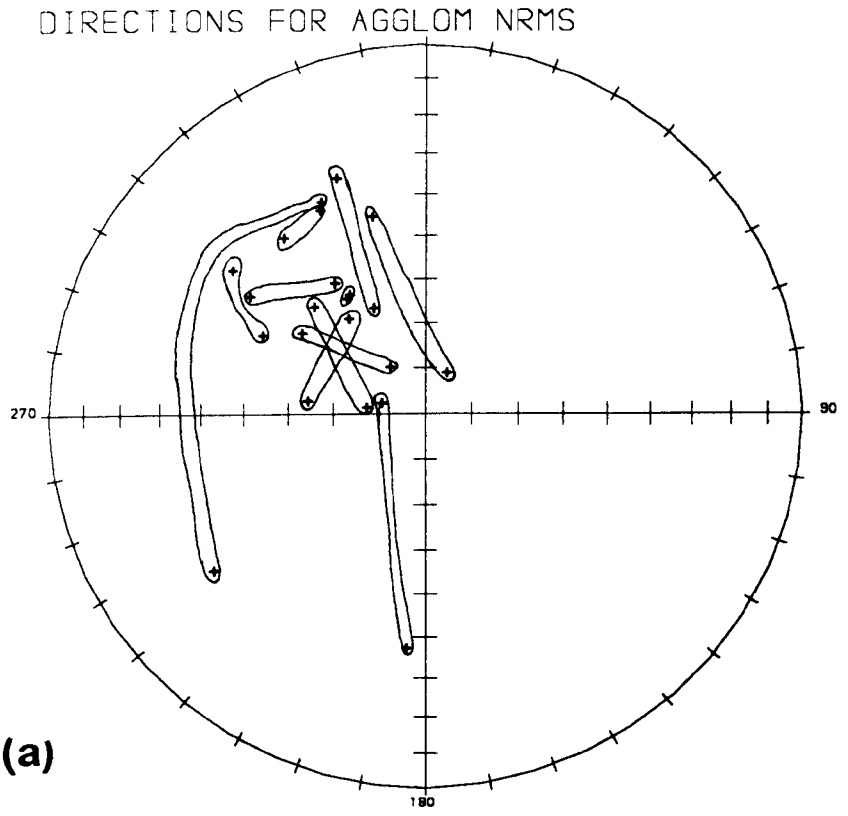

Figure 5.17a : NRM directions for samples from agglomerate clasts. Envelopes are placed around the directions for sister samples from the same clast.

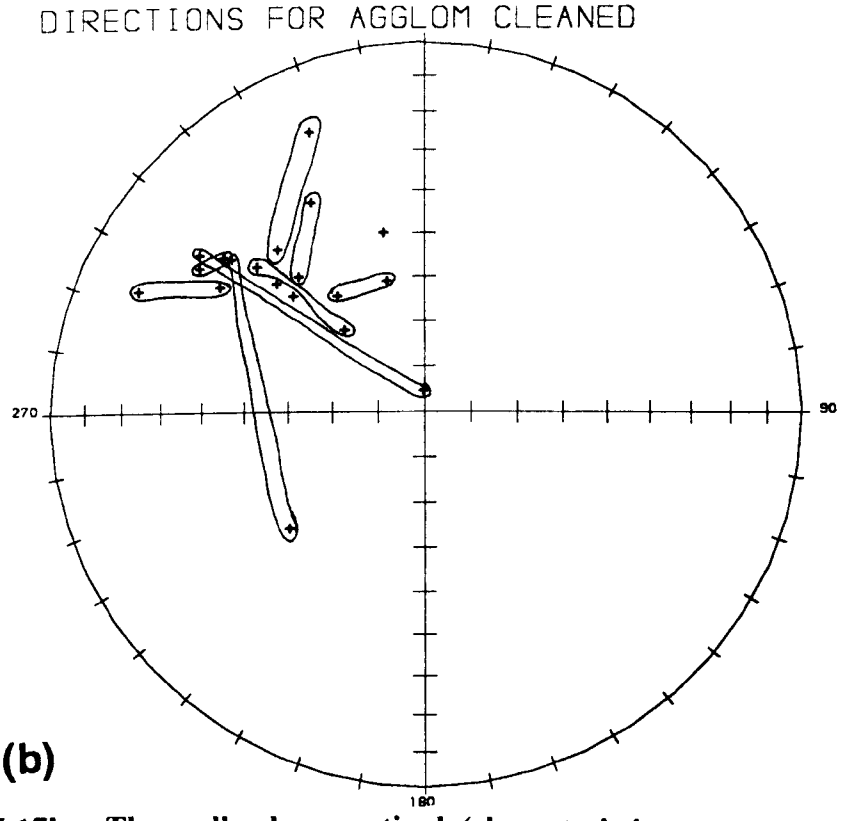

Figure 5.17b : Thermally demagnetised (characteristic remanence) directions for samples from agglomerate clasts. envelopes are placed around the directions for sister samples from the same clast.

Figure 5.18 : Palaeomagnetic plots illustrating the component structure of remanence for sister samples from three typical agglomerate clasts. Labels as for Figure 4.6.

SAMPLE A1-1

THERMAL DEMAGNETISATION

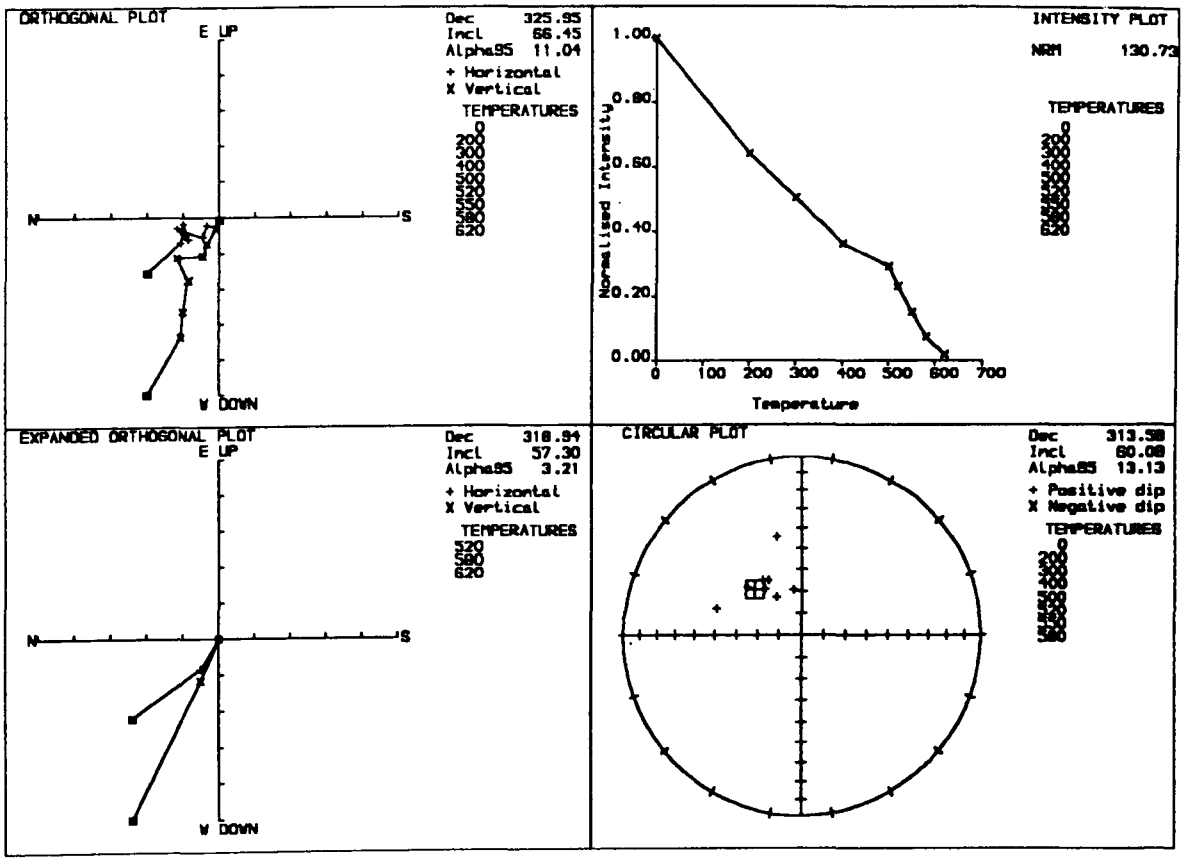

SAMPLE A1-2

THERMAL DEMAGNETISATION

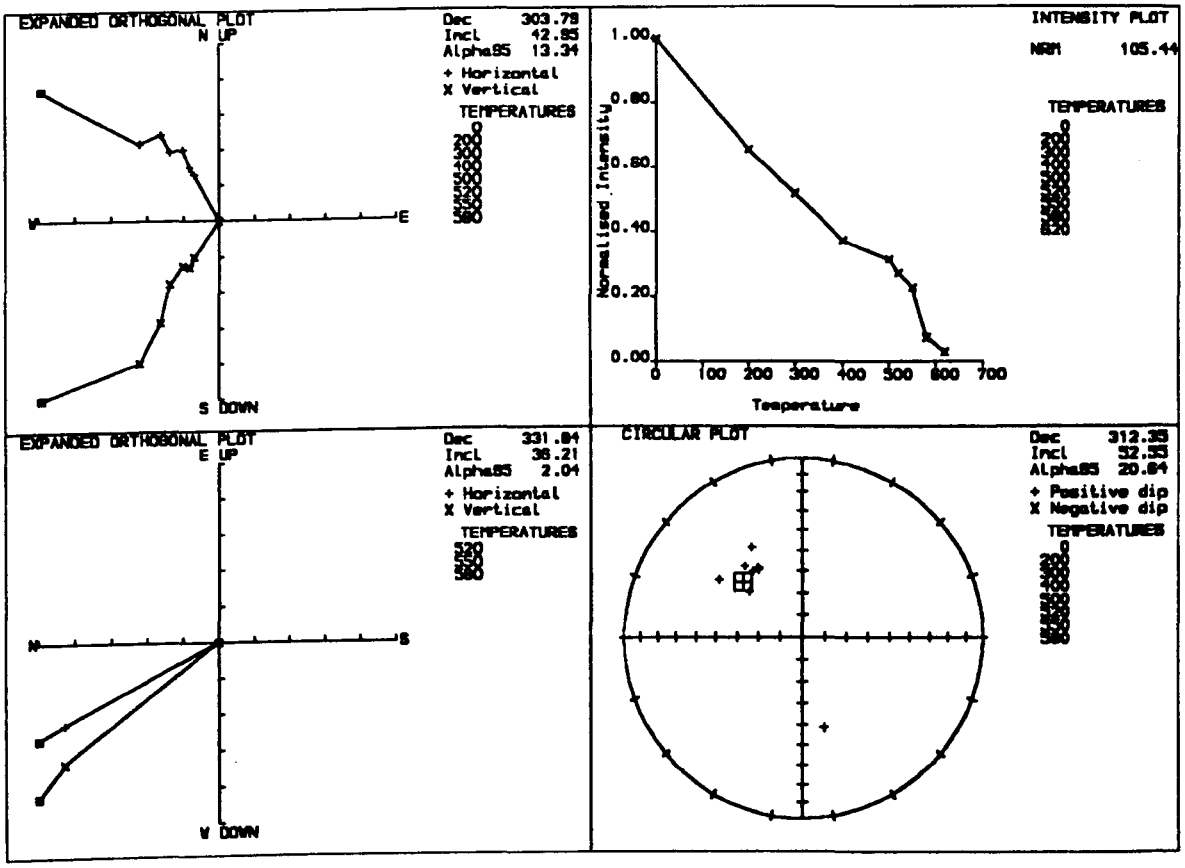

SAMPLE A2-1

THERMAL DEMAGNETISATION

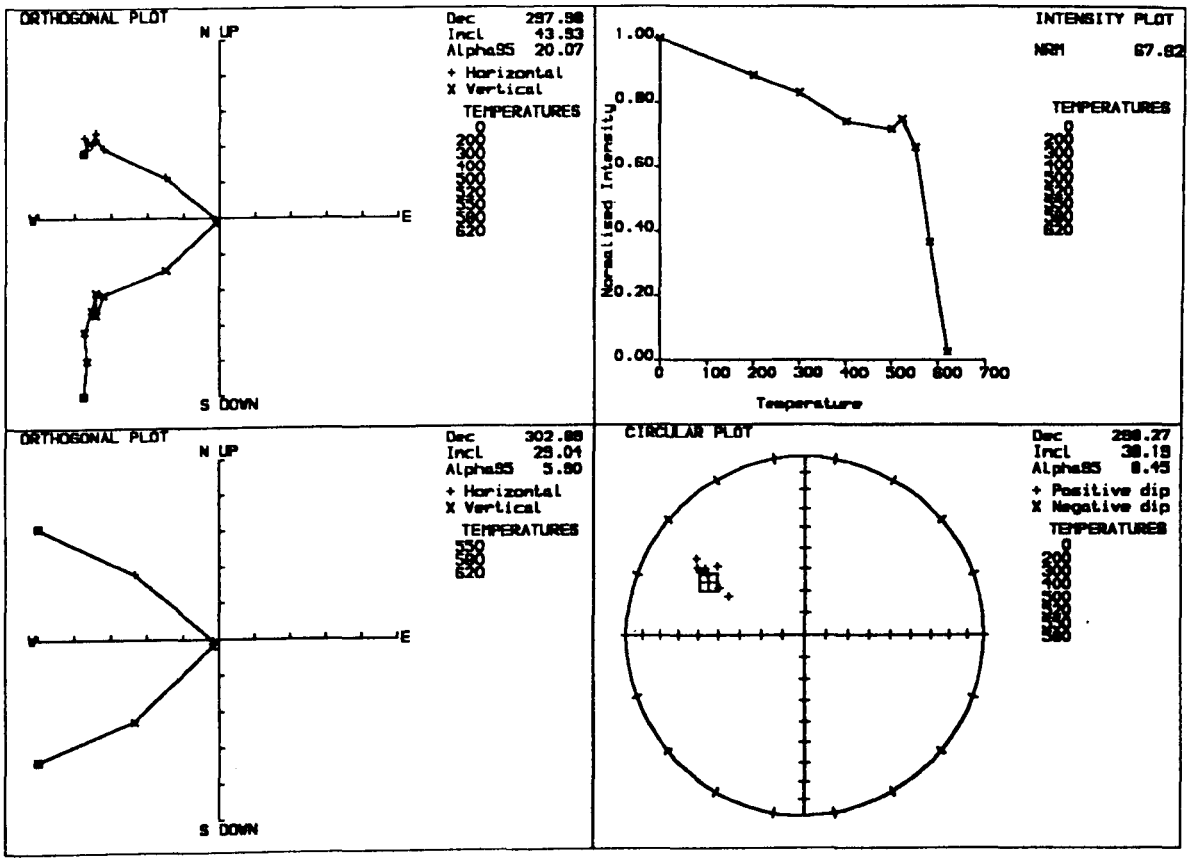

SAMPLE A2-2

THERMAL DEMAGNETISATION

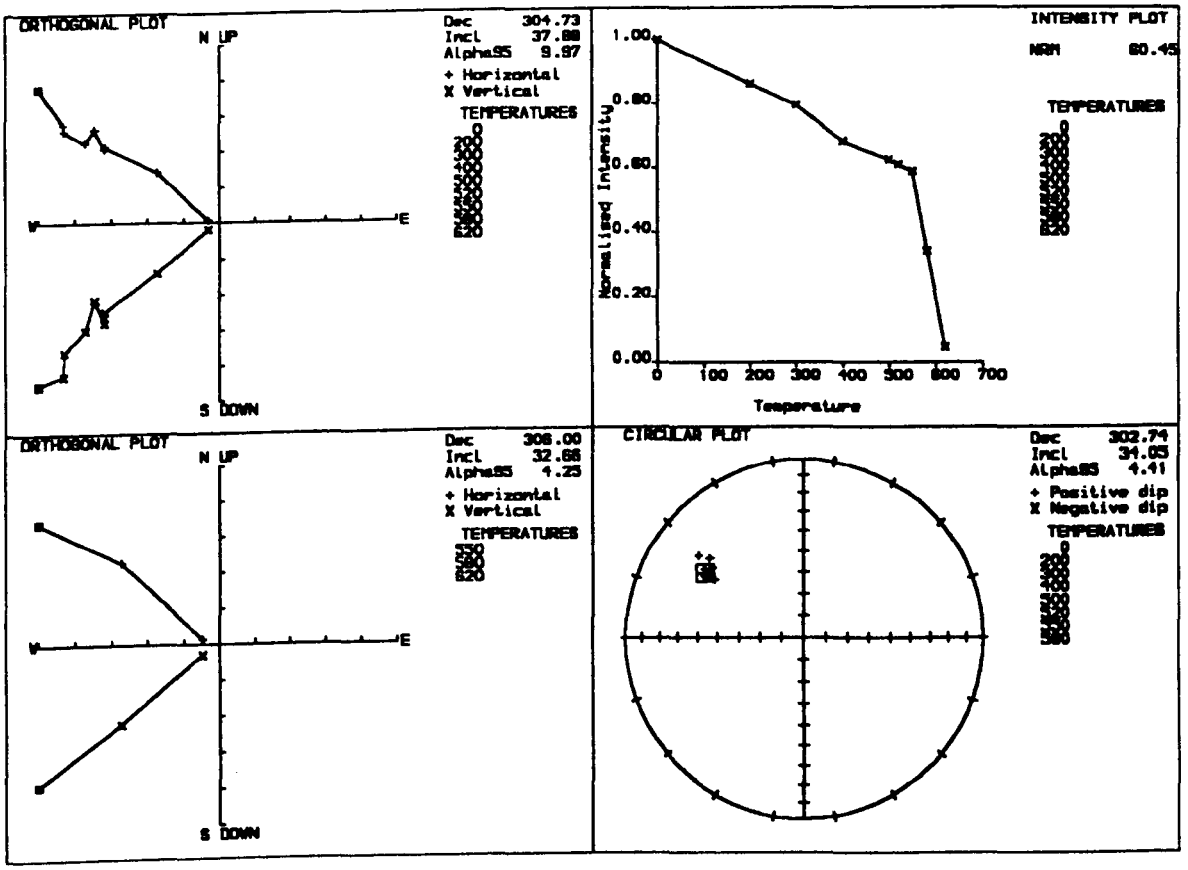

SAMPLE A9-1

THERMAL DEMAGNETISATION

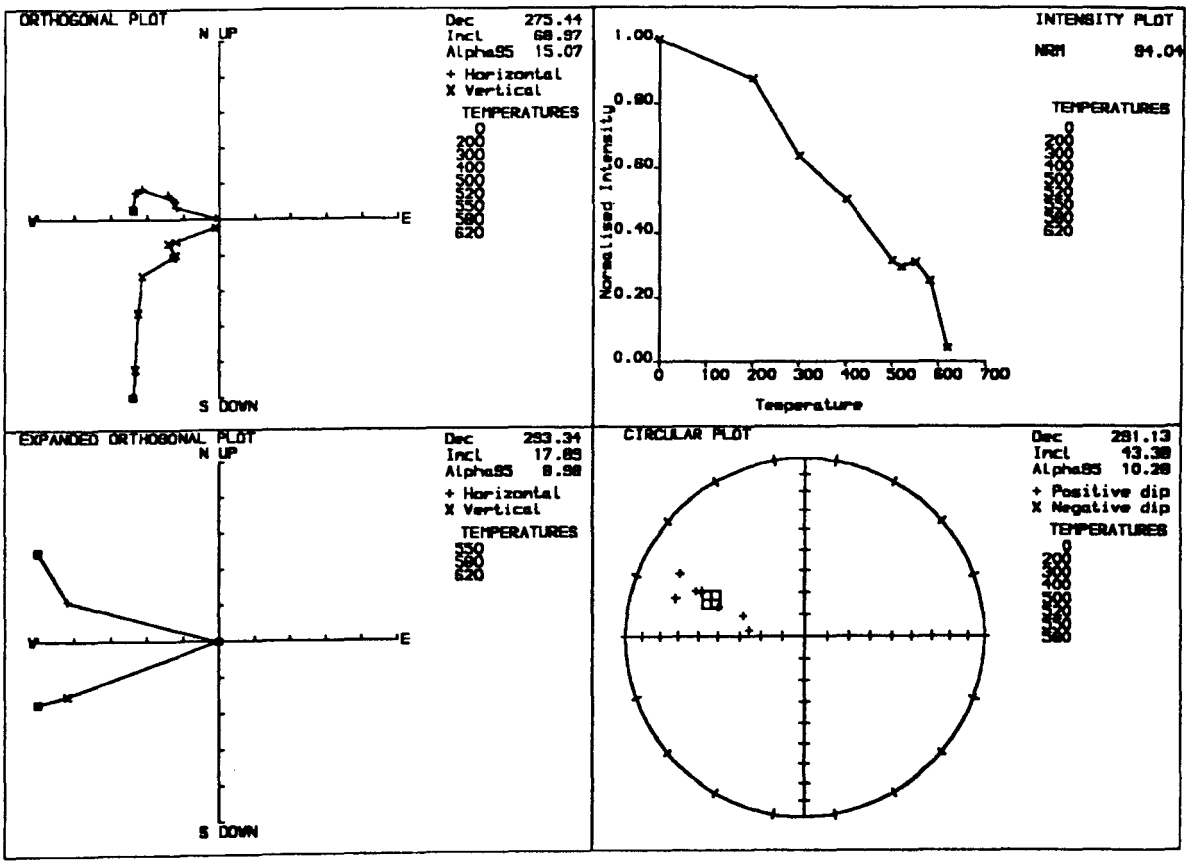

SAMPLE A9-2

THERMAL DEMAGNETISATION

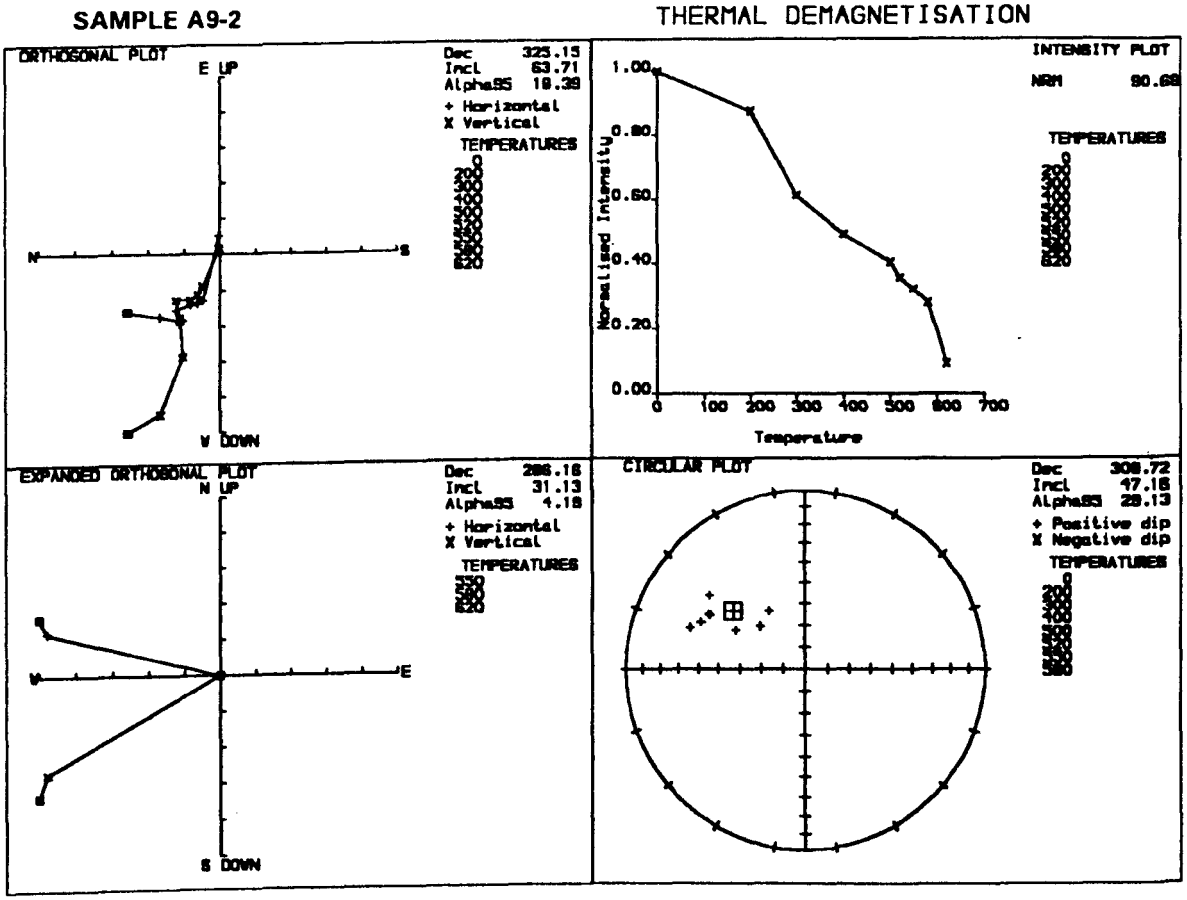

5.5 RADIOMETRIC DATING OF THE GARDAR LAVAS

Several attempts have been made to date the Gardar lavas using radiometric techniques (B.G.J. Upton, pers. comm.) but all have been unsuccessful due to the unsuitability of the rocks. This provides a problem for palaeomagnetic studies since, despite having good geological evidence which constrains the age of the lavas to within ca.1320 Ma, we are still unable to date the lavas, and hence their remanence, with more precision.

A method not previously attempted is the $^{39}Ar - ^{40}Ar$ stepwise degassing method. This section describes an attempt to date the lavas using this technique. A detailed description of this technique is given in Mussett et al (1980). This work was carried out only as a subsidiary exercise of the palaeomagnetic studies and, since it proved unsuccessful, will not be given a great deal of coverage.

Four samples were used for the dating experiments; one from the base and one from the top of the Upper Lava Formation, one from the Middle Lava Formation and one from the Lower Lava Formation in order to obtain an even spread of age determinations throughout the lava succession. The principle of the dating method is outlined briefly below and is followed by the results.

5.5.1 The method

The $^{39}Ar - ^{40}Ar$ dating method is a variant of the K-Ar method. Potassium is mostly made up of ^{39}K but approximately 0.0118% is ^{40}K. 89% of the ^{40}K decays to ^{40}Ca but 11% decays to ^{40}Ar. In the K-Ar dating method, the

K and Ar contents are determined separately (on separate portions of the sample) and the results are combined to give the date.

In the Ar-Ar dating method, a proportion of ^{39}K is converted to ^{39}Ar by bombarding the ^{39}K with fast neutrons to produce ^{39}Ar and protons. Thus, the ratio of ^{39}Ar to ^{40}Ar can be calculated. To date a rock sample, it is first irradiated with neutrons and then heated in steps of, say, 50°C in a vacuum to degass the rock. At each temperature step, the gas released is measured in a mass spectrometer and the peaks due to the various isotopes of argon are measured and an age is calculated from the ratio of the ^{39}Ar and ^{40}Ar peaks. This age is known as the "step age".

5.5.2 Results

The analyses for each sample were displayed in two ways:

1. **The age spectrum plot.** In this plot, (see, for example Figure 5.19d) a plateau must be defined for an acceptable age to be obtained. This "plateau age" is the average of the step ages for the temperature steps that define the plateau.

   In addition to the age steps (shown as long, thin rectangles) two further graphs are shown on this plot, which are used to give additional information. The solid line shows the atmospheric contamination by argon from the air. This is expected to be low for old rocks. The dashed line plots the $^{37}Ar/^{39}Ar$ ratio, which is proportional to the Ca/K ratio for the sample. This is used to give an idea of the relative K and Ca content for the sample. Minerals which have a high-K and low- Ca content will released gas at the low temperature end of the spectrum whereas those

with a low-K and a high Ca content will release gas at the high temperature end of the spectrum. The Gardar lavas, being basic rocks, have a significant Ca content and have a high 37/39 ratio at the high temperature end of the spectrum (see Figure 5.19)

2. **The correlation or isochron plot.**

This plot, seen in Figure 5.19, is used to confirm the date obtained from the age plot. Only the temperature steps which define the plateau on the age plot are used in the correlation plot. The intercepts of this plot are used to calculate the isochron age (intercept on y-axis) and the contamination ratio (intercept on x-axis). A measure of the scatter of the data points at one standard deviation is also given, by the parameter MSWD (the mean standard weighted deviate).

For a date to be acceptable, the following criteria must be satisfied by the data:

1. On the age plot, at least three successive temperature steps containing over 50% of the argon released, must define a plateau.

2. On the correlation plot:

   (a) The isochron age must equal the plateau age within error limits.

   (b) The contamination ratio must be 295.5 (the value for air).

   (c) The MSWD value must be ≤ 2.5.

Figure 5.19 (a)-(d) shows the age and correlation plots for each of the four samples and Table 5.5 lists the key results, namely the % ^{39}Ar released for the plateau steps. the age determinations their associated errors, calculated from each plot, the contamination ratio and the MSWD value.

The age spectrum plots show some evidence of plateaus for two of the four samples (U32 and L16) at ca. 700 Ma. The other two samples (U4 and M1) show no evidence of plateaus so no age can be estimated. Table 5.5 shows that all samples fail to pass the MSWD criterion, having values at least two orders of magnitude too large. Thus, over the temperature steps which define the plateau, the errors on the straight line are too large and this renders the age determinations largely meaningless.

In all plots, the atmospheric contamination is low, as expected for such old rocks. The $^{39}Ar - {}^{40}Ar$ ratio is fairly constant for sample L16 until the last few temperature steps, when it increases due to the release of gas by the Ca minerals. This increase is a feature on all four plots and correlates well with a similar rise in the age plot. This may be evidence for a heating event which is older than the 700 Ma plateaus.

5.5.3 Discussion

The analysis is complicated in the present study since whole-rock samples were used as opposed to separate minerals, which are preferable. The Ar-Ar method usually has a 1 in 3 success rate, on average, when applied to whole-rock basalt samples which may contribute to the failure to obtain a reliable age for the Gardar lavas. Since this dating study was only a subsidiary part of the project and since the analysis is very time consuming, no more samples were investigated.

SAMPLE NO.	%^{39}Ar RELEASED	AGE1	AGE2	CR	MSWD
U4	100.0	685.2±105.0	752.0±41.2	142.6±115	7521.2
U32	58.4	708.9±12.4	721.0±20.7	233.8±105	56.4
M1	64.6	786.3±62.9	823.5±67.3	79.3±329.0	4075.8
L17	55.7	784.4±21.3	769.5±33.1	408.0±236	233.4

Table 5.5 : Results of the Ar-Ar dating experiment. All errors are at ± 1σ. CR is the contamination ratio, expressed as the ratio of argon derived from the air (^{36}Ar) to the total ammount of ^{40}Ar derived from the sample. MSWD is the mean standard weighted deviate; Age1 is the plateau age calculated from the age spectrum plot; Age2 is the isochron age calculated from the intercept on the y-axis (i.e. the ^{39}Ar/^{40}Ar axis) of the isochron (correlation) plot.

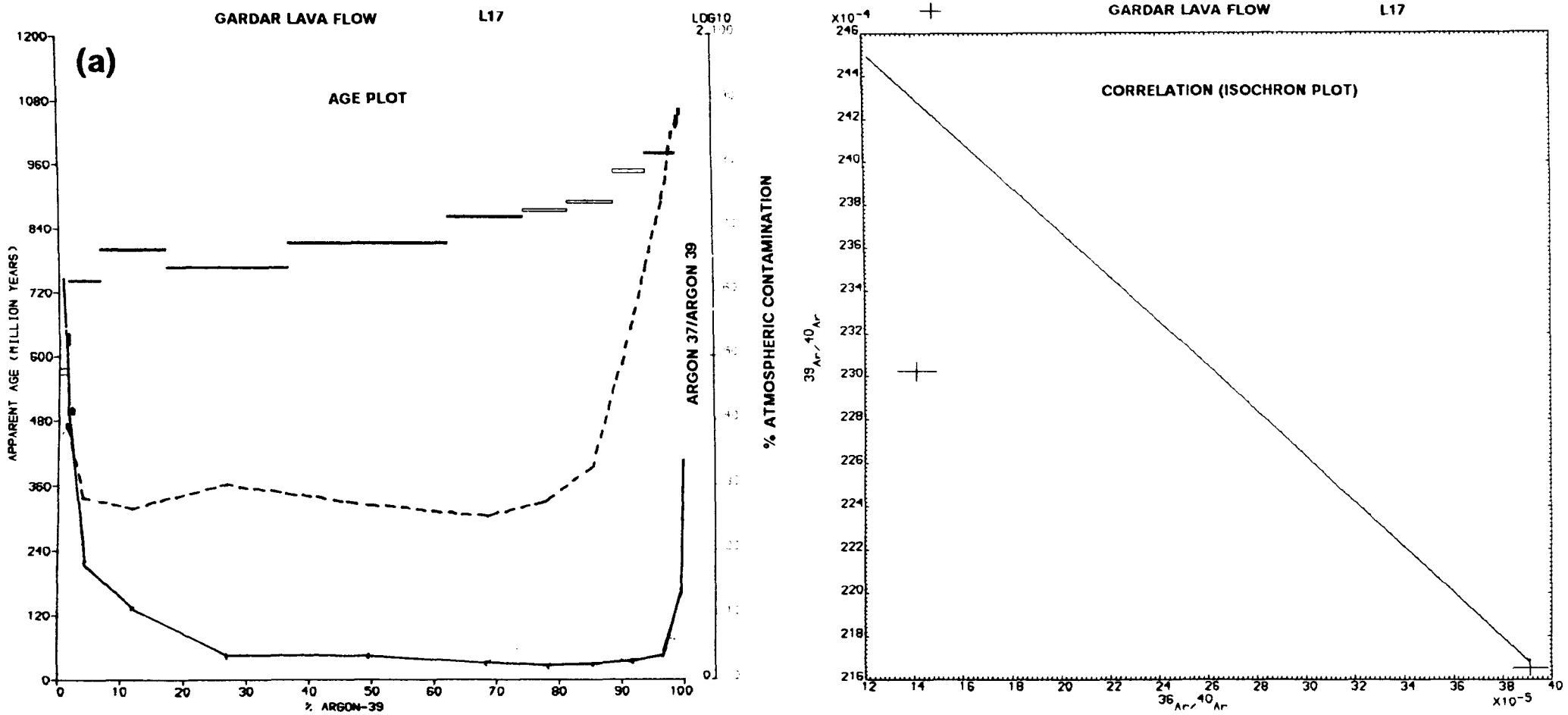

Figure 5.19 : Age spectrum and correlation ("isochron") plots for four lava flows from the Eriksfjord Group used in the ^{39}Ar -^{40}Ar dating method. The age steps are shown as long, thin rectangles, the dashed line shows the ^{37}Ar-^{39}Ar ratio and the solid line shows the contamination ratio.

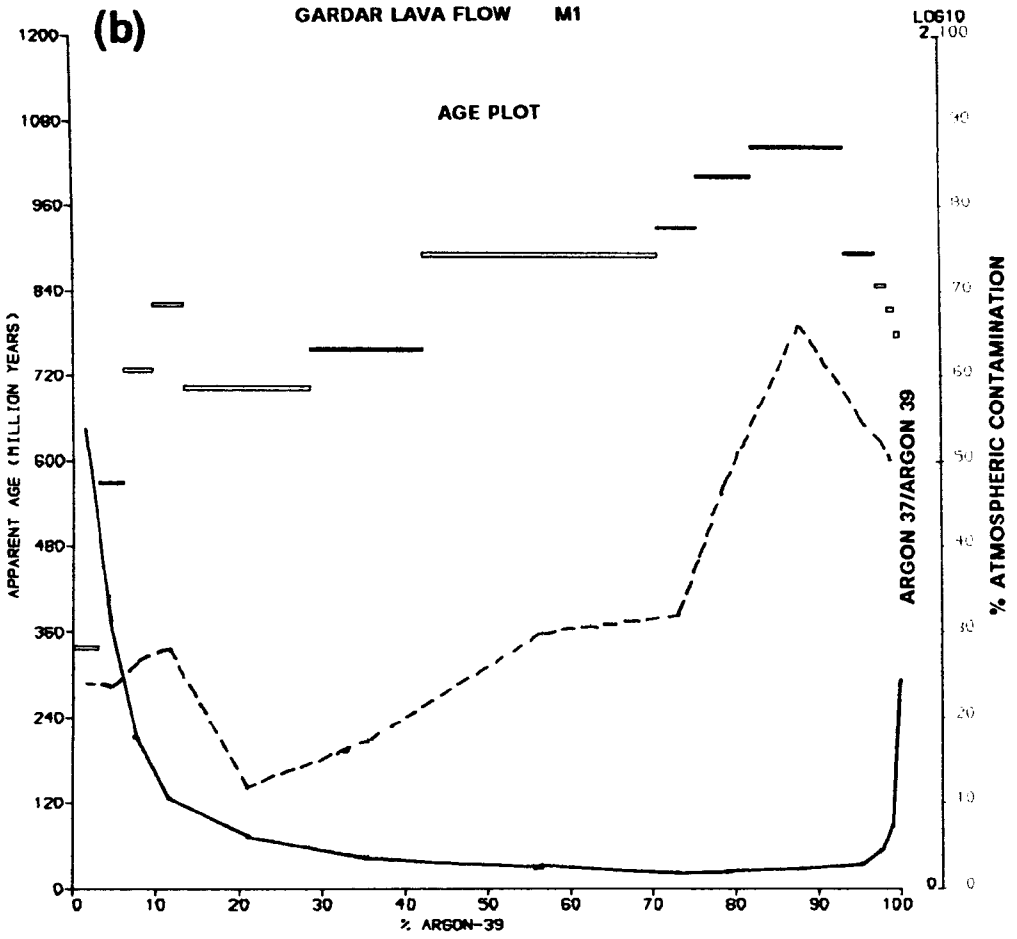
(b)
GARDAR LAVA FLOW M1
AGE PLOT
LO610
2_100
APPARENT AGE (MILLION YEARS)
% ARGON-39
ARGON 37/ARGON 39
% ATMOSPHERIC CONTAMINATION

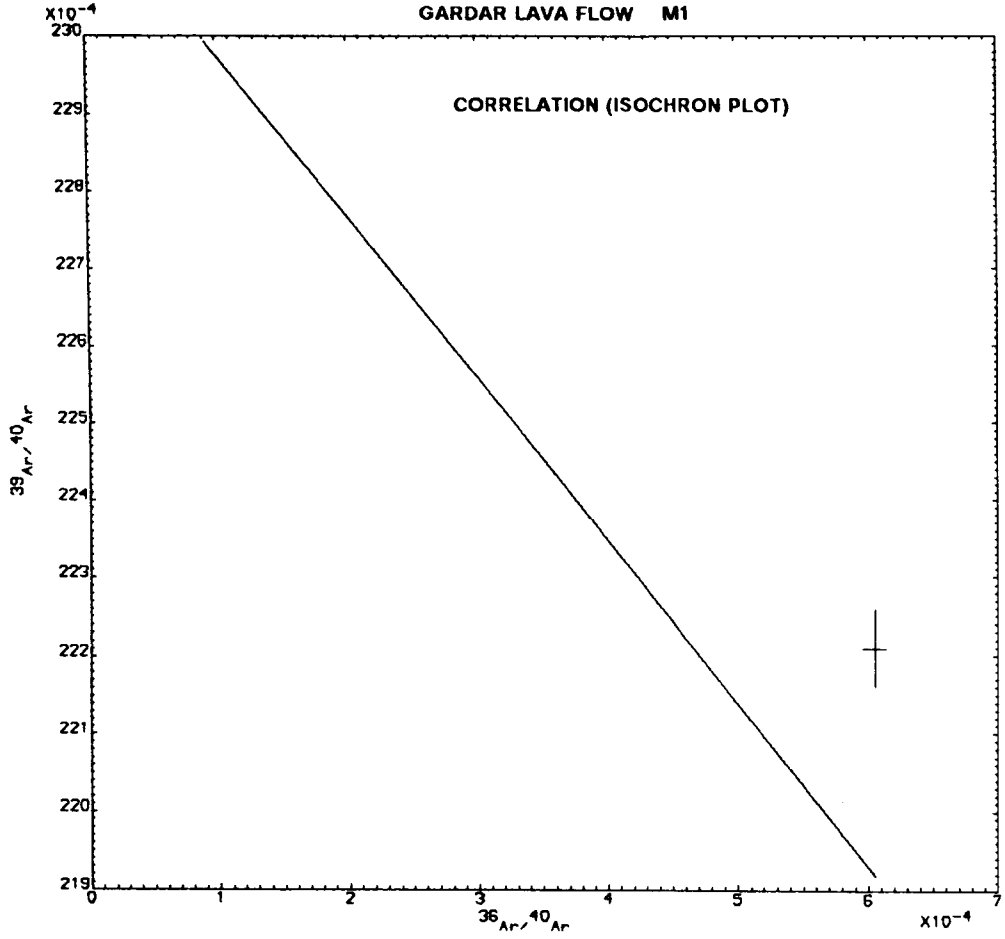
GARDAR LAVA FLOW M1
CORRELATION (ISOCHRON PLOT)
X10⁻⁴
39Ar/40Ar
36Ar/40Ar
X10⁻⁴

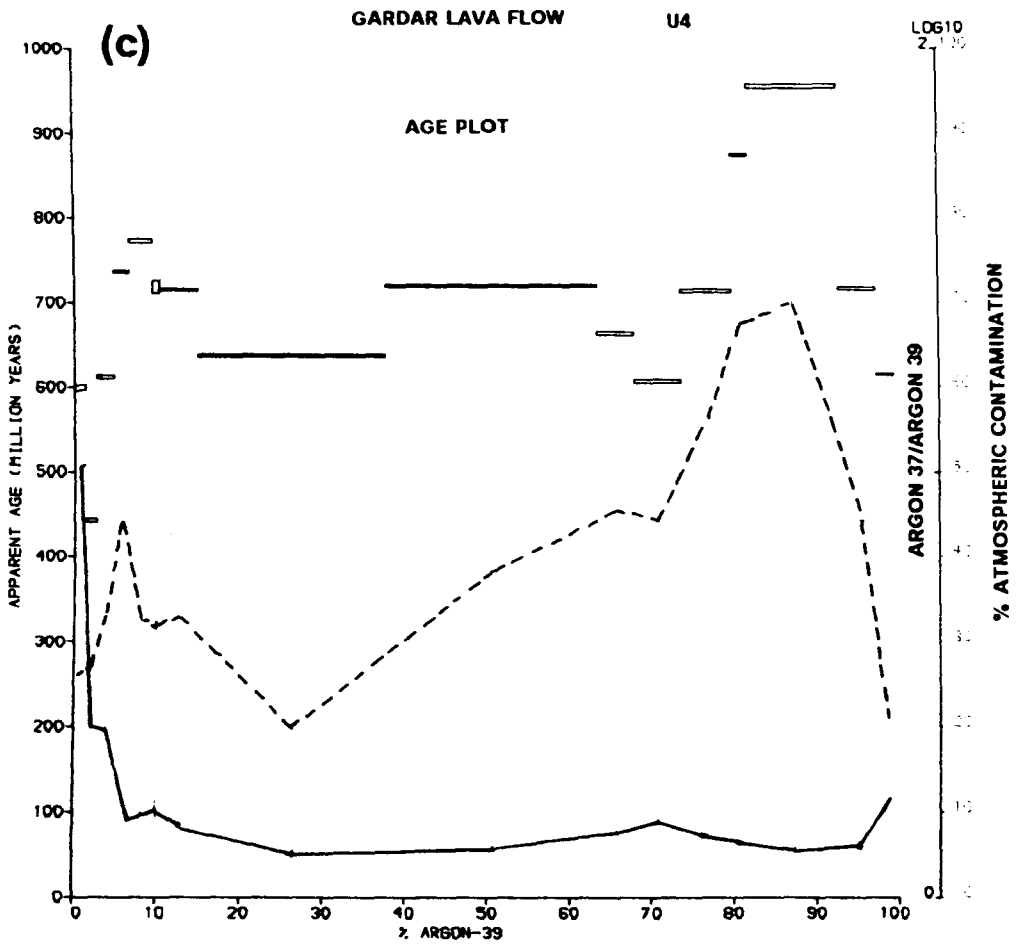
(c)
GARDAR LAVA FLOW U4
AGE PLOT
APPARENT AGE (MILLION YEARS)
% ARGON-39
ARGON 37/ARGON 39
% ATMOSPHERIC CONTAMINATION
LOG10

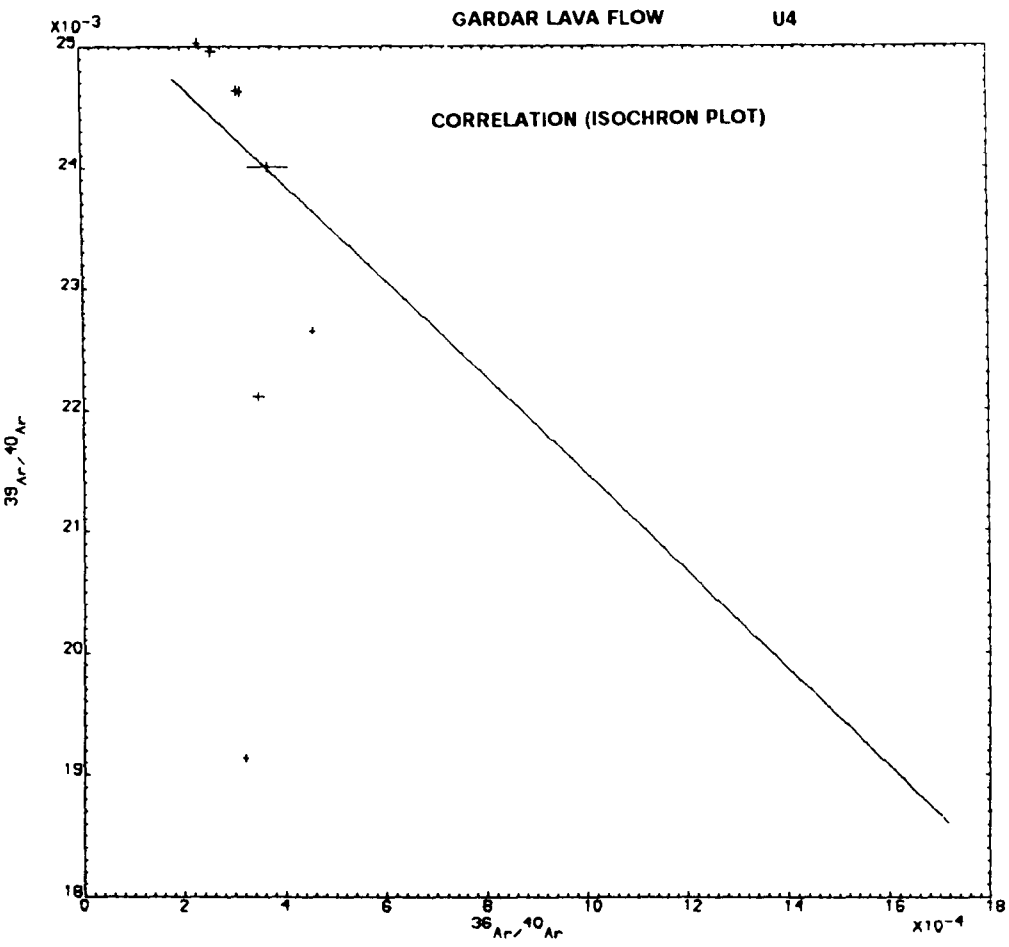
GARDAR LAVA FLOW U4
CORRELATION (ISOCHRON PLOT)
X10-3
39Ar/40Ar
36Ar/40Ar
X10-4

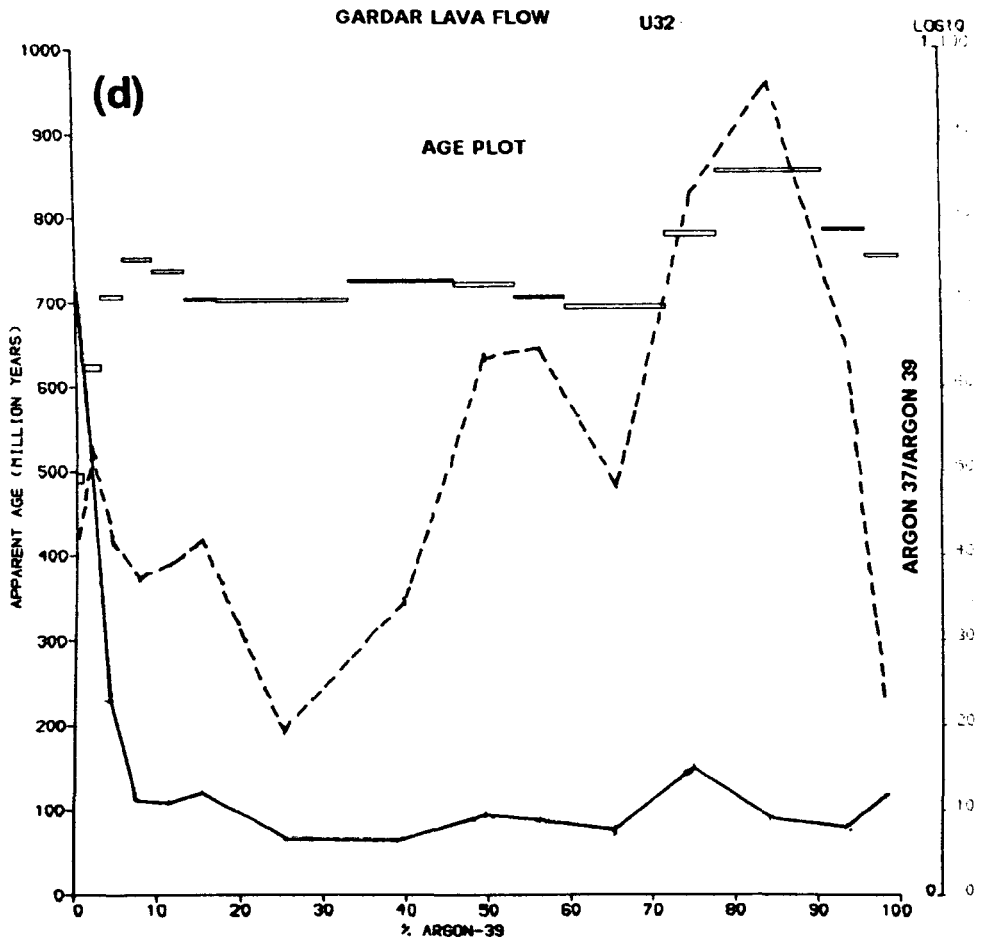
GARDAR LAVA FLOW
U32
(d)
AGE PLOT
APPARENT AGE (MILLION YEARS)
% ARGON-39
ARGON 37/ARGON 39
% ATMOSPHERIC CONTAMINATION

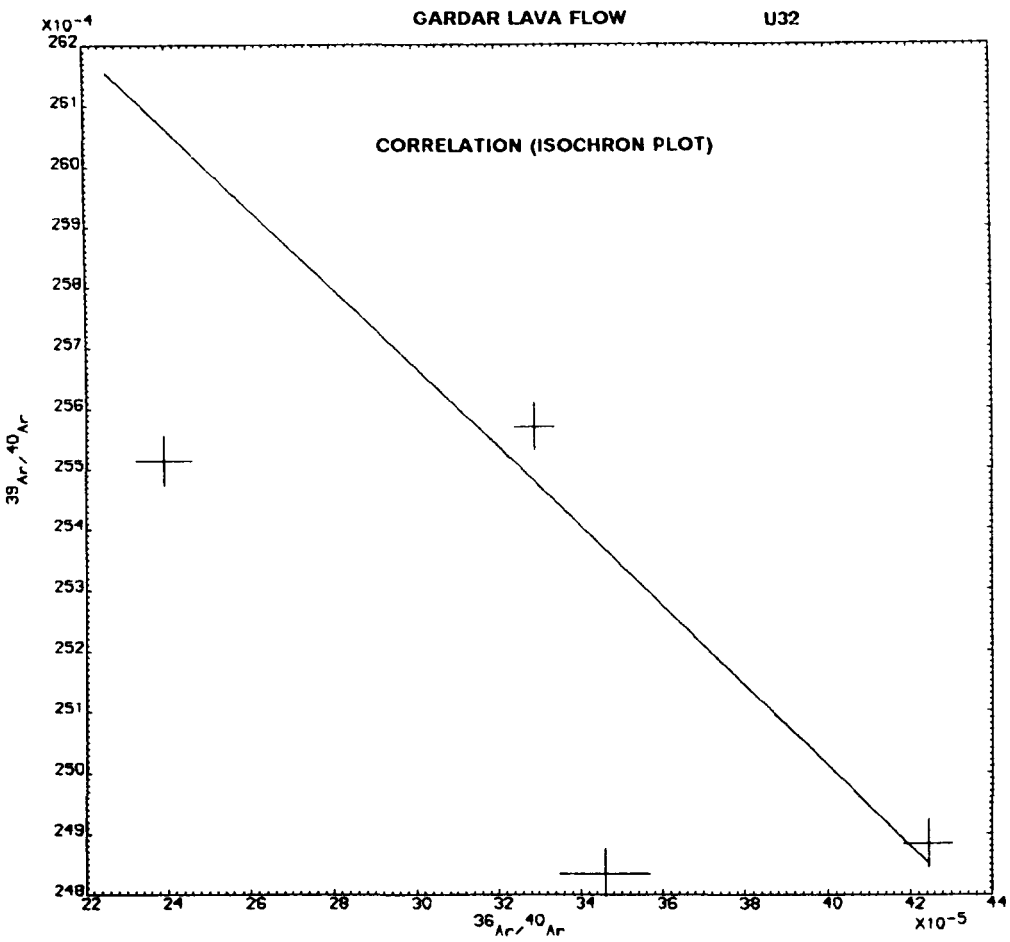
GARDAR LAVA FLOW
U32
CORRELATION (ISOCHRON PLOT)
X10⁻⁴
X10⁻⁵

5.6 DISCUSSION OF RESULTS

The results obtained in this chapter have vital importance to the project as a whole because identification of the age and nature of the characteristic remanence held by the Gardar lavas dictates the relevance of the palaeomagnetic and palaeointensity data (Chapters 4 and 6) to a study of the nature of the Mid-Proterozoic geomagnetic field.

The positive baked contact tests described in this chapter for two of the three lava formations in addition to the presence of reversals within these formations (Chapter 4), and rock magnetic evidence (Chapter 3) strongly suggests that the remanence held by the flows is a TRM acquired during (or a TCRM acquired shortly after) initial cooling. It therefore pre-dates both the Mid-Gardar and Late-Gardar phases of intrusive activity. The nature and age of the remanence held by the sandstones of the Mâjût and Mussart ût Formations has not been resolved by this study because some samples from these formations proved to be unsuitable for palaeomagnetic analysis and time constraints precluded an in-depth study of the remaining collection.

The lack of suitable clasts in the thick conglomerate bands within the Mussartût Formation neccessitated the application of a less satisfactory agglomerate test. In the event, the results of this test were equivocal. The failure of this test to produce significantly-random directions between clasts does not necessarily indicate the presence of secondary overprinting of the lower lavas. Formation of the agglomerate was contemporaneous with the onset of Mussartût volcanism and basaltic clasts within the agglomerate are fragments of material emitted from the volcanic source during an initial explosive episode. They may well have been emplaced at temperatures well

above the Curie point of magnetite in which case they will have cooled and acquired a TRM, in the direction of the post-emplacement field, comparable with the succeeding lava flows. Thus, in this instance, the ambiguity of the agglomerate test is outweighed by the more conclusive nature of results from the baked contact tests in the Lower and Upper Lava Formations.

The Argon-Argon dating analysis of four samples from the Gardar lavas did not yield any consistent and reliable dates. However, there was some evidence for plateaus at ca. 700 Ma. This age is undoubtedly too young, since evidence from reliable radiometric dating of the Gardar intrusions constrains the age of the lavas to be ca. 1320 Ma. Furthermore, the evidence from the palaeomagnetic contact tests documented in this Chapter strongly suggests that the remanence held by the lavas is older than the emplacement age of the Ilímaussaq intrusion, which is dated at 1143 Ma (Blaxland et al, (1978).

From the results described in this chapter, it is inferred that the characteristic remanence held by the Gardar lavas is a primary TRM, or TCRM acquired during initial cooling. This permits the palaeodirectional, and most particularly the palaeointensity, results of the present study to be interpreted in the context of the geomagnetic field during Early Gardar (ca. 1300 Ma) times.

CHAPTER 6 : PALAEOINTENSITY INVESTIGATIONS OF THE GARDAR LAVAS

6.1 INTRODUCTION

Palaeointensity determinations from very old rocks are sparse (Chapter 8) and of varying reliability. There are genuine problems such as the existence of secondary components of remanence which contaminate a primary TRM (e.g. Roy, 1977) or the existence of a magnetic mineralogy (i.e. multi-domain grains of magnetite) which does not lend itself to retaining stable magnetisations (e.g. Radhakrishnamurty et al, 1991). Consequently, very few workers have attempted to determine geomagnetic field intensities for the Precambrian. Nevertheless, in the context of the present study, it was important to obtain field intensity estimates from the Gardar lavas. Palaeomagnetic results (Chapter 4) indicate the presence of asymmetric fields in the Gardar lava succession, which suggest a time-averaged geomagnetic field which was more complex than a geocentric axial dipole. Palaeointensity results from lavas of both normal and reversed polarities will help to clarify the geomagnetic significance of the reversal asymmetry and the anomalous palaeodirectional results obtained from the Middle (Ulukasik) Lava Formation.

This chapter describes palaeointensity experiments on samples from all three lava formations within the Eriksfjord Group. Two techniques are used, namely the modified Thellier (Coe, 1967) and modified Shaw (Rolph and Shaw, 1985) techniques. Results obtained from sister samples and different samples from the same flow, using both techniques, are compared in an attempt to evaluate the relative suitabilities of the two techniques for use with the Gardar lavas.

6.2 THERMAL PALAEOINTENSITY TECHNIQUES

6.2.1 Introduction

Nagata (1943) developed a relationship which showed that TRM is directly proportional to the inducing field, provided that this field does not exceed 100 μT. Hence, the NRM of a rock is related to the palaeofield magnitude, B_a, by:

$$NRM = k_1 B_a \qquad [1]$$

Similarly, an artificial TRM induced in a laboratory field, B_l, is given by:

$$TRM = k_2 B_l \qquad [2]$$

k_1 and k_2 are constants which depend on the magnetic properties of the rock. If $k_1 = k_2$, then:

$$\frac{NRM}{TRM} = \frac{B_a}{B_l} \qquad [6.1]$$

Equation 6.1 will hereinafter be referred to as the palaeointensity (or B_a) equation. This equation has been shown, experimentally, to hold true for igneous rocks comprising both multi-domain (MD) and single-domain (SD) grains (Dunlop and Waddington, 1975). Importantly, $k_1 = k_2$ only if the magnetic properties of the rock have not changed since its formation, i.e. the NRM should not have decayed significantly, no secondary components of NRM should have been acquired and no physico-chemical alteration of the

rock should have occurred, either subsequent to NRM acquisition or during the heating used to impart the laboratory TRM.

These criteria are the basic requirements for a rock to satisfy the palaeointensity equation. Many workers have developed thermal techniques for measuring paleointensity, most of which are based on the original method proposed by Thellier and Thellier (1959) for use with pottery.

6.2.2 The original Thellier technique

This technique, or its derivatives, is the most widely used of all palaeointensity methods. The original form was developed by the Thelliers over a period of twenty years (Thellier, 1937, 1938; Thellier and Thellier, 1959). All forms of the Thellier technique are based on the law of additivity of partial thermoremanent magnetisation (PTRM), which states that the PTRM acquired in any temperature interval between room temperature, T_R, and the Curie temperature, T_c, is independent of the state of magnetisation outside that interval. The total TRM of a sample is thus equal to the sum of the PTRMs in the temperature interval T_R to T_c:

$$TRM_{tot} = PTRM(T_R, T_c) \qquad [6.2]$$

Experimental results support this law with a reasonable degree of accuracy (Dunlop and West, 1969; Levi, 1976). The palaeointensity equation (6.1) can thus be extended for use in any temperature interval between T_R and T_c:

$$\frac{J_N(T_1, T_2)}{J_T(T_1, T_2)} = \frac{B_a}{B_l} \qquad [6.3]$$

where J_N and J_T are the PNRM and PTRM acquired in the temperature interval T_1 to T_2.

The original Thellier method, in which the decay of NRM and acquisition of TRM are measured for each temperature interval between T_R and T_c, has the following steps:

1. The samples were allowed to stand for two weeks in the laboratory to restore the VRM components which may have been altered since sampling. The NRM was then measured.

2. The samples were rotated through 180° about the E-W axis and stored for two weeks as in (1). The NRM was measured.

3. The NRM and VRM were computed from the vector difference of (1) and (2). Samples for which the VRM was greater than a few percent of the NRM were discarded.

4. The samples were heated to an elevated temperature, T_1, where $T_c > T_1 > T_R$, cooled in the Earth's magnetic field and measured.

5. The samples were then rotated through 180° and the NRM measured as in (4).

6. Step (4) is repeated at a further elevated temperature T_2, where $T_c > T_2 > T_1$.

7. Step (5) is repeated at T_2.

8. Step (6) is repeated.

9. Step (5) is repeated.

The vector sum of steps (4) and (5) is subtracted from the vector sum of steps (6) and (7). This gives a value of double the PNRM lost between T_1 and T_2. If the vector sum of steps (6) and (7) is subtracted from the vector sum of steps (8) and (9), then the resultant value is double the PTRM gained between T_1 and T_2. These values were then used in the palaeointensity equation. The cycle of steps (4) to (9) was then repeated for a series of temperature values up to the Curie temperature, enabling a number of estimates of B_a to be made for each sample. The advantage of this method is that the onset of thermal alteration as a result of laboratory heating can be monitored and hence the temperature range over which the calculated palaeointensity is not influenced by thermal alteration can be defined.

6.2.3 Modifications of the original Thellier technique

Several authors have described modifications of the original Thellier technique, which either shorten the experimental time (Kono and Ueno, 1977) or provide further checks for thermal alteration (Coe, 1967). The most important modifications warrant description.

(a) The Coe (1967) modification

Instead of rotating the sample through 180°, Coe (1967) made a pair of heating and cooling cycles to elevated temperatures; one of which was in zero magnetic field and the other in a known weak laboratory field. His steps were:

1. Measure the NRM of a sample at T_R.

2. Heat to T ($T_c > T > T_R$) in air and cool in zero field. Measure the NRM remaining J_n (T_c,T).

3. Heat to T and cool in a known laboratory field. Measure the total remanence at T_R.

4. Steps (2) and (3) were repeated at elevated temperatures below T_c .

5. A graph of J_n (T_c,T) against J_T (T_R,T) was plotted, the slope of which was used to calculate the palaeointensity.

(b) The Kono modification

Kono and Ueno (1977) suggested a single heating technique to reduce the time required for the Thellier method. Samples were set with their (previously determined) NRM vector perpendicular to the axis of a solenoid, heated to T ($T_c > T > T_R$) and cooled to T_R in a d.c. field of 50μT. The total remanence in the interval (T_c,T) is given by:

$$J(T_c, T) = J_n(T_c, T) + J_I(T_R, T) \qquad [6.4]$$

where J_n is perpendicular to J_T. Therefore, the end points of the total remanence vector should describe a straight line whose gradient is equal to B_a/B_I. The magnetic anisotropy of a sample must be corrected for when using this technique.

(c) The Domen modification

Domen (1977) used two samples from the same core which were placed in a furnace so that the long axes of the samples were parallel and anti-parallel,

respectively, to the horizontal component of the geomagnetic field. The samples were then heated to a temperature T and cooled in the Earth's field. The combination of the measured remanences of each sample gives the PNRM lost and the PTRM gained.

(d) The Hoffman modification

In an effort to reduce the number of heatings on any one sample during the Thellier method, and thus to limit the effects of thermal alteration, Hoffman et al (1989) developed a technique of using several 9mm specimens from the same one inch core. Each of these specimens was heated to a different temperature, so that instead of heating the one inch core to increasing temperatures, each 9mm specimen from the core is heated twice to a specific temperature (once to demagnetise the sample to that temperature and once to impart the TRM at that temperature). Sherwood (1991) has used the Hoffman multi-specimen palaeointensity technique on Cretaceous basalts from Israel and has found that the results were not significantly different from those obtained using the Coe (1967) modification of the Thellier technique. The Hoffman modification was not used during the present study.

(e) The total TRM method of Wilson

The relatively low success rate of palaeointensity determinations using the time consuming PTRM method of the Thelliers encouraged Wilson (1961) to develop a method whereby the sample was heated to above its Curie temperature and cooled to room temperature in a known field, thus comparing a total TRM with the NRM of a sample. The sample was heated to successively higher temperatures in zero field, with the NRM being measured after each step, measurements being made at the raised

temperature. After reaching its Curie temperature, the sample was allowed to cool in a known applied field. The subsequently induced TRM was then treated in the same manner as the NRM and a graph was drawn of PNRM lost against PTRM lost for each heating step.

The disadvantage of Wilson's method is that results are meaningless if alteration occurs during the NRM demagnetisation. In the Thelliers' method, the comparison of NRM and TRM below the temperature at which alteration sets in is unaffected, but in Wilson's method the comparison will be affected throughout the entire range of temperatures because the sample is heated above its Curie temperature before the TRM is imparted.

6.3 EXPERIMENTAL PROCEDURE USED IN THE PRESENT STUDY.

The Thellier method with the Coe (1967) modification and "PTRM checks" (Prévot et al, 1983), hereinafter referred to as the modified Thellier method, was used in the present study for two reasons:

1. It permits palaeointensity determinations to be made from the lower blocking temperature intervals. Thus, a paleointensity estimate is made even when a sample undergoes irreversible alteration at higher temperatures, resulting in the dramatic increase in TRM capacity which is often seen in basalts (Coe et al, 1978; Grommé et al, 1979; Prévot et al, 1983).

2. Checks for non-linear alteration, i.e. that which cannot be detected by breaks of slope in the NRM-TRM plot, can be made by using the "PTRM check" (see point (6) below). If the PTRM values measured at

any temperature, T, before and after heating to a higher temperature, T_1, are within the commonly accepted value of about 15% of each other, then the level of alteration is considered acceptable. PTRM checks were made every 100°C during the present study, between 100°C and T_c.

The steps used in the modified Thellier experiments are described below, along with the equations for the total remanence, J_n, measured at each step.

1. The original NRM of the sample was measured.

$$J_o = J_n \quad (T_c, T_R) \qquad [6.5]$$

2. The sample was heated to a temperature T_1 (usually 100° C), where $T_c > T_1 > T_R$, and cooled to T_R in zero field. The remaining NRM, J_1, was then measured and is given by:

$$J_1 = J_o - J_n(T_1, T_R) = J_n(T_c, T_1) \qquad [6.6]$$

3. The sample was re-heated to T_1 and cooled to T_R in a laboratory field of 50μT, which was present throughout the entire heating and cooling cycle. The total remanence was then given by:

$$J_2 = J_n(T_c, T_1) + J_T(T_1, T_R) \qquad [6.6]$$

where J_T (T_1,T_R) is the PTRM acquired in the interval T_1 to T_R.

4. Step (2) was repeated for a temperature, T_2, where $T_c > T_2 > T_1$, and:

$$J_3 = J_o - J_n(T_2, T_R) = J_n(T_c, T_2) \qquad [6.7]$$

5. Step (3) was repeated for temperature, T_2, and:

$$J_4 = J_n(T_c, T_2) + J_T(T_2, T_R) \qquad [6.8]$$

6. A PTRM check (the third heating) was then made, where the sample was thermally demagnetised at T_1, and the remanence, J_5, measured:

$$J_5 = J_n(T_c, T_2) + J_T(T_2, T_R) - J_T(T_1, T_R) \qquad [6.9]$$

therefore,

$$J_5 = J_n(T_c, T_2) + J_T(T_2, T_1) \qquad [6.9]$$

On examination of equations 6.5-6.8, it can be seen that,

$$(J_5 - J_3) == J_3 + (J_4 - J_3) - (J_2 - J_1) \qquad [6.10]$$

If equation 6.10 is satisfied for each PTRM check, then no non-linear alteration has occurred between T_1 and T_2.

Steps (2)-(6) were repeated at progressively higher temperatures until the Curie temperature was reached, or until linear alteration set in. The results were analysed by plotting a graph of NRM remaining against TRM gained for each temperature step, T_i. This graph is known as the Arai-plot (Nagata et al, 1963). The equation of the straight line of the Arai-plot, is given by:

$$J_n(T_c, T_R) = J_o + \left(-\frac{B_a}{B_l} \right) J_T(T_i, T_R) \qquad [6.11]$$

Thus, knowing the laboratory field (50μT), the palaeointensity was estimated from the gradient of the Arai-plot, as shown in Figure 6.1.

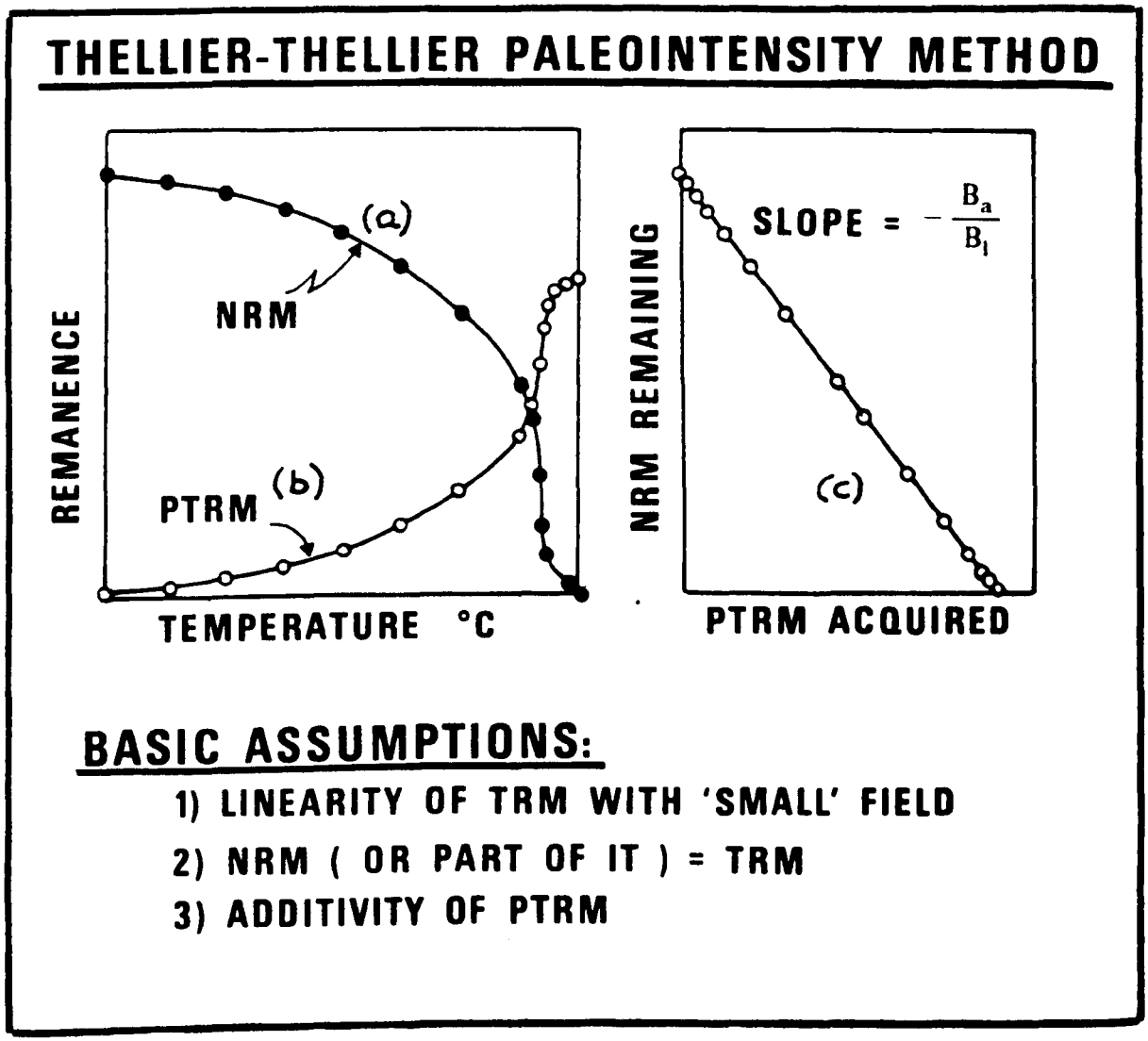

Figure 6.1 : Diagrams indicating the parameters measured during modified Thellier experiments, (a) the decay of NRM with temperature, (b) the acquisition of TRM with temperature, and (c) the Arai-plot, indicating the NRM remaining against TRM gained for each temperature throughout the experiment (from Pesonen, 1978).

6.4 EXPERIMENTAL DETAILS

1. Samples were held at the elevated temperature T_i for 20 mins. during each heating step to ensure that the whole sample reached T_i.

2. A laboratory field of 50μT was used for PTRM acquisition and was checked before each PTRM was given, using a fluxgate magnetometer.

3. All temperature steps for modified Thellier experiments were chosen after stepwise thermal demagnetisation of sister samples (described in Chapter 4) to identify the blocking temperature spectra. These steps were normally 100° , 50° or 30°, in the region 100° – 700° C.

4. All heating and cooling cycles were made in a Magnetic Measurements Thermal Demagnetiser (MMTD) and all measurements of magnetisation were made using a Molspin Spinner Magnetometer. Both were situated inside a 2m^3 Rubens coil arrangement (Rubens, 1945) which reduced the ambient magnetic field in the laboratory by more than 90%.

6.5 METHOD OF DATA ANALYSIS.

All modified Thellier data were analysed in the same way. An average of two samples from each flow were used and no pre-selection was made during pilot studies, so that the behaviour of all samples could be compared with their respective rock magnetic properties (Chapter 7). The following steps were used in the data analysis:

1. Orthogonal vector plots (OVPs) (Zijderveld, 1967), NRM intensity decay plots (J/J_0) and stereo-plots were analysed for each sample to deduce the

component structure, blocking temperature spectrum and directional stability. The ideal sample for Thellier experiments has a single, stable component of remanence with a distributed blocking temperature spectrum, so that the NRM and TRM can be compared over a wide range of temperatures. However, samples with more than one non-viscous component of magnetisation were included in the pilot experiments so that their behaviour during Thellier runs could be assessed.

This first step enabled identification of the range of temperatures which could be used to calculate the palaeointensity.

2. Arai-plots were analysed and all samples categorised according to the shape of the plots (Fig.6.2) as follows:

Class A : Arai-plot is ideal and shows only one straight line portion for all data points (Fig. 6.2a).

Class B : Arai-plot shows two portions, one linear at temperatures below 450°C, the other usually non-linear above 450°C. PTRM checks above 450°C fail (Fig. 6.2b).

Class C : Arai plot similar to Class B but only a small decrease in the original NRM ($<25\%$) is seen (Fig. 6.2c).

Class D : No linear portion was defined over any temperature range on the Arai-plot (Fig.6.2d).

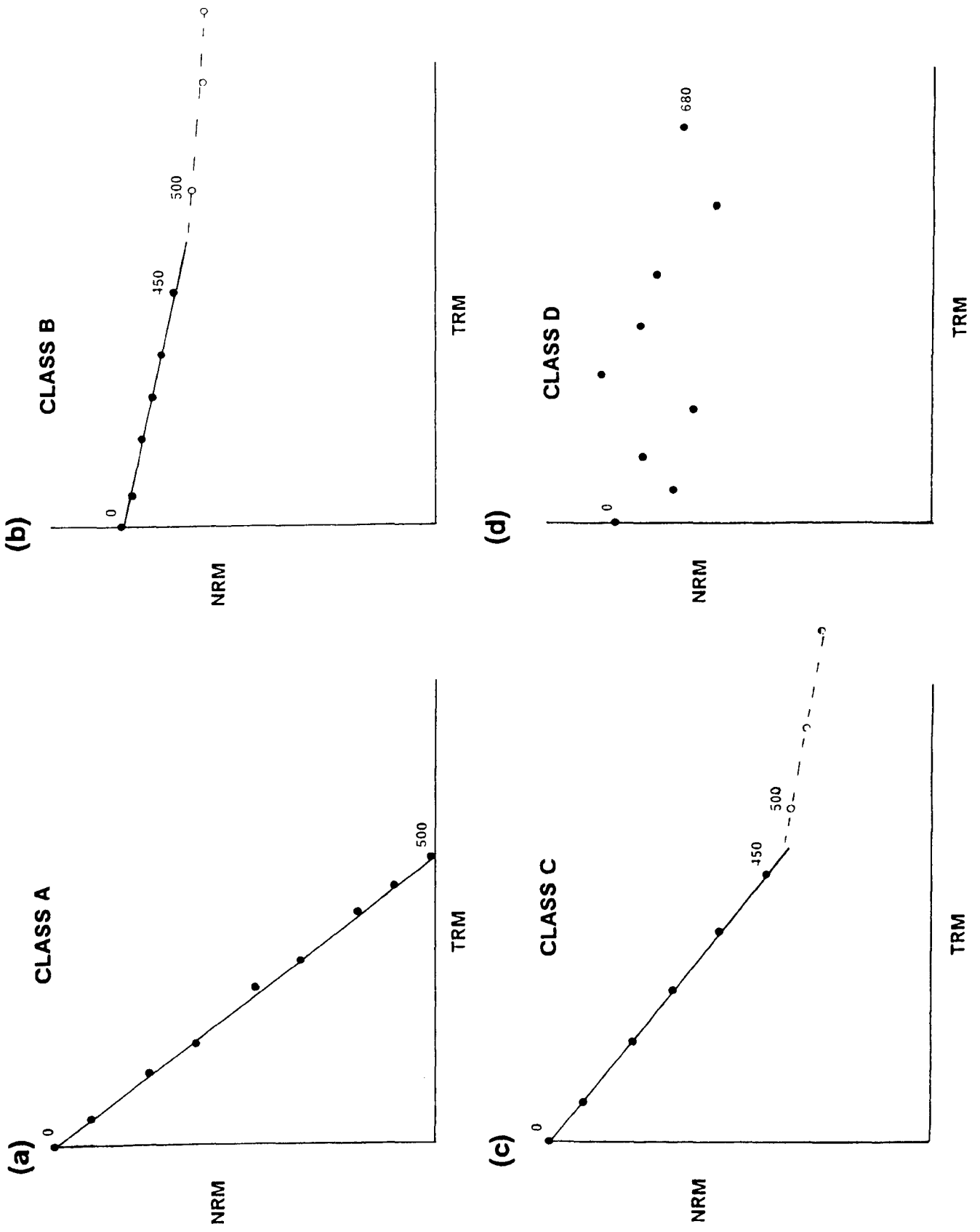

Figure 6.2 : Diagrams illustrating the four categories of Arai-plot witnessed in the present study, (a) Class A (b) Class B (c) Class C (d) Class D (see text for explanation of the classification scheme.

For Classes A, B and C, the temperature intervals over which the Arai-plot was linear (labelled DT in Tables 6.1-6.3) were noted.

3. A straight line fit (using the least squares method) was made to the selected data points on the Arai-plot, the slope of which was used in the palaeointensity equation. The straight line fit was only accepted if the criteria, outlined in Section 6.6 were satisfied.

6.6 ACCEPTANCE CRITERIA.

Samples from each of the eighty flows were used in the pilot experiments. Analysis of the results of these experiments revealed that the samples which gave acceptable Arai-plots (Classes A,B or C) were predominantly those which had non-viscous single component stable NRMs.

Samples were accepted if they satisfied the following rules:

1. Analysis of OVPs of thermal demagnetisation could identify a stable, characteristic remanence vector, preferably (but not essentially) in the higher ($>100°C$) blocking temperature region.

2. The following criteria were satisfied:

   a. At least four points were used to describe the linear segment and no anomalous data points within this segment were eliminated.

   b. The length of the segment should represent at least a 15% decrease in NRM intensity.

c. The standard deviation of the slope on the straight line fit should be $< 15\%$.

d. No segments which have unstable vectors in the OVP analysis in (1) were used to calculate the slope of the Arai-plot.

e. Any points showing evidence of P.E.F components were eliminated.

f. The PTRM checks for at least two temperatures should be within $\pm$ 15% of the original PTRM value at those temperatures.

6.7 RESULTS

One hundred and sixty six samples, from eighty flows, were used in the modified Thellier experiments.

The overall success rate, defined by the number of samples which passed the acceptance criteria described in Section 6.6, was 67 % (112 samples from a total of 166). The results from each separate formation are described, in stratigraphical order, in the following sub-sections.

6.7.1 The Lower (Mussartût) Lava Formation

Forty-eight samples from twenty-three flows were used, thirty-six of which passed the acceptance criteria described in Section 6.5. Table 6.1 gives the results of the palaeointensity experiments.

Most of the samples exhibited Class B (concave-up) Arai-plots, with curvature setting in at temperatures in excess of 400° or 450° C. This curvature is a result of a large increase in the TRM capacity of the sample

due to the onset of thermal alteration during laboratory heating. Figure 6.3 shows typical Arai-plots for samples from the Lower Lava Formation. Only six samples showed Class A Arai-plots, which usually yielded palaeointensity results in excess of 50μT. In the majority of samples, the points in the temperature interval between room temperature and 100° or 150° C were omitted from the analysis due to the presence of a component of magnetisation, possibly a burial remagnetisation, in this temperature range (e.g. Figure 6.3).

The results of PTRM checks for all samples are illustrated in Figure 6.6a. Approximately 50% of the samples used passed PTRM checks at raised temperatures of 300° and 400°C, whereas less than 20% of the samples passed the checks at 200° and 500°C. This suggests that the part of the blocking temperature spectrum most useful for determining palaeointensity results was that between about 100°C and 400 or 450°C. The 100° and 500°C points on the Arai-plot were only used for samples which passed the PTRM checks at 200° and 600°C.

The mean palaeointensity from all samples which gave a result was $37.9 \pm 2.4\mu$ T, as opposed to a mean value from the accepted samples was $34.3 \pm 2.3\mu$T. These mean palaeointensity values correspond to Virtual Dipole Moments (VDMs) of $9.1 \pm 0.7 \times 10^{22}$Am and $8.2 \pm 0.5 \times 10^{22}$Am^2 respectively.

6.7.2 The Middle (Ulukasik) Lava Formation.

Palaeointensity determinations were made for thirty-eight samples from the eighteen flows in this group, fourteen from samples which show an anomalous mean direction (the 'A' direction) of magnetisation (Chapter 4)

which may represent a transitional phase of the geomagnetic field. Table 6.2 summarises the results and Figures 6.4a-e show examples of typical Arai-plots for flows possessing the 'A' direction and Figures 6.4f-h show examples of Arai-plots for flows with the 'B' direction. Samples from flows M12 and M13 were unstable throughout the palaeointensity experiments and gave Class D Arai-plots; these samples were discarded. The palaeointensity values are among the lowest in the entire lava succession, with all but three flows having values ranging from 1.1 μT - 13.1 μ T; the mean value for the flows exhibiting the 'A' direction was 8.1 $\pm$ 0.6μT and that for flows with the 'B' direction was 9.0 $\pm$ 1.0μT. These correspond to mean VDM values of (1.7 $\pm$ 0.1) $\times 10^{22}$Am^2 and (2.3 $\pm$ 0.2) $\times 10^{22}$Am^2 respectively. The three normally magnetised flows (M1, M17 and M18) have higher palaeointensities, ranging from 34.8μT - 60.5μT. Examples of Arai-plots for these flows are shown in Figures 6.4i-k. These flows, and most of those showing the reversed ('B') direction, have magnetite as the magnetic mineral, whereas the flows giving the lowest answers have haematite as the remanence carrier. These three flows are also characterised by Class B Arai-plots, as opposed to the Class C plots shown by majority of the haematite-bearing flows.

Generally, the PTRM checks are less convincing than those witnessed from samples in the lower group; Figure 6.6b illustrates the results of these checks. As for the lower lavas, the most successful PTRM checks are those at raised temperatures of 300° and 400° with lower success rates for those at 200°, 500°, 600° and 680°C.

6.7.3 The Upper (Ilímaussaq) Lava Formation.

A great variation of behaviour is exhibited by the flows from this group. Eighty samples were used, from the forty flows, forty-six of which (58 %) gave results which passed the acceptance criteria defined in Section 6.5. Fifty-nine of the samples used were of normal polarity, four had intermediate directions and seventeen were of reversed polarity. Thirty-four of the normal flows and ten of the reversed flows passed the acceptance criteria. All intermediate flows failed to meet the acceptance criteria.

Table 6.3 details the results of the experiments and lists the class of Arai-plot for each sample. All classes (A-D) of Arai-plot were witnessed in the samples. Figure 6.5 shows typical examples from the formation. Flows which showed a variation of >15% between the palaeointensity results from sister samples were eliminated from the calculation of group mean palaeointensity and VDM values.

The normally magnetised samples, examples of which are illustrated in Figures 6.5a-k, give higher palaeointensity values (mean = $31.4 \pm 2.5\mu$T, mean VDM $= 6.9 \pm 0.3 \times 10^{22}$Am^2) than the reversely magnetised flows (mean = $10.8 \pm 1.1\mu$T, mean VDM $= 2.7 \pm 0.2 \times 10^{22}$Am^2) shown in Figures 6.5p-t. This suggests that the strength of the geomagnetic field during the reversely magnetised period may have been much less than that during the normal polarity intervals. This observation should, however, be treated with some caution since only six reversed flows occur in the formation, yielding only ten palaeointensity results.

Figure 6.6c illustrates the low success rate for PTRM checks from the

(Table 6.1 - Legend overleaf)

SAMPLE	DT	N	C/RM	F	Ba	Ba(Sh)	VDM $\times 10^{22}Am^2kg^{-1}$
L1-02**	0-450	9	D/1	22	15.9±2.1	7.2±0.6	3.4#
L2-01	250-400	5	B/1	19	41.1±2.8	----	9.9#
L3-02	150-400	6	B/1	21	33.7±3.1	28.5±2.3	8.6#
L4-02	0-400	8	B/2	22	32.7±2.1	31.0±1.7	7.0±1.5
-05	150-300	5	A/2	42	48.5±2.2	----	
-06	0-350	4	B/2	42	35.8±3.1	----	
L5-03	200-450	8	A/1	21	26.2±4.5	42.3±0.8	6.2±0.3
-06	----------					3.5±0.1	
-03	250-500	6	B/1	22	24.6±1.8		
L6-02	250-560	7	B/1	36	22.7±1.5	42.7±1.4	6.1#
L7-01	100-450	9	B1/2	55	69.5±9.3	----	
-02	150-560	10	C1/2	71	78.4±4.8	30.9±3.3	
-03**	0-300	6	B1/2	66	54.6±4.6	----	11.2±2.1
L8-02	150-450	7	B/2	23	33.5±3.2	28.7±0.3	
-03	150-450	5	B/2	33	14.5±0.6		
-06	0-450	8	B/2	59	49.9±2.0	----	8.6±4.8
-07	----------					1.8±0.1	
L9-02	150-450	7	B/1	25	36.8±3.4	50.3±1.2	
-03**	100-350	5	B/1	30	30.3±10.6	33.6±1.6	
-04	100-450	9	C/1	72	30.7±5.7	----	7.8±0.9
-07	----------					39.0±1.7	
L10-02	150-500	6	C/2	25	19.2±1.0		
-03	150-450	6	B/2	30	21.8±0.7	----	
-04	----------					----	5.4±0.4
-05	100-450	10	D/2	32	21.3±2.0	4.4±0.1	
L11-01	200-500	7	B/1	34	13.8±1.2		4.4±1.5
-02	150-400	7	A/1	33	20.9±2.0	----	
-03	150-400	6	B/1	25	27.7±0.9	----	
-05	----------					8.1±0.1	
L12-01	300-450	5	B1/2	38	26.0±1.6		9.4#

L13-01	0-450	6	B1/2	21	22.2±1.3		
-06**	100-300	5	C1/2	13	10.7±1.0		4.2±1.5
-07	200-450	4	B1/2		16.5±1.0		
-03	----------					----	
L14-01	100-400	6	B/2	27	40.2±3.6	40.9±1.4	10.1#
L15-04**	150-450	4	C/1	9	24.5±3.0	13.5±0.2	
-06	----------						
-07	----------					----	6.2#
L16-04**	300-450	4	B/1	13	10.0±0.6	----	15.5±18.7
-05**	240-400	5	A/1	26	124.7±19.7	----	
-06	----------					8.2±0.5	
L17-01	200-450	6	B/2	35	26.5±2.2	----	5.8±1.0
-02	380-560	6	B/2	24	27.5±1.3		
-03	----------					15.8±0.5	
-06	200-450	6	B/2	31	19.4±2.2	----	
L18-02	0-400	7	B/1	40	64.0±5.0	66.7±3.5	
-05	200-450	5	B/1	26	84.9±3.8	----	19.1±4.3
-07	----------					30.2±5.3	
L19-01	0-300	6	B/1	30	31.7±5.4	30.8±1.3	6.5±0.3
-02	150-500	8	B/1	56	29.4±3.0	26.5±0.4	
L20-01**	500-590	4	B1/2	25	42.5±1.2		12.8±7.2
-04	150-450	5	A1/2	36	80.8±3.6	----	
-05	----------					84.0±7.8	
-07	0-450	8	B1/2	46	26.0±1.6		
L21-02	100-380	5	B/2	37	38.9±4.4	29.9±1.3	5.8#
L22-02	100-450	8	B1/2	40	88.9±9.3	----	13.0#
L23-01**	100-300	5	D/2	5	14.7±3.8	16.1±1.2	3.7#
-02	----------					28.0±2.6	

Table 6.1 : Palaeointensity results for the lower (Mussartût) lava group. DT = Temperature range over which Ba was calculated, N = Number of data points used to calculate Ba, C = Thellier category (see text). RM = Rock Magnetic set, as defined in Chapter 7. F = % of NRM used in calculation of Ba, Ba(Th) = modified Thellier palaeointensity value, Ba(Sh) = modified Shaw palaeointensity value, VDM = Mean Virtual Dipole Moment for the flow (Smith 1967a), given in $\times 10^{22}Am^2$. # indicates that the VDM was calculated using only one sample. ** indicates sample eliminated from calculation of mean values.

SAMPLE NUMBER	DT	N	C	F	Ba	VDM $\times 10^{22}Am^2kg^{-1}$
M1-04	100-450	6	B	69	57.0±4.5	10.4±0.4
-05	100-400	8	B	72	60.5±3.1	
M2-01	500-610	7	A	88	9.5±0.4	1.8±0.3
-03	500-600	4	A	79	7.2±0.6	
M3-01	450-640	9	A	37	7.9±0.2	1.4±0.2
-03	0-680	10	A	83	6.4±0.1	
M4-05	0-590	9	A	35	9.7±0.5	1.8±0.2
-07	100-680	9	A	44	8.3±0.3	
M5-02	100-540	5	C	23	10.2±0.3	2.1#
M6-01	560-650	7	A	94	9.4±1.8	1.5±0.6
-02	400-680	8	A	96	5.5±0.1	
M7-01	530-640	6	A	99	1.3±0.1	1.4#
-02	----------					
-03	300-680	9	A	93	6.6±0.2	
M8-02	400-580	4	A	89	7.9±0.3	1.9#
M9-01	400-680	9	A	46	8.4±0.8	2.1#
M10-02	0-540	8	A	42	7.1±0.7	1.8#
M11-02	0-450	9	C	29	10.8±0.1	2.7#
M12-01	400-580	10	A	32	12.9±0.1	3.3#
M13-01	450-560	8	C	28	12.3±0.2	3.1#
M14-01	400-620	7	C	10	6.7±0.6	1.7#
M15-03	400-680	10	A	82	6.8±0.1	1.7#
M16-02	100-500	5	C	57	13.6±1.3	3.5#
M17-01	150-400	5	A	38	42.7±3.3	9.2±1.3
-05	200-300	4	A	22	34.8±5.5	
M18-07	0-300	4	A	88	41.5±0.9	9.6#

Table 6.2 : Palaeointensity results for the Middle (Ulukasik) Lava Formation. Symbols as for Table 6.1.

SAMPLE NUMBER	DT	N	C	F	Ba	VDM $\times 10^{22}Am^2kg^{-1}$
U01-04	150-400	4	B	47	32.7±2.4	6.9±1.3
-05	150-400	5	B	55	42.6±2.0	
U02-01	150-300	4	A	36	40.0±3.3	8.1±0.4
-03	150-350	5	B	48	37.3±9.4	
U03-06	0 + 450	2	A	60	33.7±1.7**	7.6±0.2
-07	0 + 450	2	A	80	34.8±4.5**	
U04-02	0-350	5	B	89	60.8±2.9	7.7±3.0
-04	200-400	5	B	35	34.7±2.5	
U05-04	450-680	6	A	88	6.0±0.3	1.3±0.2
-05	0-620	11	A	99	5.1±0.1	
U06-02	----------					----
-05	100-400	5	D	22	15.7±2.9**	3.6#
U07-01	----------					
-02	0-560	8	C	95	7.8±0.2**	1.8#
U08-02	250-450	5	B	31	13.8±1.0	2.6±0.4
-05	300-450	4	B	20	17.7±3.2	
U09-01	----------					----
-05	----------					----
U10-02	590-660	4	C	73	14.0±0.7	3.7±0.2
-03	500-620	5	C	84	10.3±0.3	
-04	350-620	10	C	99	6.8±0.4	
U11-01	530-680	7	C	94	7.9±0.4	1.3±0.1
-02	540-620	5	C	96	5.2±0.2	
-03	400-630	6	C	99	5.9±0.1	
U12-01	200-530	5	C	59	10.8±2.9	3.1±0.4
-03	300-660	10	C	99	11.4±0.9	
-06	450-580	6	C	27	14.0±0.7	
U13-01	400-680	10	C	60	7.8±0.2	2.9±1.5
-04	300-590	5	C	34	7.7±0.2	
-05	300-640	10	C	94	16.7±0.2	
U14-02	0 + 370	2	A	96	31.9±2.3**	8.4±0.5
-04	0 + 370	2	A	33	34.6±0.1**	
U15-01	0-450	9	B	91	81.4±4.2	21.3±0.5
-04	0-270	6	C	63	83.9±6.0	
U16-02	150-350	5	B	25	8.9±1.2	1.2#
-06	0-400	5	A	98	48.3±5.5**	
U17-03	0-200	4	A	15	37.9±0.6	8.2±1.6
-05	0-200	3	A	35	28.9±0.9	
U19-01	500-660	6	C	82	6.0±1.1	1.9±0.5
-03	500-660	6	C	89	7.7±0.4	
-05	300-620	8	C	86	9.8±0.4	
U20-04	----------					
-08	0-200	4	A	86	26.7±0.5**	6.2#
-03	----------					
U21-03	0-200	4	B	54	52.4±3.9	7.3±0.2
-05	0-200	4	B	46	54.1±3.6	
U22-01	0-350	7	B	56	55.5±9.0**	9.2±1.0
-06	0-200	4	B	64	47.2±4.3**	
U23-01	200-500	5	B	21	15.3±1.2	5.3±3.0
-02	0-450	5	B	43	35.8±2.5	
U24-02	150-400	3	B	35	13.3±1.0**	4.9±3.9
-07	0-400	4	B	29	48.0±7.3**	
U25-03	100-450	5	B	30	15.7±0.8**	3.4±0.1
-07	200-500	5	B	40	15.3±0.4**	
U26-02	0-450	6	B	10	17.3±1.6**	2.7#
-05	----------					
-07	----------					

U27-02	100-450	5	C	22	17.0±0.7	3.1#
-05	----------					
U28-02	150-300	4	B	31	22.3±4.2	5.7±1.2
-05	150-300	4	B	30	30.3±2.7	
U29-04	----------					
U30-01	----------					
U31-05	0-200	3	B	40	33.0±3.9**	2.5#
-07	150-300	4	B	20	14.1±0.8	
U32-04	240-500	8	B	34	15.9±1.4**	3.5#
U33-05	----------					
-07	----------					
U34-02	----------					
-03	----------					
U35-01	----------					
-02	0-300	6	A	24	15.8±2.7**	2.1#
U36-03	450-620	6	B	34	25.2±1.3	3.4±0.1
-04	500-620	4	C	23	24.3±0.8	
U37-02	100-500	6	B	43	38.5±4.7	6.6#
U38-04	450-530	3	B	37	21.5±1.7**	2.8#
U39-03	150-350	5	B	31	48.0±3.6	10.1±0.4
-06	0-200	5	B	42	50.9±1.9	
U40-01	0-400	7	B	80	49.4±6.6	11.7±0.7
-02	0-400	4	B	84	45.4±3.9	

Table 6.3 : Thellier palaeointensity results for the Upper (Ilímaussaq) Lava Formation. Symbols as for Table 6.1.

Figure 6.3 : Modified Thellier palaeointensity (Arai) plots for the Lower Lava Formation. NRM and TRM values are normalised to the initial NRM (T = TR) and TRM (T = T1) values. Each circle on the plots represents the NRM remaining and the TRM acquired at a particular temperature step. The figures next to the circles give the temperature and closed (open) circles indicate points accepted (rejected) from the calculation of the palaeointensity. Triangles indicate "PTRM checks" carried out at raised temperatures.

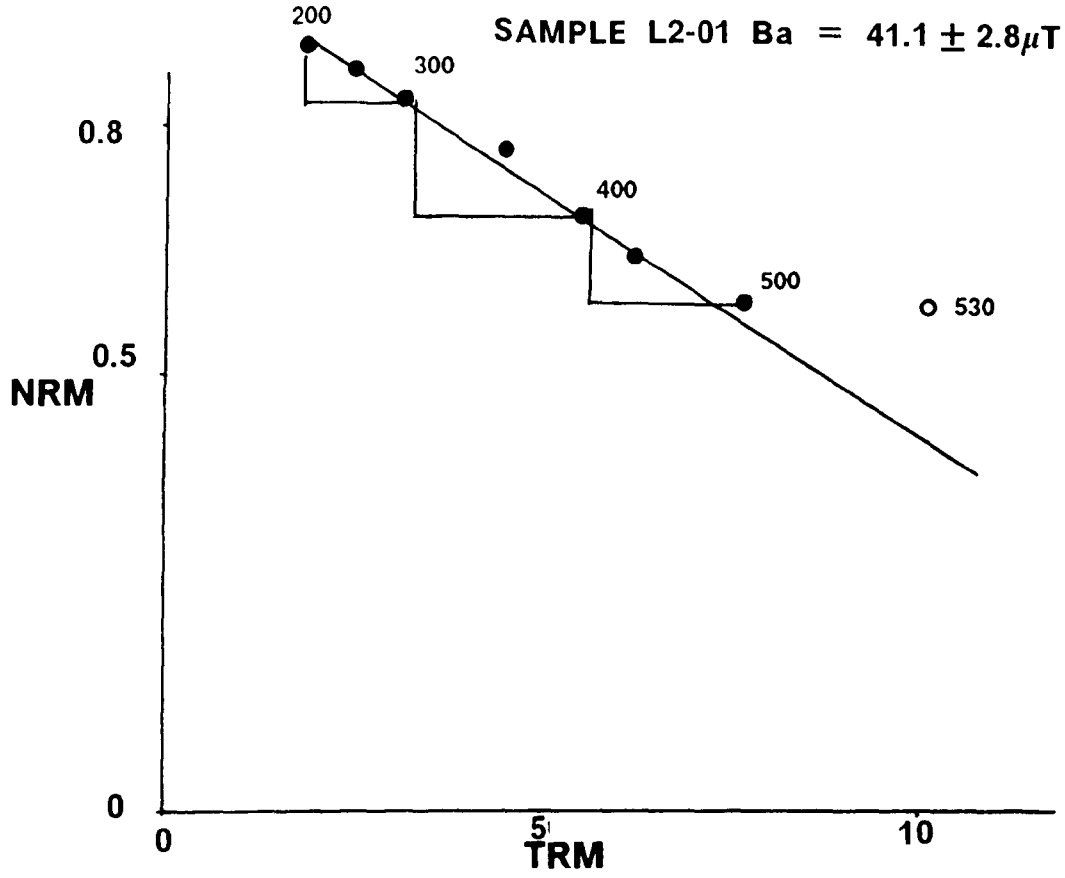
SAMPLE L2-01 Ba = 41.1 ± 2.8μT
200
300
400
500
530
0.8
0.5
NRM
0
0
5
10
TRM

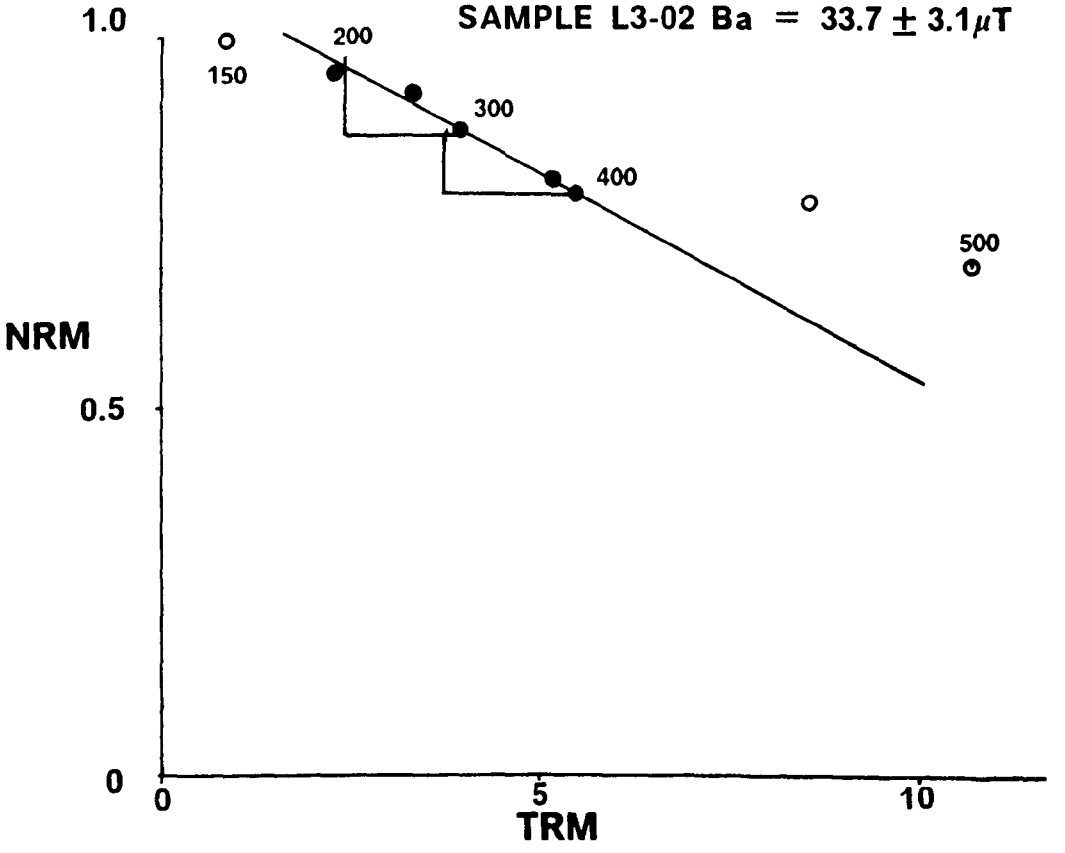
SAMPLE L3-02 Ba = 33.7 ± 3.1μT
1.0
150
200
300
400
500
NRM
0.5
0
0
5
10
TRM

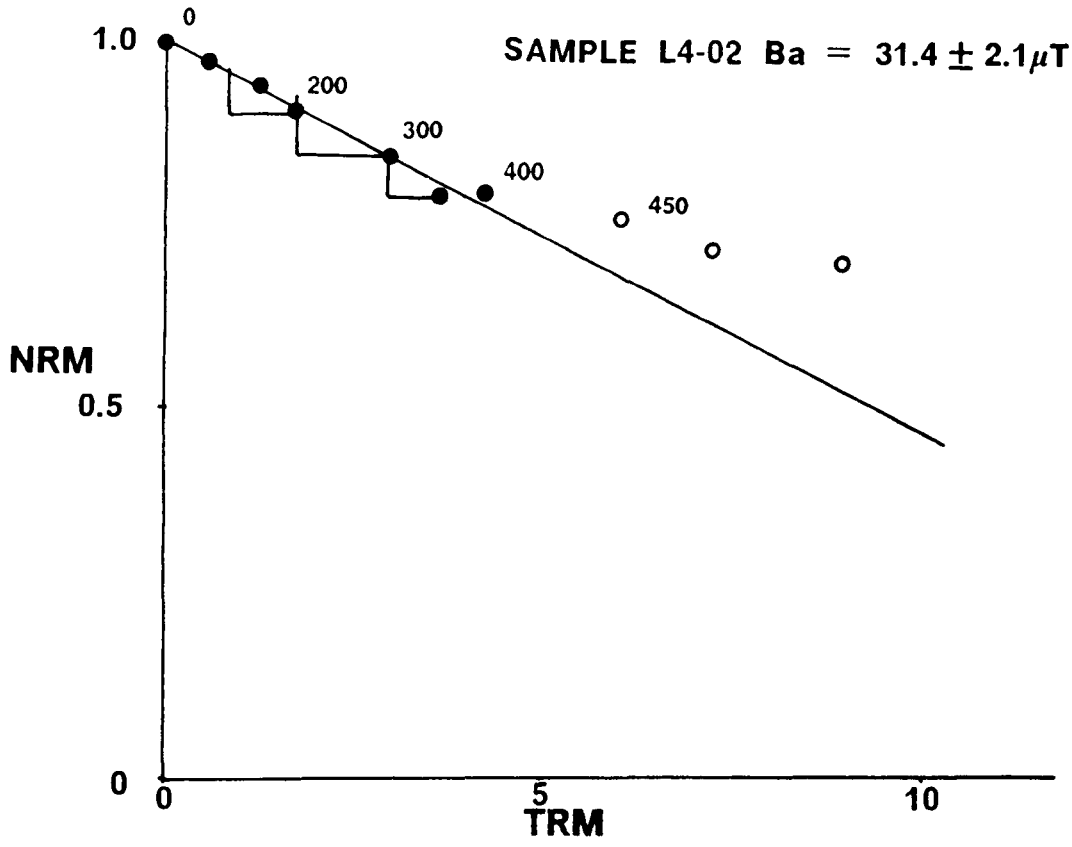
SAMPLE L4-02 Ba = 31.4 ± 2.1μT
1.0
0.5
0
NRM
0
200
300
400
450
0
5
10
TRM

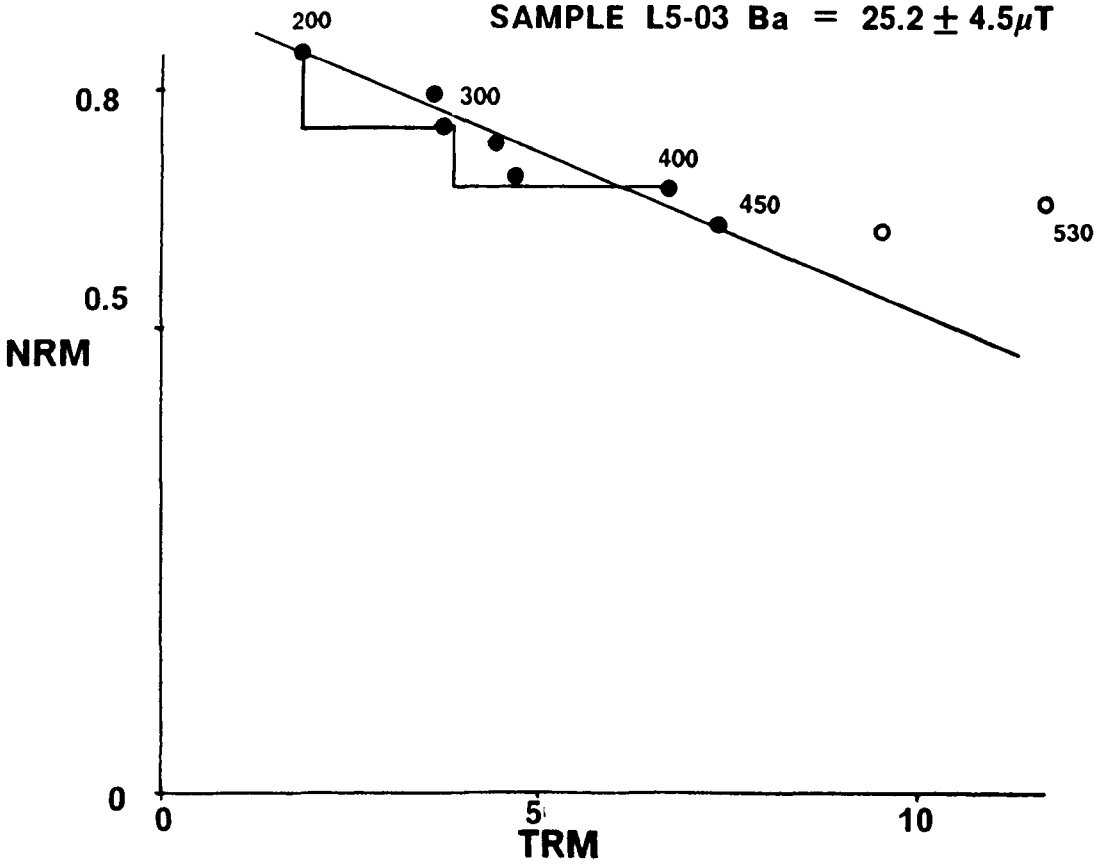
SAMPLE L5-03 Ba = 25.2 ± 4.5μT
0.8
0.5
0
NRM
200
300
400
450
530
0
5
10
TRM

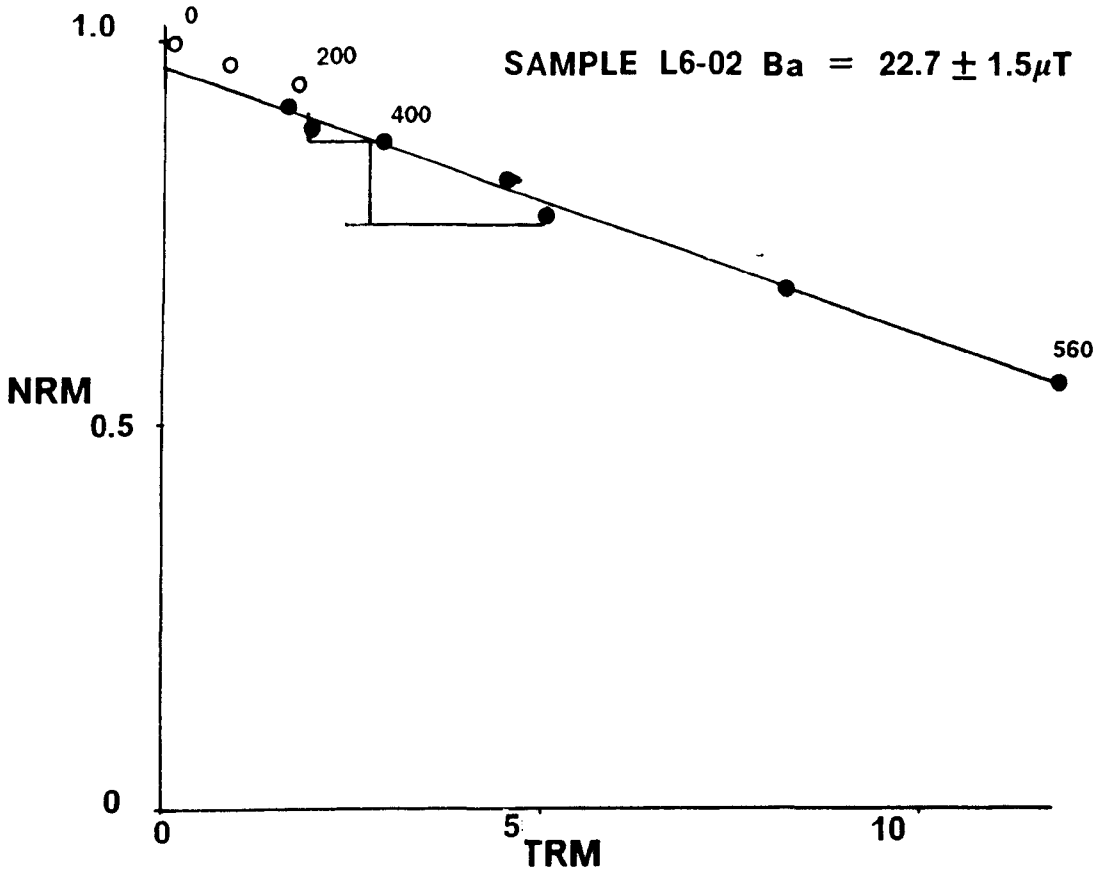
SAMPLE L6-02 Ba = 22.7 ± 1.5μT
1.0
0.5
0
NRM
0
200
400
560
0
5
10
TRM

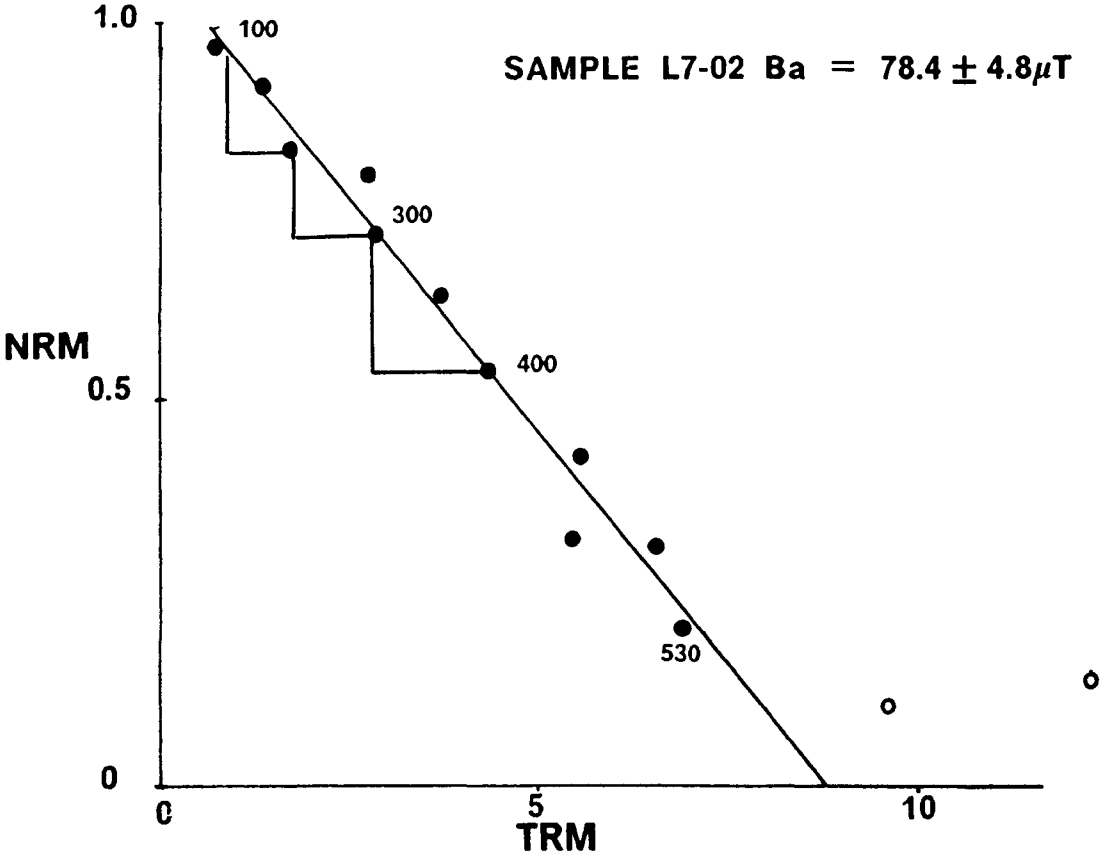
SAMPLE L7-02 Ba = 78.4 ± 4.8μT
1.0
0.5
0
NRM
100
300
400
530
0
5
10
TRM

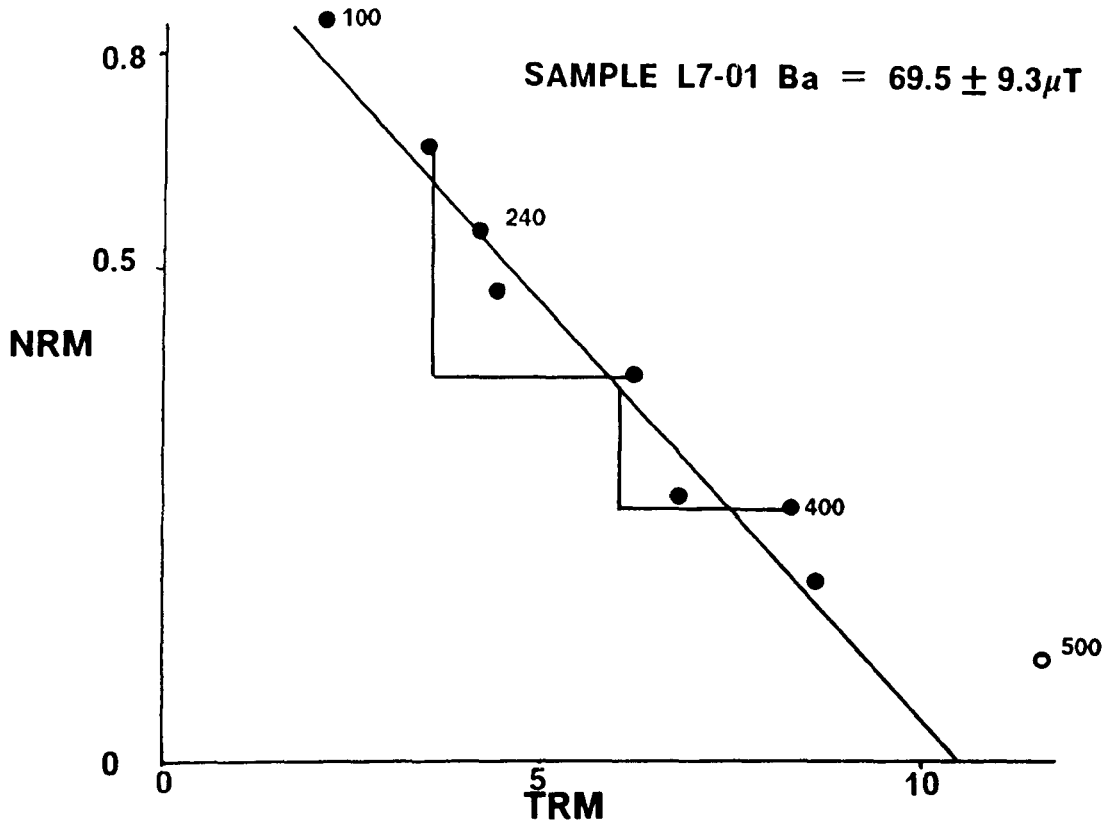
SAMPLE L7-01 Ba = 69.5 ± 9.3μT
100
240
400
500
0.8
0.5
0
NRM
0
5
10
TRM

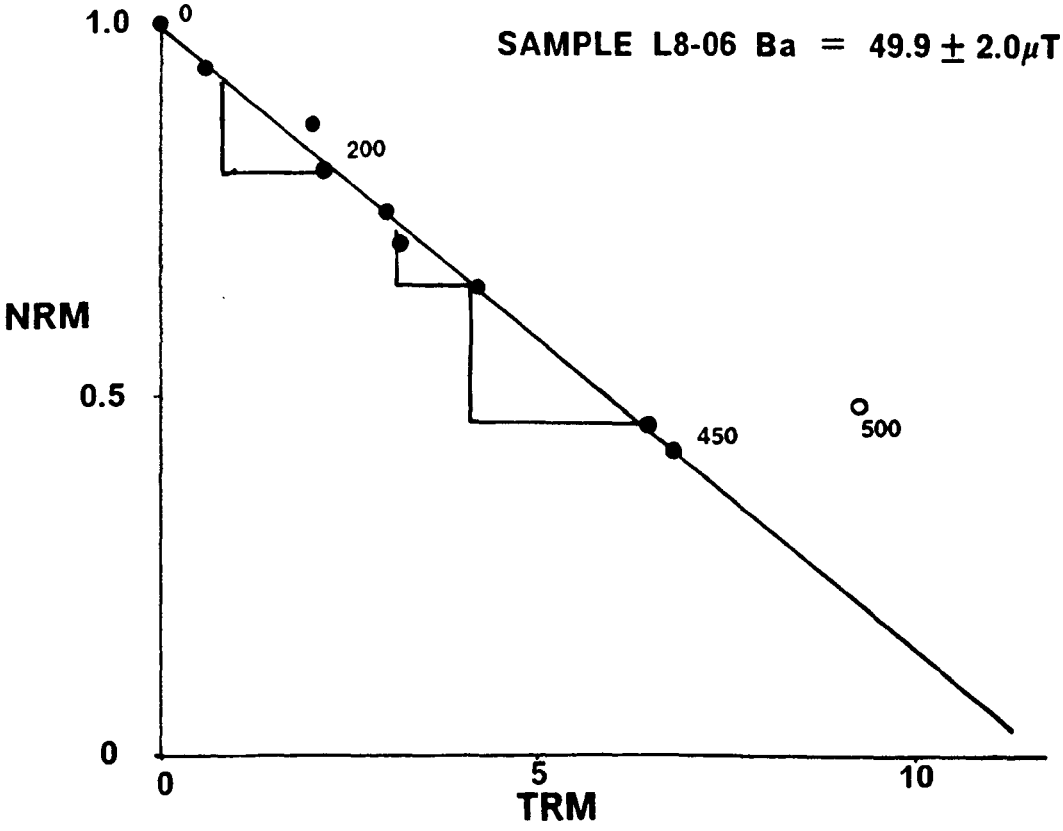
SAMPLE L8-06 Ba = 49.9 ± 2.0μT
0
200
450
500
1.0
0.5
0
NRM
0
5
10
TRM

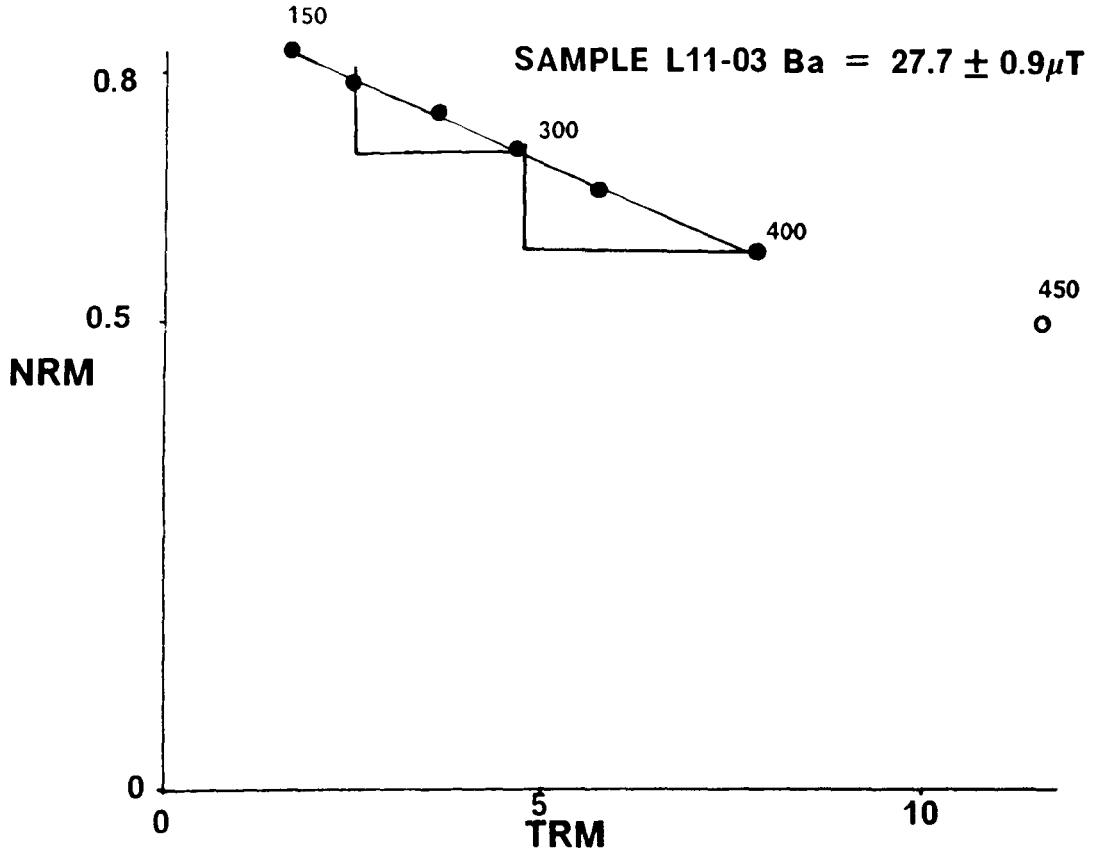
SAMPLE L11-03 Ba = 27.7 ± 0.9μT
150
300
400
450
0.8
0.5
0
NRM
0
5
10
TRM

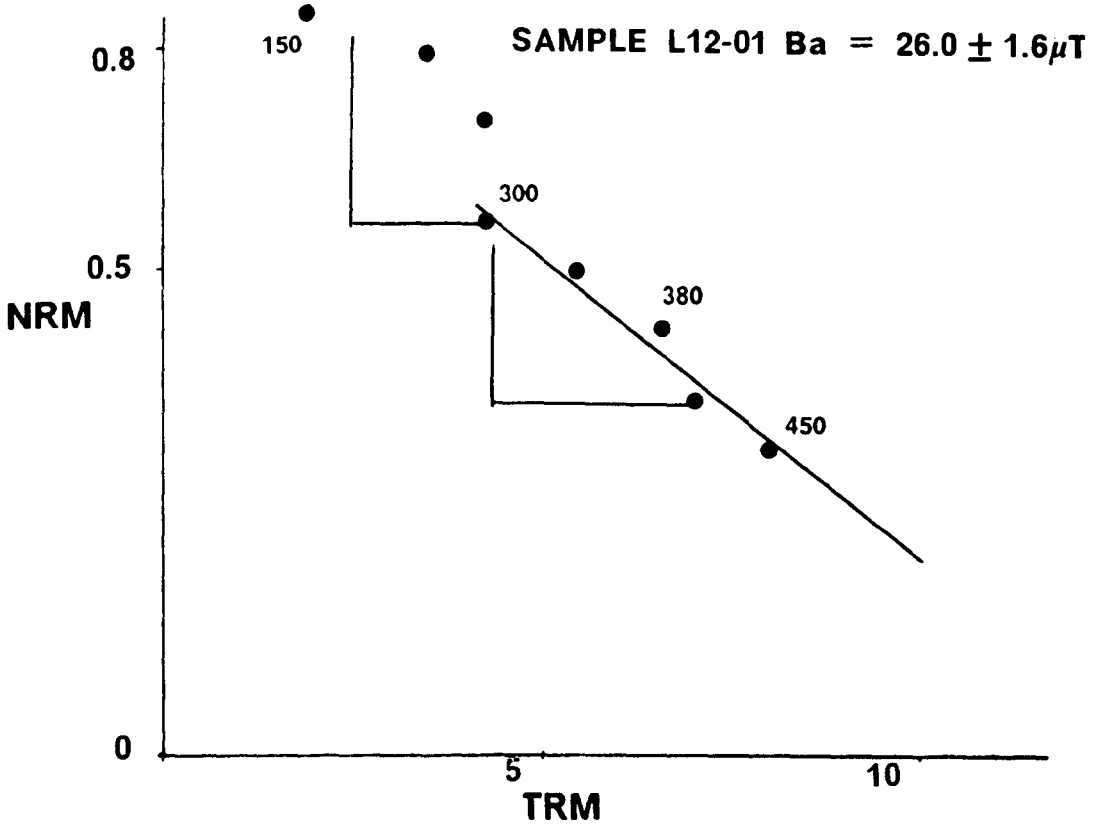
SAMPLE L12-01 Ba = 26.0 ± 1.6μT
150
300
380
450
0.8
0.5
0
NRM
5
10
TRM

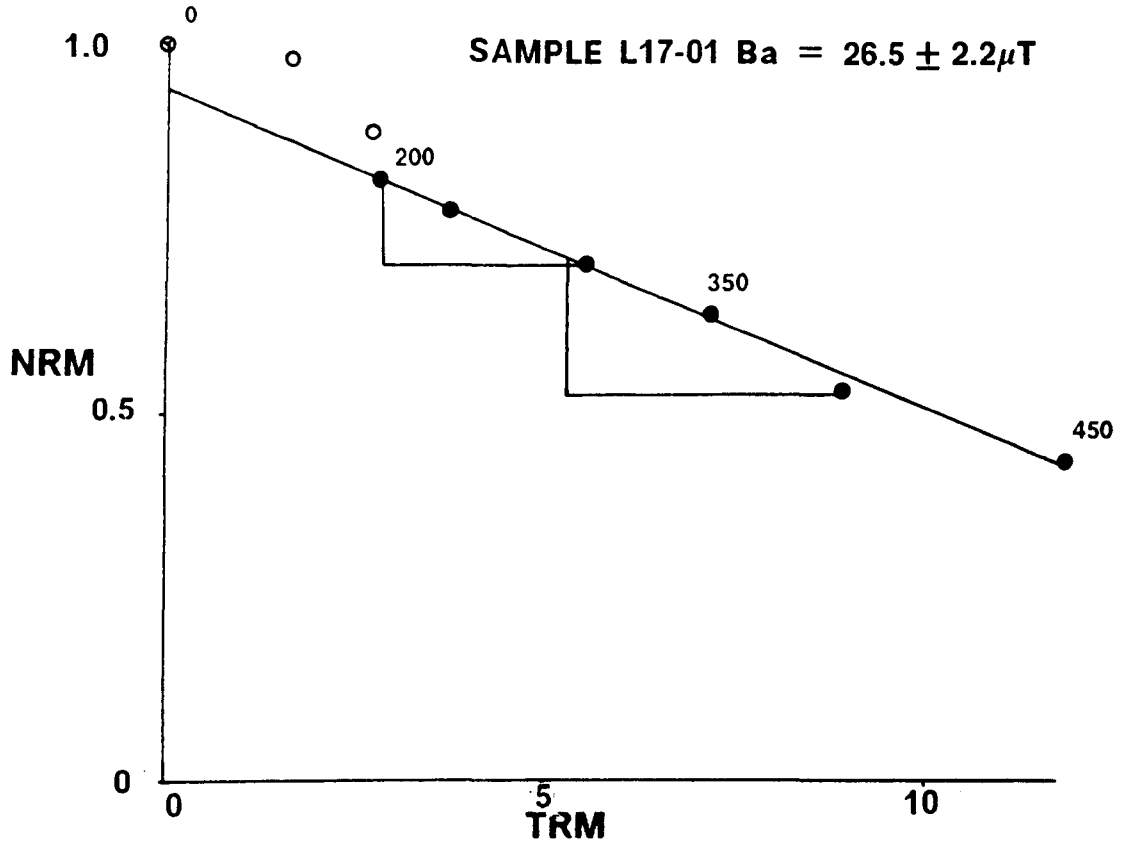
SAMPLE L17-01 Ba = 26.5 ± 2.2μT
1.0
0.5
0
NRM
0
200
350
450
0
5
10
TRM

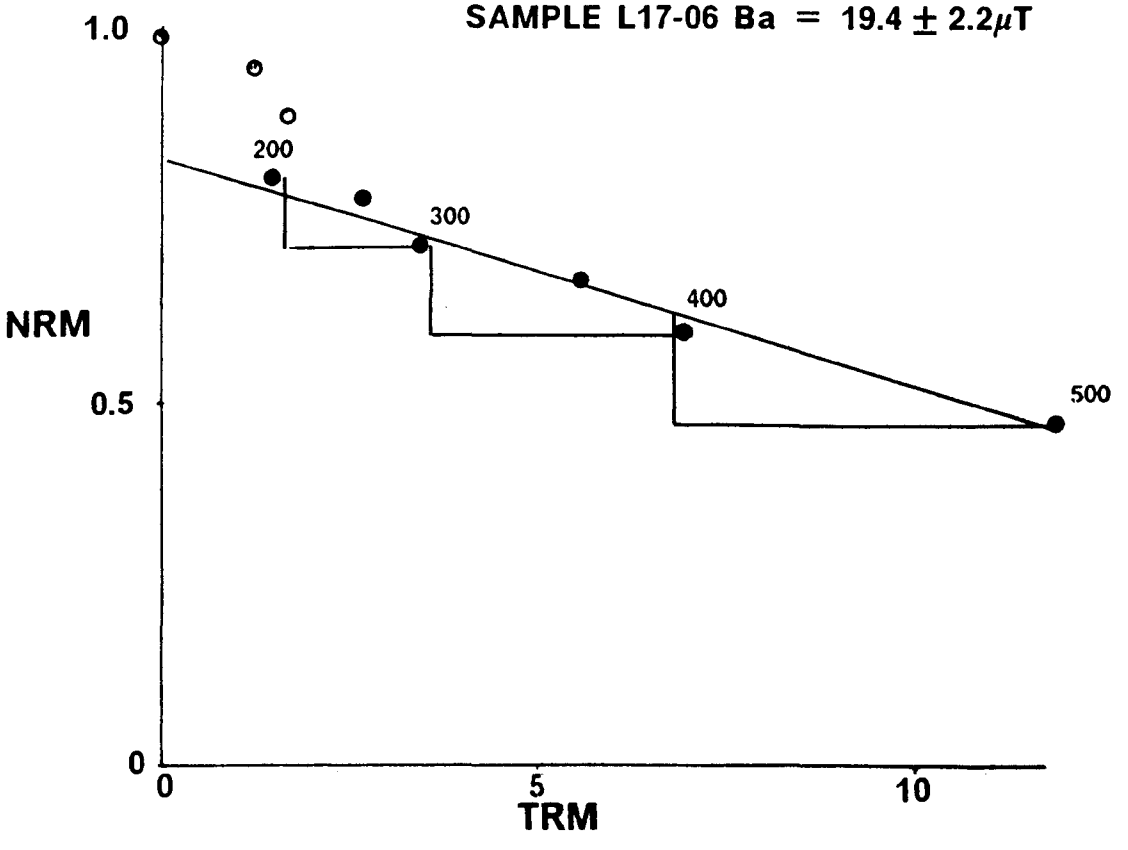
SAMPLE L17-06 Ba = 19.4 ± 2.2μT
1.0
0.5
0
NRM
200
300
400
500
0
5
10
TRM

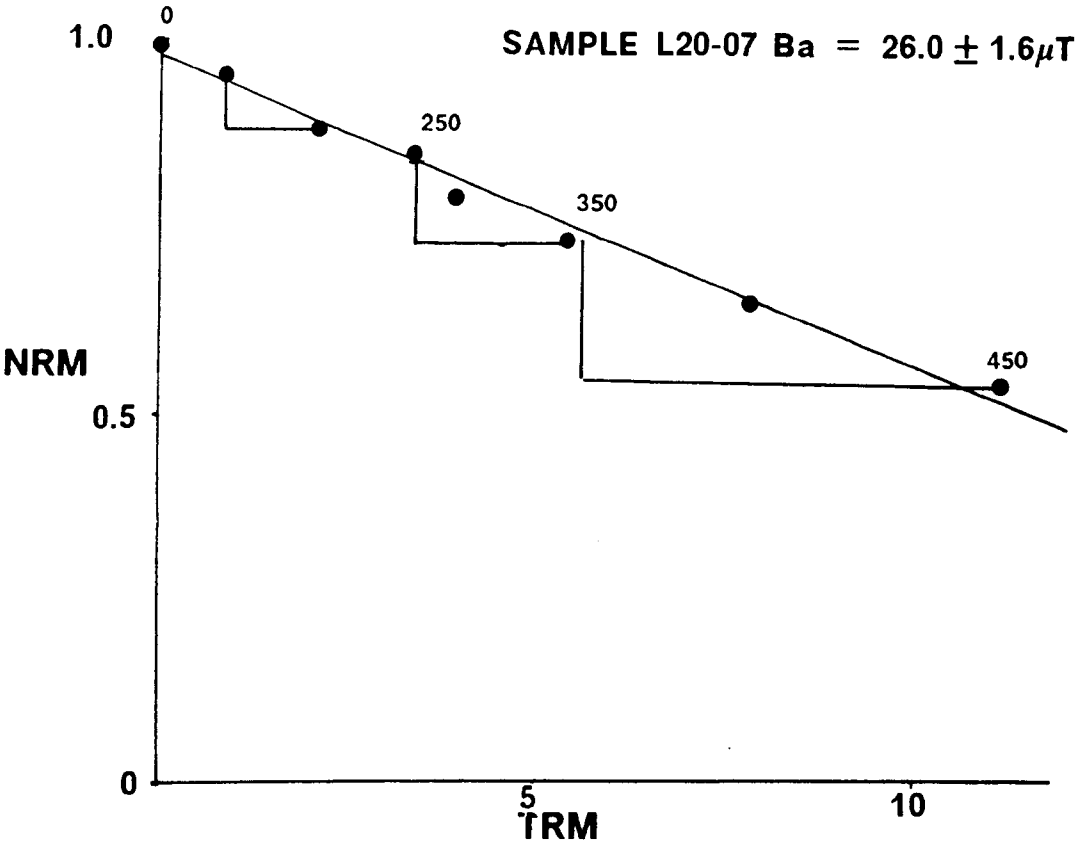
SAMPLE L20-07 Ba = 26.0 ± 1.6μT
1.0
0
250
350
450
NRM
0.5
0
5
10
TRM

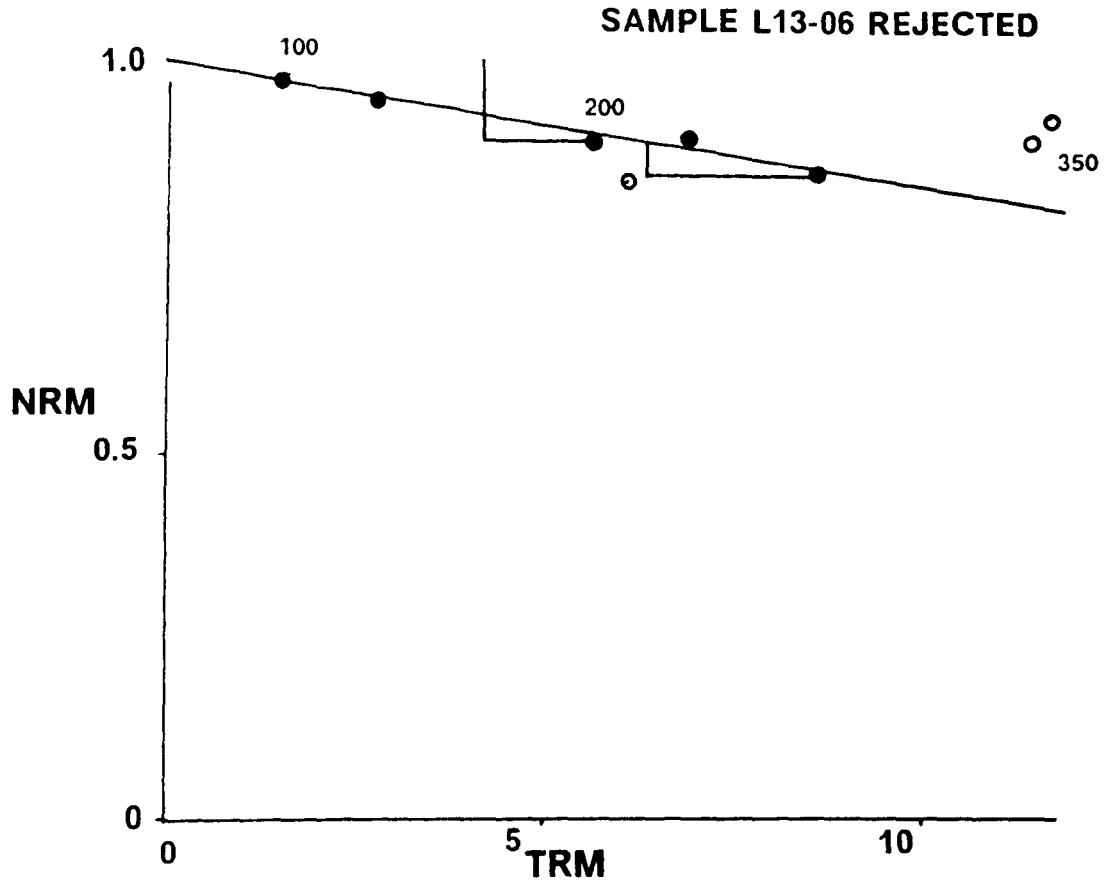
SAMPLE L13-06 REJECTED
1.0
100
200
350
NRM
0.5
0
0
5
TRM
10

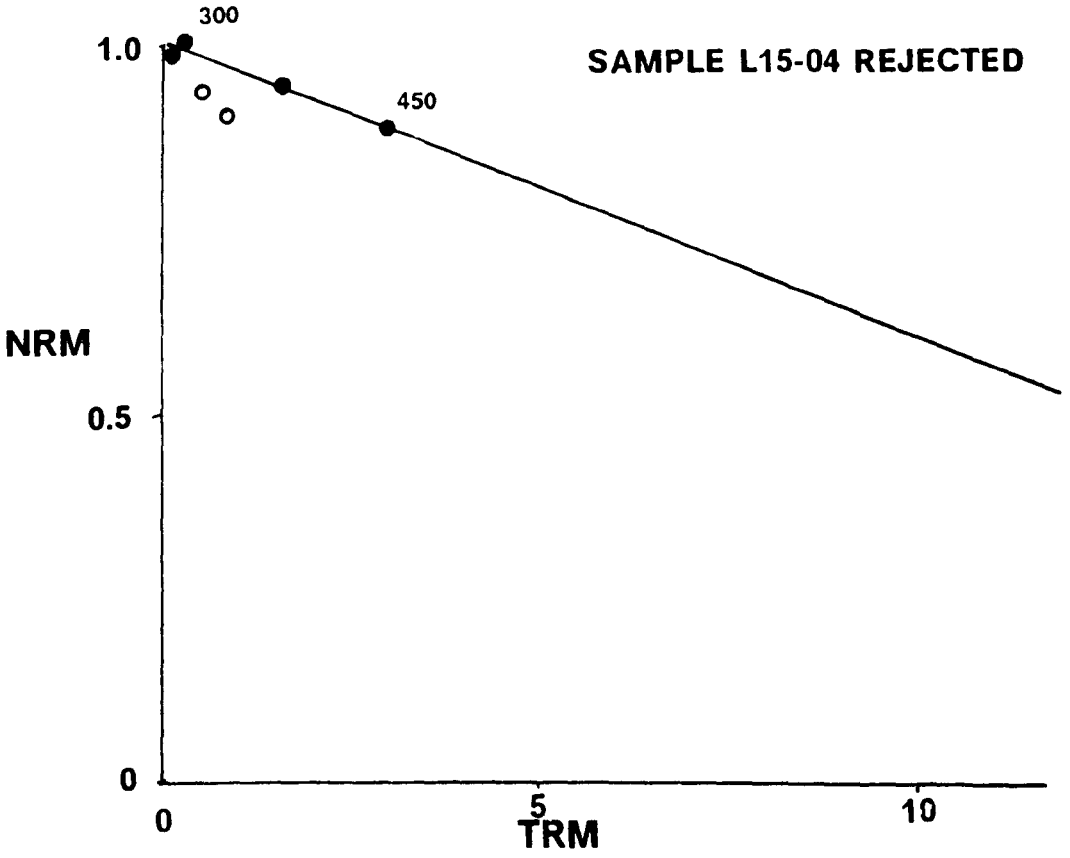
300
1.0
SAMPLE L15-04 REJECTED
450
NRM
0.5
0
0
5
TRM
10

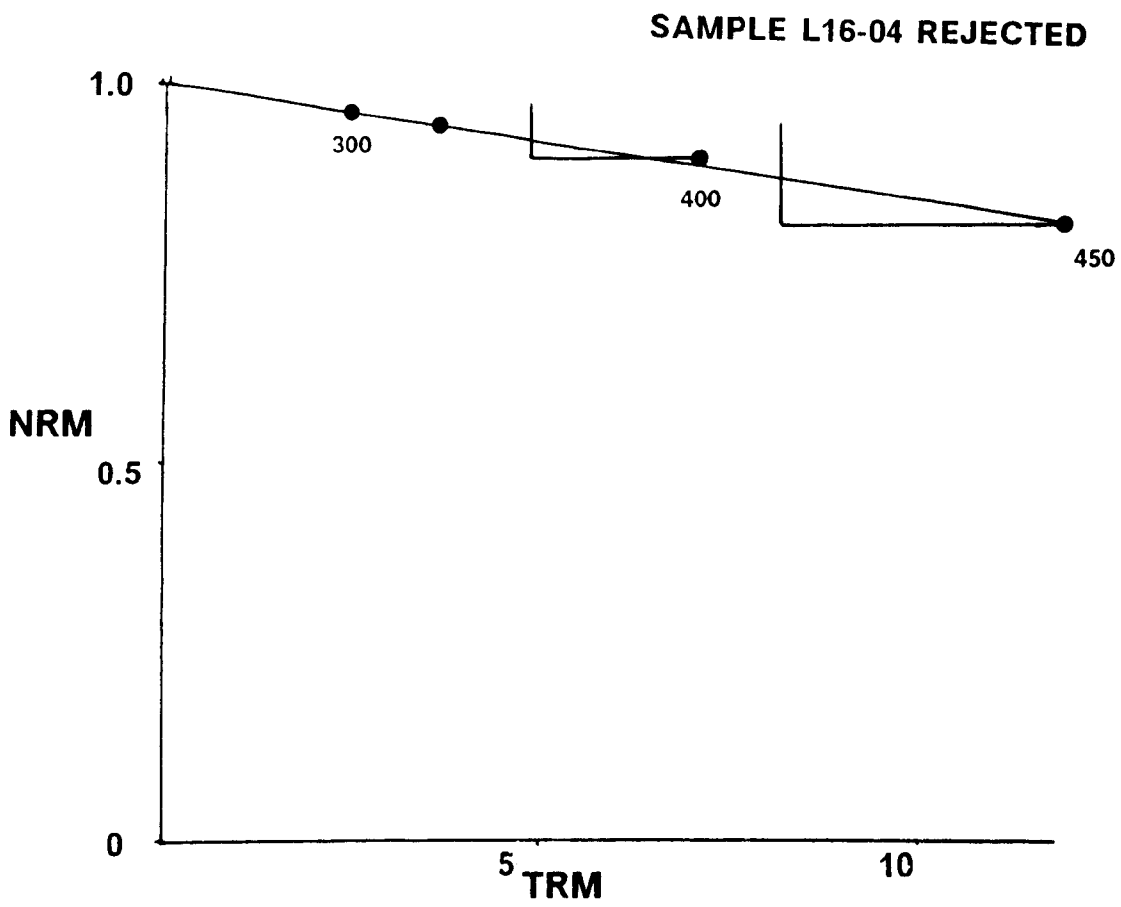
SAMPLE L16-04 REJECTED
1.0
300
400
450
NRM
0.5
0
5
TRM
10

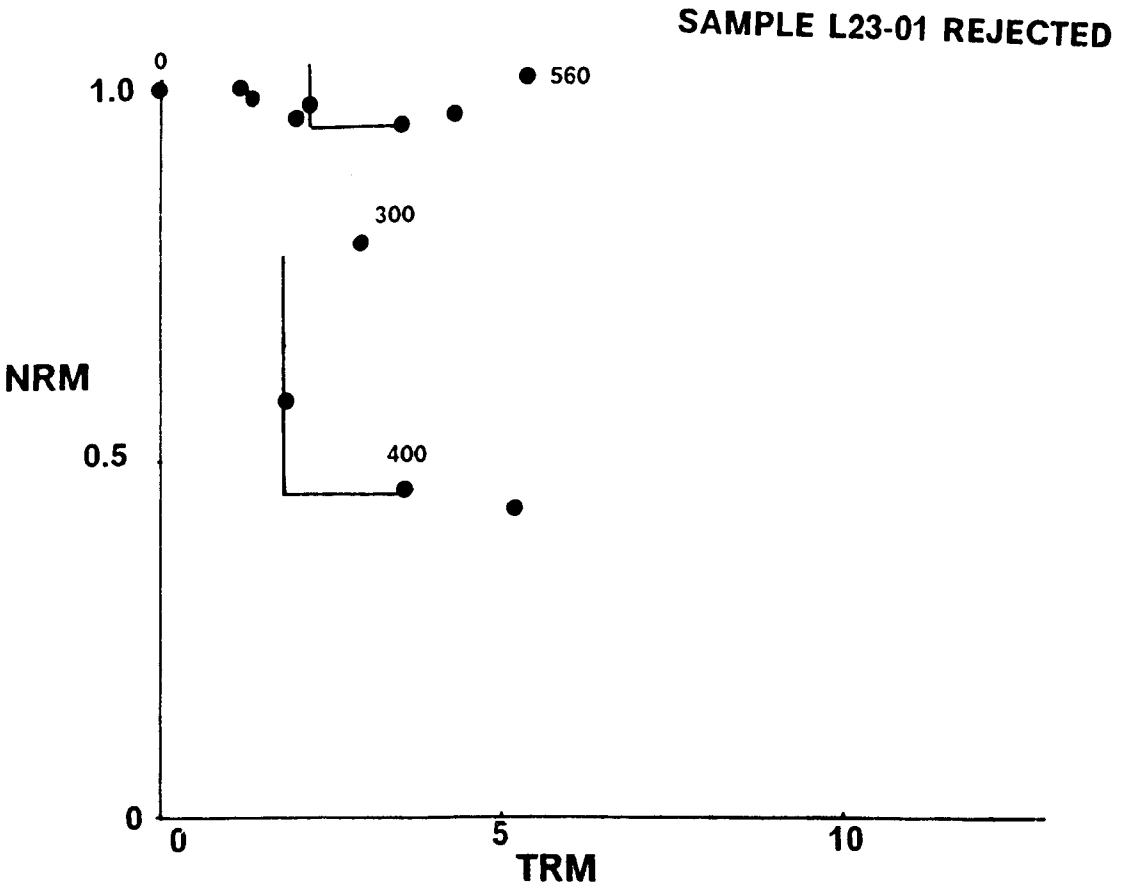
SAMPLE L23-01 REJECTED
0
1.0
560
300
NRM
0.5
400
0
0
5
TRM
10

Figure 6.4 : Modified Thellier palaeointensity (Arai) plots for the Middle Lava Formation. See Figure 6.3 caption for explanation of the plot.

Figures 6.4 a-e : Plots for samples possessing the 'A' direction

Figures 6.4 f-h : Plots for samples possessing the 'B' direction

Figures 6.4 i-k : Plots for samples possessing westerly directions

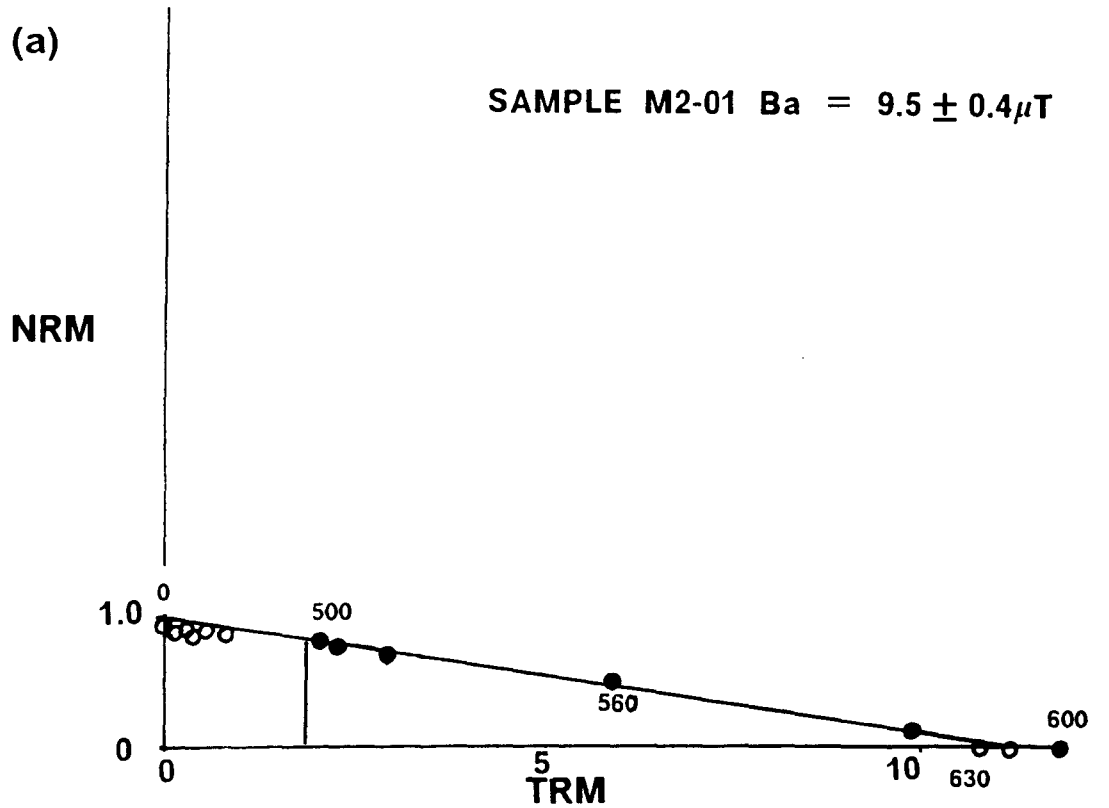
(a)
SAMPLE M2-01 Ba = 9.5 ± 0.4μT
NRM
1.0
0
0
500
560
600
0
5
10
630
TRM

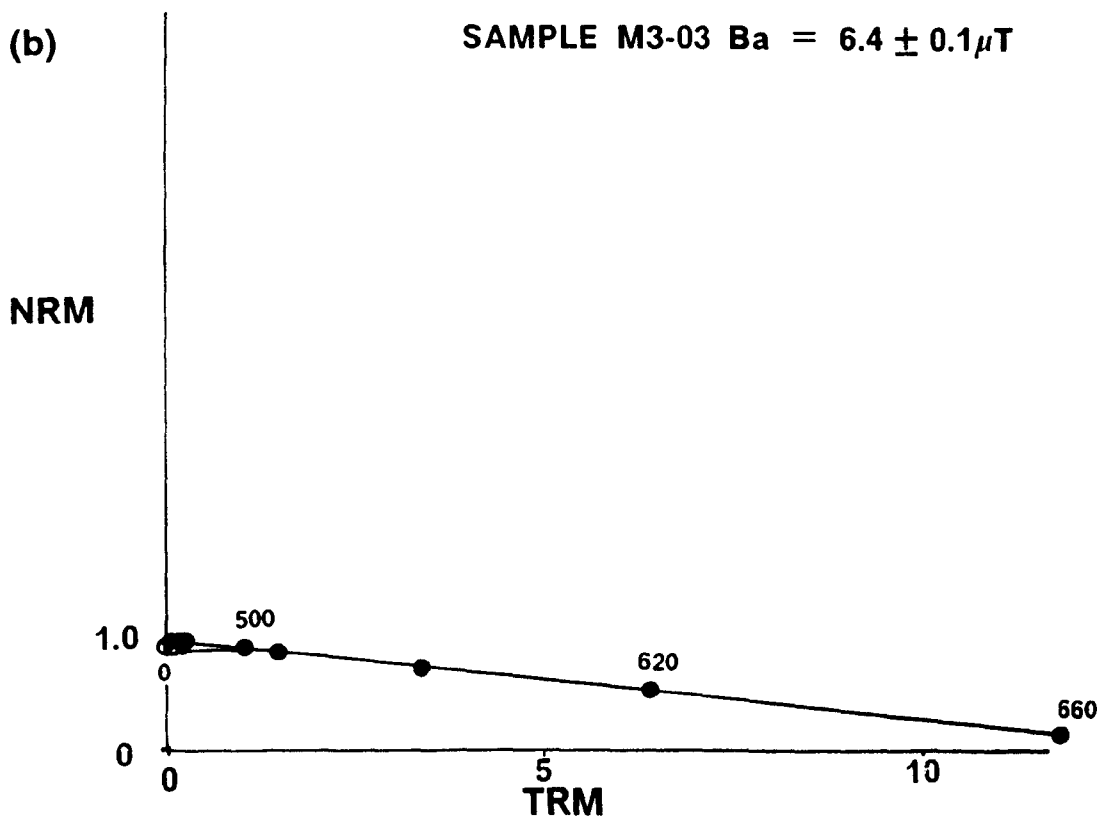
(b)
SAMPLE M3-03 Ba = 6.4 ± 0.1μT
NRM
1.0
0
0
500
620
660
0
5
10
TRM

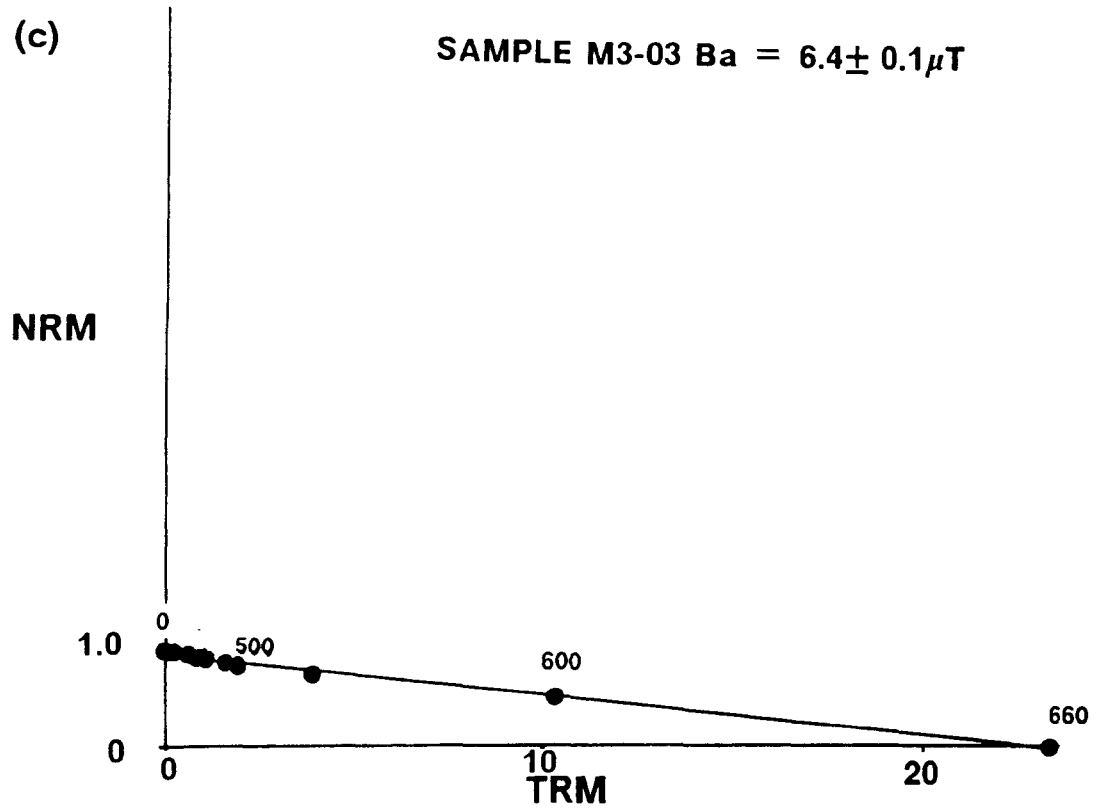
(c)
SAMPLE M3-03 Ba = 6.4± 0.1μT
NRM
1.0
0
0
500
600
660
0
10
20
TRM

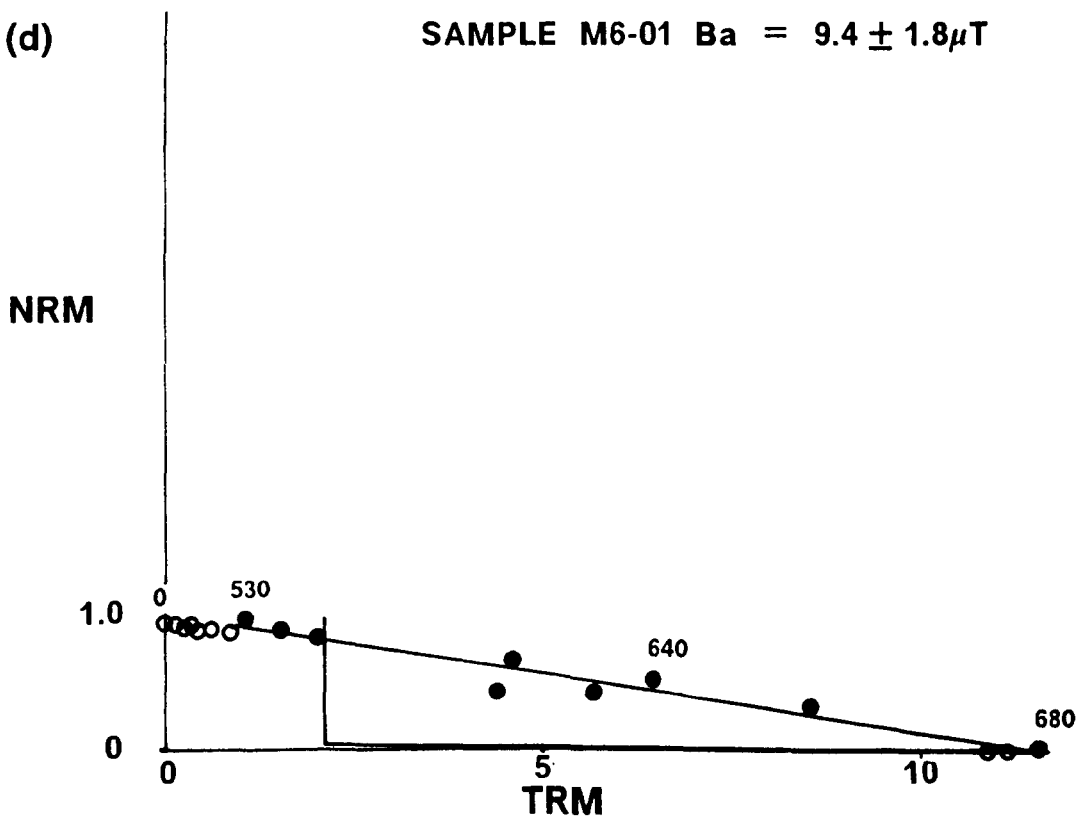
(d)
SAMPLE M6-01 Ba = 9.4 ± 1.8μT
NRM
1.0
0
0
530
640
680
0
5
10
TRM

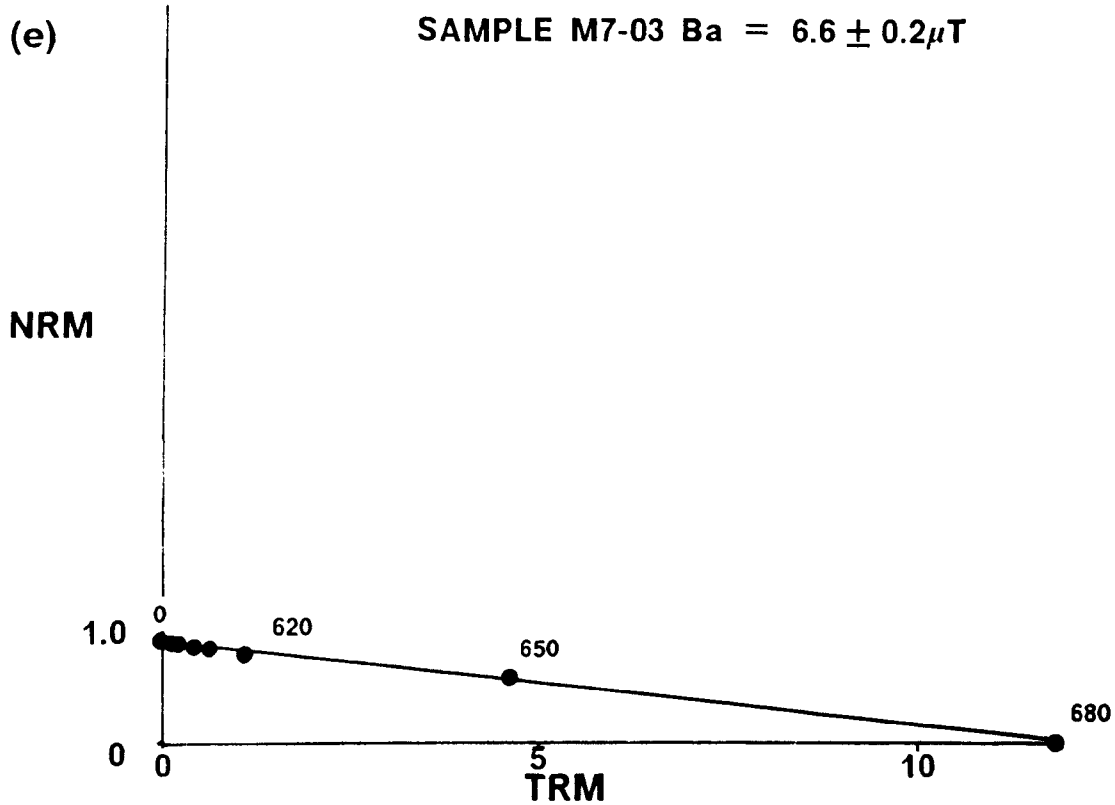
(e)
SAMPLE M7-03 Ba = 6.6 ± 0.2μT
NRM
1.0
0
0
620
650
680
0
5
10
TRM

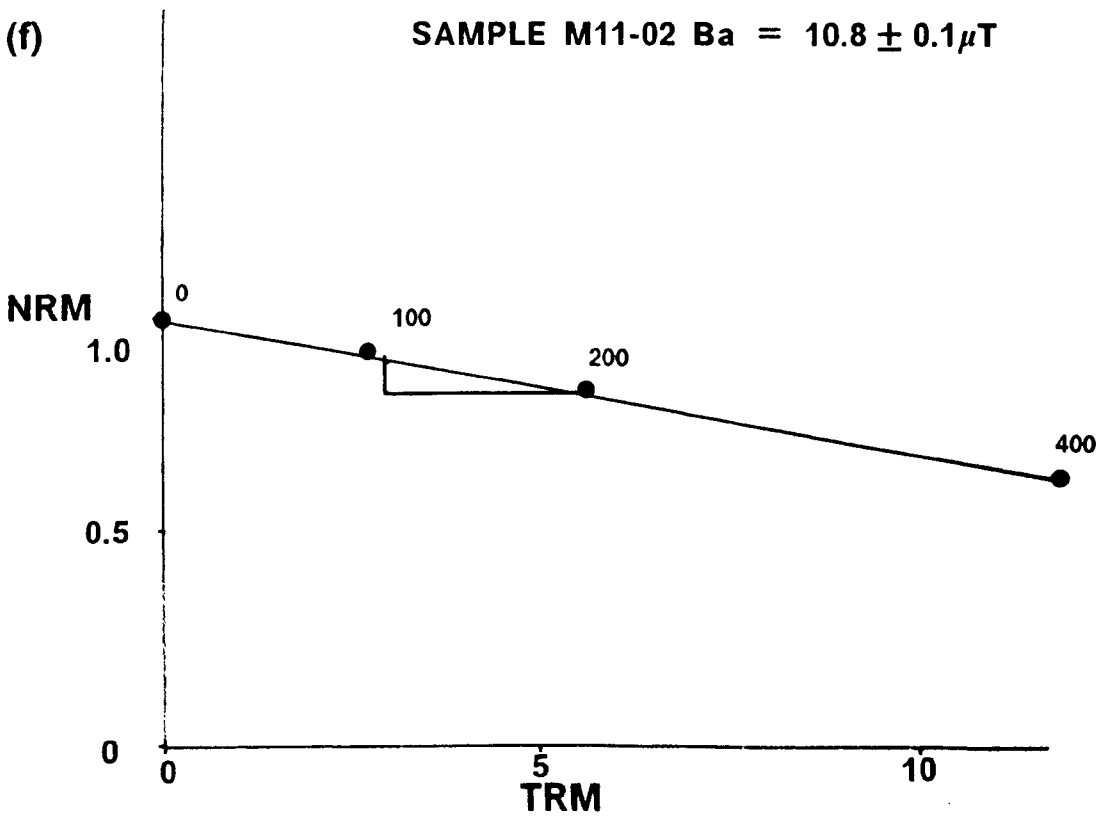
(f)
SAMPLE M11-02 Ba = 10.8 ± 0.1μT
NRM
1.0
0.5
0
0
100
200
400
0
5
10
TRM

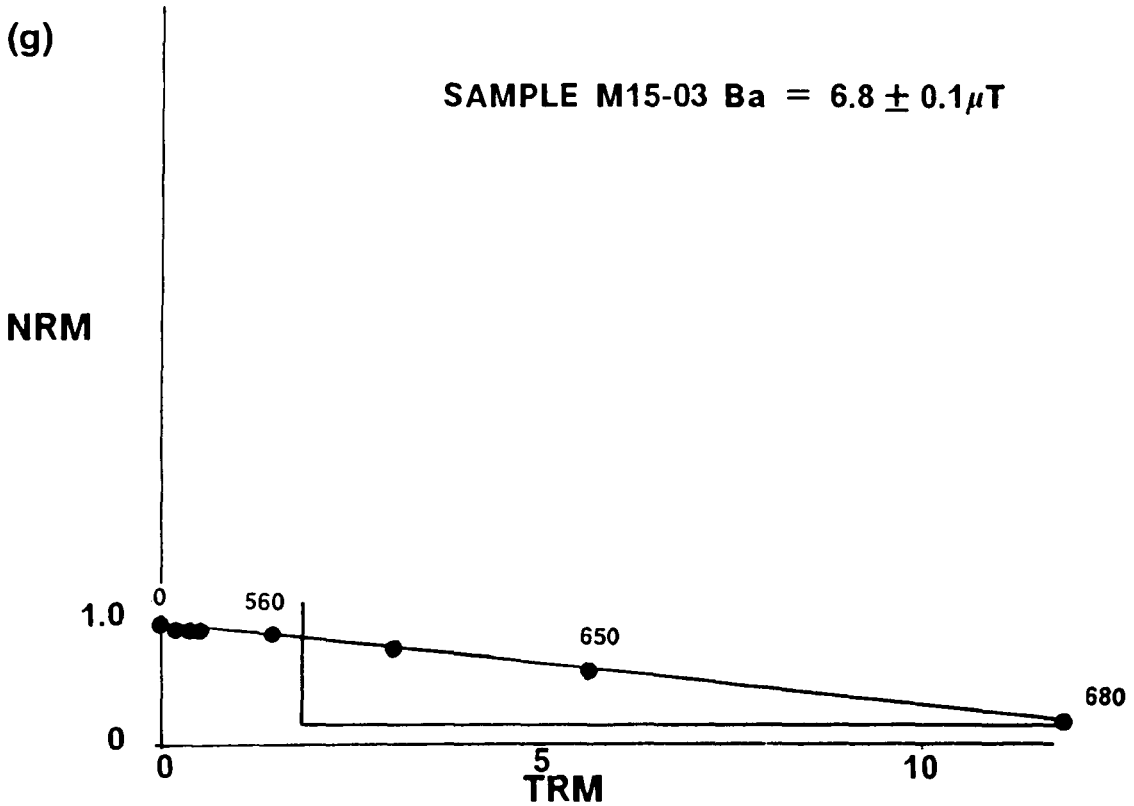
(g)
SAMPLE M15-03 Ba = 6.8 ± 0.1μT
NRM
1.0
0
0
560
650
680
0
5
10
TRM

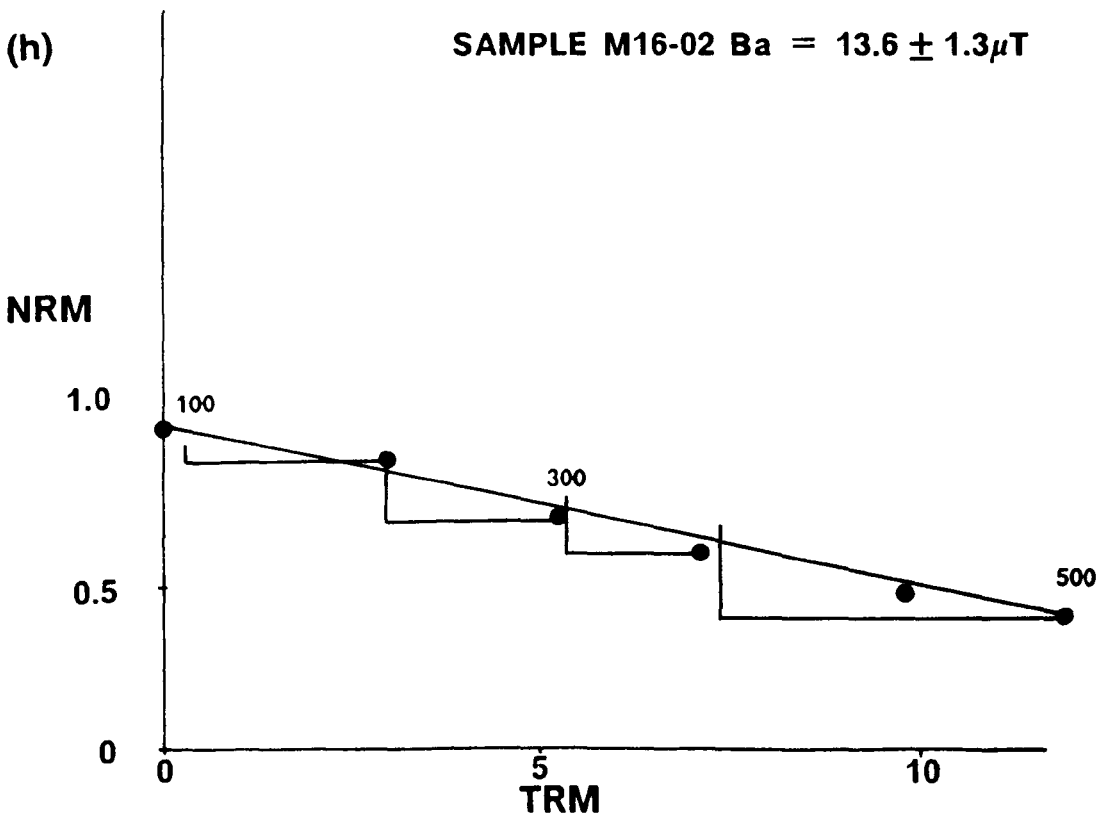
(h)
SAMPLE M16-02 Ba = 13.6 ± 1.3μT
NRM
1.0
0.5
0
100
300
500
0
5
10
TRM

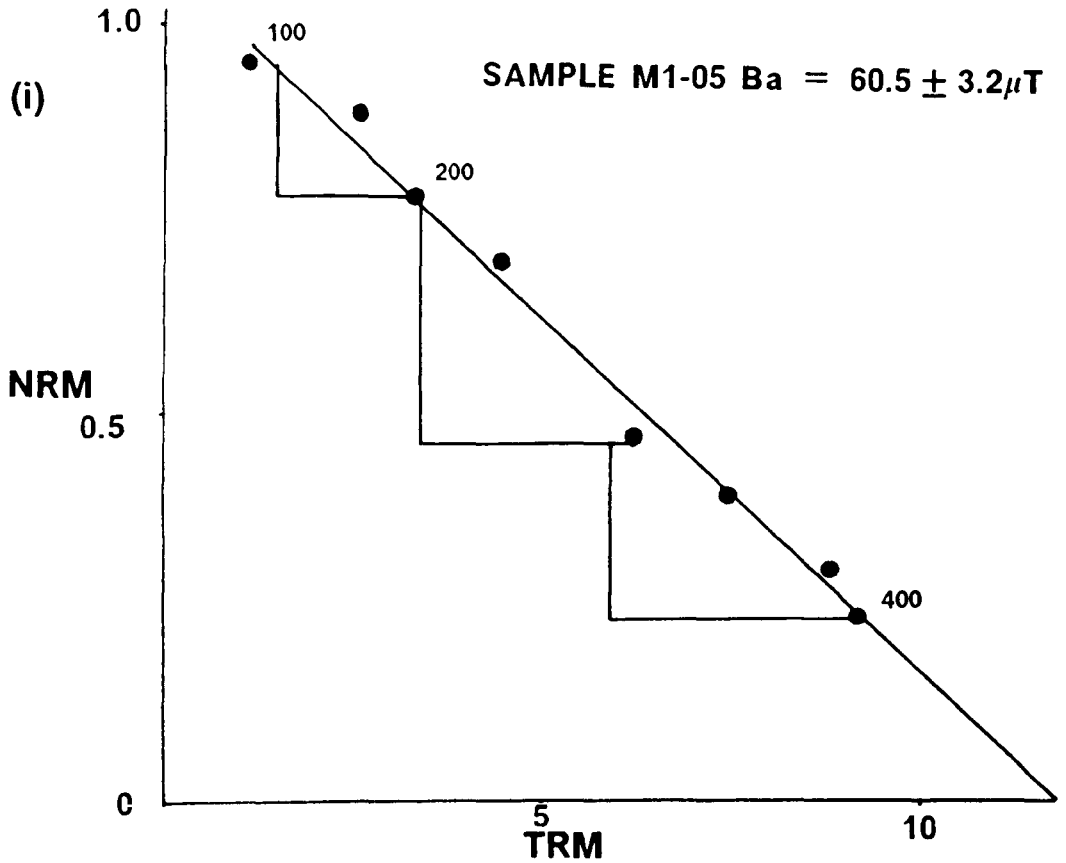
(i)
SAMPLE M1-05 Ba = 60.5 ± 3.2μT
1.0
NRM
0.5
0
100
200
400
5
10
TRM

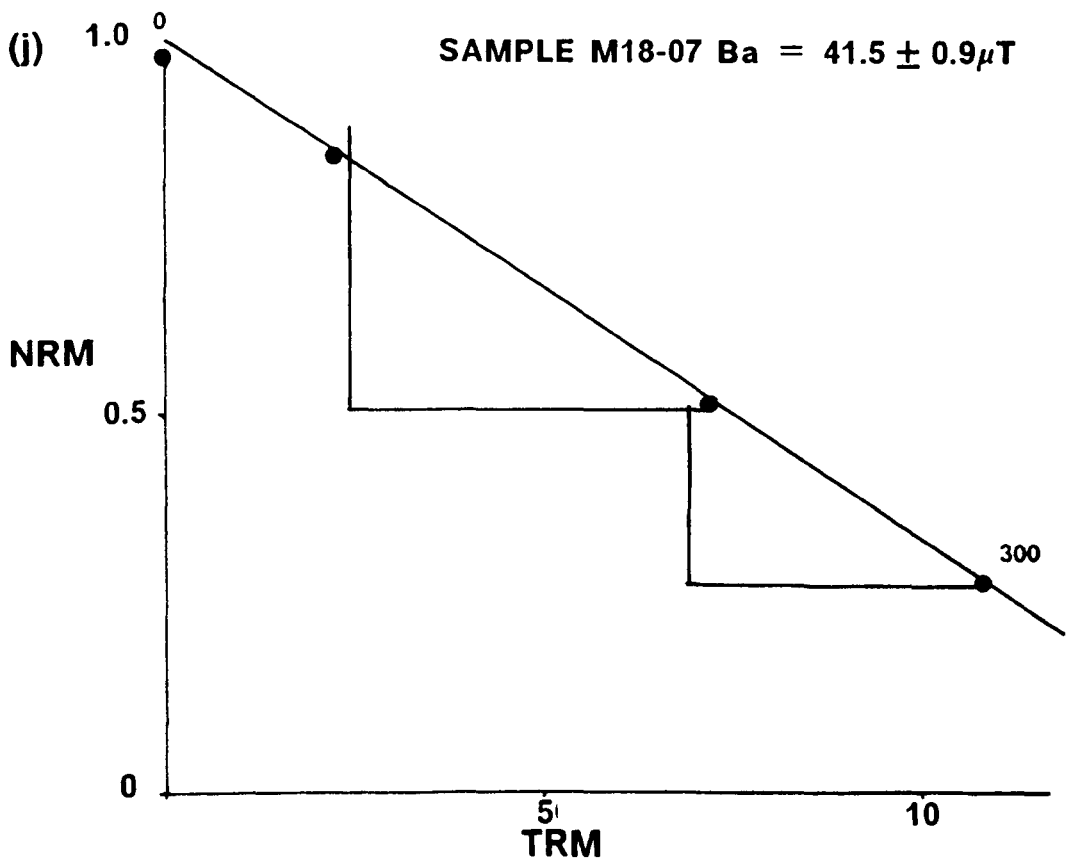
(j)
SAMPLE M18-07 Ba = 41.5 ± 0.9μT
1.0
0
NRM
0.5
0
300
5
10
TRM

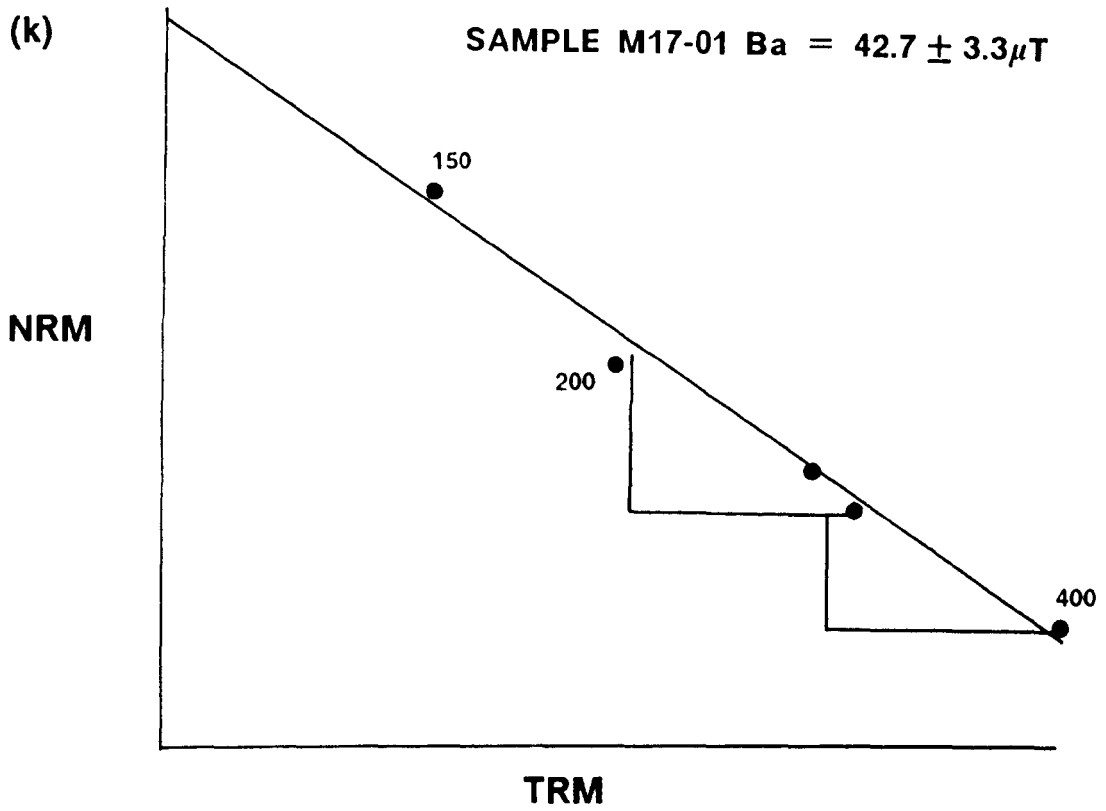
(k)
SAMPLE M17-01 Ba = 42.7 ± 3.3μT
150
200
400
NRM
TRM

Figure 6.5 : Modified Thellier palaeointensity (Arai) plots for the Upper Lava Formation. See Figure 6.3 caption for explanation of the plot.

Figures 6.5 a-k : Plots for normally magnetised samples

Figures 6.5 l-o : Plots illustrating some rejected samples

Figures 6.5 p-t : Plots for reversely magnetised samples

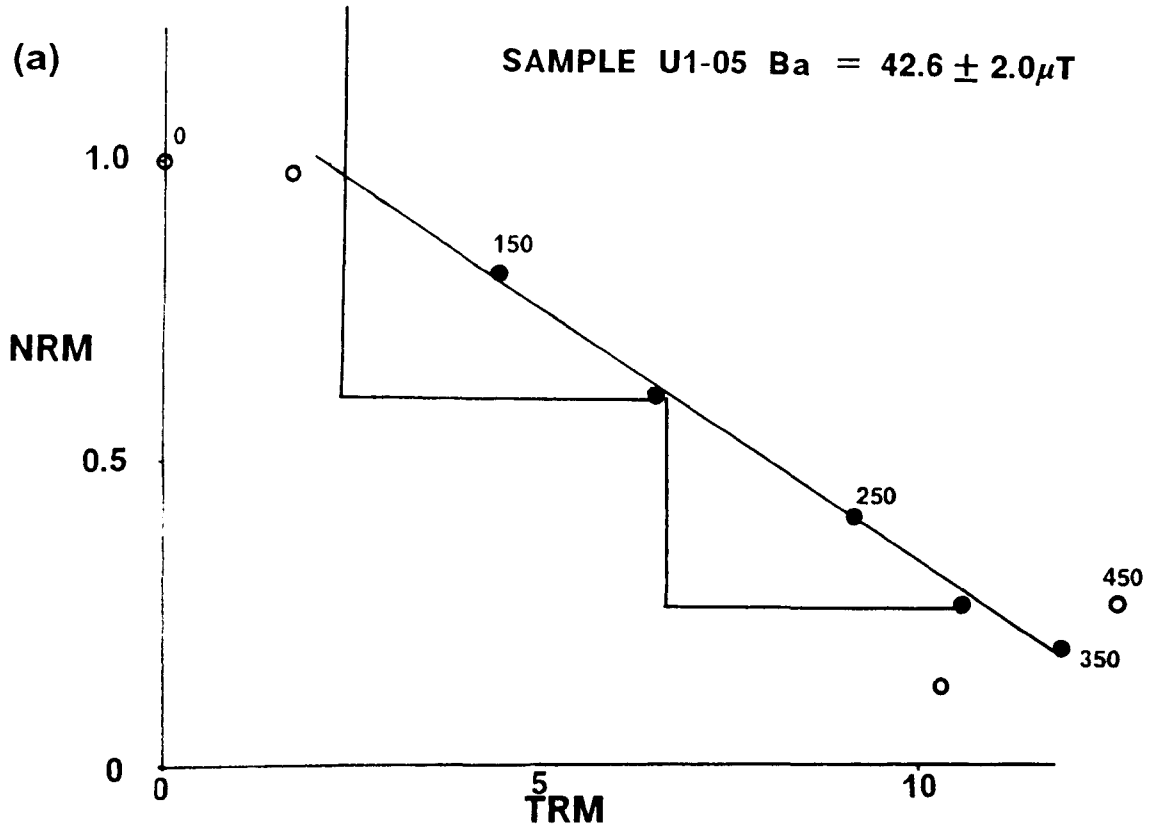
(a)
SAMPLE U1-05 Ba = 42.6 ± 2.0μT
1.0
0
NRM
0.5
0
0
5
10
TRM
0
150
250
350
450

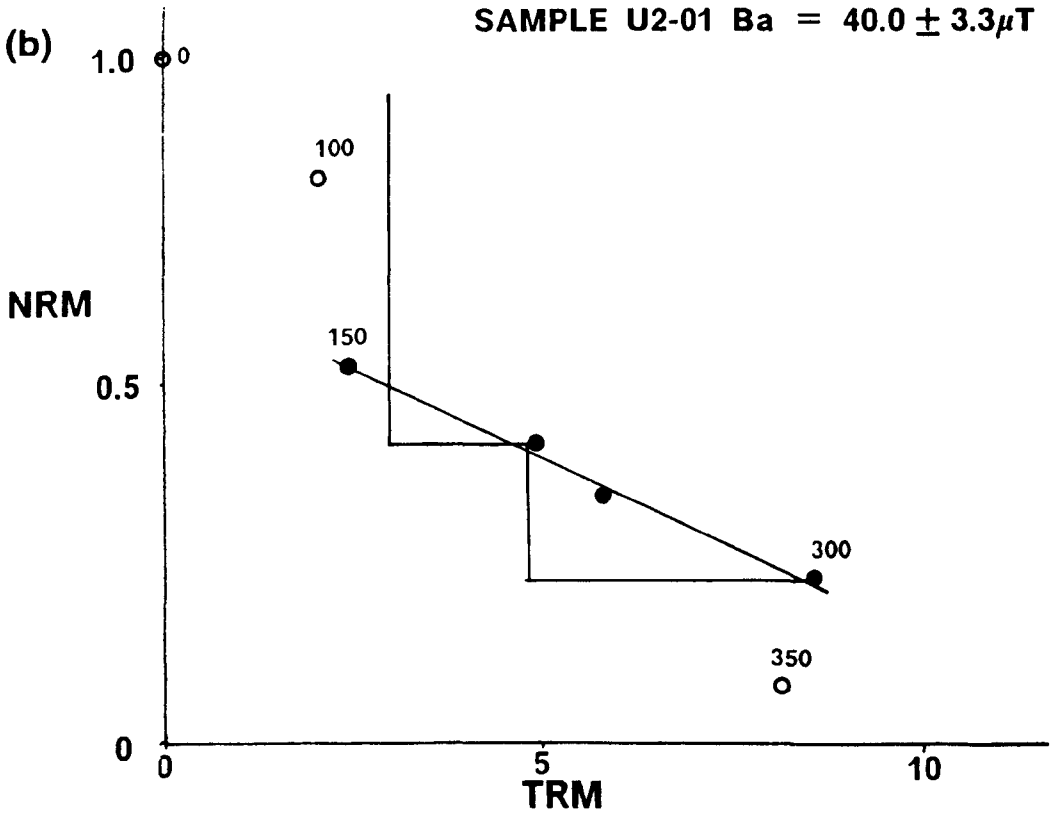
(b)
SAMPLE U2-01 Ba = 40.0 ± 3.3μT
1.0
0
NRM
0.5
0
0
5
10
TRM
0
100
150
300
350

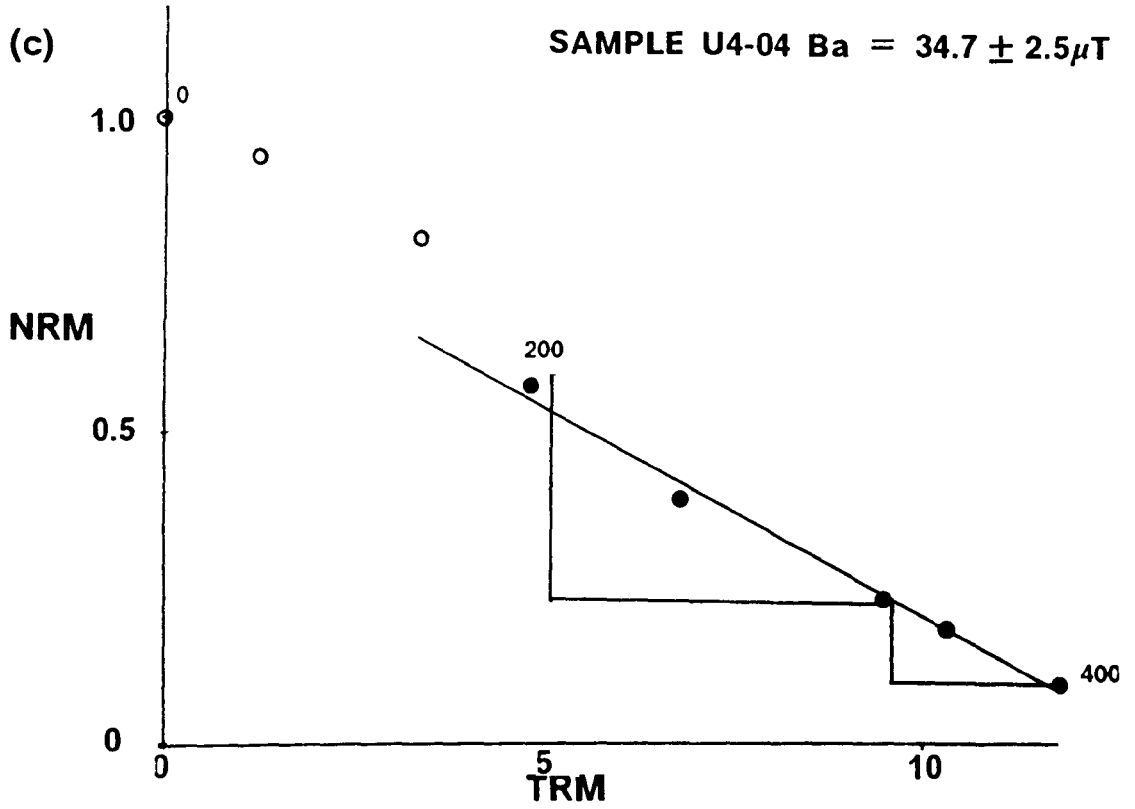
(c)
SAMPLE U4-04 Ba = 34.7 ± 2.5μT
1.0
0
NRM
0.5
0
0
200
400
5
10
TRM

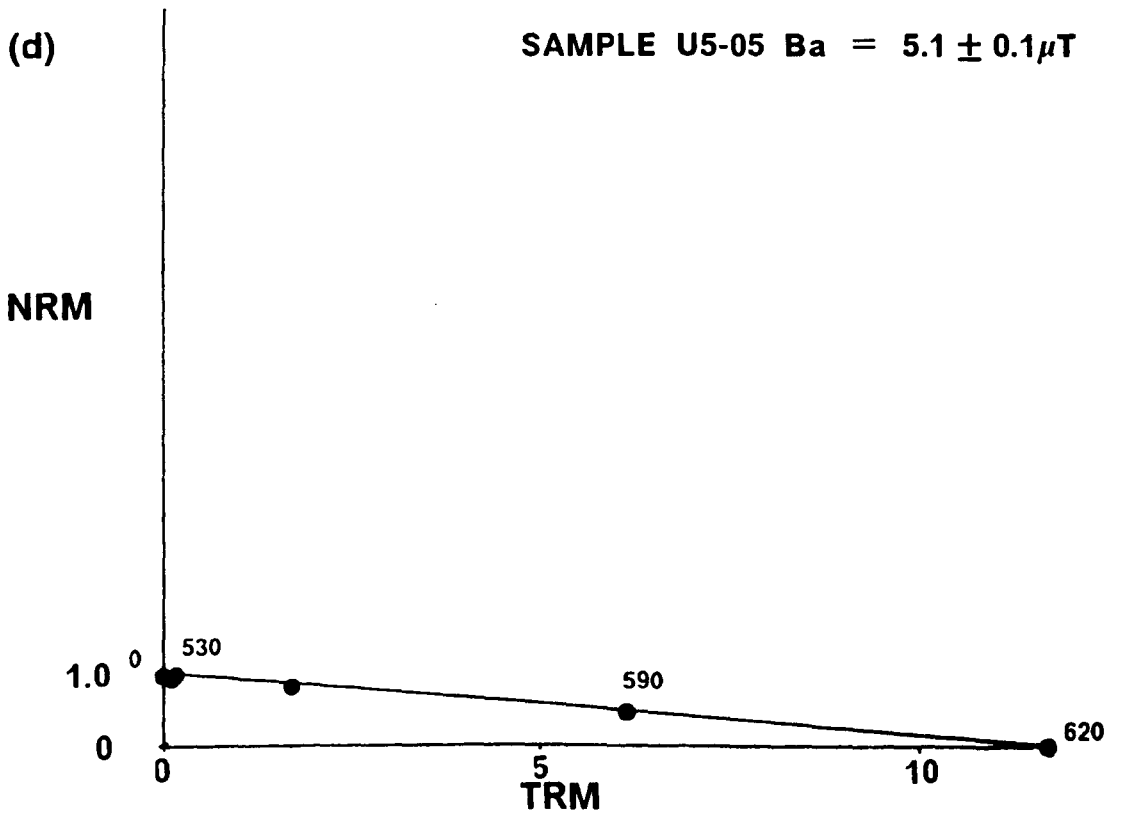
(d)
SAMPLE U5-05 Ba = 5.1 ± 0.1μT
NRM
1.0
0
0
530
590
620
0
5
10
TRM

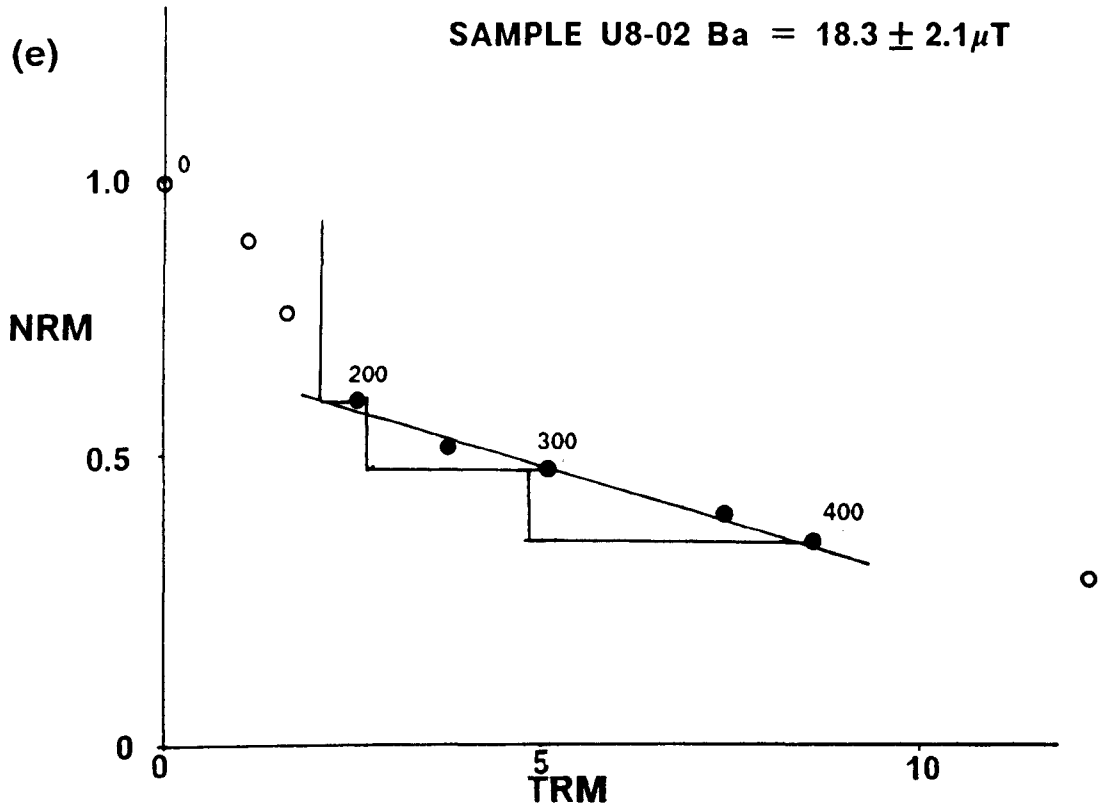
(e)
SAMPLE U8-02 Ba = 18.3 ± 2.1μT
1.0
0
NRM
0.5
0
0
200
300
400
5
10
TRM

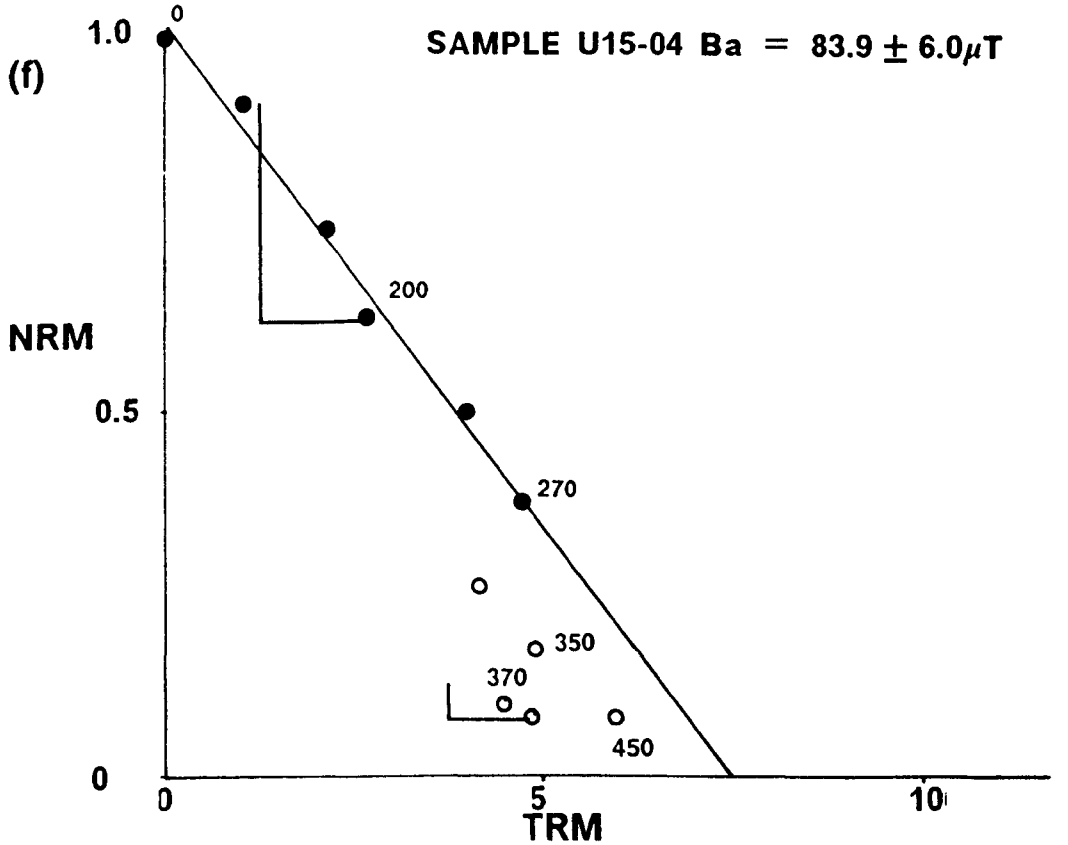
(f)
SAMPLE U15-04 Ba = 83.9 ± 6.0μT
1.0
0
NRM
0.5
0
200
270
350
370
450
0
5
10
TRM

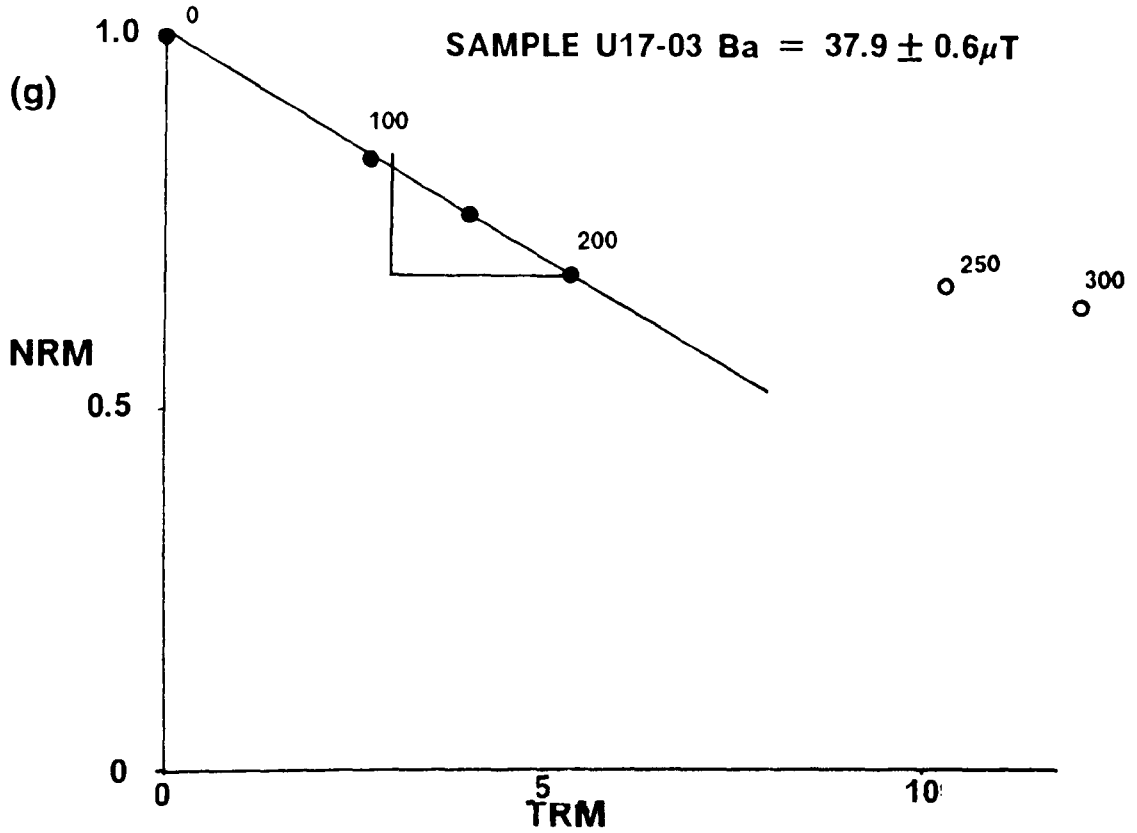
(g)
SAMPLE U17-03 Ba = 37.9 ± 0.6μT
1.0
0
100
200
250
300
NRM
0.5
0
0
5
10
TRM

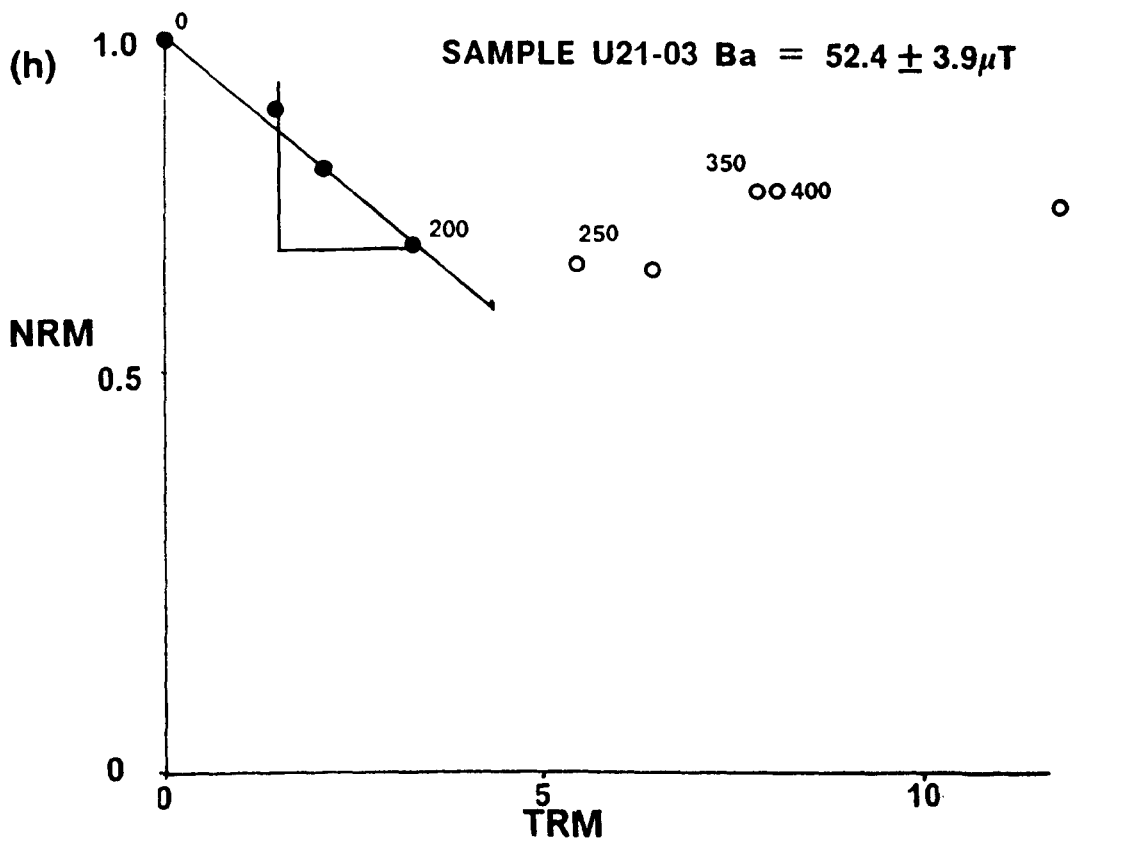
(h)
SAMPLE U21-03 Ba = 52.4 ± 3.9μT
1.0
0
350
400
200
250
NRM
0.5
0
0
5
10
TRM

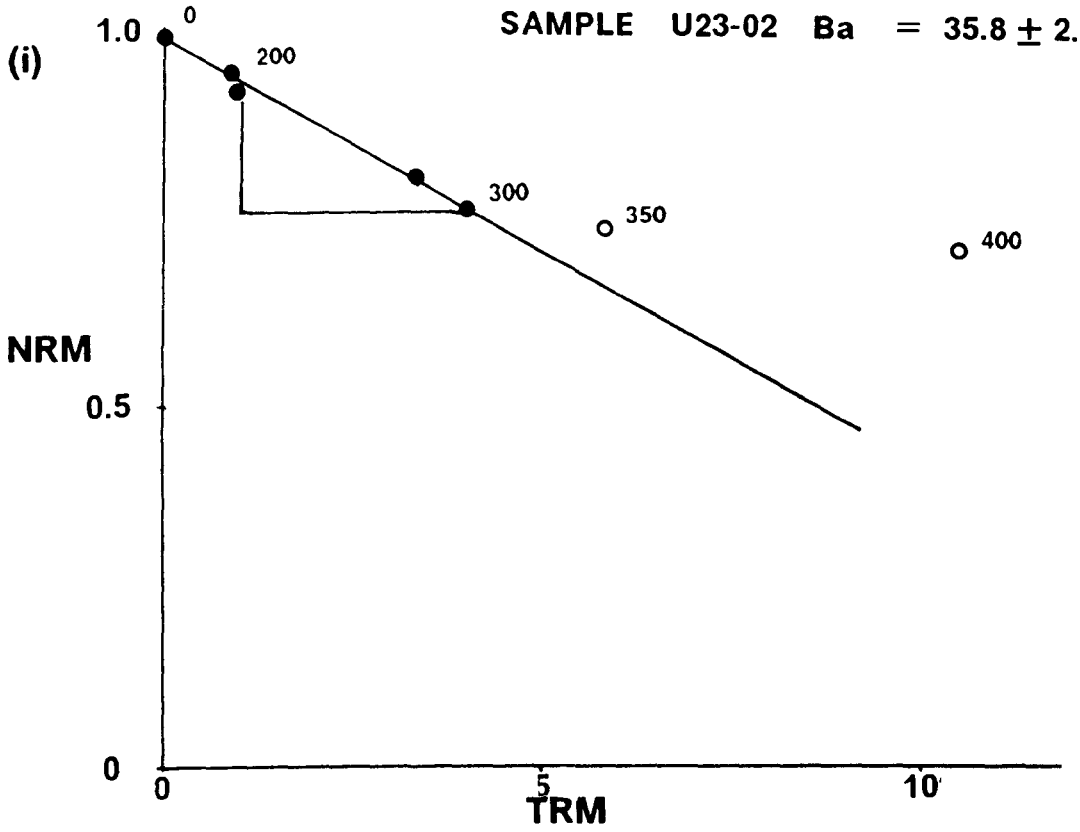
(i)
SAMPLE U23-02 Ba = 35.8 ± 2.5μT
1.0
0
200
300
350
400
NRM
0.5
0
0
5
10
TRM

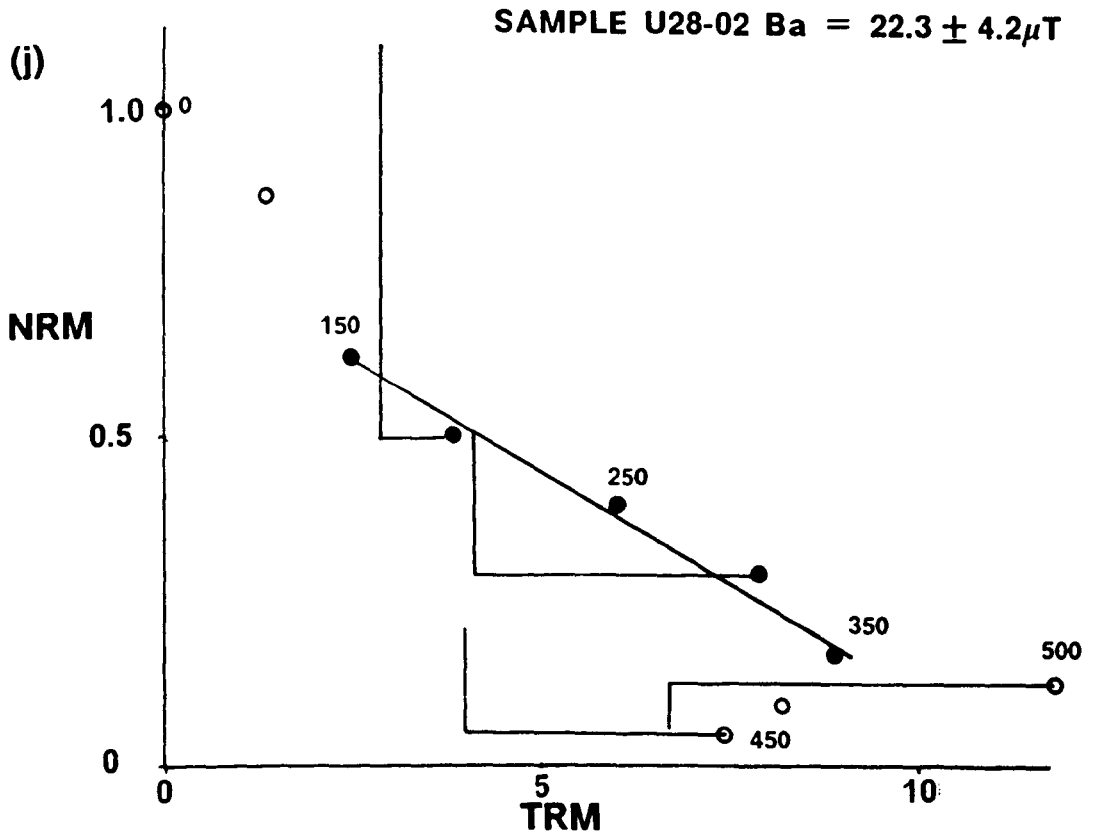
(j)
SAMPLE U28-02 Ba = 22.3 ± 4.2μT
1.0
0
150
250
350
500
450
NRM
0.5
0
0
5
10
TRM

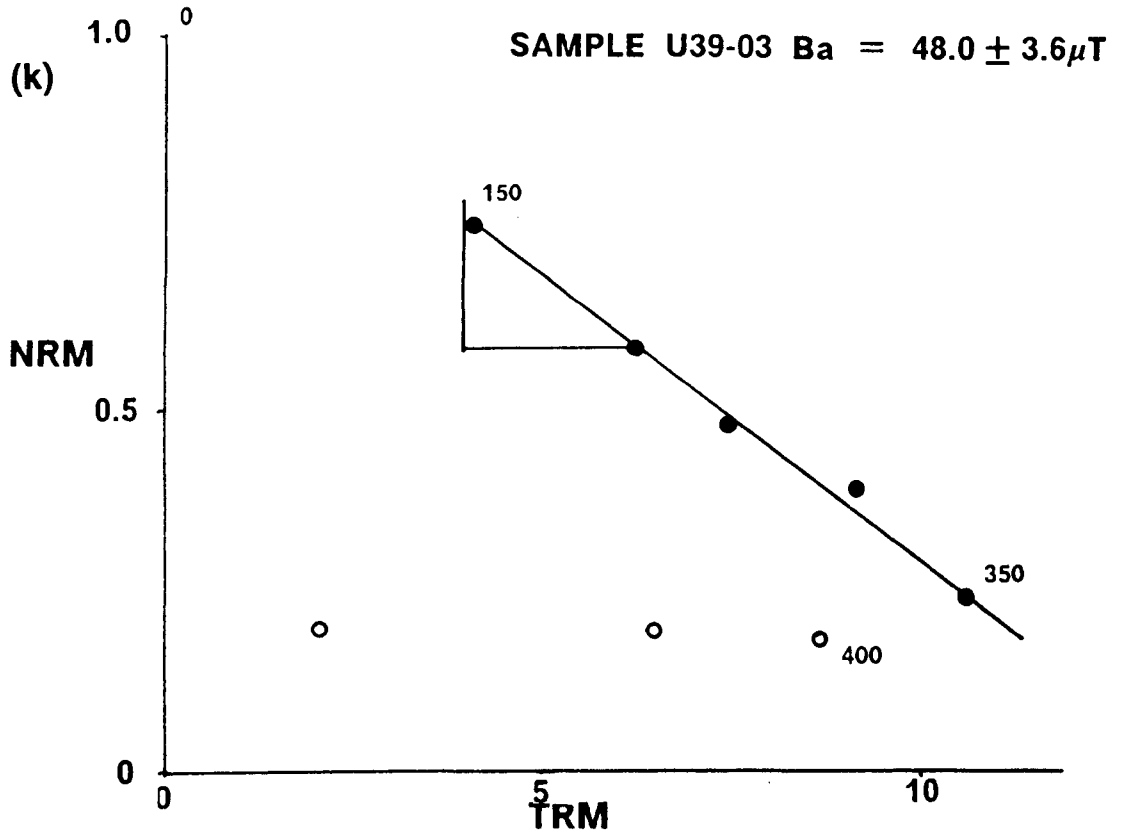
(k)
SAMPLE U39-03 Ba = 48.0 ± 3.6μT
1.0
0
NRM
0.5
0
150
350
400
0
5
10
TRM

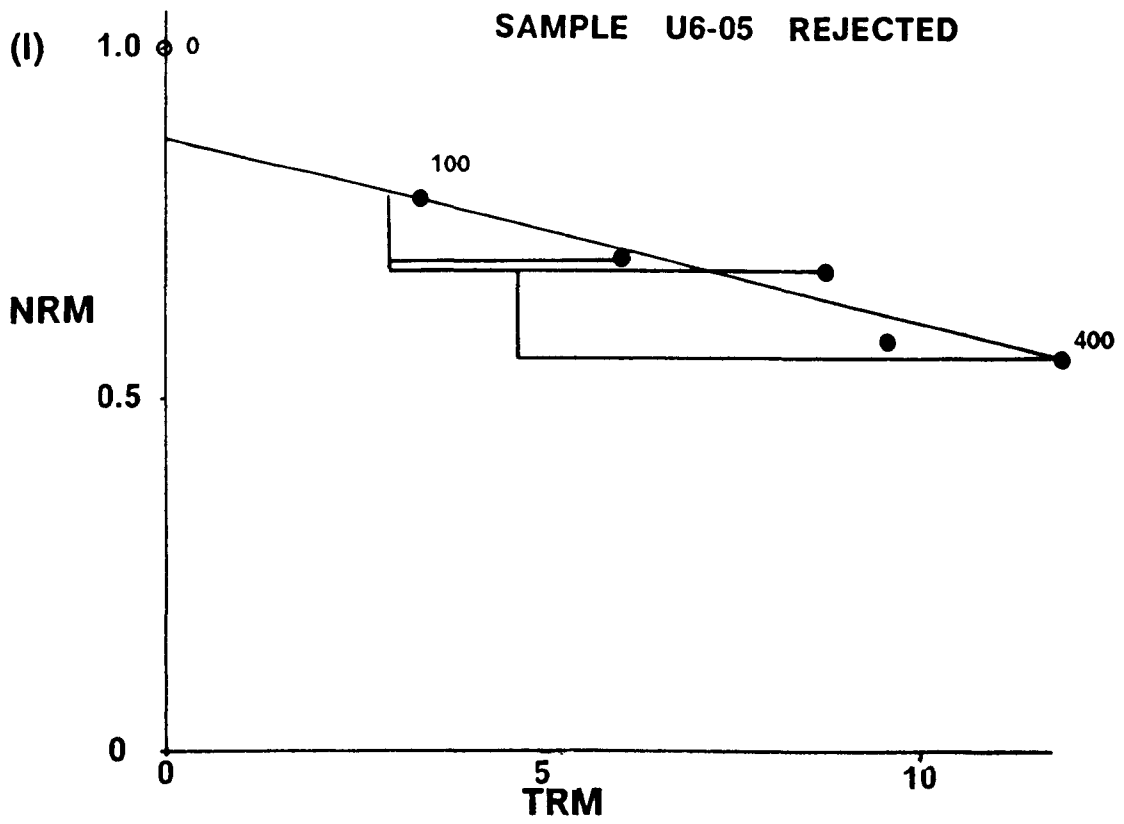
(l)
SAMPLE U6-05 REJECTED
1.0
0
NRM
0.5
0
100
400
0
5
10
TRM

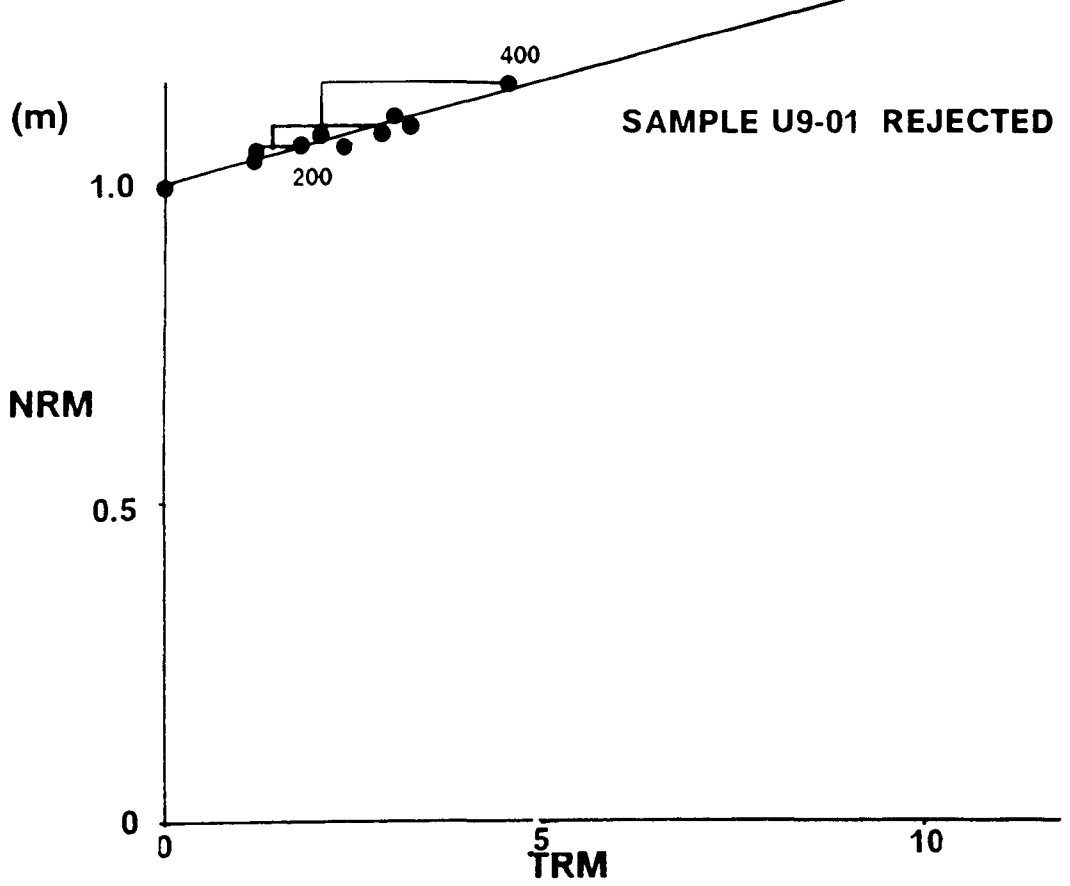
(m)
SAMPLE U9-01 REJECTED
400
200
1.0
NRM
0.5
0
0
5
10
TRM

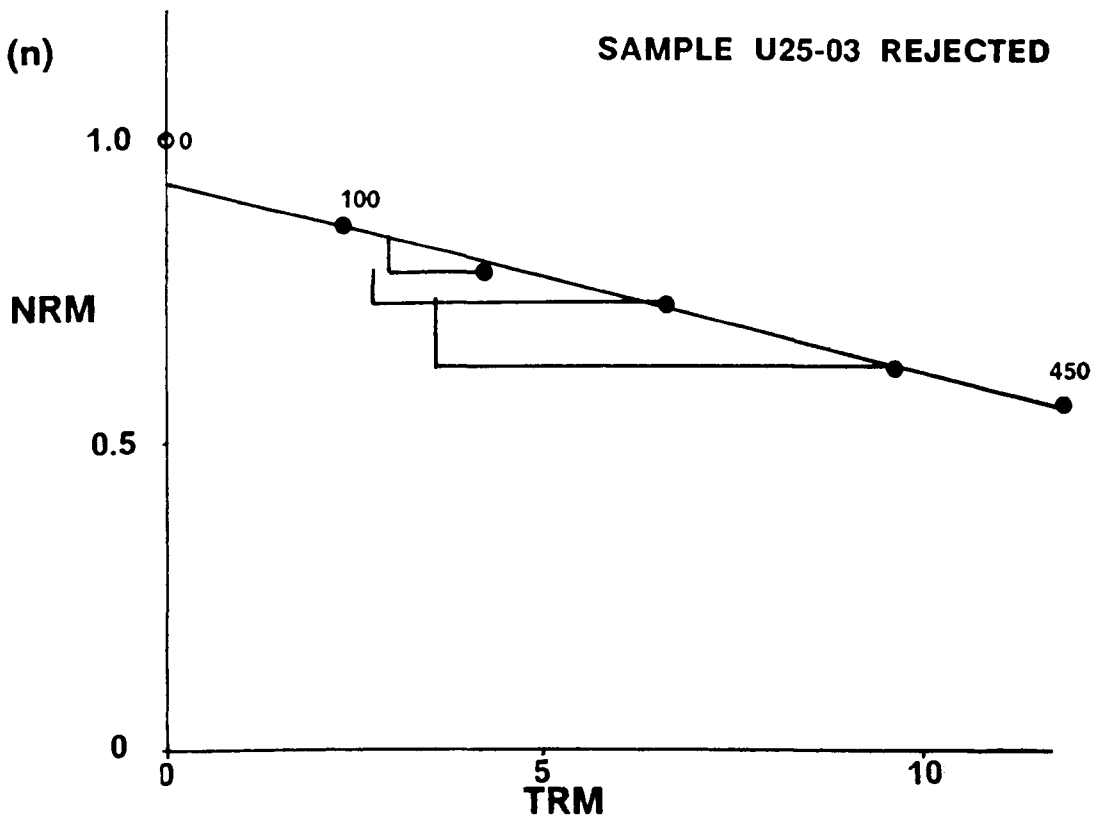
(n)
SAMPLE U25-03 REJECTED
1.0
0
100
NRM
450
0.5
0
0
5
10
TRM

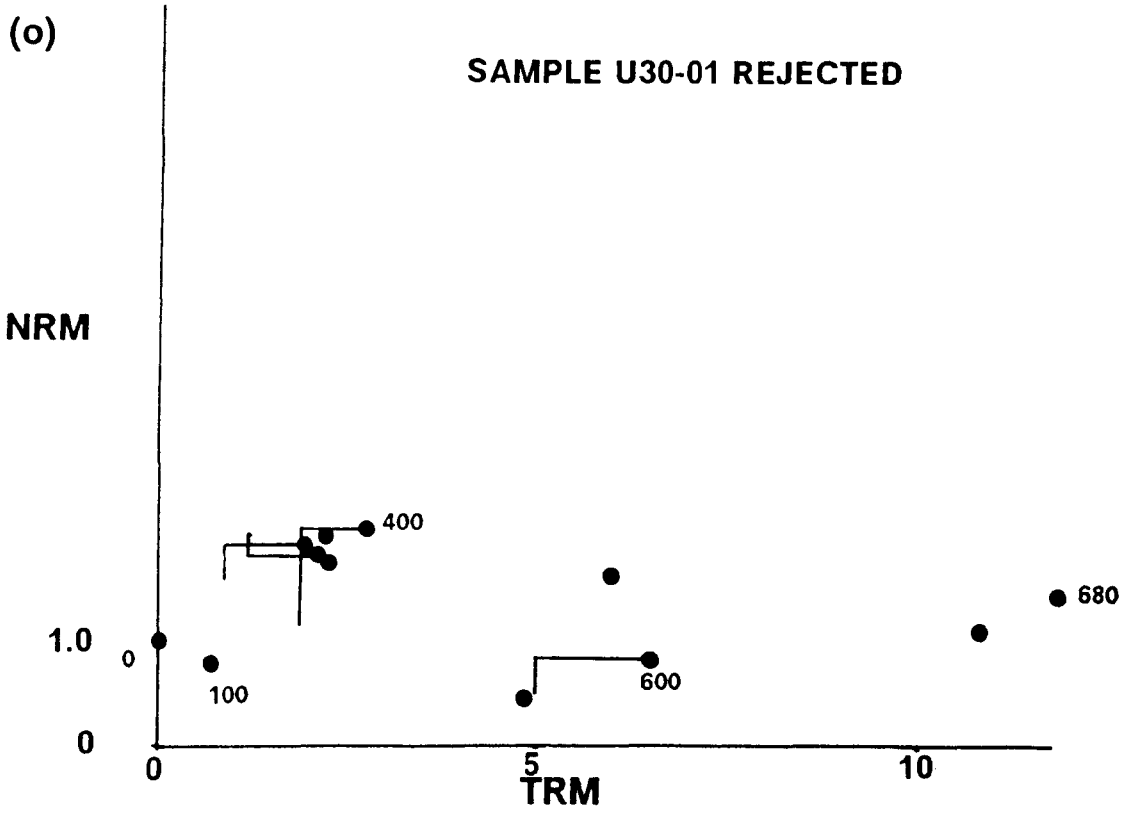
(o)
SAMPLE U30-01 REJECTED
NRM
1.0
0
0
100
400
600
680
0
5
10
TRM

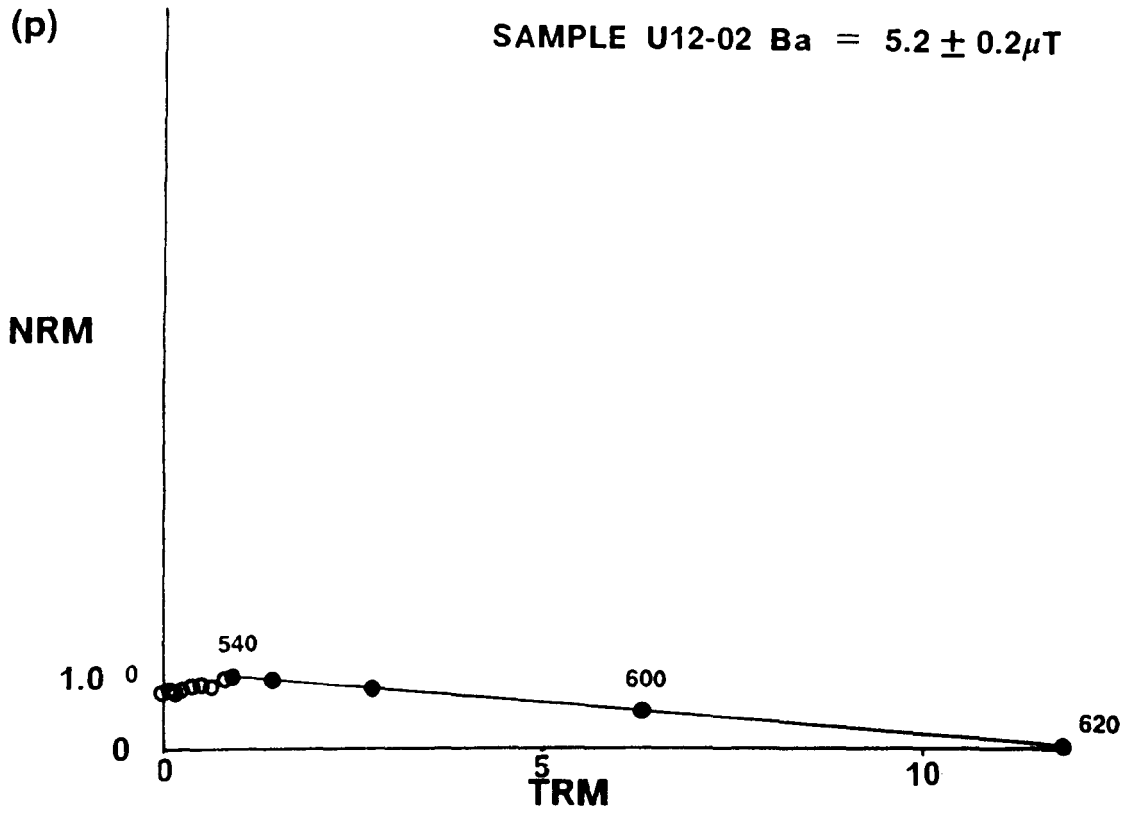
(p)
SAMPLE U12-02 Ba = 5.2 ± 0.2μT
NRM
1.0
0
0
540
600
620
0
5
10
TRM

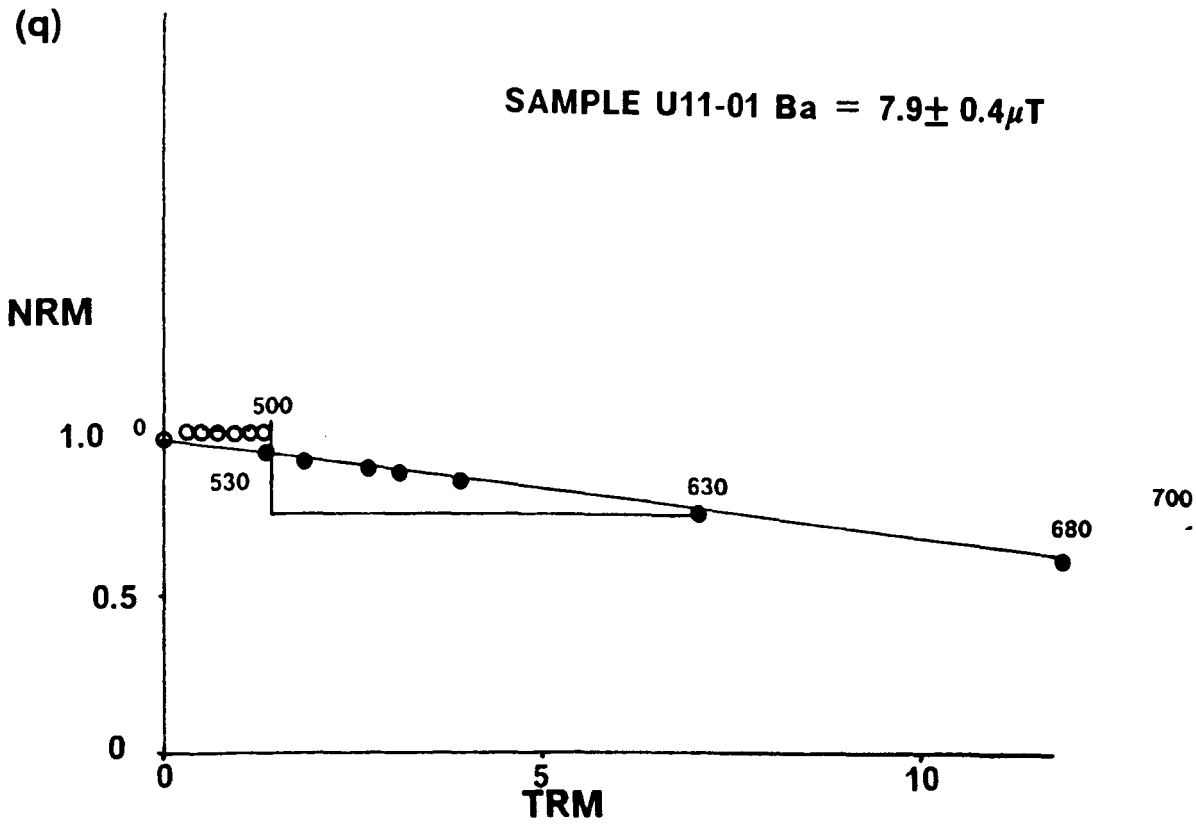
(q)
SAMPLE U11-01 Ba = 7.9± 0.4μT
NRM
1.0
0.5
0
0
500
530
630
680
700
0
5
10
TRM

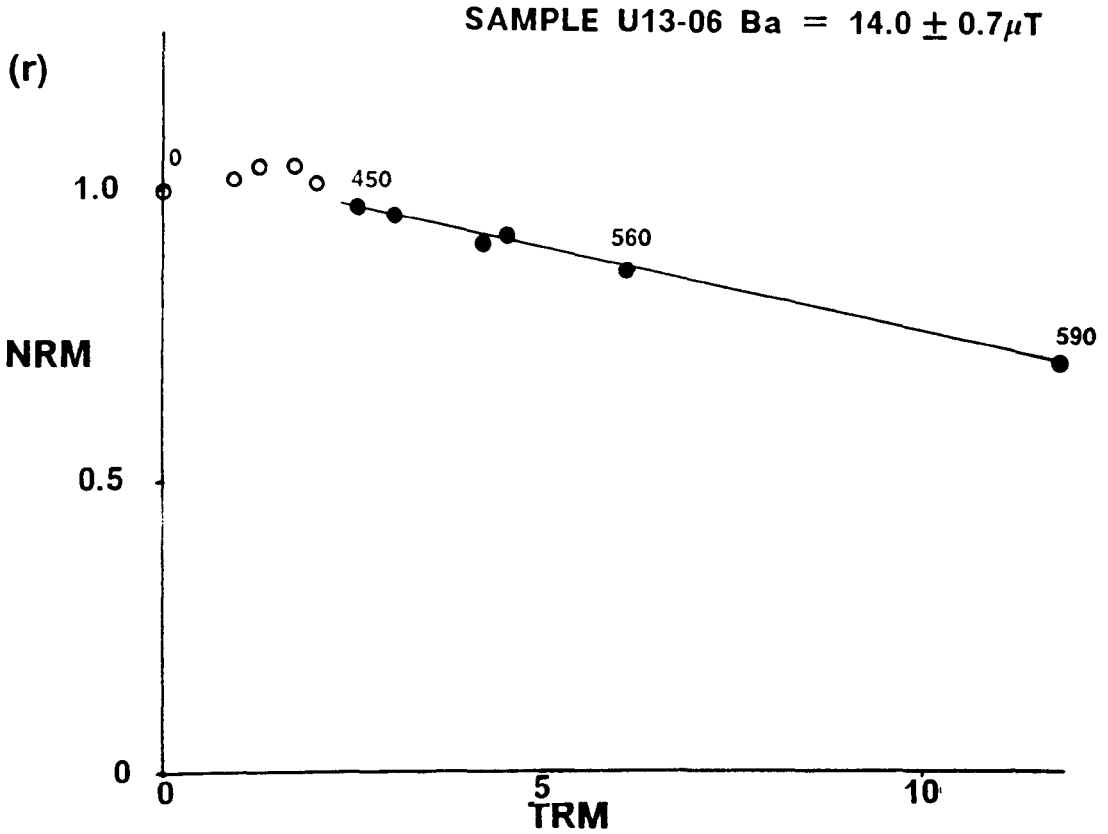
(r)
SAMPLE U13-06 Ba = 14.0 ± 0.7μT
NRM
1.0
0.5
0
0
450
560
590
0
5
10
TRM

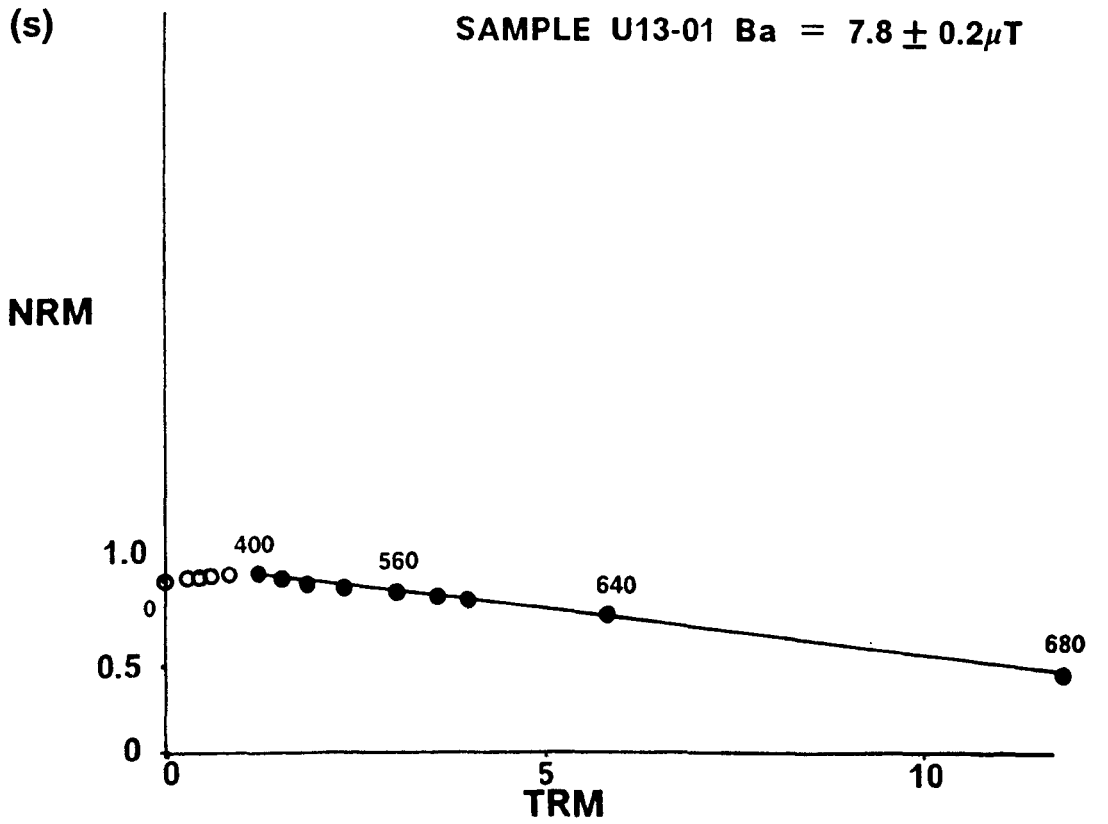
(s)
SAMPLE U13-01 Ba = 7.8 ± 0.2μT
NRM
1.0
0
0.5
0
400
560
640
680
0
5
10
TRM

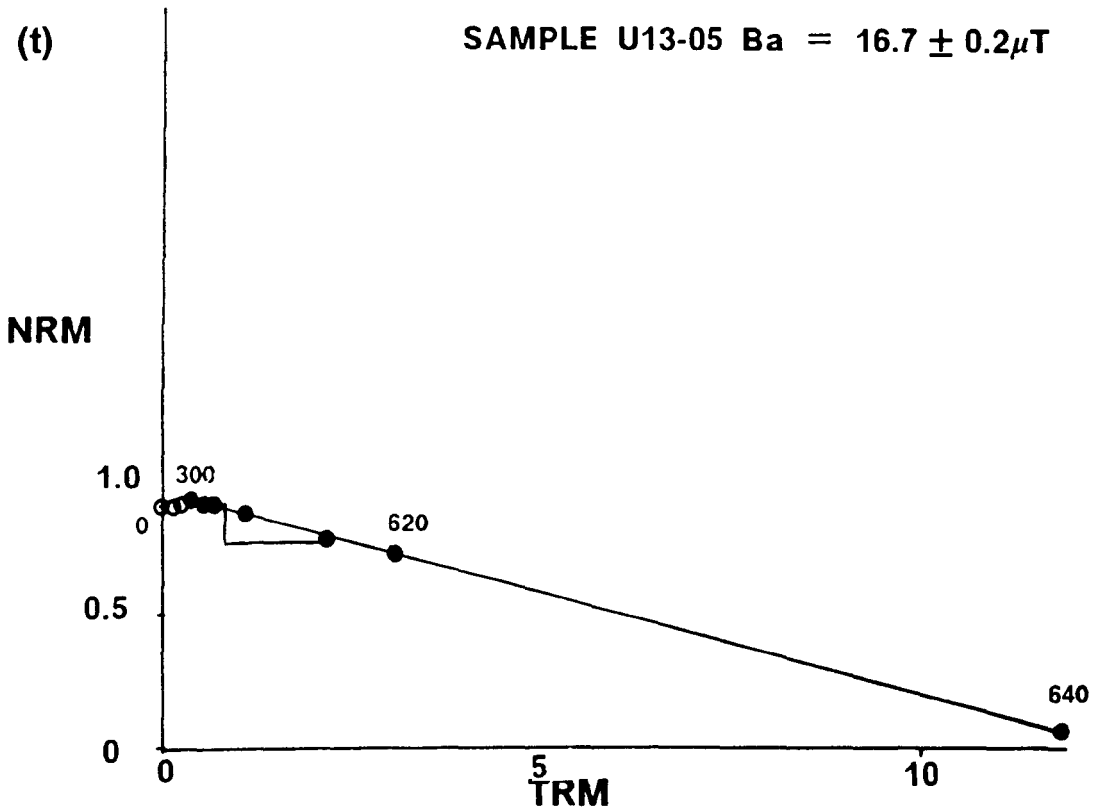
(t)
SAMPLE U13-05 Ba = 16.7 ± 0.2μT
NRM
1.0
0
0.5
0
300
620
640
0
5
10
TRM

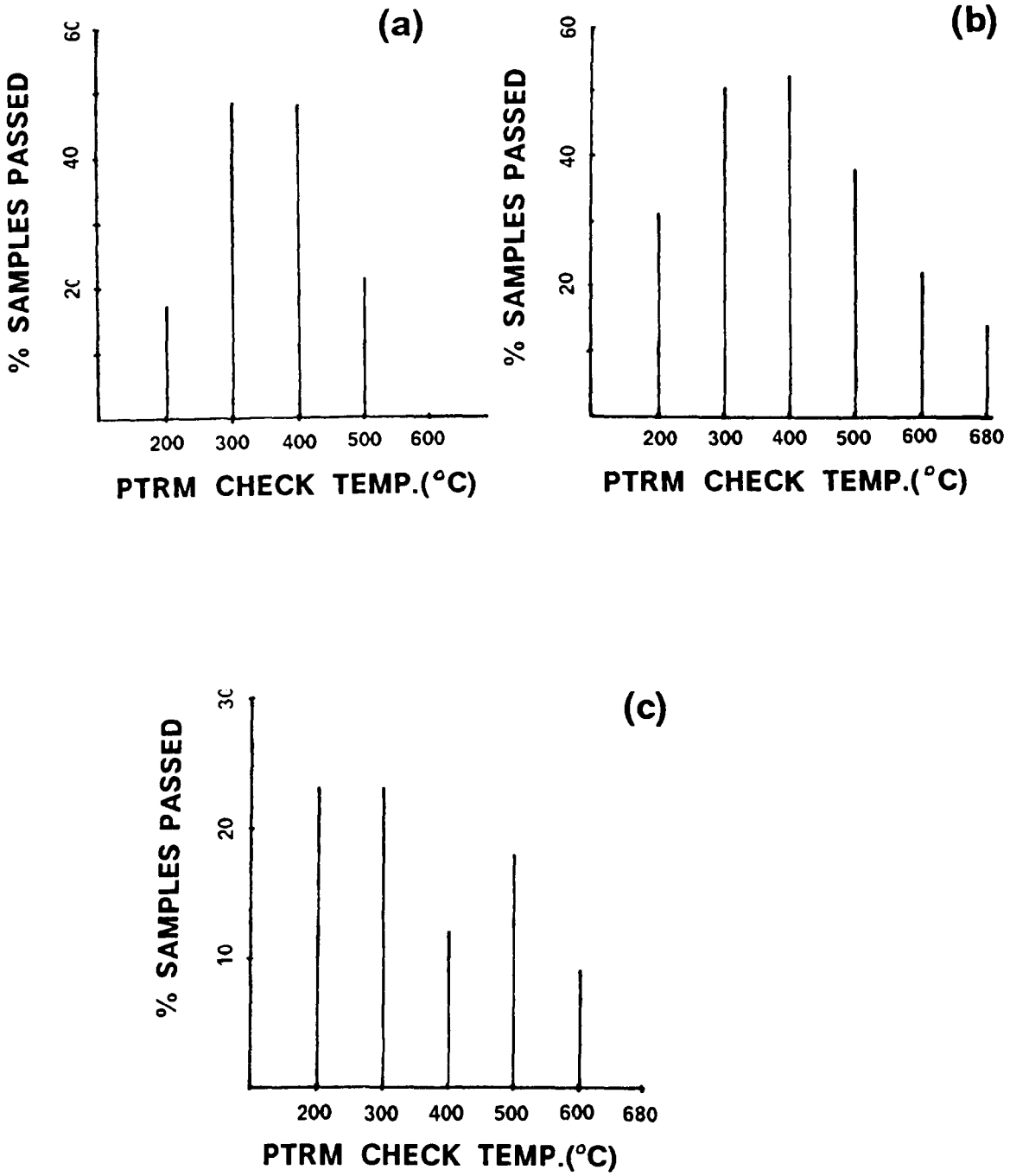

Figure 6.6 : Results of "PTRM checks" for (a) the Lower (b) the Middle, and (c) the Upper Lava Formations. Temperatures indicated are the raised temperature (e.g. the value at 200°C corresponds to a check of the TRM at 100°C).

samples in this group. These results represent the poorest checks in the entire collection and imply that some alteration process, other than that witnessed by curvature (non-linearity) of the Arai-plot, is probably taking place between successive heatings. The effect of this is alteration to increase the TRM capacity of the rock in a linear manner. The presence of linear alteration in samples casts doubt on the validity of their palaeointensity results.

6.8 DISCUSSION OF RESULTS.

6.8.1 The Lower (Mussartût) Lava Formation.

The behaviour of samples both within and between flows is very consistent. Thirty of the forty eight samples had Class B Arai-plots, indicating the onset of thermal alteration during laboratory heating at temperatures of ≃450°C, which is often witnessed for basalts (Pesonen, 1978; Prévot et al, 1985). These samples showed a characteristic linear segment between 100° or 150°C and 400° or 450° C, before an increase in PTRM acquisition capacity was observed, signifying the onset of thermal alteration due to laboratory heating (linear alteration). Data points outside these temperature intervals were rarely used. The lower temperatures (T_R-100° or 150°C) were only used if the OVP clearly showed no evidence of a low temperature secondary component of remanence. Such low temperature components may be TCRMs due to burial remagnetisation below over 2km of sediments and lavas. A similar feature was observed in Keweenawan extrusives by Pullaiah et al (1975), Merrill (1975), Dunlop and Buchan (1977) and Pesonen (1978).

There was little variation observed in the palaeointensity results which corresponds with the low scatter of flow mean directions isolated by the palaeomagnetic study (Chapter 4). This evidence suggests that the flows may have been rapidly extruded over a short time such that the characteristics of the geomagnetic field did not change greatly. Rapid extrusion rates are supported by geological evidence (Chapter 2).

The flows generally carry stable single component remanences which are almost certainly primary TRMs (confirmed by the positive baked contact test in Chapter 5). PTRM checks show the highest pass rate for the whole collection, in the region used for palaeointensity calculation. Any effect of burial remagnetisation is very limited and can be isolated from OVPs of thermal demagnetisation. Furthermore, rock magnetic tests (Chapter 3), show no evidence for low temperature oxidation (maghaemitization) in the flows.

All of the above evidence, and the discussion in Chapter 7, indicates that the flows of the lower formation give the most reliable Thellier results in the entire collection.

6.8.2 The Middle (Ulukasik) Lava Formation.

The low palaeointensity values obtained from the flows of this formation are intriguing. These low answers were obtained from flows exhibiting both the 'A' and 'B' directions of magnetisation described in Chapter 4, which have both haematite and magnetite as the respective remanence carriers. It has been suggested (Chapter 4) that flows which exhibit the anomalous 'A' direction were erupted during a period when the field was in a transitional phase, between polarity stable states. The low palaeointensity values for

these flows provides support for this suggestion, since it is well documented (e.g. Van Zijl et al, 1962; Bogue and Coe, 1982, Prévot et al, 1985) that the strength of the Earth's field, as recorded in lava sequences, decreases during a transitional phase. Jacobs (1984) recognises that the field intensity decreases by a factor of three or four for a period of several thousand years during a transition whilst the field direction remains constant. PTRM checks for flows from this formation show a reasonable success rate, which suggests that linear alteration is probably not important. The low answers could, alternatively, be the result of a secondary CRM overprint arising from hydrothermal alteration in which case the results would be meaningless. Pesonen (1978) found that lavas which have suffered hydrothermal alteration producing secondary CRM show some similarities in behaviour to that witnessed in the middle lavas; a slight increase in NRM is seen before the sample begins to demagnetise. However, as discussed in Chapter 4, the geological and palaeomagnetic evidence presents no firm support for this theory. Furthermore, the rock magnetic results for this group (Chapter 3) suggest that deuteric oxidation has occurred in all flows, with pure magnetite and haematite being the magnetic minerals. Highly oxidised lavas are generally accepted as providing the most accurate records of the ancient field characteristics. They are very suitable for palaeointensity work since they have already been heated to temperatures in excess of their Curie temperature during oxidation, thus minimising the possibilities of further alteration during laboratory heating. No evidence of low temperature oxidation (maghaemitization) was witnessed, which suggests that significant hydrothermal alteration has not occurred.

Although the existence of a CRM in flows possessing the 'A' direction of magnetisation is difficult to disprove, and the palaeointensity results are

suspiciously low, the evidence presented from all studies in this project is consistent with what would be expected if the 'A' direction was a record of a transitional field direction.

6.8.3 The Upper (Ilimaussaq) Lava Formation.

In contrast to the other two groups, a variety of behaviour was seen in this formation. The most striking difference in behaviour was observed between flows of opposite polarity (Figure 6.5). The normally magnetised flows are characterised by higher palaeointensities than those with reversed polarity, which is opposite to the findings of Pesonen (1978) for dykes from the Proterozoic Keweenawan Province, Canada. Two rejected samples from flow U9 and samples U11-1 and U13-1, all having reversed polarities, show an increase in both NRM and TRM with increasing temperature up to 400 or 450°C, resulting in a 'negative palaeointensity' (Fig. 6.5). This behaviour was witnessed in coarse grained intrusives and hydrothermally altered lavas from the Keweenawan by Buchan (1977) and Pesonen (1978). Pesonen attributed the behaviour to the presence of a 'hard VRM overprint', identified in OVPs of demagnetisation, with blocking temperatures of up to 500°C. The samples in his collection which show this behaviour all have very low median destructive fields upon a.f. demagnetisation. This is not the case in the present study where all samples showing this "negative intensity" are very resistant to a.f. demagnetisation due to the presence of haematite as the magnetic mineral. Furthermore, palaeointensity results can be obtained from most of these samples in the region above 450°C where the NRM begins to demagnetise, as indicated by the OVPs of thermal demagnetisation and the Arai plot in Figure 6.5 .

For the normally magnetised flows, most of which have magnetite as the magnetic mineral, PTRM checks are very poor compared with the samples in the other two groups. The dominance of MD grains of magnetite may well contribute to the failure of the PTRM checks; it is believed by Bolshakov and Shcherbakova (1979) that the blocking and unblocking temperatures for MD grains are not equivalent. Thus, there must be some doubt concerning the validity of the results from the magnetite-bearing flows in the upper group. Despite this, linear segments are obtained from the Arai plots of the samples, normally between 150-450°C, as for the lower group. Certain flows however, such as flows U21, U22, do not have linear segments above about 200°C. It is these samples which have the largest amount of MD material and give the highest palaeointensity values. These results must therefore be considered to be unreliable.

No results were obtained from samples which contain maghaemite, as identified from thermal rock magnetic tests (Chapter 3). This is not surprising since they have suffered low temperature oxidation which produces a CRM. This immediately renders such samples unsuitable for palaeointensity work as their NRM is not a TRM. All of these samples exhibited Class D Arai-plots where no linear segment was identified (e.g. Figs. 6.5h-k).

Generally, the results from the Upper Lava Formation are not as consistent as those from the Lower Formation, neither are they as reliable; multi-component magnetisations are often present, PTRM checks fail quite badly indicating significant linear alteration, low temperature oxidation has occurred and most magnetite-bearing flows do not contain a significant amount of SD material, which is important for palaeointensity work.

Although results are obtained from the Upper Formation, they are disappointing and must be treated with caution when used to describe the nature of the Early Gardar geomagnetic field.

6.9 ALTERNATING FIELD PALAEOINTENSITY TECHNIQUES.

6.9.1 Early methods

Several palaeointensity methods have been proposed in which progressive alternating field demagnetisation of NRM and TRM replaces the stepwise demagnetisation used in the thermal palaeointensity techniques. Alternating field techniques attempt to reduce the possibility of thermal alteration which may result from multiple heatings.

Van Zijl et al (1962) compared the progressive a.f. demagnetisation of NRM and TRM, the latter being imparted to samples by a single heating to a temperature greater than the Curie temperature of the sample. This heating took place in nitrogen to further minimise alteration. A graph of NRM against TRM was then plotted, with peak alternating field as the parameter, the slope of which was used in equation 6.1. This method, although quicker than the Thellier method since it involves only one heating, has the disadvantage of not giving a palaeointensity result if a sample alters close to the Curie temperature. The Thellier technique and its derivatives, however, may provide a result from the lower temperature region.

Smith (1967a) essentially used the van Zijl method with an added test for alteration. The saturation magnetisation (J_s) of a sample was monitored during heating to 670°C and subsequent cooling. For a sample to pass this test, the shape of the heating and cooling curves had to be similar and the J_s

value at room temperature, before and after heating, should not vary by more than 15%.

Carmichael (1967), whilst using the van Zijl method, regarded a sample to be altered if its Curie temperature changed as a result of heating and the shape of the NRM and TRM demagnetisation curves were different. In addition, the value of palaeointensity is multiplied by a correction factor which is the ratio of two saturation isothermal remanences (SIRMs), one given before heating and one after heating.

McElhinny and Evans (1968) modified the Carmichael method by progressively a.f. demagnetising SIRMs given before and after heating (SIRM1 and SIRM2) in addition to the a.f. demagnetisation of the NRM and TRM. They selected a coercivity region where the NRM/TRM and SIRM1/SIRM2 ratios were constant (and equal in the case of SIRM1 and SIRM2) and calculated the palaeointensity over this range in the usual manner.

Rigotti (1978) described a method which incorporates a.f. demagnetisation of anhysteretic remanent magnetisation (ARM) (See Section 1.2) as a correction factor. The NRM of the sample was progressively a.f. demagnetised and the a.f. value at which the NRM vector stabilised was noted. Then a pre-heating ARM - ARM1 - was given in a series of increasing alternating fields in a known d.c. field and the ARM measured at each field. The ARM was demagnetised to the field at which the NRM stabilised. A TRM was then imparted to the sample in the same d.c. field as for ARM1 and demagnetised in the same way. Finally, a second ARM - ARM2 - was introduced and demagnetised in the same manner as ARM1. The a.f. demagnetisation curves of all four remanences, normalised to the

field at which the NRM became stable, were drawn. The shapes of the NRM-TRM and ARM1-ARM2 curves were then correlated in order to make an estimate of the palaeointensity, which was given by:

$$B_a = B_l\left(\frac{NRM}{TRM}\right)\left(\frac{A1}{A2}\right) \qquad [6.12]$$

where A1 and A2 are the pre- and post-heating ARM values for the field at which the NRM became stable.

6.9.2 The original Shaw method and its derivatives.

The most widely used single-heating palaeointensity method which uses a.f. demagnetisation is that proposed by Shaw (1974). The basic principle of this method is to analyse the a.f. demagnetisation spectra of pre- and post-heating ARMs, to check for thermal alteration and to identify the part of the coercivity spectrum over which it has occurred. The original method involved the following steps:

1. The NRM of a sample was stepwise a.f. demagnetised up to a peak value of 130 mT and the NRM remaining after each demagnetisation step was measured. The same demagnetisation fields were used in subsequent demagnetisations.

2. An ARM - ARM1 - was introduced in the peak alternating field used in (1) and in a steady weak d.c. field of 50μT. This ARM1 was then a.f. demagnetised and measured as in (1).

3. The sample was then given a TRM, by heating it to a temperature greater than its Curie temperature and cooling back to room temperature in a

d.c. field of 50μT. This TRM was then a.f. demagnetised and measured as in (1).

4. A second ARM - ARM2 - was then introduced to the sample in an identical manner to ARM1. This ARM2 was subsequently demagnetised and measured as in (1).

These four steps yield four a.f. demagnetisation plots of NRM, ARM1, TRM and ARM2.

5. A graph of ARM1 against ARM2 was plotted, using a.f. demagnetisation field as the parameter. A line of slope = 1.0 was fitted to the data by the least squares method. Any data point not lying on the line, within the 95% confidence level of the chi-squared fit, was rejected. Since small portions of NRM and TRM remain after demagnetisation in steps (1) and (3), and are still present after demagnetisation of the ARMs, the line of slope = 1.0 is NOT constrained to pass through the origin. If no alteration took place during heating, all data points will lie on the line of slope = 1.0, since both ARMs were given in the same weak d.c. magnetic field.

In practise, some data points, found empirically to lie in the low coercive force region, do not lie on the line of slope = 1.0. These are rejected and the remainder of the points can be considered to lie within that part of the coercive force spectrum where alteration has not occurred and ARM1 and ARM2 are identical. Although the ARMs are not equivalent to the NRM or TRM, they reside in the same magnetic minerals and the same coercive force regions. Thus, any alteration of these magnetic minerals, due to heating, will change both the TRM and ARM2.

6. The NRM of all data points was plotted against the corresponding TRM and the best straight line was fitted (using the least squares method) only to the data points lying in the unaltered part of the coercive force spectrum identified in (5). The best fit line is constrained to pass through the origin, which is the point where the demagnetisation field is infinite. The slope of the NRM-TRM curve was then used in equation 6.1 to calculate the palaeointensity value.

In practise, alteration of samples occurs and the use of the original Shaw method becomes untenable. However, using certain corrections, involving the pre- and post-heating ARM ratios, altered samples can be used. These methods are described below:

The Kono correction

Kono (1978) developed a method for correcting for a small amount of linear alteration when using the original Shaw technique. He classified the results of his experiments on the basis of the shape of the NRM-TRM and ARM1-ARM2 curves. The criteria are:

(1) ARM1-ARM2 plot is linear with slope = 1.0

(2) ARM1-ARM2 plot is linear with slope $\neq$1.0

(3) ARM1-ARM2 plot is non-linear

AND

(a) NRM-TRM plot is linear, line goes through origin

(b) NRM-TRM plot is linear, line does not go through origin

(c) NRM-TRM plot is non-linear.

Only samples from Class 1a, which are effectively unaltered, are used in the original Shaw technique. Kono (1978) considered that samples with Class

1b characteristics may well be suitable for use in palaeointensity experiments, since alteration appears to only have occurred at coercivities higher than those used for palaeointensity determination. For class 2a and 2b samples, Kono suggested a correction which is applied to the data as a whole and not to individual data points. If the slope of the NRM-TRM plot is m1 and the slope of the corresponding ARM1-ARM2 plot is m2, then the Kono-corrected palaeointensity, B_a, is given by:

$$B_a = \frac{m1}{m2} B_l \qquad [6.13]$$

Unlike the original Shaw method, the Kono method is applicable to samples whose ARM1-ARM2 plots are linear but do not have a line of slope = 1.0. Physically, this means that the shape of the ARM coercivity spectrum is unchanged but its magnitude is different before and after heating. Senanayake et al (1982) have found, experimentally, that the Kono-corrected Shaw technique can be used provided the slope of the ARM1-ARM2 plot lies between 0.7 and 1.4. Class 3 samples, where the ARM1-ARM2 plot is non-linear, cannot be used in the Kono-corrected Shaw technique.

The Rolph and Shaw correction.

Rolph and Shaw (1985) realised that the Kono-type correction could be taken a stage further and developed a method which corrects for non-linear thermal alteration, with specific applicability for lavas which exhibit extensive thermal alteration during heating in the original Shaw technique. The difference from the Kono correction is that TRM data points are corrected individually as opposed to the whole data set. The TRM value for each data point is multiplied by the corresponding ARM1/ARM2 ratio and then plotted

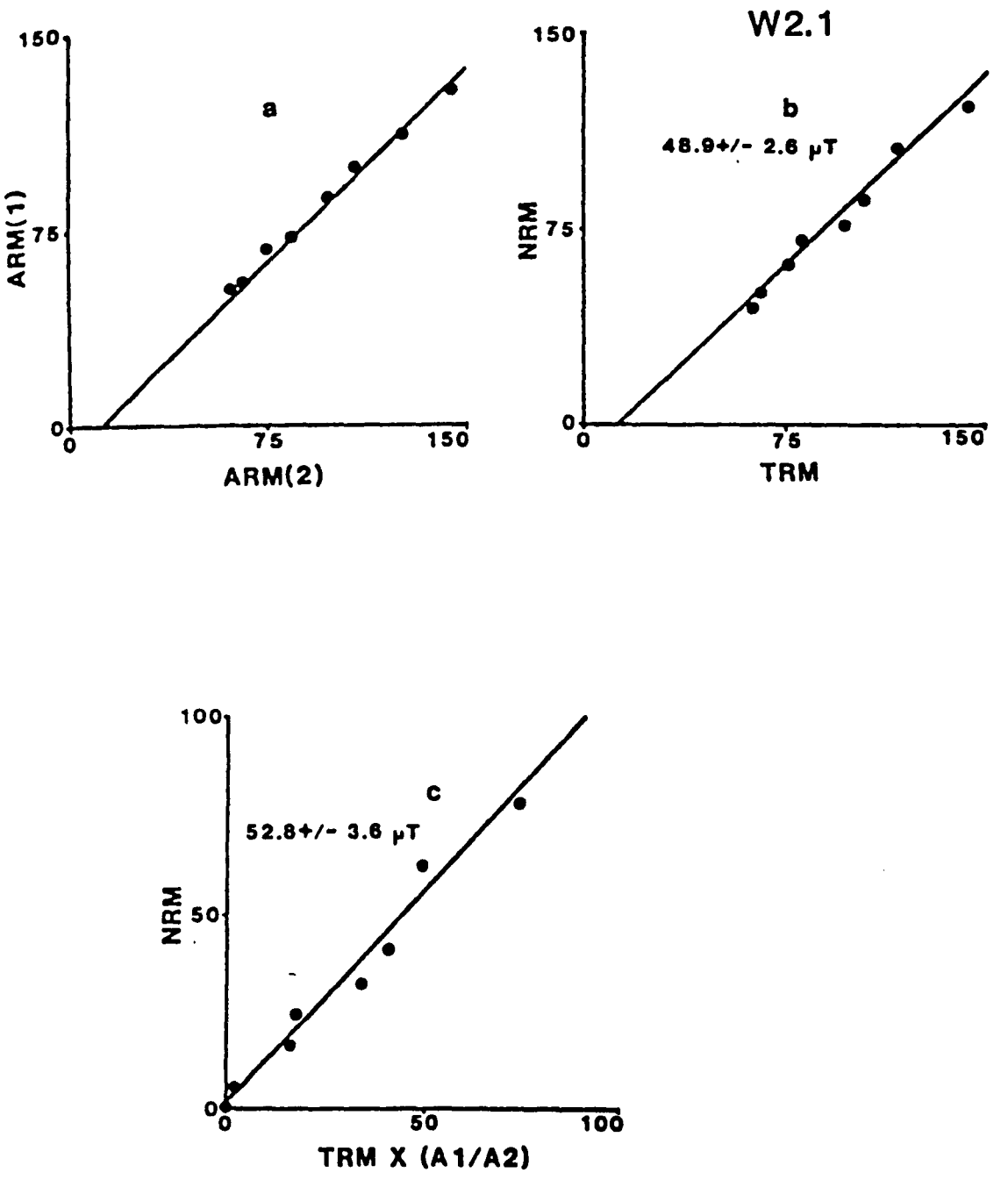

Figure 6.7 : An example of the Rolph and Shaw (1985) palaeointensity correction. The upper two diagrams show the original Shaw (1974) type plots and the lower diagram shows the corrected (R-S) plot (from Rolph and Shaw, 1985).

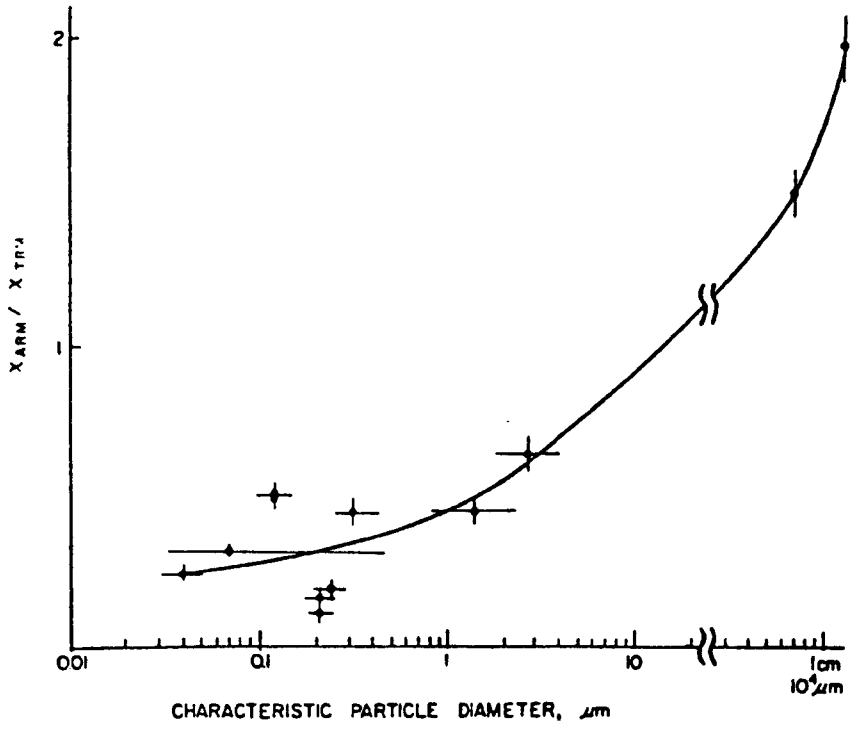

Figure 6.8 : Apparent susceptibility ratio against particle size for magnetite-bearing samples (from Levi and Merrill, 1976).

against NRM (Fig.6.7). This plot will be referred to hereafter as the Rolph and Shaw (R-S) plot. The maximum demagnetising field did not remove all the magnetisation, leaving residual moments N_{min}, $A1_{min}$, T_{min} and $A2_{min}$ in all four measurement suites. These residual moments were subtracted from all measurements. The gradient of the R-S plot is then used in equation 6.1 to calculate the palaeointensity value. The correction assumes that since both ARMs are given in the same field, then after equivalent a.f. demagnetisation the ratio ARM1/ARM2 gives directly the ratio of change, due to heating, in the ability of a particular coercive force region to acquire an induced magnetisation. The method can be used, unlike that of Kono (1978), on samples which have non-linear NRM-TRM plots, provided that the two plots have the same shape.

Rolph and Shaw (1985) describe a limitation for the use of their correction. Levi and Merrill (1976) derived a grain size dependence for the apparent susceptibility ratio of ARM/TRM for magnetite-bearing samples. This ratio increases with increasing grain size (Fig.6.8). Rolph and Shaw (1985) note that, on heating to impart the TRM, the grain size distribution of samples may change. Using the Levi and Merrill (1976) model, they infer that these changes will have little effect on the ARM/TRM ratio in the SD/PSD region, whereas in the MD region, the effect will be greater. Thus, they conclude that the use of ARM alteration to correct for TRM alteration may only be valid for grains in the SD/PSD region and consequently, they only use data for this region. The peak alternating field required to totally demagnetise MD grains is 100mT (McElhinny, 1973). Therefore only data above this value are valid for use in determination of the palaeointensity. Sherwood (1986), whilst recognising that there is a rise in the apparent susceptibility ratio with increasing grain size, notes that the data of Levi and Merril (1976)

is sparse. Their curve (Fig.6.8) gives no indication that the rate of change of the ratio is greater for MD than for SD or PSD grains. Also, the absence of typical MD size grains from the data is noted. Thus, there is an uncertainty in the grain size dependence of the apparent susceptibility ratio. In reality, many MD grains are demagnetised by fields of only a few tens of mT (Stacey, 1961) and recently, Rolph (pers. comm.) has experienced samples in which the MD fraction appears to have been completely demagnetised by fields as low as 40-50 mT. It is possible, then, that the Rolph and Shaw correction may also be valid for fields in the coercive force region from 50-100 mT.

6.10 EXPERIMENTAL DETAILS

All modified Shaw technique palaeointensity experiments performed on the spinner magnetometer incorporated the following experimental conditions:

1. All a.f. demagnetisations were performed using a two-axis tumbler in a set of Helmholtz coils (low field$\simeq$10 nT) up to a peak demagnetisation field of between 150-180 mT, the value of which depends on the stability and strength of the NRM.

2. ARM1 was given in the direction of the NRM of the sample and in a steady d.c. field of 50μT and a peak a.f. equal to the maximum a.f. in (1).

3. The TRM was imparted by heating samples to 720°C, with a hold time of 20 mins. followed by cooling to room temperature (25°C). A d.c. field of 50μT was applied to the samples throughout the heating and cooling cycles. The samples were heated inside a Magnetic Measurements Thermal Demagnetiser (MMTD), where the field inside the oven is approximately 5 nT.

4. ARM2 was given in the direction of the TRM

5. All measurements of magnetisation were performed on a Molspin spinner magnetometer.

6. Only samples which have magnetite as the single magnetic mineral were used in the modified Shaw experiments, since the maximum peak alternating fields that could be achieved by the a.f. demagnetisers (180mT for the spinner and 200mT for the SQUID) were too low to demagnetise haematite.

The cryogenic (SQUID) magnetometer developed by Shaw et al (1984) was used to perform automated palaeointensity experiments by the modified Shaw technique. This magnetometer uses a static a.f. demagnetisation system which can sometimes result in the acquisition of a gyroremanent magnetisation (GRM), particularly in samples which have a high degree of anisotropy of magnetic susceptibility.

6.11 METHOD OF DATA ANALYSIS

All data from modified Shaw experiments were analysed in the same way, using computer programmes developed at the Earth Sciences department at Liverpool University, specifically designed for analysing data obtained by the modified Shaw technique.

The following steps were used in the data analysis:

1. The NRM of a sample was analysed using orthogonal vector plots, directional plots and a.f. demagnetisation intensity plots. The ideal

sample for a modified Shaw experiment is that which has a single, hard, component of NRM which is stable to a.f. demagnetisation and has magnetite as the magnetic mineral, since the practical limit of the a.f. demagnetiser used here is 180mT. Haematite-bearing samples can be used for Shaw experiments, provided that the maximum peak alternating field of the demagnetiser is sufficiently high. Senanayake (1981) developed such a piece of apparatus and used haematite-bearing rocks from the Permian Esterel volcanics in Shaw experiments.

It was found, experimentally, that samples which possessed either multi-component NRMs or single component soft, unstable NRMs all failed to give acceptable palaeointensity estimates. However, during the majority of the experiments, this was not used as a rejection criterion because one of the major aims of the present study was to investigate the behaviour of all types of sample during palaeointensity experiments. This enabled the selection/rejection method described in Chapter 7 to be formulated empirically.

2. The characteristics (shape and median destructive field values) of the a.f. demagnetisation spectra of the NRM, ARM1, TRM and ARM2, were compared.

3. The ARM1-ARM2 and NRM-TRM plots for each sample were analysed and categorised according to the Kono (1978) classification (see Section 6.8.2).

4. The R-S plot (NRM-corrected TRM) for each sample was analysed and a best fit was obtained, regardless of the coercivity region over which this fit was obtained.

In the majority of cases, the data points removed at stage (4) were from the lowest coercive force region (0-40 mT), where the NRM shows little resistance to a.f. demagnetisation, and those in the highest part of the coercive force region (140-180 mT), where one or more of the four demagnetisations becomes unstable (i.e. the intensity is greater than that for the previous demagnetisation step)

Criteria similar to those described by Senanayake et al (1982) for determining linear segments of the NRM-TRM plot were used. A minimum of three, but preferable more than four, data points must define the linear segment, with no elimination of anomalous data points within this segment. Also, the length of the segment should be at least 15% of the length of the distance between the zero field point and the maximum demagnetisation field point. Segments with systematic curvature were avoided.

5. All palaeointensity values obtained were tabulated and compared with the rock magnetic data to assess the reasons for the suitability or otherwise of the sample for use in the palaeointensity experiment (see Chapter 7).

6.12 THE SELECTION OF SAMPLES

As previously mentioned, all samples were used in the pilot experiments regardless of their apparent suitability. At this stage, (pre)-selection criteria were not used so that a sufficiently large data set could be obtained to compile the selection/rejection criteria described in Chapter 7.

It became clear from the results of the pilot experiments that the few samples with multi-component NRMs or those which were unstable to a.f.

demagnetisation were, as suggested by Rolph and Shaw (1985), unsuitable for use in the modified Shaw experiments. Hence, in subsequent experiments, samples showing such behaviour during a.f. demagnetisation were rejected, and only samples with stable, single component NRMs were selected. This approach is satisfactory in that all samples were tested first, and only after this test were selected for or, rejected from, subsequent experiments.

6.13 RESULTS

The limited number of results obtained using the modified Shaw method are listed in Tables 6.4-6.7. Both spinner and SQUID magnetometers were used for the experiments, with the latter employed on samples from the lower lava group, since they proved to be the most suitable for use with this technique.

ARM1-ARM2 plots

Four types of ARM1-2 plot were exhibited (Figure 6.9), corresponding to all the classes defined by Kono (1978) (Section 6.8.2).

Class 1 : Linear ARM1-2 plot. (a) coercivity spectra of ARM1 and ARM2 are identical if slope = 1.0, (b) Shape of coercivity spectra are similar but the magnitudes are different if slope$\neq$1.0.

Class 2 : Non-linear, concave up. No ARM1 remains at higher fields, ARM2 is more resistant to a.f. demagnetisation due to the creation of harder magnetic material during the heating step.

Class 3 : Non-linear, convex. No ARM2 remains at higher fields, ARM1 is more resistant to a.f. demagnetisation. Magnetically softer material is created during heating.

Class 4 : Two linear segments to ARM1-2 plot.

The majority of samples have Class 3 (non-linear) ARM1-2 curves indicating thermal alteration during laboratory heating (TRM step) which has caused the second ARM to have different characteristics to the first.

NRM-TRM (Shaw) plots

All three types of NRM-TRM curve classified by Kono (1978) were witnessed (Figure 6.10). Where the NRM-TRM curves were non-linear (Class 3) their shape was always similar to that of the corresponding ARM1-2 plot. Rolph and Shaw (1985) note this as an essential factor for the use of their correction. If the ARM1-2 and NRM-TRM plots were non-linear and had different shapes, then some process other than laboratory thermal alteration was responsible for the non-linearity and the sample was rejected. In such cases, the NRM of the sample may not be a pure TRM.

A.F. demagnetisation of NRM

Tables 6.4-6.6 show analyses of the behaviour of the NRM of each sample during a.f. demagnetisation, which is classified using three parameters - interpretation of orthogonal vector plots (OVPs), directional stability (DS) and median destructive field (MDF) value.

The OVP interpretation was similar to that used for thermal demagnetisation in Chapter 4:

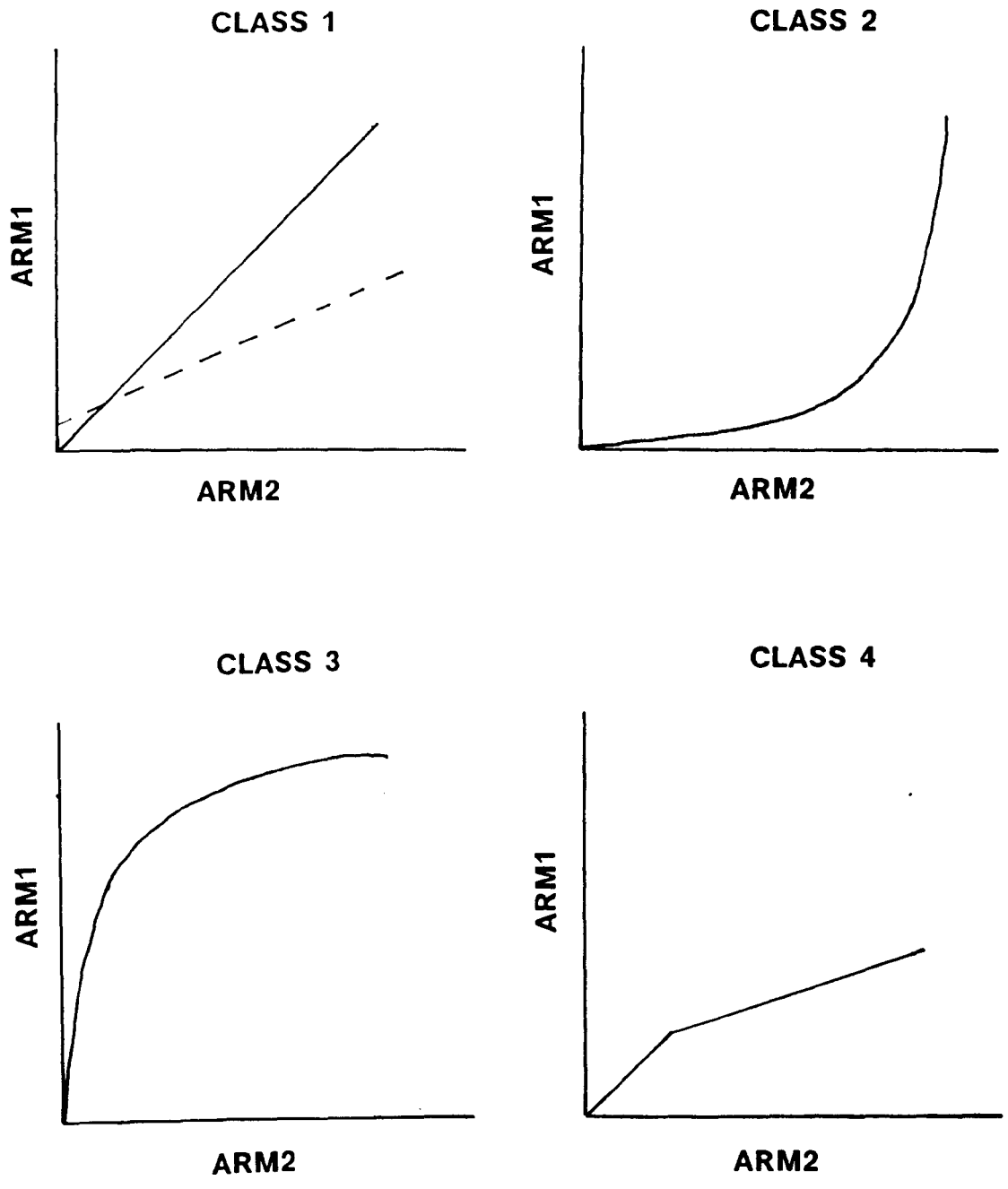

Figure 6.9 : Diagrams showing the four Classes of ARM1-ARM2 curves witnessed in the Gardar lavas. Classification is described in the text.

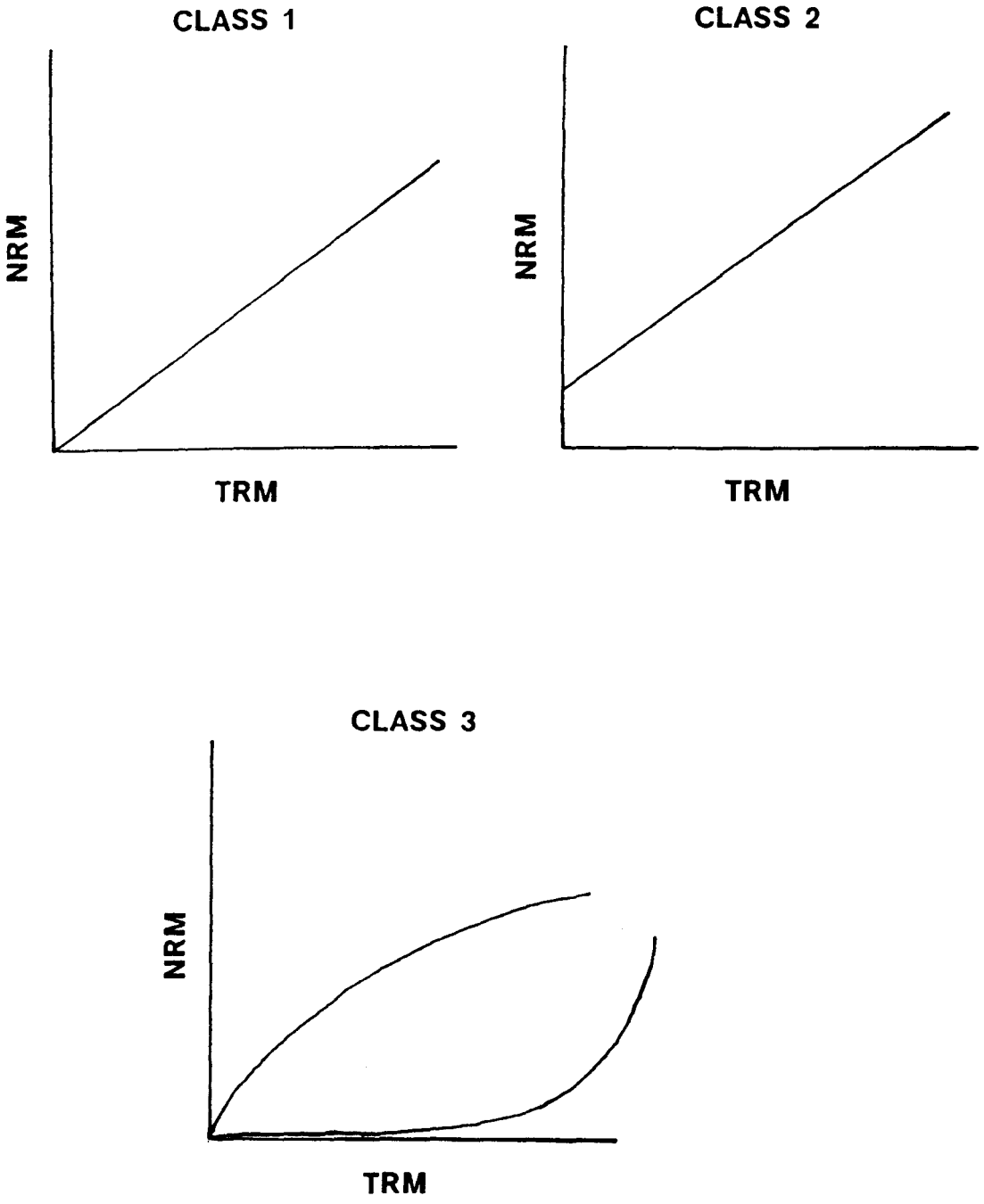

Figure 6.10 : Diagrams showing the three Classes of NRM-TRM curves witnessed in the Gardar lavas. Classes are described by Kono (1978) and in the text.

Category A : Single, non-viscous component.

Category B : Single component with small low coercivity component between 0 and 20mT, with a steep positive direction, probably in the P.E.F.

Category C : Two components, both remote from the P.E.F.

Category D : NRM shows evidence of a low coercivity component (0-20 mT) in the P.E.F. Otherwise, the component structure is the same as witnessed for Category D.

Category U : Unstable sample - no vector defined.

The DS of a.f. demagnetisation was classified as follows:

Class 1 : Stable throughout demagnetisation (to 180 mT).

Class 2 : Directions are unstable at fields above 150 mT.

Class 3 : Directions are unstable at fields above 100 mT.

Class 4 : Directions are unstable at fields above 50 mT.

Class 5 : Directions are unstable throughout demagnetisation.

Comparison of intensity decay (J/Jo) plots .

The J/Jo plots for each demagnetisation suite (NRM, ARM1, TRM and ARM2) were analysed and classified for each sample as follows:

Class a : All demagnetisation curves show the same shape and have similar MDF values.

Class b : NRM and ARM1 are softer than TRM and ARM2

Class c : NRM and ARM1 are harder than TRM and ARM2.

Median destructive field (MDF) values .

The MDF values for a.f. demagnetisation of the NRM of each sample (Section 3.7.1) are listed in milliTeslas.

The results listed in Tables 6.4-6.7 employ the classification schemes described above. In the column labelled 'curves', the two figures correspond to the Classes of ARM1-2 and NRM-TRM plots. In the column labelled 'Demag', the following sequence is listed: an upper case letter for the OVP interpretation (A,B,C,D or U), a single number for the DS of a.f. demagnetisation (1,2,3,4 or 5), a lower case letter for the J/J_o curve type (a,b or c) and another number for the MDF value (0-165). These correspond, to the classification scheme described above, in the order listed above.

6.13.1 The Lower (Mussartût) Lava Formation

Forty-seven samples, from the twenty-three flows in this formation, were used for the modified Shaw palaeointensity determinations. Fourteen of these samples possessed NRMs which proved to be unstable to a.f. demagnetisation and were not used in the ARM(1), TRM and ARM(2) steps of the technique after pilot studies. An example of this instability is shown in Fig. 6.11. Table 6.4 lists the results and Figure 6.12 illustrates typical results (R-S plots) obtained from the flows of this formation.

The majority of samples show non-linear, concave-up ARM1-2 plots (Class 2), which are quite commonly seen in ancient basalts (e.g. Senanyake, 1981, Rolph and Shaw, 1985). Seven samples have ARM1-2 plots with two linear segments (Class 4) but only two have plots which are linear throughout the entire coercivity spectrum (Class 1). In both cases, the slope of the ARM1-2 plot is not unity, hence these samples would also be suitable for application of the Kono correction (Kono, 1978).

SAMPLE NUMBER	RM	DEMAG	CURVES	Ba±SD	POL	VDM
L1-02	1	B4b11	3,3	7.2±0.6 (0-40)	R	1.6#
L2-02	1	A4b9	3,3	19.4±0.8 (40-130)	N	4.7#
L3-01	1	A4b11	3,3	4.0±0.2 (0-40)	N	1.0#
L4-01	2	U5b8	2,3	3.4±0.1 (0-150)	N	1.0±0.6
-03	2	C3b22	2,3	7.8±0.4 (0-50)	N	
-05	2	A4*12	-	-	N	
-06	2	U5*7	-	-	N	
L5-03	1	B3b24	3,3	42.3±0.8 (50-130)	N	10.3#
-06	1	A4b18	2,3	3.5±0.1 (0-40)	N	
L6-02	1	A4b10	3,3	6.8±0.5 (0-60)	N	1.6#
L7-01	1/2	U5*7	-	-	N	-
-03	1/2	A4b5	2,3	REJECTED	N	
-01	1/2	A4b11	2,3	7.7±0.1 (0-150)	N	
-02	1/2	A4b12	3,3	30.9±3.3 (40-110)		
L8-02	2	A4b10	2,3	7.4±0.3 (0-40)	I	-
-06	2	A4*11	-	-	N	-
-07	2	A3b14	2,3	1.8±0.1 (0-150)	N	
L9-01	1	B2a30	3,3	38.3±0.5 (60-110)	N	8.8±0.7
-03	1	A4b20	2,3	33.6±1.6 (80-140)	N	
-07	1	A1a38	3,3	39.0±1.7 (80-120)	N	
L10-01	2	B3a15	2,3	6.4±0.5 (0-20)	N	1.4#
-04	2	U5*5	-	-	N	
-05	2	A4a15	2,3	4.4±0.1 (0-40)	N	
L11-02	1	A4b14	2,3	REJECTED	N	
-03	1	A4*10	-	-	N	
-05	1	A4b17	3,3	8.1±0.1 (0-50)	N	-
L12-02	1/2	A4b14	2,3	8.5±0.3 (0-40)	N	1.2#
L13-02	1/2	C3b9	4,3	5.4±0.4 (50-110)	I	1.4#
-03	1/2	A4*8	-	-	I	
L14-01	2	A2a16	3,3	40.9±1.4 (40-140)	N	13.8±5.1
-02	2	B3a15	3,3	69.4±4.9 (40-90)	N	
L15-04	1	A3b22	3,3	13.5±0.3 (0-90)	N	3.4#
-06	1	A3b17	3,3	-	N	
L16-05	1	A5*21	-	-	N	
-06	1	A4b17	2,3	8.2±0.5 (0-60)	N	1.9#
L17-03	2	A3a7	2,3	15.8±0.5 (10-150)	N	3.8#
L18-01	1	B2a39	3,3	31.0±1.6 (60-130)	N	7.6±0.2
-02	1	B2a36	3,3	66.7±3.5 (70-110)	N	
-06	1	A2a28	2,3	29.6±1.3 (60-130)	N	
-07	1	A1a109	2,3	30.2±5.3 (100-140)	N	
L19-01	1	A1a15	3,3	30.8±1.3 (90-150)	N	7.2±0.2
-02	1	B3b11	3,3	26.5±0.4 (50-100)	N	
L20-02	1/2	A2c55	3,3	64.6±5.2 (60-130)	N	7.9±0.1
-03	1/2	B3a18	3,3	30.3±2.6 (50-120)	N	
-05	1/2	A1a60	3,3	84.0±7.8 (80-120)	N	
L21-02	1	U4*7	-	-	I	-
L22-02	1/2	U4*8	-	-	N	-
L23-01	1	A2c30	3,3	16.1±1.2 (60-90)	R	7.1#

Table 6.4 : Modified Shaw palaeointensity results for the Lower (Mussartût) Lava Formation using the spinner magnetometer. DEMAG column displays details of the a.f demagnetisation of the NRM of each sample (see text for details). CURVES column indicates classification of the ARM1-2 and NRM-TRM curves (see text for details). RM = Rock Magnetic set, as defined in Chapter 7. POL = Polarity of remanence. VDM values are x 10^{22}Am^2. For samples marked with a #, VDM value was calculated using only one intensity determination. SD = Standard error on the palaeointensity. Figures in brackets after the palaeointensity result and associated error refer to the coercivity range (in mT) over which the palaeointensity was calculated. Note : an asterisk (*) in the NRM Demag column indicates that the sample was not used for complete analysis in the modified Shaw experiments, hence no comparison could be made of NRM, ARM1, TRM and ARM2 demagnetisation curves.

SAMPLE	Ba±SD	POL	VDM	DEMAG	CURVES	FIELD RANGE	RM SET*
L1-02	REJECTED	R		B4b11	3,3		2
L3-02	28.5±2.3	N	7.3#	A4b10	3,3	30-90	1
L4-03	REJECTED	N		C3b22	2,3		2
L6-02	42.7±1.4	N	10.2#	A4b10	3,3	60-110	1
L7-03	7.7±0.7	N	-	A4b5	2,3	0-40	2
L8-01	28.7±1.9	I	7.4#	A4b12	2,3	90-110	1/2
L9-02	50.3±1.2	N	12.3±0.4	A4b14	3,3	70-200	1
L9-03	52.4±1.3	N		A4b20	4,3	50-200	1
L10-01	45.9±3.0	N	11.9#	B3a15	1,1	80-120	1
L11-01	REJECTED	N		A4b6	2,3		2
L12-03	REJECTED	N		A5b7	2,3		2
L13-03	REJECTED	I		A4b8	2,3		2
L14-02	36.9±1.7	N	9.3±0.9	B3a15	1,2	50-100	2
L14-03	43.6±0.7	N		B3a12	2,3	70-110	2
L16-03	REJECTED	N		A3b6	2,3		2
L17-02	REJECTED	N		A3a9	2,3		2
L18-03	26.7±0.3	N	6.7#	B2a24	2,3	90-200	1
L19-03	REJECTED	N		B3b9	2,3		2
L20-03	23.6±0.3	N	6.1#	B3a18	3,3	40-150	1
L21-01	29.9±1.3	I	4.4#	C3b10	1,2	40-80	1/2
L22-01	REJECTED	N		U5b8	2,3		2
L23-02	28.0±2.6	R	7.1#	A3c25	3,3	60-120	1

Table 6.5 : Palaeointensity results from the Lower Lava Formation obtained using the modified Shaw method on an automated cryogenic (SQUID) magnetometer. *RM sets are defined in Chapter 7. VDM values are $\times 10^{22}$Am^2. For samples indicated with a #, VDM was calculated from a single intensity determination. Other symbols are explained in Table 6.4.

SAMPLE NUMBER	DEMAG	CURVES	Ba±SD	POL	VDM
M1-05	U5*4	-	-	I	-
M11-02	U5*6	-	-	I	-
M12-03	C3*7	-	-	R	-
M16-09	U4b17	3,3	3.6±0.3 (50-110)	N	0.9#

Table 6.6 : Modified Shaw palaeointensity results for the Middle (Ulukasik) Lava Formation. NRM demagnetisation analysis symbols as defined in text. VDM values are $\times 10^{22}Am^2$. For samples marked with a #, VDM values were calculated using one intesnity determination. Other symbols are explained in Table 6.4.

SAMPLE NUMBER	DEMAG	CURVES	Ba±SD	POL	VDM
U1-03	U4b8	2,3	7.9±1.0 (30-60)	N	1.4#
U2-04	B3c13	2,3	9.4±0.3 (20-40)	N	2.0#
U4-03	B4b6	2,3	14.1±0.1 (10-40)	I	2.0±0.4
-07	B4a5	1,1	10.7±0.3 (40-70)	N	
U5-07	B1b92	3,3	20.3±0.7 (60-110)	N	4.8#
U6-02	A1**	-	-	N	-
U7-01	D2**	-	-	N	-
U8-04	U3b11	2,3	1.4±0.1 (10-150)	N	0.2#
-06	U3b11	2,2	1.1±0.1 (10-150)	N	
U9-06	C1**	-	-	R	-
U10-03	B1c110	3,3	9.8±0.8 (30-170)	R	2.5
U11-03	A1**	-	-	R	-
U13-04	A1**	-	-	R	-
U14-03	B1**	-	1.8±0.1 (10-110)	R	0.5#
-05	B1**	-	-	R	-
U15-02	D2b69	2,3	15.9±1.9 (120-150)	I	4.1#
-06	U4*7	-	-	R	-
-07	B1**	-	-	R	-
U16-02	D3b30	3,3	23.3±0.7 (90-120)	I	3.2#
-05	U4*6	-	-	N	-
U17-03	U4b8	2,3	3.5±0.3 (30-60)	N	0.9#
U18-02	A1**	-	-	N	-
U19-06	A1**	-	-	N	-
U20-03	B3c17	2,3	18.3±0.9 (100-120)	N	4.3#
U21-06	U4*5	-	-	N	-
U24-07	U5*3	-	-	N	-
U25-07	B1*165	-	-	N	-
U26-07	B1**	-	-	I	-
U27-02	B4*2	-	-	I	-
U28-02	B1*12	-	-	N	-
U30-06	A1**	-	-	I	-
U31-02	U2*9	-	-	N	-
U32-07	B2*105	-	-	N	-
U33-02	A1**	-	-	I	-
U35-04	A1**	-	-	I	-
U36-02	A1**	-	-	I	-

Table 6.7 : Modified Shaw palaeointensity results for the Upper (Ilímaussaq) Lava Formation. NRM demagnetisation analysis symbols as described in text. VDM values are $\times 10^{22}Am^2$. For samples marked with a #, VDM values were calculated from one intensity determination. Samples marked ** did not lose more than 10% of their initial moment on demagnetisation to 180mT. Other symbols are explained in Table 6.4.

Many samples give low palaeointensity results which do not agree with the Thellier results for the same flows (Section 6.8, Tables 6.1-6.3). It is also noticeable that several of these results are obtained from the low coercivity region (10-50 mT). Rolph and Shaw (1985) suggest that the use of their correction is not valid in this region of the coercive force spectrum.

Fifteen samples, however, give results which are comparable to the corresponding Thellier values. These results are generally obtained from the higher parts of the coercivity spectrum (60-150 mT) and often above 100 mT, although some are obtained from the lower coercivity region (<60 mT), the significance of which is discussed in Section 6.14. It is likely that most, if not all, MD grains are demagnetised by fields of 60 mT or less (Stacey, 1963) which enables the use of the modified Shaw method above this field (Section 6.9.2).

Several samples which possessed stable, single component NRMs with MDF values from 10-15 mT which are unstable above 100 mT (classification A3) contain a small SD magnetite fraction. However, during measurements at higher fields using the spinner magnetometer in the ambient laboratory field, the contribution of this fraction to the remanence is masked by a viscous component which is picked up after each demagnetisation at these high fields. Consequently, the remanence of the sample becomes unstable. Samples showing such behaviour would benefit from being run on the cryogenic magnetometer where all demagnetisation and measurement is carried out in zero field. This reduces the possibility of picking up viscous magnetisations at fields in excess of 100 mT. Also, the cryogenic magnetometer is able to measure the weaker magnetic moment resulting from the small SD fraction.

Table 6.5 lists the results obtained using the cryogenic (SQUID) magnetometer developed at Cardiff University by Shaw et al (1984). Examples of these results are illustrated in Fig. 6.12. A problem with using the SQUID is that it incorporates a static a.f. demagnetisation system which may result in the acquisition of a Gyroremanent Magnetisation (GRM) at higher fields in samples which exhibit a significant amount of shape anisotropy.

A GRM may be acquired by a sample in an alternating magnetic field, without rotation, and is associated with the flip of magnetic vectors within individual grains into alignment with the external field. This has the effect that, during demagnetisation of the NRM, the sample is not demagnetised but a magnetisation is induced in the direction of the last 'demagnetisation'. Figure 6.13 illustrates this effect for a lava sample. GRMs have been previously identified for samples from the Upper Lava Formation of the Eriksfjord Group (Richards, 1986) which appear to show the largest amount of AMS (Section 3.2). Fortunately, the GRM effect was found to be negligible in the samples from the lower group, since they show an insignificant AMS (Section 4.2). Consequently, no significant GRM effect was observed for the lava samples used in the present study.

6.13.2 The Middle (Ulukasik) Lava Formation.

Only five flows in this member contain magnetite as the main remanence carrier, hence the modified Shaw technique was largely useless. In total, four samples were run, three of which were unstable to a.f. demagnetisation and were rejected. One sample was used for all four demagnetisation suites and exhibited a non-linear (Class 3) ARM1-2 plot. No reliable estimate of the field intensity could be made from this sample, shown in Fig. 6.14.

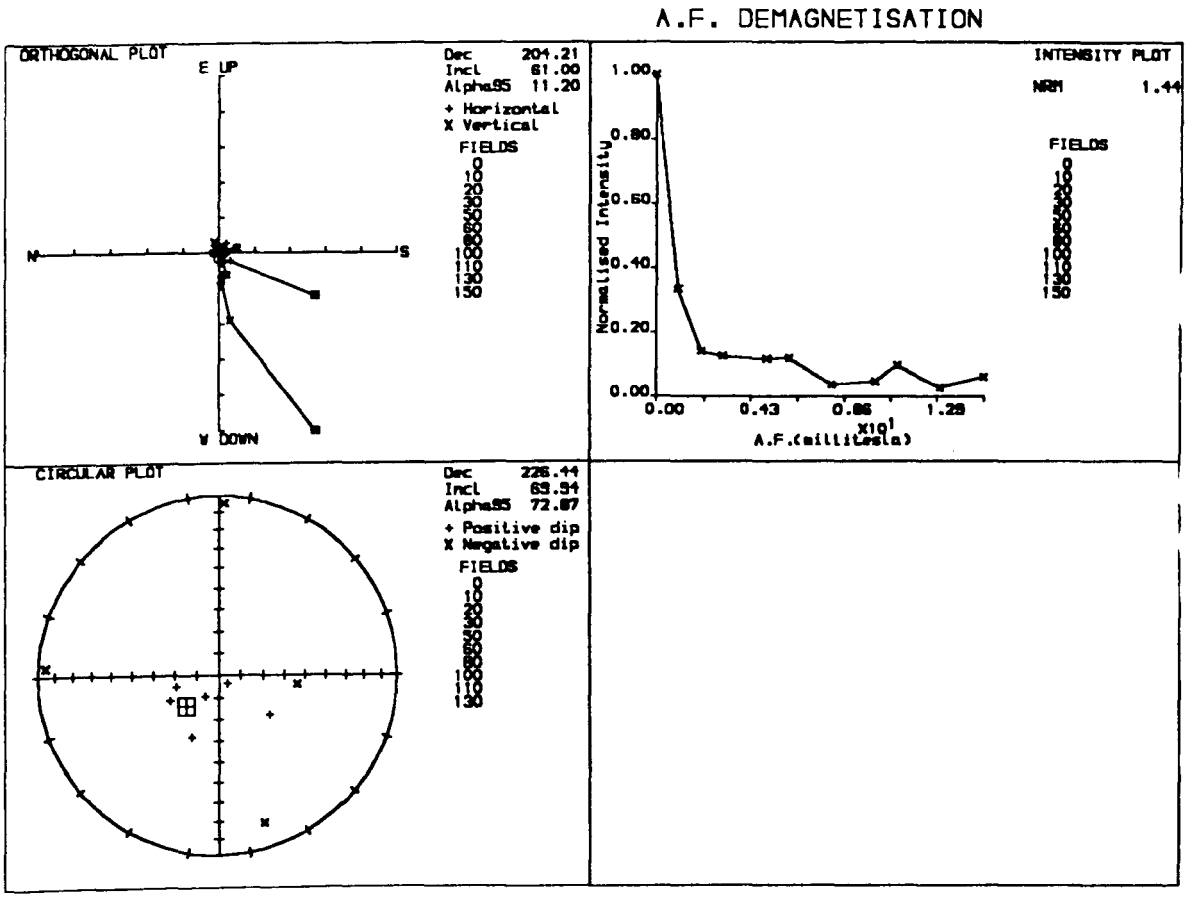

Figure 6.11 : A sample from the Lower Lava Formation which shows instability to a.f. demagnetisation.

Figure 6.12 : Modified Shaw palaeointensity (R-S) plots for the Lower Lava Formation. Samples run on the spinner magnetometer are denoted by an 'S' after the sample number and samples run on the cryogenic (SQUID) magnetometer are denoted by and 'SQ' after the sample number. The figures shown indicate the a.f. demagnetising fields between which the palaeointensity result was calculated. On the R-S plot, NRM and (TRM*(ARM1/ARM2)) are normalised to the respective intensity value at the lowest field used to define the result. ARM1-ARM2 and NRM-TRM plots are also shown, for the same fields as used in the R-S plot.

SAMPLE L4-03S Ba = 7.8 ± 0.4μT

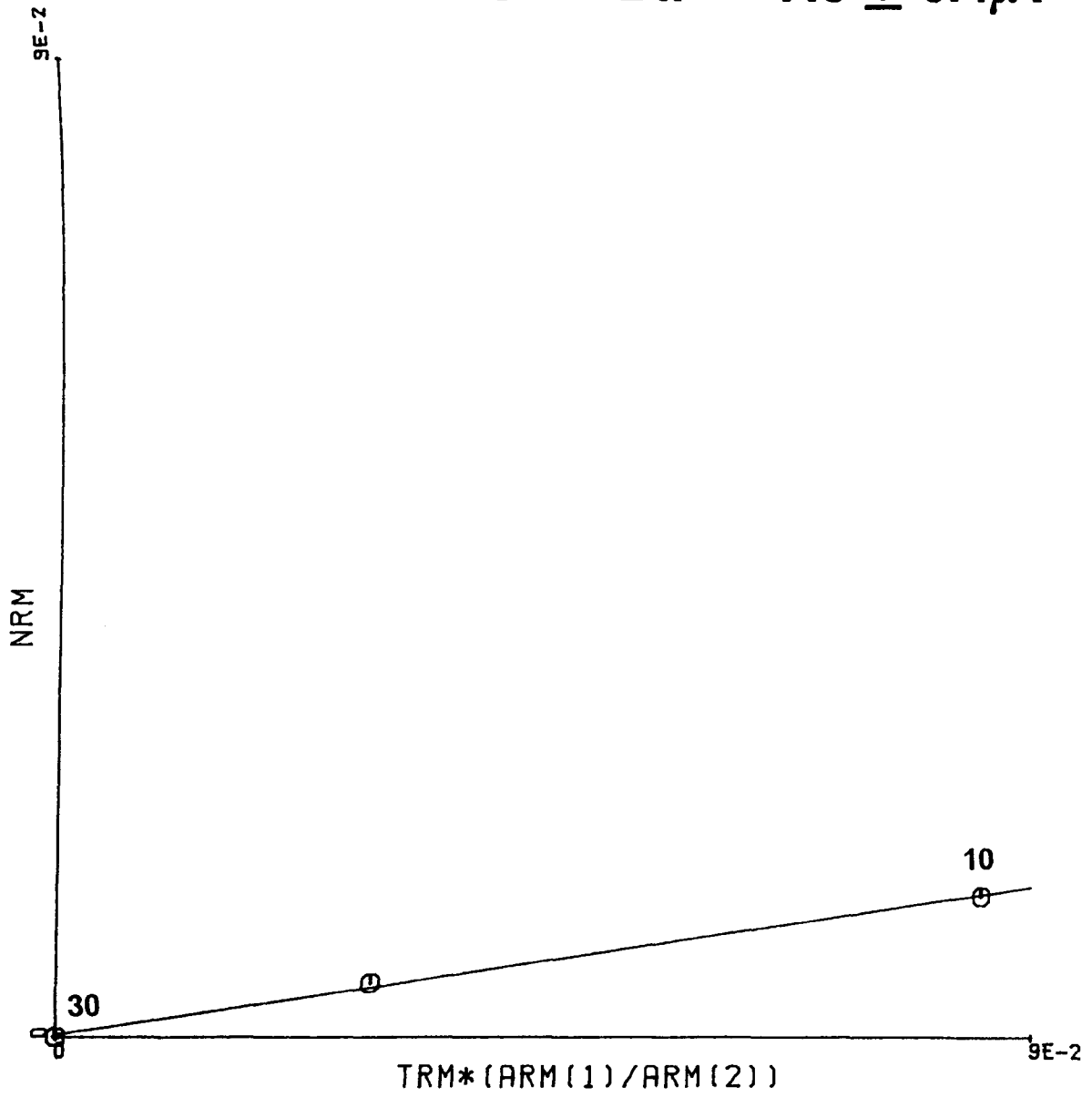

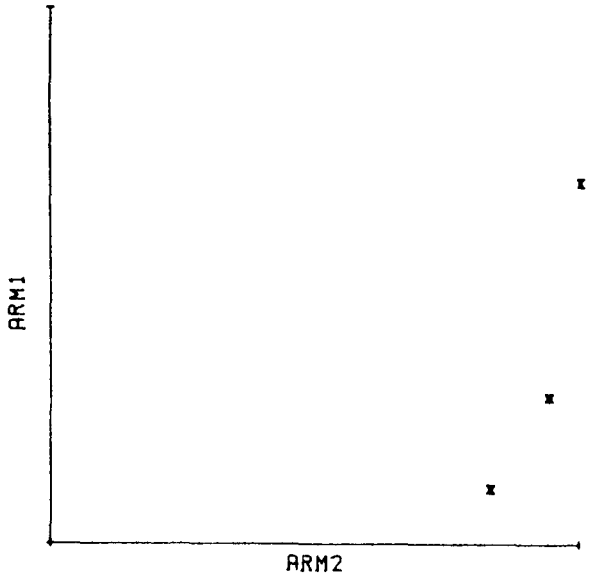

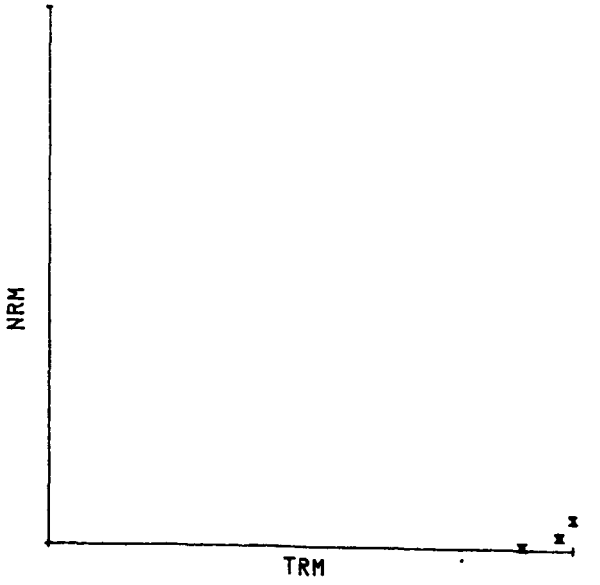

SAMPLE L5-03S Ba = 42.3 ± 0.8μT

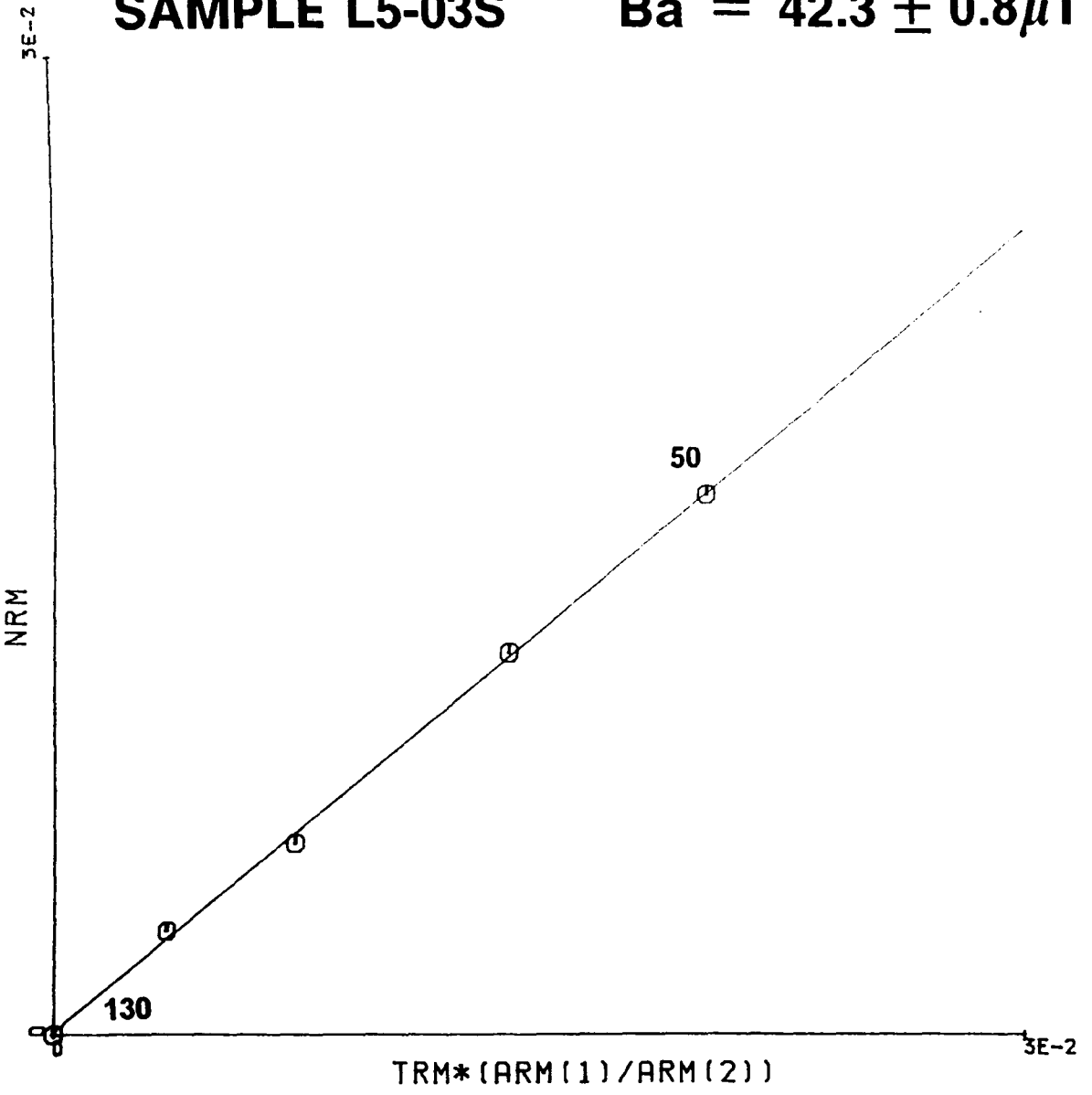

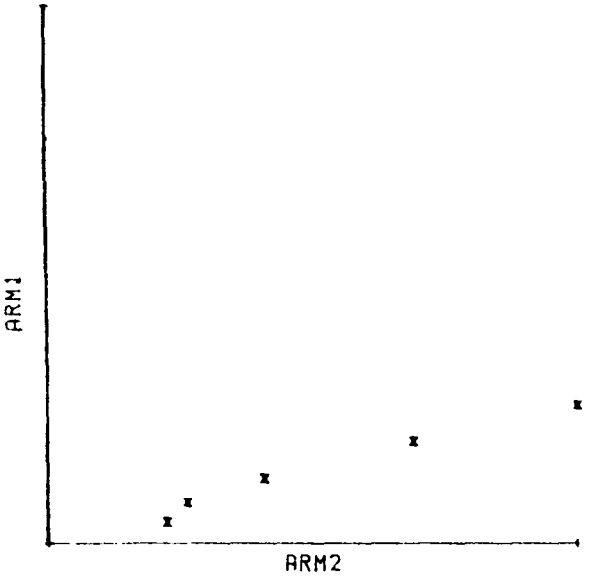

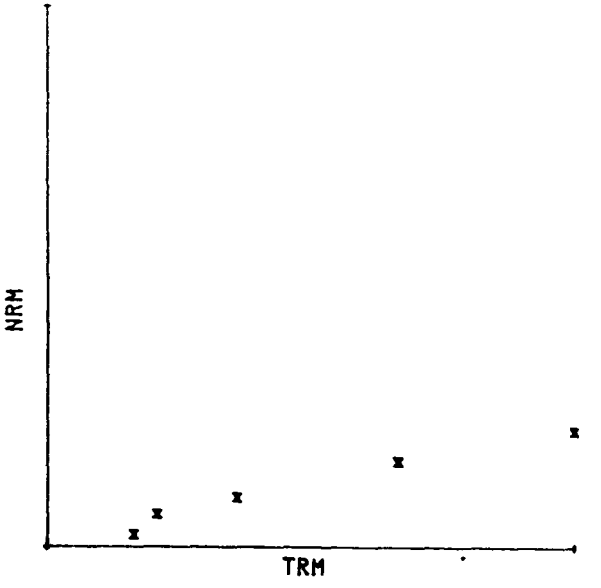

SAMPLE L5-06S Ba = 3.5 ± 0.1μT

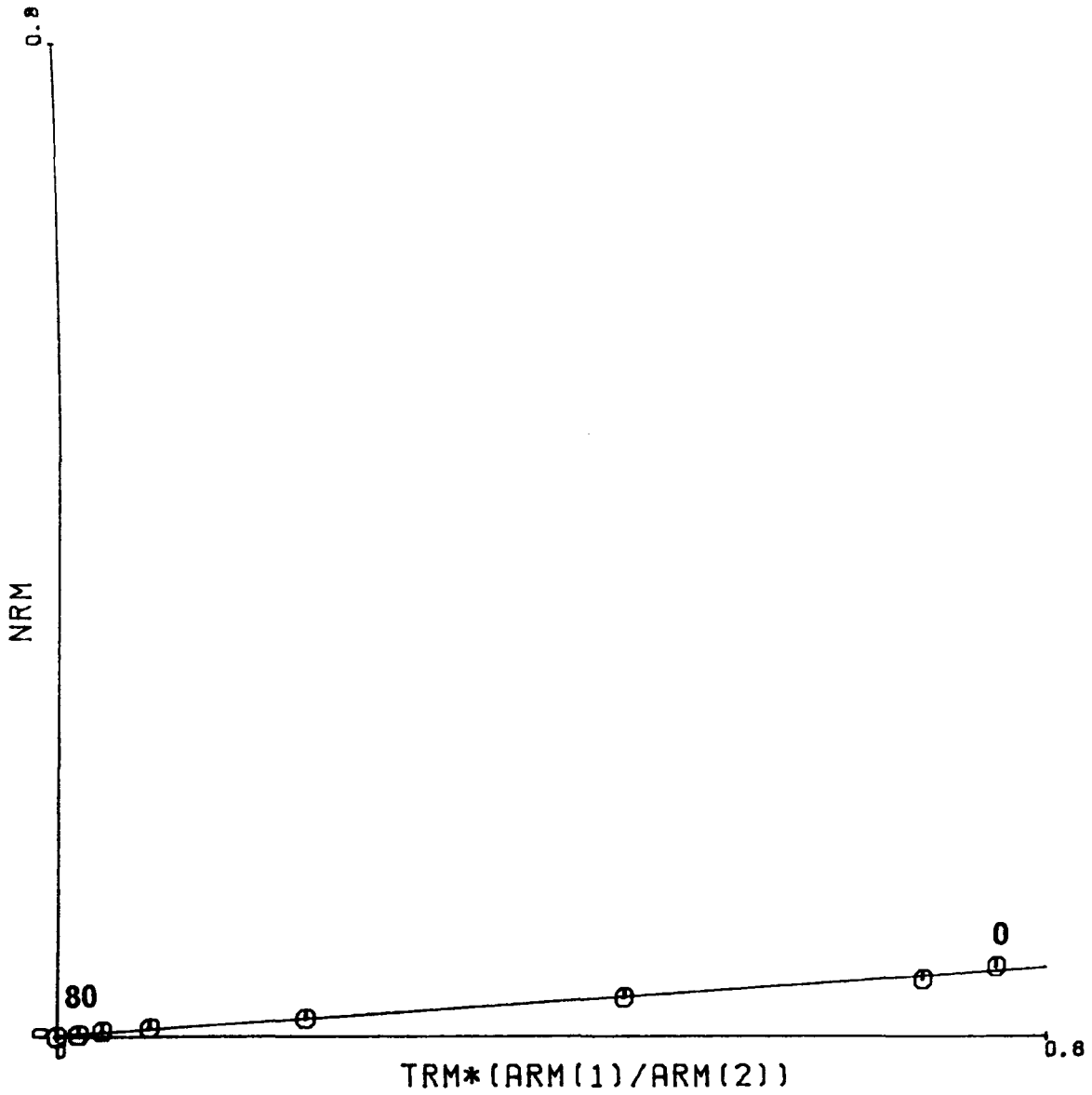

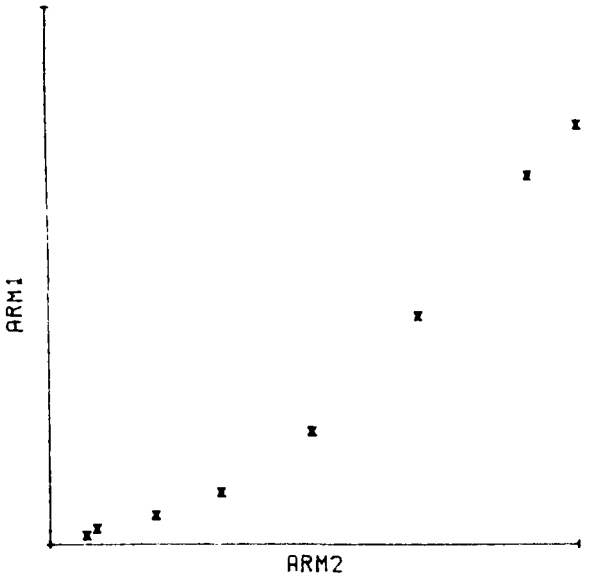

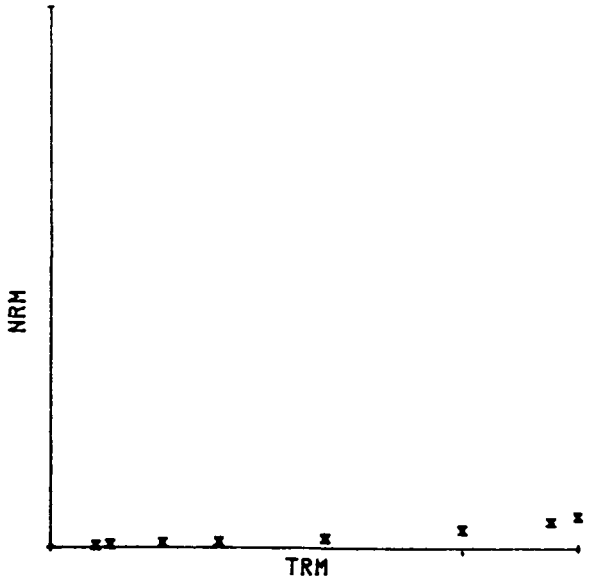

SAMPLE L7-03S REJECTED

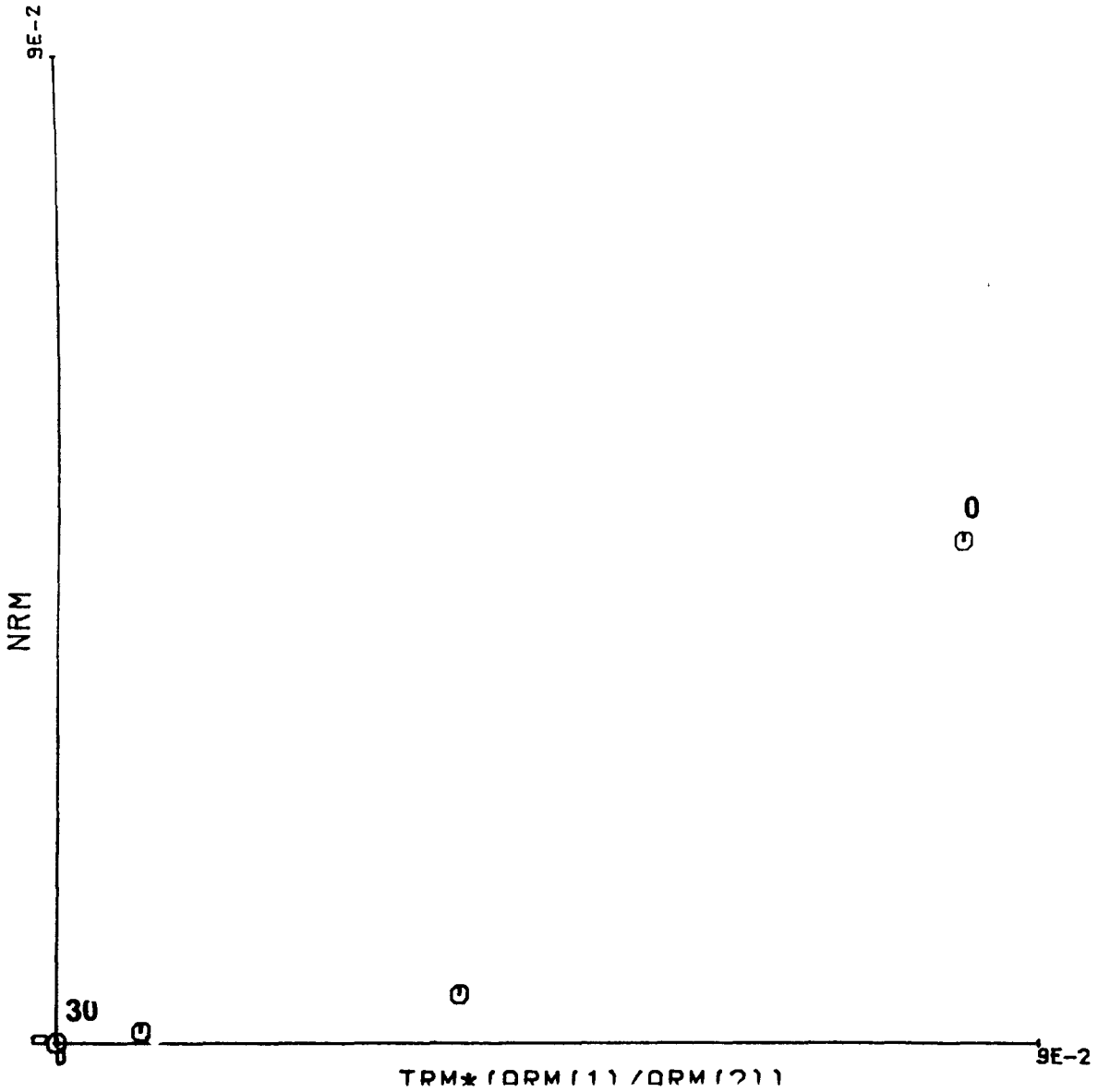

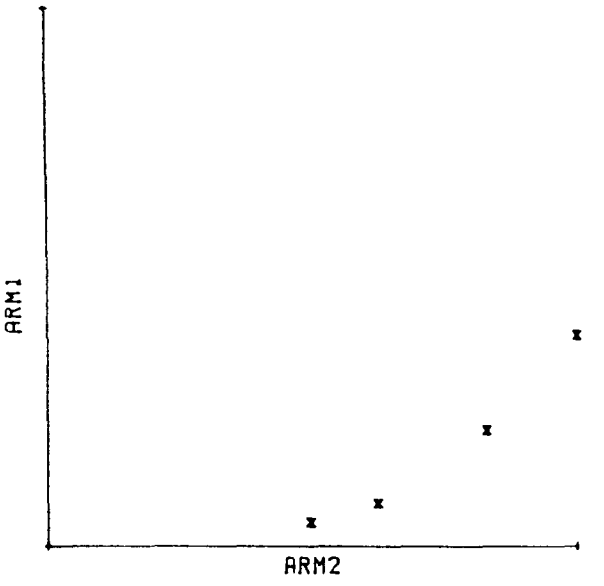

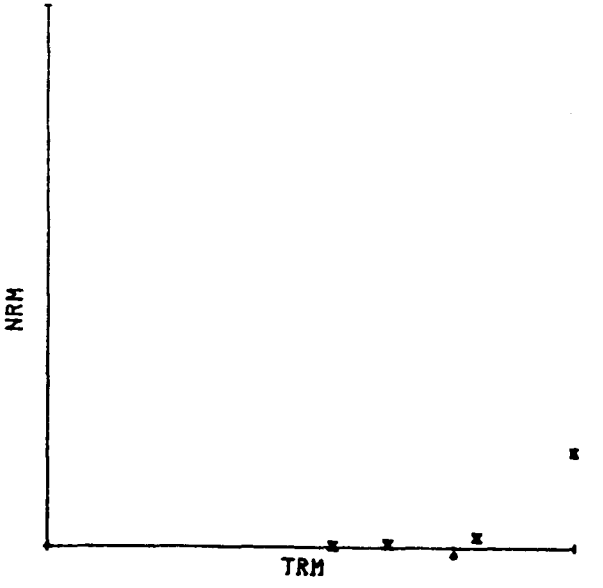

SAMPLE L8-02S Ba = 7.4 ± 0.3μT

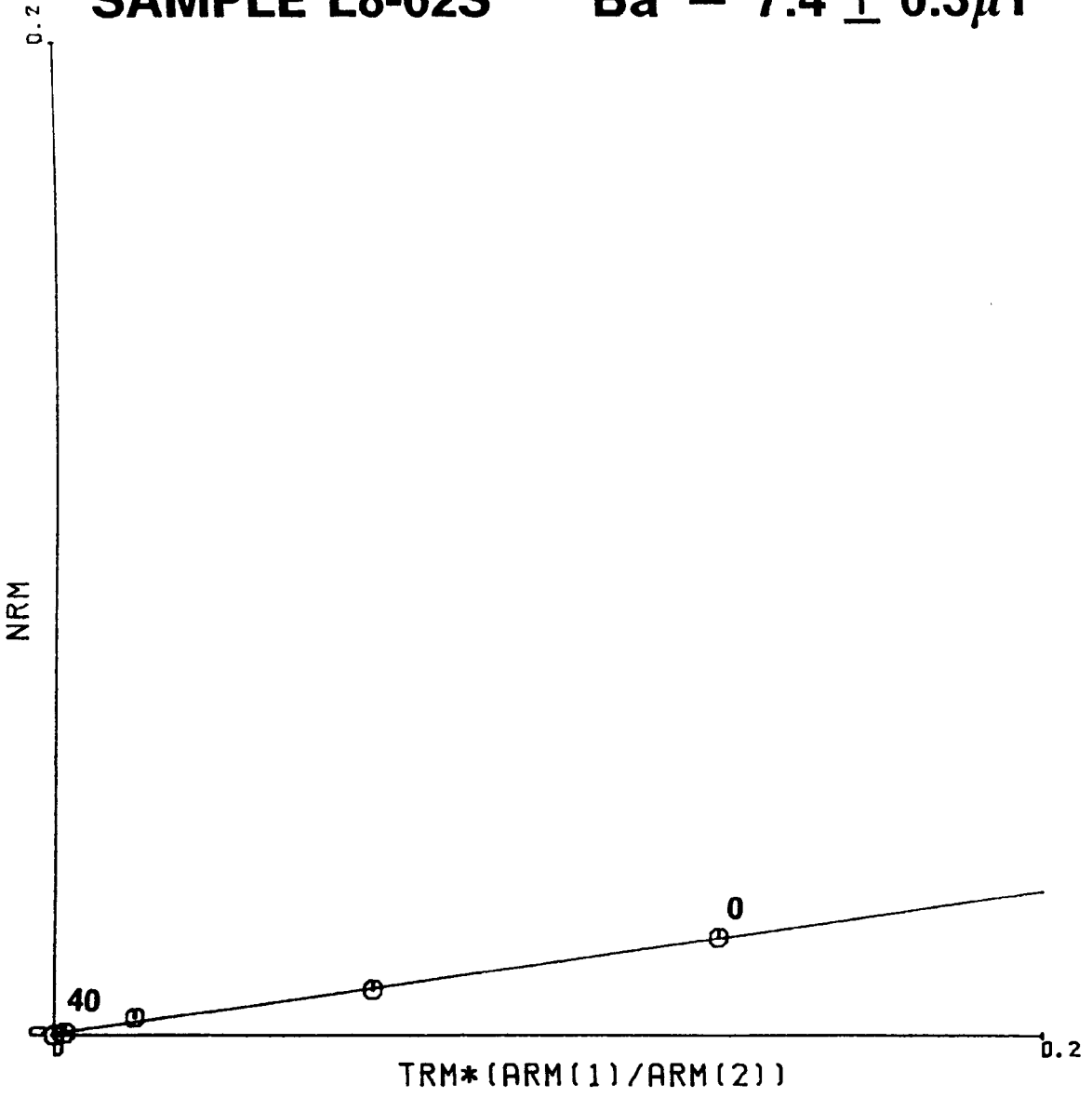

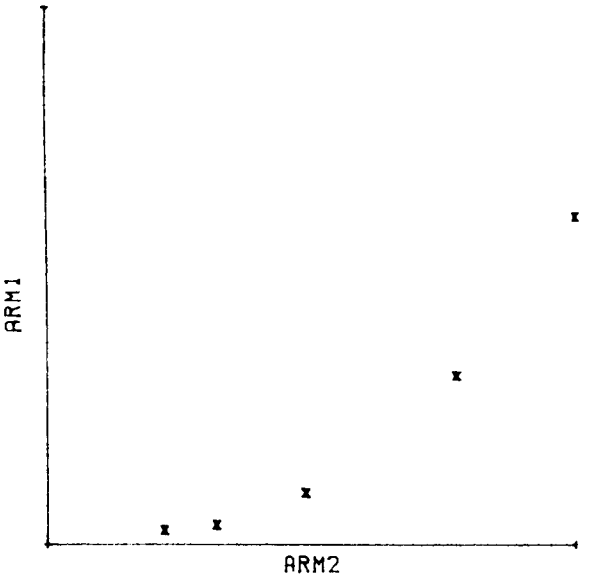

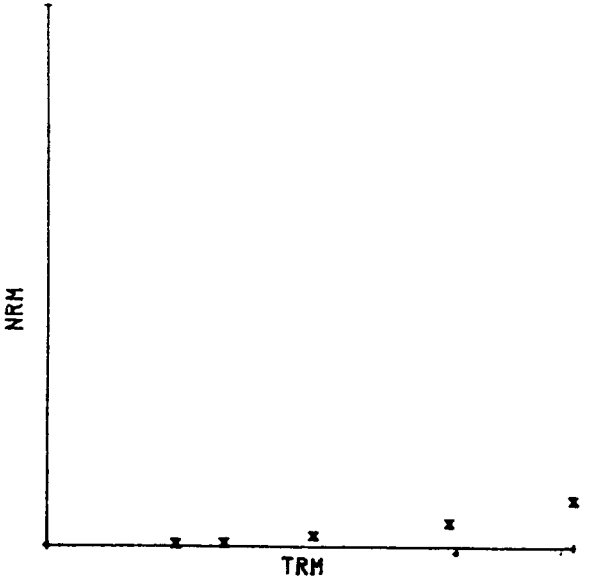

SAMPLE L9-01S Ba = 38.3 ± 0.5μT

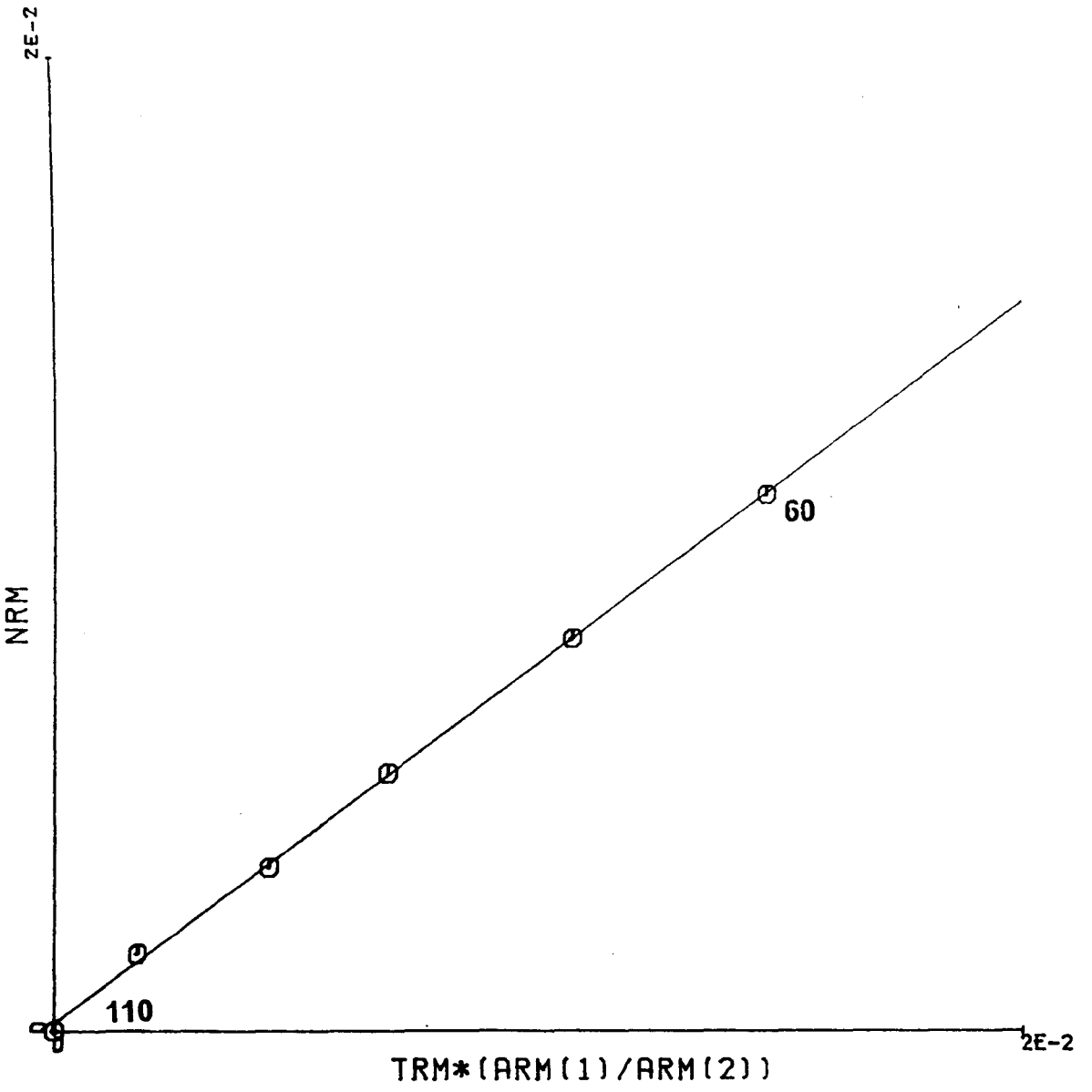

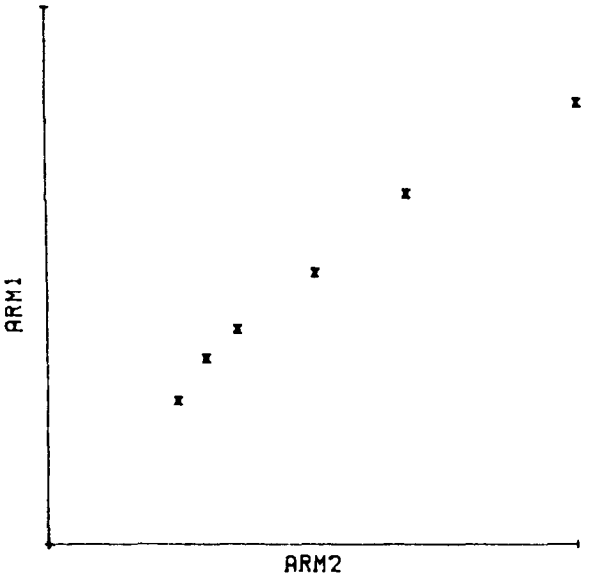

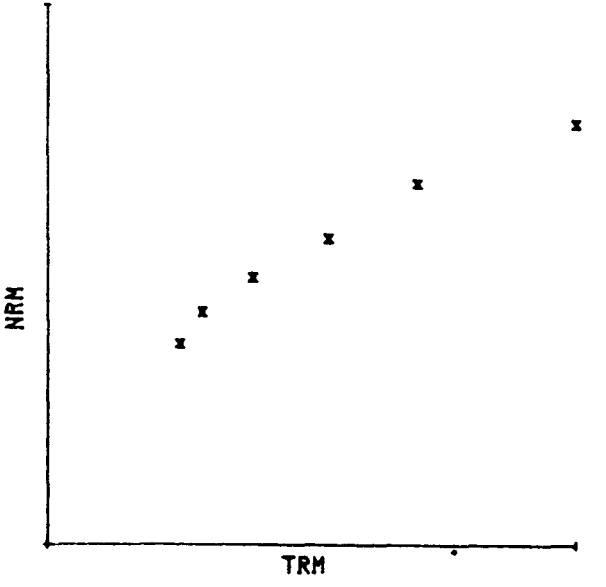

SAMPLE L10-01S Ba = 6.4 ± 0.5μT

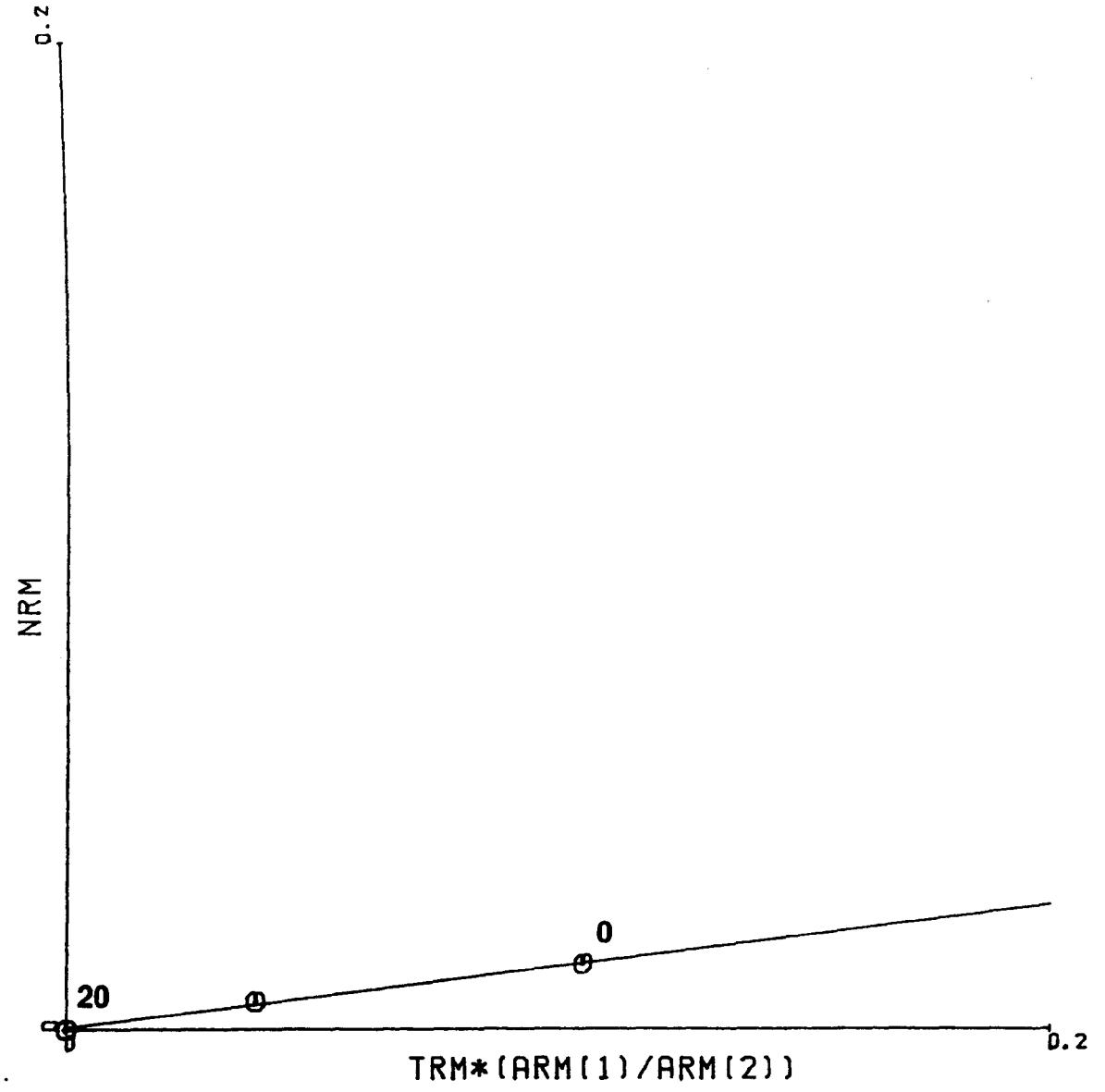

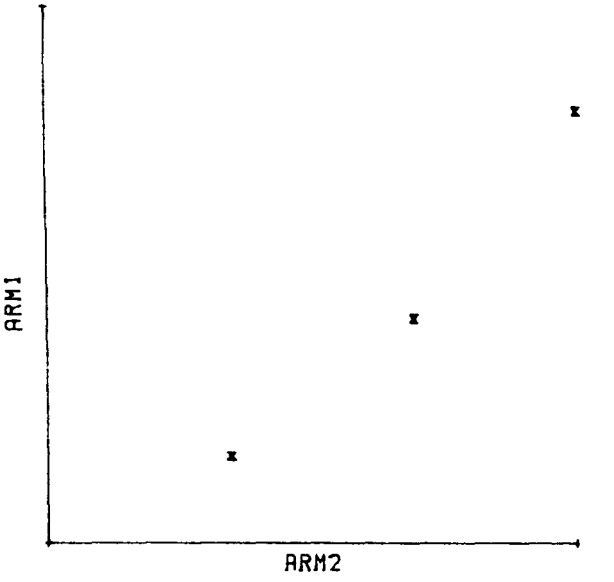

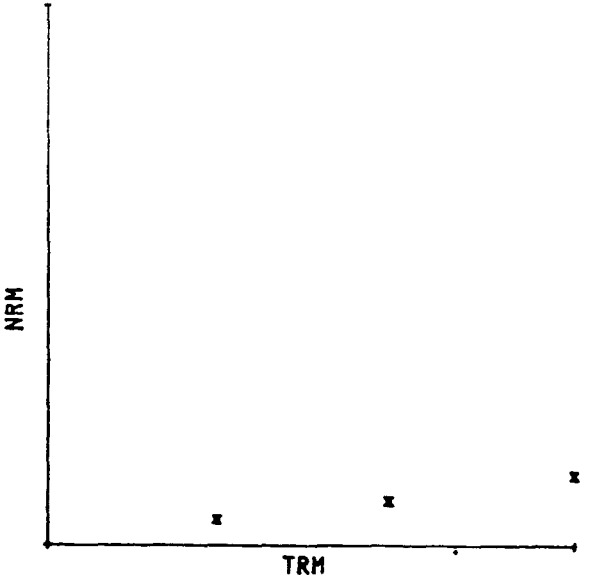

SAMPLE L13-02S Ba = 5.4 ± 0.5μT

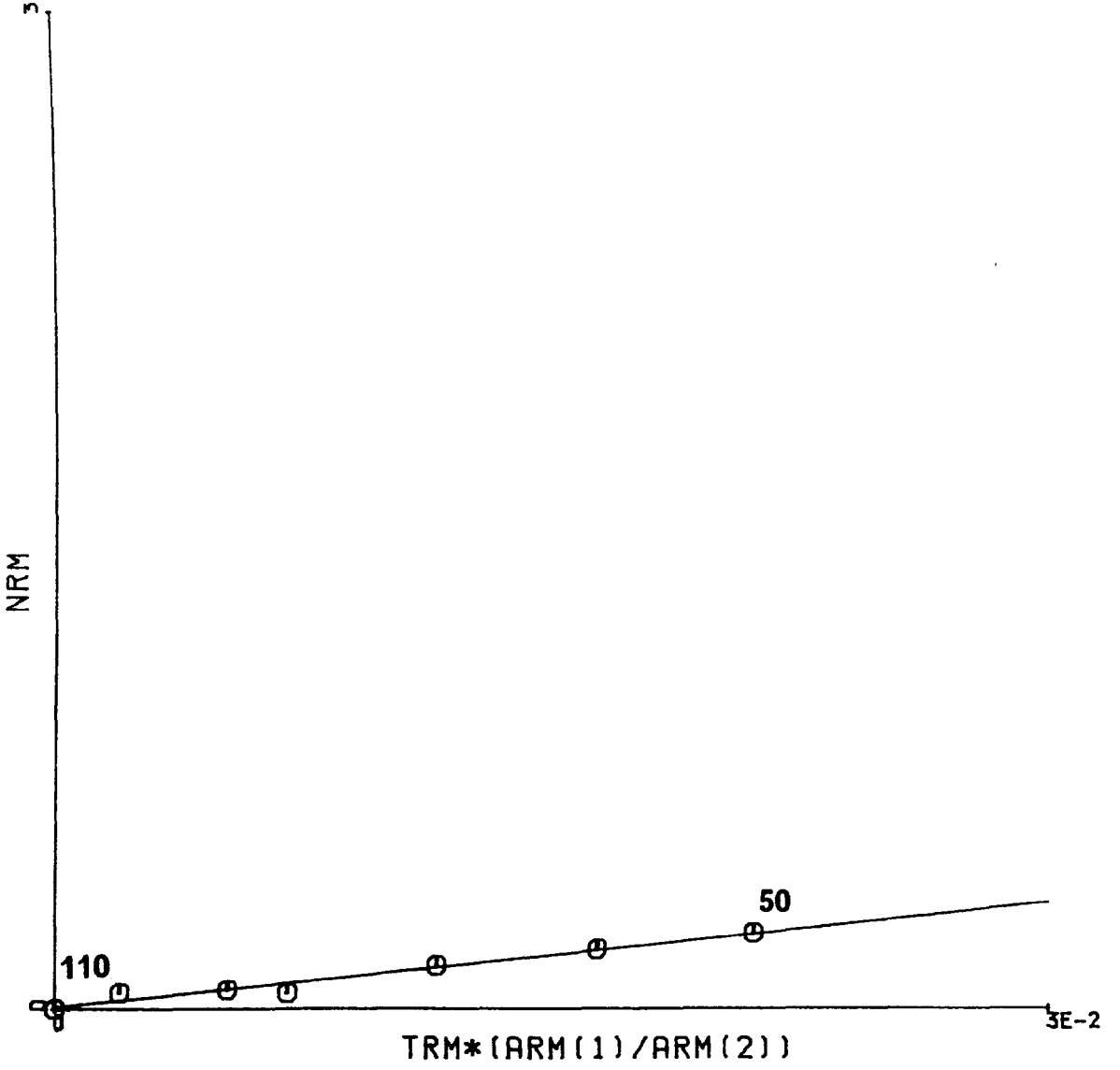

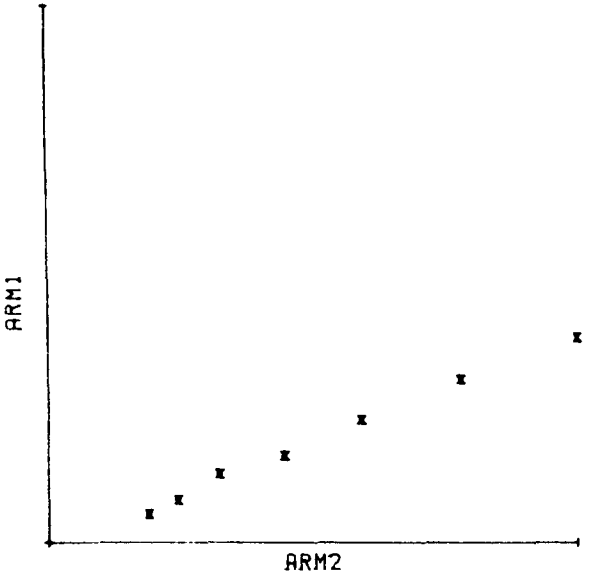

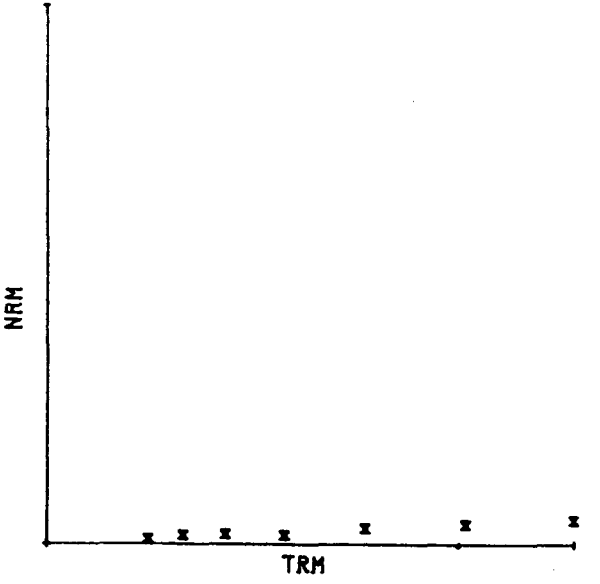

SAMPLE L14-01S Ba = 40.9 ± 1.5μT

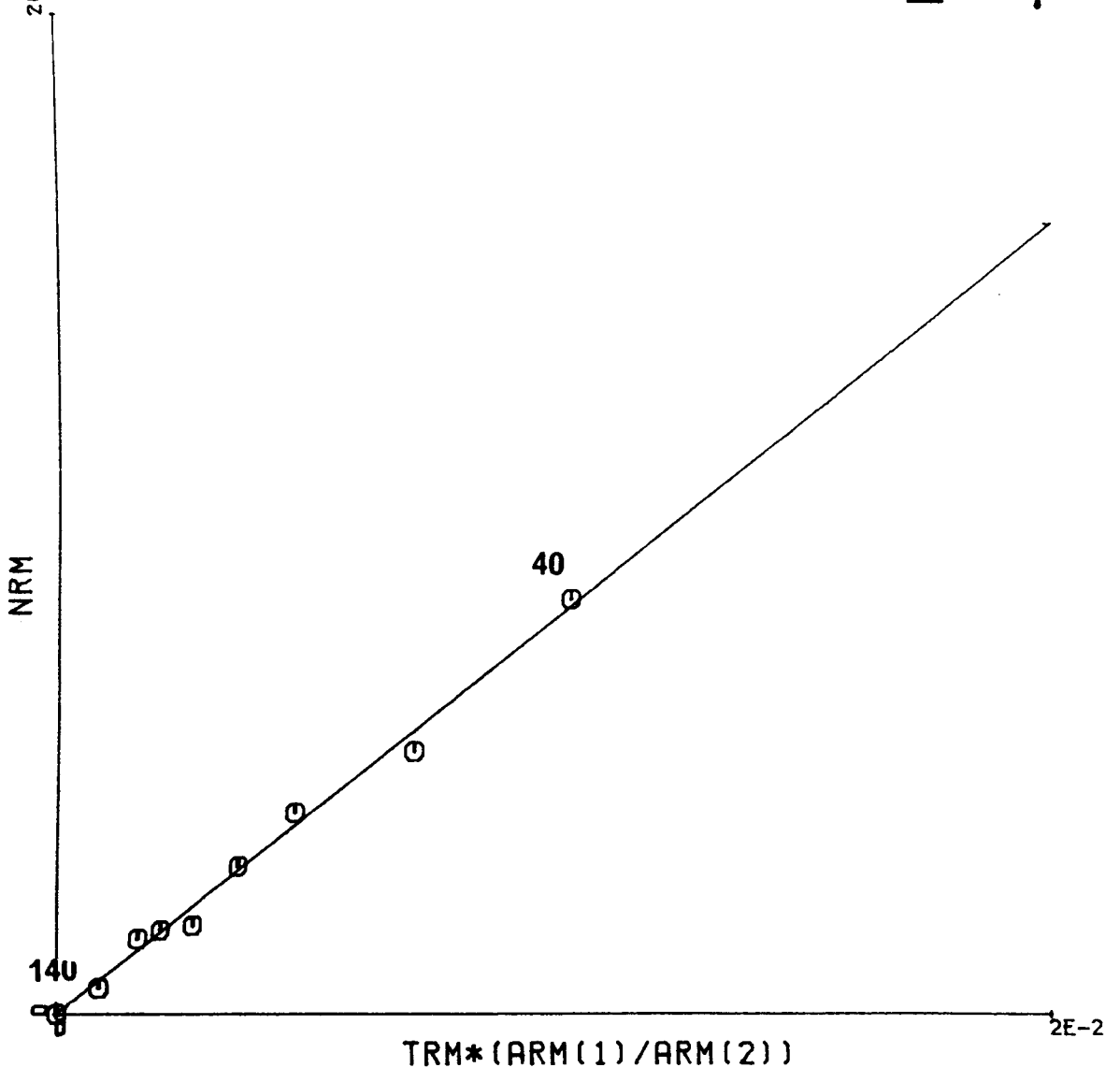

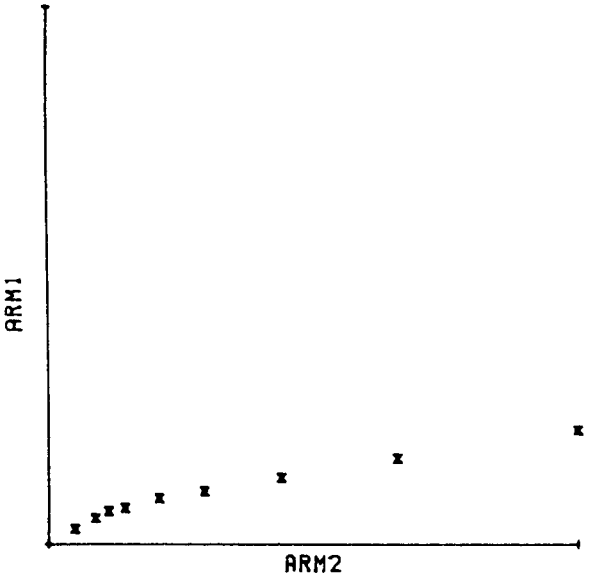

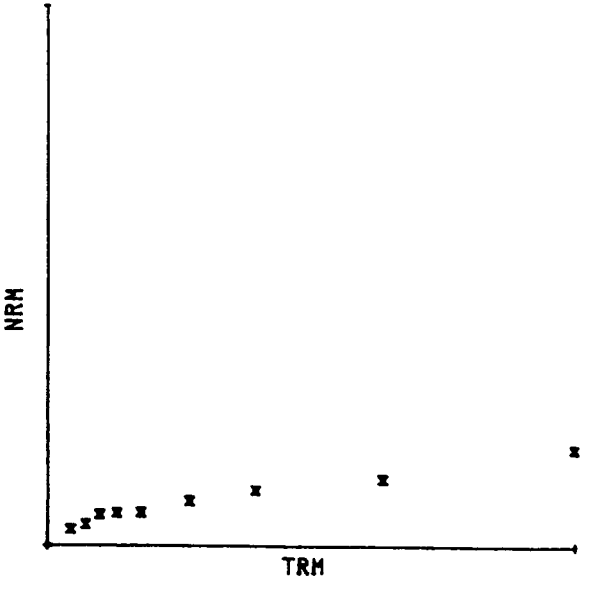

SAMPLE L18-01S Ba = 31.0 ± 1.6μT

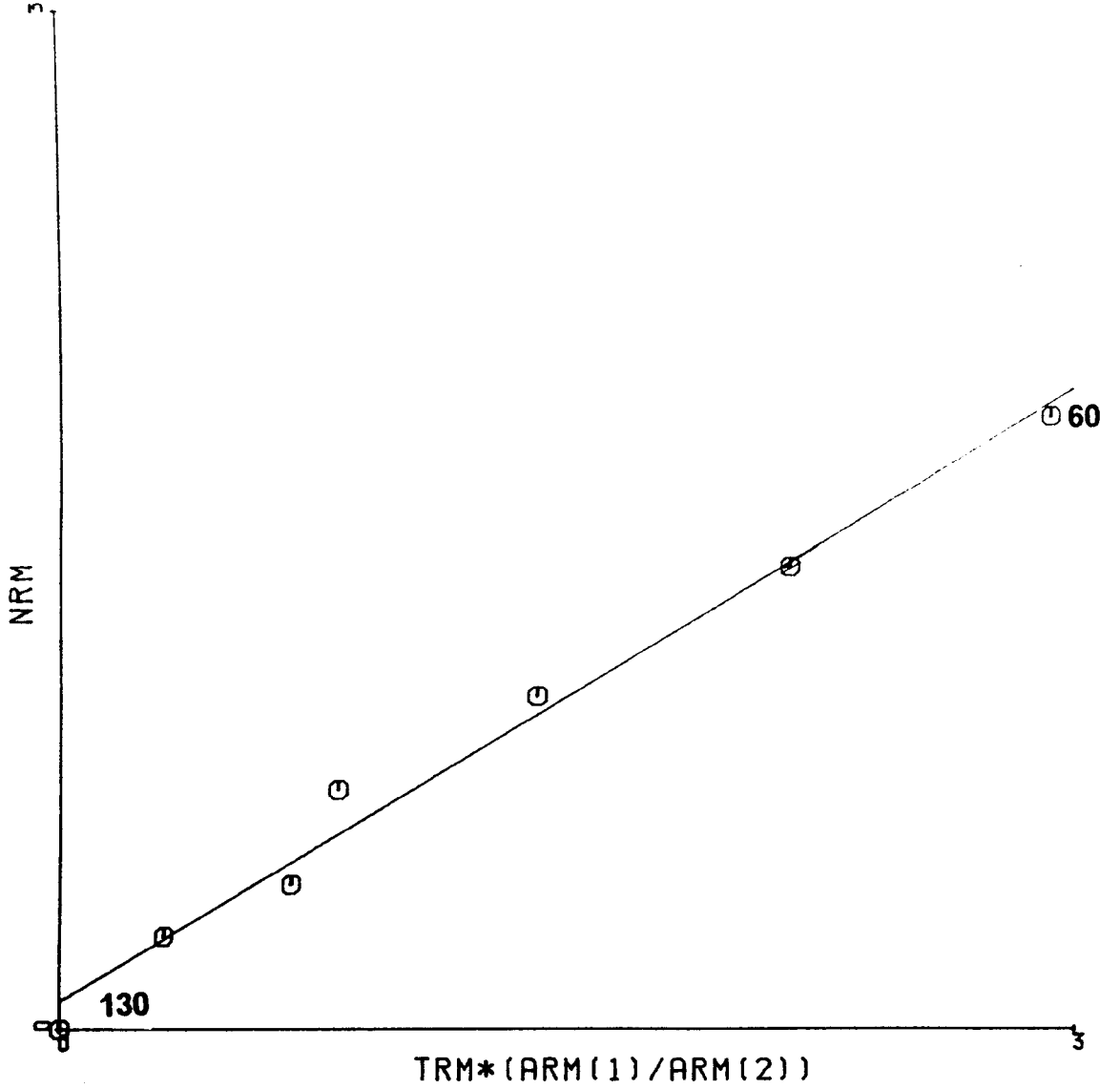

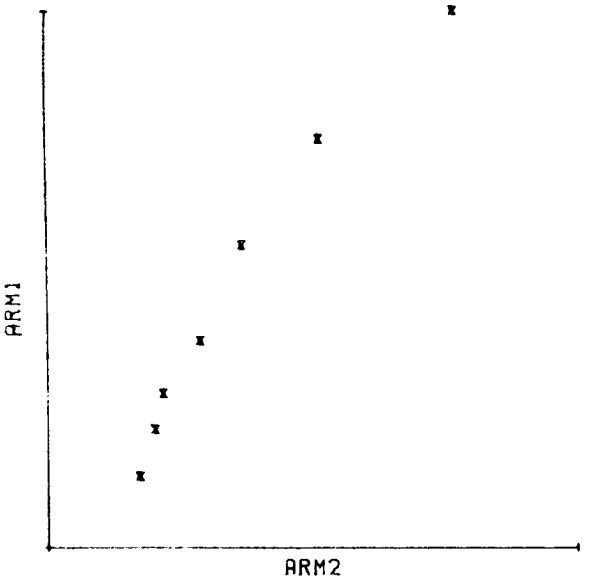

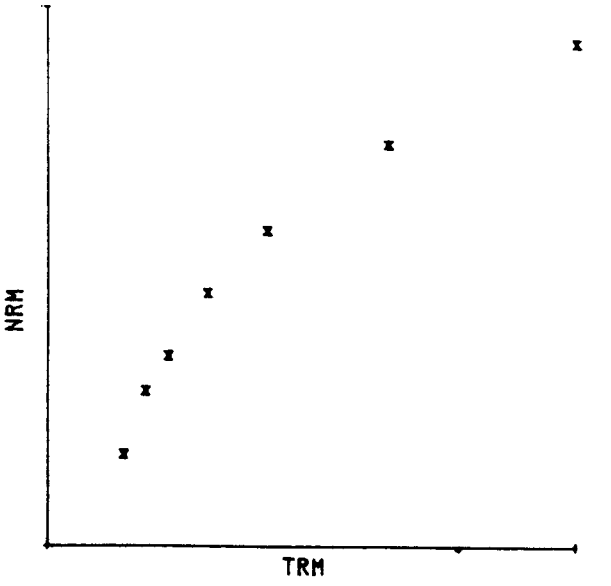

SAMPLE L18-02S Ba = 66.7 ± 3.7μT

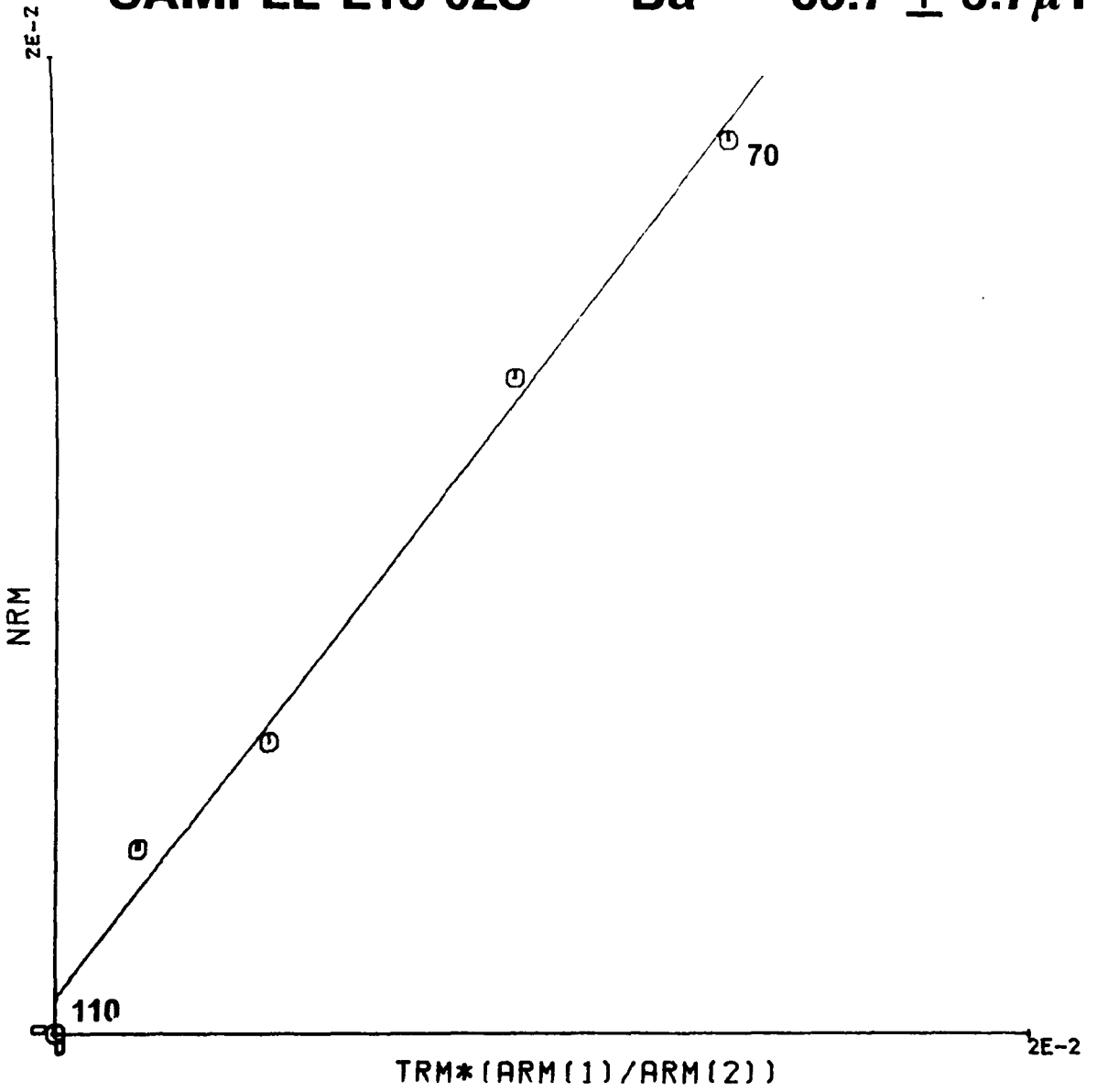

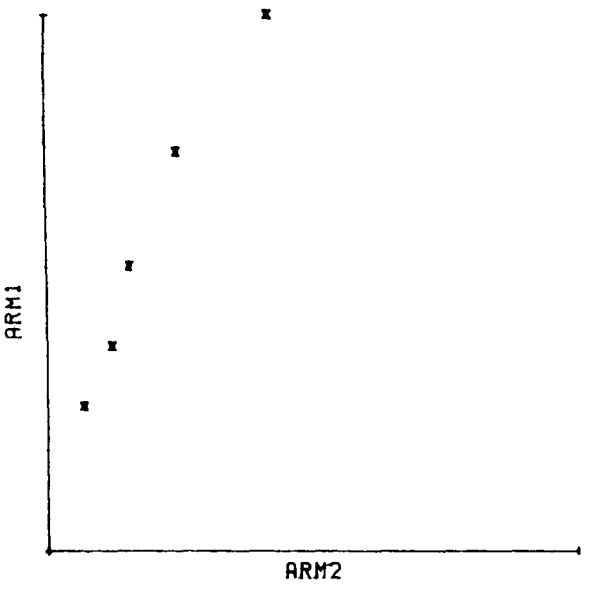

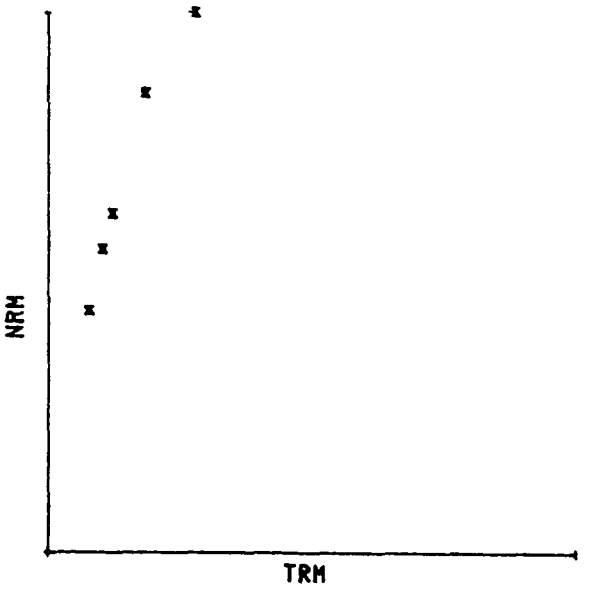

SAMPLE L20-02S Ba = 64.6 ± 5.2μT

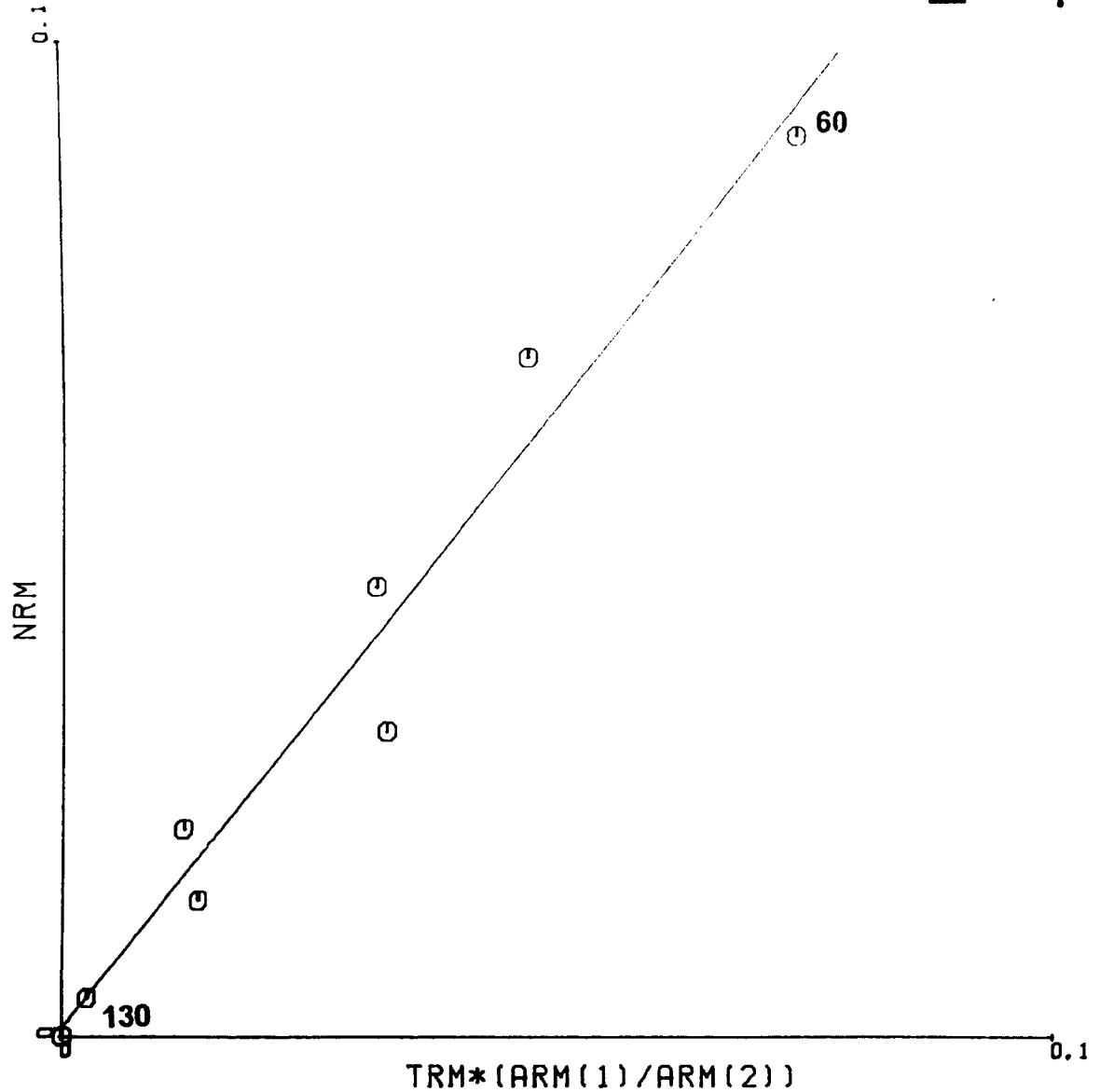

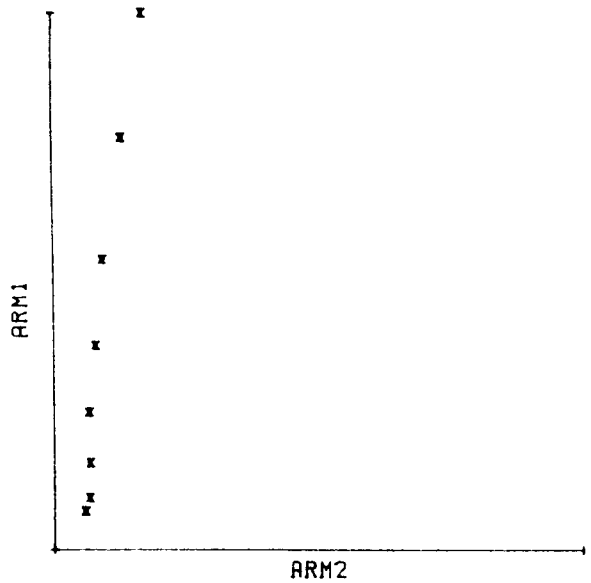

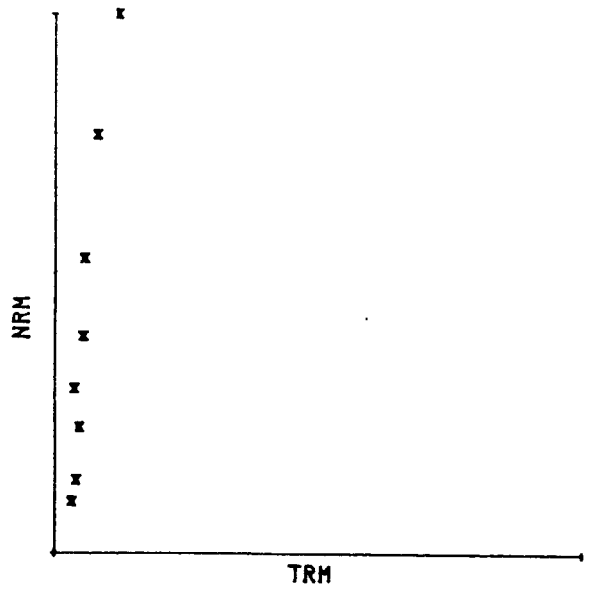

SAMPLE L23-01S Ba = 16.1 ± 1.2μT

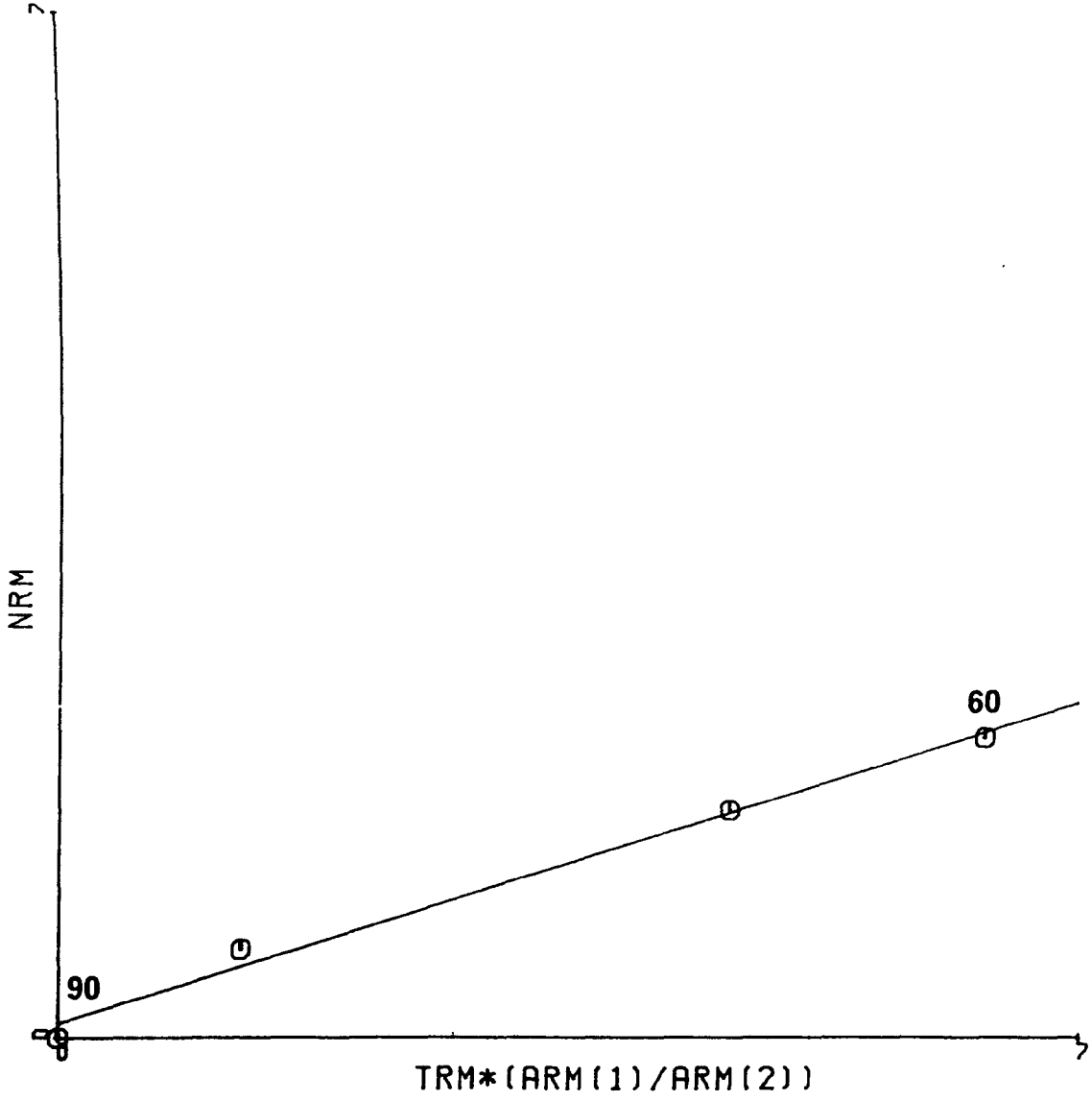

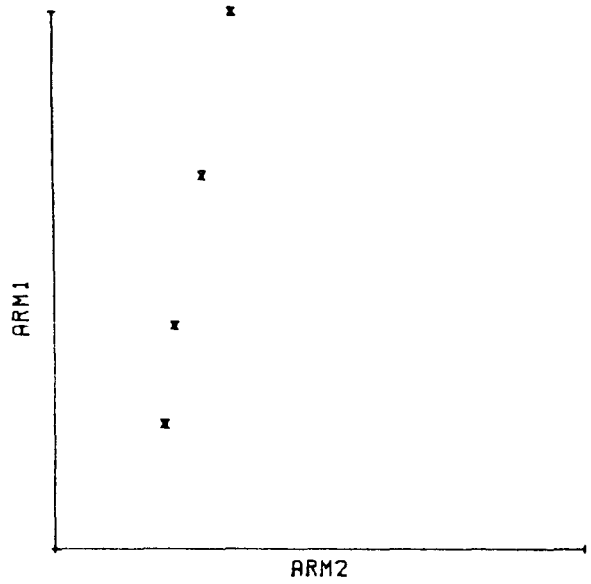

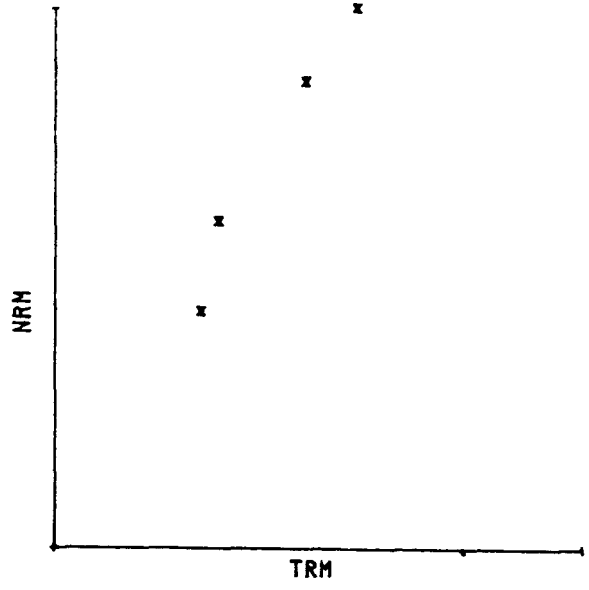

SAMPLE L4-03SQ REJECTED

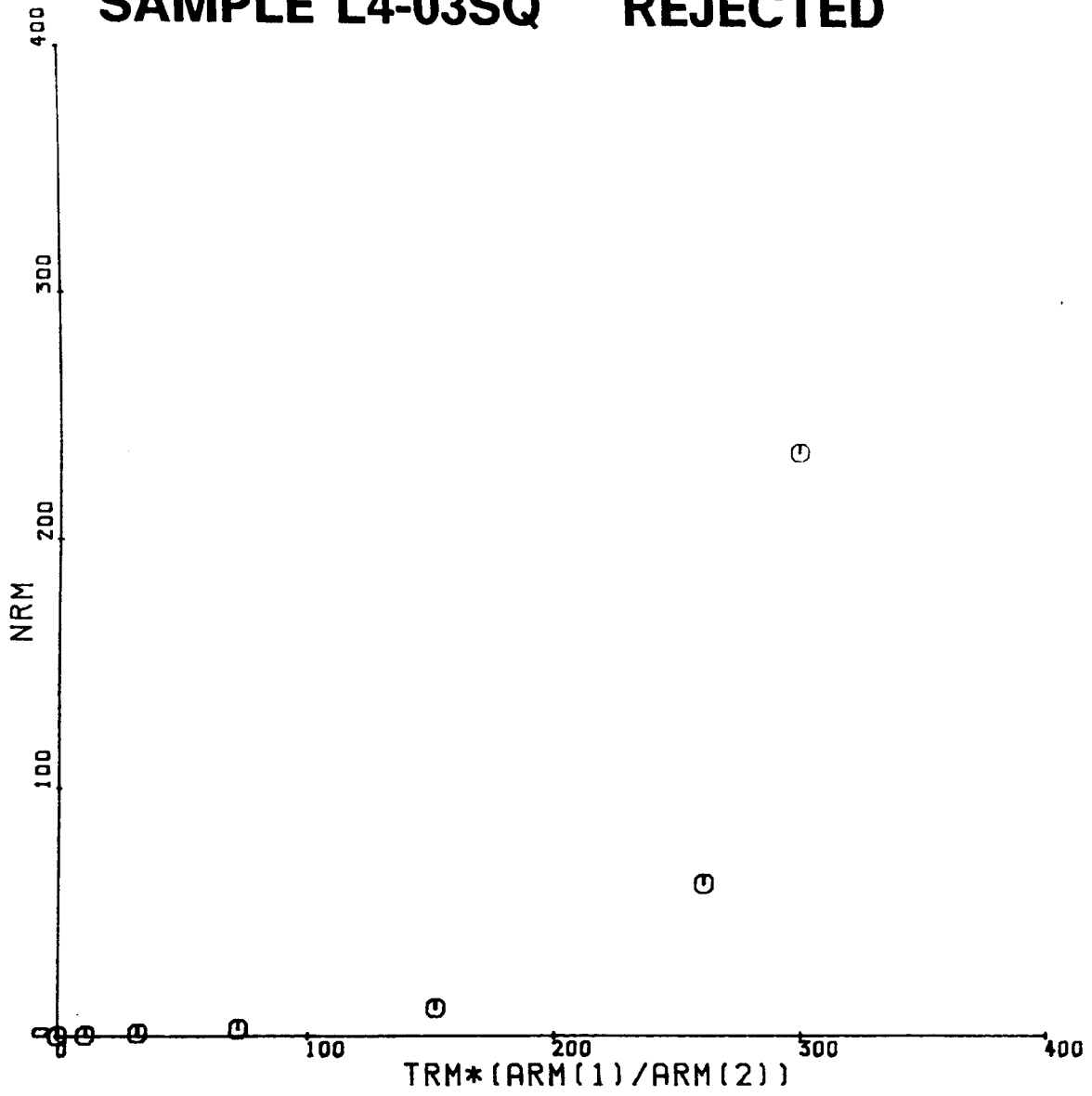

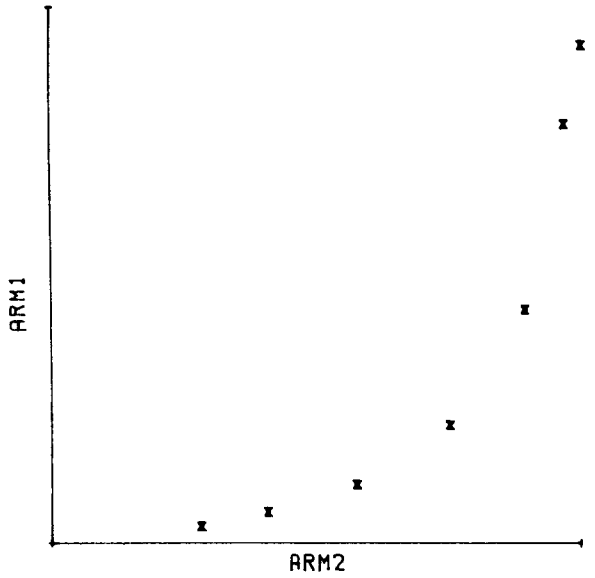

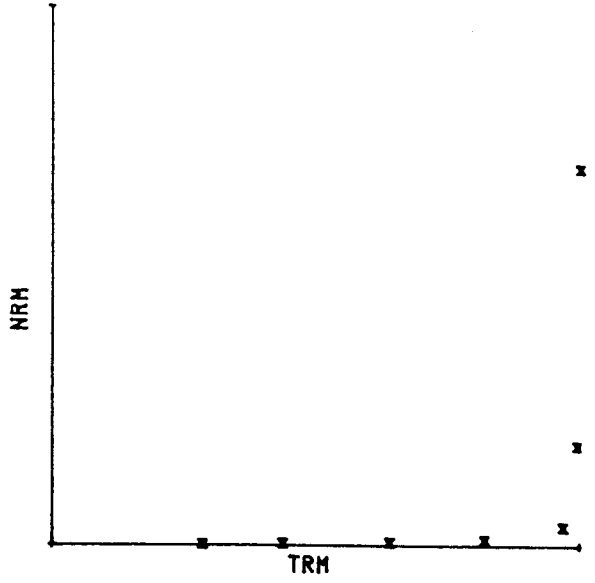

SAMPLE L6-02SQ Ba = 42.7 ± 1.4μT

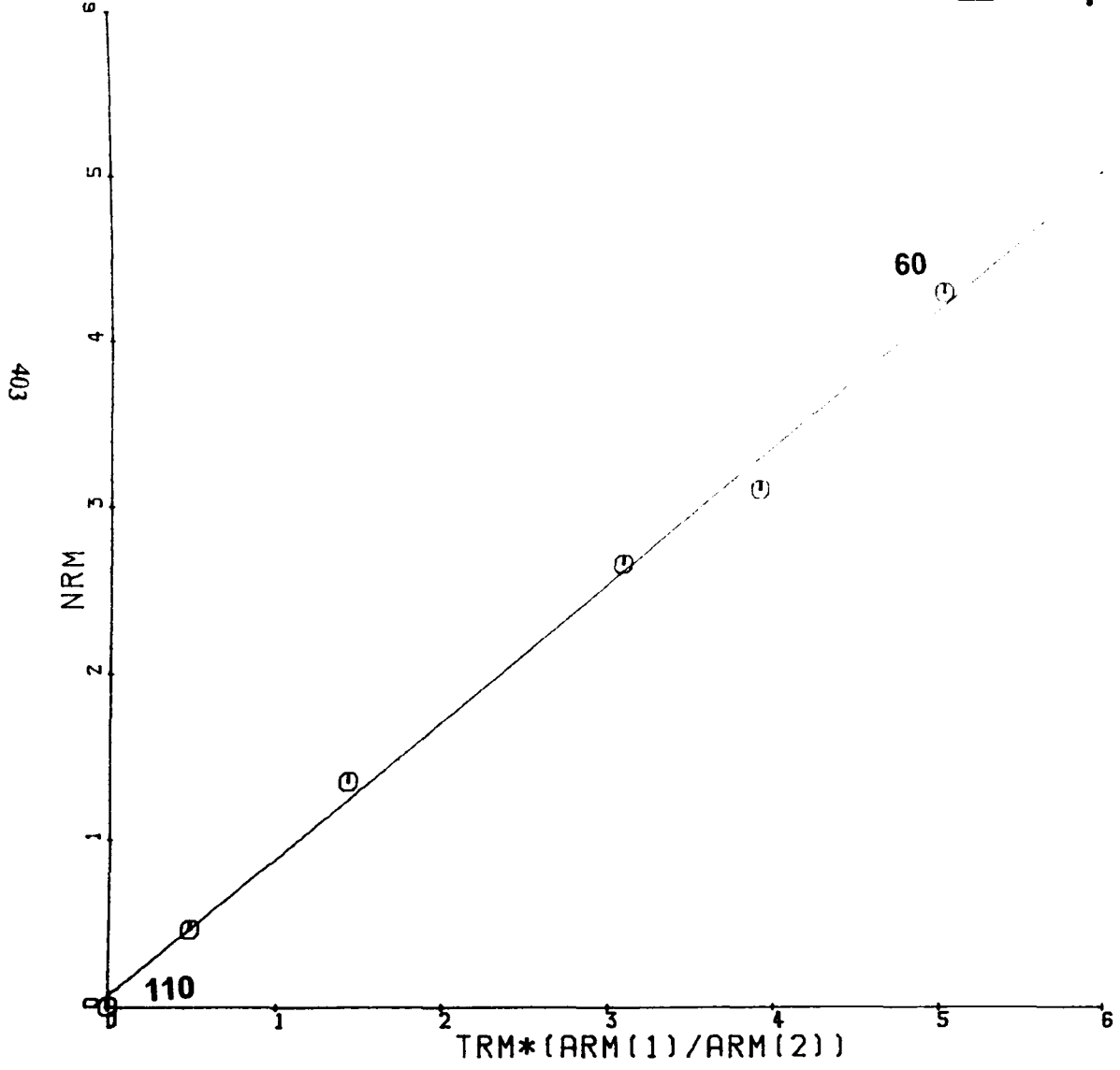

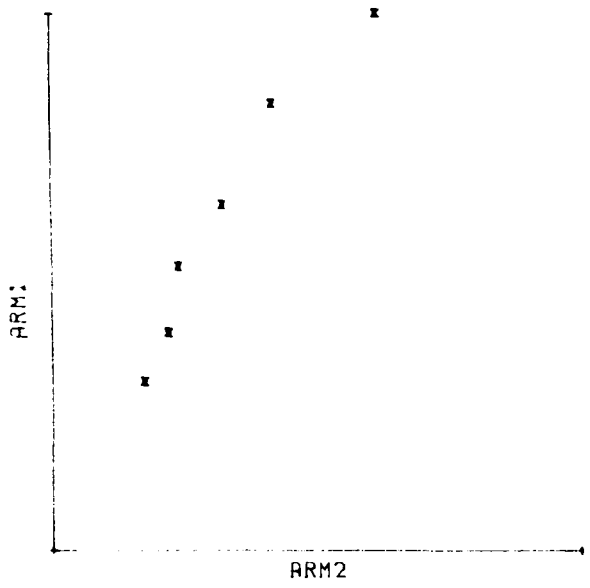

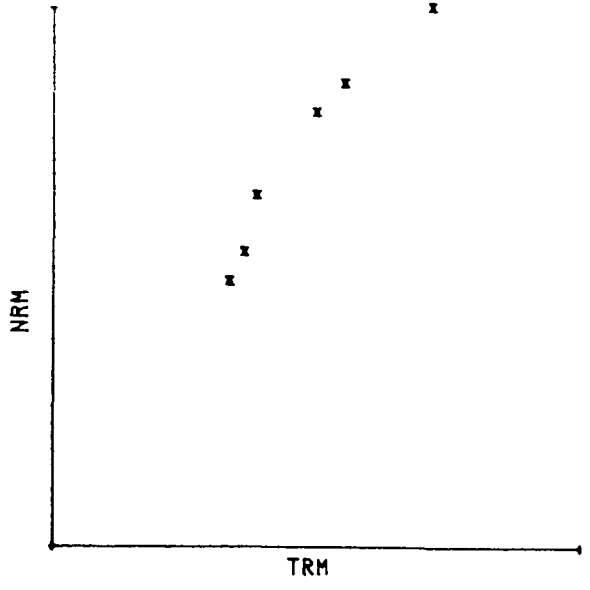

SAMPLE L7-03SQ Ba = 7.7 ± 0.7μT

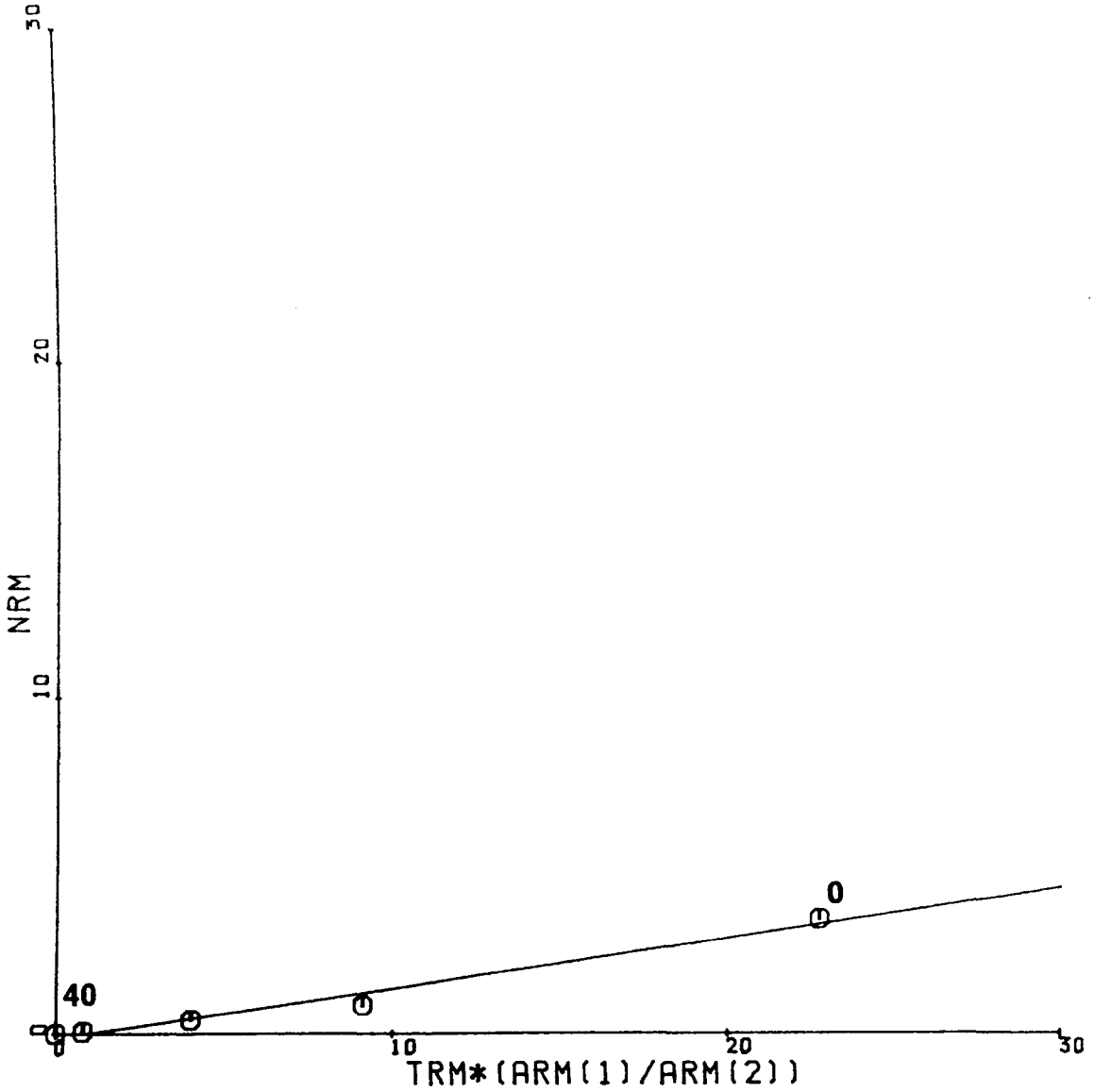

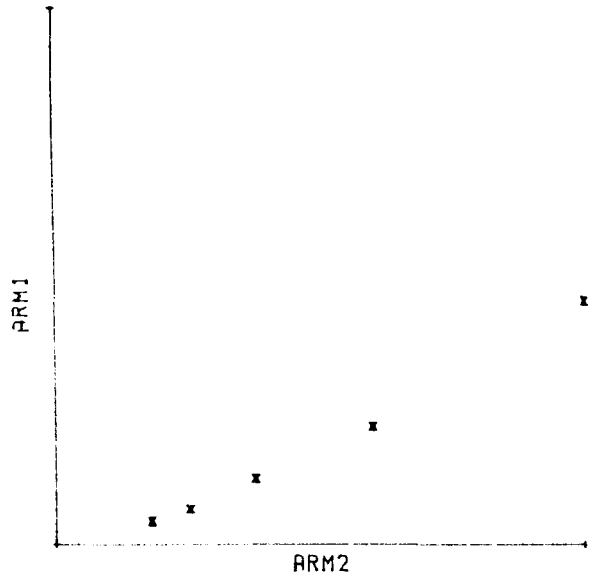

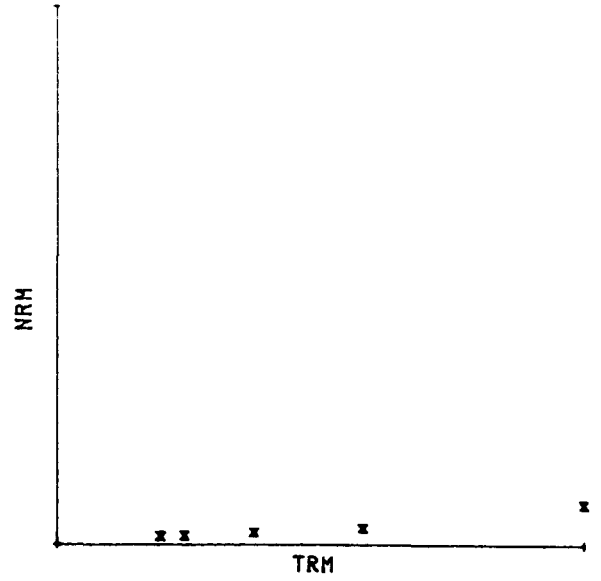

SAMPLE L9-03SQ Ba = 52.4 ± 1.3μT

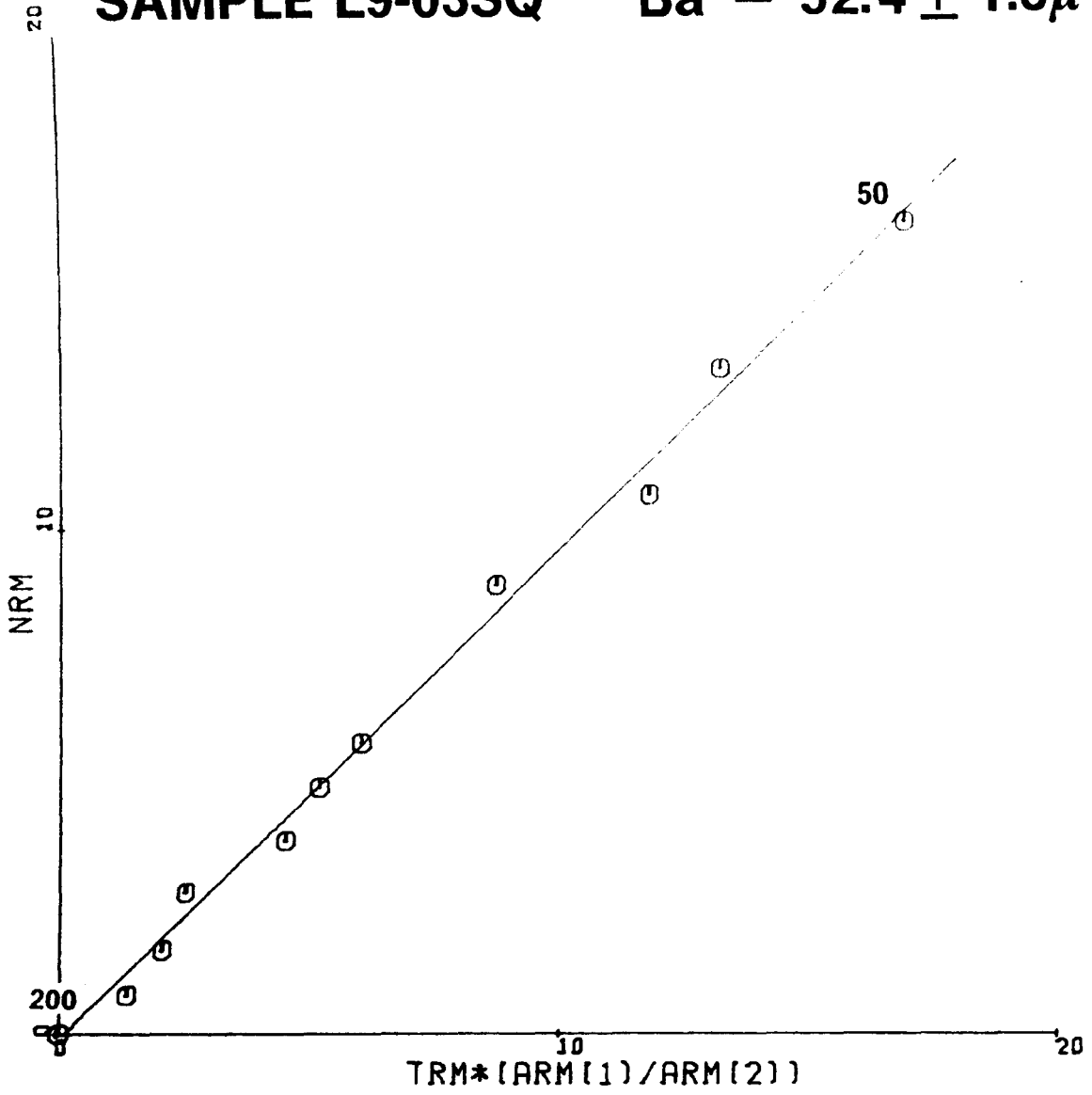

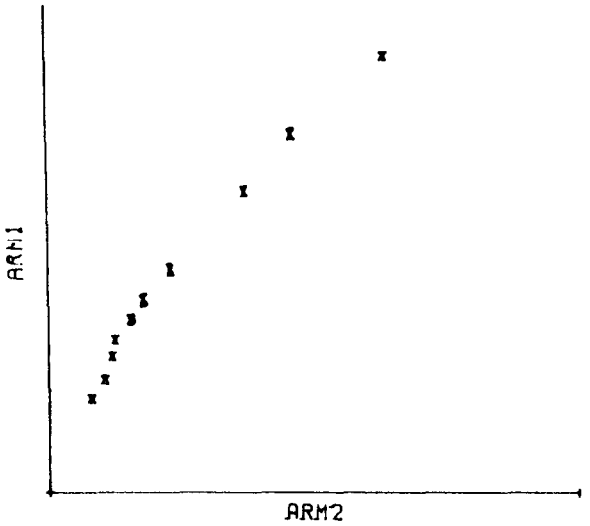

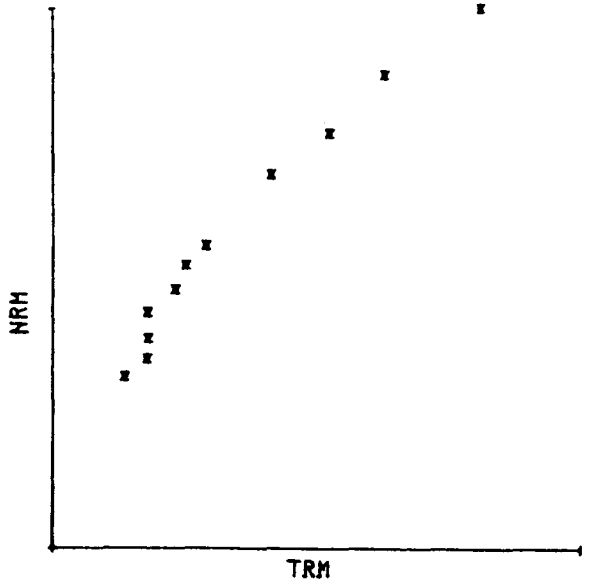

SAMPLE L8-01SQ Ba = 14.6 ± 0.5μT

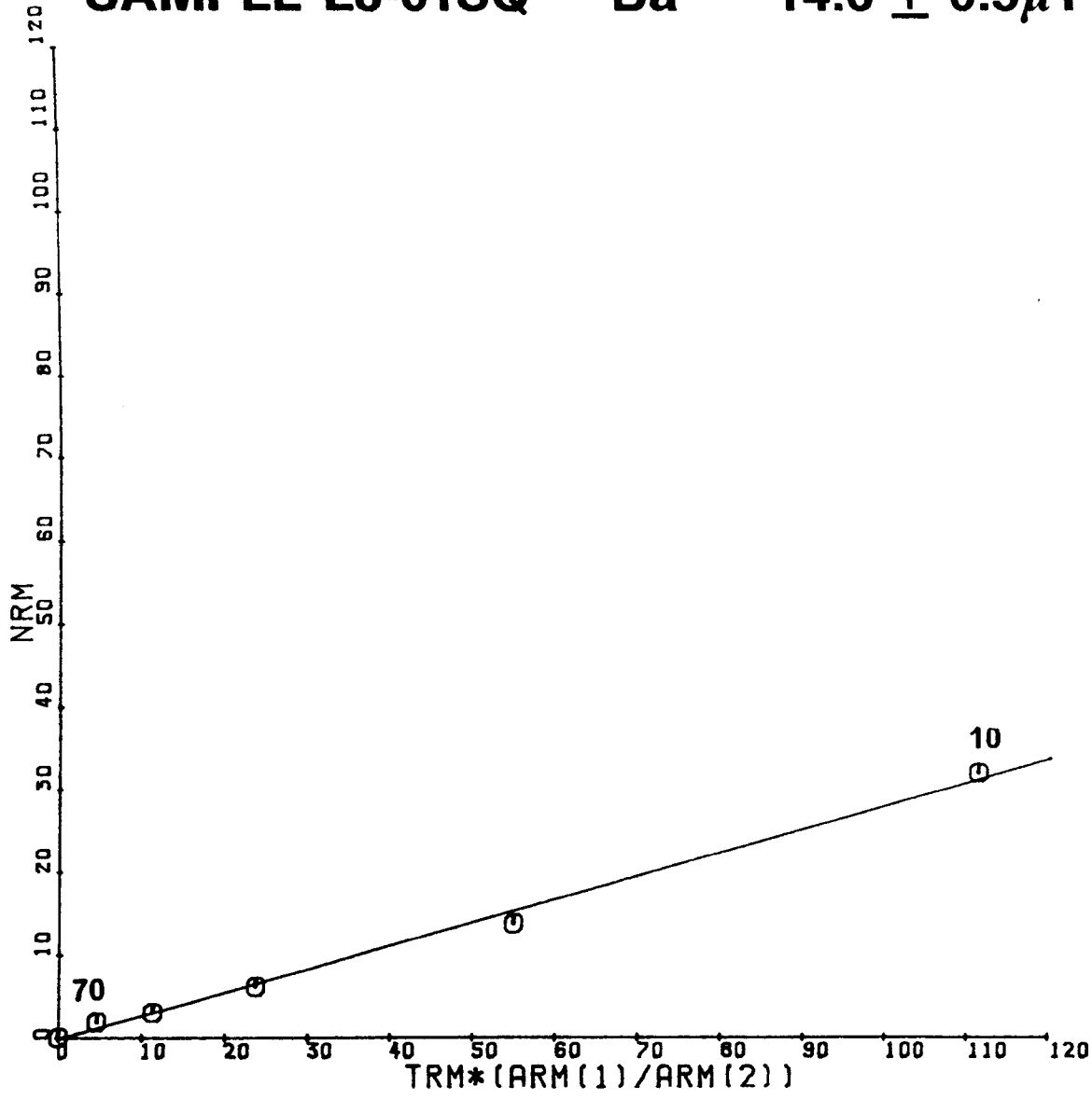

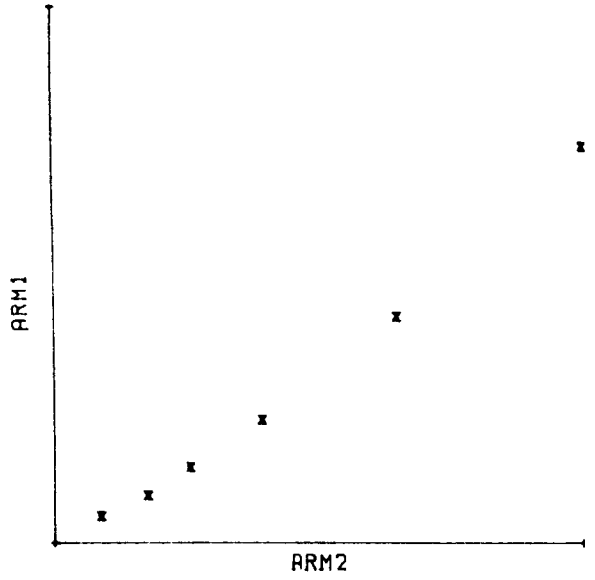

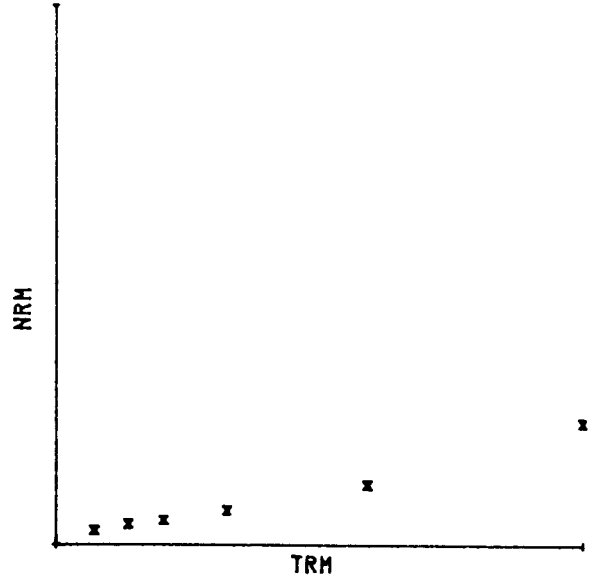

SAMPLE L10-01SQ Ba = 45.9 ± 3.0μT

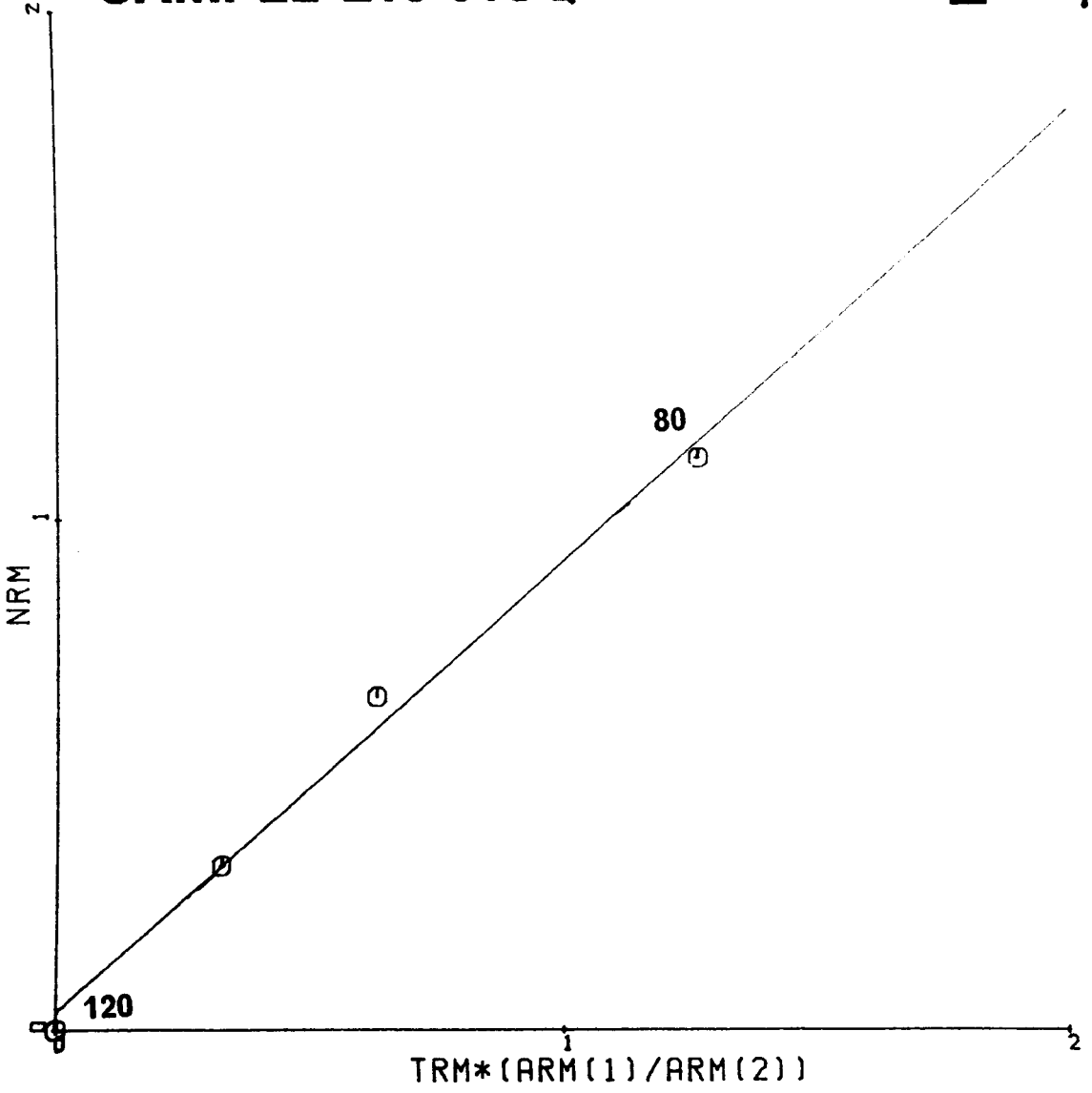

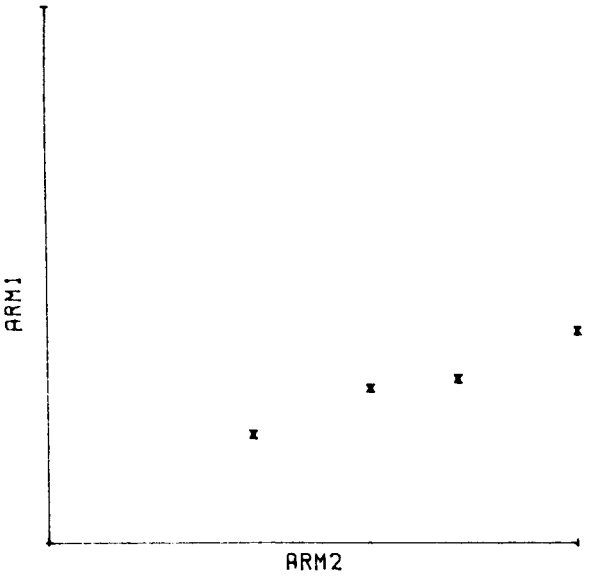

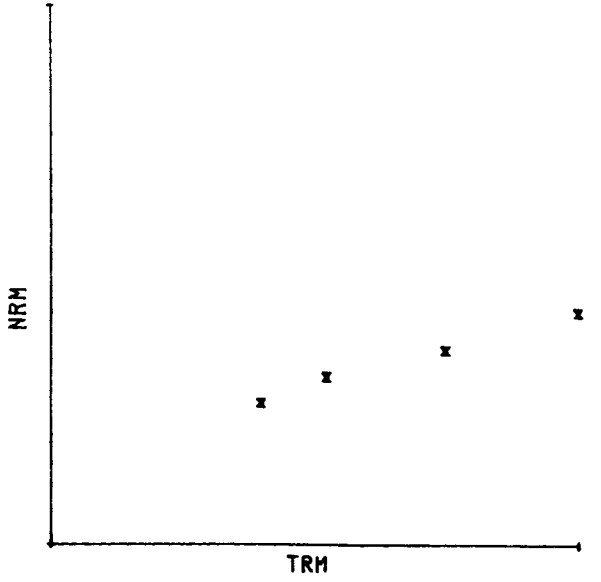

SAMPLE L14-02SQ Ba = 36.9 ± 1.7μT

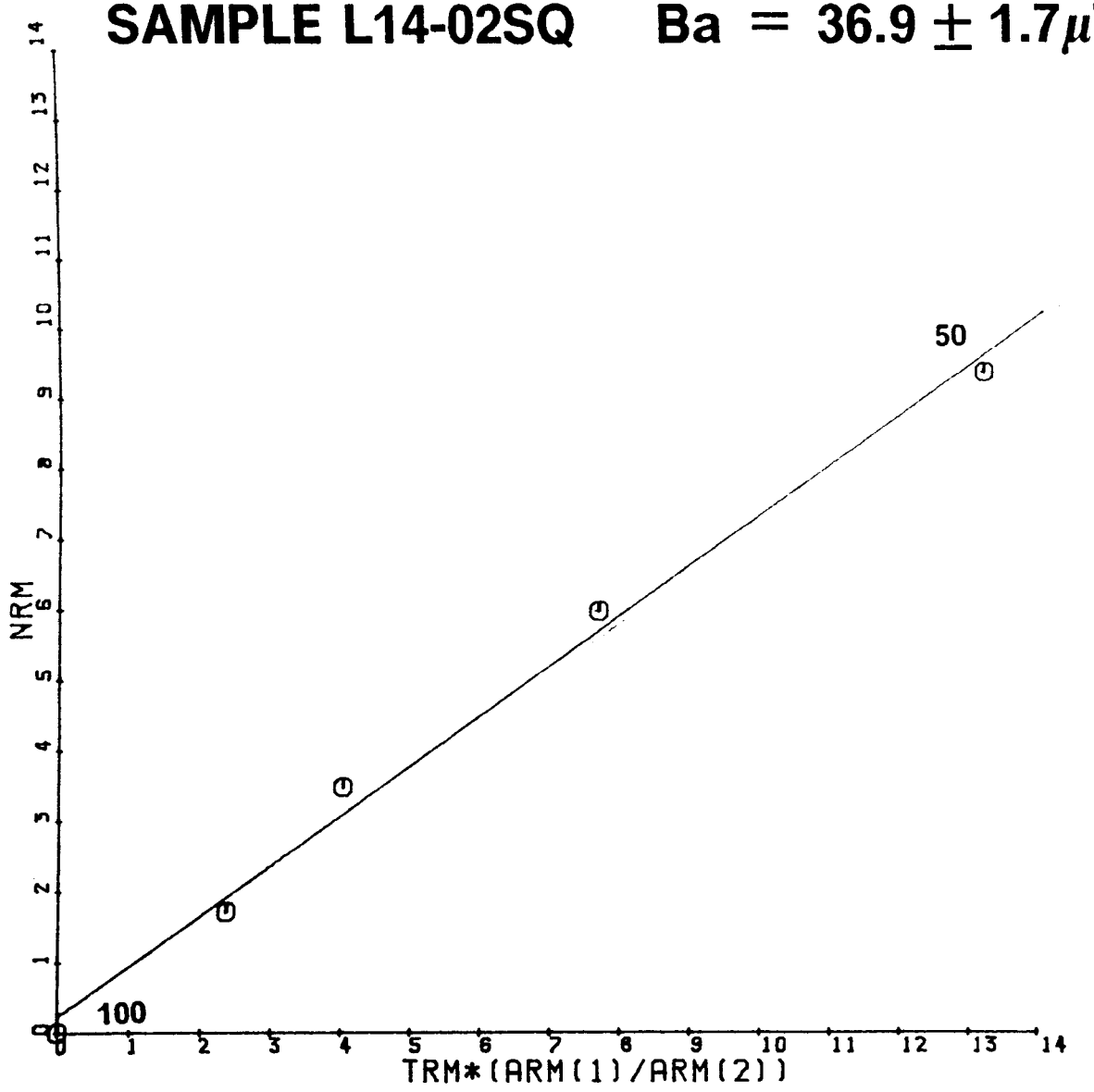

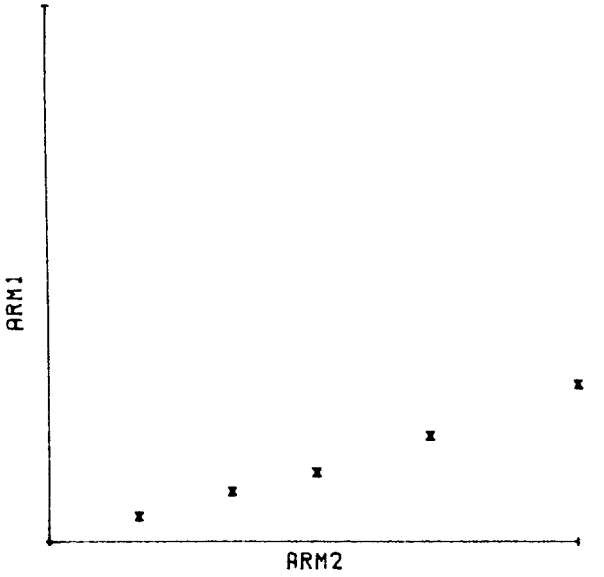

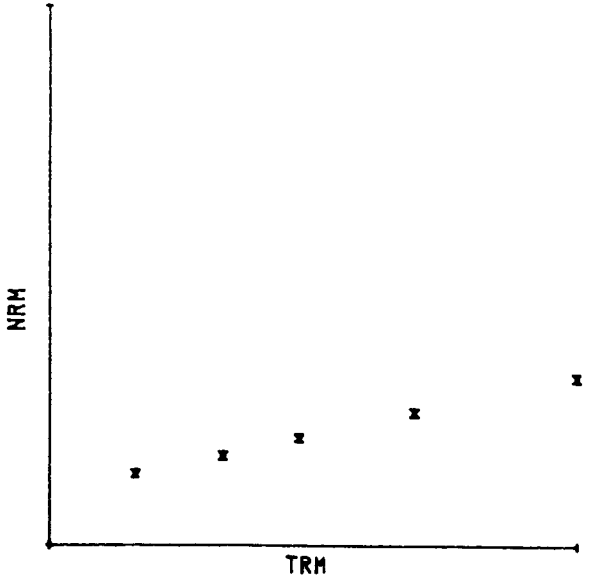

SAMPLE L14-03SQ Ba = 43.6 ± 0.7μT

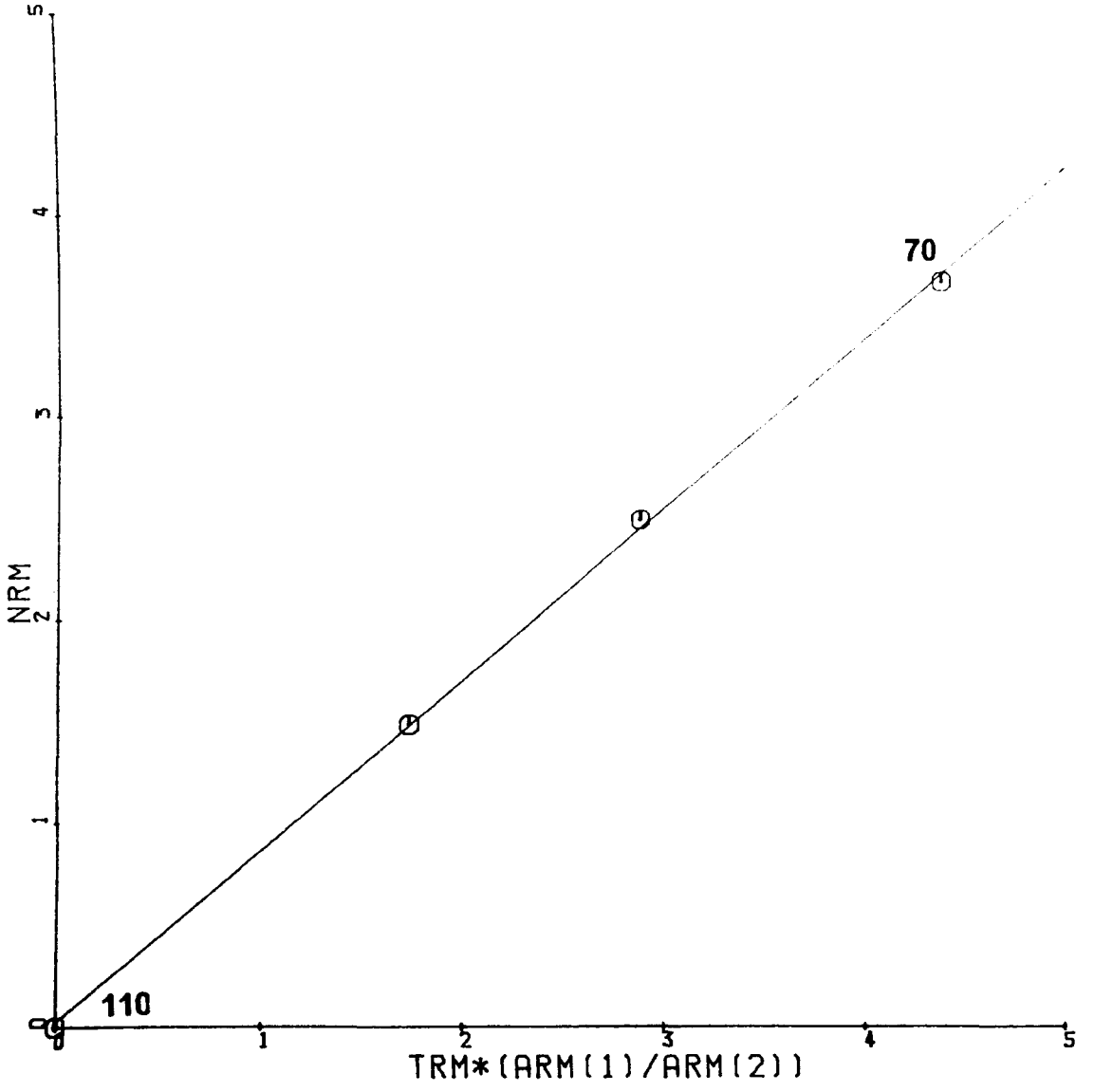

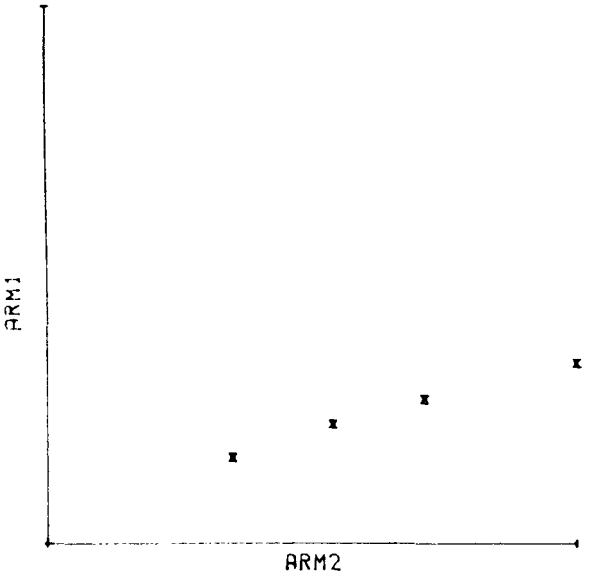

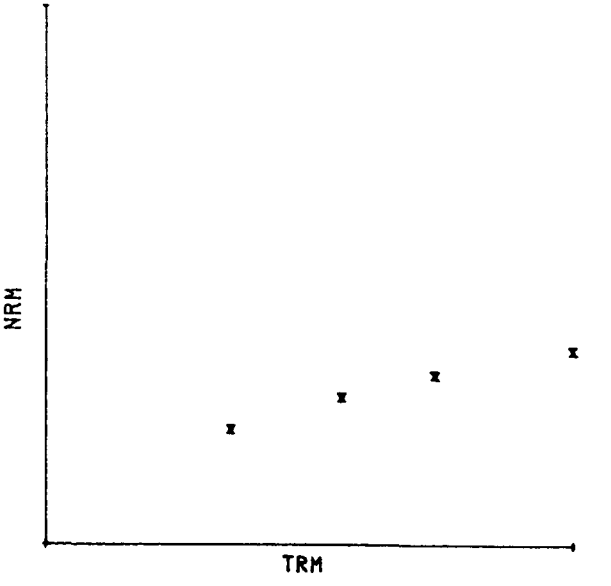

409

SAMPLE L20-03SQ Ba = 23.6 ± 0.3μT

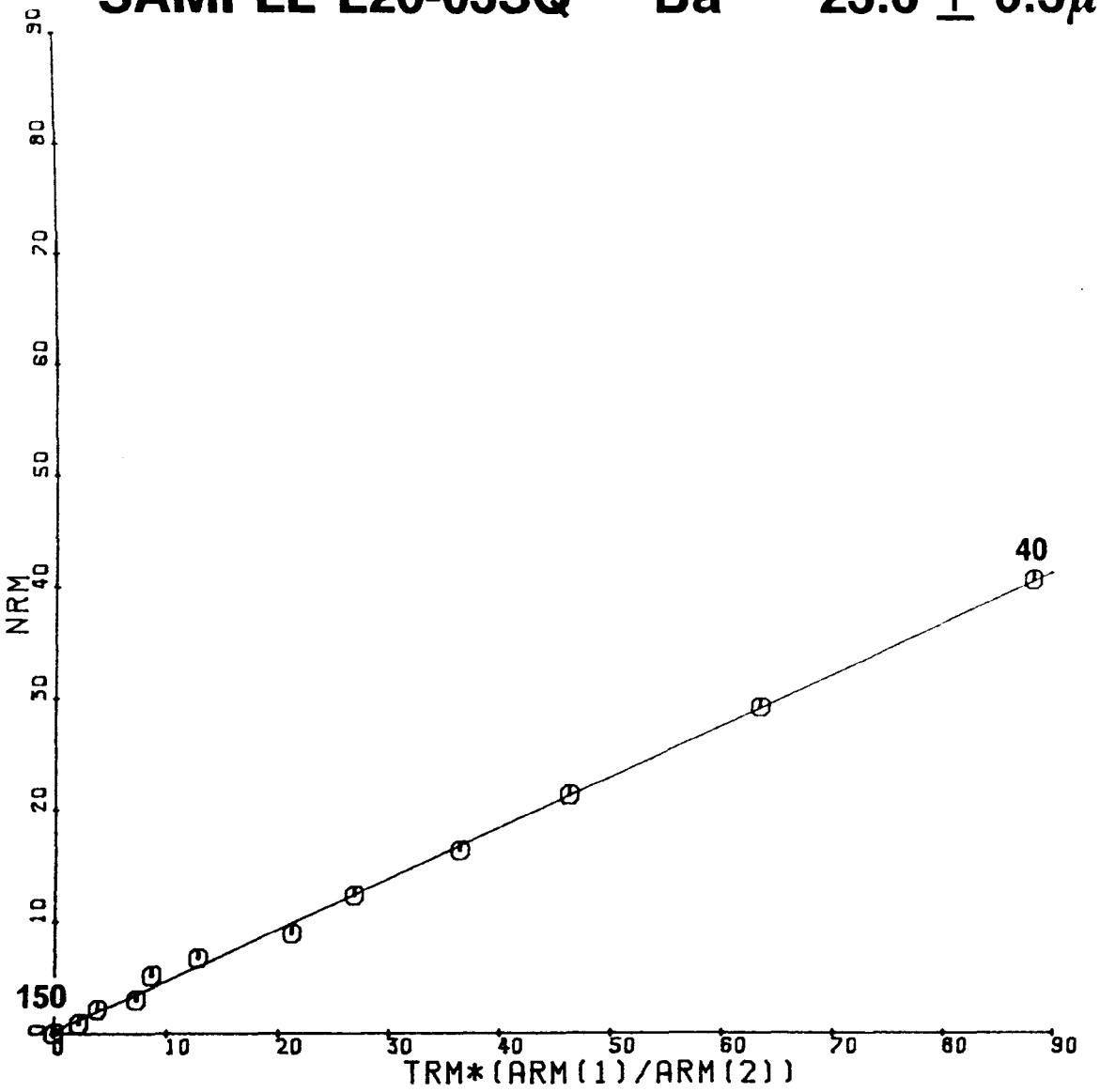

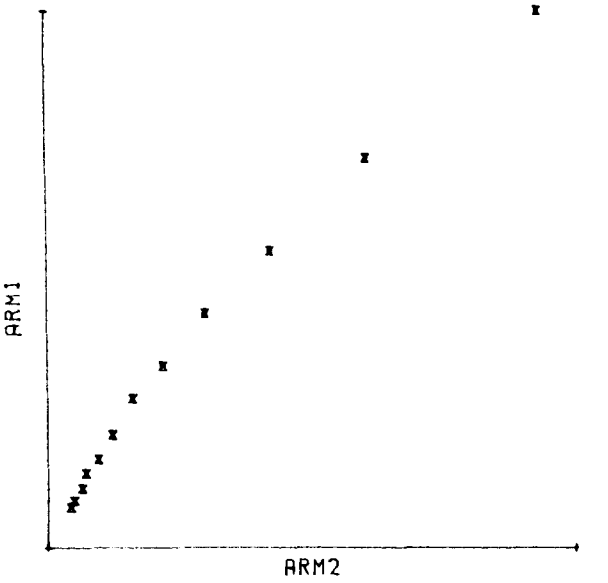

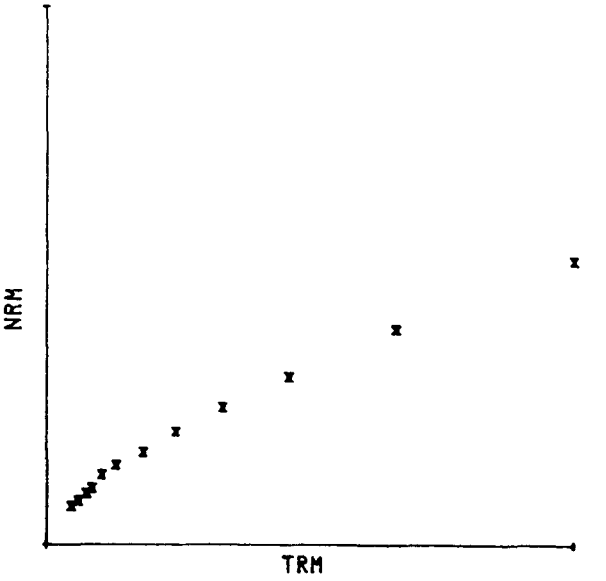

SAMPLE L21-01SQ Ba = 30.0 ± 1.3μT

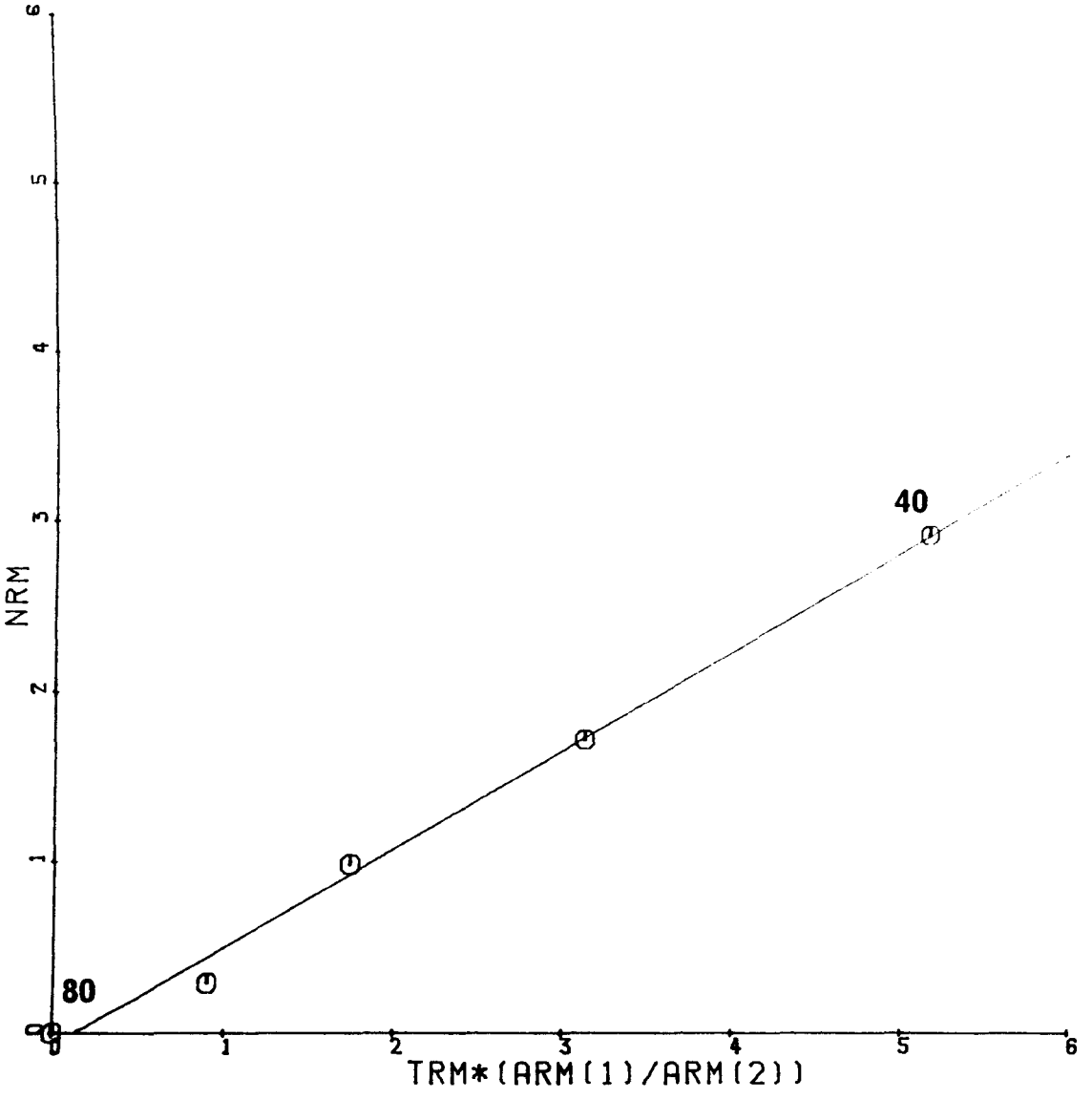

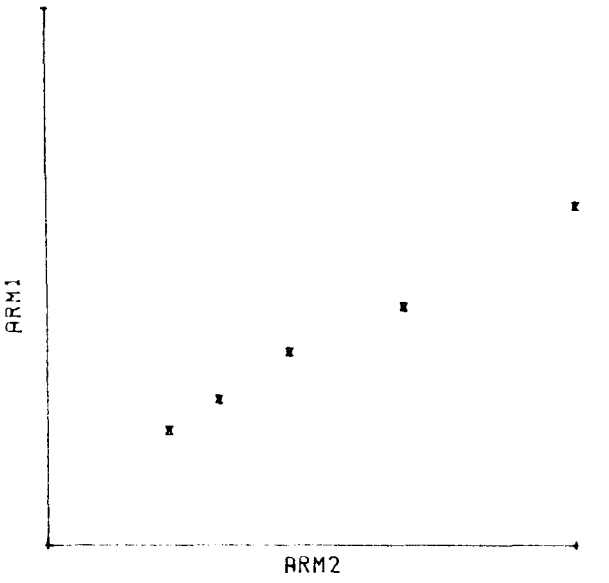

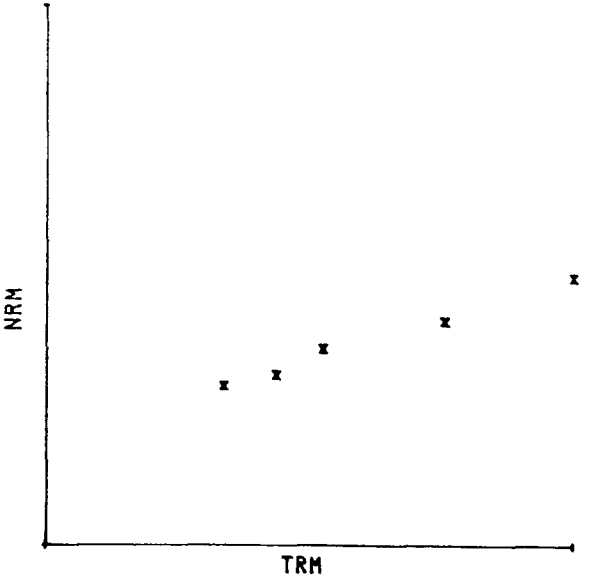

SAMPLE L23-02SQ Ba = 28.0 ± 2.6μT

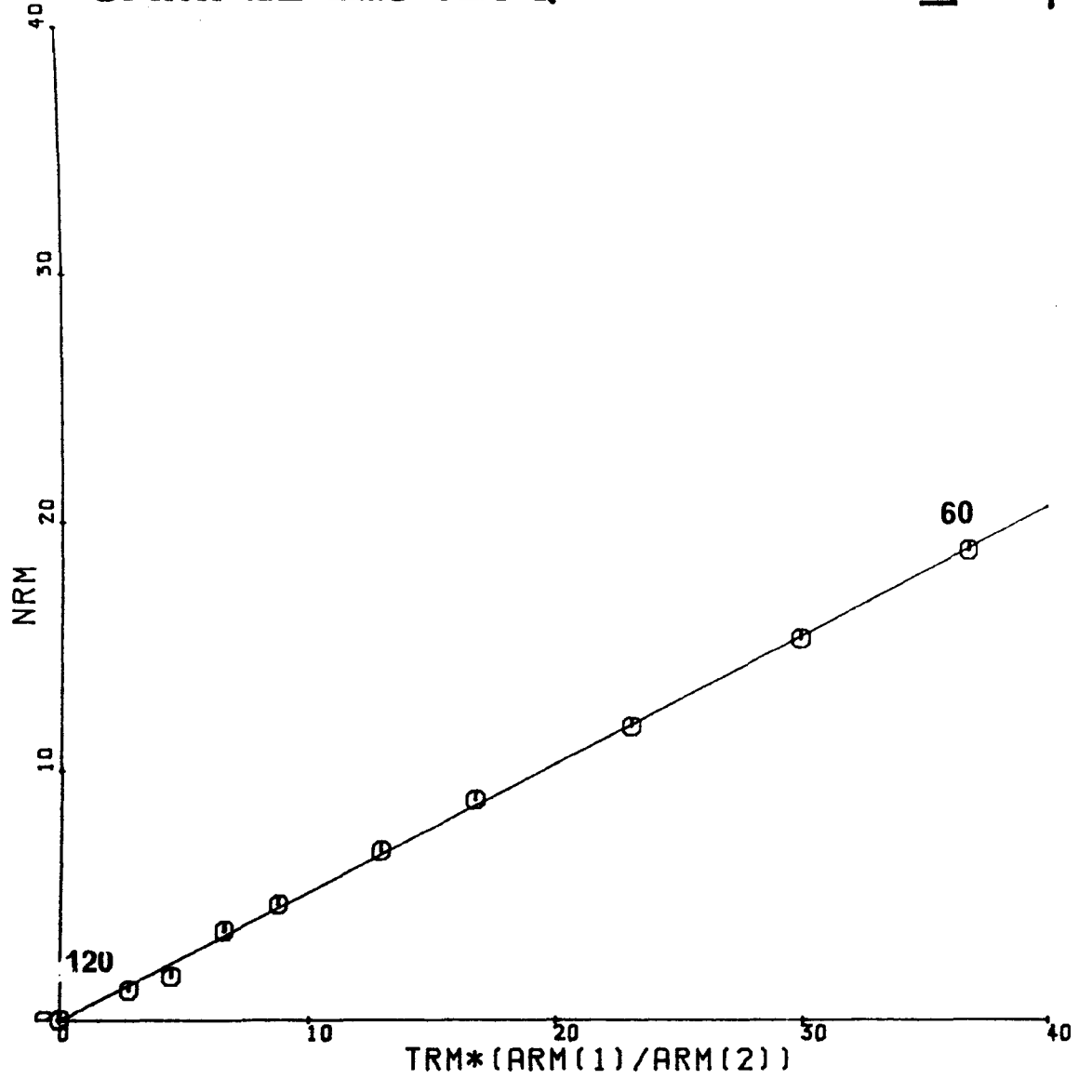

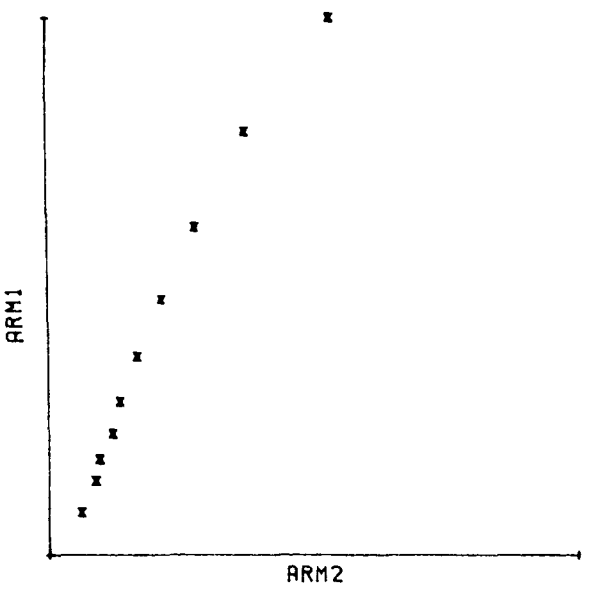

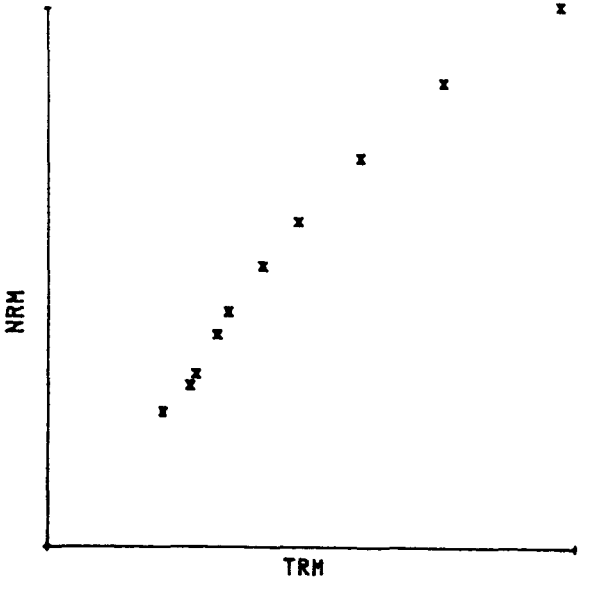

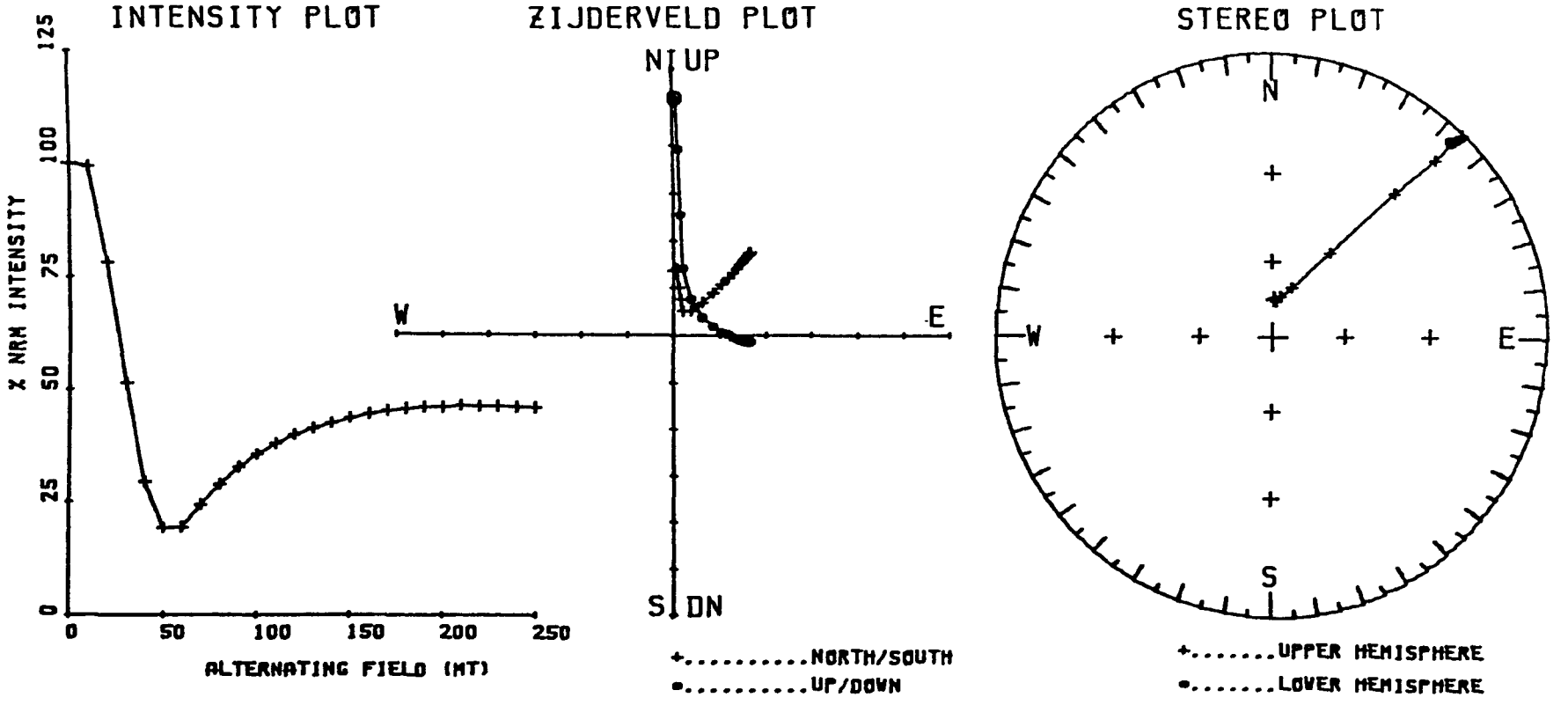

Figure 6.13 : An example of a Gyroremanent magnetisation (GRM) acquired by a lava sample during static a.f. demagnetisation in a modified Shaw experiment, using the automated cryogenic magnetometer.

Figure 6.14 : Modified Shaw palaeointensity plots (R-S) for the Middle Lava Formation. See Figure 6.12 caption for explanation of the plots.

SAMPLE M16-09S Ba = 3.6 ± 0.3μT

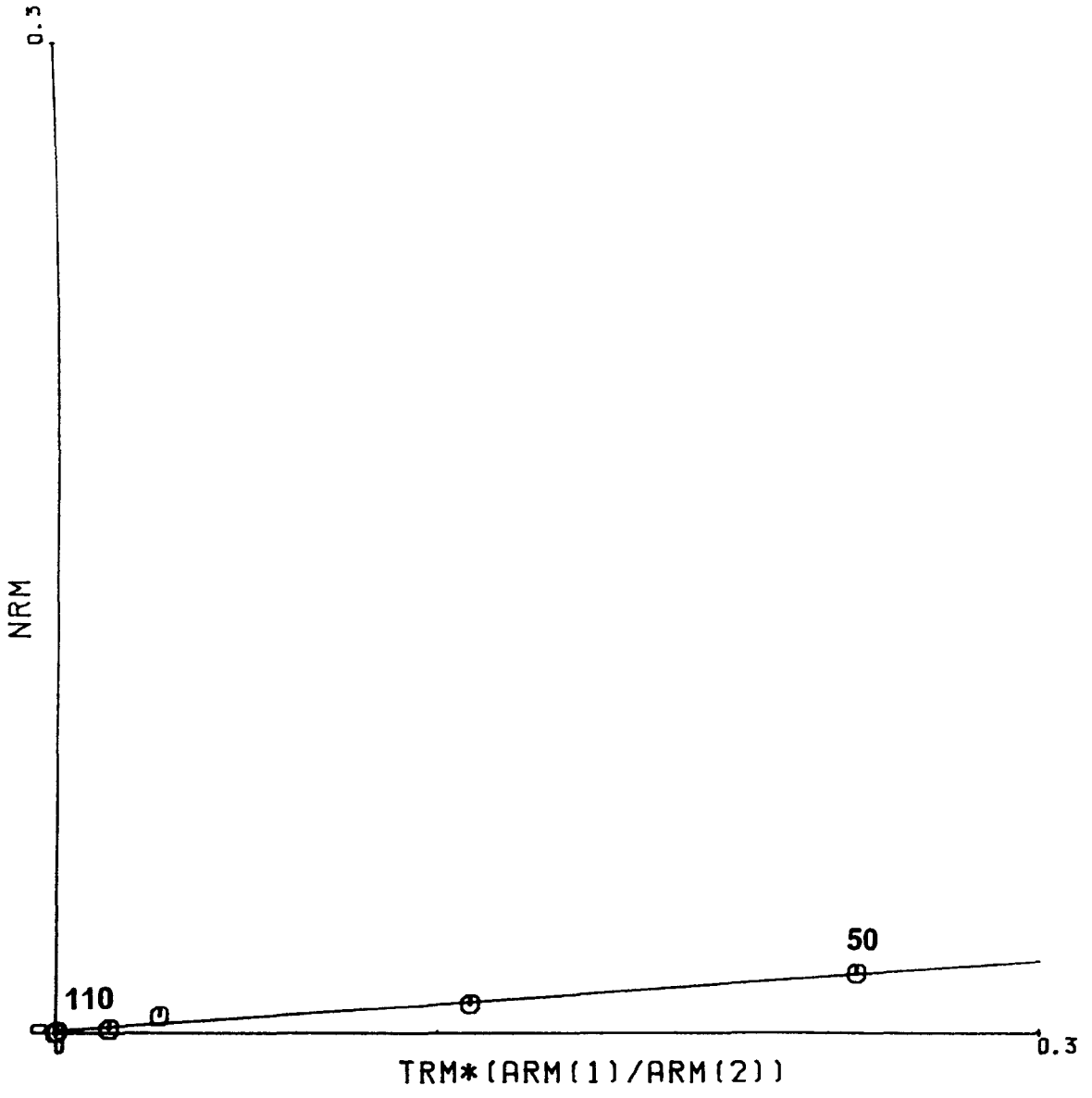

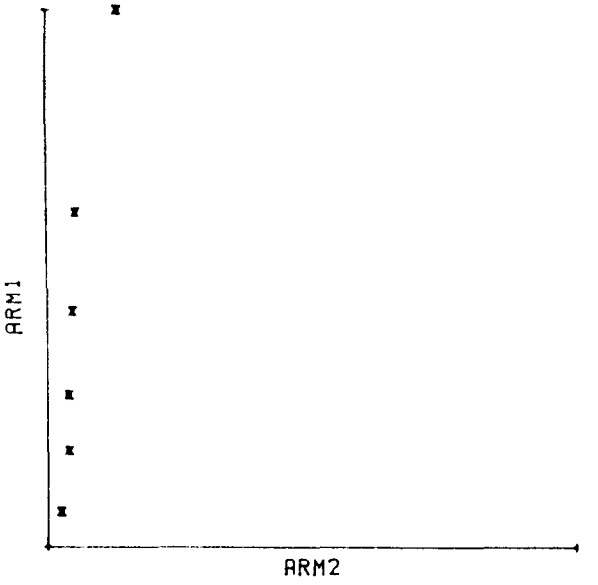

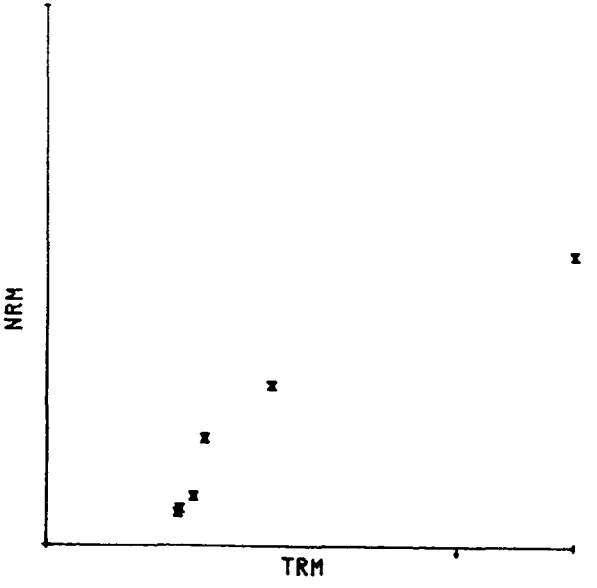

415

Figure 6.15 : Modified Shaw palaeointensity plots (R-S) for the Upper Lava Formation. See Figure 6.12 caption for explanation of plots.

SAMPLE U4-07S Ba = 10.7 ± 0.3μT

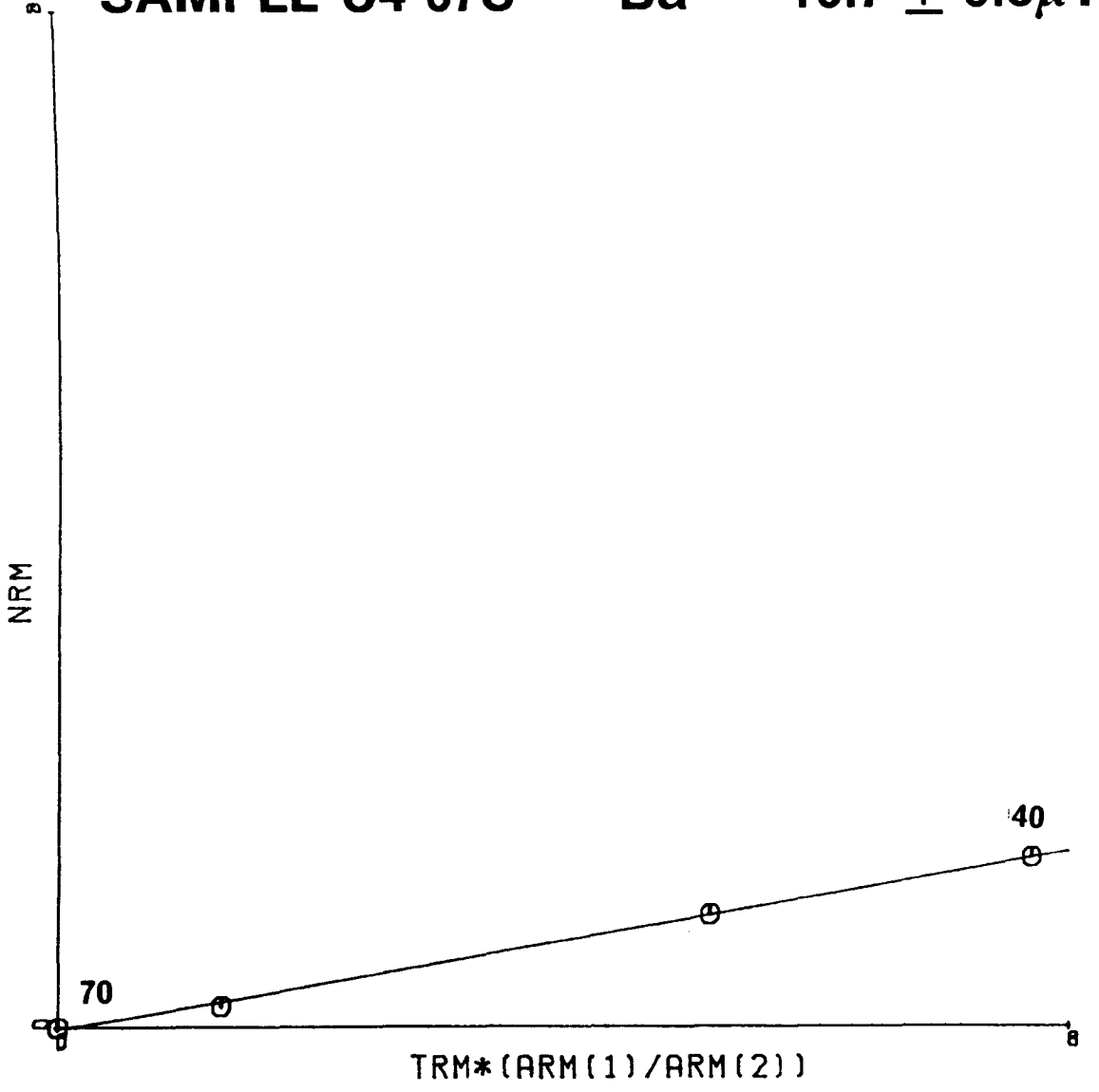

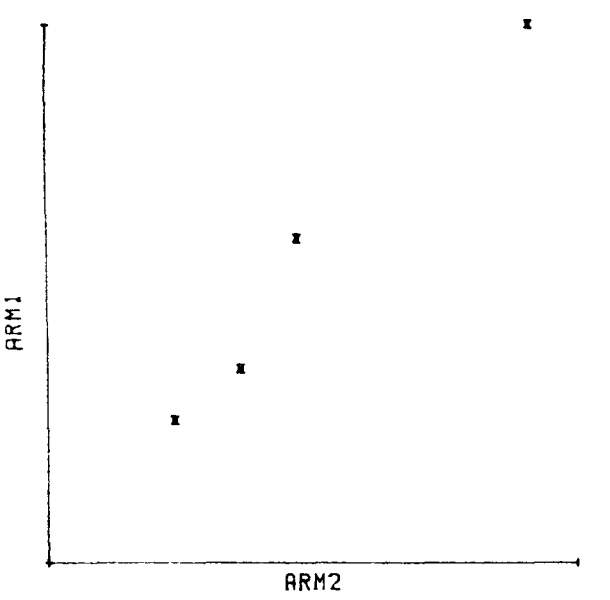

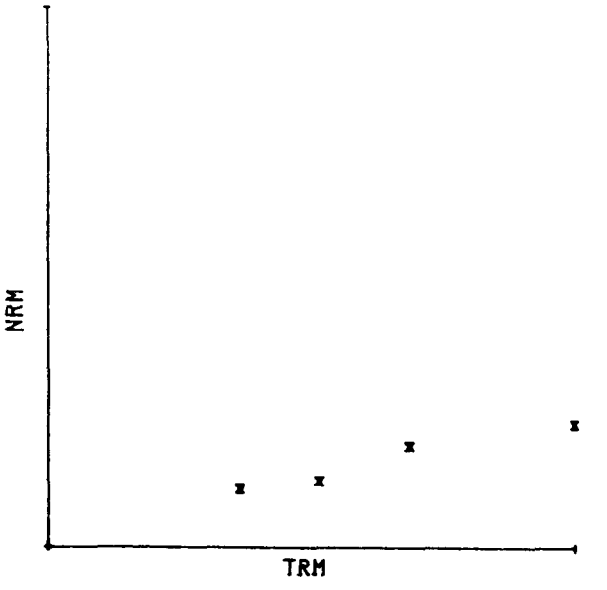

SAMPLE U5-07S Ba = 20.3 ± 0.7μT

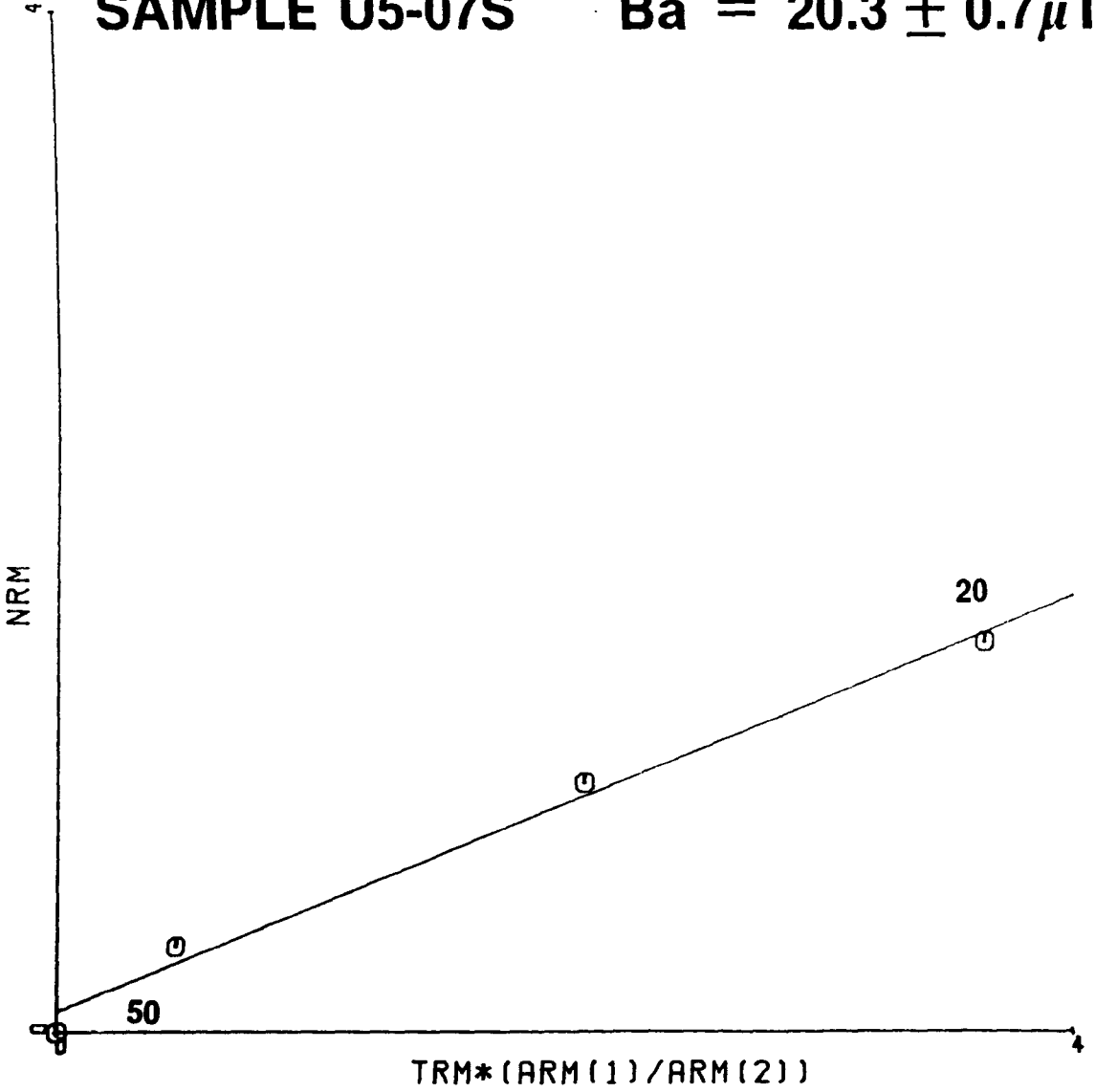

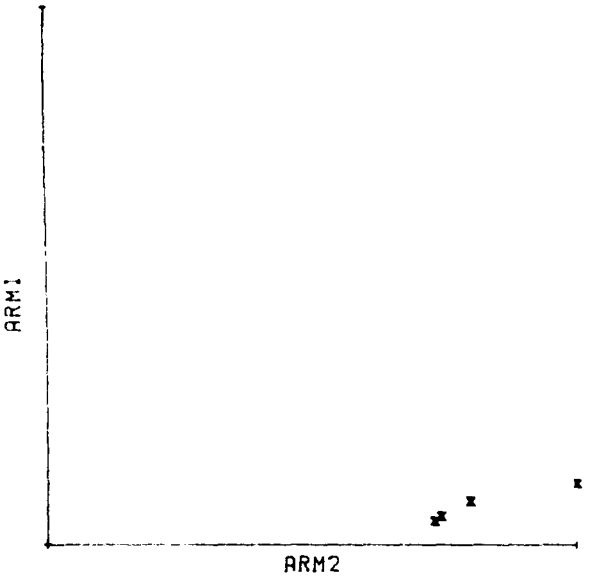

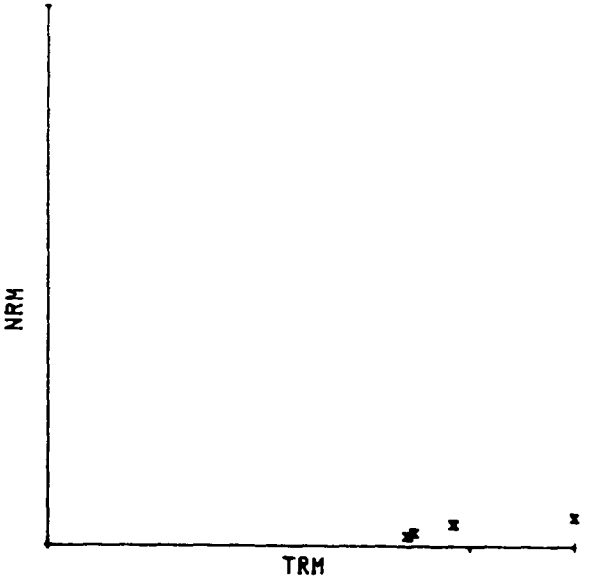

SAMPLE U8-06S Ba = 1.1 ± 0.1μT

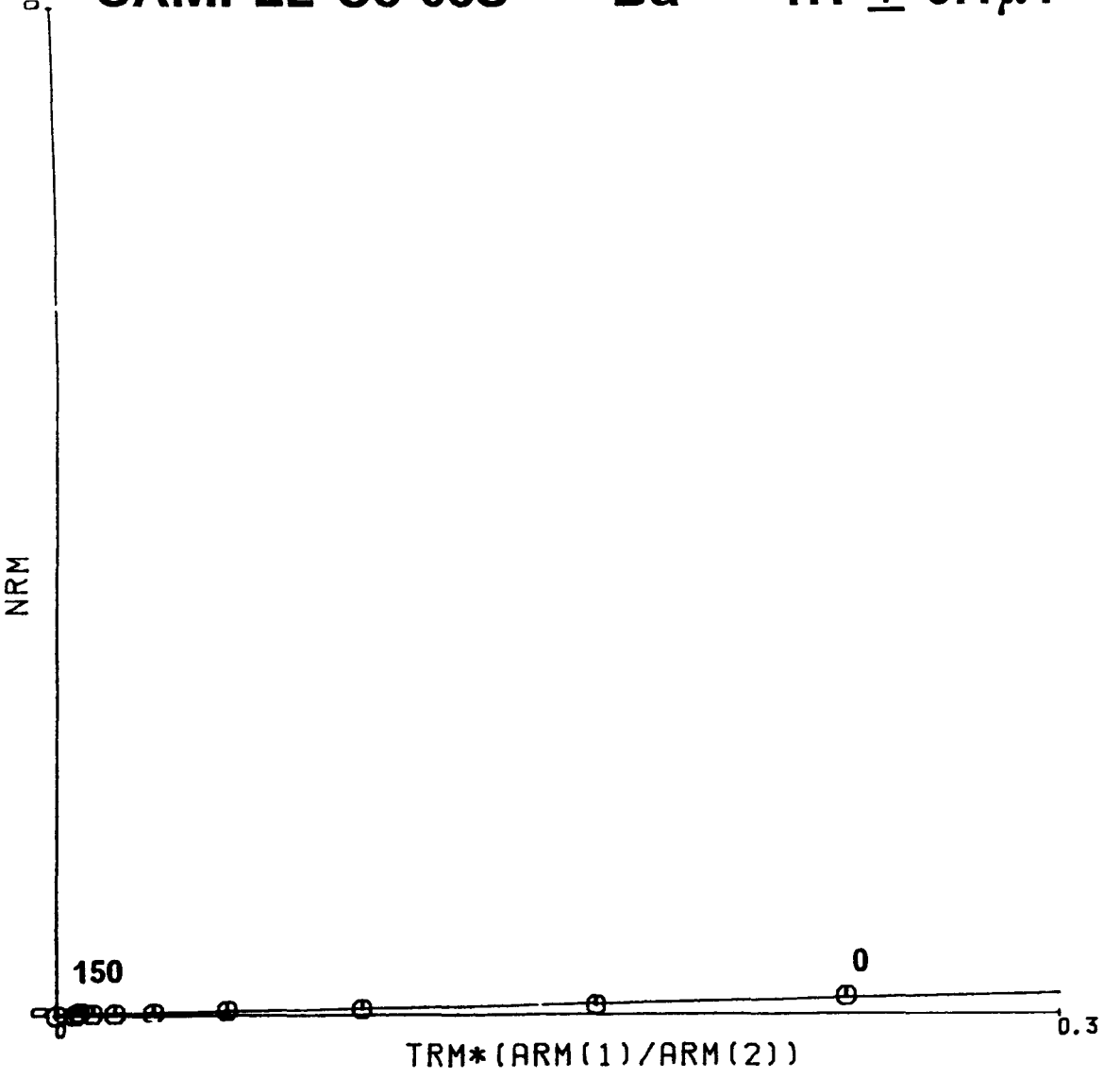

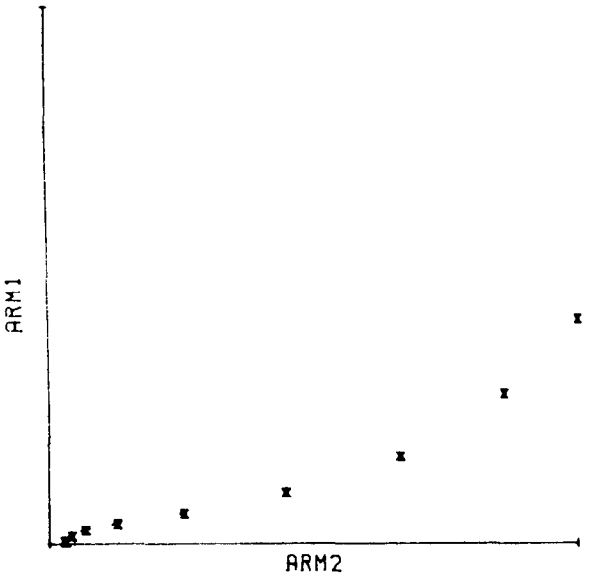

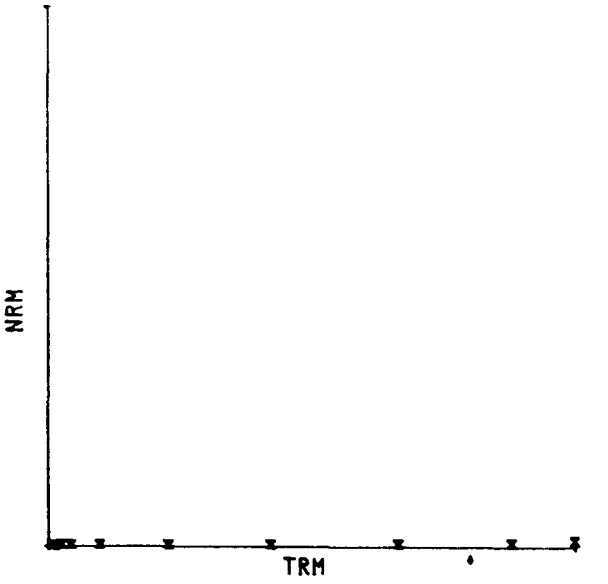

SAMPLE U16-02S Ba = 23.3 ± 0.7μT

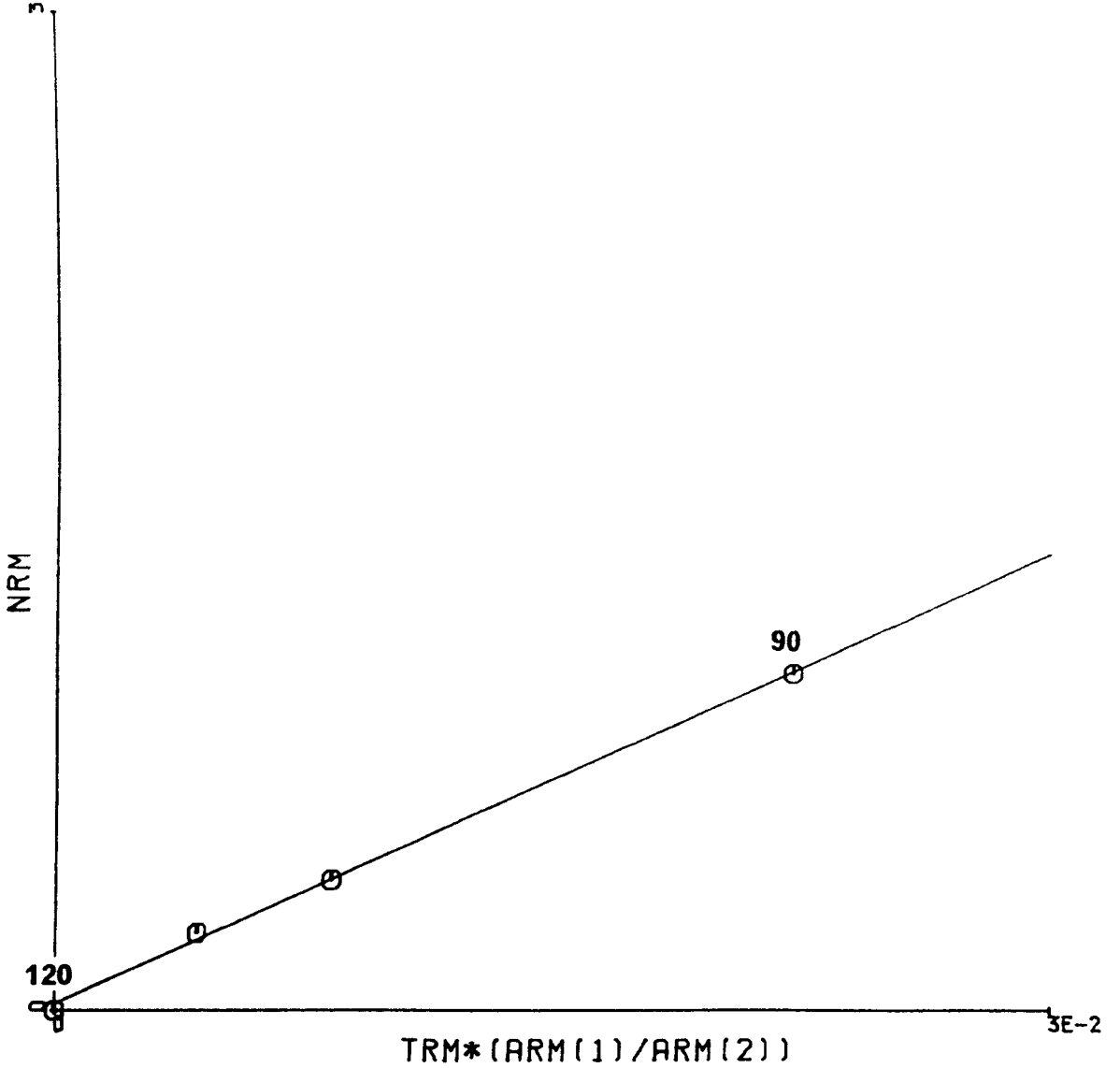

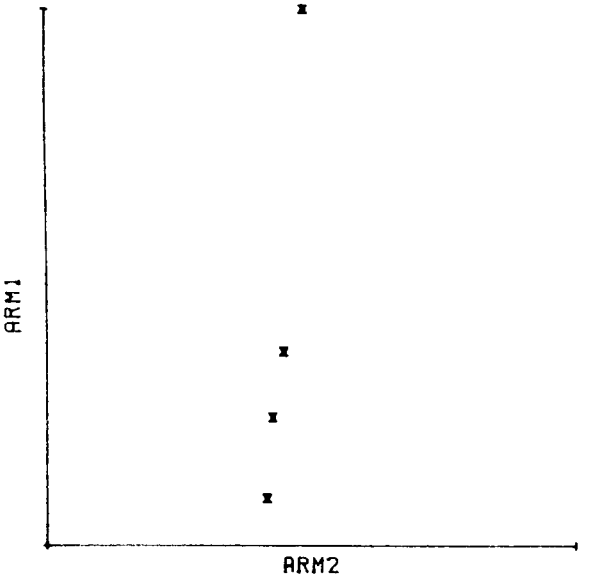

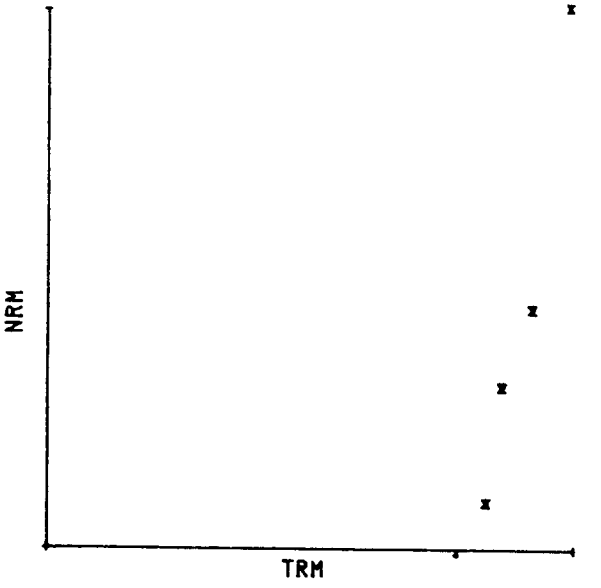

6.13.3 The Upper (Ilimaussaq) Lava Formation.

Forty-seven samples from this thickest stratigraphic formation in the EG were used, thirty-two of which were rejected on the grounds of either showing an instability to a.f. demagnetisation, or having haematite as the magnetic mineral. Of the remaining samples only six yielded results, which are listed in Table 6.7 and illustrated in Figure 6.15. These results were obtained from the lowest part of the coercivity spectrum (0-40 mT) which casts doubt upon their reliability, for the reasons previously explained. Three of the fifteen samples used gave Class 2 ARM1-2 plots, one gave a linear (Class 1) plot and eleven gave Class 3 plots, indicating the creation of softer material on heating. None of the results obtained were comparable to the corresponding modified Thellier results (Section 6.8).

6.14 DISCUSSION OF RESULTS

It is clear from the success rate of the modified Shaw experiments that the samples most suited to the use of this technique of palaeointensity determination are those from the Lower (Mussartût) Lava Formation. The reasons for this are obvious; the samples from this group show the greatest stability to a.f. demagnetisation, generally having single component remanences and rock magnetic results show that they possess the greatest amount of single-domain (SD) magnetite which is essential to the success of palaeointensity experiments.

The Upper Lavas, in contrast, are not suitable for modified Shaw experiments. Their instability to a.f. demagnetisation due to the predominance of multi-domain (MD) grains of magnetite results in their

failure to produce reliable palaeointensity estimates. Rolph and Shaw (1985) suggest that the reason for this failure is that grain size changes induced by heating in the MD coercivity region ($< \simeq 60$ mT) will probably affect the apparent susceptibility ratio of ARM to TRM more severely than those for the SD region. The Thellier results from the flows of the Upper Formation are also in doubt because it is clear that the main remanence carrier is MD magnetite, which is believed to be unsuitable for use in this palaeointensity technique since the blocking and unblocking spectra are not believed to be equivalent.

Some samples in the Lower Formation, and most in the Upper Formation, give non-linear ARM1-2 plots and low palaeointensity values. These samples contain the greatest amount of MD material and consequently most of the remanence is lost in the low coercivity region, with the result that no remanence remains in the higher coercivity region. Therefore, the gradient of the corrected NRM-TRM diagram (R-S plot), and thus the palaeointensity value, is very low. The reasons for this are not obvious but could be related to the process which results in the formation of the MD material. Results obtained from these samples should be treated with caution.

The success rate of samples run on the SQUID magnetometer was encouragingly high. Some samples, which failed to give reliable results on the spinner because they were unstable at fields above 100 mT, gave acceptable results on the SQUID (e.g. L8, L10, L13 - Tables 6.4-6.5) because the SQUID is more sensitive than the spinner so it can measure smaller amounts of SD material. Clearly then, demagnetisation and measurement in zero field, using the SQUID, improves the quality of the results from all samples

but particularly those which have only a very small fraction of SD material. In view of this, it is recommended that a SQUID magnetometer be used for all samples but especially those which are in the grey area between being stable and unstable to a.f. demagnetisation on the spinner, e.g. samples which have rock magnetic characteristics on the boundary between RM sets 1 and 2, defined in Chapter 7.

In summary, the magnetic mineralogy of the Gardar lavas ensures that most flows are not suitable for use in palaeointensity determination with the modified Shaw technique. The Upper Lavas are largely unsuitable due to the dominance of MD grains of magnetite in the magnetic mineralogy. The Middle Lavas are predominantly haematite-bearing and are thus also unsuitable. However, the greater fraction of SD material in the mixed magnetite grain size present in many flows from the lower formation makes them more resistant to a.f. demagnetisation and hence more suitable for use with the modified Shaw technique. Also, generally they have single component remanences which is preferred for the use of this technique.

A factor which will affect all intensity determinations is that due to the difference in the natural cooling rate (present during acquisition of the NRM) and the artificial cooling rate used in laboratory experiments. For example, in nature, it may take tens of years for the centre of a thick flow to reach the ambient temperature, but in the laboratory the time taken for a sample to cool from its Curie temperature is approximately 45 mins. Fox and Aitken (1980) found that intensities obtained using rapid cooling during TRM acquisition were 7% higher than the known result. McClelland-Brown (1984) obtained important results from artificial samples. For a sample containing a low concentration of SD magnetite, a 15% increase in TRM

intensity was observed for a factor of 50 increase in cooling time. However, for samples containing a high concentration of SD magnetite and those containing PSD and MD grains, the reverse was observed. Slower cooled TRMs were weaker than the rapidly cooled TRMs, a result which is not consistent with kinetic theory and is probably due to grain interactions. The implication of these observations is that palaeointensity results for MD grains will be lower than the correct value. However, the theory behind these observations is not well constrained and it is difficult to make a correction for this cooling rate difference. It is possible, though that the palaeointensity values calculated in this chapter may be underestimates of the Early Gardar field.

6.15 COMPARISON OF THELLIER AND SHAW RESULTS

Due to the small number of results obtained from the modified Shaw technique it is difficult to make meaningful comparisons for either the upper or middle lava groups. However, the acceptable results obtained from the lower group using both the spinner and SQUID magnetometers allows some comparison to be made with the results obtained by the modified Thellier technique on sister samples and separate samples from the same flow.

Of the 18 samples for which accepted results were obtained using both techniques, 12 samples gave values which were within 15% of each other. Figure 6.16 plots the palaeointensities determined from the accepted Thellier palaeointensity estimates against those obtained using the Shaw technique for a sister sample from the same core. There is an equal scattering about the 45° line which suggests that there is no systematic or significant difference in the values obtained using the two methods.

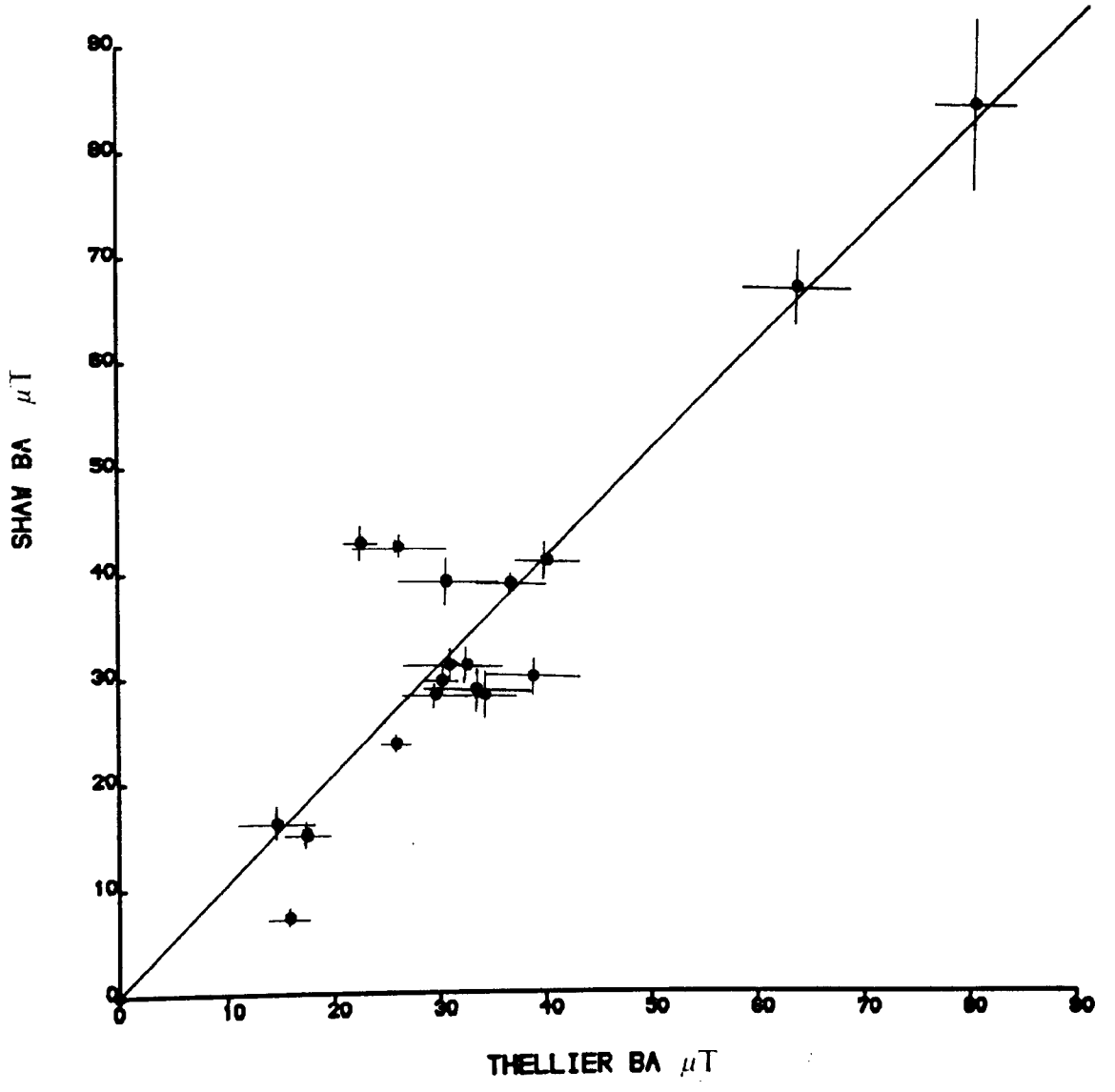

Figure 6.16 : Comparison of palaeointensity results determined by the modified Thellier and the modified Shaw techniques. For perfect agreement between results from two techniques, points should lie on the 45° line.

An interesting point arising from the comparison is that a small number of modified Shaw results, obtained from the lower coercivity region, agree well with the corresponding Thellier results (Tables 6.1, 6.4 and 6.5). Since these Shaw results are probably obtained from MD grains of magnetite, the agreement suggests that the Thellier results may also be recorded by MD grains within the mixed grain size of pure magnetite. Boshakov and Shcherbakova (1979) have suggested that MD grains are of little use in Thellier experiments because the remanence held by them does not unblock until just before the Curie temperature. This casts a doubt on the validity of the Thellier results but, in itself, may be a useful guide to the reliability of some Thellier results obtained from rocks with a magnetic mineralogy similar to that of the Gardar lavas. A useful experiment which could be performed to further analyse this would be to use low temperature demagnetisation (for example by immersing the samples in liquid nitrogen in zero field) prior to performing Thellier and Shaw experiments to eliminate the remanence held by MD grains. This would allow a direct comparison of results obtained from samples with both MD and SD grains with those containing no MD material in order to estimate how important the MD contribution is in Thellier experiments. Unfortunately, this experiment was not carried out due to time constraints.

Overall, the best agreement between results from the two techniques was obtained from samples with the characteristics of RM set 1 (Chapter 7), i.e. those containing the largest SD fraction in a mixed grain size of pure magnetite.

The palaeointensity results obtained using both techniques require thought as to what they actually represent. To avoid erroneous interpretations from

unsuitable samples, rock magnetic tests must be used to identify samples which are most likely to give reliable results, i.e. those with a significant SD fraction. Bearing this in mind, it was decided that a method for the selection and rejection of samples for use in palaeointensity experiments, which incorporates detailed rock magnetic tests, was needed. The next chapter describes such a technique and compares the Thellier and Shaw results in greater detail.

CHAPTER 7 : A NEW METHOD FOR DETERMINING THE SUITABILITY OF BASALTS FOR PALAEOINTENSITY ANALYSIS

7.1 INTRODUCTION

There are many problems associated with palaeointensity work (e.g. Coe, 1967; Pesonen, 1978) but the two which most dictate the success or failure of experiments are:

1. The failure of many rocks to comply with the fundamental requirement for palaeointensity work - namely that the natural remanent magnetisation (NRM) of a rock must be a primary unaltered thermoremanent magnetisation (TRM) (Nagata, 1943). This happens as a result of physical and or chemical changes which occur subsequent to the formation of the rock.

2. Alteration of the rock during laboratory heating, resulting in changes in the chemistry of the rock. Palaeointensity experiments involve heating the rock and this has the drawback that it provides the opportunity to alter the chemistry (usually by oxidation) and, importantly, its magnetic mineralogy.

The concept of sample selection for palaeointensity experiments is then, apparently, quite simple; a sample must have a stable NRM which is a primary TRM or TCRM (acquired during or just after initial cooling) and have a magnetic mineralogy which is less likely to undergo thermal alteration during laboratory heating. Several workers have attempted to provide criteria which can be used to isolate such samples.

Prévot et al (1985) and subsequently Derder et al (1989) used two important criteria for determining the suitability of samples for use in palaeointensity experiments: repeatability of stable NRM directions for adjacent samples

after a.f. demagnetisation and the possession of a single, high Curie temperature with a reversible curve (Type 2a of Mankinen et al, 1985). Only 18 out of 220 samples (8%) in the Derder et al (1989) study satisfied these criteria and were subsequently used. Senanayake and McElhinny (1982) suggested a simple selection criterion based on low temperature susceptibility (KLT) results only. They claim that of the three types of behaviour described by Senanayake and McElhinny (1981), Group 2 samples are the most suited because they are believed to contain deuterically oxidised titanomagnetites with exsolved ilmenite lamellae which effectively subdivide the grains into elongate SD grains of magnetite. As a result of their advanced oxidation states (Classes II and III of Wilson and Watkins, 1967), Group 2 samples show resistance to alteration during laboratory heating. Senanayake et al (1982) present palaeointensity results from Tertiary basalts selected on the basis of the KLT criterion. Out of 716 samples, only 149 (21%) were selected using this criterion. The remainder were discarded.

The common complaint with the selection procedures of both Prévot et al (1985) and Senanayake et al (1982) is that samples which did not pass their selection test were omitted, without trial, from palaeointensity experiments. This brings into question the validity of the selection procedure, which can only be judged by comparing the success of those samples selected by the technique with those samples which fail to fulfil the necessary criteria. Rolph (1984) commented that rigorous application of the Senanayake et al criterion to Carboniferous lavas would have resulted in the rejection of all but one of the 41 samples in his study. However, he investigated all samples and concluded that those which gave palaeointensity results showed no preference for any KLT group. This observation was supported by Sherwood (1986) from studies of Miocene lavas from New Zealand. Furthermore, if this

criterion had been applied to the samples of the present study, none would be selected for palaeointensity work, due to the absence of genuine Group 2 behaviour, as interpreted by Senanayake and McElhinny (1981). There is, then, evidence that (pre-) selection of samples, using only KLT results, is a wasteful approach. Rolph (1991) has found empirically that some historic lava samples which fail to give reliable palaeointensity results (based on agreement with observatory measurements) can be recognised by their a.f. demagnetisation characteristics. These samples show stable tails to their a.f. demagnetisation curves (samples ES3A(1886) and E1607.4B) but show no evidence of haematite from other rock magnetic results. These samples showed Group 2 KLT characteristics and should therefore be highly oxidised and suitable for palaeointensity work. However, the palaeointensity values yielded were too high when compared with known observatory records (Fig. 7.1) and the samples were regarded as probably possessing an NRM which is not a pure TRM and were therefore (pre-)rejected from palaeointensity work.

The aim of this chapter is to present a new approach to the problem of sample selection/rejection for palaeointensity experiments, which utilises rock magnetic results from five techniques and relates them to palaeointensity results from the same samples. This is a more thorough approach than those outlined above.

7.2 THE MATERIAL

A major problem encountered during palaeointensity experiments on ancient basalts is that ideal samples can rarely be found; the magnetic mineralogy is often complex and the thermal history usually unknown. These factors

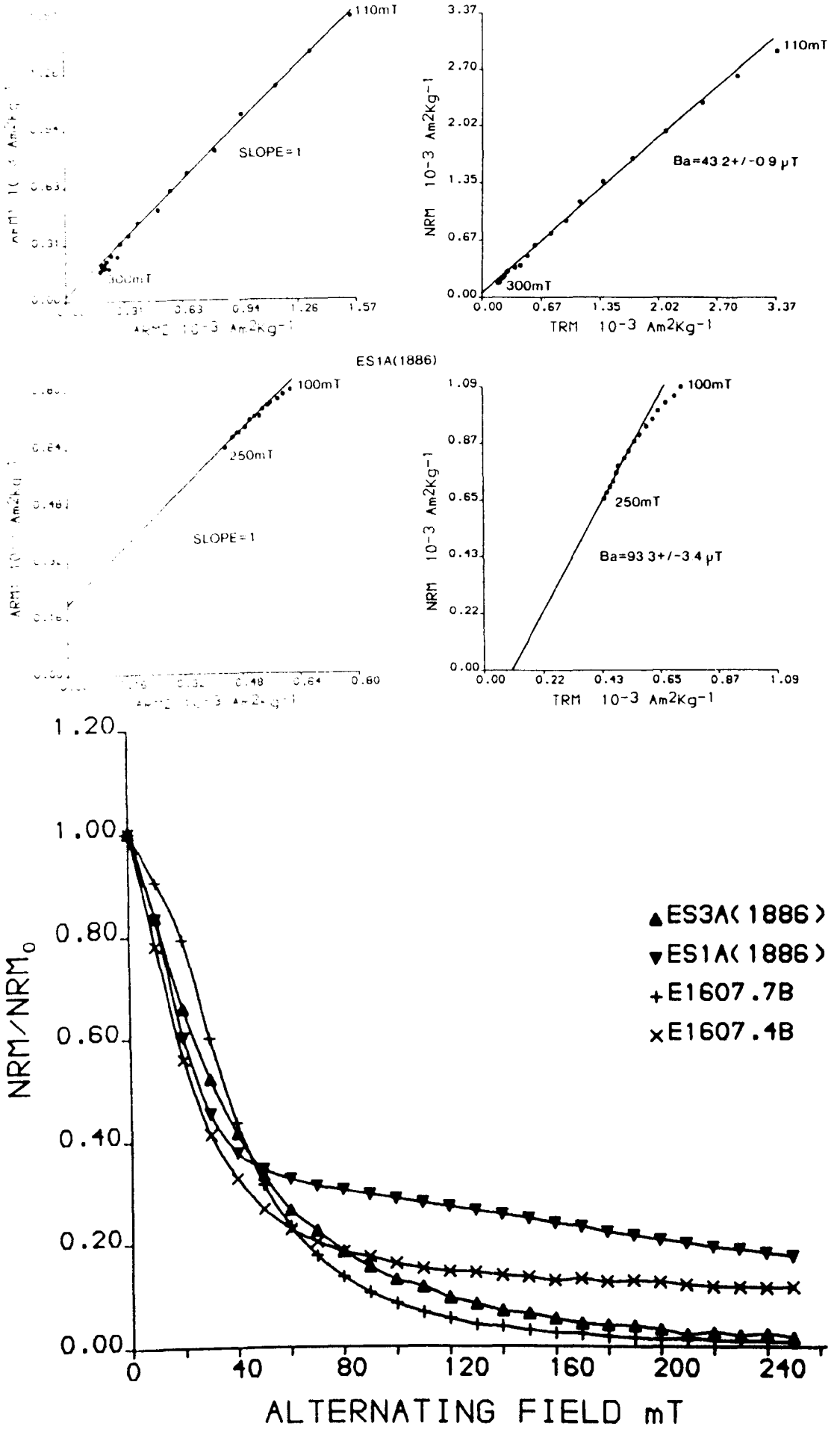

Figure 7.1 : An example of the a.f. demagnetisation characteristics of a recent lava which gives a palaeointensity value which is too high when compared with observatory measurements (from Rolph, 1991).

and the predominance of multi-domain (MD) grains of magnetite in such rocks has led palaeomagnetists to believe that it is unlikely that reliable palaeointensity estimates can be obtained from ancient basalts. Consequently, work has concentrated on younger rocks, resulting in a shortage of field intensity data for ancient rocks, particularly those from the Precambrian. However, it is common knowledge that most ancient basalts, whilst being dominated by MD magnetite, are in fact characterised by mixed grain sizes of pure magnetite where single-domain (SD) grains are also present in varying amounts (Radhakrishnamurty et al, 1991 and Chapter 3). This SD fraction is very important for palaeointensity work, since it is these grains that are more likely to carry a stable, primary TRM for which the blocking and unblocking spectra are identical and the law of additivity of TRM (Thellier, 1951) is obeyed. Thus, it is possible that consistent and acceptable palaeointensity estimates can be produced from ancient basalts, provided samples with a significant amount of SD material in the mixed grain size can be identified. It is necessary, then, to devise a method which can identify suitable samples so that palaeointensity results obtained from ancient basalts can be regarded as offering reliable estimates of the ancient geomagnetic field strength.

The suitability of the Gardar lavas for palaeomagnetic studies (discussed in Chapters 4 and 5), allied with the large amount of rock magnetic data (Chapter 3) and the palaeointensity data of varying reliability (Chapter 6) provide an ideal opportunity to discuss sample selection and rejection criteria for palaeointensity work. The new method only applies to magnetite-bearing samples since both modified Thellier and Shaw results are available for these samples. Thus, only samples from the Lower and Upper Lava Formations are used here.

7.3 THE METHOD

The principle of the method is to categorise all samples, based on information provided by their rock magnetic properties, and subsequently to analyse how each sample behaves during palaeointensity experiments. Patterns of behaviour are identified from the rock magnetic and palaeointensity results and a set of criteria are established which govern the selection and rejection of samples for either the modified Thellier (Coe, 1967) or the modified Shaw (Rolph and Shaw, 1985) palaeointensity technique. These criteria take into account the importance of mixed grain sizes of pure magnetite which is of common occurrence in ancient basalts (Radhakrishnamurty et al, 1991). Also, the inclusion of all samples in the palaeointensity analysis is a more thorough approach than previous methods. This approach minimises the possibility of overlooking suitable samples but increases the chances of selecting samples which satisfy the two requirements mentioned earlier - namely that the NRM is a primary TRM and that the magnetic mineralogy is most resistant to alteration during laboratory heating.

The new method involves the following steps:

1. **Rock magnetic experiments (Chapter 3)** : Five major rock magnetic techniques are used. They are thermomagnetic analysis, high temperature susceptibility (KHT) (the thermal methods), low temperature susceptibility (KLT), hysteresis measurements and alternating field demagnetisation (the non-thermal methods).

The critical point of this new method is to combine results from all these techniques to build a complete picture of the magnetic composition and domain state of a sample.

2. **Palaeointensity experiments (Chapter 6)** : Sister samples from each core are used to calculate palaeointensity values for each flow by the modified Thellier (Coe, 1967) and modified Shaw (Rolph and Shaw, 1985) techniques. The reliability of results obtained from these experiments is assessed using criteria similar to those defined by Coe et al (1978) for the modified Thellier method and Senanayake et al (1982) for the modified Shaw technique.

3. **Correlation of behaviour** : All rock magnetic and palaeointensity results for each sample are compared and categorised into "SETS", which reflect patterns of similar behaviour within the sample collection.

4. **Selection/Rejection criteria** : The sets defined in (3) above are used to establish criteria for the selection or rejection of samples for use in the modified versions of the Thellier and Shaw techniques.

For this integrated approach, it is important that large sample collections are used in order to fully define the range of rock magnetic behaviour, and thereby the magnetic mineralogy, of the rocks used in the study. This criterion is satisfied by the present study (Chapter 6) since over a hundred palaeointensity determinations were made from forty-one lava flows; each flow having a complete set of rock magnetic results (1, above). As a result of this large data set, the method devised in the present study can be confidently applied to basalt collections with similar magnetic mineralogy.

7.4 CORRELATION OF BEHAVIOUR - THE DEFINITION OF ROCK MAGNETIC (RM) SETS

The results of the rock magnetic and palaeointensity experiments are described in detail elsewhere in the thesis, and are summarised here in Figures 7.2-7.5 and Tables 7.1-7.3. Samples from the Gardar lavas fall into one of three rock magnetic sets, whose characteristics are shown in Figure 7.2 and defined in Table 7.1, based on their behaviour during the rock magnetic experiments. Very few samples from the collection show a set of results which do not fall into one of these RM sets. Occasionally, a small number of samples (<5%) from RM set 1 have type 2a instead of type 3 thermomagnetic curves. The palaeointensity results for each RM set are discussed in detail below:

1. **RM set 1** : The majority of samples from this set give palaeointensity results which show consistency between the two techniques and between samples from the same flow. Eighteen flows (1 from the Upper Lavas and 17 from the Lower Lavas) fall into this category, representing 38% of the entire collection. From these flows, 36 samples (2 and 34 from the Upper and Lower Formations respectively) were used in Thellier experiments and 19 (2 and 17) in Shaw experiments. Twenty-seven and twelve of these samples give acceptable results using the Thellier and Shaw techniques respectively. Ten flows give palaeointensity values which are consistent between the two techniques for the same flow. Most set 1 samples pass at least two of the PTRM checks in the temperature region over which the palaeointensity was calculated during the modified Thellier experiments and give linear R-S plots (Section 6.8.2) within the

higher coercivity (>80 mT) region during modified Shaw experiments. An important feature of set 1 samples is that they mainly comprise flows from the Lower Lava Formation. These flows, as described in Chapter 3, show the greatest amount of SD material in a mixed grain size of magnetite. Figure 7.3 shows modified Thellier and modified Shaw plots for two RM set 1 samples.

The consistency of results shown by set 1 samples within flows and between techniques suggests that samples from this set are most likely to give acceptable palaeointensity results.

2. **RM set 2** : Generally, samples belonging to this set give a limited number of reliable palaeointensity results using the Thellier technique but do not tend to give reliable results using the Shaw technique. Specifically, nineteen flows (13 from the Upper Lavas, 6 from the Lower Lavas) representing 40% of the entire collection, fall into this category. From these flows, 36 samples (23 from the Upper Lavas and 13 from the Lower Lavas) were used in Thellier experiments and 23 samples (13 and 10) for Shaw experiments. Eighteen samples give Thellier results which are considered to be reliable. On examination of the rock magnetic characteristics of set 2 samples, it becomes clear why some fail to give reliable Thellier results. The magnetic mineralogy is dominated by MD magnetite with little evidence of SD material. It is well known that pure MD magnetite is unsuitable for palaeointensity work, since the blocking and unblocking spectra of TRM in MD grains are not necessarily equivalent. Those samples from RM set 2 which do give acceptable Thellier results all show rock magnetic characteristics which indicate the presence of small amounts of SD material in the MD rich sample. Any

samples which do give a modified Shaw result have very low intensity values. These low values occur as a result of the total removal of the NRM at low demagnetising fields due to the predominance of MD magnetite in the samples, effectively leaving no NRM in the higher coercivity region. Figure 7.4 indicates the typical modified Thellier and modified Shaw plots for acceptable and unacceptable samples from RM set 2.

3. **RM set 3** : Samples from this set do not give any acceptable palaeointensity results. A total of 24 samples (from 11 flows), all from the Upper Lava Formation, were used and all failed to provide a consistent palaeointensity value, with either technique. Non-thermal rock magnetic data suggest that such samples contain a significant SD fraction, which should make them suitable for palaeointensity studies. However, the thermal results show that significant alteration has occurred during heating. The inflection in the thermomagnetic heating curve at ca.450° C suggests that the dominant magnetic phase present in samples showing set 3 behaviour is maghaemite (Readman and O'Reilly, 1970 and Chapter 3). The presence of a large peak in the KHT heating curves probably reflects the unblocking of a narrow range of SD maghaemite grains. These peaks in the KHT curves have been witnessed by Dr. P.W. Schmidt (pers. comm.) who also interprets them as being due to the presence of maghaemite. His data are supported by TEM images which clearly indicate the presence of maghaemite in samples with the hump and its absence in samples without the hump.

RM SET	THERMAL			NON-THERMAL					
	Thermomag		KHT	KLT		Hyster		AFD	
	Tc(°C)	Curve	Curve	RS	PS	Type	Mrs/Ms	MDF	Stab
1	580	3(2a)	MD/SD(H)	>0.5	1.30	3b	>0.12	>10	S
2	580	2a	H(MD/SD)	<0.5	1.15	3a	<0.12	<10	U
3	600-620	6	H′	>0.5	1.20	3b	>0.12	>10	U

Table 7.1 : Definition of characteristics of each rock magnetic (RM) set. Tc = Curie temperature, RS = Ratio K_{-196}/K_{30}, PS = Ratio K_{peak}/K_{30}, Mrs/Ms = Ratio of saturation remanence to saturation magnetisation, MDF = Median Destructive Field in mT, Stab = Stability to alternating field demagnetisation (AFD) S = Stable up to 150mT, U = Unstable throughout demagnetisation.

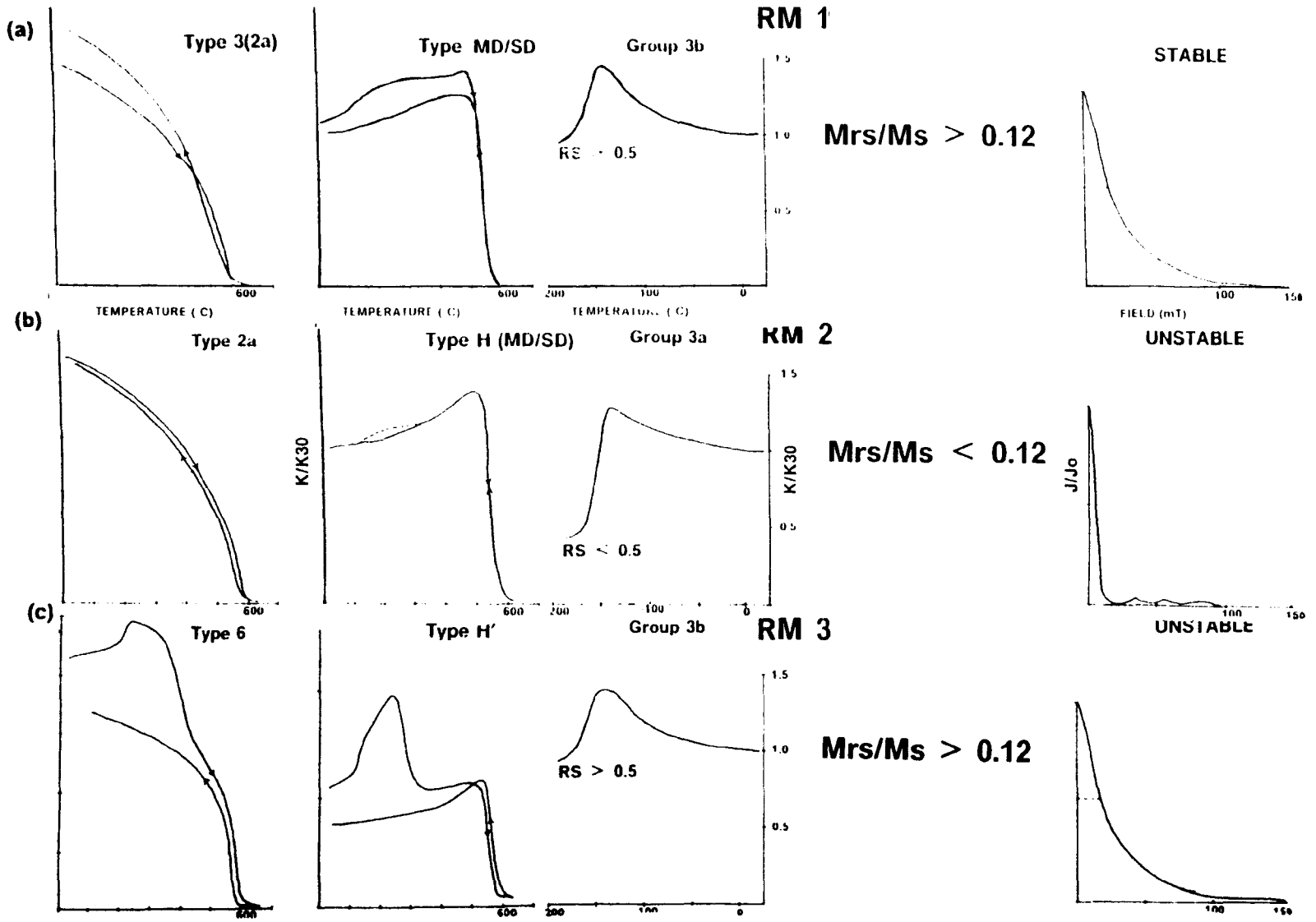

Figure 7.2 : Characteristics of the three rock magnetic (RM) 'sets' defined for the Gardar lavas : (a) RM set 1 (b) RM set 2 (c) RM set 3 (see text for explanation of symbols and sets).

The presence of maghaemite indicates that some degree of low temperature oxidation (maghaemitization) has occurred in the samples showing RM set 3 behaviour. This produces a chemical remanence (CRM) which contaminates the Primary TRM. This explains the inability of set 3 samples to produce results and immediately invalidates the use of such samples for palaeointensity work, since the NRM is not a pure TRM. Examples of modified Thellier palaeointensity plots for these unsuitable samples are shown in Figure 7.5; no results were obtained using the modified Shaw technique.

7.5 SAMPLE SELECTION AND REJECTION

The selection and rejection of samples for use in palaeointensity experiments has both advantages and disadvantages. The results of the present study can be used to highlight the major disadvantage, namely the use of an inadequate rock magnetic data set which leads to the erroneous selection/rejection of samples. Figure 7.2 illustrates three cases where use of a limited amount of available rock magnetic data would lead to an erroneous selection/rejection of a sample.

Figure 7.2(a) - The thermomagnetic curve shows that a small amount of thermal alteration has occurred during laboratory heating, which would suggest that these samples may not be suitable for palaeointensity work. However, the results of the non-thermal RM tests indicate the presence of a significant amount of SD material in a mixed grain size and a stable a.f. demagnetisation curve. These samples belong to RM set 1 and have produced reliable and consistent results with both palaeointensity techniques.

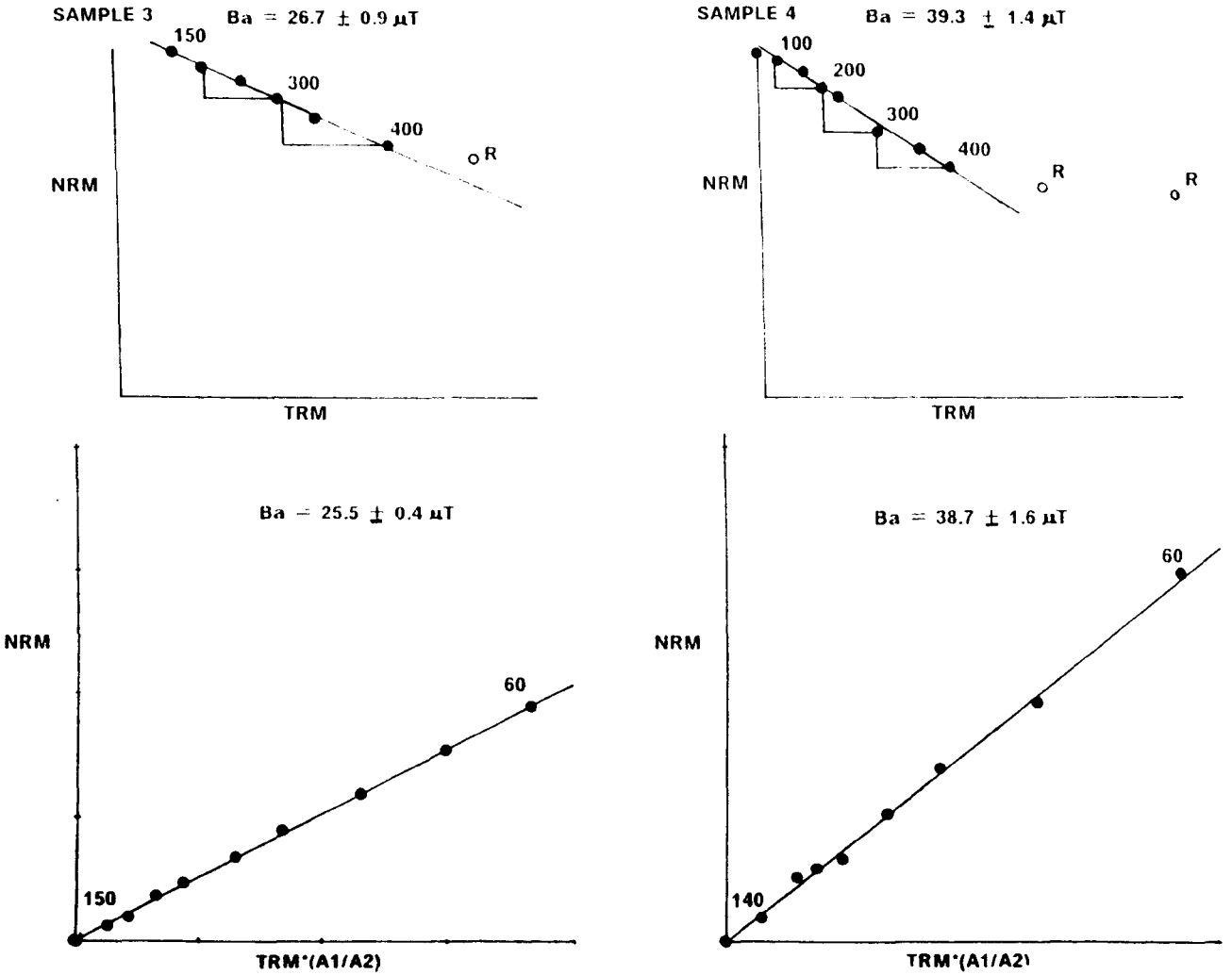

Figure 7.3 : Modified Thellier and modified Shaw palaeointensity results for two samples exhibiting RM set 1 characteristics (Symbols as for Figure 6.3).

Sample 1 : Consistent result with both methods.

Sample 2 : Consistent result with both methods

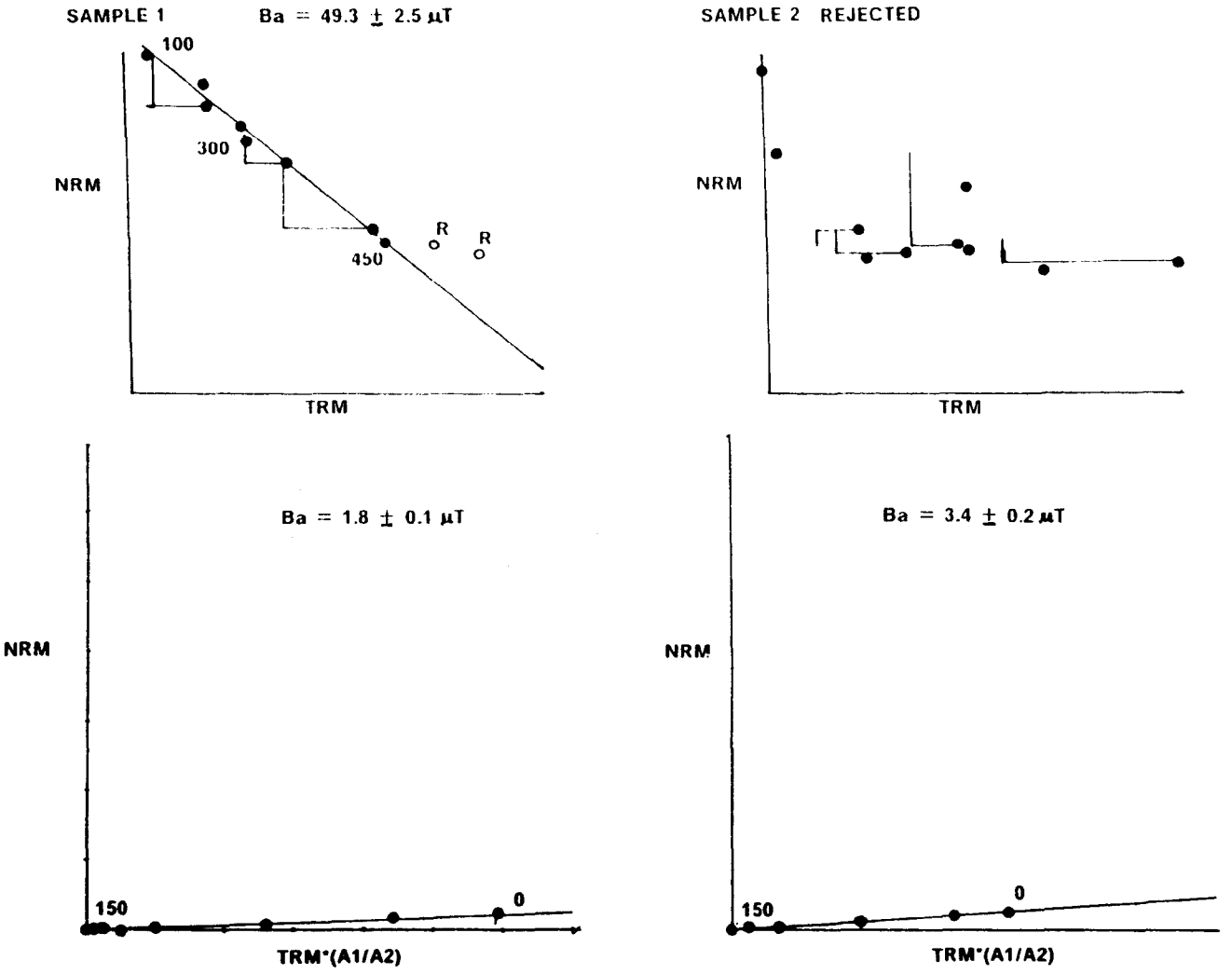

Figure 7.4 : Modified Thellier and modified Shaw palaeointensity results for two samples exhibiting RM set 2 characteristics (Symbols as for Figure 6.3). Sample 3 : Thellier accepted, Shaw rejected. Sample 4 : No result obtained with either method.

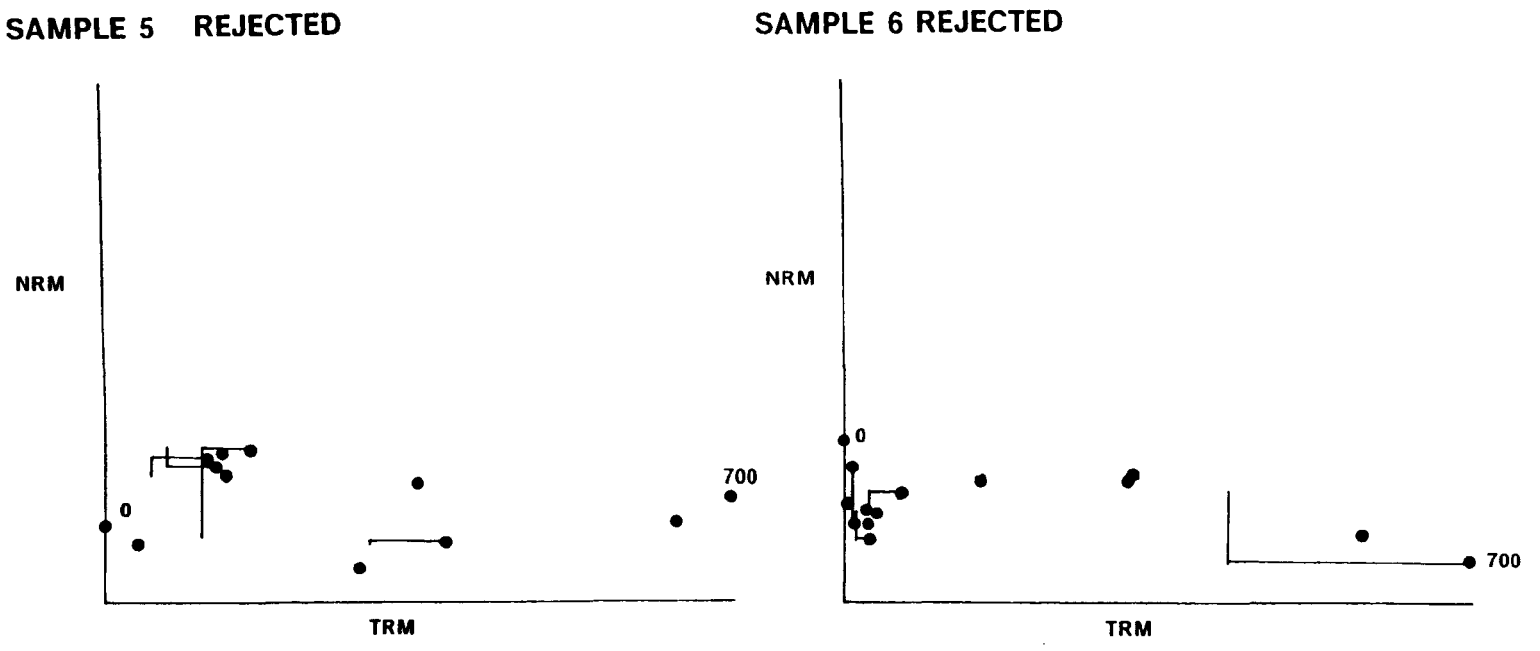

Figure 7.5 : Modified Thellier and modified Shaw palaeointensity results for two samples exhibiting RM set 3 characteristics (Symbols as for Figure 6.3).

Sample 5 : No result obtained with either method.

Sample 6 : No result obtained with either method.

RM SET	No. samples used (Thellier)		No. samples used (Shaw)	
	Upper Lavas	Lower Lavas	Upper Lavas	Lower Lavas
1	2 (2)	34 (25)	2 (0)	17 (12)
2	23 (11)	13 (7)	13 (0)	10 (3)
3	24 (0)	0 (0)	11 (0)	0 (0)

Table 7.2 : Success rate statistics for palaeointensity experiments. Figures not in brackets represent the number of samples used in experiments. Figures in brackets represent the number of samples for which results were accepted.

LAVA GROUP	N/n	Mean Thellier Ba (μT)	Mean Shaw Ba (μT)
Upper (Normal)	13/0	31.4±3.0	-
Upper (Reversed)	10/0	10.8±1.1	-
Lower	32/15	34.3±1.0	33.8±2.1

Table 7.3 : Results of modified Thellier and modified Shaw palaeointensity experiments. N/n = Number of accepted samples used in modified Thellier experiments / Number of accepted samples used in modified Shaw experiments. Errors are quoted to 1σ

Figure 7.2(b) - The thermomagnetic curve which characterises RM set 2 behaviour indicates a single, high Curie temperature and a reversible curve. This evidence suggests that the sample does not alter significantly on heating and would be likely to give an acceptable palaeointensity result (e.g. Prévot et al, 1985; Derder et al, 1989). While in some cases this assumption would be correct, the results of the non-thermal RM tests indicate that such samples are, in fact, completely dominated by MD magnetite and are thus unsuitable for both the modified Thellier and modified Shaw palaeointensity techniques.

Figure 7.2(c) - The results of the non-thermal RM tests for set 3 suggest that these samples have a mixed grain size with a significant amount of SD material present. On this evidence alone, the samples would be expected to give an acceptable palaeointensity result with both methods. However, the results of the thermal RM tests show that maghaemite is present, indicating that low temperature oxidation has occurred. Thus, samples showing this behaviour would not give an acceptable palaeointensity result with either technique.

These three examples clearly indicate the danger of using a limited amount of rock magnetic data to assess the suitability of samples for use in palaeointensity experiments. A better approach is to consider results from as many RM tests as possible, at least one of which should be thermal and at least one non-thermal.

From the rock magnetic and palaeointensity results described, in this thesis, the following set of selection/rejection criteria is proposed for identifying suitable samples for use in the modified versions of the Thellier and Shaw palaeointensity techniques. These criteria apply to basalts whose magnetic mineralogy comprises pure ($Ti < 0.1$) magnetite with a mixed grain size, with

1. **SELECTION (SAMPLES MOST LIKELY TO GIVE ACCEPTABLE RESULTS USING THELLIER OR SHAW METHODS)**

   - Samples with RM SET 1 characteristics.

2. **REJECTION (SAMPLES WHICH FAIL TO GIVE ACCEPTABLE RESULTS WITH EITHER METHOD)**

   - Samples with RM SET 3 characteristics.
   - Samples with all the following non-thermal RM characteristics, regardless of their thermal RM characteristics:
   - Mrs/Ms ratio < 0.08
   - Group 3a KLT curve (RS < 0.5)
   - Median destructive field (MDF) < 8 mT.

3. **REJECTION FROM SHAW EXPERIMENTS (SAMPLES WHICH INVARIABLY ARE UNSTABLE TO A.F. DEMAGNETISATION)**

   - Samples with RM SET 2 characteristics.

4. **POSSIBLE SELECTION (SAMPLES HAVING ROCK MAGNETIC CHARACTERISTICS WHICH DO NOT FALL INTO ONE OF THE THREE DEFINED RM SETS)**

   - Samples with all the following RM characteristics:
   - Type 2 (a) thermomagnetic curves
   - Group 3 (a) or 3 (b) KLT curves
   - Mrs/Ms ratios between 0.08 and 0.12

varying amounts of SD material in MD-dominated samples and are thus designed for use with ancient basalts.

The fourth criterion listed here represents a grey area in the method, where certain samples possess rock magnetic characteristics which do not fall into any of the three defined RM sets (Section 7.4). In the present study, such samples represent only 7% of the collection (ten samples) and hence are relatively unimportant. Of these ten samples six gave palaeointensity estimates which comply with the reliability criteria mentioned in Section 7.3 and four did not.

It must be stressed that caution should be exercised when applying selection/rejection criteria to basalt collections. The criteria listed above are applicable only to basalts with a mixed grain size of pure magnetite. The

magnetic mineralogy of younger basalts and their behaviour during palaeointensity experiments is likely to be very different. Thus, although the technique of grouping results into characteristic "rock magnetic sets" is a valid approach for basalts of any age, the conclusions reached from such a classification, and hence the resulting selection/rejection criteria, are likely to differ for basalts of different ages.

7.6 DISCUSSION

The large amount of data accumulated in the present study have demonstrated that, provided an integrated rock magnetic approach is used, sample selection rejection provides a useful addition to palaeointensity studies. The behaviour of each sample during rock magnetic experiments is correlated with that during palaeointensity experiments so that patterns of behaviour can be identified within the rock collection. These patterns can then be used to establish criteria which define the sets of samples which give the most reliable results in the present study and are thus most suitable for future palaeointensity work.

The magnetite-bearing ancient basalts which are most likely to give consistent and acceptable field intensity determinations are those which belong to RM set 1, which is characterised by samples containing significant amounts of SD grains in a mixed grain size of pure magnetite, i.e. those with the smallest amount of MD grains.

Although a large volume of rock magnetic data is used in the new method, the results can be obtained speedily since the tests themselves are quick and a number of tests can be performed simultaneously.

There are of course, as in most scientific techniques, limitations to the use of the new selection/rejection method. The major limitation at present is the lack of precise quantitative estimates of the rock magnetic parameters which characterise a sample which is suitable for palaeointensity work. Specifically, we require a precise knowledge of the M_{rs}/M_s, RS and MDF values which a sample needs before it can be classed as suitable.

Ideal behaviour in basalts, especially ancient ones, is rare. Thus, any selection/rejection method is subject to a certain degree of inconsistency. However, the present study has shown that an integrated rock magnetic approach is a thorough, effective and accurate method of assessing the suitability of samples, with mixed grain sizes of pure magnetite, for palaeointensity work.

Palaeointensity techniques tend to be labour intensive and time consuming. Provided that the integrated approach is followed, the advantages of sample selection/rejection are clear. Large rock collections can be rapidly investigated and the suitable samples identified, thus saving a significant amount of laboratory time. This is a good example of a positive use of rock magnetism in palaeomagnetism, increasing the efficiency and reliability of palaeointensity techniques. Furthermore, the advantages over previous methods are important. The previous methods described here use a limited amount of rock magnetic data; they reject samples on limited practical criteria, consequently performing palaeointensity experiments only on selected samples. In the integrated method, many rock magnetic techniques are used and palaeointensity experiments are performed on all samples. Consequently, samples are rejected on empirical and theoretical grounds which is a much more thorough approach.

CHAPTER 8 : GEOMAGNETIC SIGNIFICANCE OF THE RESULTS

8.1 INTRODUCTION

The palaeomagnetic results from Chapter 4 show that two reversals are recorded by the flows of the Upper (Ilímaussaq) Lava Formation. Significantly, the mean inclination for reversely magnetised units ($I_R = -17°$) is shallower than that for the normally magnetised units ($I_N = +37°$). Also, the results from Chapter 6 indicate that the palaeointensity values for reversely magnetised flows ($Ba_R = 10.8\mu T$) are appreciably lower than those for flows with normal polarity ($Ba_N = 31.4\mu T$). These results indicate a considerable degree of asymmetry between the normal and reversed field states at this time.

The occurence of asymmetric fields in Proterozoic rocks is not uncommon. Palmer (1970) found asymmetric fields associated with three successive reversals (R → N → R → N) in the Mamainse Point area of the ca.1200-1000 Ma Keweenawan Igneous Province of Canada. The sign of this asymmetry is opposite to that witnessed for the Gardar lavas, with normal directions having shallower inclinations than reversed directions ($I_N = +42°$ and $I_R = -67°$; Pesonen, 1978). Furthermore, the normal/reversed palaeointensity ratio is much lower (0.8) than that for the Gardar lavas (2.9). Thus, the field model which can account for the asymmetry in the Keweenawan will be very different from that which satisfies the asymmetry recorded by the flows from the Gardar lava succession.

The aim of this chapter is to attempt to explain the differences in normal and reversed palaeodirectional and palaeointensity data obtained for the Upper Lava Formation by considering various geomagnetic field models which have been suggested in the literature and to establish which model(s) best explain the Gardar results.

8.2 THE STRENGTH OF THE PRECAMBRIAN FIELD : A SUMMARY OF CURRENTLY AVAILABLE DATA.

Compared with the amount of palaeointensity data available for the Phanerozoic, particularly the last 5 Ma (Merrill and McElhinny, 1983), very few estimates of the Precambrian geomagnetic field strength have been made. The contributions of Carmichael (1967), Smith (1967b), McElhinny and Evans (1968), Kobayashi (1968), Schwarz and Symons (1969), Bergh (1970), Senanayake (1981), Pesonen and Halls (1983), Roberts (1983) and Hale (1987) are the only documented records. Of these studies, that by Pesonen and Halls (1983) is the most comprehensive, and subsequent work by Nevanlinna and Pesonen (1983) used the data from this original study to model the Keweenawan (1200-1000 Ma) geomagnetic field.

To make a meaningful comparison of these available field intensity estimates, which originate from rocks in different geographical localities, a method must be used which takes into account the different palaeolatitudes of the rocks. Smith (1967a) used a parameter called the Virtual Dipole Moment (VDM) which is defined as the equivalent dipole moment which would have produced the measured palaeointensity at a palaeolatitude,λ, and is given by:

$$VDM = \frac{4\pi R^3 B_a}{\mu_0}\left(4 - 3\cos^2\lambda\right)^{-1/2} \qquad [8.1]$$

or, in terms of the inclination,I, from $\tan I = 2\tan\lambda$, we get:

$$VDM = \frac{2\pi R^3 B_a}{\mu_0}\left(1 + 3\cos^2 I\right)^{1/2} \qquad [8.2]$$

where, R = radius of the earth (= 6371 km)
B_a = palaeointensity value
μ_0 = permeability of free space.

The variation of mean VDM throughout the Precambrian and Phanerozoic, using time intervals of 200 Ma, is illustrated in Figure 8.1. The lack of data in certain time intervals makes it difficult to average the data over smaller time windows. Table 8.1 summarises the data used to construct Figure 8.1 and includes the results from the present study. For comparison, the data for the past 500 Ma are also presented. The early and mid Precambrian data are seen to fluctuate about the present day VDM value of $\simeq 8 \times 10^{22} Am^2$, with a mean VDM of $(7.7 \pm 4.1) \times 10^{22} Am^2$ from 54 results (Merrill and McElhinny, 1983). During the late Precambrian, the VDM value dropped markedly and has since been rising again to the present value.

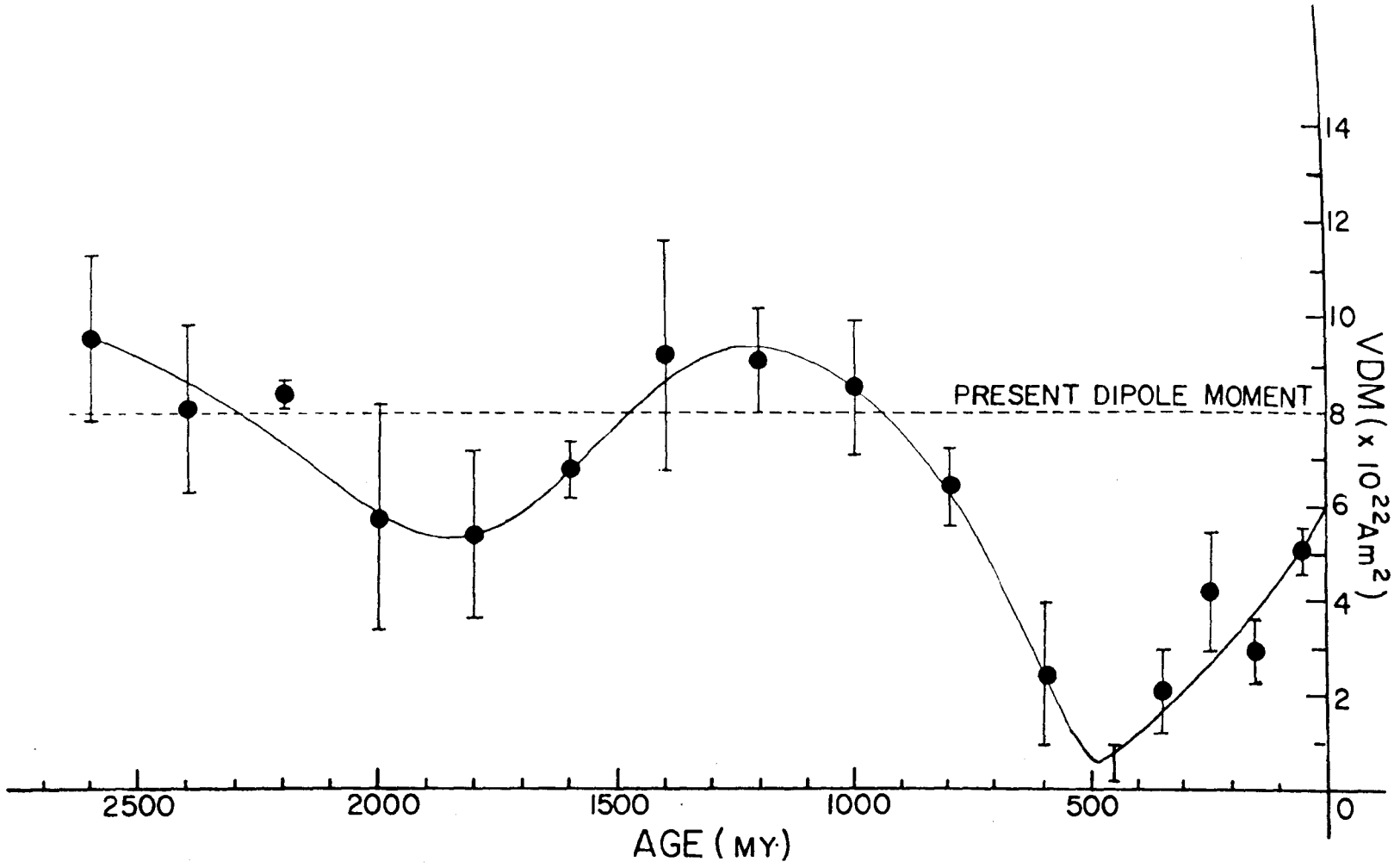

Figure 8.1 : The variation of VDM from 2700 Ma to the present (from Senanayake, 1981).

Age	N	VDM ($\times 10^{22}Am^2$)	SD ($\times 10^{22}Am^2$)
0-100	13	5.1	0.43
100-200	8	3.0	0.68
200-300	8	4.2	1.25
300-400	12	2.1	0.88
400-500	3	0.6	0.4
500-700	2	2.4	1.55
700-900	8	6.4	0.85
900-1100	14	8.5	1.47
1100-1300	6	10.3	2.36
1300-1500	7	9.1	2.49
1500-1700	5	6.8	0.58
1700-1900	5	5.4	1.83
1900-2100	3	5.8	2.47
2100-2300	2	8.4	0.29
2300-2500	4	8.1	1.85
2500-2700	2	9.6	1.83
2700-3500	1	2.7	-

Table 8.1 : A summary of the Precambrian VDM data. Sources : Carmichael (1967); Smith (1967); Kobayashi (1968); McElhinny and Evans (1968); Schwarz and Symons (1969); Bergh (1970); Senanayake (1981); Pesonen and Halls (1983); Roberts (1983); Hale (1987) and the present study (1300-1500 Ma). N = Number of VDM determinations in each time interval.

8.3 POSSIBLE MODELS TO ACCOUNT FOR FIELD ASYMMETRY

Nevanlinna and Pesonen (1983) described four possible models to account for the asymmetry witnessed in the Keweenawan. Although the asymmetry is different, these models may also be relevant for the Gardar and are discussed in this context in Section 8.4.

8.3.1 Model 1 - The secondary component model

Palmer (1970) discovered non-random NRM directions in Keweenawan conglomerates and suggested that a secondary component of magnetisation was superimposed on the original random NRM directions in the pebbles. He proposed a model which accounted for the asymmetry by partial overprinting by a secondary component of magnetisation (Figure 8.2a). This model is geologically feasible since low temperature alteration has been witnessed in Keweenawan rocks (Ade-Hall et al, 1971) which could be associated with the production of a secondary component of remanence, which would be a chemical remanence (CRM). This type of alteration is also a common feature in all Precambrian rocks, including the Gardar lavas (Chapters 3 and 4).

The validity of this model can be tested by detailed thermal and a.f. demagnetisation of samples to isolate the component structure of NRM. For the Keweenawan, Pesonen and Halls (1979) found no evidence of a secondary component on detailed demagnetisation studies, which was interpreted as indicating that the blocking temperature and coercivity spectra for the primary and secondary components were identical. Consequently, the

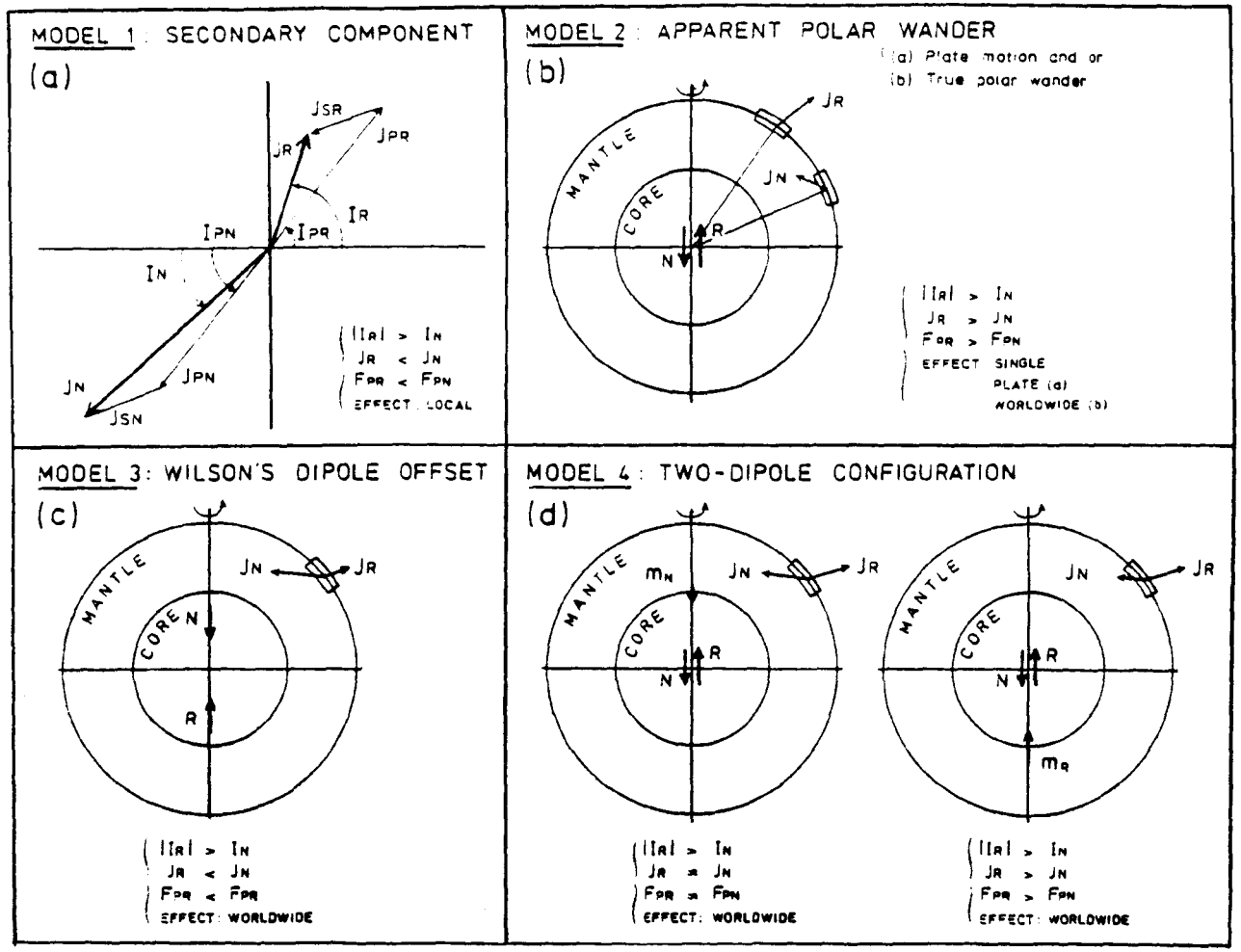

Figure 8.2 : Four models for explaining the field asymmetry observed in Keweenawan rocks (from Pesonen and Halls, 1983). (a) Model incorporating a secondary magnetisation component with a direction of 293°/+25°, recognised in Keweenawan conglomerates, (b) Apparent Polar Wander model, (c) Wilson's offset dipole model (d) the two dipole configuration of Pesonen and Nevanlinna (1981). The predicted NRM intensity (J), inclination (I) and palaeointensity (Fp) are shown for each model.

two components could not be separated and the secondary component became known as the "non-removeable" secondary.

8.3.2 Model 2 - The Apparent Polar Wander (APW) model.

The Keweenawan asymmetry was interpreted by Dubois (1962) and Robertson and Fahrig (1971) as being a signature of apparent polar wander during igneous activity. The normal and reversed units are often separated by stratigraphic breaks, e.g. clastic sediments, representing a sizeable time gap between the units. It is therefore possible that movement of the North American plate before the onset of igneous activity in the opposite polarity could explain the asymmetry. Figure 8.2b illustrates this model for a R → N reversal, where the plate would move from high (R) towards lower latitudes (N).

8.3.3 Model 3 - The Offset Dipole Model

Palaeomagnetic poles from Tertiary and Quarternary rocks have been shown to plot systematically on the far side and to the right of the geographic pole when viewed from the sampling locality (e.g. Wilson, 1970, 1971; Hailwood, 1977). Analyses of these data have indicated that the "far-sidedness" is not a result of APW, true polar wander (TPW) or the magnetic properties of the rocks (Wilson, 1970,1971; Wilson and McElhinny, 1974).

Wilson proposed that the farsidedness (but not the right-handedness) could be explained if the geomagnetic field source was not a GAD but an offset axial dipole (OAD) (Figure 8.2c), with an offset equivalent to a 285 km northwards movement of the dipole. The consequence of this OAD would be to make all inclinations in the N hemisphere too shallow and those in the

S hemisphere too steep. Thus, palaeomagnetic poles calculated using the GAD model, will become farsided when viewed from the sampling site.

Both normal and reversed poles will be farsided, but Wilson (1972), and Merrill and McElhinny (1977) showed that the reversed poles will be more farsided than the normal poles. Specifically, the reversed dipole source will be axially offset (farsided) by ca. 1000 km whereas the normal source has an offset of ca. 200 km. Thus, the Tertiary field is intrinsically asymmetric, requiring no APW or secondary component for explanation.

8.3.4 Model 4 - The two-dipole configuration

This model, proposed by Pesonen and Nevanlinna (1981), consists of an axial geocentric dipole and an axially offset dipole, with the latter located at either the northern or southern core-mantle boundary (CMB) (Figures 8.2d). The geocentric dipole (main dipole) has two polarity states - normal and reversed, where the dipole moments of these states are equal ($M_N = M_R$) but antiparallel. The offset dipole (minor dipole, m), represents the long term zonal average of the non-dipole (Nd) field, the physical source of which is presumably large-scale eddies at the CMB (Cox, 1975). Asymmetric fields occur when the geocentric dipole reverses polarity while the offset dipole, which can be of either polarity, retains its constant polarity.

Four possible models arise from the two-dipole configuration. The minor dipole may be situated at either the north or the south CMB and could have either a normal or a reversed polarity.

8.4 GEOMAGNETIC FIELD MODEL FOR THE EARLY GARDAR PERIOD

Despite the large palaeomagnetic and palaeointensity data set obtained in the present study, no meaningful global field model can be proposed for the Early Gardar period for three reasons:

1. There are no palaeointensity results from rocks of a comparable age to the Gardar lavas.

2. The Gardar lava succession is not accurately dated, thus even if data were available for other Mid-Proterozoic rocks, no direct comparison could be made.

3. The palaeointensity results for the Upper Lavas may be unreliable, as discussed in Chapter 6.

Consequently, any field model proposed here to account for the observed inclination and palaeointensity anomalies for normal and reversed flows within the Gardar lavas must be treated with caution. The following sections analyse the evidence for each of the field models suggested in Section 8.3, in the context of the Upper Gardar Lavas.

8.4.1 The secondary component model

The effect that a secondary component has on the original remanence depends on the direction of this secondary. For the Gardar lavas, the most likely secondary component would be acquired due to the thermal effect of the Ilimaussaq intrusion, which has a steep, NE positive direction of

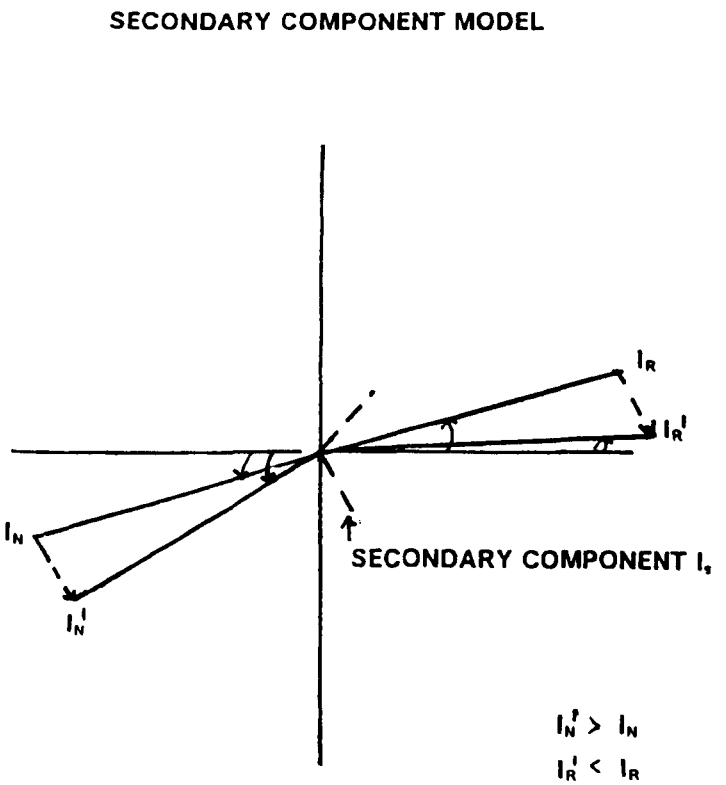

Figure 8.3 : The situation incorporating the secondary component model as a possible explanation for the field asymmetry witnessed in the Gardar lavas. Direction of secondary is that corresponding to the mean direction isolated in Chapter 5 for the Ilímaussaq intrusion. I_N ,I_R and I_S are the mean inclinations of the normally magnetised lavas, the reversely magnetised lavas and the secondary component respectively.

magnetisation (Chapter 5). Figure 8.3 shows that a secondary component in this direction would have the effect of steepening the normal inclinations and shallowing the reversed inclinations. This condition is satisfied by the data. If the blocking temperature and coercivity spectra of the two components completely overlapped, the NRM intensity would be greater for the normal polarity than for the reversed polarity, a condition which is also satisfied by the data.

In the palaeodirectional study, described in Chapter 4, characteristic flow directions are isolated by component analysis. Thus any contamination of this remanence was removed and secondary magnetisations are not important, assuming that their blocking temperature spectra do not totally overlap with that of the primary, and will not have a bearing on the mean magnetisation directions calculated. Furthermore, the positive baked contact test with the Ilímaussaq intrusion (Chapter 5) demonstrates that the remanence held by the flows of the upper lava group is a primary TRM or TCRM. Therefore, despite the fact that the inclination condition is satisfied, other evidence suggests that a secondary overprint is not responsible for the reversal asymmetry witnessed.

8.4.2 The APW model

Unlike the Keweenawan, the reversals of magnetisation in the Gardar lavas occur within a continuous lava sequence (Figure 4.15a - Chapter 4) comprising thin flows which, as suggested by geological evidence, are known to have erupted in a short period of time. Thus, it is unlikely that the sample locality could have had enough time to move a distance, during a reversal, which would be large enough to produce the observed inclination anomaly.

A useful method for examining the difference between normal and reversed palaeointensity values is to reduce all palaeointensities to the equator by using equation 8.1.

If the geomagnetic field was that due to a GAD, and if the difference in palaeointensity values was caused by plate motion during a polarity change, the palaeointensity difference should be eliminated when the in situ N and R values are reduced to the equator. When the mean in situ N and R palaeointensity values for the Gardar lavas (31.4μT and 10.8μT respectively) are substituted into equation 8.1, the resulting equatorial values are 26.0μT and 10.2μ T respectively. Therefore, the asymmetry cannot be explained by plate motion between successive polarity states (APW model).

From the above analyses, it is clear that an alternative explanation is neccessary to explain the reversal asymmetry witnessed. There are two ways of approaching the problem; to consider the hypothetical situation of having an axial dipole, or a configuration of dipoles, offset from the geocentre, or to represent the field in terms of Spherical Harmonic Analysis (Section 1.1.2). Both are convenient mathematical ways of representing physical processes occurring within the Earth's core.

For completeness, the following sections include analysis of both offset dipole models and SHA representation of the field.

8.4.3 Spherical Harmonic Analysis (SHA) Models

As explained in Section 1.1.2, the inclination of the Earth's magnetic field can be described in terms of zonal harmonic (g_n^0) terms (where n is the harmonic degree; the harmonic order is 0).

The inclination anomaly, which is the difference between the observed inclination and that due to a GAD, is dependent on the relative strength of the dipole and the higher order terms (g_2^0, g_3^0, g_4^0 etc..). For a GAD field, the inclination is given by the equation $\tan I = 2 \cot \theta$. If the g_2^0 and g_3^0 terms are included, then the inclination I′ at a colatitude θ, will be given by:

$$\tan I' = \frac{2\cos\theta + g_2^0/g_1^0(4.5\cos^2\theta - 1.5) + g_3^0/g_1^0(10\cos^3\theta - 6\cos\theta)}{\sin\theta + g_2^0/g_1^0(3\cos\theta\sin\theta) + g_3^0/g_1^0(7.5\cos^2\theta\sin\theta - 3\sin\theta)} \quad [8.3]$$

(Merrill and McElhinny, 1983)

If we assume, in the simplest case, that the higher order terms (g_3^0, etc..) have a minor influence on the inclination, the inclination I′ observed at a colatitude θ is given by:

$$\tan I' = \frac{2\cos\theta + 3g_2^0/g_1^0(1.5\cos^2\theta - 1)}{\sin\theta + 3g_2^0/g_1^0(\sin\theta\cos\theta)} \quad [8.4]$$

where $180° \leq \theta \leq 0°$

Since the assumption that the inclination is exactly half the difference between the observed N and R inclinations is unlikely to be true, the site colatitude, θ, must be calculated by changing the g_2^0/g_1^0 ratio iteratively according to equation 8.4, until the correct N and R inclinations are seen.

The value of g_2^0/g_1^0 which satisfies this equation can then be used to calculate the required dipole offset for the colatitude and observed inclinations.

For the Gardar lavas data set, where $I_N = +36.9$ and $I_R = -17.4$, g_2^0/g_1^0 values of -0.130 and -0.133 for normal and reversed polarity respectively satisfy the equation when the colatitude is 75.6° for normal polarity and 104.4° for reversed polarity. Thus, the quadrupole strength is ≃13% of that for the dipole and since the sign of g_2^0/g_1^0 was negative for both polarities, the quadrupole must also reverse in addition to the dipole. Merrill and McElhinny (1983) show that, for the past 5 Ma, the quadrupole has both a reversing and a non-reversing part, with the intensity of the non-reversing part ≃ 34% of that of the reversing part. Therefore, the simple model which satisfies the Gardar lavas data is feasible.

This simple analysis of the field is equivalent to an offset axial dipole model. The values of g_2^0/g_1^0 and θ calculated above are equivalent to a dipole which is offset from the geocentre by 414km southwards for the normal polarity and 424km northwards for the reversed polarity.

This simple model cannot account, however, for the differences in the normal and reversed palaeointensity values calculated in Chapter 6. Thus, assuming that the palaeointensity values are reliable, it is likely that higher order terms are important. If we consider the field to be represented by dipole, quadrupole and octupole terms, a model can be proposed by changing the values of θ, g_2^0/g_1^0 and g_3^0/g_1^0 in equation 8.3, until the required normal and reversed inclination values are obtained. Also, by adapting equation 8.3, the intensity and reversed palaeointensity values can be calculated.

The above analysis was performed and in this case, both the inclination anomaly and the palaeointensity anomaly were satisfied by a field model which has the following set of non-unique solutions:

Palaeolatitude : 15°N. ($\theta = 75.0°$)

Normal field : $g_2^0/g_1^0 = -0.152$ $g_3^0/g_1^0 = -0.141$

Reversed field: $g_2^0/g_1^0 = -0.056$ $g_3^0/g_1^0 = +0.215$

It should be noted that these values for the harmonics define only one model which satisfies the field asymmetry witnessed in the Gardar lavas. Many more solutions to equation 8.3 may exist. The physical meaning of the solutions listed above is that the field has a reversing dipole term, a reversing or partly reversing quadrupole term (since the sign of g_2^0/g_1^0 is the same for both polarities) and a partly reversing octupole term. The low palaeointensity value for the reversed field means that the octupole term is more important than the quadrupole term for this polarity, where it is approximately four times as strong as the quadrupole term.

8.4.4 Axial offset dipole models.

1. The co-axial two dipole configuration.

Pesonen and Nevanlinna (1981) proposed that their two dipole model (Section 8.3) would satisfy the Gardar lavas data and have $I_N > I_R$ if the minor dipole (m) was either situated on the northern CMB with a reversed polarity or on the southern CMB with a normal polarity (Figure 8.2d).

Nevanlinna and Pesonen (1983) developed equations to determine the offset parameter q (where q = offset distance/radius of the earth) and the dipole strength ratio m/M, for a known site colatitude θ, given the observed normal and reversed inclinations I_N and I_R. A detailed description of the derivation of these equations, which is based on a consideration of the vertical and horizontal components of the field at a point on the Earth's surface, can be found in their original paper. They derive:

$$\tan I_\varepsilon = \left[\frac{(\varepsilon MF(\theta, 0) + mF(\theta, q))}{(\varepsilon MG(\theta, 0) + mG(\theta, q))} \right] \qquad [8.5]$$

M = Strength of the geocentric dipole
m = Strength of the minor dipole

$$F(\theta, q) = -\delta \left[P - 3(P - q)(1 - qP)\rho^{-2} \right]$$
$$G(\theta, q) = -\delta Q \left[1 + 3q(P - q)\rho^{-2} \right]$$

$$P = \delta \cos \theta$$
$$Q = -\delta \sin \theta$$
$$\rho^2 = 1 + q^2 - 2qP$$

δ = 1(−1) for a dipole located at the geocentre or in the northern
= (southern) hemisphere.
ε = 1(−1) for normal (reversed) polarity of the geocentric dipole.

By definition, the ratio (m M) is equal for both polarities of the field, i.e. $(m/M)_N = (m\ M)_R$. Thus, a quadratic equation in the offset parameter, q, can be constructed:

$$-2Aq^2 + (AP + B/P)q + (A - B) = 0 \qquad [8.6]$$

where,

$$A = C(Q\text{-}P) + Q \tan I_N - P$$
$$B = -3P(1+C)$$
$$C = \frac{(2 \cot \theta - \tan I_N)}{(2 \cot \theta - \tan I_R)}$$

If the assumption is made that the minor dipole is situated on the northern CMB, then the offset parameter, q, is 0.55. Thus, using equation 8.6, the value of colatitude, θ, which satisfies the inclination anomaly would be $\theta = 83.0°$.

2. The Wilson (1972) offset dipole model.

A limiting case of the two dipole model is where both dipoles coincide and only one single offset dipole describes the field for each polarity. This model is essentially the same as that used by Wilson (1972) for Tertiary data. For only one dipole, the quadratic equation in 8.6 reduces to:

$$2q^2(L\text{-}P) + (P^2 - LP + 3)q - (2P + L) = 0 \qquad [8.7]$$

where $L = Q \tan I_\lambda$

If the quadratic equation 8.7 is solved for normal and reversed polarities (palaeolatitude $\lambda = 15°N$) the values of q are +0.07 and -0.06 respectively. This represents an offset for the normal dipole of 446 km southwards and 382 km northwards for the reversed dipole.

8.5 DISCUSSION

The most detailed mathematical analysis of the Precambrian geomagnetic field, prior to this study, was that described by Nevanlinna and Pesonen

(1983) who modelled the field based on the palaeomagnetic results of Pesonen and Halls (1979,1983) for rocks from the Lake Superior area, belonging to the ca. 1200-1000 Ma Keweenawan Igneous Province. In those studies, the inclination anomaly and palaeointensity data were consistent with a field model, based on SHA, comprising a reversing dipole term, and non-reversing quadrupole and octupole terms ($g_2^0/g_1^0 = 0.16$ and -0.225; $g_3^0/g_1^0 = 0.132$ and -0.186). This model is quite different from that proposed in the present study for the Early Gardar period, a fact which is chiefly due to the high N/R palaeointensity ratio witnessed in the present study (2.9) compared with a value of 0.8 observed by Pesonen and Halls (1983). The high ratio for the Gardar imposes great physical demands on a field model and, although the model proposed is realistic it may also arise from the use of unreliable palaeointensity data. The concerns over the reliability of the palaeointensity results for the Upper Lava Formation have already been discussed in Chapters 6 and 7 and it is stressed here that any field model proposed, which uses these data, is totally dependent on their reliability.

The analysis in this Chapter has shown that the simplest representation of a non-GAD field, namely that which incorporates an offset axial dipole (Wilson, 1971, 1972) which is equivalent to an axial dipole and a quadrupole, accounts for the inclination anomaly witnessed in the Upper Lava Formation but cannot account for the high N/R palaeointensity ratio. Therefore, higher order harmonics appear to be important. After many studies into the time-averaged palaeomagnetic field, such as those of Wells (1973), Coupland and Van der Voo (1980) and Merrill and McElhinny (1983), it is now accepted that normally the only zonal harmonics which are significant are the g_1^0, g_2^0 and g_3^0 terms. Using these terms, the Gardar data are consistent with a geomagnetic field model which comprises a reversing dipole, a reversing (or

partly reversing) quadrupole and a partly reversing octupole, with the octupole being weak in the normal field but strong in the reversed field.

The two-dipole configuration proposed by Nevanlinna and Pesonen (1983) can explain the Gardar asymmetry where the minor (offset) dipole, which represents the long-term average of the zonal non-dipole field, is located at the northern core-mantle boundary and has a constant reversed polarity. The positioning of this minor dipole is chosen to represent the large-scale eddies which occur at the CMB (Cox, 1975). This model requires the Gardar sampling site to be situated at a palaeocolatitude of 83°.

The difference in the field models described here indicates that it is important to obtain both directional and intensity results for asymmetric fields and even with these data, any solution has limitations since we have discounted the effects of non-zonal and higher order zonal terms. Merrill and McElhinny (1983) note that the g_2^1, g_3^1, h_1^1 and h_3^1 terms are important in the present field and may also have been important in Proterozoic times. Nevertheless, the proposed dipole-quadrupole-octupole model, described by SHA, provides a physically acceptable situation which describes the Early Gardar field.

GENERAL DISCUSSION

The primary objective of the present study was to analyse the geomagnetic field during a short period of Mid-Proterozoic times, which is uniquely well recorded by the lavas of the early Gardar (ca. 1320 Ma) Eriksfjord Group. Although both direction and intensity results have been documented, the project has focussed primarily on the intensity (strength) of the field.

The results are discussed at the end of each chapter in order to promote the continuity of the thesis and a repetition of specific results here would be superfluous. However, the most important points warrant general discussion.

Probably the most important contribution to emerge from the project is a new method for assessing the suitability of basalt samples containing mixed grain sizes of magnetite, for application to palaeointensity investigations. This method (Chapter 7) has evolved from comparison of rock magnetic properties with behaviour during palaeointensity experiments. Three distinct patterns of behaviour have been identified and are used to assess the suitability of individual samples for palaeointensity determinations. This is an important advance in palaeointensity studies because, unlike previous methods of sample selection, palaeointensity experiments were performed on all samples, to which multiple rock magnetic techniques were also applied. Consequently, samples are rejected on more empirical grounds than in previous methods. Furthermore, the new integrated method is an important development in Precambrian palaeomagnetism. For the first time, basalts of this age have been selected for palaeointensity experiments on the basis of having a suitable magnetic mineralogy, i.e. a SD grain size fraction in a deuterically oxidised sample. Previously, results from Precambrian basalts have been questioned on the assumptions that their geological history is so complex and that their magnetic mineralogy so altered that they could not possibly have preserved

the geomagnetic field strength from the time of formation. In many cases, such as a number of those documented in Chapter 8, earlier results have not been accompanied by detailed rock magnetic investigations to identify the magnetic mineralogy. Hence, the palaeointensity values obtained cannot be fully understood and the confidence in their reliability is decreased. Whilst these reservations may not have been fully countered, the present study has produced a body of well-supported and internally-consistent results of comparable quality to the best studies of young Phanerozoic rocks.

Another interesting observation to emerge from this project is the variable quality and reliability of the palaeointensity results. The flows of the Upper (Ilímaussaq) Lava Formation provide the least reliable results and consequently little confidence is placed in most of the intensity values from this formation. This is a disappointing result which is due to unsuitability magnetic mineralogy; MD magnetite dominates, and there is little or no sign of SD magnetite which is essential for successful palaeointensity work. Also, maghaemite is present in some flows possessing a secondary CRM. The Middle (Ulukasik) Lava Formation yields low palaeointensity values compared with the rest of the collection. As discussed in Chapter 6, these results are believed to represent reliable estimates of field intensity during a polarity inversion of the ancient field. The Lower (Mussartût) Lava Formation provided the palaeointensity values of highest quality and greatest reliability. We have no way of unequivocally proving that these lavas record the geomagnetic field at the time of their formation. However, the palaeomagnetic studies show that the remanence held by many of these flows is single component and pre-dates later intrusive activity. Furthermore, rock magnetic evidence suggests that the magnetic mineralogy comprises deuterically oxidised magnetite with predominantly MD grains but,

importantly, includes a significant SD fraction essential for palaeointensity work. Hence, the only interpretation which can be made is that the flows of the Lower Lava Formation record the geomagnetic field at the time of their formation.

The predominance of MD magnetite throughout the Gardar lavas presents problems for palaeointensity studies. In the Lower Lava Formation, certain samples possessing only a small SD fraction gave results of higher quality when the automated cryogenic magnetometer was used in preference to the spinner magnetometer to perform intensity determinations using the modified Shaw technique. This is likely to occur because the cryogenic magnetometer (unlike the spinner) is more sensitive and performs demagnetisation and measurement in zero field. Consequently, at higher fields (> 100 mT) when all MD grains are demagnetised and only a small magnetic moment due to the SD fraction remains, the sample is less likely to acquire a VRM than when being measured in the ambient laboratory field as is the case when the modified Shaw experiments are performed on the spinner magnetometer. Therefore, future Shaw palaeointensity investigations on rocks with this mineralogy would best be undertaken with a cryogenic magnetometer. Furthermore, to reduce the problems presented by MD grains, it might be useful to incorporate low temperature demagnetisation in Thellier and Shaw experiments, by immersing samples in liquid nitrogen in zero field (e.g. Merrill, 1970; Dunlop and Argyle, 1991). This would demagnetise only MD grains and is more practical than using a.f. demagnetisation for this purpose since one is never certain at which peak a.f. all MD grains are demagnetised without affecting any SD grains.

The possible identification of a Mid-Proterozoic transitional field direction, as recorded by the flows of the Middle Lava Formation is a very important result of this project. The anomalous directions obtained from a number of flows in this Formation in the previous palaeomagnetic study (Piper, 1977) stimulated these further investigations. Similar anomalous directions were obtained in the present study using thermal demagnetisation, between flows of opposite polarity. When analysed using a transformed directions plot (Hoffman, 1984,1986) the anomalous directions are found to plot remote from the defined GAD axis for the remainder of the collection. Rock magnetic results indicate that these flows are highly deuterically oxidised and show no evidence of low temperature oxidation which could lead to secondary CRM acquisition. Palaeointensity results from these flows are consistently the lowest of the entire collection and geological evidence suggests very rapid extrusion. Collectively, this evidence strongly suggests that flows recording the anomalous 'A' direction were extruded during a period when the geomagnetic field was executing a transition. If this is true, then the present study has identified one of the oldest transitional directions on record.

The most important feature of the new palaeodirectional study was the isolation of the component structure of the remanence for the Gardar lavas. Many of the eighty flows held single component remanences and those which did not had secondary components which either possessed Present Earth's Field (P.E.F.) directions or directions similar to that which prevailed during the cooling of the Ilímaussaq intrusion. This body intrudes the top of the Upper Lava Formation and thus offers an opportunity to perform a large-scale palaeomagnetic baked contact test. The results of this test (Chapters 4 and 5) show that the remanence in the lavas is older than the Ilímaussaq intrusion, which is one of the youngest known Gardar intrusion

(Blaxland et al, 1978). The intrusion is therefore a crucial part of the magnetisation story and the only drawback of its presence is the total overprinting of a few flows near the top of the lava pile, which results in a gap in the magnetostratigraphic record here.

As a measure of the reliability of the directional results, the Gardar lavas have a Q (quality) factor (Van der Voo, 1989) of 6 out of a possible 7 and must therefore be regarded as highly reliable.

The quality and reliability of the palaeomagnetic (direction and intensity) results obtained in the present study have been rigorously discussed throughout, with both good and poor results being highlighted. Overall, however, despite the inability to test proposed field models on rocks from different geographic localities, the project has confirmed that the Gardar lavas present an ideal situation for a study of the Earth's Magnetic Field during part of Mid-Proterozoic times for the following reasons:

1. The rocks form part of a stable Precambrian shield and have remained unaffected by later orogenic events.

2. Palaeomagnetic field tests have shown that the age of remanence within the lavas is older than later intrusions and is thus a part of the Gardar history.

3. Rock magnetic evidence strongly suggests that the remanence is a TRM or a TCRM acquired during or shortly after initial cooling of the lavas, and is thus likely to be primary.

In Chapter 8, the geomagnetic significance of the palaeomagnetic results was analysed. Several possible explanations for the observed field asymmetry were discussed and a field model was proposed (based on Spherical Harmonic Analysis) which was consistent with the data. This model comprises a reversing axial geocentric dipole, a reversing quadrupole and a partly reversing octupole, with the latter being stronger than the quadrupole during the reversed polarity state. However, since zonal harmonic terms higher than order 3 and non-zonal harmonics were ignored, the field model has limitations. Furthermore, the relatively low quality of the palaeointensity results from the Upper Lava Formation (which record the asymmetric fields) introduce further uncertainties. The lack of an accurate age for the Gardar lavas precludes the possibility of testing the field model on contemporaneous rocks from different geographic localities. In any case, the eruption of the lavas represents a time interval so short that it would be almost impossible to locate a sequence of rocks formed during the same interval.

CONCLUSIONS

Conclusions of the present study, are those which are (i) directly relevant to the palaeomagnetic study of the Gardar Province and the geomagnetic field during Mid-Proterozoic times, and (ii) those which are of more general significance and relevant to palaeomagnetism as a whole.

Conclusions relevant to the Gardar Province

1. Rock magnetic investigations have indicated that most flows contain a single magnetic mineral. This is either magnetite in some flows, or haematite in others. Both have no recognisable titanium substitution and were probably formed as a result of high temperature (deuteric) oxidation of original titanomagnetites shortly after initial cooling.

2. The remanence within the majority of flows is a TRM or a TCRM formed during initial cooling, with evidence of secondary CRMs only seen in the top of the Upper Lava Formation in flows nearest to the invading Ilímaussaq intrusion. The remanence within the flows of the Upper and Lower Lava Formations pre-dates intrusion of the Ilímaussaq complex and the NE-SW trending Late Gardar dyke swarm respectively.

3. Two reversals (R-N and N-R) were identified in the Lower Lava Formation and two complete reversals (N-R and R-N) were identified in the Upper Lava Formation. The latter shows a reversal asymmetry of 20° in inclination, with the mean inclinations for normal and reversed flows being +37° and -17° respectively. This anomaly is satisfied by a field source model comprising a reversing axial geocentric dipole, a reversing quadrupole and a partly reversing octupole (g_1^0, g_2^0 and g_3^0) terms, with the octupole being stronger than the quadrupole during the reversed polarity state.

4. The Shaw technique yielded no palaeointensity results from the Upper and Middle Lavas since the flows possess an unsuitable magnetic mineralogy. The mean Thellier palaeointensity values calculated for the normal and reversed flows in the Upper lavas are $31.4 \pm 2.5\mu T$ and $10.8 \pm 1.1\mu T$ respectively, although limited confidence is placed in these results. The large N/R palaeointensity ratio may be real or it could be due to the low reliability of either, or both, the normal and reversed mean palaeointensity values. The mean Thellier palaeointensity value for the Middle lavas is $8.4 \pm 0.5\mu T$. The flows of the Lower Lava Formation gave acceptable results with both the modified Thellier and Shaw techniques; the mean Thellier palaeointensity value was $34.3 \pm 2.3\mu T$ and the mean Shaw result was $33.8 \pm 2.1\mu T$. These results are believed to be the most reliable of the entire collection.

5. The mean VDM values for the normally magnetised flows in the Lower and Upper Lava Formations are $(8.2 \pm 0.5) \times 10^{22} Am^2$ and $(6.9 \pm 0.3) \times 10^{22} Am^2$ respectively. These compare favourably with previous estimates for the Proterozoic field (Chapter 8). The mean VDM values for the 'A' and 'B' directions of the Middle Lava Formation are $(1.7 \pm 0.1) \times 10^{22} Am^2$ and $(2.3 \pm 0.2) \times 10^{22} Am^2$ respectively. These values are much lower than the previous estimates of the Proterozoic VDM. The mean VDM value for the reversely magnetised lavas of the Upper Lava Formation is also low ($2.7 \pm 0.2 \times 10^{22} Am^2$).

6. Geological and palaeomagnetic evidence strongly suggests that seven flows within the Middle Lava Formation which carry an anomalous direction of magnetisation were erupted and magnetised when the geomagnetic field was in a transitional phase. If this is true, then this

transition (the Ulukasik transition) would be one of the oldest field transitions on record, although some earlier reversals have been recorded in sedimentary sequences (e.g. Bingham and Evans, 1975).

7. The global significance of the geomagnetic field model proposed in this project cannot be tested satisfactorily until accurate age determinations are available for the Gardar lavas. Attempts to obtain ages are in progress in the U.K. but were not completed by the time of presentation of this thesis.

General Conclusions and recommendations

1. It is important to perform detailed rock magnetic investigations on old rocks prior to performing palaeomagnetic investigations in order to identify the composition, domain state and oxidation states of the magnetic minerals. This information allows the palaeomagnetic results to be fully understood in the context of the thermomagnetic history of the rocks.

2. In palaeointensity experiments, all samples should be used initially, i.e. there should be no pre-rejection on the evidence of limited rock magnetic data, so that the behaviour of samples during experiments can be correlated with their rock magnetic properties. This allows selection/rejection criteria to be established for use in later studies which assess sample suitability on empirical grounds.

3. Ancient basalts often yield palaeointensity results of limited reliability due to the predominance of MD magnetite in their magnetic mineralogy.

The most reliable field intensity estimates are obtained from basalts with a significant SD fraction in a mixed grain size of magnetite.

4. At present, we cannot identify the amount of SD material necessary for a rock to record and preserve a reliable palaeointensity estimate. A useful piece of future research would be to extend the analysis presented in Chapter 7 to incorporate other ancient basalts in an attempt to confirm that the values of M_{rs}/M_s, MDF, RS and PS, recognised here as describing the SD fraction necessary for a sample to be suitable for palaeointensity work, are of general application.

5. It is recommended that future palaeointensity work on ancient basalts should:

   a. Perform both Thellier and Shaw experiments wherever possible for comparative purposes.

   b. Use a cryogenic magnetometer so that the magnetic moment resulting from very small SD fractions can be accurately measured.

   c. Assess the benefits of using low temperature demagnetisation in zero field to eliminate MD grains of magnetite from palaeointensity analysis. A comparison could also be made with the use of a.f. demagnetisation for this purpose.

   d. Undertake detailed rock magnetic investigations of all samples prior to palaeointensity analysis.

REFERENCES

Ade-Hall, J.M., Khan, M.A., Dagley, P & Wilson, R.L. (1968). A detailed opaque petrological and magnetic investigation of a single Tertiary lava from Skye, Scotland. Part I: Iron-titanium oxide petrology. Geophys. J. R. Astr. Soc., 16, 375-395.

Ade-Hall, J.M., Palmer, H.C., & Hubbard, T.P.. (1971). The magnetic and opaque petrological response of basalts to regional hydrothermal alteration. Geophys. J. R. Astr. Soc., 24, 137-174.

Aitken, M.J. & Hawley, H.N. (1971). Archaeomagnetism. Evidence for magnetic refraction in kiln structures. Archaeometry 13 (1), 83-85.

Akimoto, S & Katsura, T. (1959). Magneto-chemical study of the generalised titanomagnetite in volcanic rocks. J. Geomag. Geoelect., 10, 69-90.

Allart, J.H., (1970). Geological map of Greenland, 1:100,000 Julianehåb, 60 V.2 Nord. Geological Survey of Greenland, Copenhagen.

Appel, E. & Soffel, H.C. (1985). Domain state of Ti-rich titanomagnetites deduced from domain structure observations and susceptibility measurements. J. Geophys., 56, 121-132.

As, J.A. & Zijderveld, J.D.A. (1958). Magnetic cleaning of rocks in palaeomagnetic research. Geophys. J.R. Astr. Soc.,1, 318-319.

Barbetti, M.F. & McElhinny, M.W. (1972). Evidence of a geomagnetic excursion 30,000 yr BP. Nature 239, 327-329.

Barbetti, M.F. & McElhinny, M.W. (1976). The Lake Mungo geomagnetic excursion. Phil. Trans. R. Soc. A 281, 515.

Barraclough, D.R. (1974). Spherical Harmonic analysis of the geomagnetic field for eight epochs between 1600 & 1910. Geophys. J.R. Astron. Soc. 36, 497-512.

Bergh, H.W. (1970). Palaeomagnetism of the Stillwater Complex Montana. In Palaeogeophysics, Runcorn, S.K., ed.. Academic Press, 143-158.

Berthelsen, A. & Henriksen, N., (1975). Geological map of Greenland, 1:100,000 Ivigtut 61 V.1 Syd. The Orogenic and Cratogenic Geology of a Precambrian Shield Area, 169pp. Geological Survey of Greenland, Copenhagen.

Bickford, L.R. (1950). Ferromagnetic resonance absorption in a magnetite single crystal. Phys. Rev., 78, 449-457.

Bingham, D.K. & Evans, M.E. (1975). Precambrian geomagnetic field reversal. Nature 253, 332-333.

Blaxland, A.B., van Breeman, O., Emeleus, C.H. & Anderson, J.G., (1978). Age and origin of the major syenite centres in the Gardar province of South Greenland: Rb-Sr studies. Geol. Soc. Am. Bull. 89, 231-244.

Bogue, S.W. & Coe, R.S. (1981). Thellier palaeointensity results from a R-N transition zone on Kauai, Hawaii. EOS 62, 853-855.

Bohse, H., Brooks, C.K. & Kunzendorf, K. (1971). Field observations on the kakortokites of the Ilímaussaq intrusion, South Greenland. Rapp. Grønlands Geol. Unders. 38, 43pp.

Bolshakov, A.S. & Shcherbakova, V.V. (1979). Thermomagnetic test for determining the domain structure of ferrimagnetics. Izv. Akad. Nauk USSR. Solid Earth 15, 111-117.

Bonhommet, N & Babkine, J. (1967). Sur la présence d'aimantations inversées dans la Châine des Puys. C.R. Acad. Sci. Paris 264, 92-103.

Briden, J.C. & Mullan, A.J. (1984). Superimposed Recent, Permo-Carboniferous and Ordovician palaeomagnetic remanence in the Builth Volcanic Series, Wales. Earth Planet. Sci. Lett. 69, 413-421.

Brunhes, B. (1906). Reserches sur la direction d'aimantation des roches volcaniques. J. Phys. 5, 705-724.

Buchan, K.L. (1977). Palaeomagnetic and rock magnetic studies of multicomponent remanences in metamorphosed rocks of the Grenville

Province of the Canadian Shield. Unpublished Ph.D. thesis, University of Toronto, Ontario.

Buddington, A.F. & Lindsley, D.H. (1974). Iron-titanium oxide minerals and synthetic equivalents. J. Petrol. 54, 310-357.

Bullard, E.C., Freedman, C., Gellman, H & Nixon, J. (1950). The westward drift of the earth's magnetic field. Phil. Trans. Roy. Soc. A 243, 67-92.

Bullard, E.C., Everitt, J.E. & Smith, A.G. (1965). A Symposium on Continental Drift IV. The fit of the Continents around the Atlantic. Phil. Trans. Roy. Soc. Lond. A258, 41-51.

Butler, R.F. & Banerjee, S.F. (1975). Theoretical single-domain grain size range in magnetite and titano-magnetite. J. Geophys. Res. 80, 4049.

Carmichael, C.M. (1967). An outline of the intensity of the palaeomagnetic field of the Earth. Earth Planet. Sci. Lett. 3, 351-354.

Coe, R.S. (1967). The determination of palaeointensities of the earth's magnetic field with emphasis on mechanisms which would cause nonideal behaviour in the Thelliers method. J. Geomag. Geoelect. 19, 157-179.

Coe, R.S., Grommé, C.S. and Mankinen, E.A. (1978). Geomagnetic palaeointensities from radiocarbon-dated lava flows on Hawaii and the question of the Pacific nondipole low. J. Geophys. Res. 83, 1740-1756.

Cox, A (1961). Anomalous remanent magnetisation of basalt. U.S. Geol. Surv. Bull. 1083-E, 131-160.

Cox, A. (1975). The frequency of geomagnetic reversals and the symmetry of the non-dipole field. Rev. Geophys. Space Phys. 13, 35-51.

Coupland, D.H. & Van der Voo, R. (1980). Long-term non-dipole components in the geomagnetic field during the last 130 Ma. J. Geophys. Res. 85, 3529-3548.

Creer, K.M. (1959). A.C. demagnetisation of unstable Triassic Keuper marls from S.W. England. Geophys. J. Astr. Soc., 2, 261-275.

Creer, K.M. & Ibbetson, J.D. (1970). Electron microprobe analyses and magnetic properties of non-stoichiometric titanomagnetites in basaltic rocks. Geophys. J.R. Astr. Soc., 21, 485-511.

Dagley, P., Wilson, R.L., Ade-Hall, J.M., Walker, G.P.L., Haggerty, S.E., Sigurgeirsson, T., Watkins, N.D., Smith, P.J., Edwards, J. & Grasty, R.L. (1967). Geomagnetic polarity zones for Icelandic lavas. Nature 216, 25-29.

Dagley, P. & Wilson, R.L. (1971). Geomagnetic field reversals - a link between strength and orientation of a dipole source. Nature Phys. Sci. 232, 16

Dagley, P. & Lawley, E. (1974). Palaeomagnetic Evidence for the Transitional Behaviour of the Geomagnetic field. Geophys. J.R. Astron. Soc. 36, 577-598.

Day, R. (1973). The effect of grain size on the magnetic properties of the magnetite-ulvospinel solid solution series. Ph.D. thesis (Unpublished), Univ. of Pittsburgh, Pittsburgh, Pa., U.S.A.

Day, R., Fuller, M. & Schmidt, V.A. (1976). Magnetic hysteresis properties of synthetic titanomagnetites. J. Geophys. Res., 81, 989-994.

Day, R., Fuller, M. & Schmidt, V.A. (1977). Hysteresis properties of titanomagnetites: grain size and composition dependence. Phys. Earth Planet. Inter., 13, 260-267.

Derder, M.E., Thompson, J., Prévot, M. and McWilliams, M. (1989). Geomagnetic field intensity in Early Jurassic: investigation of the Newark Supergroup (eastern North America). Phys. Earth Planet. Inter. 58, 126-136.

Domen, H. (1977). A single heating method of palaeomagnetic field intensity determination applied to old roof tiles and rocks. Phys. Earth Planet. Inter. 13, 315-318.

Dickson, G.O., Everitt, C.W., Parry, L.G. & Stacey, F.D. (1966). Origin of thermoremanent magnetisation. Earth Planet. Sci. Lett., 1, 222-233.

Dubois, P.M. (1962). Palaeomagnetism and correlation of Keweenawan rocks. Bull. Geol.Surv. Can. 71, 1-75.

Duff, B.A. (1979). Peaked thermomagnetic curves for haematite-bearing rocks and concentrates. Phys. Earth Planet. Inter., 19, P1-P4.

Dunlop, D.J. (1969). Hysteresis properties of synthetic and natural monodomains. Phil. Mag., 19, 329-338.

Dunlop, D.J. (1971). Magnetic properties of fine-particle haematite. Ann. Geophys., 27, 269-293.

Dunlop, D.J. (1972). Magnetite: behaviour near the single domain threshold. Science, 176, 41-43.

Dunlop, D.J. (1973). Superparamagnetic and single domain threshold sizes in magnetite. J. Geophys. Res., 78, 1780-1793.

Dunlop, D.J. (1974). Thermal enhancement of magnetic susceptibility. J. Geophys., 40, 439-451.

Dunlop, D.J. (1979). On the use of Zijderveld vector diagrams in multi-component palaeomagnetic studies. Phys. Earth Planet. Inter., 20, 12-24.

Dunlop, D.J. (1981). The rock magnetism of fine particles. Phys. Earth Planet. Inter. 26, 1-26.

Dunlop, D.J. & Buchan, K.L. (1977). Thermal remagnetisation and the palaeointensity record of metamorphic rocks. Phys. Earth Planet. Inter. 13, 325-331.

Dunlop, D.J. & Waddington, D. (1975). The field dependence of thermoremanent magnetisation in igneous rocks. Earth Planet Sci. Lett, 25, 11-25.

Dunlop, D.J. & West, G.R. (1969). An experimental evaluation of single-domain theories. Rev. Geophys. Space Phys. 7, 709-757.

Dunlop, D.J. & Argyle, K.S. (1991). Separating Multidomain and Single-Domain-Like Remanences in Pseudo-Single Domain Magnetites (215-540 nm) by Low Temperature Demagnetisation. J. Geophys. Res. 96, 2007-2017.

Emeleus, C.H. & Upton, B.G.J., (1976). The Gardar period in Southern Greenland. In: Escher, A. & Watt, S.W. (Eds) The Geology of Greenland, 153-181. The Geological Survey of Greenland, Copenhagen.

Evans, M.E. & McElhinny, M.W. (1969). An investigation of the origin of stable remanence in magnetite-bearing igneous rocks. J. Geomag. Geoelec. 21, 757-773.

Everitt, C.W.F. & Clegg, J.A. (1962). A field test for palaeomagnetic stability. Geophys. J.R. Astron. Soc. 6, 312-319.

Ferguson, J. (1964). Geology of the Ilímaussaq alkaline intrusion, South Greenland. Bull. Gronlands Geol. Unders. 39, 82pp.

Ferguson, J. (1970). The differentiation of agpaitic magmas: the Ilímaussaq intrusion, South Greenland. Can. Miner. 10, 335-349.

Fisher, R.A. (1953). Dispersion on a Sphere. Proc. Roy. Soc. Lond. A217, 295-305.

Fox, J.M.W. & Aitken, M.J. (1980). Cooling rate dependence of thermoremanent magnetisation. Nature 283, 462-463.

Graham, J.W. (1949). The stability and significance of magnetism in sedimentary rocks. J. Geophys. Res., 54, 131-167.

Graham, K.W.T. (1961). The remagnetisation of a surface outcrop by lightening currents. Geophys. J.R. Astron. Soc. 6, 85-102.

Grommé, C.S., Wright, T.L. & Peck, D.L. (1969). Magnetic properties and oxidation of iron-titanium oxide minerals in Alae and Makaoputi lava lakes, Hawaii. J. Geophys. Res. 74, 5277-5293.

Grommé, C.S., Mankinen, E.A., Marshall, M & Coe, R.S. (1979). Geomagnetic palaeointensities by the Thelliers method from submarine pillow basalts: effects of seafloor weathering. J. Geophys. Res. 84, 3553-3575.

Gubbins, D. (1984). The earth's magnetic field. Contemp. Phys. 25, 269-290.

Haggerty, S.E. (1976). Oxidation of opaque mineral oxides in basalts. Oxide Minerals (short course notes), (ed. D. Rumble). Mineralogical Soc. Amer. 3, 1-100.

Hailwood, E.A. (1977). Configuration of the geomagnetic field in early Tertiary times. J. Geol. Soc. Lond. 133, 23-36.

Hailwood, E.A. (1989). Magnetostratigraphy. Blackwell Scientific for the Geol. Soc., Oxford.

Hale, C.J. (1987). The intensity of the geomagnetic field at 3.5Ga: palaeointensity results from the Komati Formation, Barberton Mountain Land, South Africa. Earth Planet. Sci. Lett. 86, 354-364.

Hamilton, E.I. (1964). The geochemistry of the northern part of the Ilímaussaq intrusion, S.W. Greenland. Bull. Grmnlands Geol. Unders. 42, 104pp.

Hoffman, K.A. (1984). A method for the display and analysis of transitional palaeomagnetic data. J. Geophys. Res. 89, 6285-6292.

Hoffman, K.A. (1986). Transitional field behaviour from southern hemisphere lavas: evidence for two stage reversals of the geodynamo. Nature 320, 228-232.

Hoffman, K.A., Constantine, V.L. & Morse, D.L. (1989). Determination of absolute palaeointensity using a multi-specimin procedure. Nature 339, 295-297.

Hopkinson, J. (1889). Magnetic and other physical properties of iron at a high temperature. Phil. Trans. R.S. (London), A180, 443-465.

Irving, E., Robertson, W.A., Scott, P.M., Tarling, D.H. & Ward, M.A. (1961). Treatment of partially stable sedimentary rocks showing planar distribution of directions of magnetisation. J. Geophys. Res. 66, 1927-1933.

Jacobs, J.A. (1984). Reversals of the Earth's Magnetic field. Adam Higler, Bristol.

Kirschvink, J.L. (1980). The least squares line and plane and the analysis of palaeomagnetic data. Geophys. J. Royal Astr. Soc. 62, 699-718.

Kobayashi, K. (1968). Palaeomagnetic determination of the intensity of the geomagnetic field in the Precambrian period. Phys. Earth Planet. Inter. 1, 387-395.

Koenigsberger, J.G. (1938). Natural residual magnetism of eruptive rocks, parts I and II. Terr. Magn. Atmos. Elec. 43, 119-127, 299-330.

Kono, M. (1978). Reliability of palaeointensity methods using alternating field demagnetisation and anhysteretic remanences. Geophys. J.R. Astr. Soc. 54, 241-261.

Kono, M & Ueno, N. (1977). Palaeointensity determination by a modified Thellier method. Phys. Earth Planet. Inter. 13, 305-314.

Larsen, J.G., (1977). Petrology of the late lavas of the Eriksfjord Formation, Gardar Province, South Greenland. Geological Survey of Greenland Bulletin 125, 31pp.

Larson, E.M., Ozima, M, Nagata, T & Strangway, D.W. (1969). Stability of remanent magnetisation of rocks. Geophys. J.R. Astr. Soc., 17, 263-292.

Lawson, C.A., Nord, G.L., Dowty, E. & Hargreaves, R.B. (1981). Antiphase domains and reverse thermoremanent magnetism in ilmenite-haematite minerals. Science 213, 1372-1374.

Levi, S. (1976). The additivity of partial thermoremanence. EOS, Trans. Act. Am. Geophys. Un. 57, 12, 905.

Levi, S & Merrill, R.T. (1976). A comparison of ARM and TRM in magnetite. Earth Planet. Sci. Lett. 32, 171-184.

Levi, S & Merrill, R.T. (1978). Properties of single domain, pseudo-single domain and multi domain magnetite. J. Geophys. Res. 85, 3690-3698.

Liddicoat, J.C. & Coe, R.S. (1979). Mono Lake Geomagnetic excursion. J. Geophys. Res. 84, 261-271.

Lowrie, W. & Fuller, M. (1971). On the alternating field demagnetisation characteristics of multi-domain thermoremant magnetisation in magnetite. J. Geophys. Res., 78, 6339-6349.

Maher, B. (1988). Magnetic properties of some synthetic sub-micron magnetites. Geophys. J.R. Astr. Soc. 94, 83-96.

Mankinen, E.A., Prévot, M. & Grommé, C.S. (1985). The Steens Mountain (Oregon) geomagnetic polarity transition 1: directional history, duration of episodes and rock magnetism. J. Geophys. Res. 90, 10393-10416.

McElhinny, M.W. (1973). Palaeomagnetism and Plate Tectonics. University Press, London. 358pp.

McElhinny, M.W. & Evans, M.E. (1968). An investigation of the strength of the geomagnetic field in the early Precambrian. Phys. Earth Planet Inter. 1, 485-497.

McFadden, P.L. & McElhinny, M.W. (1982). Variations in the geomagnetic dipole 2: statistical analysis of VDMs for the past % million years. J. Geomag. Geoelectr. 34, 163-189.

McClleland-Brown, E. (1984). Experiments on TRM intensity dependence on cooling rate. Geophys. Res. Lett. 11, 205-208.

Merrill, R.T. (1970). Low temperature treatment of magnetite and magnetite-bearing rocks. J. Geophys. Res., 75, 3343-3349.

Merrill, R.T. & McElhinny, M.W. (1977). Anomalies in the time-averaged palaeomagnetic field and their implications for the lower mantle. Rev. Geophys. Space Phys. 15, 309-323.

Merrill, R.T. & McElhinny, M.W. (1983). The Earth's Magnetic Field - its history, origin and planetary perspective. Academic Press. 401pp.

Molyneux, L. (1971). A complete result magnetometer for measuring the remanent magnetisation of rocks. Geophys. J.R. Astr. Soc. 24, 429-433.

Mussett, A.E., Ross, I.G. & Gibson, I.L. (1980). 40Ar-39Ar dates of eastern Iceland lavas. Geophys. J.R. Astron. Soc. 60, 37-52.

Nagata, T. (1943). The natural remanent magnetism of volcanic rocks and its relation to geomagnetic phenomena. Bull. Earthquake Res. Inst. Tokyo Univ. 21, 1.

Nagata, T., Arai, Y & Momose, K. (1963). Secular variation of the geomagnetic total force during the last 5000 years. J. Geophys. Res. 68, 5227-5242.

Nevanlinna, H. & Pesonen, L.J. (1983). Late Precambrian Keweenawan asymmetric polarities as analysed by axial offset dipole geomagnetic models. J. Geophys. Res. 88, 645-658.

Néel, L (1949). Théorie du trainage magnétique des ferromagnétiques en grains fins avec applications aux terres cuites. Ann. Geophys. 5, 99-136.

Néel, L. (1955). Some theoretical aspects of rock magnetism. Phil. Mag. Suppl. Adv. Phys. 4, 191-243.

Nishitani, T. & Kono, M. (1983). Curie temperature and lattice constant of oxidised titanomagnetite. Geophys. J. R. Astron. Soc. 74, 585-600.

O'Reilly, W. (1983). The identification of titanomaghaemites: model mechanisms for the maghaemitization and inversion processes and their magnetic consequences. Phys. Earth Planet. Inter. 31, 65-76.

O'Reilly, W. (1984). Rock and mineral magnetism. Blackie, 220pp.

Ozdemir, O. & Banerjee, S.K. (1981). An experimental study of magnetic viscosity in synthetic monodomain titanomaghaemites: implications for the magnetisation of the ocean crust. J. Geophys. Res. 86 (11), 864-868.

Palmer, H.C. (1970). Palaeomagnetism and some correlation of some Middle Keweenawan rocks, Lake Superior. Can. J. Earth Sci. 7, 1410-1436.

Parry, L.G. (1965). Magnetic properties of dispersed magnetite powders. Phil. Mag. 11, 303-312.

Parsons, J. (1989). A palaeomagnetic study of the ca. 1300 Ma Lower Sandstone Group of the Eriksfjord Formation, South Greenland. Unpublished undergraduate honours year project, University of Liverpool.

Patchett, P.J., Bylund, G. & Upton, B.G.J., (1978). Palaeomagnetism and the Grenville orogeny : new Rb-Sr ages from dolerites in Canada and Greenland. Earth Planet. Sci. Lett. 40, 349-364.

Pesonen, L.J. (1978). Palaeomagnetism, palaeointensity and palaeosecular variation studies of Keweenawan igneous and baked contact rocks. Unpublished Ph.D. thesis, Univ. of Toronto, Toronto, Ontario, Canada.

Pesonen, L.J. & Halls, H.C. (1979). The palaeomagnetism of Keweenawan dykes from from Baraga and Marquette counties, northern Michigan. Can. J. Earth Sci. 16, 2136-2149.

Pesonen, L.J. Halls, H.C. (1983). Geomagnetic field intensity and reversal asymmetry in late Precambrian Keweenawan rocks. Geophys. J.R. Astr. Soc. 73, 241-270.

Pesonen, L.J. & Nevanlinna, H. (1981). Late Precambrian Keweenawan asymmetric reversals. Nature 294, 436-439.

Piper, J.D.A. (1975). The palaeomagnetism of Precambrian igneous and sedimentary rocks of the Orange River belt in South Africa and South West Africa Geophys. J. R. Astron. Soc. 40, 313-344.

Piper, J.D.A. (1976). Palaeomagnetism of marginal syenites and fractionated rocks of the Ilímaussaq intrusion, South Greenland. Bull. Geol. Soc. Denmark 25, 89-97.

Piper, J.D.A. (1977). Magnetic Stratigraphy and Magnetic-Petrologic properties of Precambrian Gardar lavas, South Greenland. Earth Planet. Sci. Lett. 34, 247-263.

Poulsen, V. (1964). The sandstones of the Precambrian Eriksfjord Formation in South Greenland. Geological Survey of Greenland report 2, 16pp.

Prévot, M., Mankinen, E.A., Grommé, C.S. & Lecaille, A. (1983). High palaeointensities of the geomagnetic field from thermomagnetic studies on rift valley pillow basalts from the Mid-Atlantic Ridge. J. Geophys. Res. 88, 2316-2326.

Prévot, M., Mankinen, E.A., Coe, R.S. & Grommé, C.S. (1985). The Steens Mountain (Oregon) Geomagnetic Polarity Transition 2. Field intensity variations and discussion of reversal models. J. Geophys. Res. 90, 10417-10448.

Pullaiah, G., Irving, E, Buchan, K.L. & Dunlop, D.J. (1975). Magnetisation changes caused by burial and uplift. Earth Planet. Sci. Lett. 28, 133-143.

Radhakrishnamurty, C. (1985). Identification of titanomagnetites by simple magnetic techniques and application to basalt studies. J. Geol. Soc. India 26, 640-651.

Radhakrishnamurty, C. (1989). Developments in rock (basalt) magnetism. Geophysics in India 1, 39-45.

Radhakrishnamurty, C. (1990). Mixed domain states of magnetic grains in basalts and implications for palaeomagnetism. Phys. Earth Planet. Inter. 64, 348-354.

Radhakrishnamurty, C. & Likhite, S.D. (1970). Hopkinson effect, blocking temperature and Curie point in basalts. Earth Planet. Sci. Lett. 7, 389-396.

Radhakrishnamurty, C. & Likhite, S.D. (1987). A pulsed field technique for the study of magnetic grains in rocks. Phys. Earth Planet. Inter. 46, 259-262.

Radhakrishnamurty, C., Likhite, S.D. & Sahasrabhude, P.W. (1970). Some curious magnetic properties of rocks. In Palaeogeophysics, Runcorn, S.K. ed.. Academic Press, London, 166-168.

Radhakrishnamurty, C., Likhite, S.D. & Sahasrabudhe, P.W. (1977). Nature of magnetic grains and their effect on the remanent magnetisation of basalts. Phys. Earth Planet. Inter. 13, 289-300.

Radhakrishnamurty, C., Likhite, S.D., Deutch, E.R. & Murthy, G.S. (1978). Nature of magnetic grains in basalts and implications for palaeomagnetism. Proc. Indian Acad. Sci. A87, 235-243.

Radhakrishnamurty, C., Likhite, S.D., Deutch, E.R. & Murthy, G.S. (1981). A comparison of the magnetic properties of synthetic titanomagnetites and basalts. Phys. Earth Planet. Inter. 26, 37-46.

Radhakrishnamurty, C., Likhite, S.D. & Sahasrabudhe, P.W. (1991). Domain states of magnetic grains in basalts and palaeointensity techniques. J. Geomag. Geoelec. 43, 1-15.

Rahman, A.A. & Parry, L.G. (1978). Titanomagnetites prepared at different oxidation conditions: Hysteresis properties. Phys. Earth Planet. Inter. 16, 232-239.

Readman, P.W. & O'Reilly, W. (1970). The synthesis and inversion of non-stoichiometric titanomagnetites. Phys. Earth Planet. Inter. 4, 121-128.

Reubens, S.M. (1945). Cube-surface coil for Producing a Uniform Magnetic Field. Rev. Sci. Instr. 16 (9), 243-245.

Richards, A. (1986). A study of the palaeointensity and reversal asymmetries of the geomagnetic field using 1300 Ma Gardar lavas from South Greenland. Unpublished undergraduate honours year project, University College, Cardiff.

Rigotti, P.A. (1978). The ARM correction method of palaeointensity determination. Earth Planet. Sci. Lett. 39, 417-426.

Rikitake, T. (1966). Electromagnetism and the Earth's interior. Elsevier, Amsterdam.

Roberts, N. (1983). The Earth's Magnetic Field during Reversals. Unpubl. Ph.D. thesis. University of Wales.

Roberts, N & Shaw, J. (1984). The relationship between the magnitude and direction of the geomagnetic field during the Late Tertiary in eastern Iceland. Geophys. J. R. Astron. Soc. 76, 637-651.

Robertson, W.A. & Fahrig, W. (1971). The great Logan Palaeomagnetic Loop - the polar wandering path from Canadian shield rocks during the Neohelikian era. Can. J. Earth Sci. 8, 1355-1372.

Rolph, T.C. (1984). The determination of ancient, historic and modern geomagnetic field intensities from thermally altered lavas. Unpublished Ph.D. thesis. Univ. of Wales.

Rolph, T.C. (1991). High field intensity results from recent and historic lavas. PEPI Conference edition (In press).

Rolph, T.C. and Shaw, J. (1985). A new method of palaeofield magnitude correction for thermally altered samples and its application to Lower Carboniferous lavas. Geophys. J.R. Astron. Soc. 80, 773-781.

Roy, J.L. (1977). Problems in determining palaeointensities from very old rocks. Phys. Earth Planet. Inter. 13, 319-324.

Roy, J.L. & Robertson, W.A. (1978). Palaeomagnetism of the Jacobsville Formation and the apparent polar wander path for the interval -1100 to -670 m.y. for North America. J. Geophys. Res. 83, 1289-1304.

Sanver, M. & O'Reilly, W. (1970). Identification of naturally occurring non-stoichiometric titanomagnetites. Phys. Earth Planet. Inter. 2, 166-174.

Scherbakov, V.P. & Lamash, B.E. (1988). Metastability threshold sizes in single domain magnetite particles. Geophys. Res. Lett. 15 (5), 526-529.

Schwartz, E.J. & Symons, D.T.A. (1969). Geomagnetic intensity between 100 million and 2500 million years ago. hys. Earth Planet. Inter. 2, 11-18.

Senanayake, W.E. (1981). Geomagnetic field intensity in the geological past. Unpublished Ph.D. thesis, Australian National University, Canberra, Australia.

Senanayake, W.E. & McElhinny, M.W. (1981). Hysteresis and susceptibility characteristics of magnetite and titanomagnetites: interpretation of results from basaltic rocks. Phys. Earth Planet. Inter. 26, 47-55.

Senanayake, W.E. & McElhinny, M.W. (1982). The effects of heating on low temperature susceptibility and hysteresis properties of basalts. Phys. Earth Planet. Inter. 30, 317-321.

Senanayake, W.E., McElhinny, M.W. & McFadden, P.L. (1982). Comparisons between the Thelliers' and Shaw's palaeointensity methods using basalts less than 5 million years old. J. Geomag. Geoelectr. 34, 141-163.

Shaw, J. (1974). A new method of determining the magnitude of the palaeomagnetic field. Application to five historic lavas and five archaeological samples. Geophys. J.R. Astron. Soc. 39, 133-144.

Shaw, J. (1975). Strong geomagnetic field during a single Icelandic polarity transition. Geophys. J. R. Astron. Soc. 40, 345-350.

Shaw, J. (1977). Further evidence for a strong intermediate state of the palaeomagnetic field. Geophys. J. R. Astron. Soc. 48, 263-269.

Shaw, J., Dagley, P. & Mussett, A.E. (1982). The magnitude of the palaeomagnetic field in Iceland between 2 and 6 Myr ago. Geophys. J. 68, 211.

Shaw, J., Share, J.A. & Rogers, J. (1984). An automated superconducting magnetometer and demagnetising system. Geophys. J.R. Astron. Soc. 78, 209-217.

Sherwood, G.J. (1986). The Middle to Late Miocene Geomagnetic field: Implications of new results from New Zealand lavas. Unpublished Ph.D. thesis, University of Wales.

Sherwood, G.J. (1988). Rock magnetic studies of Miocene volcanics in eastern Otago and Banks Peninsula, New Zealand: comparison between Curie temperature and low temperature susceptibility behaviour. New Zealand J. Geol. Geophys. 31, 225-235.

Sherwood, G.J. (1989). MATZIJ - A Basic Program to determine Palaeomagnetic Remanence Directions Using Principal Component Analysis. Computers & Geosciences 15, 1173-1182.

Sherwood, G.J. (1990). A palaeomagnetic and rock magnetic study of Tertiary volcanics from the Vogelsberg (Germany). Phys. Earth Planet. Inter. 62, 32-45.

Sherwood, G.J. (1991). Evaluation of a Multi-Specimen Approach to Palaeointensity Determination. J. Geomag. Geoelec. 43, 341-349.

Smith, P.J. (1967a). The intensity of the Tertiary geomagnetic field. Geophys. J. R. Astron. Soc. 12, 239-258.

Smith, P.J. (1967b). On the suitability of igneous rocks for ancient geomagnetic intensity determination. Earth Planet. Sci. Lett. 2, 99-105.

Soffel, H & Appel, E. (1982). Domain structure of small synthetic titanomagnetite particles and experiments with IRM and TRM. Phys. Earth Planet. Inter. 30, 348-355.

Sørensen, H., Hansen, J. & Bondesen, E. (1969). Preliminary account of the geology of the Kvanefjeld area of the Ilímaussaq intrusion, South Greenland. Rapp. Grmnlands Geol. Unders. 18, 40pp.

Sørensen, H. (1970). Internal structures and geological settings of three agpaitic intrusions - Khibina and Lovozero of the Kola peninsula and Ilímaussaq, South Greenland. Can. Miner. 10, 299-334.

Stacey, F.D. (1961). Theory of the magnetic properties of igneous rocks in alternating magnetic fields. Phil. Mag. 6, 1241-1260.

Stacey, F.D. (1963). The physical theory of rock magnetism. Adv. Phys. 12, 45-133.

Stacey, F.D. (1967). The Koenigsberger ratio and the nature of thermoremanence in igneous rocks. Earth Planet. Sci. Lett. 2, 67-68.

Stacey, F.D. & Banerjee, S.K. (1974). The Physical Principles of Rock Magnetism. Elsevier Scientific Publishing Co., London and New York. 195pp.

Starkey, J., & Palmer, H.C. (1971). The sensitivity of the conglomerate test in palaeomagnetism. Geophys. J.R. Astr. Soc. 71, 235-240.

Stewart, J.W. (1964). The earlier Gardar igneous rocks of the Ilímaussaq area, South Greenland. Unpublished Ph.D. thesis. Univ. of Durham, England.

Stewart, J.W. (1970). Precambrian alkaline-ultramafic carbonatite volcanism at Qagssiarssuk, South Greenland. Geological Survey of Greenland Bulletin 84, 70pp.

Steiger, R.J., & Jager, E., (1977). Subcommision on geochronology: Convention on the use of decay constants in geo- and cosmochronology. Earth Planet. Sci. Lett. 36, 359-375.

Stoner, E.C. & Wohlfarth, E.D. (1948). A mechanism of magnetic hysteresis in heterogeneous alloys. Phil. Trans. Roy. Soc. London Ser. A A240, 599-642.

Syono, Y & Ishikawa, Y. (1963). Magnetocrystalline anisotropy of $\times Fe_2TiO_4(1 - x)Fe_3O_4$ J. Phys. Soc. Japan 18, 1230-1232.

Thellier, E. (1937). Recherche de l'intensité du champ magnétique terrestre dans le passé: Premiers résultats. C.R. Acad. Sci. Paris 204, 184-186.

Thellier, E. (1938). Sur l'animation des terres cuites et des applications géophysique. Ann. Inst. Phys. Globe 16, 157-302.

Thellier, E. (1951). Propriétés magnétiques des terres cuites et des roches. J. de Phys. et Radium. 12, 205-218.

Thellier, E. and Thellier, O. (1959). Sur l'intensité du champ magnétique terrestre dans le passé historique et géologique. Ann. Geophys. 15, 285-376.

Thompson, R & Oldfield, F. (1986). Environmental Magnetism. Allen & Unwin, London, 227pp.

Trench, A., Torsvik, T.H., Smethhurst, M.A., Woodcock, N.H. & Metcalfe, R. (1991). A palaeomagnetic study of the Builth Wells-Llandrindod Wells Ordovician inlier, Wales: palaeogeographic and structural implications. Geophys. J. Int. 105, 477-489.

Upton, B.G.J. & Blundell, D.J. (1978). The Gardar igneous province: evidence for Proterozoic continental rifting. In: Neumann, E.R. & Ramberg, I.B. (Eds). Petrology and Geochemistry of Continental Rifts. Reidel, Dordrecht. 163-172.

Upton, B.G.J. & Emeleus, C.H. (1987). Mid-Proterozoic alkaline magmatism in southern Greenland: the Gardar province. In: Fitton, J.G. & Upton, B.G.J. (Eds). Alkaline Igneous Rocks. Geological Society Special Publication No. 30, 449-471.

Upton, B.G.J., Macdonald, R. & Pinkerton, H. (1974). Early lavas of the Precambrian Eriksfjord Formation - South Greenland. Bull. Geol. Soc. Denmark. 32, 123-141.

Upton, B.G.J., Stephenson, D. & Martin, A.R. (1985). The Tugtutôq older giant dyke complex: mineralogy and geochemistry of an alkali-gabbro-augite-syentite-foyaite association in the Gardar province of South Greenland. Mineral. Mag. 49, 623-642.

Ussing, N.V. (1912). Geology of the country around Julianehåb, Greenland. Meddr. Grønland 38, 376pp.

van Breeman, O., Aftalion, M. & Allart, J.H. (1974). Isotope and Geochronologic Studies on Granites from the Ketilidian Mobile Belt of South Greenland. Bull. Geol. Soc. Amer. 85, 403-412.

van der Voo, R. (1989). Palaeomagnetism of North America: The craton, its margins and the Appalachian Belt. Geol. Soc. Am. Mem. 172, 447-470.

van Zijl, J.S.V., Graham, K.W.T & Hales, A.L. (1962). The palaeomagnetism of the Stormberg lavas of South Africa, 1 and 2. Geophys. J.R. Astron. Soc. 7, 23-39 and 169-182.

Vlasov, A Ya. & Popova, A.V. (1968). Palaeomagnetism of Precambrian deposits of the Yenisei Ridge, Izv. Acad. Sci. USSR Phys. Solid Earth. Engl. Trans. 2, 99-104.

Walton, D. (1980). Time-temperature relations in the magnetisation of assemblies of single-domain grains. Nature 286, 245-248.

Watkins, N.D. & Haggerty, S.E. (1968). Oxidation and magnetic polarity in single Icelandic lavas and dykes. Geophys. J. R. Astron. Soc. 15, 305-315.

Watson, G.S. (1956). A test for randomness of direction. Mon. Not. R. Astr. Soc. Geophys. Suppl. 7, 160-161.

Wegmann, C.E. (1938). On the structural divisions of southern Greenland. Meddr. Grønland 113 (2) 148pp.

Wells, J.M. (1973). Non-linear spherical harmonic analysis of palaeomagnetic data. In Methods in Computational Physics Vol. 13, ed. Bolt, B.A., p239. Academic Press, New York and London.

Wilson, R.L. (1961). Palaeomagnetism in Northern Ireland, Part 1: The thermal demagnetisation of natural magnetic moments in rocks.

Wilson, R.L. (1962a). The palaeomagnetic history of a doubly baked rock. Geophys. J. R. Astron. Soc. 6, 397-399.

Wilson, R.L. (1962b). An instrument for measuring vector magnetisation at high temperatures. Geophys. J. Royal Astr. Soc. 7, 125-130.

Wilson, R.L. (1970). Permanent aspects of the earth's non-dipole magnetic field over upper tertiary times. Geophys. J.R. Astron. Soc. 19, 417-437.

Wilson, R.L. (1971). Dipole offset. The time average palaeomagnetic field over the last 25 million years. Geophys. J.R. Astron. Soc. 22, 491-504.

Wilson, R.L. (1972). Palaeomagnetic differences between normal and reversed field sources, and the problem of far-sided and right-handed pole positions.

Wilson, R.L. & Watkins, N.D. (1967). Correlation of magnetic polarity and petrological properties in Columbia Plateau basalts. Geophys. J.R. Astr. Soc. 12, 405-424.

Wilson, R.L. & McElhinny, M.W. (1974). Investigation of the large-scale palaeomagnetic field over the past 25 million years; eastward shift of the Icelandic spreading ridge. Geophys. J.R. Astr. Soc. 39, 570-586.

Wilson, R.L., Dagley, P. & McCormack, A.G. (1972). Palaeomagnetic evidence about the source of the geomagnetic field. Geophys. J.R. Astr. Soc. 28, 213.

Yukutake, T. (1962). The westward drift of the magnetic field of the earth. Bull. Earthquake Res. Inst. 40, 1.

Zijderveld, J.D.A. (1967). A.C. demagnetisation of rocks: analysis of results. In Methods in Palaeomagnetism (Collinson, D.W., Creer, K.M. & Runcorn, S.K. eds.) Elsevier, 254-286.

APPENDIX 1 :

THERMAL DEMAGNETISATION RESULTS FOR ALL SAMPLES IN THE LOWER LAVA FORMATION

SAMPLE	D	I	α95	T	CAT	POLARITY
L1-01	337.6	58.1	1.7	300-540	B	N
	(347.0	65.8	4.2	0-200)		
-02	52.1	8.8	8.8	500-600	A	N*
L2-01	324.2	22.7	6.1	560-630	A	N
-03	292.2	23.8	2.2	560-660	A	N
L3-01	299.1	14.3	5.5	400-520	B	N
	(302.2	28.8	9.7	0-300)		
-02	308.1	7.9	6.8	530-600	A	N
L4-01	339.1	47.1	3.6	300-530	A	N*
-02	328.0	44.0	3.2	300-530	A	N*
-03	357.0	55.3	5.9	200-520	A	N*
-04	80.9	38.2	6.0	500-530	A	I*
L5-01	301.8	22.5	3.9	500-540	C	N
	(307.4	29.5	7.0	0-400)		
-02	299.5	21.7	4.5	510-560	C	N
	(302.5	29.2	4.9	0-500)		
-05	303.6	19.1	3.6	510-560	C	N
	(309.3	32.1	8.6	0-500)		
-07	306.5	26.8	4.5	300-540	B	N
	(308.1	36.8	2.8	0-200)		
L6-01	298.4	18.7	3.9	500-580	C	N
	(305.2	32.1	7.8	0-400)		
-02	286.9	39.9	7.8	400-600	A	N
-03	299.4	20.1	4.4	500-600	A	N
L7-02	316.1	77.0	4.0	0-540	A	N
-04	334.6	-30.8	4.8	400-600	A	I*
-06	343.6	82.1	4.9	300-510	A	N*
-07	325.7	87.7	6.4	0-510	A	N*
L8-01	54.2	-19.0	1.0	520-620	A	I
-02	52.4	-17.0	3.7	510-560	A	I
-04	328.3	20.6	1.4	400-530	C	N
	(326.2	28.9	6.4	0-300)		
-05	325.5	36.7	3.6	400-560	C	N
	(328.6	46.9	6.0	0-300)		
L9-01	291.7	24.9	1.8	400-540	A	N
-02	296.9	29.1	1.2	500-580	A	N
-05	Unstable					
-06	286.5	23.9	1.6	300-530	A	N

L10-01	287.2	4.9	1.7	520-600	A	N
-02	281.6	7.7	1.7	500-550	C	N
	(284.2	18.0	9.5	100-400)		
-06	282.9	-11.4	2.4	400-550	A	I
-07	331.6	-13.0	5.0	530-540	C	I
	(13.6	-29.1	23.0	100-500)		
L11-01	257.2	84.1	2.8	500-580	C	N
	(27.1	78.0	6.0	0-400)		
-04	209.1	23.5	4.9	520-550	C	I*
	(225.8	49.8	30.9	0-400)		
-06	299.0	20.6	2.5	500-560	C	N
	(300.7	26.3	4.5	100-400)		
-07	283.0	18.2	0.5	540-580	A	N
L12-01	340.4	75.2	6.1	0-400	A	N
-02	343.5	71.5	3.5	100-300	A	N
L13-01	66.0	13.5	1.7	500-580	A	I
-02	68.7	5.8	3.3	500-580	A	I
-04	71.5	6.0	1.9	500-580	A	I
-05	70.2	-4.7	1.9	530-580	A	I
L14-01	297.0	16.9	2.8	500-580	A	N
-02	Unstable					
L15-01	294.5	16.3	2.3	520-580	A	N
-02	295.7	16.0	0.6	500-540	A	N
-06	296.6	14.4	0.9	500-560	A	N
-07	297.8	16.7	0.8	400-540	A	N
L16-01	297.8	30.7	1.3	400-560	A	N
-02	295.6	30.9	1.2	300-520	A	N
-03	294.9	29.1	1.7	400-530	A	N
-07	298.8	34.9	2.9	400-540	A	N
L17-02	298.3	25.3	3.8	500-550	A	N
-04	305.2	29.3	1.8	520-580	C	N
	(311.9	44.8	9.0	0-500)		
-05	287.5	24.7	2.2	520-570	C	N
	(296.8	35.0	8.4	100-500)		
-07	296.6	26.5	4.0	520-570	C	N
	(301.1	36.2	7.3	100-500)		
L18-03	285.2	14.7	1.3	540-560	A	N
-06	287.5	15.4	1.6	520-680	A	N
-07	292.5	16.9	1.3	500-600	A	N
L19-02	308.3	38.1	5.9	400-540	A	N
-03	313.8	43.2	4.2	250-450	A	N
L20-01	288.2	10.4	1.0	400-680	A	N
-02	286.3	10.0	0.9	450-680	A	N
-03	292.3	10.9	0.9	500-660	A	N
-06	293.9	2.9	3.3	520-660	A	N

L21-02	83.2	71.0	6.3	500-540	C	I
	(51.4	79.3	7.0	0-400)		
-03	Unstable					
L22-02	305.6	72.3	2.2	300-540	B	N
	(302.1	2.1	2.1	0-200)		
-03	Unstable					
L23-01	94.4	-2.2	2.4	300-700	A	R
-02	106.5	-5.8	2.2	560-700	A	R
-03	113.8	-26.9	2.8	560-660	A	R

APPENDIX 2 :

THERMAL DEMAGNETISATION RESULTS FOR ALL SAMPLES IN THE MIDDLE LAVA FORMATION

SAMPLE	D	I	α95	T	CAT	POLARITY
M1-01	158.9	60.0	2.5	300-560	A	I
-02	163.3	58.4	3.0	300-560	A	I
-03	Unstable					
-06	167.4	58.0	8.5	540-580	C	I
	(237.2	76.1	2.4	0-500)		
M2-01	151.2	44.3	3.3	560-700	A	I
-02	149.7	38.8	2.3	580-700	A	I
-04	148.7	44.3	2.4	610-640	A	I
-05	152.6	38.7	1.8	530-630	A	I
M3-01	154.8	47.0	1.5	560-700	A	I
-02	152.5	47.8	1.6	560-700	A	I
-04	144.9	46.0	2.0	600-700	A	I
-05	145.4	48.5	1.4	620-700	A	I
M4-01	146.9	44.8	3.4	560-660	A	I
-02	165.5	61.4	2.4	610-660	A	I
-03	147.7	47.0	1.5	610-680	A	I
-06	156.9	44.0	1.2	620-700	A	I
M5-01	158.7	41.9	2.6	530-660	A	I
-02	153.9	47.4	1.3	580-680	A	I
-03	150.8	44.5	3.2	560-700	A	I
-04	160.5	41.5	3.7	590-660	A	I
M6-01	163.0	42.9	2.8	530-600	A	I
-02	157.7	41.6	1.7	560-600	A	I
-03	153.1	52.6	4.4	520-660	A	I
-06	154.1	48.1	2.4	560-680	A	I
M7-03	149.6	47.0	2.2	580-620	A	I
-04	150.9	47.4	2.9	540-620	A	I
-05	147.7	25.2	5.4	400-560	A	I
-07	145.0	38.3	4.0	620-700	A	I
M8-01	302.2	-25.4	3.6	620-720	A	I
-02	310.5	-24.6	0.9	620-680	A	I
M9-01	141.5	-15.5	0.9	620-680	A	R
-02	141.6	-16.9	3.0	0-680	A	R
M10-01	159.7	-6.6	2.2	530-640	A	R
-02	157.7	-12.5	2.0	540-620	A	R
M11-02	257.6	-4.5	8.2	580-650	C	I
	(48.6	50.0	3.8	400-540)		

-03	273.4	34.7	5.9	500-600	C	N
	(145.4	75.0	3.7	0-400)		
M12-01	134.5	-10.4	4.9	500-620	A	R
-03	142.1	-14.0	0.9	580-650	A	R
M13-02	142.3	-9.0	1.7	560-680	A	R
-03	139.4	-15.8	4.8	620-680	C	R
	(127.2	11.0	11.8	100-300)		
M14-01	137.0	-14.6	3.5	620-680	A	R
-02	134.7	-17.3	0.4	600-660	A	R
M15-01	141.0	-18.7	2.0	560-640	A	R
-03	135.6	-16.7	3.6	580-680	A	R
M16-02	294.6	27.2	5.4	530-600	A	N
-03	289.8	27.3	10.3	500-620	A	N
M17-03	320.8	-8.7	0.6	610-700	A	I
-05	315.3	-6.9	1.8	580-700	A	I
-06	312.3	-10.6	1.5	610-700	A	I
-07	315.8	-7.7	1.0	610-700	A	I
M18-01	161.6	26.0	2.5	610-700	A	I
-03	346.1	19.6	9.3	600-700	A	N
-05	311.5	31.8	4.0	500-640	A	N
-06	309.5	42.7	4.0	500-610	A	N
-04	102.1	-25.5	1.4	500-670	A	R

APPENDIX 3 :

DEMAGNETISATION DATA FOR ALL SAMPLES IN UPPER LAVA FORMATION

SAMPLE	D	I	α95	T	CAT	POLARITY
U1-01	324.2	44.4	3.5	400-560	B	N
	(330.5	58.5	7.0	0-300)		
-02	345.7	50.0	2.8	500-560	B	N
	(334.5	71.8	2.3	0-300)		
-03	293.8	59.3	1.7	500-560	B	N
	(315.8	78.5	3.4	0-300)		
-04	358.5	54.3	3.4	500-620	B	N
	(1.0	60.0	2.5	0-300)		
U2-02	332.3	31.2	3.7	500-560	B	N
	(337.2	55.3	9.1	0-300)		
-03	332.5	30.8	5.8	500-620	B	N
	(344.1	51.0	6.4	0-300)		
-05	330.3	50.9	4.1	300-530	A	N
-06	306.1	54.6	2.3	400-530	B	N
	(317.7	63.0	6.1	0-300(		
U3-01	308.8	28.5	2.4	560-680	C	N
	(338.7	77.1	1.7	0-530)		
-02	335.2	73.6	1.5	200-590	A	N
-03	309.9	21.6	3.3	560-680	C	N
	(329.7	68.3	2.1	0-500)		
-04	296.6	20.6	4.1	590-680	C	N
	(329.6	69.5	1.9	0-560)		
U4-02	284.3	60.9	6.6	500-590	C	N*
	(324.8	60.7	9.9	200-500)		
-03	348.4	61.6	2.5	200-560	A	I
-04	331.7	64.8	1.5	100-530	A	N
-05	311.4	21.6	1.5	530-620	C	N
	(332.2	68.1	3.9	100-500)		
U5-01	303.9	28.3	1.1	500-620	A	N
-02	308.1	20.5	0.2	590-640	A	N
-03	321.1	26.6	1.4	590-640	A	N
-07	313.6	33.4	3.8	500-620	A	N
U6-01	318.5	33.7	4.1	590-640	A	N
-04	313.3	29.3	3.2	0-590	A	N+
-06	Unstable					
-07	320.6	26.7	4.6	620-680	A	N*
U7-01	306.9	33.6	2.0	0-640	A	N+
-02	303.4	33.1	2.3	0-640	A	N+
-06	303.5	21.7	2.0	590-680	A	N
-07	309.9	35.2	7.5	530-620	A	N

U8-01	292.9	63.7	3.8	400-560	C	N
	(308.5	69.6	5.7	0-400)		
-02	277.6	50.2	2.8	500-590	C	N
	(295.1	72.6	6.0	0-400)		
-03	352.0	76.0	1.8	0-530	A	I
-05	248.6	58.1	3.1	500-590	C	N
	(227.2	41.7	9.7	0-300)		
U9-01	93.3	-20.6	3.7	590-680	A	R
-02	92.4	-21.6	3.2	590-680	A	R
-03	98.2	-21.1	2.9	590-680	A	R
-06	100.0	-19.9	3.6	590-680	A	R
U10-01	100.9	-14.4	1.2	560-680	A	R
-03	98.1	-12.7	1.1	590-640	A	R
-05	98.7	-16.3	0.9	590-640	A	R
-06	93.1	-17.5	0.7	530-640	A	R
U11-01	107.1	-28.2	1.6	500-620	A	R
-04	100.7	-34.3	0.8	530-620	A	R
-05	109.8	-21.0	2.5	530-620	A	R
-06	109.9	-51.7	0.9	560-620	A	R
U12-01	95.0	-22.1	3.0	530-620	A	R
-02	99.0	-18.1	2.1	530-640	A	R
-04	102.1	-25.5	1.4	500-670	A	R
-05	101.4	-24.3	1.8	500-670	A	R
U13-01	98.7	-25.6	1.4	590-670	A	R
-02	100.7	-24.7	2.4	500-640	A	R
-03	104.7	-28.7	0.7	530-640	A	R
-06	103.9	-31.4	1.4	500-620	A	R
U14-01	100.2	-4.9	6.3	560-620	C	R
	(93.3	41.1	30.9	0-530)		
-02	97.8	-21.5	1.4	560-620	A	R
-03	112.3	-24.0	3.7	590-640	D	R
	(101.6	-15.2	10.1	400-560)		
	(101.4	27.0	22.3	0-300)		
-04	108.1	-9.5	1.9	560-620	C	R
	(95.3	56.2	12.2	300-530)		
U15-02	12.3	75.1	1.0	200-590	A	I
-03	116.9	-19.3	1.0	560-670	C	R
	(284.0	64.0	3.2	200-530)		
-05	86.4	-29.0	6.1	560-670	C	R
	(64.5	16.2	37.0	200-530)		
-06	Unstable					
U16-01	331.1	78.0	1.4	300-560	A	N
-02	358.0	80.0	0.7	300-590	A	I
-03	265.0	69.9	2.5	200-530	A	N
-04	14.6	78.1	1.9	0-400	A	I
U17-01	306.8	24.0	1.0	560-620	C	N

	(318.5	26.4	6.3	0-530)		
-02	303.9	21.2	3.2	500-620	C	N
	(323.5	64.1	3.6	0-400)		
-04	304.2	25.8	3.1	530-620	C	N
	(312.9	69.2	5.1	0-400)		
-07	307.8	11.2	2.3	560-640	C	N
	(313.0	77.2	2.9	100-400)		
U18-01	284.4	28.0	5.0	560-640	A	N
-03	281.7	16.5	3.7	560-640	A	N
-04	281.6	27.2	2.7	530-700	A	N
-06	275.5	16.0	0.7	590-700	A	N
U19-01	273.2	33.5	3.3	500-640	A	N
-02	273.4	8.5	2.3	530-640	A	N
-04	276.6	28.8	2.1	300-630	A	N
-06	280.1	20.4	2.2	400-620	A	N
U20-01	270.8	33.0	3.0	530-620	A	N
-02	270.7	29.2	6.2	560-620	B	N
	(292.4	74.8	8.9	0-200)		
-06	278.2	30.6	1.1	560-620	C	N
	(269.1	28.4	4.8	0-530)		
-07	285.4	24.7	4.8	500-620	C	N
	(297.4	21.2	12.3	0-400)		
U21-01	80.2	-7.0	0.9	200-590	A	R
-02	Unstable					
-04	321.9	82.6	1.5	200-560	A	N
-07	256.7	74.9	4.6	0-500	A	N
U22-02	221.1	58.6	1.2	0-680	A	I
-03	199.7	47.8	1.7	300-680	A	I
-04	4.3	47.3	2.9	200-400	A	I
-07	309.0	-32.3	3.8	200-560	A	I
U23-03	326.0	48.9	5.2	590-660	A	N
-04	339.3	46.7	1.4	500-560	C	N
	(340.1	36.2	10.4	0-400)		
-05	334.4	38.2	3.7	400-640	A	N
-06	317.6	36.3	6.7	400-620	A	N
U24-03	45.1	-27.3	2.2	100-560	A	I
-04	145.5	19.8	4.0	100-530	A	I
-05	327.1	52.1	3.7	300-560	B	N
	(318.1	68.9	1.7	0-200)		
-06	296.6	58.4	2.4	400-530	C	N
	(308.0	71.9	4.4	0-300)		
U25-01	335.0	36.8	4.4	500-620	A	N
-04	324.6	41.9	2.1	400-620	A	N
-05	310.0	41.9	4.5	500-640	C	N
	(336.2	54.6	6.3	0-400)		
-06	334.6	27.2	2.7	400-560	C	N
	(347.2	26.8	9.0	0-300)		

U26-01	256.2	75.9	4.7	100-500	A	N
-03	333.2	45.3	4.2	400-630	C	N
	(195.2	69.2	4.3	0-300)		
-04	347.2	36.4	10.3	500-620	C	I
	(Unstable)					
-06	198.4	66.8	2.2	400-560	C	I
	(Unstable)					
U27-01	4.6	37.7	2.3	560-615	A	I
-03	346.3	70.1	1.8	540-615	C	I
	(105.1	35.1	16.8	100-500)		
-06	289.8	43.1	8.8	400-590	A	N
-07	357.9	48.3	2.5	540-680	C	N
	(278.1	21.2	10.2	0-520)		
U28-01	297.3	65.6	4.7	400-590	C	N
	(307.2	72.8	5.6	0-400)		
-03	280.6	52.5	4.4	200-420	A	N
-04	272.3	47.5	6.4	400-575	B	N
-07	327.8	-40.7	7.0	500-560	A	N
U29-01	67.6	65.3	2.4	560-680	C	I
	(75.1	58.8	7.3	0-530)		
-02	29.4	66.1	1.6	575-630	A	I
-03	48.7	70.4	2.5	540-630	B	I
-05	46.5	-16.8	4.6	0-300	C	I
	(30.2	45.9	14.1	540-590)		
U30-04	Unstable					
-05	9.1	74.4	7.5	560-680	C	I
	(268.4	28.4	5.1	0-530)		
-06	336.5	-58.2	0.9	0-560	C	I
	(320.9	42.2	12.0	575-630)		
-07	337.0	-69.2	3.1	0-560	C	I
	(318.7	33.2	16.8	575-615)		
U31-01	298.7	65.0	2.7	600-680	B	N
-03	295.6	52.7	3.4	615-680	C	N
	(278.8	33.1	12.0	400-600)		
	(278.8	-33.5	7.5	100-300)		
-04	318.0	69.4	1.8	560-640	C	N
	(113.3	-23.2	3.9	0-530)		
-06	284.3	48.1	4.8	600-660	C	N
	(167.1	57.0	3.4	0-400)		
U32-01	271.1	41.8	1.2	575-680	A	N
-02	275.0	31.1	2.5	500-590	C	N
	(246.0	4.8	5.3	0-400)		
-03	282.6	38.5	2.4	600-700	A	N
-05	Unstable					
U33-01	215.3	-62.0	1.8	200-575	A	I
-02	6.4	84.0	4.7	200-590	B	I
-03	259.1	63.2	9.6	400-575	B	N
-06	284.1	62.4	1.9	590-660	D	N

	(260.2	25.8	8.9	520-575)		
	(280.0	43.1	17.7	300-500)		
U34-01	323.9	74.2	4.7	620-660	D	N
	(0.6	77.0	1.7	400-590)		
	(25.6	79.5	1.5	0-200)		
-04	29.2	84.0	3.8	500-680	C	I
	(177.0	-38.7	8.5	0-300)		
-05	295.5	59.9	1.6	620-680	B	N
-06	24.1	74.8	4.4	560-660	A	I
U35-03	302.4	76.8	2.0	590-680	C	N
	(312.4	33.2	5.8	0-300)		
-04	21.4	83.1	1.5	560-680	A	I
-05	347.0	77.0	1.5	575-680	A	I
-06	345.0	77.8	0.5	560-680	A	I
U36-01	302.7	52.8	6.1	530-620	C	N
	(335.9	59.9	2.6	0-500)		
-02	49.3	68.8	2.9	560-680	A	I
-05	291.2	84.3	1.6	590-680	C	N
	(14.6	86.8	2.0	0-575)		
-06	32.4	76.7	5.9	0-680	A	I
U37-02	Unstable					
-03	308.8	69.4	2.5	600-680	C	N
	(74.1	52.4	9.4	500-575)		
	(17.5	21.3	9.2	0-400)		
-04	291.9	63.3	5.2	600-680	C	N
	(281.6	72.0	5.0	0-575)		
-05	285.8	46.2	3.0	530-680	B	N
	(293.8	56.1	6.6	0-200)		
U38-01	232.4	81.1	1.8	530-640	A	I
-02	313.7	88.4	3.4	560-680	C	N
	(352.0	87.4	2.2	0-540)		
-03	294.5	82.8	8.4	0-640	A	N
U39-01	302.4	22.7	10.5	500-590	C	N
	(329.6	-20.9	6.5	100-400)		
-02	276.0	55.8	4.5	400-660	C	N
	(278.0	67.7	3.6	0-300)		
-04	270.6	56.2	4.8	560-660	C	N
	(50.4	60.2	5.6	100-540)		
U40-03	285.5	19.4	4.5	500-590	C	N
	(308.9	37.8	2.0	0-300)		